# Insights into the Mechanisms of Asymmetric Phase-Transfer Catalysis

**Katrina Anne Badiola**

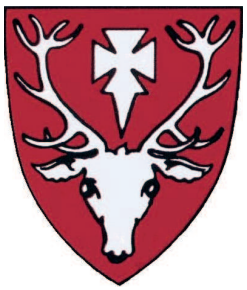
*A dissertation presented in partial fulfilment of the requirements for the award of the degree of*

**Doctor of Philosophy**

*of the*

**University of Oxford**



Chemistry Research Laboratory
12 Mansfield Road
Oxford, OX1 3TA

Hertford College
Catte Street
Oxford, OX1 3BW

*This thesis is dedicated to my parents, Maria and Wil Badiola.*

# Declaration

This dissertation describes work carried out in the Chemistry Research Laboratory at the University of Oxford between October 2014 and September 2019. The dissertation is a product of my own work and includes no results obtained through collaboration, except where specifically indicated in the text.



Katrina Anne Badiola

# Acknowledgements

First and foremost, I would like to acknowledge my supervisor, Professor Martin Smith. Without you, I would not have had the opportunity to work in such a great environment. Thank you for allowing me to be a member of your group. I am truly grateful for your support, guidance, wise words, and for the tremendous amount of assurance that really has kept me on track.

I would also like to thank Dr Martin Galpin without whom I would still be running around in circles of experiments. Thank you for your time and effort into making all those Mathematica notebooks, translating really very particular experimental procedures into solvable differential equations, and patient explanations.

Thanks must go to Yao and Ben, who I have collaborated with somewhat lately. Thank you for making the material, and doing all the optimisation that goes with it. Without your efforts, we wouldn't have had the spirok project! Ben, I had a really great time working with you, and will miss the time we were Team Kinetics.

Al and Minh (and Ben again). Thank you for your friendship and support, particularly through some of the tougher times. Thank you for understanding and being there when I needed you guys the most. I'll always remember the times we had here together.

To all other MDS group members, past and present. All those that I've had the fortune to know. Thank you for being a wonderful and terrific bunch. There are far too many of you to mention everyone, but special thanks goes to Roly, Jamie, and Bryony, for your guidance and help along the way.

Thank you to Liam, Roly, Tudor, Al, BAJer, Michael, and Nick for proof-reading my thesis. Your assistance is *greatly* appreciated.

To my parents, I am eternally grateful for your ceaseless and unconditional support, love, and encouragement. I would not have made it to where I am today without you.

Last, but certainly not least. Liam. I am truly grateful to have you in my life. I can't fully express my appreciation, particularly over the last couple of years, and when things have been tough. Your support, guidance, company, not to mention considerable proof-reading, have been an immeasurably positive influence in my life, and I look forward to see what the future holds.

# Abbreviations

| | |
|---|---|
| °C | degrees Celsius |
| ⌀ | diameter |
| % (v/v) | percent volume per volume |
| % (w/v) | percent weight per volume |
| % (w/w) | percent weight per weight |
| ® | registered |
| σ | standard deviation |
| 9MA | 9-methylanthracene |
| Ac | acetyl |
| AM | Dr Aroonroj Mekareeya |
| approx. | approximately |
| aq | aqueous |
| ATR | attenuated total reflection |
| BFR | Dr Benjamin Rahemtulla |
| Boc | *tert*-butoxycarbonyl |
| br | broad |
| brd | broad doublet |
| BrNaph | 1-bromonaphthalene |
| brs | broad singlet |
| brt | broad triplet |
| Bu | butyl |

| | |
|---|---|
| calcd. | calculated |
| cm | centimetre(s) |
| d | doublet |
| DABCO | 1,4-diazabicyclo[2.2.2]octane |
| DBU | 1,8-diazabicyclo[5.4.0]undec-7-ene |
| dd | doublet of doublets |
| ddd | doublet of doublet of doublets |
| dddd | doublet of doublet of doublet of doublets |
| ddddd | doublet of doublet of doublet of doublet of doublets |
| dddt | doublet of doublet of doublet of triplets |
| ddm | doublet of doublet of multiplets |
| decomp. | decomposed |
| dm | doublet of multiplets |
| DMF | dimethylformamide |
| DMSO | dimethylsulfoxide |
| dp | decimal place(s) |
| *d*-TFA | $CF_3CO_2D$ |
| ee | enantiomeric excess |
| eq. | equivalent(s) |
| equiv. | equivalent(s) |
| ESI | electrospray ionisation |
| Et | ethyl |
| g | gram(s) |
| h | hour(s) |
| HPLC | high-performance liquid chromatography |
| HRMS | high-resolution mass spectrometry |

| | |
|---|---|
| iPr | isopropyl |
| IR | infrared |
| ISC | internal standard curve |
| IUPAC | International Union of Pure and Applied Chemistry |
| kcal | kilocalorie(s) |
| KIE | kinetic isotope effect |
| $k_{obs}$ | observed rate |
| $l$ | length |
| L | litre(s) |
| ln | natural logarithm |
| LRMS | low-resolution mass spectrometry |
| µ | micro |
| m | multiplet |
| M | mole(s) per litre |
| Me | methyl |
| mg | milligram(s) |
| MHz | megahertz |
| min | minute(s) |
| µL | microlitre(s) |
| mL | millilitre(s) |
| mm | millimetre(s) |
| mM | millimole(s) per litre |
| mmol | millimole(s) |
| mol | mole(s) |
| mp | melting point |
| MRG | Dr Martin Galpin |

| | |
|---|---|
| MVK | methyl vinyl ketone |
| N/A | not applicable |
| nm | nanometre(s) |
| NMR | nuclear magnetic resonance |
| PFPOK | potassium 2,3,4,5,6-pentafluorophenolate |
| Ph | phenyl |
| ppm | parts per million |
| PTC | phase-transfer catalysis |
| quant. | quantitative |
| rac | racemic |
| RDS | rate-determining step |
| reXST | recrystallised |
| rpm | revolution(s) per minute |
| rt | room temperature (20–22 °C) |
| *rxn.code* | reaction code |
| s | second(s) |
| s | singlet |
| sat. | saturated |
| SD | standard deviation |
| sf | significant figure(s) |
| *t* | time |
| TBME | *tert*-butyl methyl ether |
| TLC | thin layer chromatography |
| UV | ultraviolet |
| vs | versus |
| wt% | weight percent |

# Abstract

This thesis describes work conducted towards the study of the mechanisms of asymmetric cation-directed phase-transfer catalysis (PTC).

Chapter 1 introduces the field of PTC, including its general mechanisms, utility in an asymmetric context, and previous kinetic and mechanistic studies. Despite being a well-established technique in organic chemistry, the precise mechanisms of enantioselective phase-transfer reactions, particularly those effected by cinchona alkaloid-derived catalysts are not fully understood.

In Chapter 2, we found that studying enantioselective phase-transfer reactions effected by cinchona alkaloid-derived catalysts proved to be both practically and intellectually demanding. The manner in which the reactions were practically conducted had significant bearings on the kinetic behaviour that was exhibited. Primarily, we developed robust methods that enabled the collection of reliable, reproducible kinetic data from polyphasic heterogeneous reaction systems.

Chapter 3 describes the kinetic and mechanistic study of a phase-transfer catalysed intramolecular *C*-acylation reaction. Deconvolution of the mechanism involved a series of practical kinetic investigations, evaluation of theoretical models, and further experimental interrogation. The final mechanistic hypothesis highlighted a series of processes concerning catalyst activation and regeneration, which were rate-determining in this system.

Chapter 4 presents a concise summary and conclusion to the thesis, and Chapters 5 to 10 describe experimental details and provide supporting information.

# Table of Contents


**Declaration** iii
**Acknowledgements** v
**Abbreviations** vii
**Abstract** xi
**Table of Contents** xiii
**1 Introduction** 1
1.1 Cation-directed phase-transfer catalysis (PTC) . . . 1
1.1.1 General introduction to PTC . . . 1
1.1.2 Mechanisms and reactivity of general PTC . . . 2
1.2 Asymmetric PTC . . . 7
1.2.1 Introduction to asymmetric PTC . . . 7
1.2.2 Cinchona alkaloid-derived catalysts in PTC . . . 9
1.2.3 Previous kinetic and mechanistic studies . . . 13
1.3 Previous work in the Martin Smith group . . . 23
1.4 Summary and impetus of the projects . . . 24
**2 Project 1: Developing Methods for Kinetic Studies of Asymmetric PTC** 25
2.1 Introduction . . . 25
2.1.1 Physical criteria for a model reaction . . . 25
2.1.2 Selection and precedence of a model reaction . . . 26
2.1.3 Initial mechanistic hypothesis . . . 31
2.2 Preliminary results . . . 33
2.2.1 Identifying conditions for a model reaction . . . 33
2.2.2 Establishing a quantitative assay . . . 36
2.2.3 Analysing the results . . . 38
2.3 Efforts to obtain kinetically reproducible results . . . 39
2.4 Investigating the reaction mechanism . . . 46
2.4.1 Isotope effects and further protocol optimisation . . . 46
2.4.2 Illuminating a rate-determining step . . . 54
2.5 Further protocol optimisation . . . 58
2.6 Attempts to delineate the reaction mechanism . . . 63
2.7 Summary and conclusions . . . 66
**3 Project 2: Elucidating the Mechanism of an Intramolecular *C*-Acylation Reaction Model** 68
3.1 Introduction . . . 68
3.1.1 Background to the reaction model . . . 68

3.1.2 Project approach . . . 69
3.1.3 A note on collaboration . . . 70
3.2 Preliminary preparations . . . 71
3.2.1 Sourcing equipment and planning . . . 71
3.2.2 Material syntheses and preparation . . . 72
3.2.3 Quantitative assay development . . . 75
3.3 Establishing protocols . . . 79
3.3.1 Standard reaction protocol . . . 79
3.3.2 Sampling protocol . . . 80
3.3.3 Data analysis protocol . . . 81
3.4 Initial hypothesis . . . 81
3.5 Preliminary reaction monitoring . . . 82
3.6 Viability of initial rate studies . . . 86
3.7 Preliminary investigations . . . 87
3.7.1 Investigating the transport reaction mechanism . . . 87
3.7.2 Investigating the catalyst and its effect on the rate . . . 89
3.7.3 Investigating the order in substrate . . . 95
3.7.4 Investigating the order in base . . . 97
3.7.5 Enantioenriched substrates under the reaction conditions . . . 100
3.8 Revising the mechanistic hypothesis . . . 103
3.9 Commencing a theoretical approach . . . 105
3.9.1 Numerical evaluation of the mechanistic hypothesis . . . 114
3.10 Investigating the revised mechanistic hypothesis . . . 122
3.10.1 The effect of chloride in the system . . . 122
3.10.2 Revisiting the order in base . . . 124
3.10.3 Ammonium phenolate as a mechanistic probe . . . 126
3.11 Investigating the burst phase . . . 135
3.12 Isotope effects . . . 140
3.13 Further revision of the mechanistic hypothesis . . . 147
3.13.1 Refining the theoretical model . . . 149
3.13.2 Final mechanistic hypothesis . . . 170
3.14 Final investigations . . . 172
3.14.1 Investigating the effect of 2,3,4,5,6-pentafluorophenolate on the reaction 172
3.14.2 Evaluating bases as additives in the reaction . . . 177
3.15 Availability of data . . . 180
3.16 Summary and conclusions of the project . . . 181
3.17 Future work . . . 184
**4 Summary and Conclusions 186**
**5 General Experimental Details 190**
5.1 General information relevant to material syntheses and characterisation . . . 190
5.2 General information relevant to the kinetic studies in project 1 (additions) . . . 192
5.3 General information relevant to the kinetic studies in project 2 (spirok) . . . 193
**6 Project 1: Experimental 194**

6.1 Material syntheses and characterisation . . . 194
6.2 Preliminary kinetic results . . . 198
6.3 Quantitative HPLC assay . . . 200
6.4 General protocols . . . 206
6.5 Results obtained using protocol 1 . . . 208
6.6 Effect of pre-stirring the catalyst and substrate . . . 210
6.7 Results obtained using protocol 2 . . . 212
6.8 Results obtained using protocol 3 . . . 215
6.9 Initial results obtained using deuterated substrate . . . 219
6.10 Results obtained using protocol 4 . . . 222
6.11 Evaluating the effect of deuterated substrate . . . 226
6.12 Illuminating a rate-determining step . . . 231
6.13 Results obtained using protocol 5 . . . 235
6.14 Evaluating the reaction order with respect to the substrate . . . 240
**7 Project 2: Experimental 248**
7.1 Material syntheses and characterisation . . . 248
7.2 Determination of p$K_a$ values . . . 262
7.3 Quantitative HPLC assay . . . 267
7.4 Reaction protocols . . . 273
7.5 Evaluating the extended reaction . . . 278
7.6 Viability of initial rate kinetic studies . . . 281
7.7 Evaluating the effect of stirring speed . . . 283
7.8 Evaluating the reaction order with respect to the ammonium chloride catalyst . . . 286
7.9 Evaluating the reaction order with respect to the substrate . . . 291
7.10 Evaluating the reaction order with respect to $K_3PO_4$ at constant volume . . . 295
7.11 Evaluating the reaction order with respect to $K_3PO_4$ at constant aqueous concentration . . . 299
7.12 Evaluating the effect of enantioenriched substrates . . . 304
7.13 Evaluating the effect of added KCl . . . 307
7.14 Evaluating the ammonium phenolate catalyst . . . 310
7.15 Evaluating the effect of LiCl with the ammonium phenolate catalyst . . . 316
7.16 Evaluating the effect of base with the ammonium phenolate catalyst . . . 318
7.17 Reaction order with respect to substrate during the burst phase . . . 321
7.18 Evaluating the effect of added surfactant . . . 325
7.19 Evaluating the effect of deuterated substrate . . . 327
7.20 Evaluating the effect of added 2,3,4,5,6-pentafluorophenolate . . . 333
7.21 Evaluating the effect of bases as additives . . . 338
7.22 Theoretical kinetics . . . 341
**8 R Scripts 361**
8.1 General information . . . 361
8.2 Processing data in project 1 . . . 361
8.3 Processing data in project 2 . . . 374
**9 Mathematica Scripts 383**

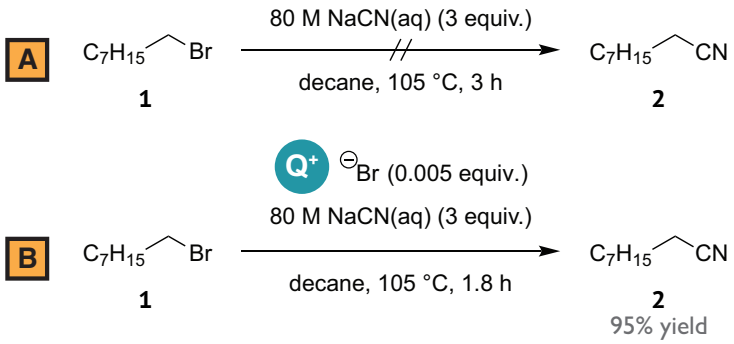
9.1 General information . . . . . 383
9.2 Mathematica scripts for model 1 . . . . . 383
9.3 Mathematica scripts for model 2 . . . . . 385
9.4 Mathematica scripts for model 3 . . . . . 387
9.5 Mathematica scripts for model 4 . . . . . 389
9.6 Mathematica scripts for model 5 . . . . . 393
9.7 Mathematica scripts for model 6 . . . . . 398
**10 References** **406**

# 1. Introduction

## 1.1 Cation-directed phase-transfer catalysis (PTC)

### 1.1.1 General introduction to PTC

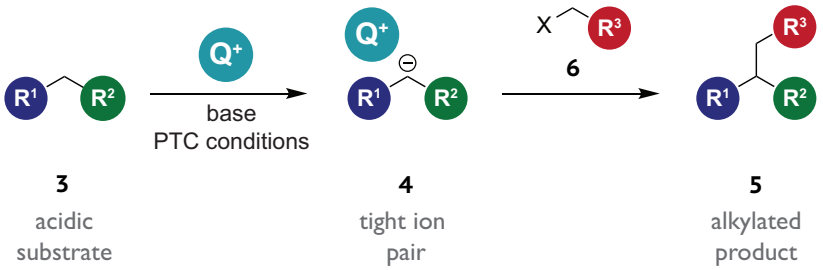
Cation-directed phase-transfer catalysis (PTC) is a powerful method for accessing a variety of structural moieties under reaction conditions that are typically mild, practically facile, and industrially viable.[1–4] To obtain reactivity between components that remain in otherwise immiscible phases, a catalyst is required, which is responsible for (1) transporting ions across phases and (2) increasing their reactivity. A classic example of PTC is the reaction of cyanide with 1-bromooctane **1**.[5] In the absence of a catalyst, the desired reaction did not proceed (A, Scheme 1.1), even after 2 weeks at 100 °C. However, introduction of a phase-transfer catalyst—a quaternary phosphonium ion—resulted in formation of the product 1-cyanooctane **2** in 95% yield after 1.8 h (B, Scheme 1.1). The catalyst was responsible for transporting the cyanide anion into the organic phase where it was then desolvated, hence increased in reactivity, and made available to react with 1-bromooctane **1**.[6]




**Scheme 1.1: The reaction of 1-bromooctane with cyanide. A)** No reaction occurred in the simple biphasic system. **B)** Addition of a phase-transfer catalyst ( = $C_{16}H_{33}(C_4H_9)_3P^+$) gave the displacement product **2** in 95% yield after 1.8 h.

While anions such as cyanide can be used, acidic substrates have recently become more common

in PTC; one general example is described in Scheme 1.2. In the presence of solid or aqueous inorganic base, the substrate **3** is deprotonated to generate the reactive anion. Coordination of the catalyst to the substrate anion results in the formation of a tight ion pair **4** which migrates deep into the organic layer, enabling the anion to undergo the requisite reaction, for example an $S_N2$ displacement to form a C−C bond.




**Scheme 1.2: Example PTC reaction using an acidic substrate.** Q+ corresponds to a phase-transfer catalyst; X indicates a leaving group.

By tuning the catalyst and reaction conditions, a myriad of reactivity modes can be accessed.[1,2,7] A few examples include $S_N2$ displacement reactions of alkyl halides,[2,6,7] base-mediated alkylation reactions,[2,8,9] elimination,[10] oxidation,[11] reduction,[1,12–14] and deuterium exchange reactions.[15] This means that PTC is immensely versatile in the types of products that it can access. This is not meant to be a comprehensive review of all phase-transfer reactions, but rather a demonstration of its breadth as an applied reaction.

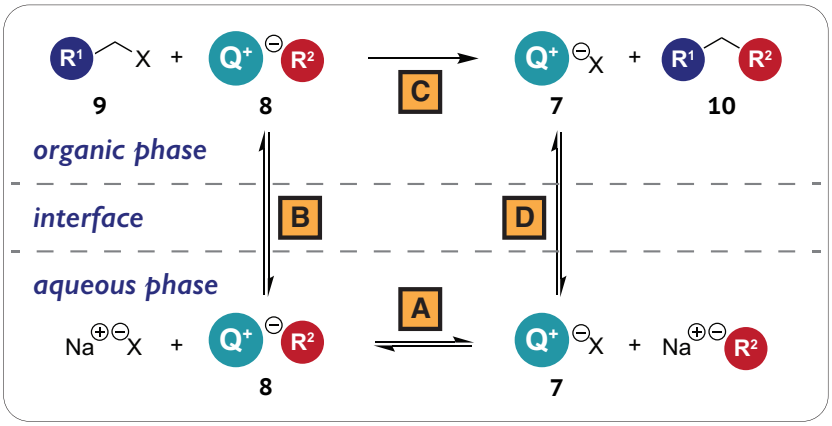
### 1.1.2 Mechanisms and reactivity of general PTC

#### Extractive and interfacial mechanisms

The mechanisms of PTC may be divided into two broad types: extractive and interfacial, with modifications and variations of both these mechanisms.[1] The key features of the extractive and interfacial reaction mechanisms are how and where the transfer event takes place. In both mechanisms, the intrinsic reaction occurs in the organic phase.

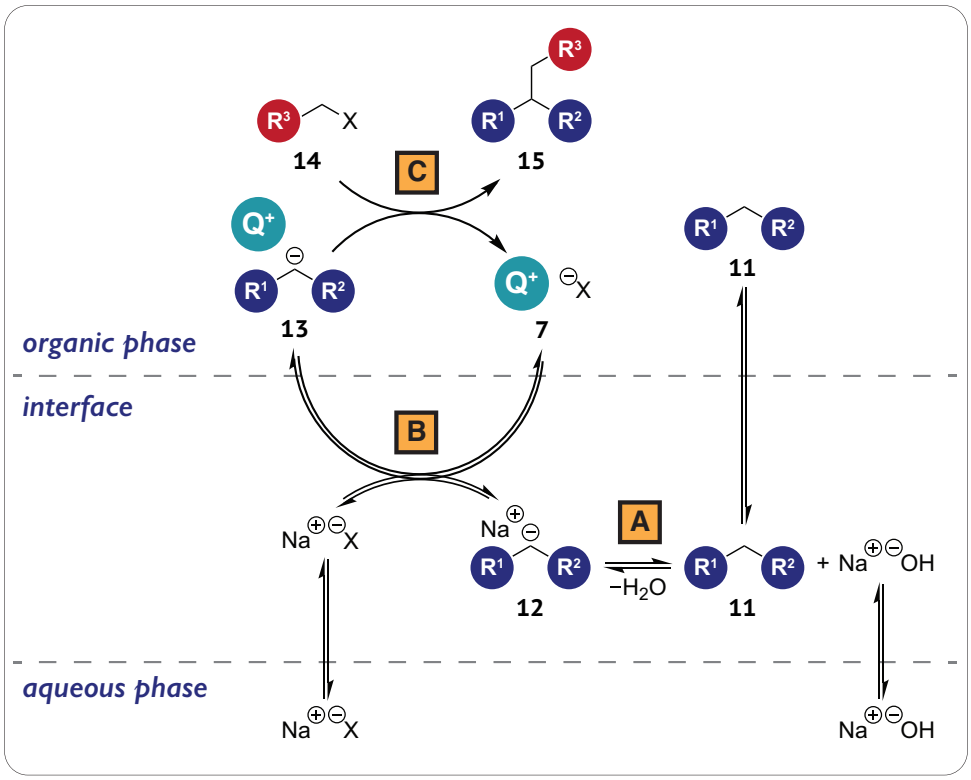
In the general extractive mechanism, an organophilic and hydrophilic catalyst (Q+) formally

transfers the product and substrate anions, as **7** and **8**, across the boundary separating the organic and aqueous phases—the interface (Scheme 1.3). Reaction of the substrate **9** to generate the product **10** subsequently occurs. The catalyst may be introduced into the reaction as the product anion salt **7** e.g. an ammonium halide salt.




**Scheme 1.3: Extractive mechanism of phase-transfer catalysis.** Followed in the clockwise direction starting from the bottom right hand corner: **A)** the catalyst cation coordinates to the currently unreactive anion in the aqueous phase; **B)** the catalyst cation transports the anion to the organic phase to form a desolvated tight ion pair; **C)** the substrate anion is then able to react with the electrophile to give the product and regenerated catalyst; **D)** the catalyst then migrates to the aqueous phase to restart the catalytic cycle. $Q^+$ Corresponds to a phase-transfer catalyst; X indicates a suitable leaving group, e.g. a halide.

The interfacial reaction mechanism is most easily represented by a reaction system involving an acidic substrate under basic biphasic conditions (e.g. an organic solvent in the presence of aqueous NaOH) (Scheme 1.4). Firstly, the substrate **11** is deprotonated by base at the interface to generate the substrate anion **12** (A, Scheme 1.4). Secondly, the substrate anion **12** coordinates to the catalyst **7** forming a tight ion pair **13** that migrates into the organic layer (B, Scheme 1.4). Lastly, the intrinsic reaction takes place, where the desolvated anion reacts with a suitable electrophile **14** to give the product **15** and the non-substrate bound catalyst **7** (C, Scheme 1.4).




**Scheme 1.4: Interfacial reaction mechanism with overall reaction of substrates 11 and 14 to give product 15 catalysed by 7. A)** Deprotonation of the substrate occurs at the interface; **B)** the phase-transfer catalyst coordinates to the substrate anion at the interface before transporting it to the organic phase; **C)** reaction of the substrate occurs in the organic phase, regenerating the phase-transfer catalyst salt, which is then able to interact with substrate. $Q^+$ Corresponds to a phase-transfer catalyst; X indicates a suitable leaving group, e.g. a halide.

Whilst these are the two simplest explanations of the main mechanisms behind PTC, there are modifications of both, which depend on other factors that include but are not limited to the lipophilicity and hydrophilicity of the catalyst, the p$K_a$ of the substrate, and the extractability of anions.[1,15–19]

### Factors that govern the mechanism

Distinguishing the precise mechanisms of phase-transfer catalysed reactions, with an emphasis on base-mediated processes, can be a non-trivial process. The factors that dictate which mechanism is dominant in a reaction system remain in contention; there is evidence to support both extractive[6,20–24] and interfacial mechanisms.[1,15,25–28]

There are several contributors to the type of reactivity of reaction systems; these are not limited to the propensity for mass transfer across phases, diffusion, solubility in the organic phase, and the nature of the intrinsic reaction.[1]

When considering base-mediated phase-transfer reactions, there are a number of factors that may affect or indicate the type of mechanism that is in operation (Figure 1.1). For example, a reaction with an overall kinetic first order, and an order with respect to the catalyst of one, with a strong dependence of the rate on catalyst organophilicity may be indicative of an extractive mechanism. Further experiments to verify the transport mechanism would do well to evaluate the rate-dependence of the reaction on its stirring speed, and to examine the p$K_a$ values of the substrates involved.

| **characteristic** | **extraction mechanism (controlled by intrinsic reaction)** | **extraction mechanism (controlled by diffusion)** | **interfacial mechanism** |
|---|---|---|---|
| catalyst structure | organophilicity | organophilicity | electrostatic availability |
| general kinetic order | simple (pseudo-first or second order) | zeroth order | complicated |
| catalyst kinetic order | first order | fractional | fractional |
| stirring speed | independent | varying dependence | very strongly dependent |
| substrate p$K_a$ | <16, 23–37 | <16, 23–37 | 16–23 |

**Figure 1.1: Characteristics of base-mediated PTC mechanisms.**

A general consensus is that the p$K_a$ of the substrate provides a good indication of which reaction mechanism might be occurring.[1,15,19] At p$K_a$ values below 16 (in DMSO), an extractive mechanism is likely. At p$K_a$ values between 16 to 23, an interfacial mechanism is favoured. At p$K_a$ values of 23 to 37, an extractive mechanism is again, more likely to be in operation. The reasons for this are that the catalyst extracts hydroxide into the organic phase, rather than the substrate anion. Only once hydroxide is in the organic phase, and desolvated, is it

basic enough to deprotonate substrates with p$K_a$ values of 23 to 37. Above p$K_a$ values of 37, phase-transfer is unlikely to be effective as a method for obtaining reactivity.

A strong but not absolute indicator of what transport mechanism might be in operation is the rate-dependence of a reaction on its stirring speed. If a transport process is rate-determining and an interfacial reaction mechanism in operation, there is typically a strong dependence of the rate on the stirring speed.[1,15,29] Stirring speeds may influence the rate of reactions proceeding via extraction mechanisms, but the rate-dependence typically plateaus above a certain threshold (usually 250 rpm),[6,30] which is that required for critical mass transfer.[1,5,15]

### Reactivity matrix of PTC

The modes of reactivity of phase-transfer reactions may be represented by the reactivity matrix of PTC (Figure 1.2).[1] Depending on the two rates—that of the intrinsic reaction and that of any transport processes—a reaction system may fall into any one of the four described quadrants: transport-limiting (1), fast (2), slow (3), or intrinsic reaction-limiting (4) regions.

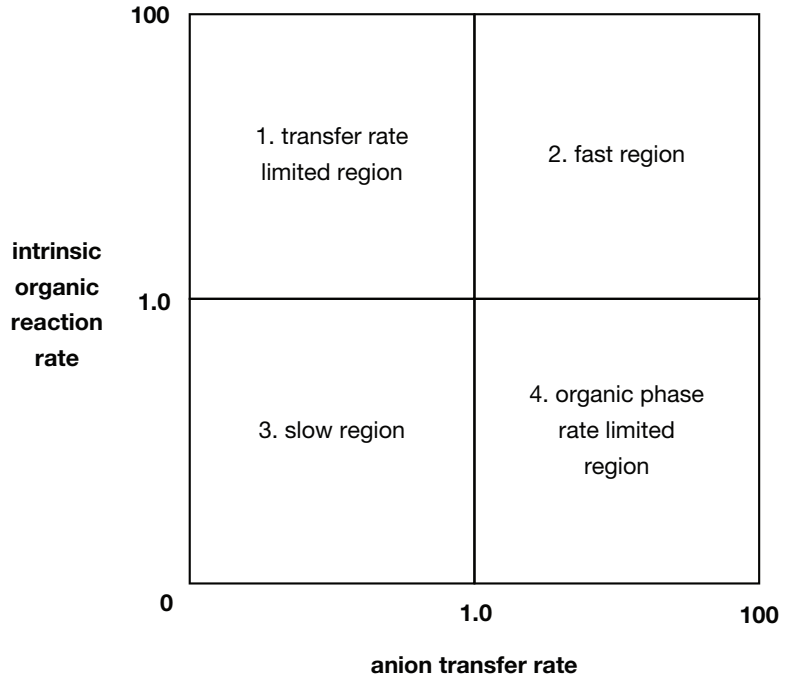


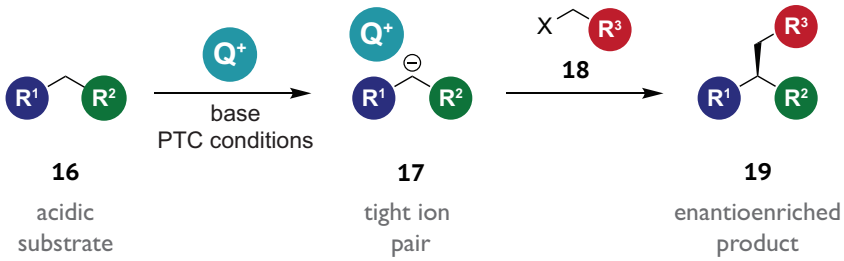

**Figure 1.2: Reactivity matrix of phase-transfer catalysis.** The $x$-axis describes the anion transfer rate and the $y$-axis is the rate of the intrinsic reaction.

By identifying where a reaction falls, and what mechanism may be operating, one can tune the reaction conditions to alter the rate. For example, in a transport-limiting regime with an interfacial-type reaction mechanism, the rate of the reaction may be increased simply by increasing the rate or efficiency of agitation.[1,31] For an extractive-type mechanism, changing the organophilicity of the catalyst may be impactful on the rate.[1,15]

## 1.2 Asymmetric PTC

### 1.2.1 Introduction to asymmetric PTC

In stereoselective PTC, a chiral and non-racemic catalyst is deployed. Selectivity is obtained by exploiting the tight ion pair between the catalyst cation and substrate anion in the non-coordinating organic phase; the catalyst directs the bond forming event, stereoselectively.[8,9,32–34] A general example of this process is described by Scheme 1.5, where an acidic substrate is used in base-mediated enantioselective PTC.




**Scheme 1.5: Generic example of an enantioselective phase-transfer catalysed reaction.** The acidic substrate is first deprotonated under the reaction conditions. Coordination of the catalyst cation to the substrate anion results in the formation of a tight ion pair. The catalyst cation then stereoselectively directs the bond-forming event to generate enantioenriched product. Q+ Corresponds to a chiral phase-transfer catalyst; X indicates a suitable leaving group, e.g. a halide.

The potential of phase-transfer catalysis as a vehicle for accessing enantioenriched molecules is exemplified by some of the enantioenriched architectures that are made available using PTC (Figure 1.3). Amino acid derivatives **20**, non-biaryl atropisomers **23**, and complex heterocycles **25** are three examples that can be enantioselectively constructed using asymmetric phase-transfer catalysis.

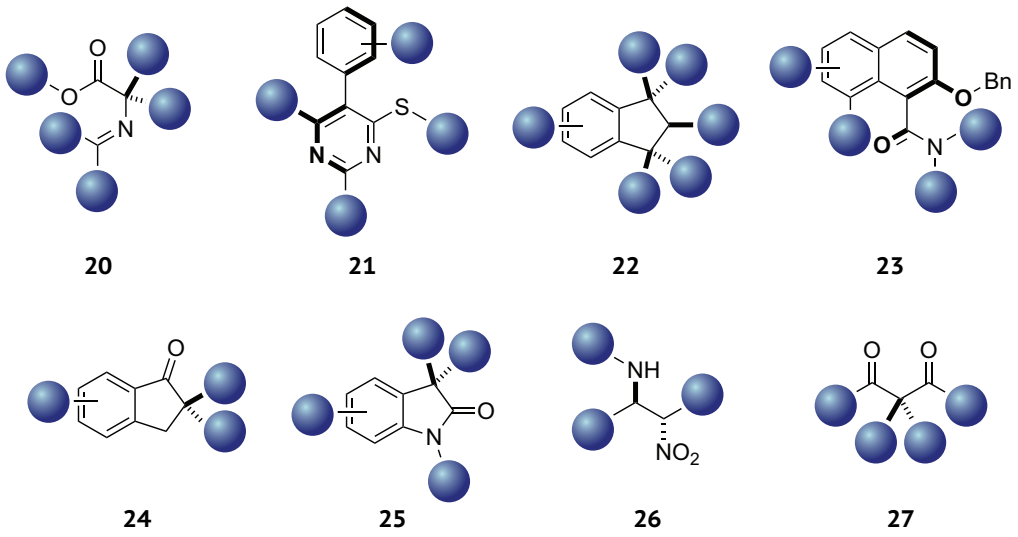



**Figure 1.3: Examples of enantioenriched scaffolds that are accessible using asymmetric PTC.** Examples include: **20**,[8,9,35,36] **21**,[37] **22**,[38] **23**,[39] **24**,[34,40–43] **25**,[42,44,45] **26**,[42,46,47] **27**.[9,42]

The catalysts that are used to effect stereoselective PTC are arguably as diverse as the reactions that have been reported (selected examples are shown in Figure 1.4). The chiral scaffolds that these catalysts are derived from are predominantly from cinchona alkaloids (A, Figure 1.4), biaryl frameworks (B, Figure 1.4), and other systems (C, Figure 1.4). Quaternary ammonium catalysts dominate the known examples, but phosphonium and sulfonium salts have been shown to be effective as chiral catalysts (D, Figure 1.4).

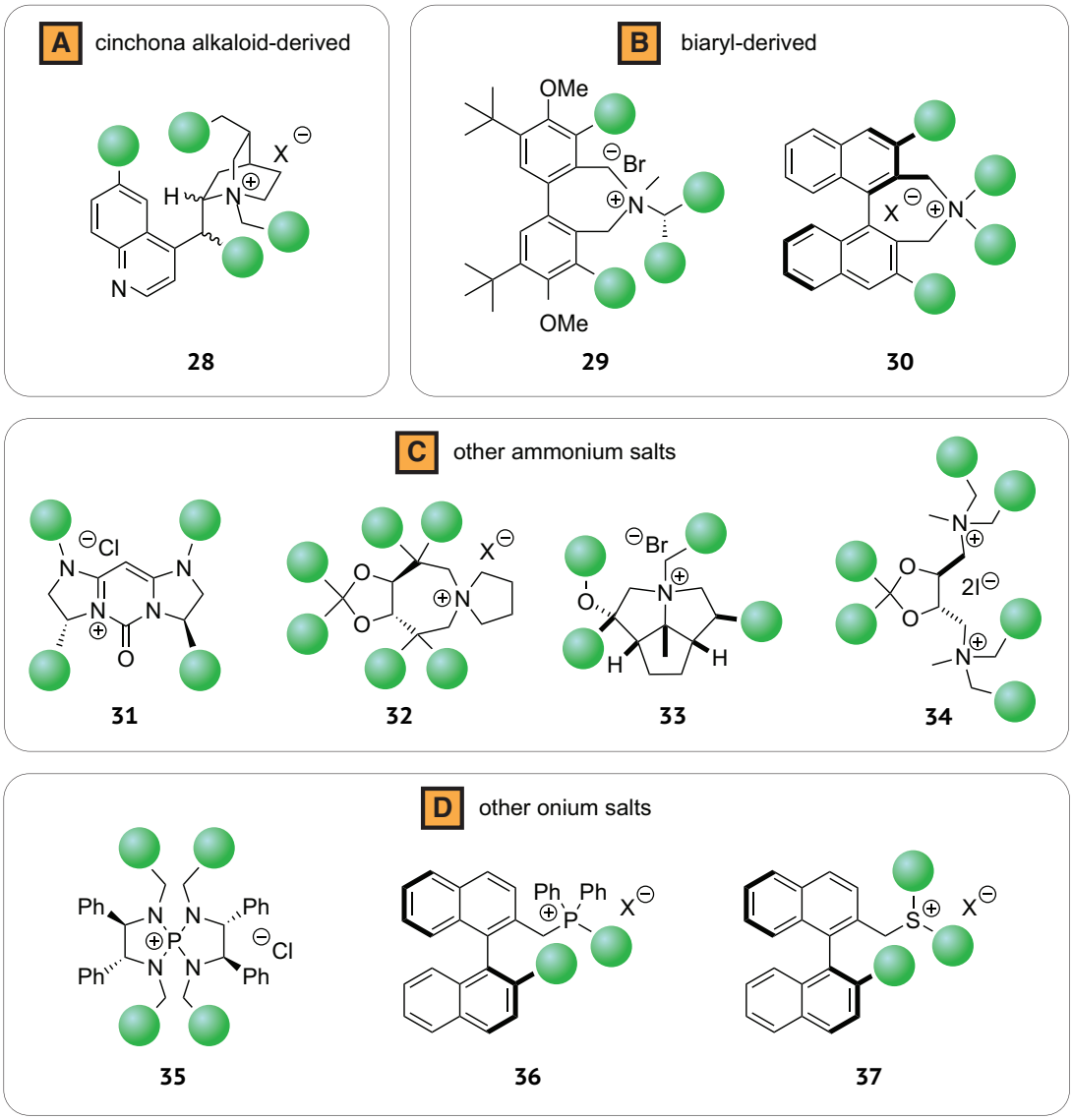
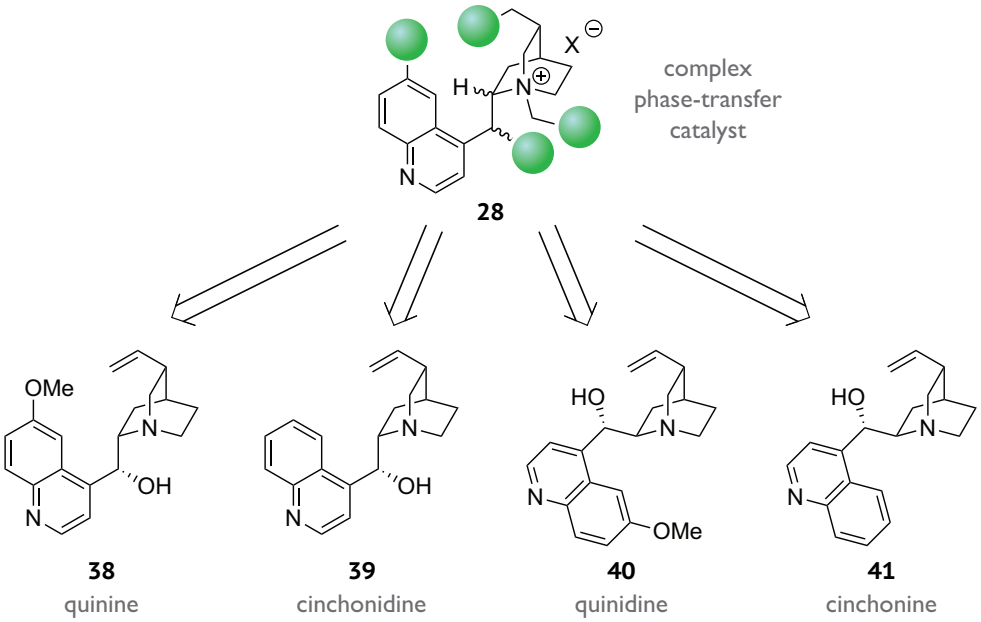



**Figure 1.4: Examples of chiral phase-transfer catalysts. A)** Cinchona alkaloid-derived catalysts (**28**[34,48]); **B)** biaryl-derived catalysts (**29**,[49] and **30**[50]); **C)** other ammonium salt catalysts (**31**,[51,52] **32**,[53,54] **33**,[55,56] and **34**[57–60]); **D)** other onium salt catalysts (**35**,[61,62] **36**,[63] and **37**[64]).

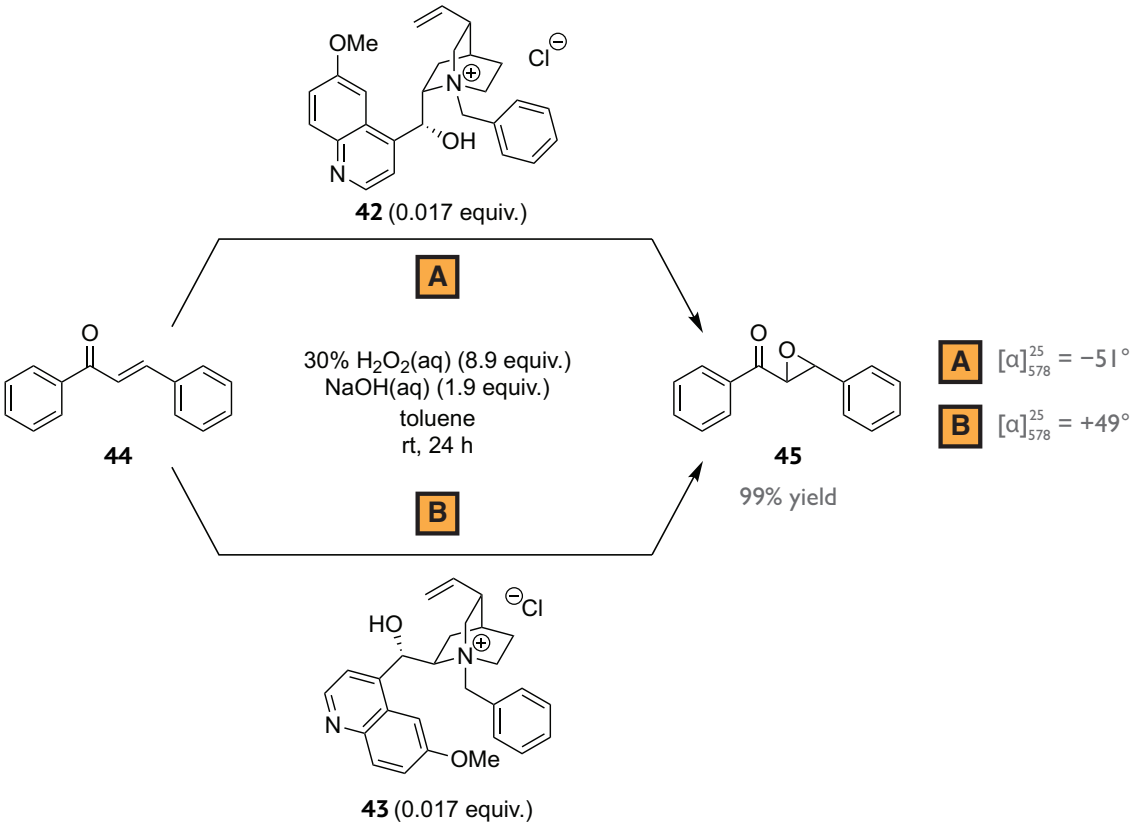
### 1.2.2 Cinchona alkaloid-derived catalysts in PTC

The most developed and used chiral phase-transfer catalysts are those derived from the four main cinchona alkaloids (Scheme 1.6).[34,48] Quaternisation of the quinuclidine nitrogen affords phase-transfer catalysts that may be easily accessed.



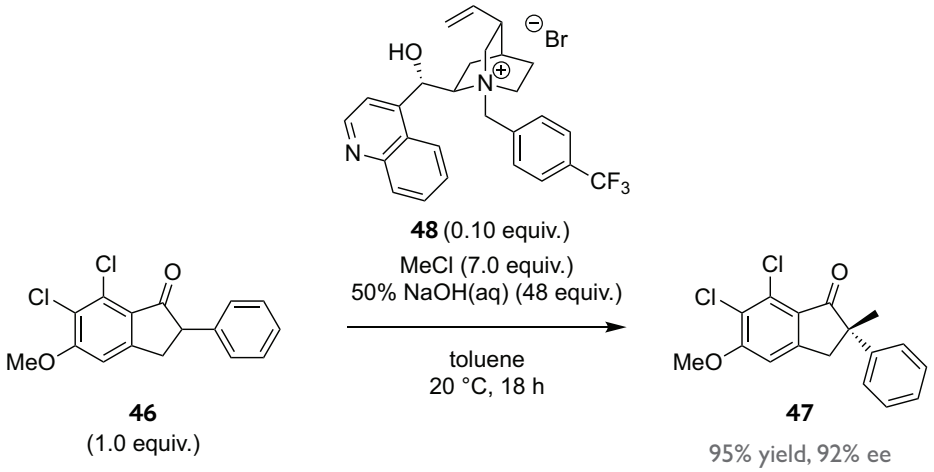

**Scheme 1.6: Complex phase-transfer catalysts may be obtained from the four main cinchona alkaloids: quinine 38, cinchonidine 39, quinidine 40, or cinchonine 41.** The green icons indicate typical sites of variation where different functionalities are commonly installed.

The application of cinchona alkaloid-derived catalysts dates back to the first examples of enantioselective phase-transfer catalysis. In 1976, Wynberg and co-workers demonstrated the use of *N*-benzylquininium chloride **42** as a catalyst in a phase-transfer reaction to generate optically active epoxides (A, Scheme 1.7). Use of the pseudoenantiomeric catalyst, *N*-benzylquinidinium chloride **43**, gave the product with the opposite enantiomeric excess, as determined by optical rotation (B, Scheme 1.7).



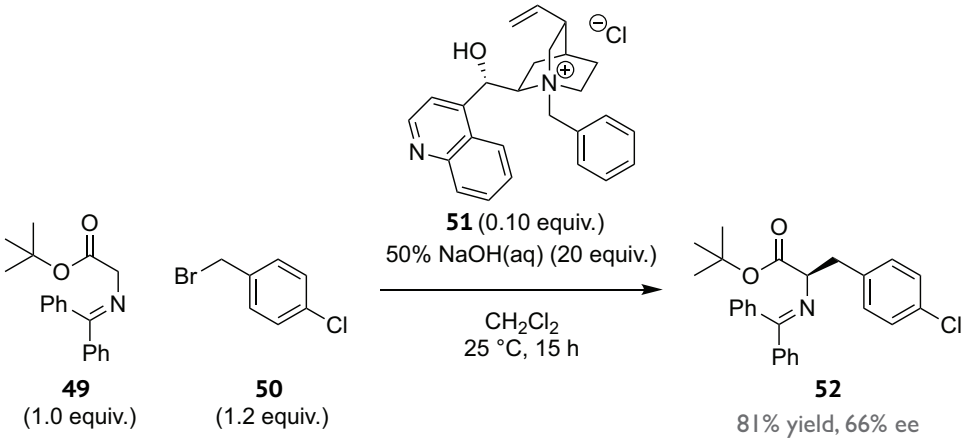

**Scheme 1.7: Phase-transfer catalysed enantioselective epoxidation of chalcone 44 effected by pseudoenantiomeric catalysts 43 and 42.** The reaction proceeded to give enantioenriched product **45** in 99% yield.

The first *highly* enantioselective phase-transfer reaction was published in 1984. It was from the Merck laboratories that the alkylation of indanone **46** was reported to give the corresponding product **47** in 95% yield and an ee of 92% (Scheme 1.8).[40] *N*-Benzylated cinchoninium **48** was deployed as the catalyst in the reaction. A thorough investigation of the reaction was subsequently performed, the details of which will be discussed later (in 1.2.3).[29]




**Scheme 1.8: First highly enantioselective phase-transfer reaction: alkylation of indanone 46 to give 47, catalysed by 48.** The reaction proceeded with 95% yield and an ee of 92% after 18 h.

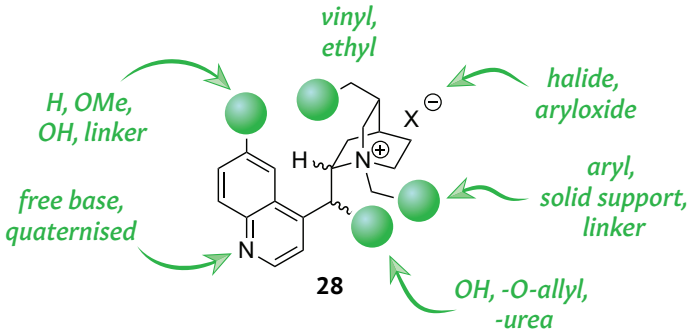
In the years following, several founding works demonstrated the use of PTC effected by cinchona alkaloid-derived catalysts in the synthesis of enantioenriched small molecules. O'Donnell and co-workers established the application of PTC in the synthesis of enantioenriched α-amino acid derivatives (Scheme 1.9),[33,35,65–67] whilst further work from the Merck laboratories explored the alkylation of indanone-derived substrates.[29,41,68]




**Scheme 1.9: One example of the phase-transfer reaction to generate enantioenriched α-amino acid derivatives.[66]** The reaction proceeded to give protected chloro-D-phenylalanine **52** in 81% yield with 66% ee.

Practically, the complexity of the cinchona alkaloid scaffold means that countless variations can be installed in derived phase-transfer catalysts (Figure 1.5).[3,8,9,48] Typical sites of variation include the quaternising group on the quinuclidine nitrogen,[8,9,40,48,69] functionalisation of the

hydroxy group,[47,70–72] identity of the counterion,[73–75] and modification of the vinyl[69,76–78] and quinoline moieties;[45,79] these are examples of modifications used to generate different cinchona alkaloid-derived phase-transfer catalysts, but is by no means an exhaustive list.



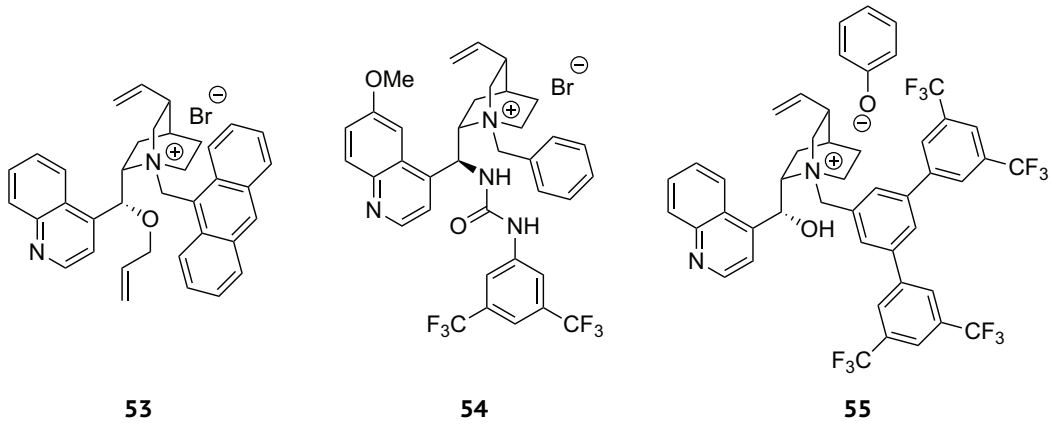



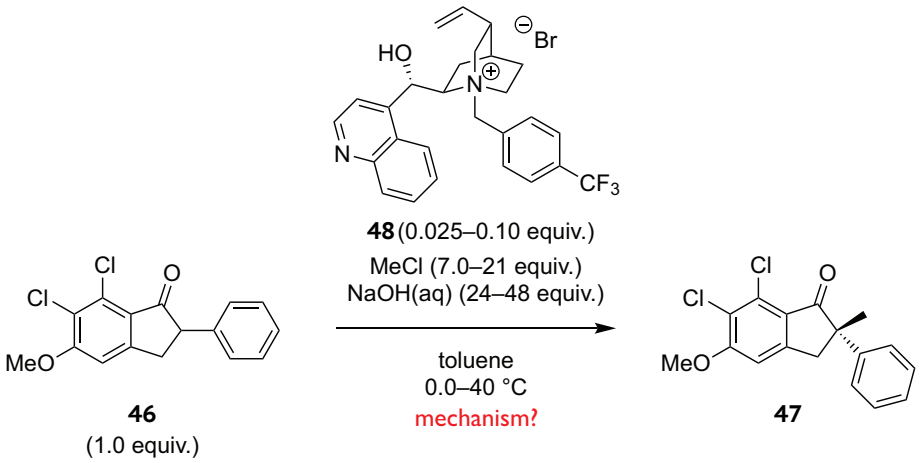

**Figure 1.5: Typical examples of modifications introduced into cinchona alkaloid-derived phase-transfer catalysts with three specific examples: 53,[70] 54,[47] and 55.[80]**

### 1.2.3 Previous kinetic and mechanistic studies

Despite their widespread use, the exact behaviour of cinchona alkaloid-derived catalysts in phase-transfer reactions remains unclear. Whilst there have been investigations examining structure-selectivity relationships,[71,76,81,82] substrate binding and induction of enantioselectivity,[46,70,83–85] there are relatively few kinetic and mechanistic studies that have focussed on the roles of these catalysts in reaction systems.[29,46,84,86]

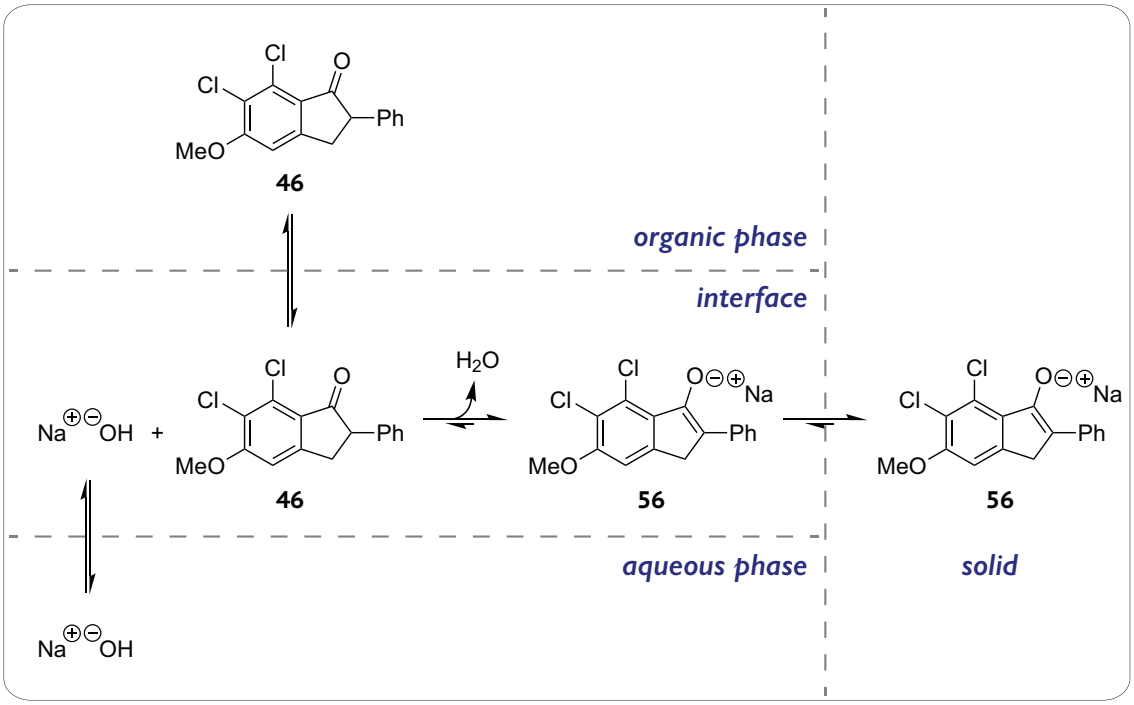
In 1987, Hughes and co-workers published a comprehensive study of the alkylation of indanone **46** by methyl chloride effected by the cinchona alkaloid-derived catalyst **48** under phase-transfer reaction conditions (Scheme 1.10).[29] Aspects of the reaction were examined in multiple stages:

substrate **46** deprotonation, catalyst behaviour and substrate anion extraction, and enantioselective methylation.



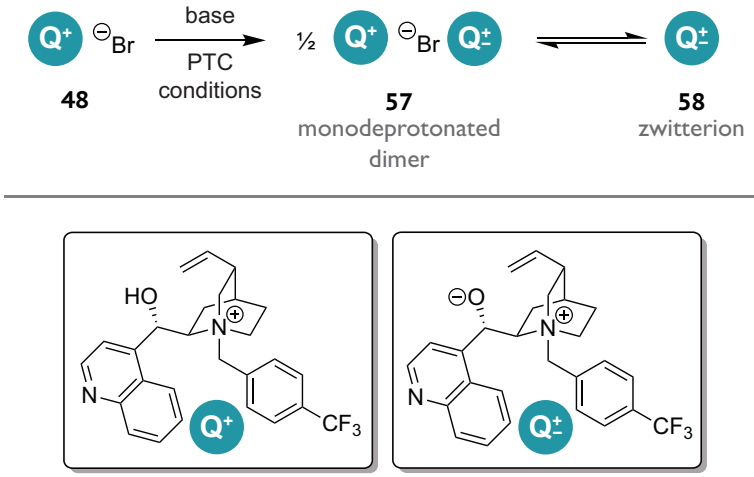

**Scheme 1.10: Investigation of the mechanism of the phase-transfer alkylation of indanone 46.**

Deprotonation of the substrate **46** by sodium hydroxide to form the corresponding sodium enolate **56** occurred via an interfacial mechanism (Scheme 1.11). The substrate predominantly existed as sodium enolate **56** as a separate solid phase in the reaction mixture. Residual indanone **46** remained present in the organic phase.



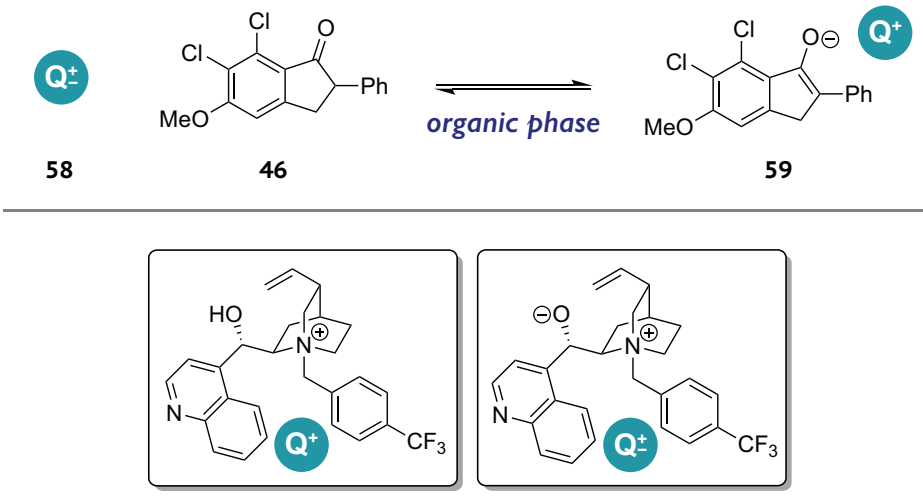

**Scheme 1.11: Formation of enolate 56 via an interfacial mechanism.**

The catalyst existed in the organic phase as a dimer **57** in equilibrium with its zwitterionic oxide **58** (Scheme 1.12). They proposed formation of the dimer occurred via dissolution of small quantities of catalyst **48** in the aqueous phase, followed by partial deprotonation, then extraction of the dimeric complex **57** into the organic phase.




**Scheme 1.12: Formation of catalyst dimer 57 and zwitterion 58 under phase-transfer reaction conditions.**

A potential pathway for the reaction was deprotonation of residual indanone **46** by the catalyst zwitterion **58** in the organic phase (Scheme 1.13). Alternatively, the substrate enolate was extracted into the organic phase either via a solid-liquid interaction, or, if small amounts of the enolate were dissolved in the aqueous layer, by liquid-liquid extraction.




**Scheme 1.13: Deprotonation of indanone 46 by zwitterion 58 in the organic phase.**

Evidence suggested that the reaction proceeded via an interfacial-type mechanism that was

not rate-determining. The rate of the reaction was independent to the stirring speed. They proposed that all rate-determining steps occurred solely in the organic phase.

The reaction order with respect to methyl chloride was 0.67. They suggested this result was due to competition between methylation and a step prior to methylation, but ruled out a rate-determining interfacial process.

They also examined the reaction in the presence of 30% NaOH(aq) and observed different mechanistic behaviour, which highlights the complexity of the system under investigation. Indeed, they found the mechanism was "more complex than that of a simple phase-transfer reaction."

In 2013 and 2016, Martins and Pliego reported computational studies of the same reaction system.[84,87] They first considered possible transition states for the enantioselective reaction (Figure 1.6). Key features of the favourable transition states were strong hydrogen bond interactions between the catalyst hydroxy group with the substrate enolate oxygen, and electrostatic interactions between the chloride leaving group and the catalyst cationic centre.[87]

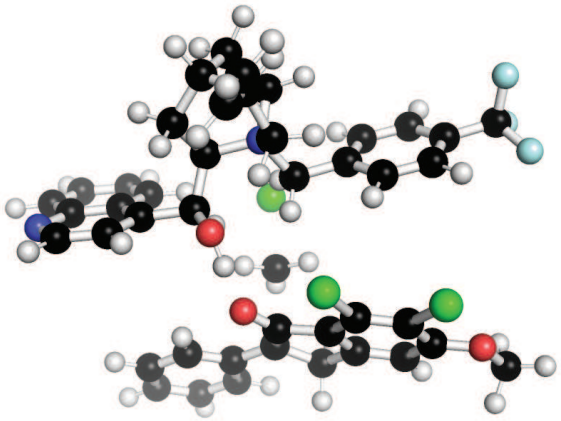
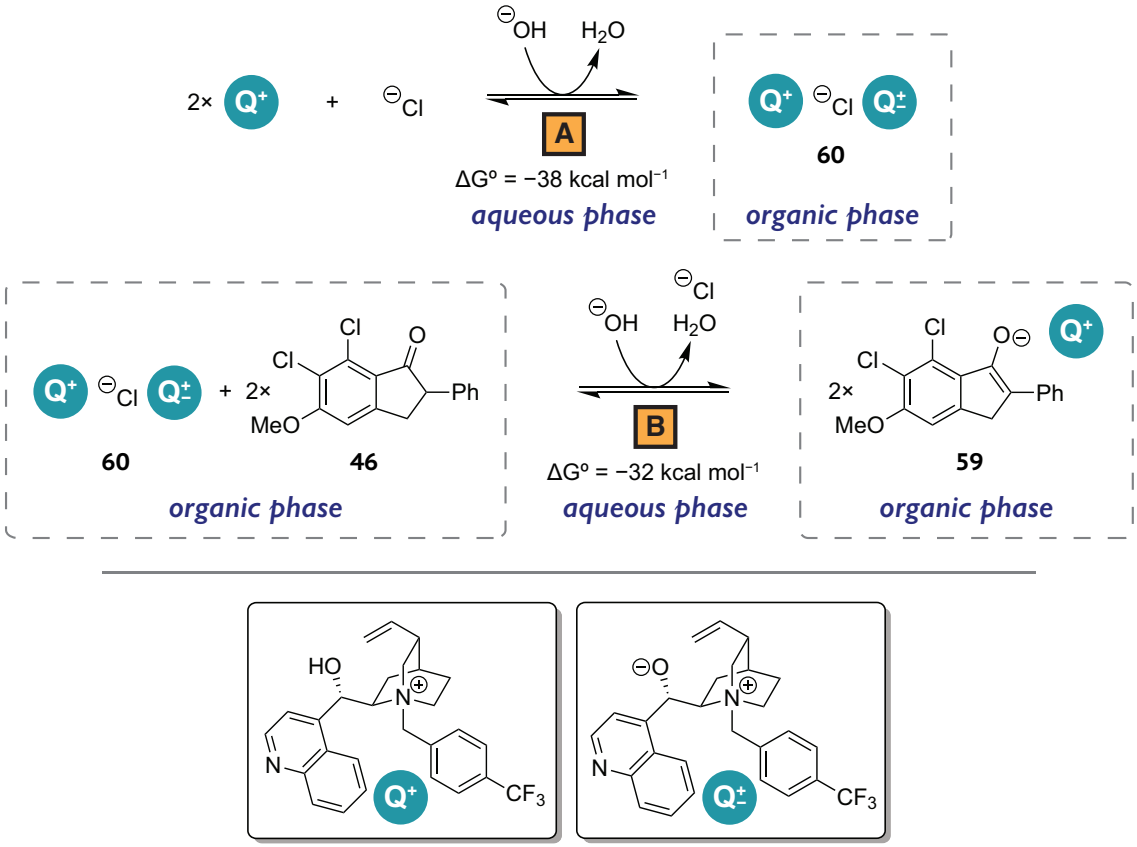


**Figure 1.6: Example transition state for the phase-transfer catalysed alkylation of indanone 46 by methyl chloride.[87]**

Furthermore, they evaluated equilibria describing transport and chemical processes relevant to

the alkylation reaction.[84] These included partitioning of the indanone substrate **46** between the organic and aqueous phase, deprotonation of the indanone in either phase (organic or aqueous) by hydroxide, formation of the ammonium enolate complex **59**, and association and dissociation steps concerning the catalyst dimer.

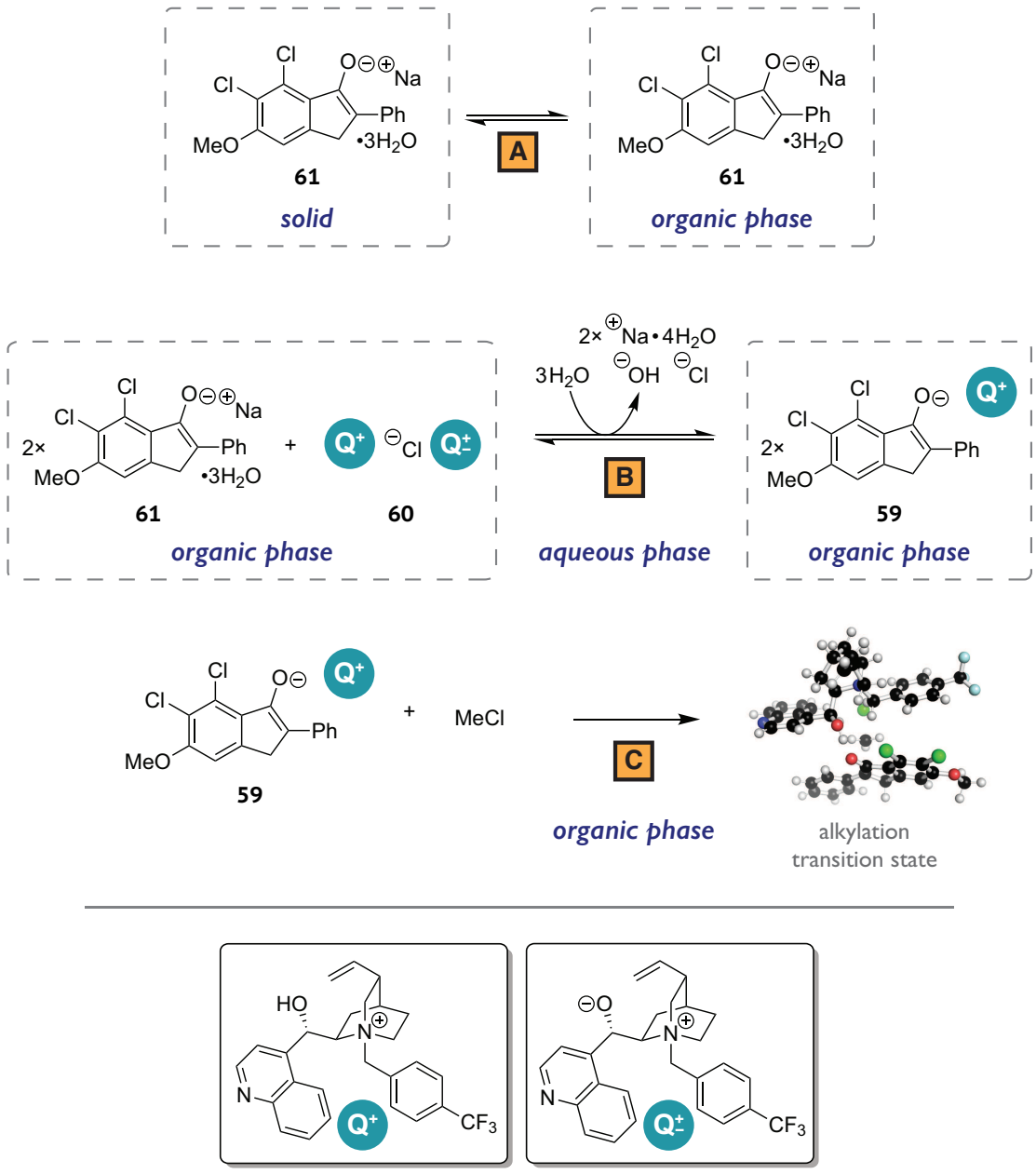
They found that formation of the catalyst dimer **60** in the organic phase was favourable compared to free ammonium, hydroxide, and chloride ions in the aqueous phase (A, Scheme 1.14). In the presence of aqueous hydroxide, indanone **46** in the organic phase readily dissociated the catalyst dimer **60** to generate ammonium enolate **59** in the organic phase (B, Scheme 1.14). Other processes included formation of sodium enolate in the organic phase and the organic phase dissociation of the catalyst dimer by the substrate enolate. All of these processes were energetically favourable. However, their results were obtained assuming infinite dilution, which did not account for the presence of solids (e.g. solid ammonium halide **48** or sodium enolate **56**), the dissolution of solids, and any solid-liquid interactions. They also did not consider the formation of zwitterion **58** in the organic phase, or the potential for the zwitterion to deprotonate the substrate in the organic phase.





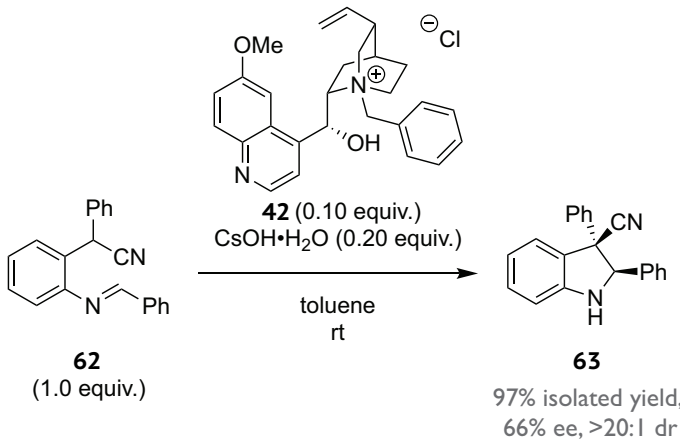

**Scheme 1.14: Example equilibria of the A) catalyst dimer formation and B) indanone 46 deprotonation.** [84]

To describe the overall reaction, they proposed a simple kinetic model comprised of three steps leading to formation of the lowest energy transition state for the alkylation (Scheme 1.15). They assumed that residual indanone in the organic phase was present as the sodium enolate **61** (A, Scheme 1.15). The next step was formation of the ammonium enolate complex **59** from the sodium enolate **61** (B, Scheme 1.15). Finally, methyl chloride in the organic phase reacted with the ammonium enolate complex **59** (C, Scheme 1.15), resulting in formation of the most favourable transition state, which led to enantioenriched alkylated product **47**.



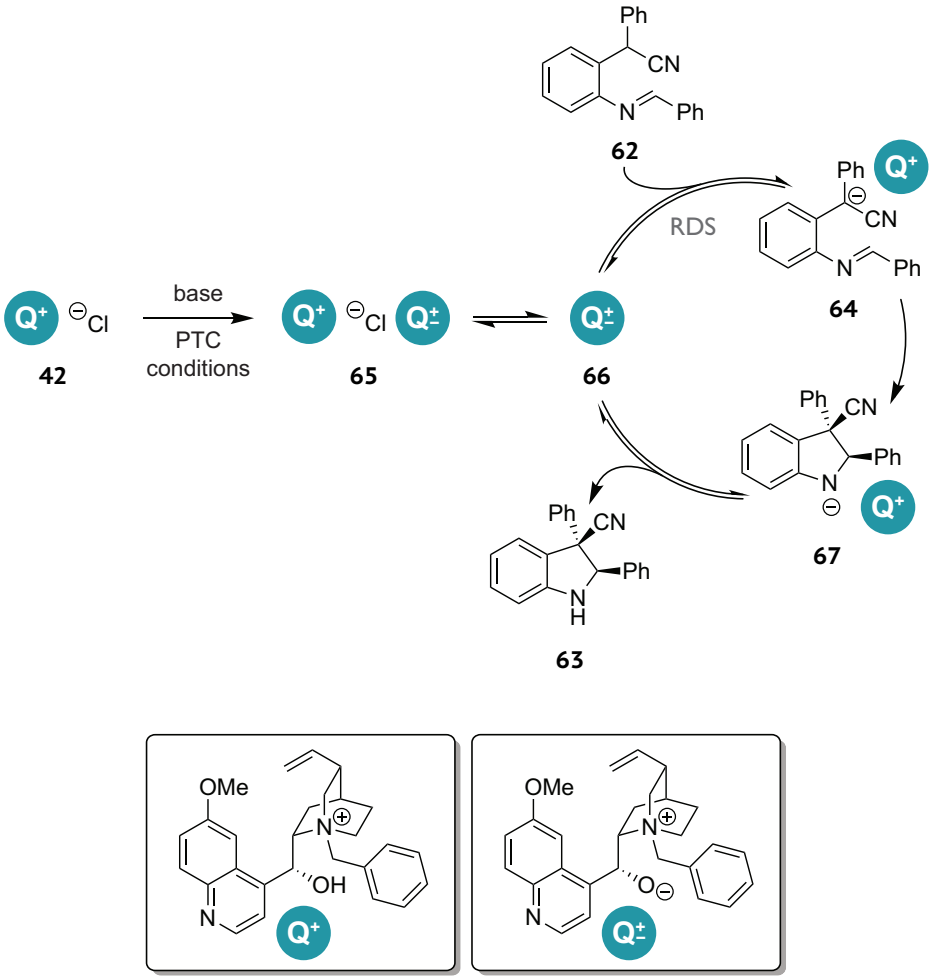

**Scheme 1.15: Kinetic model for the phase-transfer alkylation of indanone 46 by Martins and Pliego.** [84]

Another example of a kinetic and mechanistic study of an asymmetric phase-transfer reaction was carried out within the Martin Smith group; in work published in 2015 on an asymmetric phase-transfer cyclisation to give indolines.[86] The model reaction used in the mechanistic study deployed the substrate **62**, *N*-benzylquininium **42** as the catalyst, and catalytic quantities of CsOH (Scheme 1.16). The reaction was proposed to proceed via an interfacial type mechanism that was not rate-limiting under the standard reaction conditions.



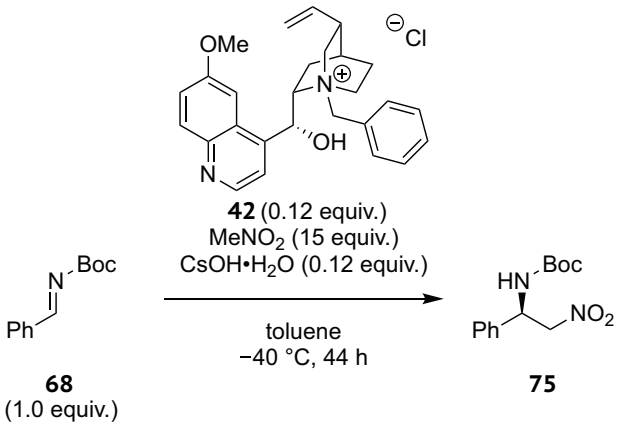

**Scheme 1.16: System used to evaluate the cyclisation reaction mechanism.** [86]

Interestingly, the kinetic profile of the reaction—the rate of formation of product **63**—was sigmoidal. The induction period in the system was attributed to an "auto" effect where the product anion deprotonated the catalyst scaffold to generate the corresponding catalyst zwitterion in the organic phase (Scheme 1.17). It was proposed that the zwitterion was responsible for deprotonating the substrate in the rate-determining step. Alternatively, the substrate was deprotonated via a classical interfacial reaction mechanism, and the resulting substrate anion reacted directly with the ammonium halide **42** to form the corresponding complex (i.e. **64**). In accordance with the work by Hughes and co-workers,[29] the reaction order with respect to the catalyst **42** was 0.56; this was consistent with the hypothesis that the catalyst was dimeric in the resting state and in equilibrium with an active monomeric species.

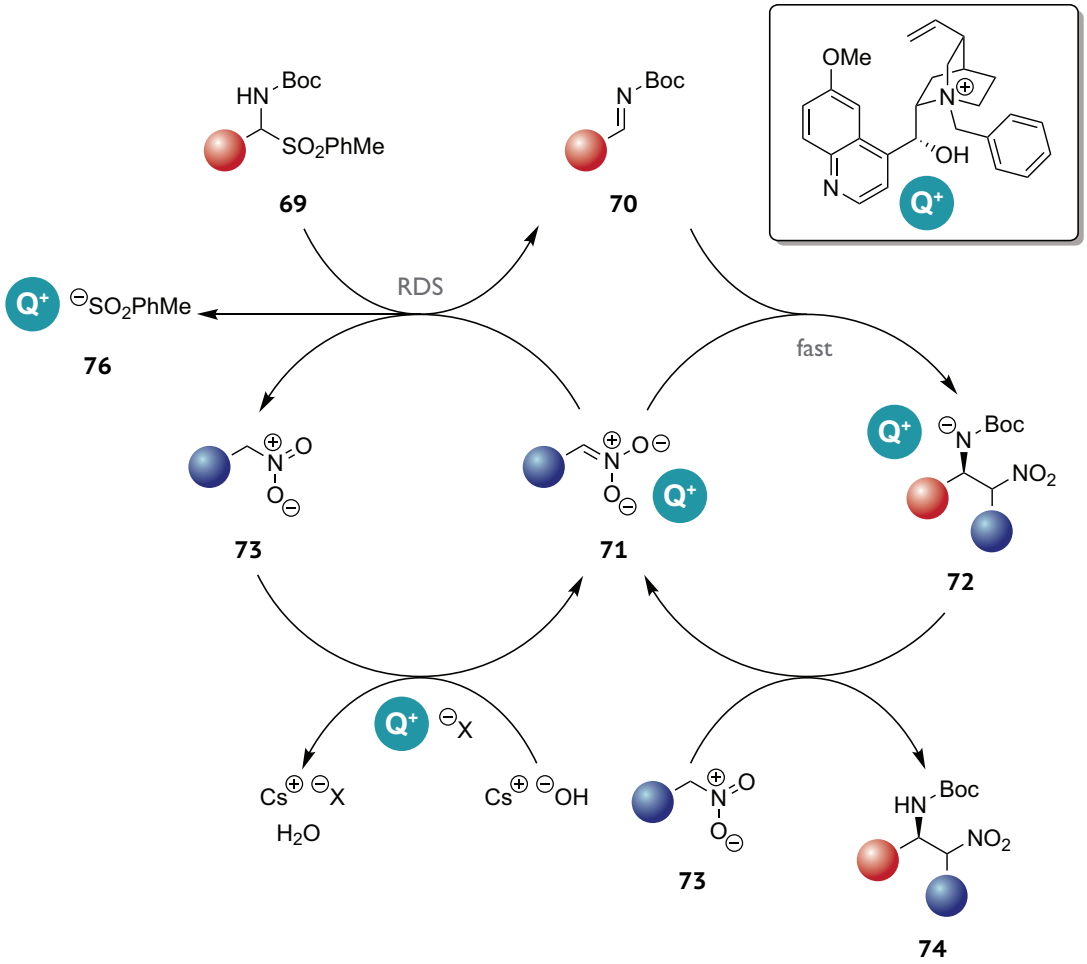



**Scheme 1.17: Proposed mechanism for the phase-transfer mediated cyclisation to give indolines.[86]**

As part of their investigations into phase-transfer catalysed aza-Henry reactions of α-amido sulfones, Palomo and co-workers conducted a brief kinetic study of the reaction of imine **68** with nitromethane (Scheme 1.18).[46] The reaction was effected using *N*-benzylquininium chloride **42** as the catalyst. They reported the reaction was first order with respect to both substrate **68** and catalyst **42**. The scope of the kinetic study did not examine the effects of nitroalkane—due to volatility—or base concentration. Overall, they proposed a general catalytic cycle for the transformation from amido sulfones **69** (Scheme 1.19). This involved the relatively slow formation of imine **70** mediated by ammonium nitronate **71**. Formation of the C−C bond subsequently occurred resulting in generation of the product anion **72**, which then reacted with nitroalkane **73** to generate product **74** and ammonium nitronate **71**.




**Scheme 1.18: Model reaction used in the kinetic study of a phase-transfer catalysed aza-Henry reaction.** [46]



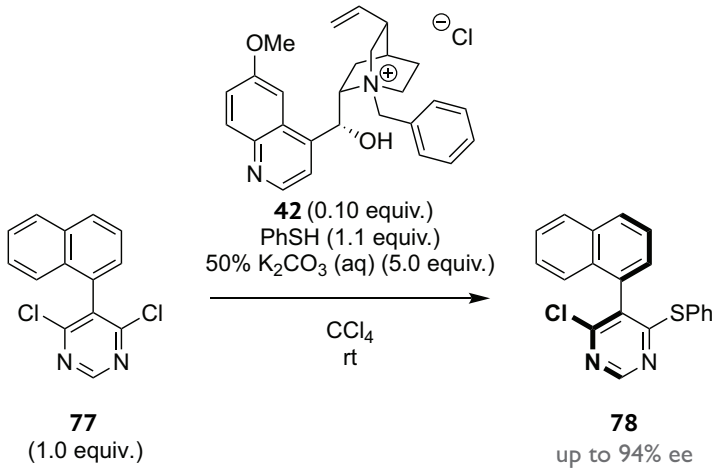

**Scheme 1.19: Proposed catalytic cycle for the aza-Henry reaction of α-amido sulfones 69 and nitroalkanes 73.** [46]

The prolific modification, application and deployment of cinchona alkaloid-derived ammonium salts as catalysts in phase-transfer reactions is not reflected in the kinetic and mechanistic

understanding of precisely how they behave in chemical systems. The handful of studies directly examining their roles in reactions has revealed potentially interesting behaviour, in addition to the presence of multiple catalyst species. However, in context, asymmetric catalysis effected by cinchona alkaloid-derived catalysts is effectively a "black box technique," which was a factor we wanted to address.

## 1.3 Previous work in the Martin Smith group

Previous work in the Martin Smith group concerning phase-transfer catalysis has primarily focused on developing methods to generate structurally diverse chiral scaffolds.[38,39,78,86] Recently, we have conducted kinetic studies with the aim of better understanding the way in which this catalysis proceeds. In addition to the cyclisation example (described in 1.2.3),[86] work by Roly Armstrong examined the mechanism of the de-symmetrising nucleophilic aromatic substitution reaction of dichloropyrimidine **77** effected by *N*-benzylquininium chloride **42** (Scheme 1.20).[37,88] Preliminary investigations of this system indicated the reaction order with respect to catalyst **42**, was 0.55, which was again consistent with the hypothesis that the cinchona alkaloid-derived catalysts exist as dimeric species under phase-transfer reaction conditions.




**Scheme 1.20: Previously investigated reaction system within the Smith group.[37,88]**

We sought to build on these previous studies, and further explore the behaviour of cinchona alkaloid-derived catalysts in phase-transfer reactions.

## 1.4 Summary and impetus of the projects

Despite the prominence of cinchona alkaloid-derived catalysts in asymmetric PTC, remarkably little is known about how these catalysts actually behave in reactions. To address this, we aimed to use general but interesting reaction systems. We wanted to explore the mechanisms of enantioselective phase-transfer catalysis in more detail. This required, firstly, identifying suitable model systems to explore, and as we discovered, developing practical methods for scrutinising our chosen systems. The goal was to gain a better understanding of how enantioselective PTC proceeds with an overarching aim to improving the way we exploit this tool and its catalysts.

# 2. Project 1: Developing Methods for Kinetic Studies of Asymmetric PTC

## 2.1 Introduction

We were interested in studying asymmetric phase-transfer catalysis generally. To do so, we required a model reaction to direct our focus. We also needed to identify phase-transfer reaction conditions that would be conducive to reproducible results, which will be discussed below. A reaction that might provide insight into asymmetric PTC generally would be ideal.

### 2.1.1 Physical criteria for a model reaction

To conduct kinetic studies of phase-transfer reactions, we required a method to monitor the concentration of reaction components over time. We were limited by the physical nature of the reactions that we wanted to monitor. For example, the requirement of constant mechanical agitation precluded NMR spectroscopy as a tool for monitoring reactions. Preliminary data obtained using ReactIR exhibited an unacceptably large signal-to-noise ratio from polyphasic, heterogeneous reaction mixtures. As such, we elected to use HPLC with a chiral stationary phase as the platform for assaying our reaction mixtures. This method would also enable the monitoring of enantioenrichment of any chiral molecules over time. To monitor the amounts of substrate and product from reaction mixtures by HPLC, the molecules needed to contain chromophores.

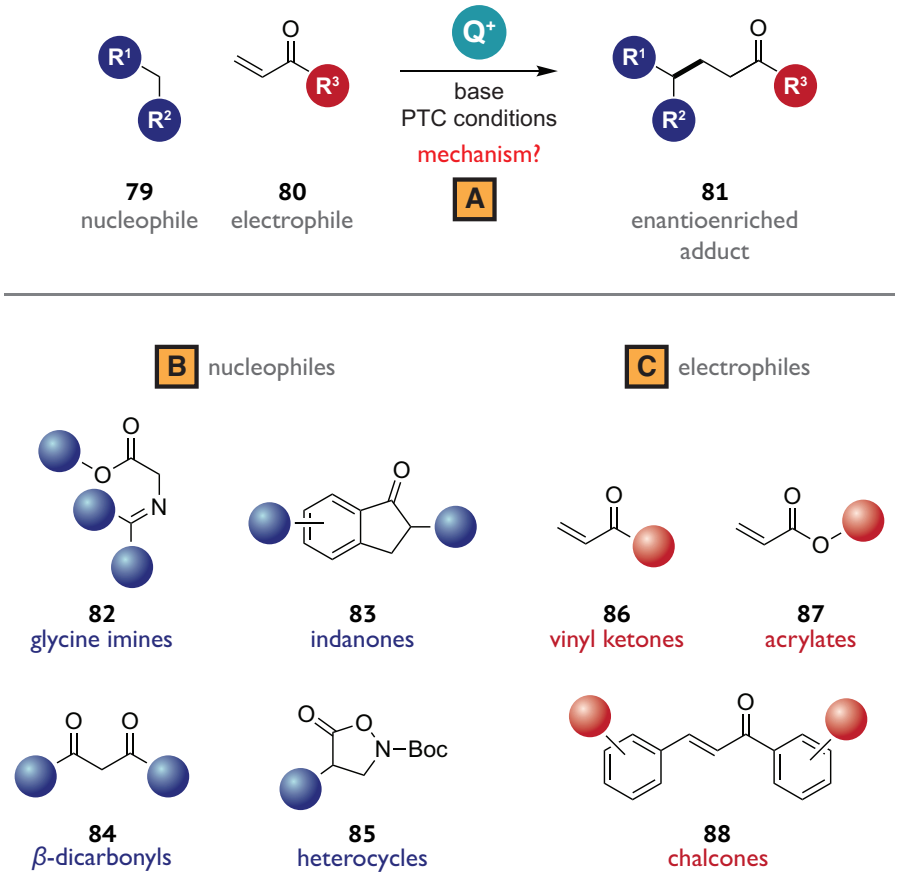
With respect to the reaction conditions, there were several criteria that we wanted the reaction to fulfil. The conditions must be such that we would maximise the probability for reproducible results. For example, we wanted the reaction to be amenable to aqueous base in order to

avoid the batch variabilities associated with solid inorganic bases. Furthermore, the reaction would ideally be carried out at room temperature due to the manner in which we would sample the reaction over time i.e. manually, by extracting aliquots from the stirred reaction mixtures. We wanted a reactive system with total reaction times of around 60 to 180 min at room temperature, but one that was easily accessible; that is, the substrates and catalyst were commercially available or obtainable on scale so that sufficient material would be on hand for the duration of the study.

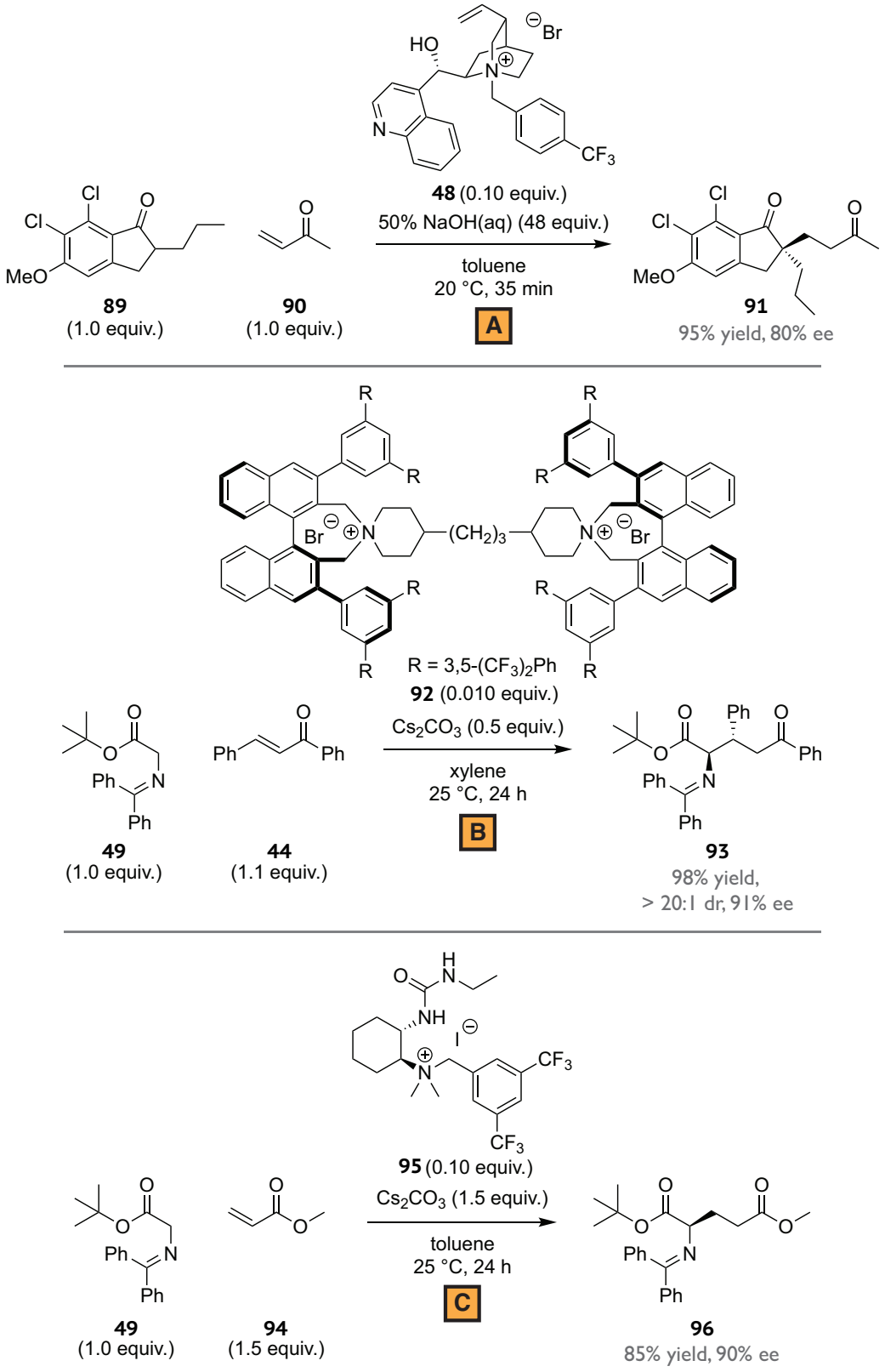
With these criteria in mind, we surveyed the literature in search of a suitable reaction on which to base our investigations.

### 2.1.2 Selection and precedence of a model reaction

We were, at the outset, interested in the mechanisms behind enantioselective phase-transfer catalysed 1,4-addition reactions (A, Scheme 2.1). This reaction model was attractive for a number of reasons. It was well-precedented in the literature.[9,34,89,90] There were a number of different reaction partners that we were able to select from (B, Scheme 2.1) and good enantiomeric excesses (80–91%) were demonstrable in a variety of systems carried out at ambient temperature (three examples are shown in Scheme 2.2).[41,91,92] Most reactions that achieve high enantioenrichment of products were carried out at temperatures below 0 °C and used highly complex catalysts.[93–95] Lastly, depending on p$K_a$ values of the reaction components, we might observe interesting kinetic behaviour (the details of which are discussed in section 2.1.3).

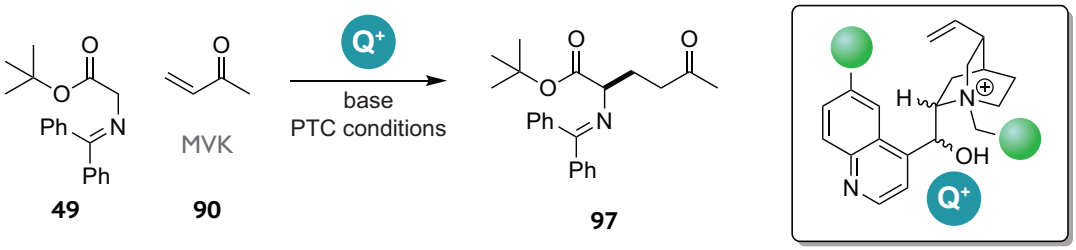



**Scheme 2.1: A) Generic enantioselective 1,4-addition reaction under PTC; B) examples of nucleophiles 82–85 and electrophiles 86–88 that have been used in this reaction.** Selected references for systems deploying nucleophiles are given as follows: glycine imines,[91,94,96–98] indanones,[43,99] dicarbonyls,[93] and other heterocycles.[100]




**Scheme 2.2: Examples of enantioselective phase-transfer catalysed 1,4-addition reactions carried out at ambient temperature. A)** Alkylation of indanone **89** using MVK **90**;[41] **B)** reaction of with glycine imine **49** with chalcone **44**;[91] **C)** reaction of glycine imine **49** with methyl acrylate **94**.[92]

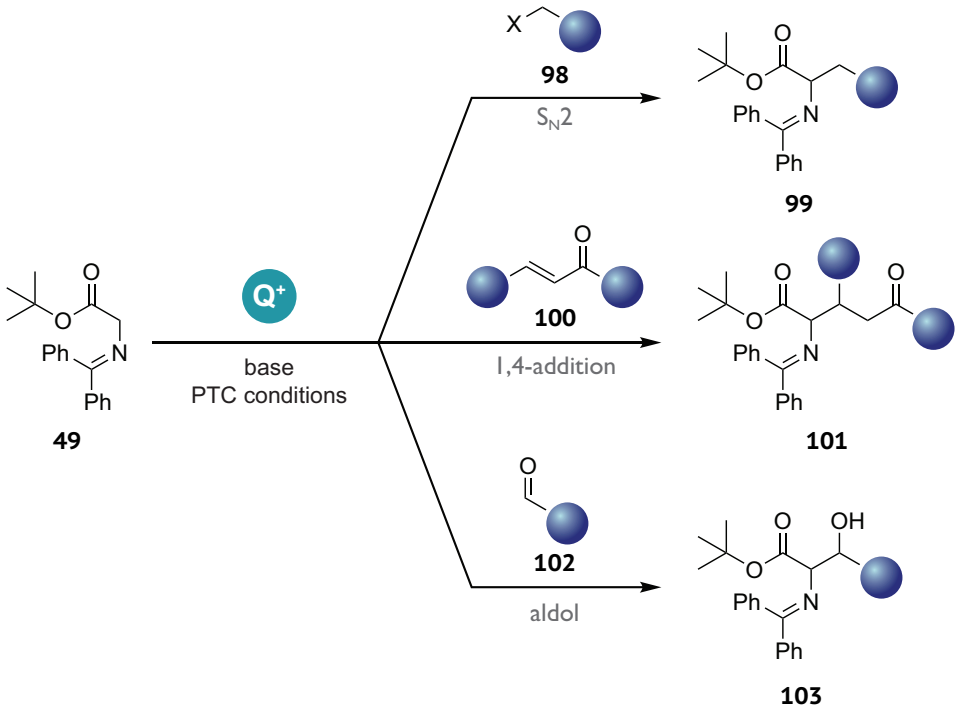
Whilst we anticipated enantioselectivity would not be high when carried out at room temperature,[89,95,98,101] we chose to investigate the reaction of glycine imine **49** with methyl vinyl ketone (MVK) **90** effected by a simple cinchona alkaloid-derived phase-transfer catalyst (Scheme 2.3). The reasons why we elected to study this particular reaction are not obvious and require some explanation.




**Scheme 2.3: Selected PTC model reaction to investigate.** The reaction between imine **49** and MVK **90** effected by a simple cinchona alkaloid-derived phase-transfer catalyst.

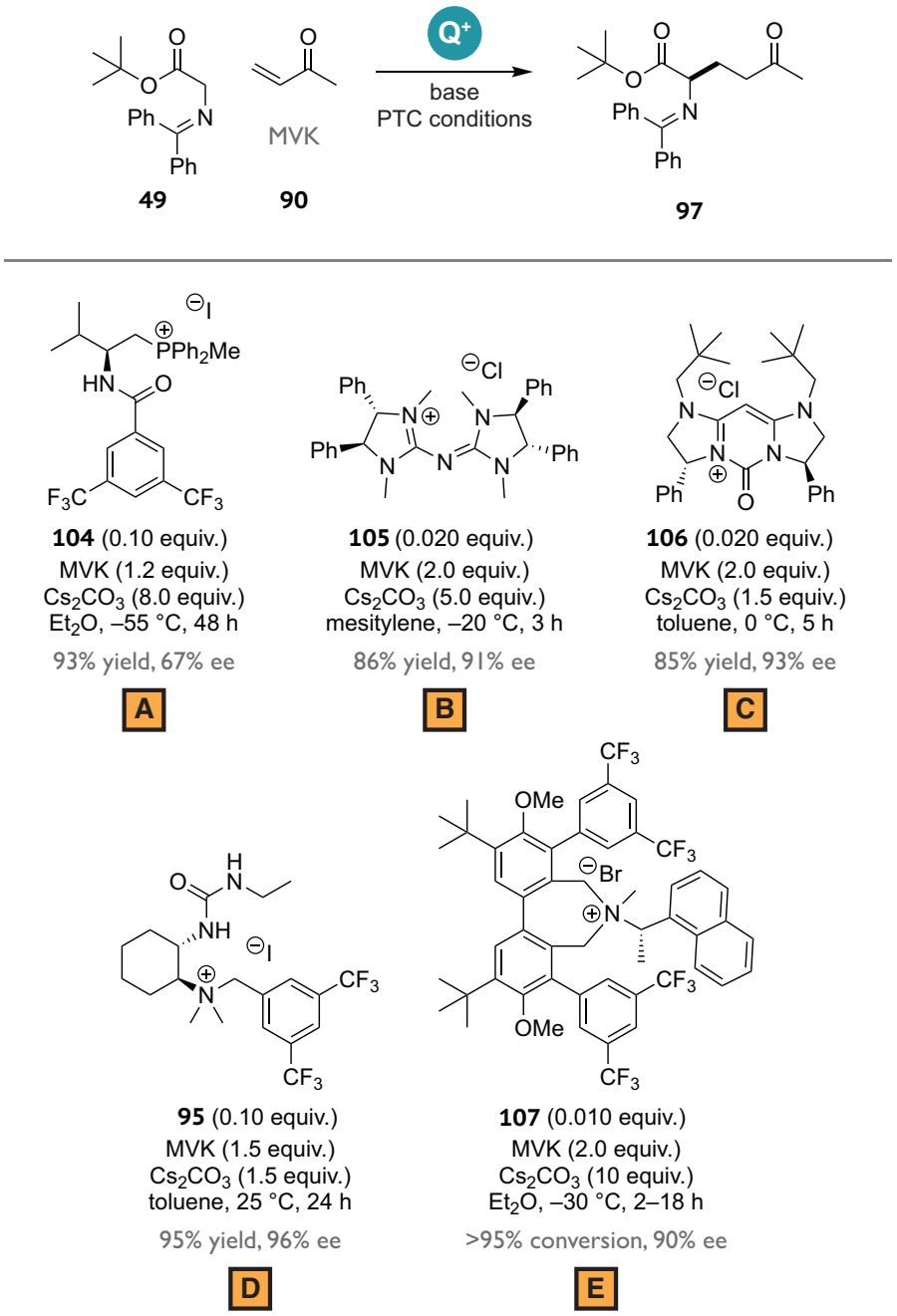
Firstly, MVK **90** was selected because it was anticipated to be a highly reactive reaction partner, particularly in reactions carried out at ambient temperature. We wanted to use a cinchona alkaloid-derived phase-transfer catalyst to better understand the nature of these catalysts in phase-transfer reaction systems. A commercially available *N*-benzyl scaffold bearing a free hydroxyl group would be ideal.

Glycine imine **49** is a ubiquitous substrate in asymmetric phase-transfer catalysis.[8,9,35,36] It was first used in PTC in the synthesis of racemic amino acids,[65] and has since been extensively exploited as a substrate in asymmetric PTC; it has been used in >1000 different reactions;[102] most of which generate intermediates for further use (three general examples are highlighted in Scheme 2.4). The enantioselective alkylation of **49** using benzyl bromide has become the benchmark reaction for novel phase-transfer catalysts.[8,9,49,50,53,94,103] Despite the widespread use of glycine imine **49**—including studies examining enantioinduction from this substrate with cinchona alkaloid-derived catalysts[83,104]—a precise understanding of how it behaves under PTC reaction conditions in asymmetric PTC remains mostly unclear.




**Scheme 2.4: Three general transformations of glycine imine 49 using base-mediated phase-transfer catalysis. A)** General $S_N2$ reaction, where X corresponds to a suitable leaving group;[8,9,35] **B)** general 1,4-addition reaction;[9,91,94,105] **C)** general aldol reaction.[9,35,106–108]

The exact reaction of **49** with methyl vinyl ketone remains one of the more challenging systems to obtain high enantiomeric excesses of the product.[51,92,94,98,109] General trends suggest low temperatures and highly complex catalysts are required to obtain selectivity (Scheme 2.5). Interestingly, excess solid $Cs_2CO_3$ appeared to be the base of choice in a number of systems evaluating the reaction of **49** with MVK. With these considerations in mind, we decided to proceed with the study of our selected reaction model.

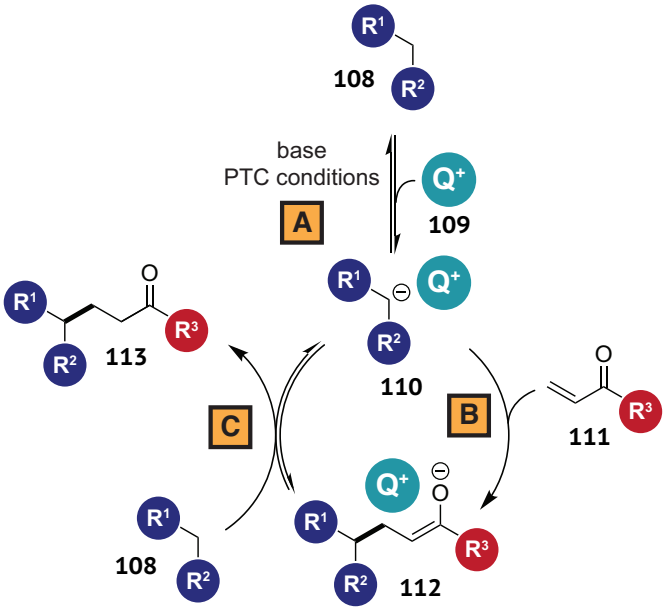



**Scheme 2.5: Five examples of systems enantioselectively reacting glycine imine 49 with MVK 90 using PTC.** The stereochemistry depicted in product **97** is arbitrary. The phase transfer catalyst ( Q+ ) and its corresponding counterion used initially in each reaction is shown as the drawn structure. The corresponding reaction conditions for each example are described below the catalyst structure, followed by the reaction outcomes. The references corresponding to the described each reaction are given as follows: **A)** [98]; **B)** [94]; **C)** [51]; **D)** [92]; **E)** [109].

### 2.1.3 Initial mechanistic hypothesis

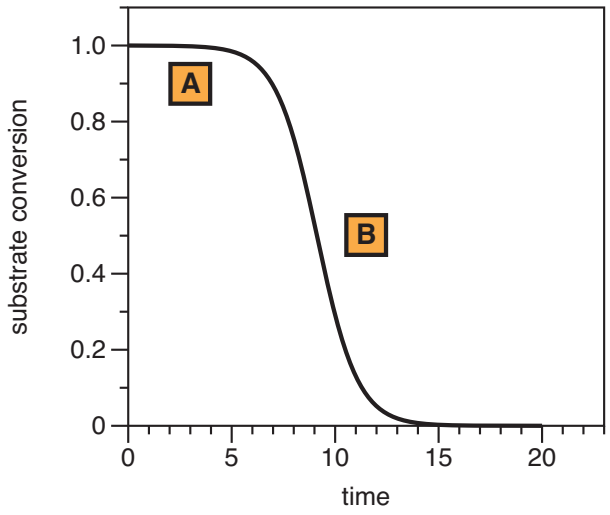
We hypothesised that there may be some interesting mechanistic possibilities going on, particularly as the product anion has a predicted p$K_a$ value higher than the substrate. This may

result in the deprotonation of the substrate by the product anion, assisting turnover of the catalytic cycle (Scheme 2.6).




**Scheme 2.6: A mechanism for the phase-transfer catalysed 1,4-addition reaction. A)** The substrate **108** is deprotonated under the reaction conditions before coordinating to the chiral phase-transfer catalyst cation **109** to generate the substrate-catalyst complex **110**; **B)** subsequent addition of the anion of **110** to the electrophile **111** generates the product anion-catalyst complex **112**; **C)** deprotonation of the substrate **108** by product anion-catalyst complex **112** generates enantioenriched product **113** and closes the catalytic cycle.

We hypothesised that this type of behaviour may manifest itself in kinetics characterised by a sigmoidal temporal concentration profile with an induction period followed by rapid conversion to product (Scheme 2.7). If this mechanism were in operation, we hypothesised that only catalytic base would be required to effect the reaction.



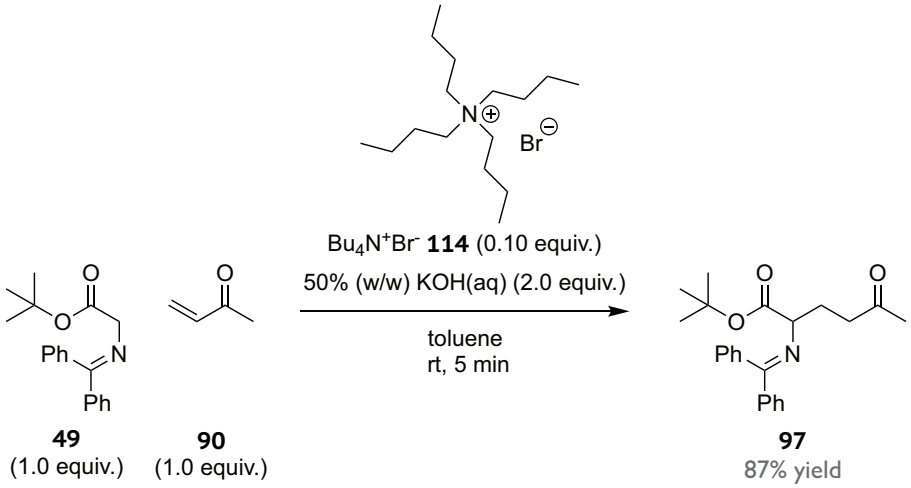

**Scheme 2.7: An example of kinetic behaviour arising from an autocatalytic mechanism.** Key features include **A)** a slow, initial induction period followed by **B)** rapid consumption of the substrate.

With an appropriate hypothesis for the reaction mechanism we began evaluating conditions for the reaction of glycine imine with MVK.

## 2.2 Preliminary results

### 2.2.1 Identifying conditions for a model reaction

We commenced our study by assessing the outcomes of our selected model reaction using an achiral phase-transfer catalyst (Scheme 2.8). In the presence of $Bu_4N^+Br^-$ **114** (0.10 equiv.) and excess base, the desired product **97** was formed within 5 min with an isolated yield of 87%. We had clearly identified a reactive system.




**Scheme 2.8: Initial result for the non-stereoselective phase-transfer reaction of glycine imine 49 with MVK 90.** Equivalents (equiv.) are reported with respect to substrate **49**.

The substrate **49** and product **97** were easily separated and visualised by HPLC at 254 nm (Figure 2.1). Importantly, we were able to obtain complete separation of the organic solvent, the substrate **49** and product **97** enantiomers. Thus, enabling the qualitative monitoring of conversion over time; by comparing the ratio of the raw signal integrals corresponding to the substrate **49** and product **97** enantiomers.

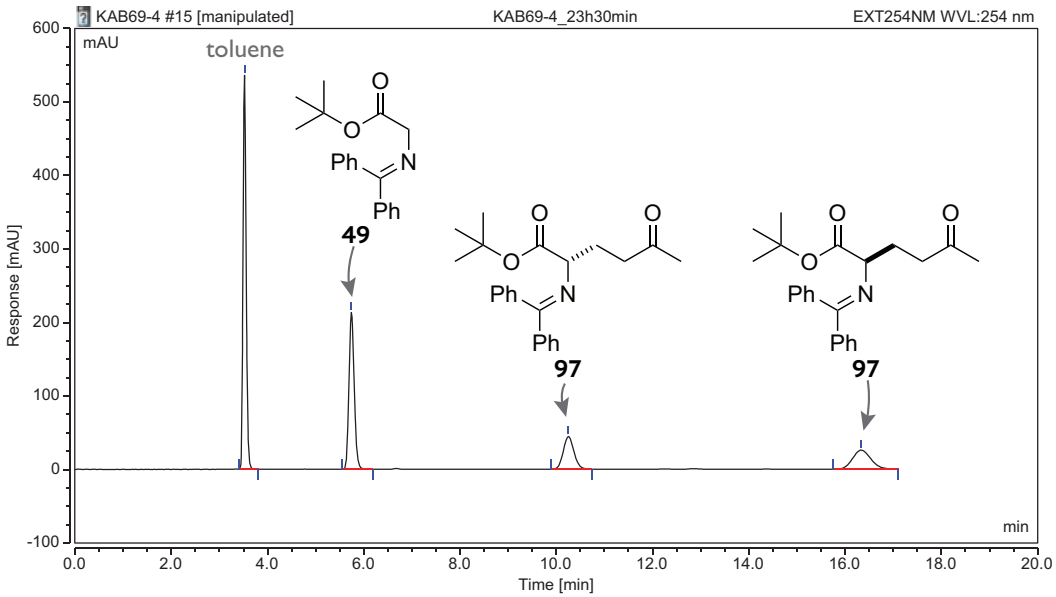
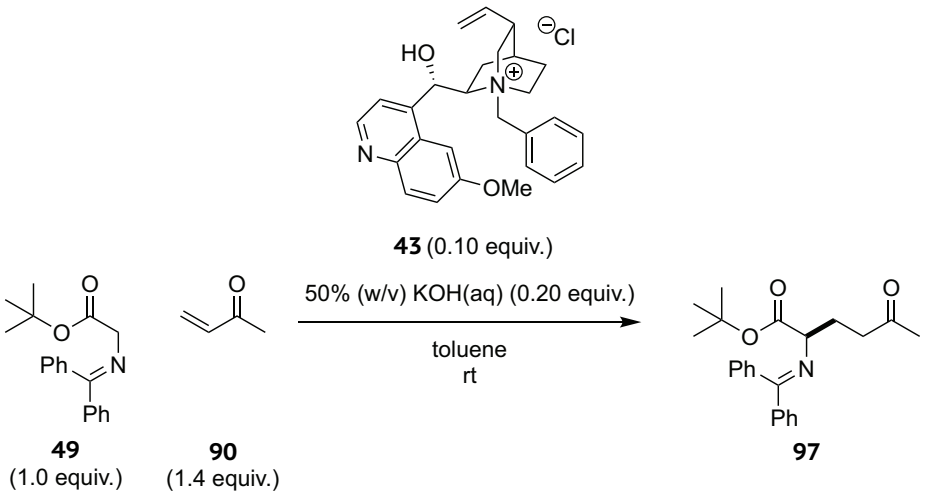



**Figure 2.1: Representative HPLC chromatogram of an aliquot extracted from a reaction mixture.** The $x$-axis represents retention time, and the $y$-axis UV absorption at the extracted wavelength (254 nm). Peak identities are indicated on the chromatogram. Depiction of stereochemistry is arbitrary.

To monitor the reaction, we found that extracting aliquots (1.5 µL) from the reaction mixtures,

filtering through a short plug of silica, eluting with 30% (v/v) 2-propanol/hexane (∼1.6 mL), then analysing the filtrate directly by HPLC was suitable. The filtration through silica was important because simply diluting the aliquots in 2-propanol/hexane did not quench reactivity.

We proceeded with the evaluation of a cinchona alkaloid-derived catalyst using catalytic hydroxide as the base. 1,4-Addition reactions carried out at ambient temperature and catalysed by cinchona alkaloid-derived salts using catalytic base were demonstrated previously to proceed quickly (see A, Scheme 2.2).[41] We elected to use catalyst **43** with a catalytic amount of aqueous KOH (Scheme 2.9).




**Scheme 2.9: Preliminary conditions for evaluating the selected model reaction.** Equivalents (equiv.) are reported with respect to substrate **49**.

Excitingly, we observed complete conversion to product **97** within 60 min, with an induction period, which was consistent with our initial hypothesis; a repeat of the reaction confirmed this behaviour (A and B, Figure 2.2). The final enantiomeric excess of the product was only 12% but this was to be expected given the literature precedent concerning vinyl ketones under rt PTC reaction conditions.

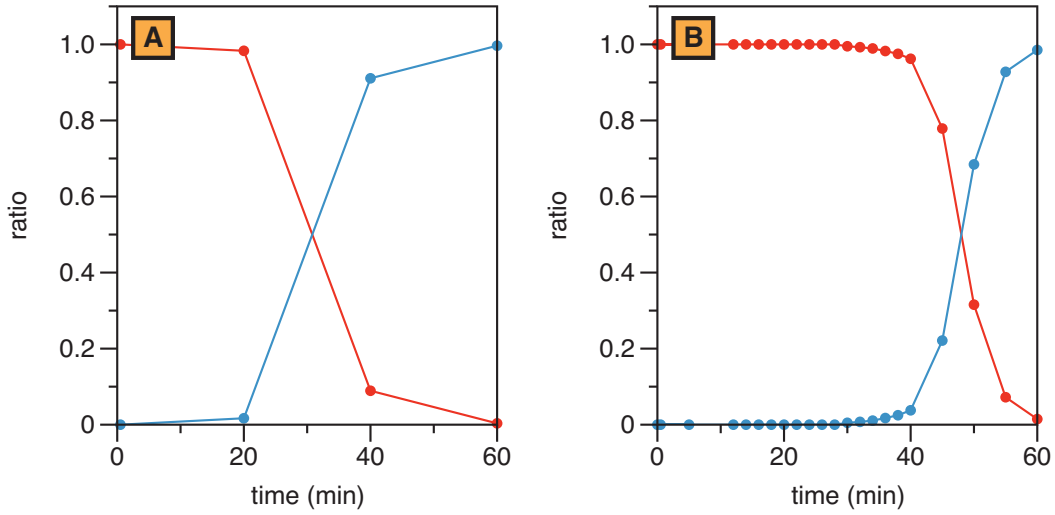



**Figure 2.2: Qualitatively gauging conversion of substrate 49 (red) to product 97 (blue) under the reaction conditions described by Scheme 2.9.** Two repeat reactions **A** and **B** were carried out. The $x$-axis in both graphs corresponds to the time following initiation of the reaction, the $y$-axes correspond to the ratio of signals corresponding to the substrate **49** and product **97** by HPLC. The lines are guides for the eye.

We had identified good candidate reaction conditions which we could vary to probe the reaction mechanism. Before we could continue, we needed to develop a quantitative assay in order to monitor the reactions.

### 2.2.2 Establishing a quantitative assay

Fortunately, we had identified suitable HPLC conditions that separated substrate **49** from the product **97** enantiomers (ChiralPak® IC, 1.0 mL $min^{-1}$, 30% (v/v) 2-propanol/hexane, 25 °C). In order to develop a quantitative assay, we required calibration curves with an internal standard. The internal standard would enable the comparison of the analyte peaks with the standard peak by HPLC thereby providing a point of reference.

The challenge with identifying a suitable internal standard was that it needed to be inert to the reaction conditions, not affect the solvent polarity significantly, contain a chromophore for HPLC analysis, and be separable from the organic solvent by HPLC. 1-Bromonaphthalene **115** (BrNaph) was found to be an adequate standard with which to compare our substrate and product peaks. We next needed to construct standard curves of the substrate **49** and product

**97** against the internal standard BrNaph **115**.

To construct the standard curves, we first prepared different mixtures with relatively constant amounts of BrNaph **115**, and varying amounts of substrate **49** and racemic product **97**. The mixtures were dissolved in toluene before dilution in 30% (v/v) 2-propanol/hexane and subsequent analysis using the identified instrument method. By comparing the mole ratio of the samples to the HPLC signal integrals we were able to construct standard curves for each analyte and identify the calibration factors corresponding to the analyte in question.

Standard curves were thus constructed for each analyte (Figure 2.3). We obtained a linear response for each analyte. By taking the slopes of each graph, and the known amounts of internal standard present in each reaction mixture (the calibration factors), we would be able to calculate the analyte amount present in the reaction mixture over time.

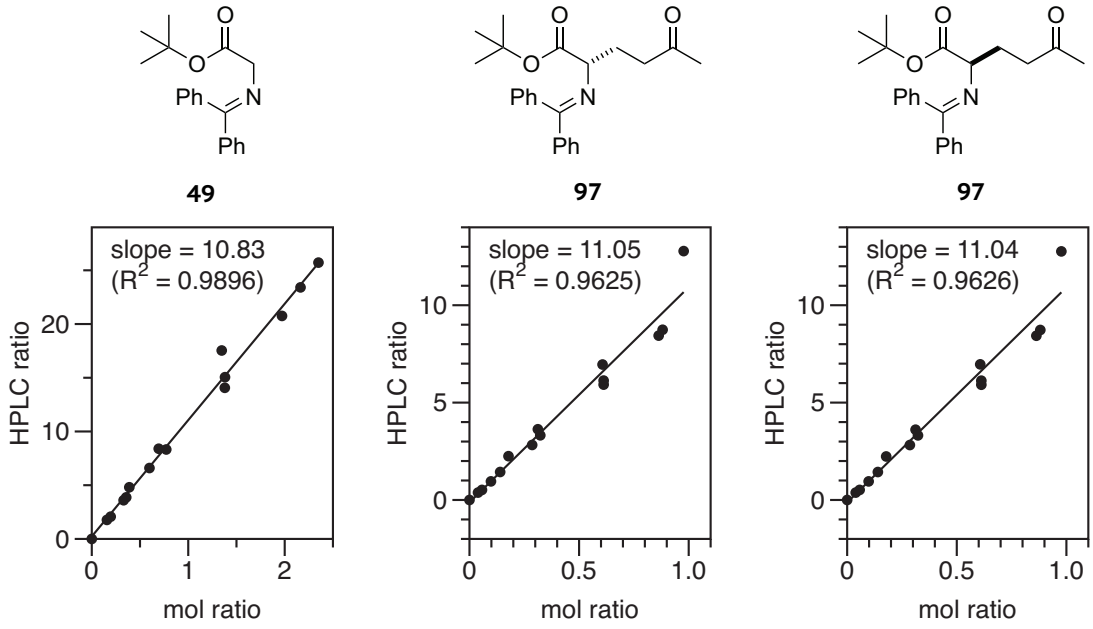



**Figure 2.3: Standard curves for each analyte (49, and the enantiomers of 97).** The $x$-axis corresponds to the mole ratio of the analyte to the internal standard BrNaph, and the $y$-axis corresponds to the HPLC signal integral ratio of the analyte to BrNaph. The lines are the slopes obtained from linear regression analyses of each data set. The drawn enantiomers of product **97** indicate arbitrary stereochemistry, and are in order (from left to right) of retention time by HPLC (ChiralPak® IC 1.0 mL $min^{-1}$, 30% (v/v) 2-propanol/hexane, 25 °C).

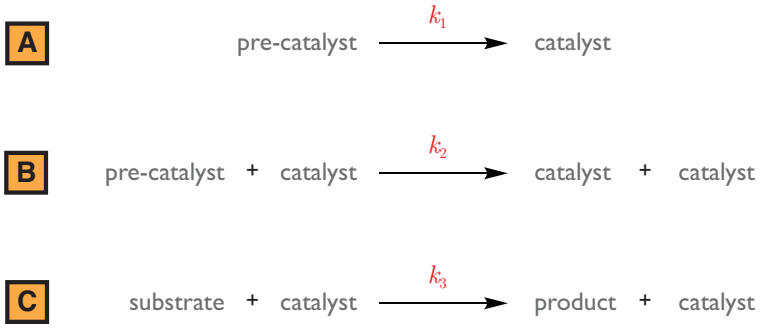
### 2.2.3 Analysing the results

The sigmoidal behaviour of the reaction model presented a challenge in how to analyse the results. If we were to fit the data linearly around the point of inflexion, we would be excluding the majority of the data collected. The extracted data would also vary depending on where we were to take the point of inflexion.

Although our reaction was unlikely to proceed via a simple autocatalytic mechanism, we found that fitting our data to the autocatalytic function described by Watzky and Finke was an appropriate method for quantifying our results.[110] Applying this function, the concentration of substrate **49** at time $t$ may be described by equation 2.1,[111] where $[\mathbf{49}]_0$ is the initial concentration of substrate **49**, and $k_1$ and $k_2$ are parameters describing particular steps in the assumed reaction process.

$$[\mathbf{49}] = \frac{\frac{k_1}{k_2} + [\mathbf{49}]_0}{1 + \frac{k_1}{k_2[\mathbf{49}]_0} \times \exp(k_1 + k_2[\mathbf{49}]_0)t} \tag{2.1}$$

In the autocatalytic model, the $k_1$ and $k_2$ parameters broadly describe two rate-limiting regimes (Scheme 2.10). The first parameter $k_1$ predominantly corresponds to the induction period, which consists of a "lag" phase and "jerk" into the growth phase.[112] The induction period is the step where active catalyst is formed from a pre-catalyst (A, Scheme 2.10). The second, so-called autocatalytic step—characterised mostly by $k_2$—describes the self-catalysed formation of catalyst (B, Scheme 2.10). The non-rate-limiting step, which is also operating in this model, is the conversion of substrate to product, effected by the active catalyst (C, Scheme 2.10); this step is characterised by the rate-constant $k_3$, and in the autocatalytic model, $k_3 >>> k_2 > k_1$.

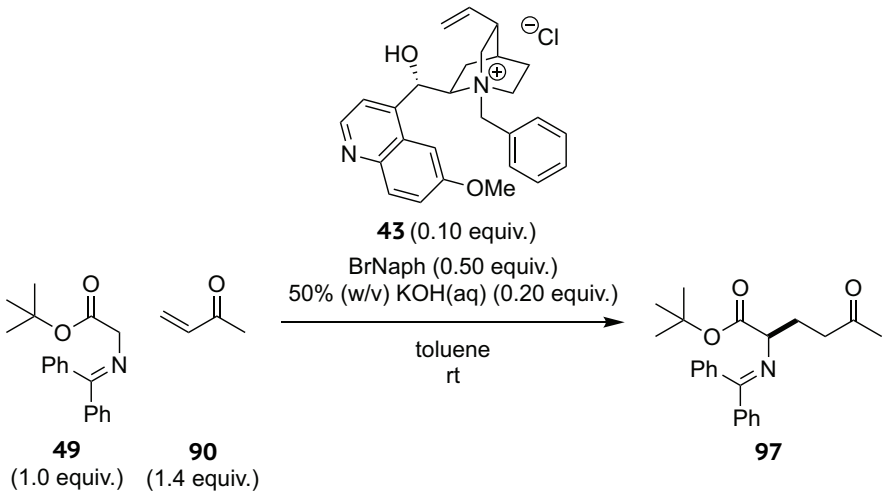



**Scheme 2.10: General steps in the Watzky and Finke autocatalytic model.**[110] **A)** The pseudoelementary step predominantly describing the induction period; **B)** the autocatalytic step, where the catalyst forms itself; **C)** the reaction step where the catalyst mediates the formation of product from substrate. The red text corresponds to the rate constants describing the appropriate step.

Using this function, we would be able to fit the whole data set acquired from each reaction, instead of the two or three data points that may be evaluated over the point of inflexion. The two parameters ($k_1$ and $k_2$) that would be extracted from the data might provide points of reference when comparing different data sets.

## 2.3 Efforts to obtain kinetically reproducible results

With methods for assaying the reaction and analysing the results, we next examined the reaction under a set of conditions we set to be standard (Scheme 2.11). The rationale was that we would then vary the conditions with the aim of elucidating the reaction mechanism.




**Scheme 2.11: Initial conditions used to kinetically evaluate the phase-transfer catalysed reaction of glycine imine 49 with MVK 90 using cinchona alkaloid-derived catalyst 43 (protocol 1).** Equivalents (equiv.) are reported with respect to the substrate **49**.

Immediately, we found that reproducing the kinetic behaviour was not a simple task. The initial three data sets that we collected varied wildly (Figure 2.4). The induction period—as observed graphically—changed from being 30 to 40 min from our initial results (see Figure 2.2) to between 10 and 40 min (indicated roughly by the dotted lines, Figure 2.4). The values for the rate constants extracted from fitting the function described by equation 2.1 were similarly spread; the average values of the calculated $k_1$ and $k_2$ were $3 \times 10^{-7} \pm 2 \times 10^{-7}$ min$^{-1}$ and $0.5 \pm 0.3$ min$^{-1}$, respectively.

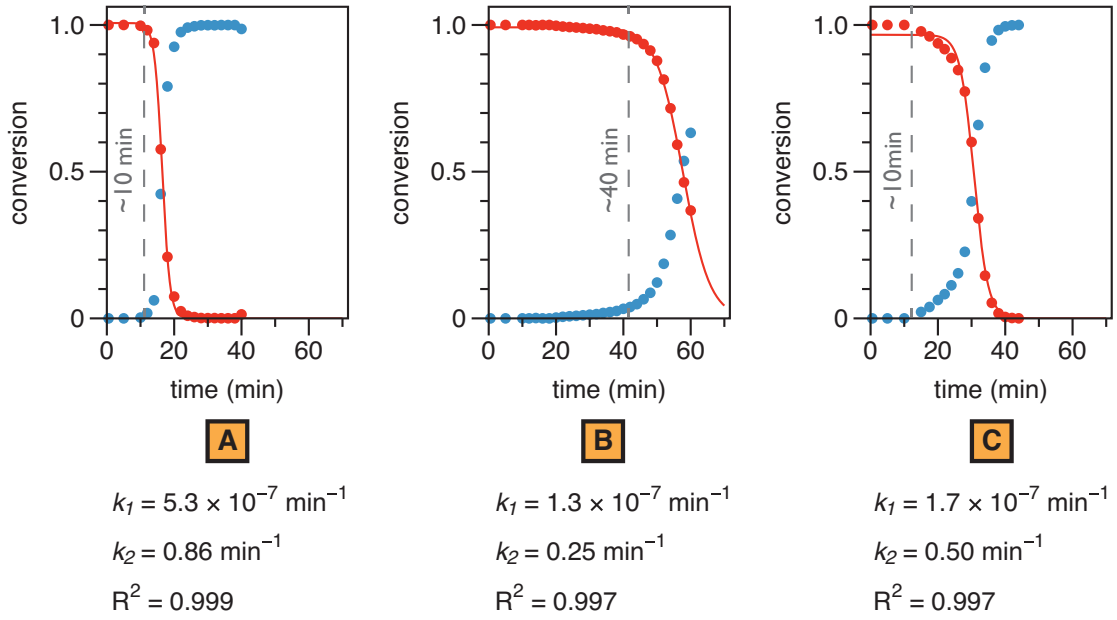
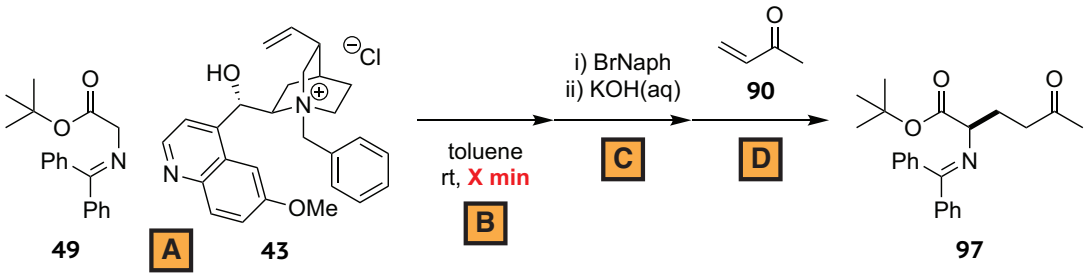


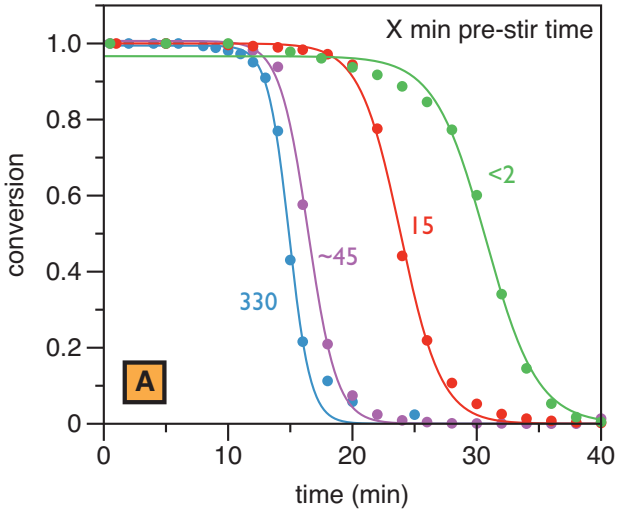

**Figure 2.4: Data obtained from the three reactions (A to C) carried out according to Scheme 2.11.** In each graph, the $x$-axis corresponds to time following initiation of the reaction by the addition of MVK; the $y$-axis corresponds to conversion as a ratio of the total amount (in mol) of substrate **49** and product **97**; the red data corresponds to the substrate **49**; the blue data analogously corresponds to the relative amount of product **97**. The red lines in each graph correspond to the fitting of equation 2.1, the extracted values for the parameters $k_1$ and $k_2$ and their goodness of fit ($R^2$) are displayed below the appropriate graph. In all cases, the initial value for the concentration of substrate $[\mathbf{49}]_0$ as described in the equation 2.1 was initially set to the unitless value of 1.0. The grey dotted lines in each graph were manually drawn to give an indication of the duration of the induction period (sideways grey labels) for each reaction.

The results forced us to examine exactly *how* we had conducted the reactions in order to pin down the cause of the variability. We had stirred the catalyst and substrate in toluene before the sequential addition of the internal standard BrNaph, KOH(aq), and finally MVK **90** to initiate the reaction (Scheme 2.12).




**Scheme 2.12: Reaction setup steps. A)** Substrate **49** and catalyst **43** are added to the reaction vial before **B)** toluene is introduced and the mixture stirred for X min; **C)** next, the internal standard BrNaph, then aqueous KOH(aq) are added and stirring is continued; **D)** MVK **90** is added to initiate the reaction at the designated time zero.

It was hypothesised that the variation in the induction period may be due to the length of time the catalyst and substrate were stirred in the organic solvent prior to the addition of the internal standard BrNaph, aqueous base, and MVK (i.e. X min, Scheme 2.12). Indeed, when we stirred the catalyst and substrate for increasing periods of time, we consequently observed a decrease in the magnitude of the induction period (Figure 2.5).




B

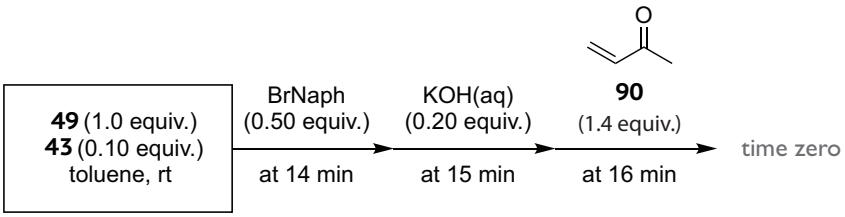
| | $k_1$ ($min^{-1}$) | $k_2$ ($min^{-1}$) | $R^2$ |
|---|---|---|---|
| ● | $1.7 \times 10^{-7}$ | 0.50 | 0.997 |
| ● | $3.0 \times 10^{-7}$ | 0.61 | 0.999 |
| ● | $5.3 \times 10^{-7}$ | 0.86 | 0.999 |
| ● | $3.6 \times 10^{-8}$ | 1.2 | 0.994 |

**Figure 2.5: Summary of data obtained when varying the substrate 49 and catalyst 43 pre-stir time (i.e. X min in Scheme 2.12). A)** Overlay of kinetic data obtained when varying the pre-stir time: <2 min (green data), 15 min (red data), ~45 min (purple data), and 330 min (blue data). The lines correspond to the fitting of equation 2.1 to the appropriately coloured data set. The $x$-axis corresponds to time following initiation of the reaction by the addition of MVK, the $y$-axis corresponds to conversion of substrate as a ratio of the total amount (in mol) of substrate **49** and product **97**. **B)** Values obtained following fitting of equation 2.1 to each data set. In all cases, the initial value for the concentration of substrate $[\mathbf{49}]_0$ as described in the equation 2.1 was initially set to the unitless value of 1.0.

The graphical trend of induction time (A, Figure 2.5)—decreasing magnitude with increased

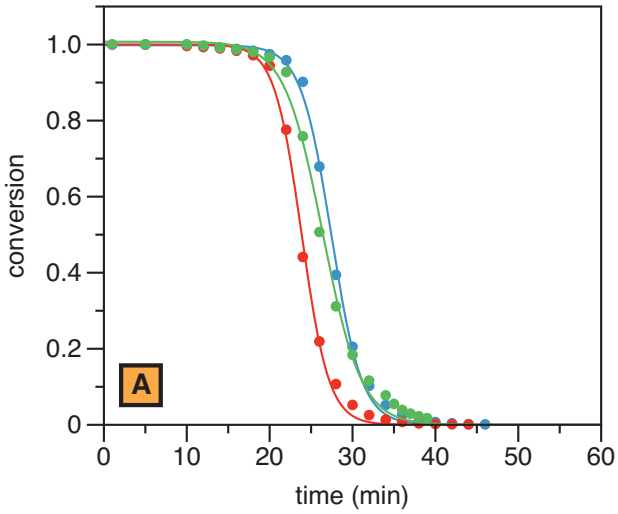
pre-stir time—was reflected in values of the $k_2$ parameter. An increase in the value of $k_2$ was observed with increasing pre-stirring time. There was no obvious trend associated with the values for the $k_1$ parameter.

To minimise the variability of the observed rate behaviour associated with the pre-stirring time, we implemented a strict protocol before initiation of the reaction by the addition of MVK (Scheme 2.13). The protocol involved stirring the substrate **49**, catalyst **43**, and toluene in a reaction vial before the sequential addition of the other reaction components at set intervals. This was to ensure that the same stirring time was achieved between samples before commencing the reaction.




**Scheme 2.13: Latest reaction protocol to control pre-stirring time (protocol 2).** The catalyst **43** and substrate **49** were stirred for a strict period of 14 min prior to the sequential addition of BrNaph, KOH(aq), and MVK over intervals of strictly 1 min. Initiation of the reaction and designation of time zero was on addition of MVK to the reaction mixture.

Three reactions were carried out using the second generation protocol, and the kinetic data was collected and analysed (Figure 2.6). Whilst the triplicate results exhibited greater coherence than those obtained previously, the data were still unacceptably inconsistent.




B

| | $k_1$ ($min^{-1}$) | $k_2$ ($min^{-1}$) | $R^2$ |
|---|---|---|---|
| ● | $4.9 \times 10^{-6}$ | 0.43 | 0.999 |
| ● | $3.0 \times 10^{-7}$ | 0.61 | 0.999 |
| ● | $1.7 \times 10^{-7}$ | 0.55 | 0.999 |

**Figure 2.6: Data obtained from three apparently identical reactions. A)** Overlay of kinetic data obtained; the different colours correspond to individual reactions within the set. The lines correspond to the fitting of equation 2.1 to the appropriately coloured data set. The $x$-axis corresponds to time following initiation of the reaction by the addition of MVK, the $y$-axis corresponds to conversion of substrate as a ratio of the total amount (in mol) of substrate **49** and product **97**. **B)** Values obtained following fitting of equation 2.1 to each data set. In all cases, the initial value for the concentration of substrate $[\mathbf{49}]_0$ as described in the equation 2.1 was initially set to the unitless value of 1.0.

We suspected the variability in mechanical agitation and heat generated from persistent use of the stirrer plate might be affecting the observed kinetic behaviour. Inconsistent stirring was previously found to affect the rate behaviour of other systems. To obtain a consistent shearing motion of stirring, we commissioned the fabrication of a custom holder to fit the reaction vial centrally across the stirrer plate (A, Figure 2.7). The same stirrer bar was to be used in all subsequent reactions. The stirring rates were verified using a stroboscope and set to 1000 rpm for the remainder of the experiments. To minimise heat transfer from the stirrer, the reaction vial was installed so as to be suspended above the surface of the holder (B, Figure 2.7).

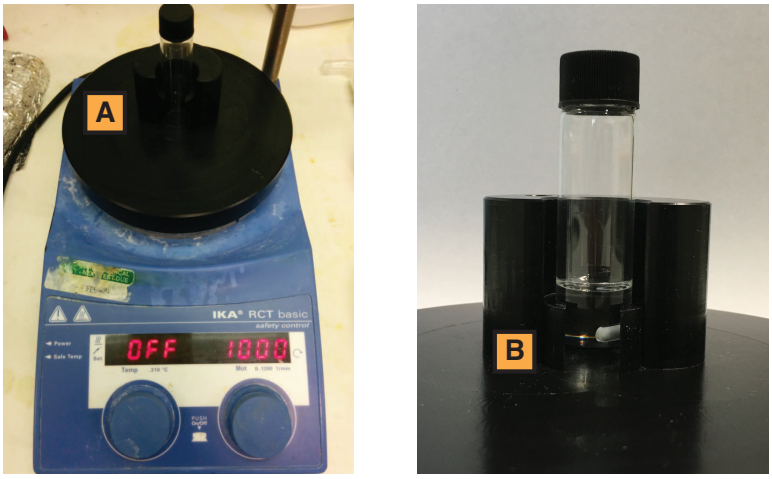



**Figure 2.7: Custom fabricated reaction vial holder. A)** Holder installed on a stirrer plate and fitted with an empty vial; **B)** reaction vial suspended above the surface of the holder.

Additionally, it was at this point in time that we suspected the water content of the organic solvent might be affecting the observed rate. A reaction carried out using anhydrous toluene resulted in complete retardation of the reaction; no product was formed over 45 min. It was therefore necessary to control the water content of the solvent, without being completely anhydrous. To this end, pre-dried, anhydrous toluene, was exposed to air for precisely 15 min, before commencing the reaction protocol (Figure 2.8).

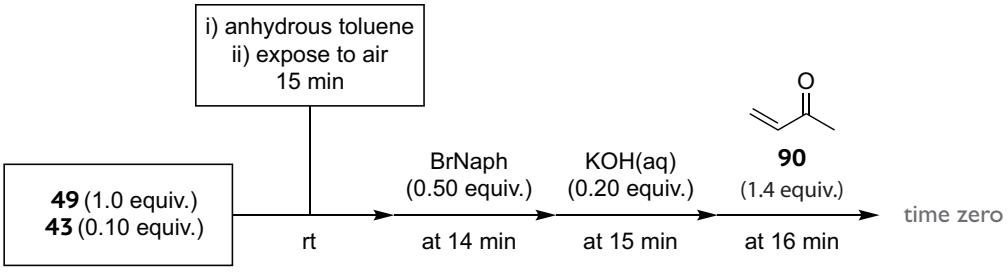
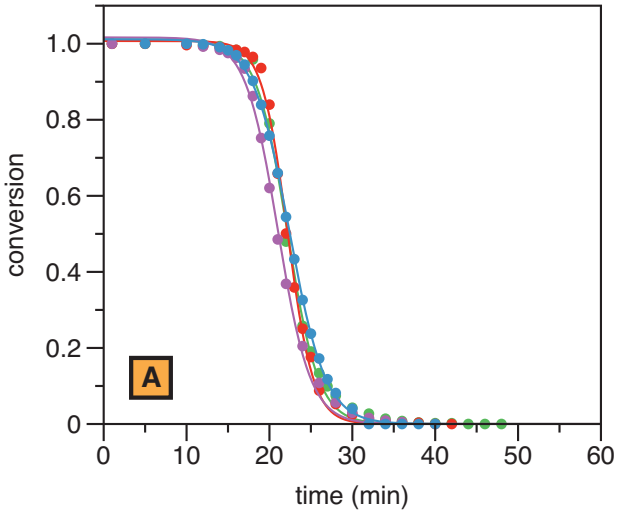



**Figure 2.8: Latest reaction protocol using semi-dry toluene (protocol 3).**

Using this optimised protocol, we were able to obtain four, graphically consistent results (Figure 2.9). Each of the four results exhibited roughly the same induction period. Despite the appearance of the overlay of the data, the extracted values of for the $k_1$ parameter differed significantly; the average value for the $k_1$ parameter from the four reactions was $7.9 \times 10^{-6} \pm 6 \times 10^{-6}$ min$^{-1}$. Because each extracted value was very small, we suspected subtle changes

in the kinetic data resulted in huge differences in the $k_1$ value obtained from fitting equation 2.1. The $k_2$ values obtained from the graphically consistent results exhibited a more acceptable range with an average value of $0.53 \pm 0.07$ min$^{-1}$.




B

| | $k_1$ (min$^{-1}$) | $k_2$ (min$^{-1}$) | $R^2$ |
|---|---|---|---|
| ● | $4.0 \times 10^{-6}$ | 0.54 | 0.998 |
| ● | $3.9 \times 10^{-7}$ | 0.64 | 0.998 |
| ● | $1.1 \times 10^{-5}$ | 0.50 | 0.998 |
| ● | $1.6 \times 10^{-5}$ | 0.45 | 1.00 |

**Figure 2.9: Summary of data obtained when carrying out identical reactions using the newly applied protocol described in Figure 2.8. A)** Overlay of kinetic data obtained; the different colours correspond to individual reactions within the set. The lines correspond to the fitting of equation 2.1 to the appropriately coloured data set. The $x$-axis corresponds to time following initiation of the reaction by the addition of MVK, the $y$-axis corresponds to conversion of substrate as a ratio of the total amount (in mol) of substrate **49** and product **97**. **B)** Values obtained following fitting of equation 2.1 to each data set. In all cases, the initial value for the concentration of substrate $[\mathbf{49}]_0$ as described in the equation 2.1 was initially set to the unitless value of 1.0.

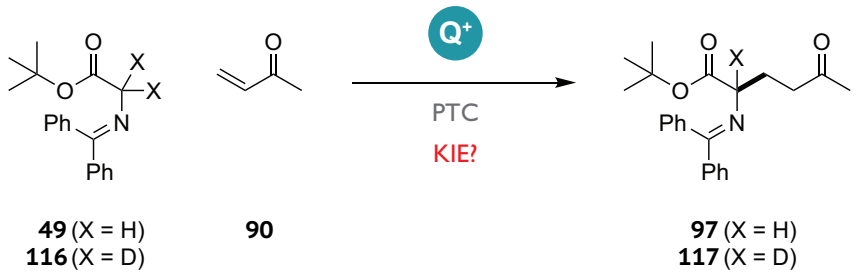
Despite the somewhat variable response in consistency with respect to the values extracted from fitting equation 2.1 to our obtained data, we had obtained results that were adequately consistent in kinetic behaviour. If our current method of analysis proved to be insufficient when probing the reaction mechanism, we would amend the data fitting model and re-assess the data acquired thus far.

The important thing to note here is that we obtained graphically consistent results using a very particular reaction protocol. We were now ready to apply our protocol in order to evaluate the reaction mechanism.

## 2.4 Investigating the reaction mechanism

### 2.4.1 Isotope effects and further protocol optimisation

We thought that an appropriate next step was to identify what might be occurring during the steps associated with both extracted rate parameters ($k_1$ and $k_2$) from our applied function. Subjecting deuterated substrate **116** to the reaction conditions might provide information as to the nature of the rate-determining steps (Scheme 2.14). For example, if we observed normal primary kinetic isotope effects (KIEs) when evaluating the induction period, or $k_1$ and $k_2$, the result may be suggestive that deprotonation of the substrate was a rate-limiting factor with respect to the overall process associated with that parameter.



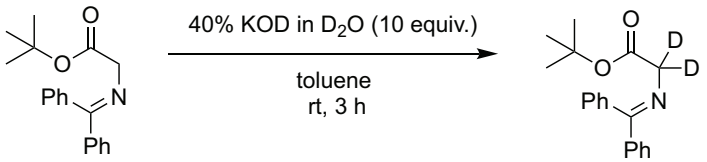

**49** (X = H)
**116** (X = D)

**90**

**97** (X = H)
**117** (X = D)

**Scheme 2.14: Ideal substrates and experiment to evaluate isotope effects in the PTC reaction system.** Q+ corresponds to the chiral quaternary ammonium ion catalyst.

We thus synthesised deuterated substrate **116** to evaluate under our optimised conditions (Scheme 2.15). By treating substrate **49** to biphasic reaction conditions, in the presence of KOD in $D_2O$, we were able to obtain substrate **116** in 32% yield with >95% deuterium incorporation.

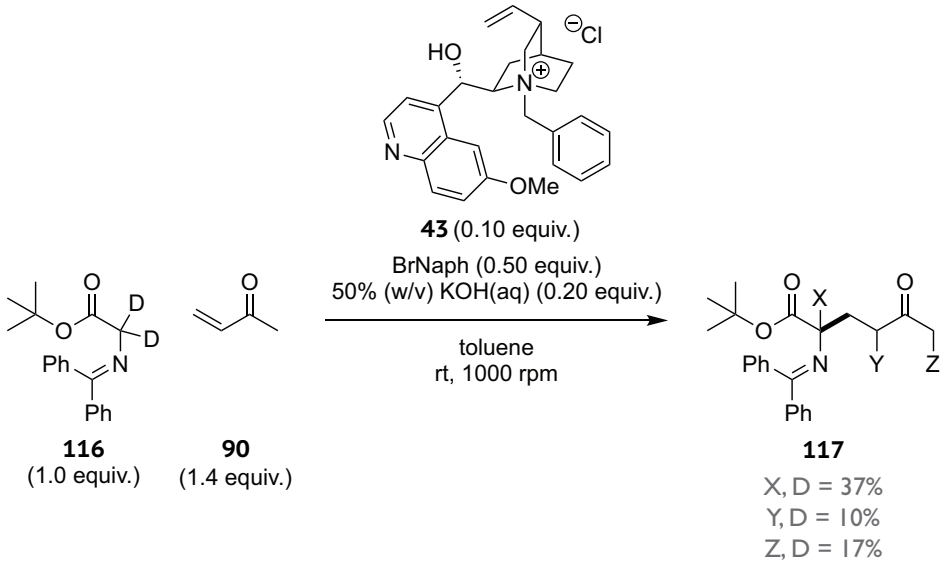



**49**
(1.0 equiv.)

**116**
32% yield
>95% deuteration

**Scheme 2.15: Synthesis of $\alpha$-deuterated material 116.** Equivalents are reported with respect to substrate **49**.

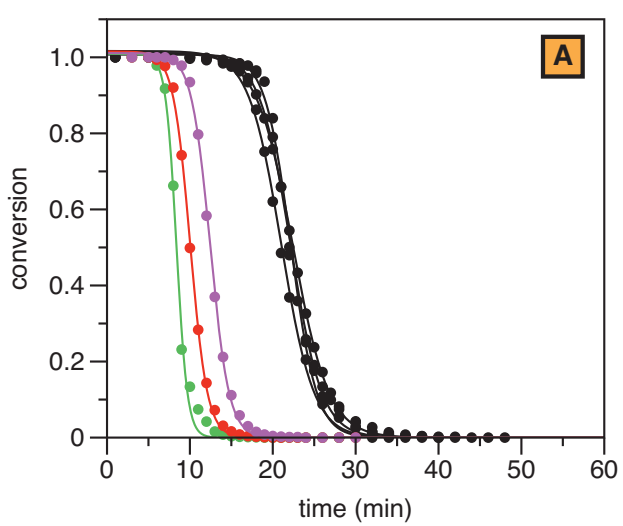
We then subjected substrate **116** to the reaction conditions (Scheme 2.16). The isolated product exhibited deuterium incorporation at the positions alpha to the carbonyls, which suggested the product anion might be involved in deprotonation of the substrate. This might occur either via deprotonation of the substrate by the product enolate formed during the addition step (i.e. at position Y). Additionally, the product **117** ketone may be deprotonated to form the terminal enolate, which might then be involved in deprotonation of the substrate (i.e. at position Z). This was consistent with our initial hypothesis. Alternatively, the deuterium at Y and Z in product **117** could be obtained indirectly from the substrate via exchange with the reaction environment. Given the reduced deuteration at the position alpha to the ester (at position X, 37% compared to >95%), the substrate likely underwent proton-deuterium exchange in the presence of aqueous KOH prior to the reaction with MVK.




**Scheme 2.16: Conditions evaluating deuterated substrate 116 to give product 117.** Equivalents (equiv.) are reported with respect to substrate **116**. The amount of deuteration in product **117** is indicated on the scheme.

Kinetically, a triplicate set of data using **116** was acquired and compared to that previously obtained using substrate **49** (Figure 2.10). The reactions carried out using deuterated **49** exhibited faster overall rates of reactions. The induction times for the three reactions were smaller than what was observed using the non-deuterated substrate **49**. Again, the values

obtained for the $k_1$ parameter were unaccountably fluctuating. The values for the $k_2$ revealed an increase in magnitude when comparing reactions using deuterated **116** to non-deuterated **49**. It appeared we were observing an inverse KIE. Unfortunately, we again observed irregularity in the obtained results from identical reactions; for example, graphically (green, purple, and red data in Figure 2.10), and from the average $k_2$ from the triplicate set using deuterated **116**, which was 1.1 ± 0.3 $min^{-1}$. Before we could address the KIE, or rely on the result, we first needed to solve the issue of reproducibility.




B

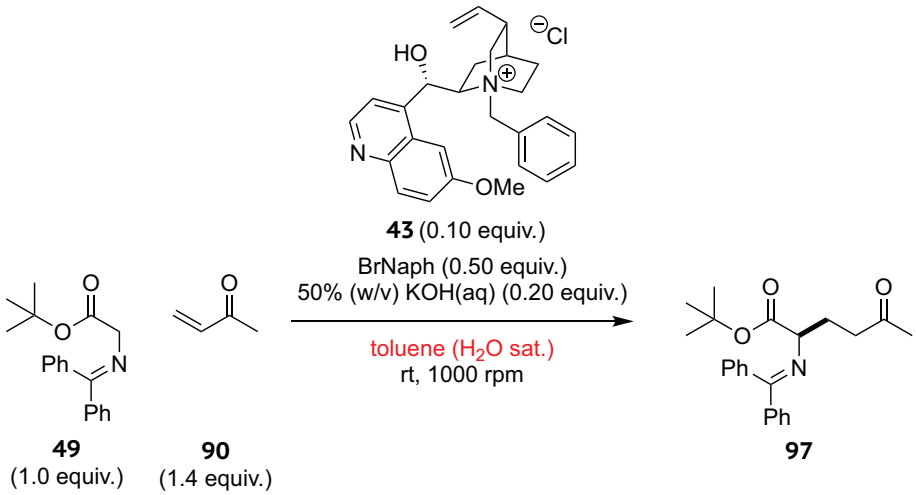
| | $k_1$ ($min^{-1}$) | $k_2$ ($min^{-1}$) | $R^2$ |
|---|---|---|---|
| **49** | $4.0 \times 10^{-6}$ | 0.53 | 0.998 |
| | $3.9 \times 10^{-7}$ | 0.64 | 0.998 |
| | $1.1 \times 10^{-5}$ | 0.50 | 0.998 |
| | $1.6 \times 10^{-5}$ | 0.45 | 1.00 |
| **116** | $4.2 \times 10^{-6}$ | 1.5 | 0.997 |
| | $5.5 \times 10^{-5}$ | 0.96 | 0.999 |
| | $1.5 \times 10^{-5}$ | 0.87 | 0.999 |

**Figure 2.10: Summary of data obtained when subjecting deuterated 116 or non-deuterated substrate 49 to the optimised reaction conditions. A)** Overlay of kinetic data obtained. The black data set corresponds to data previously described in Figure 2.9 using substrate **49**. The green, purple, and red data were collected from apparently identical reactions using deuterated substrate **116**. The lines correspond to the fitting of equation 2.1 to the appropriately coloured data set. The $x$-axis corresponds to time following initiation of the reaction by the addition of MVK, the $y$-axis corresponds to conversion of substrate as a ratio of the total amount (in mol) of substrate **49** and product **97**. **B)** Values obtained following fitting of equation 2.1 to each data set. In all cases, the initial value for the concentration of substrate $[\mathbf{49}]_0$ or $[\mathbf{116}]_0$ as described in the equation 2.1 was initially set to the unitless value of 1.0. The data are colour-coded. For exact details of the individual reactions obtained from the black set, see Figure 2.9.

We suspected the amount of water present in our organic solvent was again the cause of our reproducibility issues. When we exposed anhydrous toluene to air for 15 min then measured the amount of water in the organic solvent by Karl Fischer titration, we found it varied from 60 to 100 ppm. To fully control the quantity of water in the organic solvent, we saturated it with water (approximately 30 mL of water per 1000 mL of toluene; titrated to >300 ppm).

A batch of water-saturated toluene was prepared, which was to last for the duration of the remainder of the study.

We again evaluated the reaction using substrate **49** in triplicate (Scheme 2.17). The protocol implemented in these reactions was analogous to that described in Scheme 2.13, but using the wet organic solvent.




**Scheme 2.17: Latest conditions used to evaluate the model reaction (using protocol 4).** Equivalents (equiv.) are reported with respect to substrate **49**. The reaction setup protocol that was used is analogous to that described in Scheme 2.13.

Immediately, we obtained results we deemed—from a graphical perspective—to be adequately consistent (Figure 2.11). The triplicate set exhibited good coherence for the majority of the time course, with a slight deviation between results towards the end of the reaction. The data extracted from fitting equation 2.1 gave average values for $k_1$ and $k_2$ of $4.5 \times 10^{-4} \pm 1 \times 10^{-4}$ min$^{-1}$ and $4.3 \pm 0.04$ min$^{-1}$, respectively.

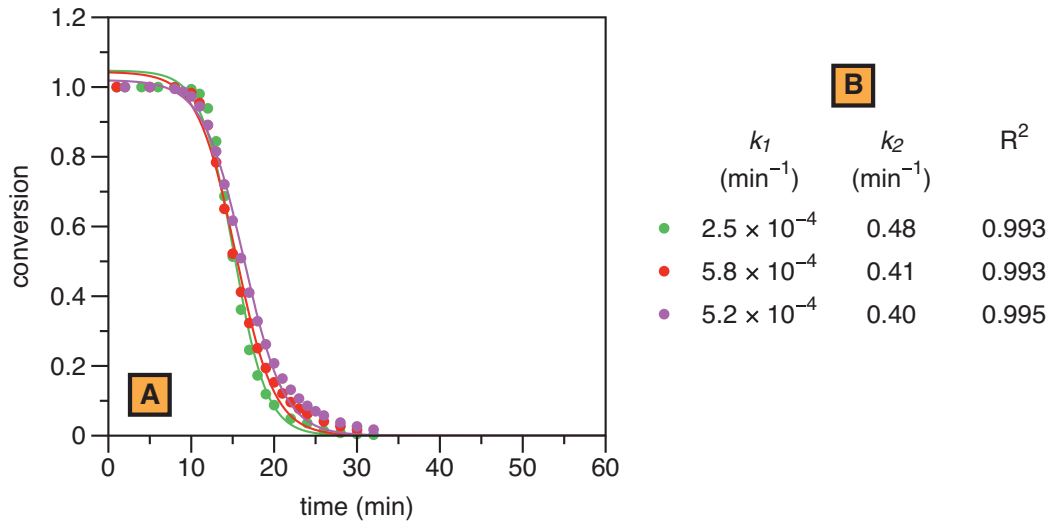



**Figure 2.11: Summary of data obtained when using toluene saturated with water. A)** Overlay of kinetic data obtained. The different colours correspond to repeats of the same reaction. The lines correspond to the fitting of equation 2.1 to the appropriately coloured data set. The $x$-axis corresponds to time following initiation of the reaction by the addition of MVK, the $y$-axis corresponds to conversion of substrate as a ratio of the total amount (in mol) of substrate **49** and product **97**. **B)** Values obtained following fitting of equation 2.1 to each data set. In all cases, the initial value for the concentration of substrate $[\mathbf{49}]_0$ as described in the equation 2.1 was initially set to the unitless value of 1.0. The data are colour-coded.

When we compared the data to that previously obtained, we found that the water content of the organic solvent had a significant effect on the observed kinetic behaviour (Figure 2.12). With greater amounts of water present in the organic solvent, increased values for both $k_1$ and $k_2$ were obtained. The precise reasons behind this effect were not explored, however we suspected it may be due to increasing the concentration of active catalyst in the organic layer by solvation.[16]

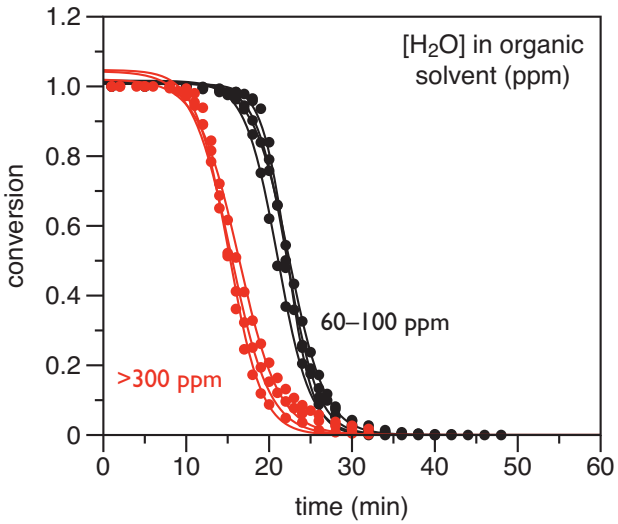



**Figure 2.12: Overlay of results obtained when using toluene of different wetness.** The overlays are of the data described in Figure 2.9 and Figure 2.11. The amount wetness of the solvent used in the reactions is indicated on the graph. The lines correspond to the fitting of equation 2.1 to each reaction. The $x$-axis corresponds to time following initiation of the reaction by the addition of MVK, the $y$-axis corresponds to conversion of substrate **49** as a ratio of the total amount (in mol) of substrate **49** and product **97**.

We were now able to re-address the observed kinetic isotope effect obtained. We subjected the deuterated substrate **116** to the latest reaction protocol, collected the kinetic data, carried out the fitting to equation 2.1, and then evaluated the extracted parameters $k_1$ and $k_2$ (Figure 2.13).

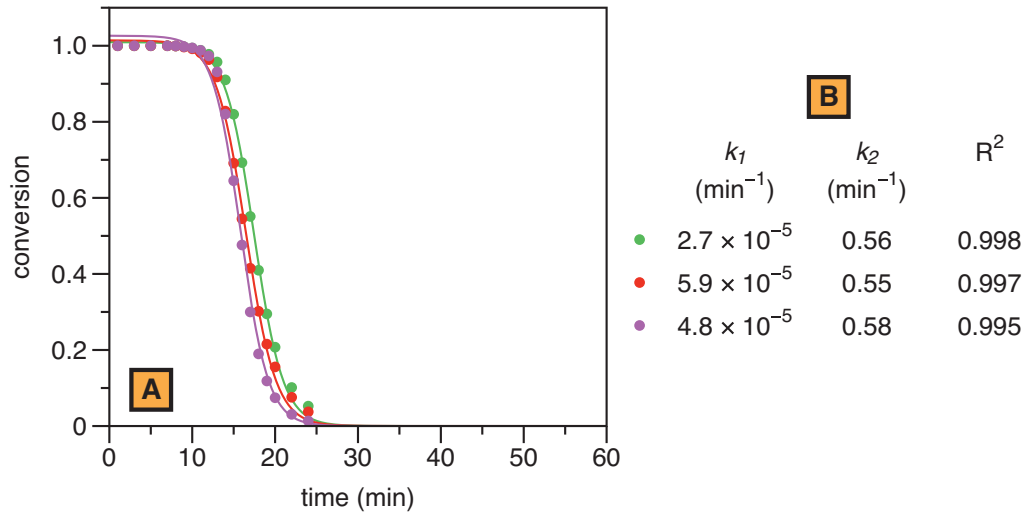



**Figure 2.13: Summary of data acquired when subjecting deuterated substrate 116 to the latest reaction protocol (i.e. using toluene ($H_2O$ sat.) as the organic solvent). A)** Overlay of kinetic data obtained. The different colours correspond to repeats of the same reaction. The lines correspond to the fitting of equation 2.1 to the appropriately coloured data set. The $x$-axis corresponds to time following initiation of the reaction by the addition of MVK, the $y$-axis corresponds to conversion of substrate **116** as a ratio of the total amount (in mol) of substrate **116** and product **117**. **B)** Values obtained following fitting of equation 2.1 to each data set. In all cases, the initial value for the concentration of substrate $[\mathbf{116}]_0$ as described in the equation 2.1 was initially set to the unitless value of 1.0. The data are colour-coded.

The rate behaviour obtained from subjecting deuterated **116** to the latest protocol was only subtly different to that observed when using the protonated substrate **49**. An overlay of the two triplicate sets (i.e. from Figure 2.11 and Figure 2.13) does not adequately depict the differences in kinetic behaviour. Thus, as a tool for comparison, the average values for the parameters extracted from the corresponding data sets (triplicate reactions using substrate **49** or **116**) were re-inputted into the function used to fit the data (i.e. equation 2.1), and the result plotted (Figure 2.14).

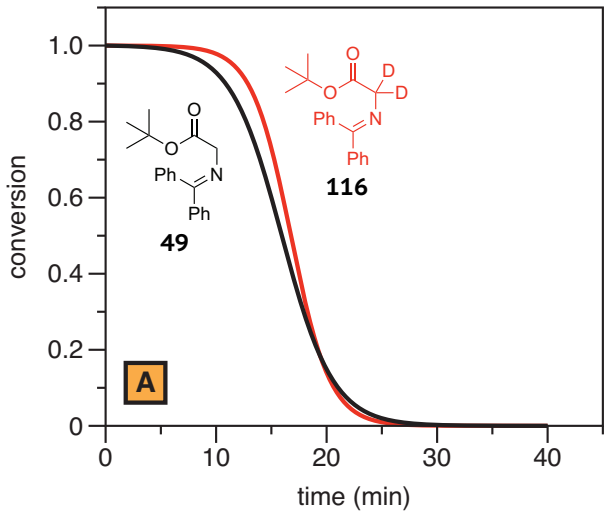
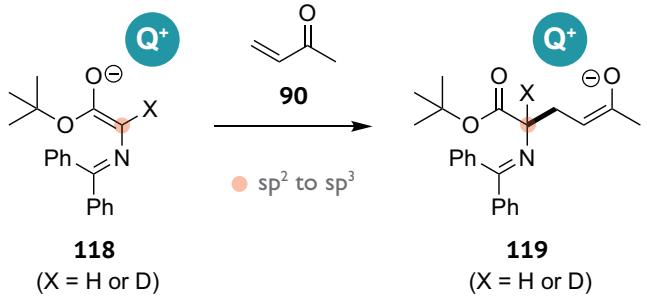



**Figure 2.14: Overlay of data comparing the kinetic behaviour of reactions using isotopically labelled substrates 49 (black) and 116 (red). A)** Comparing the graphical kinetic behaviour of results obtained using substrates **49** (black) and **116** (red). The $x$-axis corresponds to time following initiation of the reactions, the $y$-axis corresponds to conversion of the appropriate substrate (**49** or **116**) based on the ratio of the amount (in mol) of substrate to the combined amount of substrate and product. The lines are the result of inputting the parameters detailed in **B** into equation 2.1, and plotting the respective result. The data are colour-coded. **B)** Average values for the parameters $k_1$ and $k_2$ obtained from fitting the respective kinetic data to the model described by equation 2.1 and the KIE values associated with each parameter.

We obtained a primary KIE of 10 with the respect to $k_1$. This value suggested that deprotonation of the substrate nucleophile may be a rate-limiting factor in the steps associated with the $k_1$ parameter. However, we typically observed large variations of the $k_1$ values extracted from the data obtained from identical reactions; the absolute value for the primary KIE needs to be considered with caution. An inverse KIE of 0.76 was obtained with respect to the $k_2$ parameter. We suspected this was a secondary KIE corresponding to the addition step: the reaction of the substrate anion **118** with MVK (Scheme 2.18). The inverse nature and magnitude of the KIE was consistent with a hybridisation change of sp$^2$ to sp$^3$,[113] which was consistent with nucleophilic attack of an $\alpha$-labelled enolate. This suggested that the 1,4-addition step may be a rate-limiting factor in the steps associated with the $k_2$ parameter. Due to the deuteration observed in the product **117** (Scheme 2.16), the calculated KIE values need to be interpreted with caution; if proton exchange of the substrate **116** occurred prior to the reaction with MVK, the magnitude of the observed KIE would be less than what would be truly obtained if

no exchange occurred.



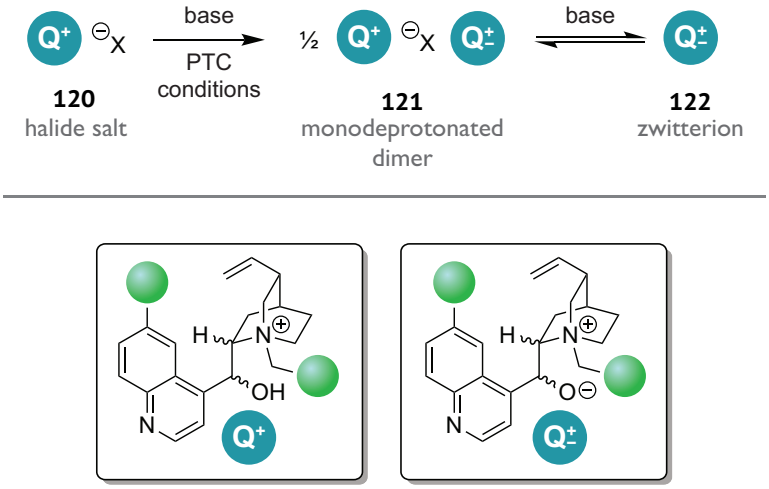

**Scheme 2.18: Bond-forming event giving rise to the secondary inverse kinetic isotope effect.**

Thus far, we had primarily focussed on obtaining graphically, and kinetically consistent results from our standard reaction conditions. With adequate protocols in place for generating good, reliable data, we then began probing the reaction mechanism. Subjecting isotopically labelled substrate to the reaction conditions gave results that were consistent with two distinct steps, which were probable in our reaction.

Whilst we had some insight as to what might be rate-limiting with respect to the extracted rate parameters of our applied kinetic model, we had very little information as to why the kinetic profile of our reaction model exhibited sigmoidal behaviour. This facet was the next subject of our investigations.

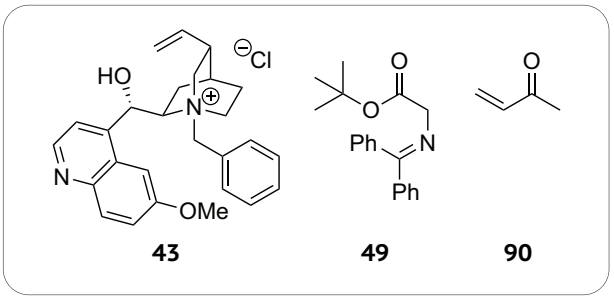
### 2.4.2 Illuminating a rate-determining step

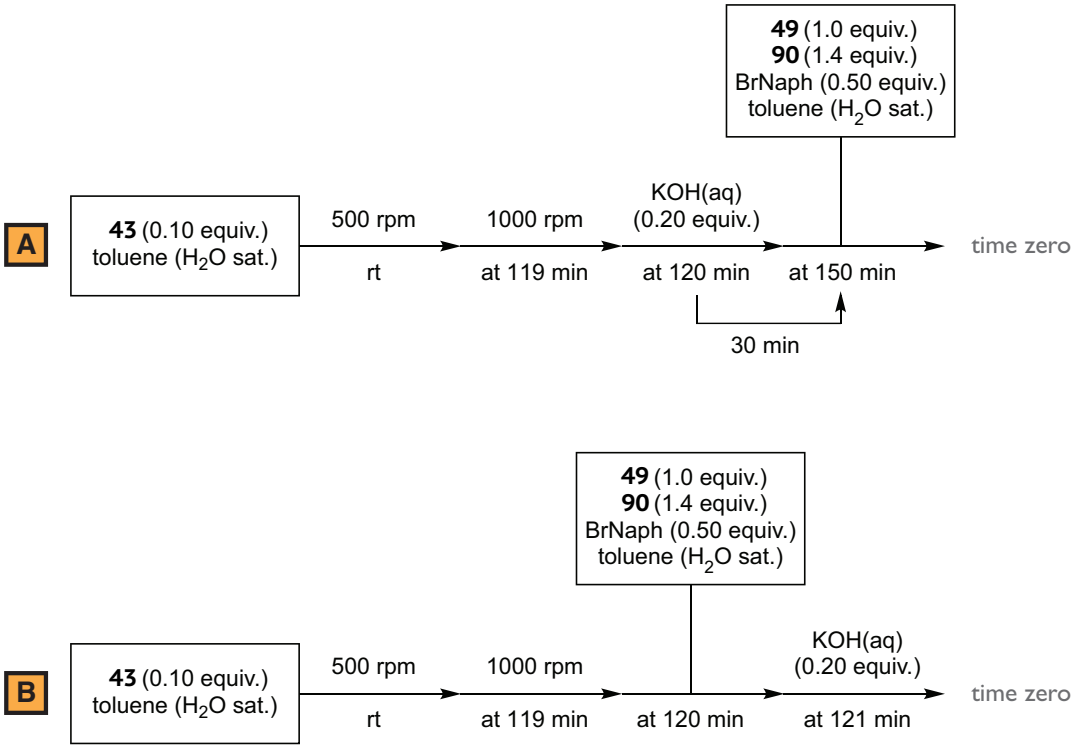
Previous work revealed that under basic phase-transfer conditions, cinchona alkaloid-derived catalysts bearing free hydroxyl groups likely exist as monodeprotonated dimers (e.g. from halide salt **120** to dimer **121**) in equilibrium with the corresponding zwitterion oxide monomer **122** (Scheme 2.19, and see 1.2.3).[29,84] The corresponding halide salt (e.g. **120**) was proposed to be a pre-catalyst, while the zwitterionic species was responsible for deprotonating the substrate in a PTC reaction system involving the alkylation of an indanone-derived substrate.[29]




**Scheme 2.19: General schematic for the formation of a dimeric cinchona alkaloid-derived salt 121 in equilibrium with the proposed active zwitterionic monomer 122.** The green balls indicate sites of variation, and X corresponds to a halide counterion, typically Cl or Br.

To test whether chloride catalyst **43** used in our system was a pre-catalyst, we carried out a reaction where the salt **43** was pre-stirred with base before initiating the reaction with a solution of the substrate materials MVK and **49** (A, Scheme 2.20). A corresponding control reaction was additionally carried out (B, Scheme 2.20). In both reactions, the salt **43** was first stirred in toluene for 120 min. This was to ensure adequate dispersion of the solid occurred before commencing subsequent steps. In the experiment, the base was added 30 min prior to the addition of the substrates and internal standard as a solution. In the control, the base was added last.




**Scheme 2.20: Protocol to evaluate the potential for catalyst activation. A)** The experiment, which included pre-stirring halide salt **43** with base prior to initiation of the reaction; **B)** the corresponding control reaction. Both reactions were otherwise carried out identically (e.g. amounts of reagents added, preparation of the substrate solution, methods for handling materials). Equivalents (equiv.) are reported with respect to substrate **49**.

When we collected the data and plotted the temporal concentration profiles, we obtained two completely different results (Figure 2.15). In the experiment where we pre-stirred the halide salt **43** with base prior to the addition of the substrates, we observed complete eradication of the induction period and apparent pseudo-first order behaviour. The control reaction revealed the same sigmoidal behaviour that we had previously observed.

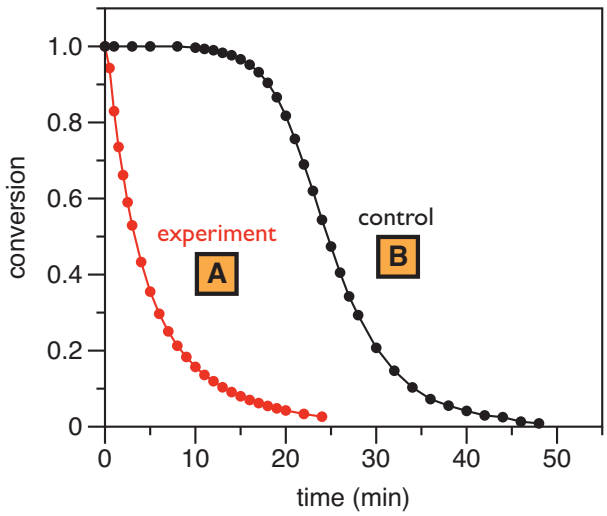



**Figure 2.15: Evaluating the potential for catalyst activation by A) pre-stirring halide salt 43 with base prior to initiation of the reaction (red data); B) carried out as an appropriate control (black data).** The red data correspond to the protocol described in A, Scheme 2.20; the black data correspond to the protocol described in B, Scheme 2.20. The $x$-axis corresponds to time following initiation of the reactions at the designated time zeros, the $y$-axis corresponds to conversion of substrate **49** taken as a ratio of the total amount (in mol) of substrate **49** and product **97**. The lines are guides for the eye.

Pre-stirring the halide salt **43** with base prior to initiating the reaction resulted in data that was simpler to analyse. Assuming a pseudo-first order reaction was in operation (with respect to the substrate **49**), we could now use either equation 2.2 or equation 2.3 to fit the data. In both equations, the concentration of substrate [**49**] at time $t$ depends on the rate constant $k$ and the initial concentration of substrate $[\mathbf{49}]_0$.

$$[\mathbf{49}] = [\mathbf{49}]_0 \times \exp(-kt) \tag{2.2}$$

$$\ln[\mathbf{49}] = \ln[\mathbf{49}]_0 - kt \tag{2.3}$$

We evaluated both equations against the data shown in A, Figure 2.15, and obtained rate constants ($k$) of comparable magnitude (Figure 2.16).

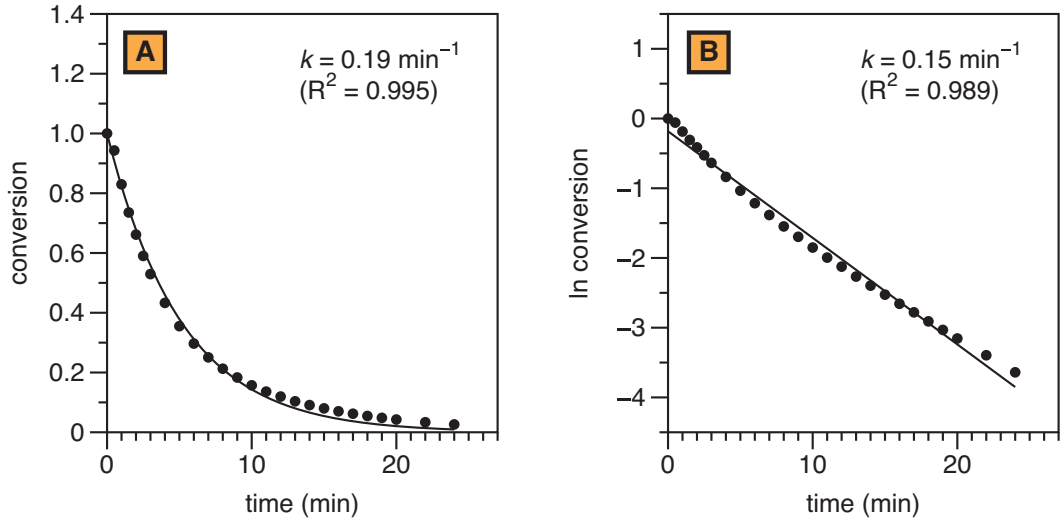



**Figure 2.16: Two methods for analysing the apparently pseudo-first order reaction data described in Figure 2.15.** In both graphs, the $x$-axis corresponds to time following initiation of the reactions at the designated time zeros. **A)** The $y$-axis corresponds to conversion of substrate **49** as a ratio of the total amount (in mol) of substrate **49** and product **97**. **B)** The $y$-axis corresponds to the natural logarithm of substrate **49** conversion, analogous to the data described in **A**. In both graphs, the lines correspond to the fitting of equation 2.2 or 2.3, in **A** and **B**, respectively. The extracted values for the $k$ parameter from fitting the data and the goodness of fit ($R^2$) are displayed on each graph.

Despite the ease of fitting a linear function to the concentration data (i.e. using equation 2.3), we decided to use equation 2.2 in the evaluation of subsequent reactions. The fit was slightly better using equation 2.2 and the integrated data for the amount of substrate **49** was not exactly linear, which suggested that we were not quite within the parameters for a pseudo-first order reaction. Nonetheless, we proceeded with the use of equation 2.2 for subsequent data analysis.

## 2.5 Further protocol optimisation

We had identified a reaction protocol that enabled the acquisition of relatively simple kinetic data for easy analysis. However, aspects of the protocol remained cumbersome or unreliable. We eventually developed a protocol and employed practical measures, which were somewhat elaborate, but necessary for the reasons we had thus far described and for additional reasons that will be described below.

Stirring the halide salt **43** for 120 min as the first step was a prohibitively time-consuming

exercise. An additional problem with this stage of the protocol was that clumps of solid catalyst would uncontrollably collect in the corner of the reaction vial, effectively reducing the surface area of catalyst available to react with the added KOH. Another physical issue was that solid catalyst would again aggregate, but on the inside surface of the vial at the air-liquid interface. To solve these issues, reduce the pre-stirring time, and maintain consistency of results, the catalyst-hydroxide-toluene mixture was treated in an ultrasound bath at precise intervals over a period of 30 min; stirring was continued between the sonication events.

We had thus far carried out reactions without knowing the total volume of the reaction mixtures. This was due to the substrate being weighed out as a solid and the solvent added to an estimated concentration of 0.1 M. This meant that obtaining correct concentration data for the substrate **49** was impossible. To enable the collection of quantitative kinetic data, we subsequently handled the substrates as solutions in toluene. The substrate **49** and MVK **90** remained completely inert in solutions made up in toluene with the internal standard BrNaph (in the absence of catalyst or base). By using a 1 mL volumetric flask, we prepared solutions with known concentration of substrate **49**, MVK **90** and BrNaph **115**. A known volume of this stock solution was then added to the stirred catalyst mixture to initiate the reactions at the designated time zero.

To facilitate the handling of solutions and solvent we used specifically acquired automatic pipettes. We found handling toluene and solutions made up with toluene using the pipettes gave consistent results as long as the disposable pipette tips were not pre-wetted before extracting the desired volume of solution.

We had thus far used the same stirrer bar for all experiments. However, we found that on occasion, solid material—presumably catalyst species—would collect on the edges of the stirrer bar, escape cleaning with water and acetone, and contribute to the next reaction. This was discovered when we were required to scrape the stirrer bar thoroughly to avoid this scenario. A

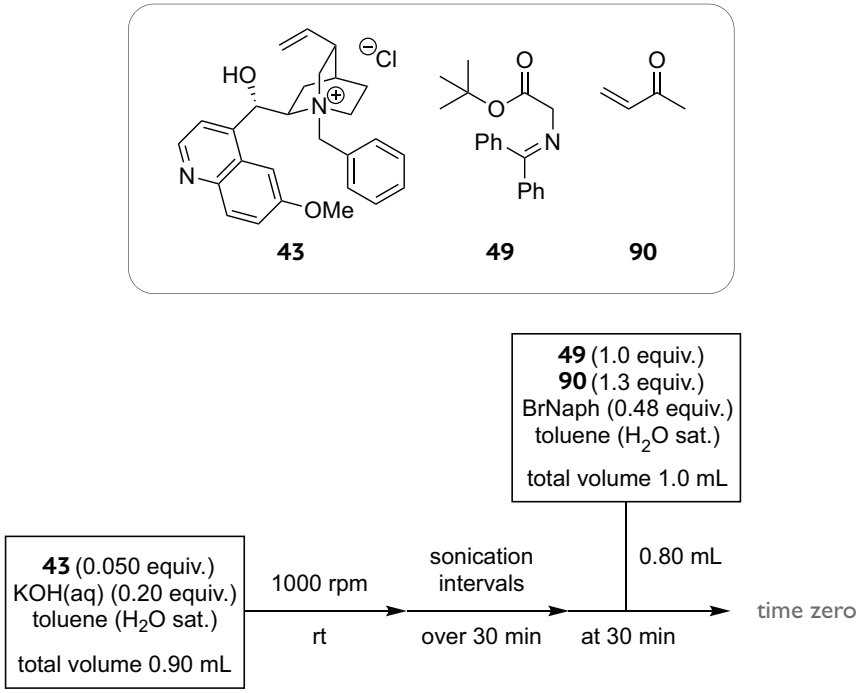
simpler solution was thus employed, and that was to deploy an unused stirrer bar in each new reaction. The new stirrer bars were acquired in bulk and were of the same model. Similarly, unused vials were used as the vessel for each new reaction.

On the unusual occasion that the ambient temperature of the laboratory reached 26 °C, we observed a considerable increase in the rate of the reaction. Reactions were subsequently only carried out when the environment was at a stable 20–22 °C (rt). On a similar note, we again found that with prolonged stirring, heat would transfer from the stirrer plate to the vial holder. To completely eliminate this unwanted effect, we installed insulation between the stirrer plate and the vial holder. Movement of the vial holder due to this change was inconsequential due to calibration of stirring using a stroboscope.

When we first started this project, the total reaction times were anywhere between 20 and 60 min, which enabled the collection of an adequate number of data points for analysis. Whilst developing our final protocol, with catalyst loadings of 0.017 mM (0.10 equiv. with respect to substrate **49**), complete consumption of substrate **49** occurred within about 5 min. This was problematic from the perspective of monitoring the reactions and acquiring a sufficient quantity of data points. We were limited by how quickly we could sample the reactions due to the requirement of quenching extracted reaction mixture aliquots through a plug of silica. We expected the rate of the reaction to be strongly dependent on the concentration of catalyst. As such, we thus amended our standard reaction conditions to be carried out with an initial catalyst concentration of 0.0084 M (0.062 equiv. with respect to substrate **49**).

The final protocol that we would use for the collection of data was thus developed (Scheme 2.21). It involved first preparing a mixture of salt **43**, toluene (saturated with water), and KOH(aq). The mixture was stirred at 1000 rpm, before being treated at regular, known, intervals in an ultrasound bath (for no more than 3 s). Meanwhile, a substrate solution (with a total volume of 1.0 mL) was prepared by dissolving the substrate **49**, MVK **90**, and internal standard BrNaph,

in toluene (saturated with water). At exactly 30 min following preparation of the salt **43** mixture, 0.80 mL of the substrate solution was added to initiate the reaction at the designated time zero.




**Scheme 2.21: Final protocol used for the evaluation of the model reaction (protocol 5).** General features include pre-treatment of the catalyst **43** with base with sonication over set intervals before initiating the reaction by the addition of the substrates **49** and **90** as a solution in toluene.

Practically the reactions were setup as precisely as possible. Solid materials were weighed out to the nearest 0.1 mg. Liquid volumes were handled with automatic pipettes or volumetric flasks of appropriate capacity. Agitation of the reaction mixtures was via a magnetic stirrer and bar; calibration of the stirring rate was carried out using a stroboscope. The reactions were carried out in non-rounded 7 mL screw-cap vials ($\varnothing$ = 1.5 cm) (A, Figure 2.17), which were to be held consistently in a specifically fabricated holder, which positioned the reaction vial centrally over the stirrer (B, Figure 2.17). Data collection involved manually sampling the reaction mixtures over time—without ceasing stirring or disturbing the stirrer bar—by extracting aliquots at precise, and known intervals. The aliquots were quenched through a short plug of silica (C, Figure 2.17), then directly analysed by HPLC.

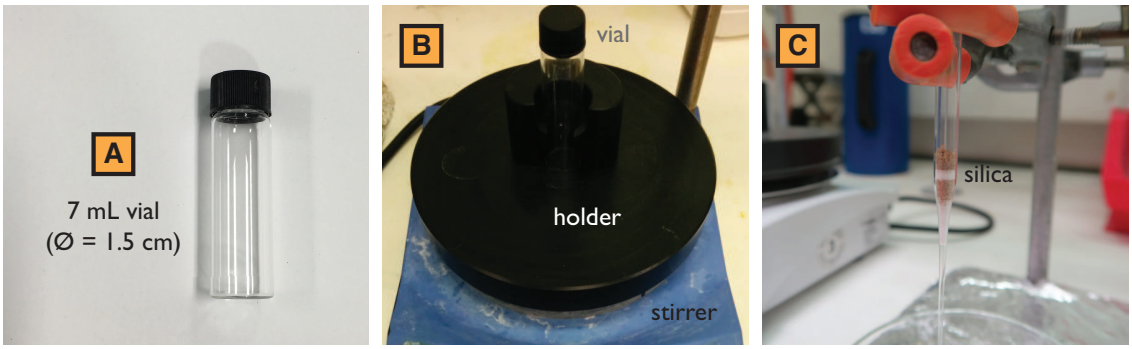
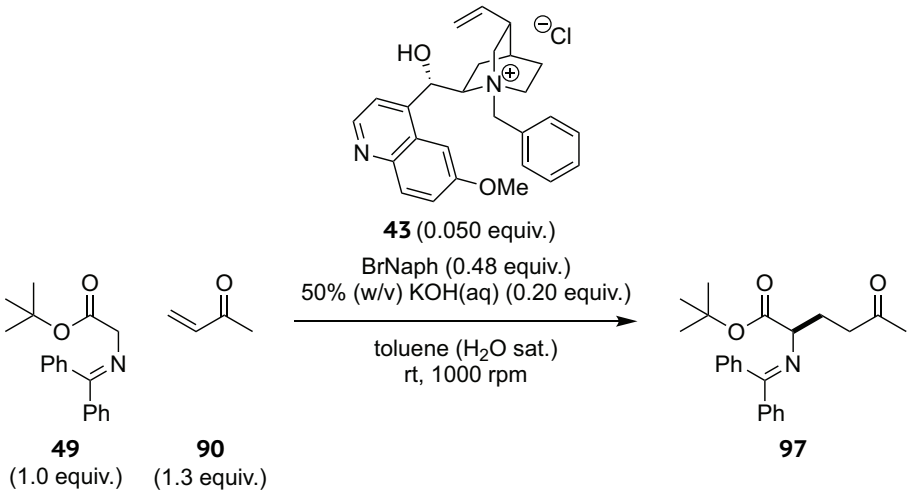



**Figure 2.17: Examples of practical considerations. A)** Single use reaction vials; **B)** vial fitted into the holder installed on a stirrer plate; **C)** example silica gel plug used to quench aliquots extracted from reaction mixtures.

We established standard conditions from which to vary the reaction (Scheme 2.22). Taking into consideration almost every practical aspect with respect to reaction setup and progression, we were able to consistently obtain reproducible results (Figure 2.18). The set of four identical reactions exhibited comparable kinetic behaviour, with an average $k$ value of 0.55 $\pm$ 0.04 $min^{-1}$.




**Scheme 2.22: Standard reaction conditions for the model reaction.** Carried out according to the protocol described in Scheme 2.21. Equivalents (equiv.) are reported with respect to substrate **49**.

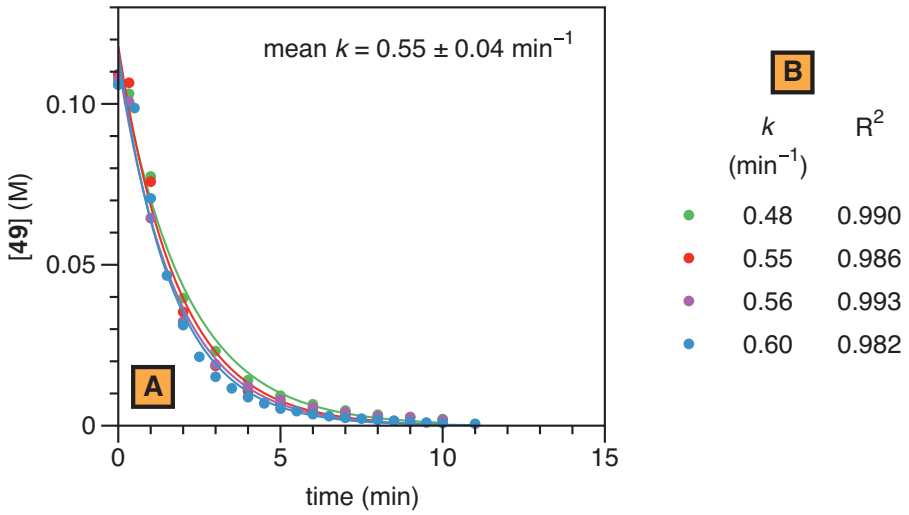
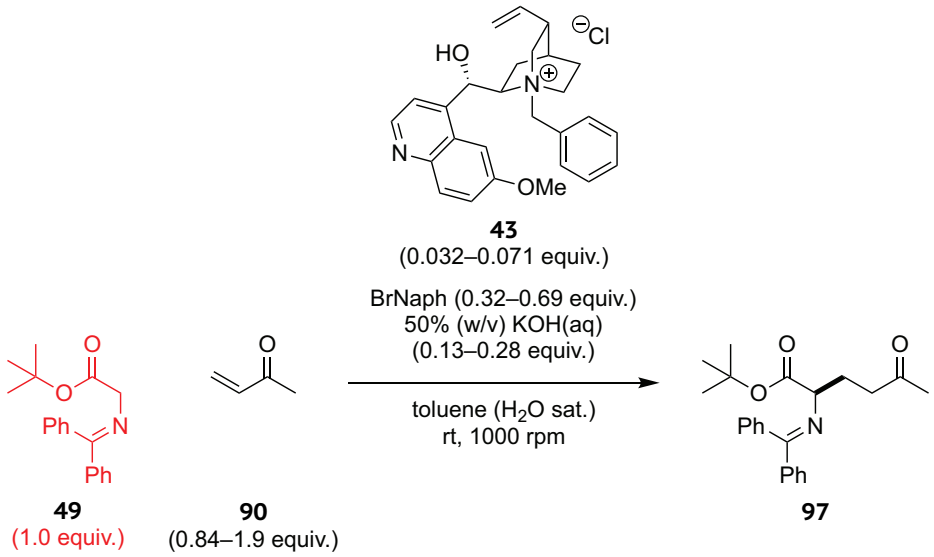



**Figure 2.18: Data acquired from four identical reactions.** The reactions were carried out according to the details in Scheme 2.21 and Scheme 2.22. **A)** Overlay of concentration data obtained from the four reactions. The $x$-axis corresponds to time following initiation of the reaction by the addition of the substrates to the reaction mixture, the $y$-axis corresponds to the concentration of substrate **49**. The different colours correspond to each of the four reactions. The coloured lines correspond to fitting of the function described by equation 2.2 corresponding to the appropriately coloured data set. **B)** Values obtained following fitting of equation 2.2 to each data set, which follows the same colour convention as in **A**.

## 2.6 Attempts to delineate the reaction mechanism

With the optimised setup and sampling protocols, we turned our attention to once again, attempting to elucidate the mechanism of this particular model reaction. Given the KIEs obtained when subjecting isotopically labelled substrate **49** to the reaction conditions (see 2.4.1), we decided to evaluate the kinetic effects of substrate **49** concentration.

Taking the standard conditions (described in Scheme 2.22), we then varied only the initial concentration of substrate **49**. A series of reactions were carried out with initial concentrations of substrate **49** of 0.070 to 0.15 M (Scheme 2.23). The kinetic data were collected and each data set analysed using equation 2.2 to extract the value for the $k$ parameter.




**Scheme 2.23: Conditions used to evaluate the reaction order with respect to substrate 49.** Carried out according to the protocol described in Scheme 2.21. Equivalents (equiv.) are reported with respect to substrate **49**.

To evaluate the rate dependence of the reaction on the concentration of substrate **49**, a double logarithmic plot of the $k$ values for the rate of each reaction against the initial substrate **49** concentration was constructed (Figure 2.19). Linear regression analysis of the double logarithmic plot revealed a slope with a value of $-0.73$. This suggested the order with respect to substrate was negative and partial, and indicated complex kinetic behaviour.

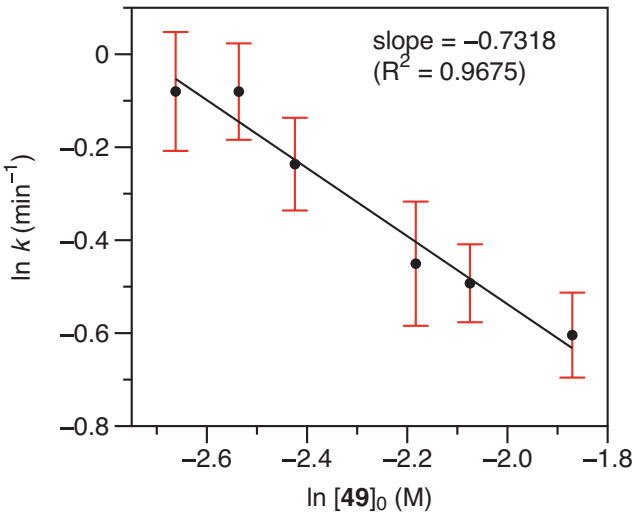



**Figure 2.19: Double logarithmic plot to evaluate the rate-dependence on the concentration of substrate 49.** The $x$-axis corresponds to the natural logarithm of the initial concentration of substrate **49** in M, the $y$-axis corresponds to the natural logarithm of the extracted $k$ value from each reaction set in $\text{min}^{-1}$. The line is from linear regression analysis of the data, which gave a slope of $-0.73$ with an $R^2$ value of 0.968.

When we examined the data as the natural logarithm of the concentration of substrate **49** over time, we found it exhibited non-linear behaviour under conditions that strayed further from what might be considered pseudo-first order (i.e. not in vast excess of MVK **90**) (Figure 2.20). This suggested the application of a first order analysis to our kinetic data might not be appropriate, which was not unexpected given conditions that we predominantly examined.

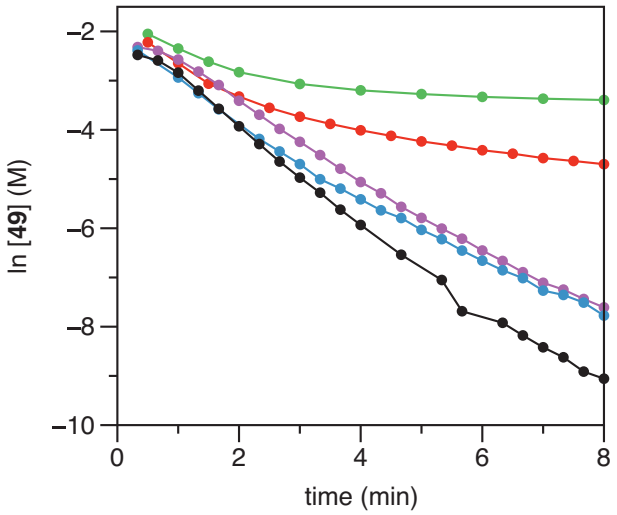
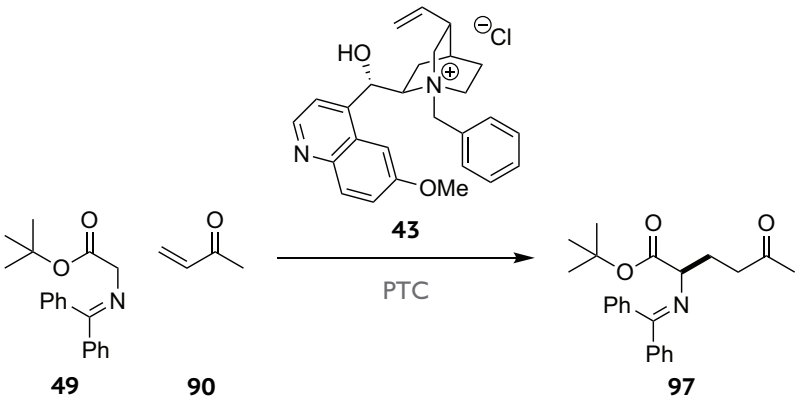



**Figure 2.20: Example of data visualised as the natural logarithm of the concentration of substrate 49 over time.** The reaction conditions corresponding to the data obtained in each example differed only by the initial concentration of substrate **49**: 0.15 M (green), 0.11 M (red), 0.13 M (purple), 0.089 M (blue), 0.079 M (black). The $x$-axis corresponds to time following initiation of the reaction, the $y$-axis corresponds to the natural logarithm of the concentration substrate **49**. The lines are guides for the eye.

The complex role of substrate **49** and the overall deviation from simple pseudo-first order behaviour led us to re-evaluate our position on attempting to deconvolute the reaction mechanism of our selected model. The complexity of the reaction model, i.e. bimolecular, catalytic in base, and pre-catalyst vs catalyst effects, in addition to the reproducibility issues that we had solved presented, overall, a significant challenge. The inability to monitor the concentration of MVK **90**, and the fast nature of the reaction further hindered our ability to collect data and conduct analyses. It was at this point in time that we made a conscious decision to halt further investigations of this particular reaction model. It was deemed to be non-productive, and at the time, we lacked the tools to adequately model the complex kinetic data.

## 2.7 Summary and conclusions

We were initially interested in the general mechanisms behind enantioselective 1,4-addition reactions effected by cinchona alkaloid-derived phase-transfer catalysts. Following evaluation of the literature, we selected a reaction model to serve as the foundation for our investigations: the 1,4-addition reaction between glycine imine **49** and methyl vinyl ketone, effected by *N*-benzylquinidinium chloride **43** (Scheme 2.24). Preliminary kinetic investigations found an induction period in the conversion of substrate **49** to product **97** (Figure 2.21), which was consistent with the initial hypothesis of the presence of "auto" effects.




**Scheme 2.24: Selected model reaction for study.**

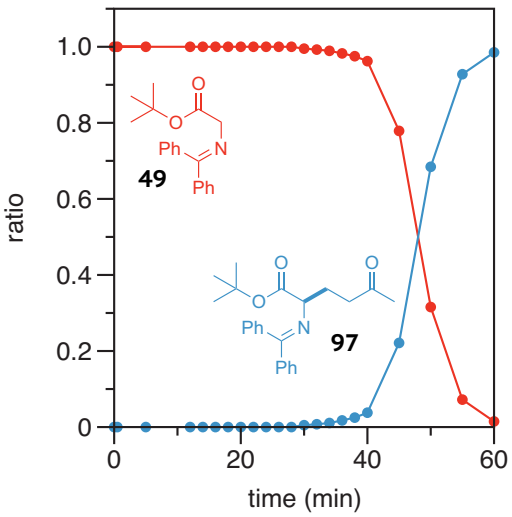



**Figure 2.21: Preliminary kinetic results from the model reaction.**

Significant protocol optimisation was required in order to obtain reproducible and consistent

kinetic results. For example, pre-stirring of the substrate and catalyst influenced the observed rate behaviour of the reaction, as did the water content of the organic solvent used; as such, we implemented controls over most feasible practical considerations. These included fabrication of custom reaction vial holders, use of a stroboscope to quantify reaction agitation, and storage of the organic solvent over water. The result was the development of solid and reliable methods to kinetically probe enantioselective phase-transfer reactions.

In the sigmoidal kinetic regime, given the KIE values obtained, the rate-determining step described by $k_2$ was likely the 1,4-addition step. The $k_1$ was related to deprotonation of the substrate, and the induction period was due to pre-catalyst activation in the presence of KOH(aq). By pre-stirring the ammonium halide salt **43** with KOH(aq) prior to initiating the reaction, a simpler pseudo-first order kinetic profile was obtained, and was thus used for subsequent investigations.

Further protocol optimisation was implemented, before our attention was turned to the investigation of the reaction mechanism itself. Evaluation of the effects of substrate **49** found deviations from pseudo-first order behaviour, revealing complex kinetics. At the time, we deemed the current investigations to be unproductive, thus concluded the project, and refocused on an alternative reaction model.

The 1,4-addition reaction proved to be quite sensitive to even the smallest changes. This made it difficult to study. However, the sensitivity of the reaction made it an ideal platform for developing solid methods to study asymmetric phase-transfer catalysis. We realised that by controlling almost every practical aspect of the reaction, we could obtain data of excellent quality, considering we were analysing polyphasic, heterogeneous reaction mixtures. Ultimately, the project was an exercise in developing methods to scrutinise enantioselective phase-transfer catalysis, which were subsequently used in the deconvolution of an alternative reaction model: the subject of Chapter 3.

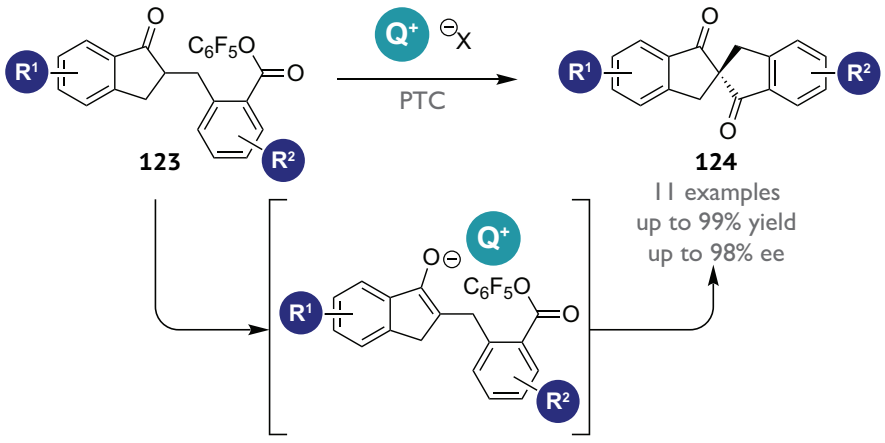
# 3. Project 2: Elucidating the Mechanism of an Intramolecular *C*-Acylation Reaction Model

## 3.1 Introduction

As a model reaction, the previous system proved to be too complicated. We rationalised that an intramolecular reaction might be simpler to study. To assist our investigations, we turned our attention towards a reaction that had been previously developed in the group.

### 3.1.1 Background to the reaction model

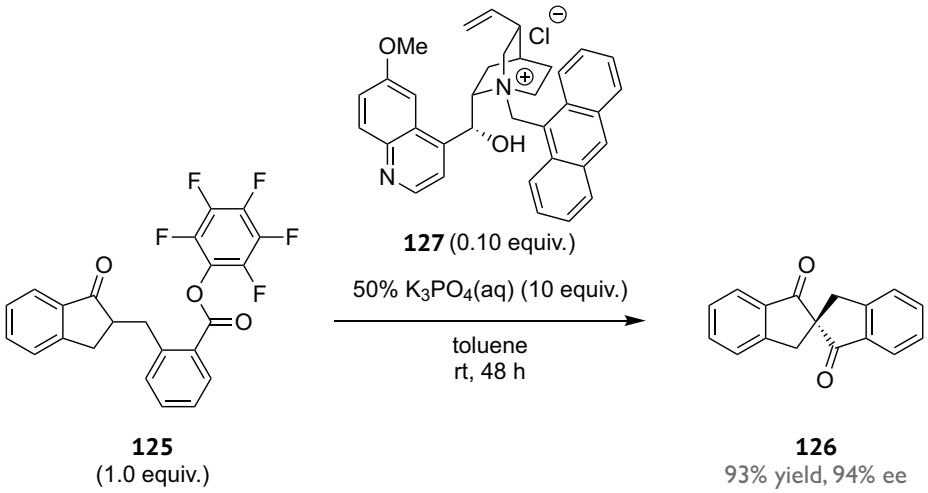
The intramolecular *C*-acylation to give spirobiindanones is a reaction that was developed in the group (Scheme 3.1).[114] Under phase-transfer reaction conditions, the substrate **123** is deprotonated, and subsequent cyclisation affords the corresponding spirocyclic product **124** with good yield and enantiomeric excess (ee).




**Scheme 3.1: General scheme for the synthesis of spirobiindanones using phase-transfer catalysis.** The reaction proceeds via an ion pair that cyclises selectively to give enantioenriched product. Several examples were reported with good yields and enantioselectivities.[114]

We rationalised that this cyclisation reaction would be a good candidate model due to the reduced complexity compared to a bimolecular reaction model. We elected to examine the

reaction that used the flagship substrate **125** to generate enantioenriched, axially chiral spirobiindanone **126** (Scheme 3.2). The reaction was previously optimised to use *N*-alkylated quinine **127** as the catalyst and aqueous potassium phosphate as the base. This parent reaction proceeded with excellent enantioselectivity and good yield over 48 h.[114]




**Scheme 3.2: Selected reaction to study.** Conditions described are from previously published results.[114] Equivalents (equiv.) are reported with respect to substrate **125**.

### 3.1.2 Project approach

The approach to project 1—Chapter 2: Developing methods for kinetic studies of asymmetric PTC—was a fluid process where the direction of the project was predominantly dictated by the variability of results that we were initially bombarded with. Our strategy to investigate this new selected model—the spirocyclisation—was to be a far more ordered advance (Figure 3.1).

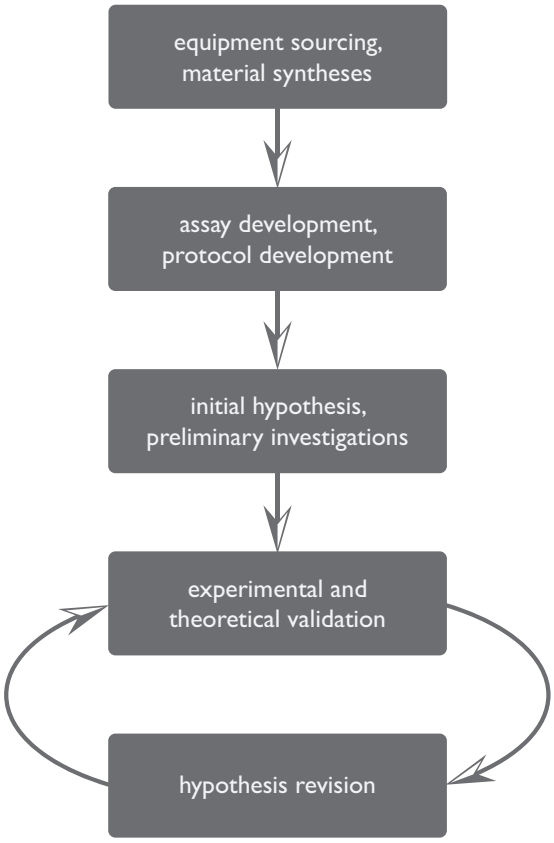



**Figure 3.1: General approach to the project.** Following initial set up, preliminary preparations and investigations, we used a hypothesis-driven strategy to drive the theoretical and practical experiments.

We were aware that almost every variable involved in the practical aspects of the reaction needed to be controlled as much as possible to minimise variation in the kinetic behaviour of experiments upon repetition. Equipment to facilitate this was acquired (reaction vial holders, reaction vials, stirrer bars, etc). We developed protocols from the outset to make sure that we were carrying out reactions consistently. An assay was developed to facilitate the quantitative monitoring of reactions. To explore the reaction itself, our progress was largely hypothesis driven. Following the acquisition of preliminary data, we focused on scrutinising particular aspects of evolving hypotheses using theoretical and experimental approaches.

### 3.1.3 A note on collaboration

The work described in this chapter was carried out in collaboration with a number of individuals. In summary, the preliminary investigations were carried out with Dr Benjamin Rahem-

tulla (BFR) (sections 3.2 to 3.8). Additional experiments were carried out with Dr Aroonroj Mekareeya (AM) (detailed in text). All theoretical aspects of this project were carried out in collaboration with Dr Martin Galpin (MRG), who constructed and solved the kinetic models, conducted treatments of derived rate equations, and carried out data fitting.

## 3.2 Preliminary preparations

Before we could explore the reaction, we sourced the equipment necessary to proceed with the kinetic study. We then needed to synthesise enough material for the entire study. Finally, as part of our pre-study preparations, we required a quantitative assay to determine concentrations of the substrate **125** and product **126** over time.

### 3.2.1 Sourcing equipment and planning

We planned to carry out all reactions at room temperature (rt), which was consistently maintained at 20–22 °C. To mechanically agitate the reactions, we used magnetic stirrers. Three identical stirrer plates were acquired and used for the duration of the study. All stirring speeds were calibrated using a stroboscope. Single use reaction vials of one batch were acquired—the shape of which were rounded so that no corners were present for solid material to collect into. Stirrer bars were selected so that an optimal shearing motion of stirring was obtained; they were deployed for single use to prevent cross-contamination between reactions. Vial holders were constructed to perfectly fit our selected reaction vials; the holders were designed to centrally position the vials over the stirrer plates to obtain consistent stirring between experiments. In addition, the holders suspended the vials above the bottom surface to minimise heat transfer from the stirrer plate (Figure 3.2). Insulation was installed between the holder and the stirrer plate to further minimise this effect.

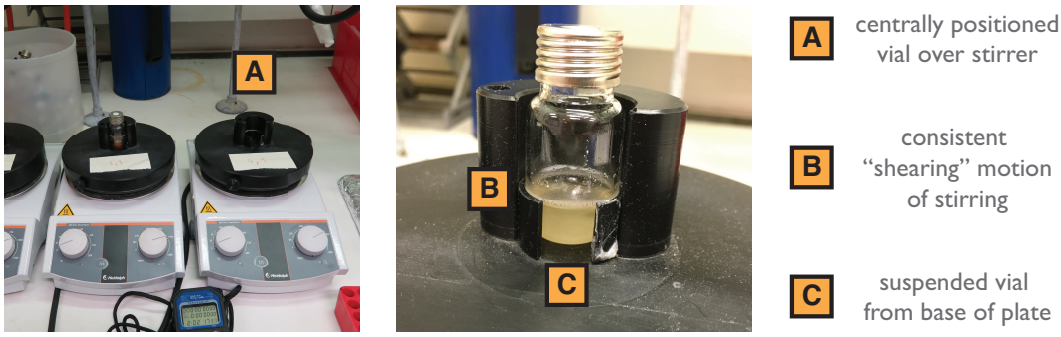


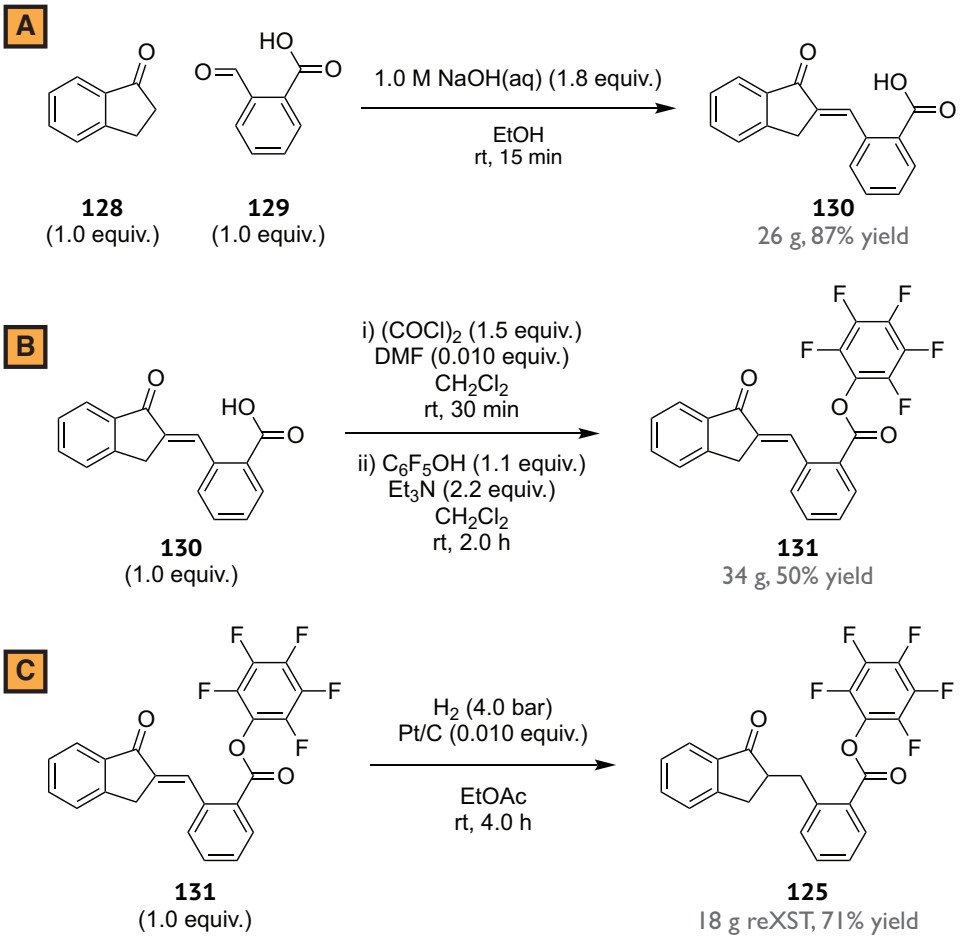

**Figure 3.2: Example reaction station set up showing a vial holder installed on a magnetic stirrer plate.** The holders were designed to be **A)** centrally positioned over the stirrer to give a **B)** consistent shearing motion of stirring, and **C)** hold vials above the base of the plate.

### 3.2.2 Material syntheses and preparation

Due to the vial size we required reaction volumes of roughly 2 mL. As such, the predicted scale of the reactions meant we needed approximately 60–70 mg of substrate per reaction (about 0.08 M reaction scale), with up to 210 mg required for triplicate experiments. Hence, we required a bulk substrate pool of at least 15 g to ensure enough material would be available for the duration of the study (up to approximately 70 triplicate experiments). We also needed a large quantity of the catalyst **127**, which was also required to be synthesised in bulk (at least 3 g).

Bulk syntheses of the starting materials were carried out by BFR using conditions modified from the literature;[114] all optimisations for preparing the substrate **125** and catalyst **127** on multigram scales were carried out by BFR.[115]

The substrate **125** was prepared in three steps (Scheme 3.3). Aldol condensation of indanone **128** with 2-carboxybenzaldehyde **129** to give the adduct **130** (A, Scheme 3.3) was followed by formation of the pentafluorophenolate ester **131** (B, Scheme 3.3). Subsequent hydrogenation of **131** yielded the crude model substrate **125**; purification of the crude material by flash chromatography followed by recrystallisation from 2-propanol afforded the substrate in a bulk pool of 18 g with adequate purity for our studies (>99% purity by HPLC at 254 nm) (C, Scheme 3.3 and Figure 3.3).




**Scheme 3.3: Three-step synthesis of the substrate 125. A)** Aldol condensation to give intermediate **130**; **B)** formation of ester **131** via the corresponding acid chloride; **C)** enone hydrogenation to give model substrate **125**.

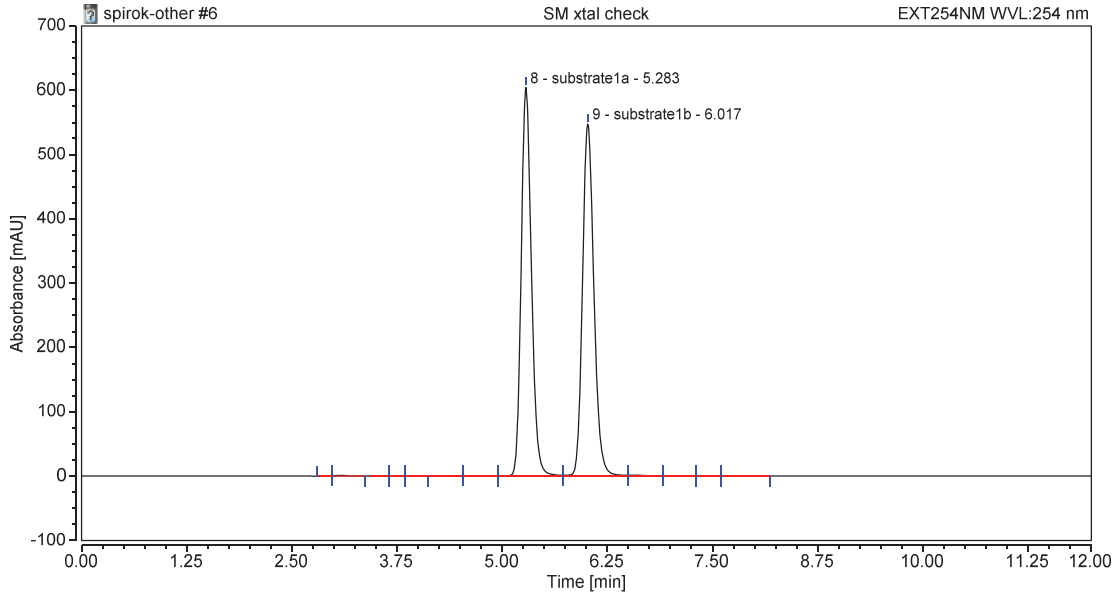
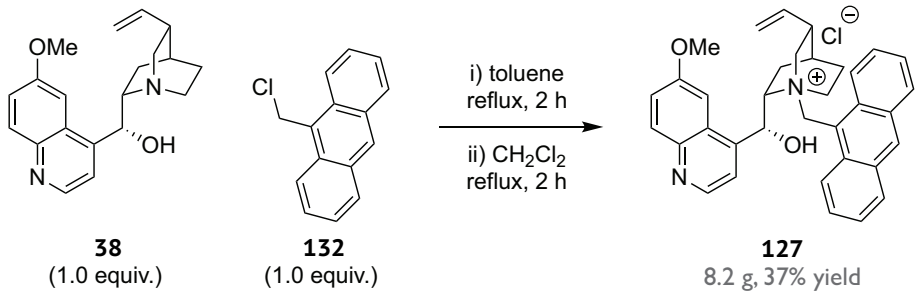



**Figure 3.3: HPLC chromatogram of the batch synthesised substrate 125.** The $x$-axis represents retention time; the $y$-axis shows UV absorption at the extracted wavelength. Data are extracted at 254 nm to give an indication of the purity of the material; the signal integral areas corresponding to the substrate enantiomers (−)-**125** and (+)-**125** were >99% of the total.

The catalyst **127** was prepared by alkylation of quinine **38** with chloromethyl anthracene **132** (Scheme 3.4).[114,115] Unfortunately, we were unable to recrystallise the material and it was used without further purification.




**Scheme 3.4: Synthesis of the catalyst starting material, compound 127.** Two-step procedure to prepare the reaction model catalyst via the alkylation of quinine **38** using chloride **132**.

Whilst the literature reaction was initially effected using 50% (w/w) aqueous $K_3PO_4$,[114] we used a saturated solution of aqueous $K_3PO_4$ (titrated to 4.77 M) as the base in our study. We anticipated changes in the concentration of base over time might affect the kinetic behaviour of the reaction model; it was more practical to keep a saturated solution on hand for use in the study. The organic solvent used was toluene, which was prepared as a water saturated solution

and was stored over water (approximately 30 mL of $H_2O$/1000 mL).

### 3.2.3 Quantitative assay development

With bulk quantities of the required materials obtained, we turned our attention to quantifying mixtures of the substrate and product by chiral HPLC using an internal standard. Our internal standard was 9-methylanthracene **133** (9MA), obtained from Sigma-Aldrich (45793-250MG) as a crystalline solid with analytical grade purity, which was ideal for our purposes. Due to the sheer quantity of data we expected to generate, we required HPLC run times of ideally, less than 15 min. The challenge was to obtain complete separation of the solvent, the internal standard **133**, the substrate **125** enantiomers, and the product **126** enantiomers within that period. After screening various HPLC conditions, we were able to obtain complete separation of the described components within 11 min using data extracted at 240 nm (Figure 3.4). The absolute configurations of the product **126** and identification of the corresponding peaks by HPLC were determined in previous work.[114,115] Optical activity of the substrate was determined following the isolation of small quantities of enantioenriched material (see 3.7.5).

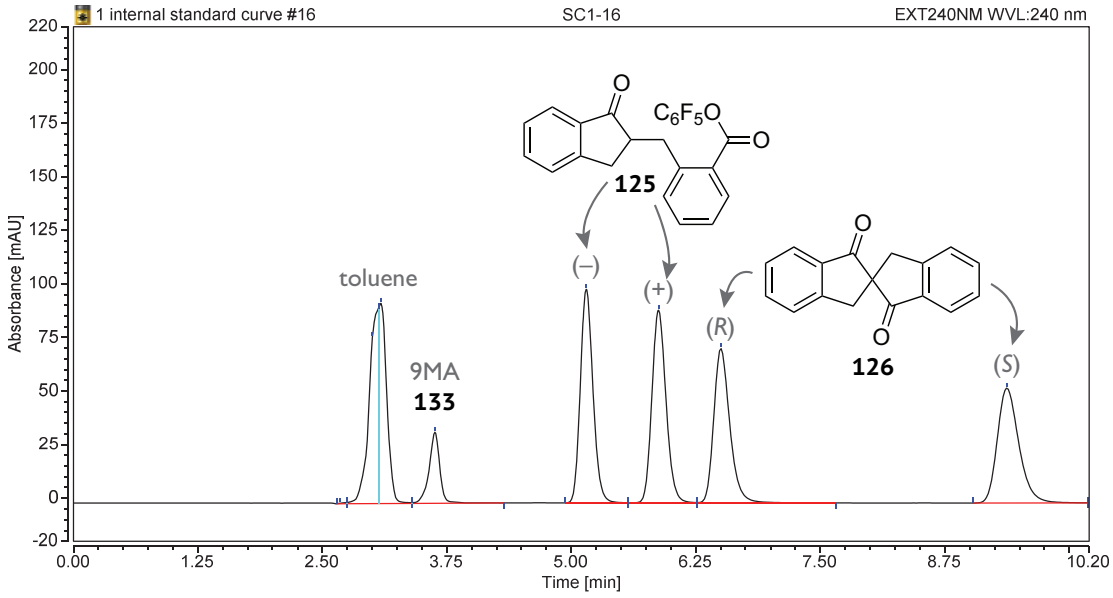



**Figure 3.4: HPLC chromatogram of a sample mixture.** Instrument conditions: injection volume 50 µL; ChiralPak® IA, 1.100 mL $min^{-1}$, 30% (v/v) 2-propanol/hexane, 25 °C. The data are extracted at 240 nm. The $x$-axis represents retention time; the $y$-axis shows UV absorption at the extracted wavelength. Peak identities are marked on the chromatogram.

With a suitable HPLC method identified, we constructed standard curves for each analyte (substrate enantiomers (−)-**125**, (+)-**125**, and product enantiomers (*R*)-**126**, and (*S*)-**126**) against our selected internal standard **133** (9MA). We prepared analytical samples containing racemic substrate **125** and racemic product **126** across the concentration space expected for a reaction profile. We anticipated that we would require initial rate kinetic studies to assist further studies of the reaction mechanism. We therefore increased the number of data points in the region of high substrate concentration and low product concentration.

The concentrations and composition of the standard, solvent, and analyte present in the samples were set to what we would expect from an extracted aliquot (2.0 µL) from a genuine reaction mixture. To facilitate handling of small amounts of material, the analytes were manipulated as stock solutions in 2-propanol. The samples for the standard curves were prepared by adding the desired amount of stock solution to each sample; the remaining volume was then made up with hexane and 2-propanol before the addition of toluene, sufficient mixing, and analysis by HPLC.

Three standard curves were constructed for each analyte (Figure 3.5). In all cases, we obtained a linear response for the analyte. The amounts of analyte in a sample could be calculated using the slope of each graph and the known amount of standard present in a reaction mixture. We next wanted to validate the assay by comparing its calculated yield to an isolated yield of a reaction mixture sample.

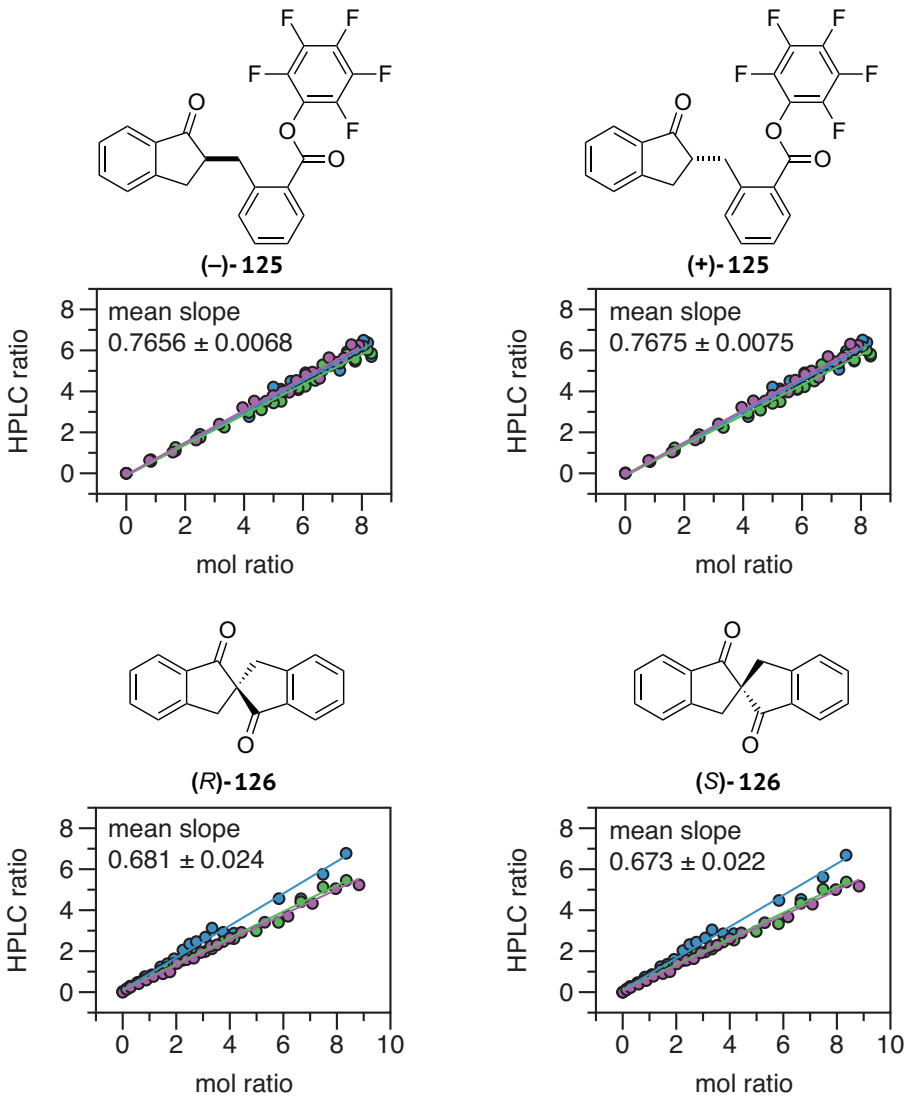



**Figure 3.5: Standard curves for each analyte ((−)-125, (+)-125, (*R*)-126, and (*S*)-126).** The $x$-axis corresponds to the mole ratio of the analyte to the internal standard 9MA, and the $y$-axis corresponds to the HPLC signal integral ratio of the analyte to 9MA. The blue, green, and purple dots indicate different standard curve sets. The lines are the slopes from linear regression analyses of the corresponding set of the same colour. The mean slope of the sets were calculated for each analyte to give the assay conversion factor for the analyte.

Whilst validating our quantitative assay, we encountered a slight issue: at extended reaction times (>18 h), an additional peak appeared in the HPLC chromatogram, interfering with the data analysis of (+)-**125** and (*R*)-**126**. This minor peak was attributed to anthracen-9-ylmethanol, presumably from catalyst degradation over time.

To address this issue, we extracted the data at both 240 nm and 292 nm. All analytes exhibited good absorption at 240 nm, whilst only the substrate **125** enantiomers and product **126** enantiomers absorbed at 292 nm (Figure 3.6). The data for the obscured peaks ((+)-**125** and

(*R*)-**126**) were extrapolated at 240 nm using the data obtained at 292 nm. This was possible because the enantiomeric ratio must remain constant at all wavelengths. The data at 240 nm were then used to calculate the amount of each analyte present in the reaction mixture. We were unable to use data solely obtained at 292 nm due to the poor absorption of the standard 9MA at that wavelength. Details for the calculation of analyte amounts in a sample may be found in 7.3.4.

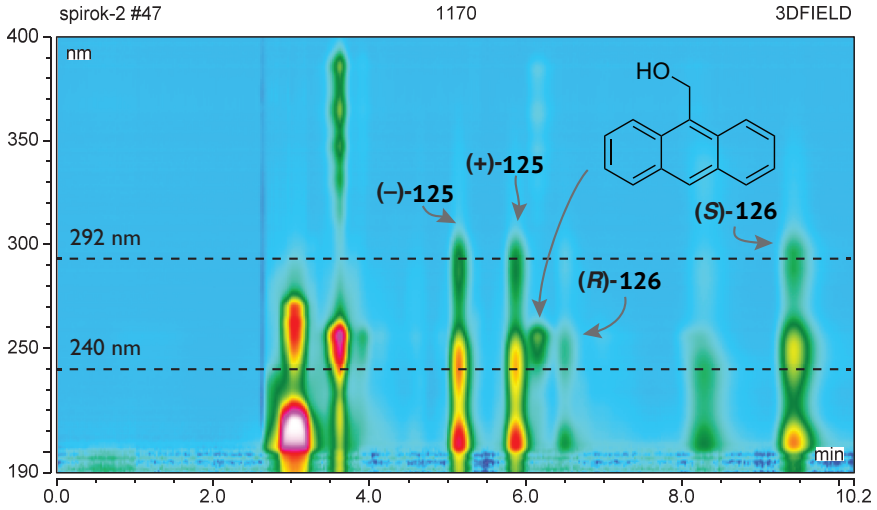
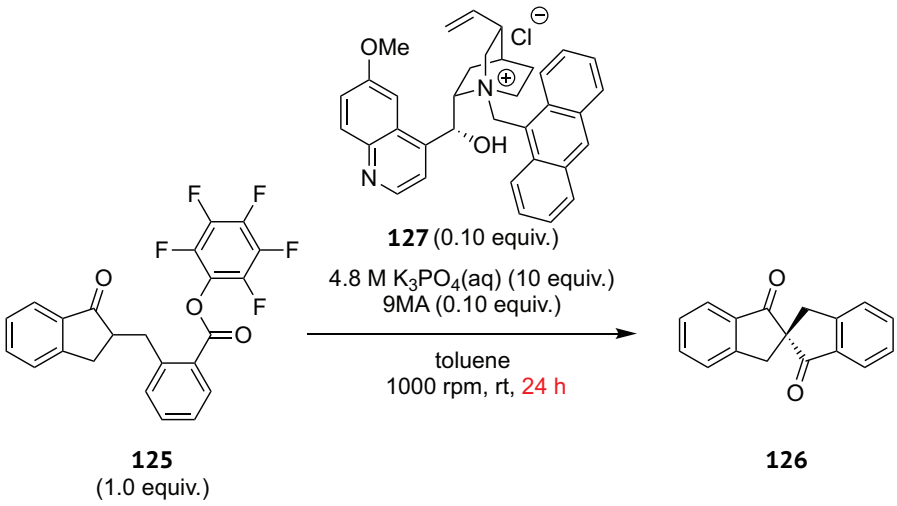



**Figure 3.6: HPLC 3D field of the reaction sample.** The $x$-axis corresponds to retention time in min, the $y$-axis corresponds to wavelength in nm, and the contours (from blue to red) represent absorption intensity.

With our optimised method developed, we carried out an experiment to validate the calibration. A reaction was set up on the scale that we expected to carry out subsequent kinetic experiments. After 24 h, an aliquot was extracted from the reaction mixture before it was immediately quenched and the substrate **125** and product **126** isolated (Scheme 3.5). The aliquot itself was quenched then analysed using our assay to give the calculated yields for the substrate **125** and product **126**. Good agreement was obtained between the two values, validating our assay as a method for quantifying these reaction mixtures.




| | 125 | 126 |
|---|---|---|
| *calculated* | 27.5 mg (55% yield) | 8.5 mg (30% yield) |
| *isolated* | 29.8 mg (60% yield) | 9.2 mg (32% yield) |

**Scheme 3.5: Validating the HPLC assay.** The substrate **125** was subjected to the reaction conditions described, quenched at 24 h, and the product **126** and remaining substrate **125** isolated. The isolated yield was then compared to that calculated at 24 h.

## 3.3 Establishing protocols

Before we could begin analysing reaction mixtures, we needed to establish reaction and sampling protocols and decide how we would practically handle the reactions. The protocols were designed with considerations from project 1 in mind.

### 3.3.1 Standard reaction protocol

To carry out the majority of our reactions, we implemented a pre-stirring protocol (see 7.4.1) (Figure 3.7). This involved stirring the catalyst **127** with some organic solvent and the desired amount of aqueous $K_3PO_4$. The protocol ensured any catalyst activations steps occurred prior to the addition of our substrate, hence potentially simplifying the kinetic behaviour for analysis. The procedure was carried out according to a strict schedule. In summary, the catalyst was added to the reaction vial before toluene was added, followed by the aqueous base. A pre-reaction schedule was then carried out, which involved treating the mixture in an ultrasound

bath at regular intervals; stirring at 1000 rpm was continued between treatments. This was to ensure maximum dispersion of the solid catalyst to minimise any variances in rate behaviour due to uneven dispersions between reaction sets. After the set 30 min, the substrate was added as a solution in toluene to initiate the reaction at the designated time zero.

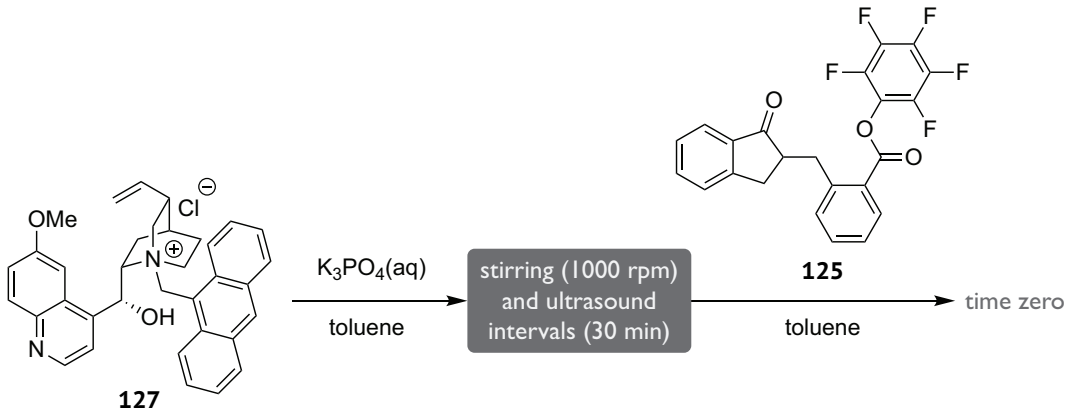



**Figure 3.7: Schematic representation of the standard reaction protocol.** General setup involved pre-stirring the catalyst with base under phase-transfer conditions before initiating the reaction by the addition of substrate.

All reagents were handled as solutions in toluene as much as was practically feasible to ensure concentration values for the analytes could be calculated appropriately. Unfortunately, the catalyst **127** was completely insoluble in the solvent, so was consistently handled as a solid; the volume contribution of the solid was considered to be negligible. All volumes were handled using automatic pipettes of appropriate capacity.

### 3.3.2 Sampling protocol

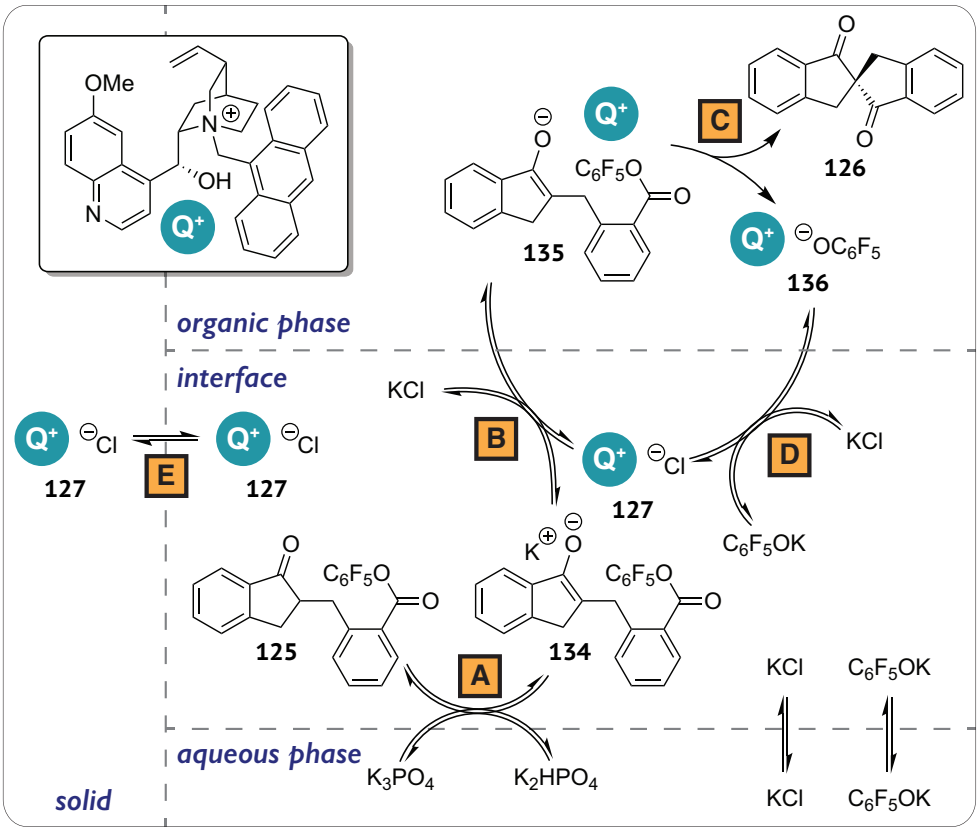
The reactions were sampled by extracting aliquots from reaction mixtures without ceasing stirring or disturbing the stirrer bar. The aliquots were immediately quenched by filtering through a short plug of silica gel, eluting with a 50% (v/v) mixture of 2-propanol/hexane. The filtrate was collected in a sample vial, which was directly analysed by HPLC using the optimised instrument method (injection volume 50 µL; ChiralPak® IA, 1.100 mL $min^{-1}$, 30% (v/v) 2-propanol/hexane, 25 °C).

### 3.3.3 Data analysis protocol

In order to minimise errors introduced through manual handling of data, the raw HPLC data were processed using R scripts, which were written specifically for this project (for all scripts, see 8.3). R is a freely available software environment typically used for statistical computing.[116] The reaction conditions were imported as input files, and in addition to the raw HPLC data, were subjected to processing. The R scripts applied the quantitative assay to generate the kinetic data (concentration of analytes over time) for the specified reaction.

## 3.4 Initial hypothesis

With the pre-study preparations complete, we turned our attention to the reaction itself. Our initial hypothesis for the reaction model was that it proceeded via an interfacial mechanism (Scheme 3.6). Following deprotonation of the substrate **125**, the potassium enolate **134** undergoes metathesis with the chiral ammonium salt **127** to generate the ammonium enolate complex **135**. The chiral framework then directs the cyclisation of the enolate to give the major product (*S*)-**126** and an ammonium phenolate **136**. Subsequent metathesis with KCl to regenerate the ammonium halide **127** or metathesis with the potassium enolate **134** to obtain the ammonium enolate **135** might occur to close the catalytic cycle.

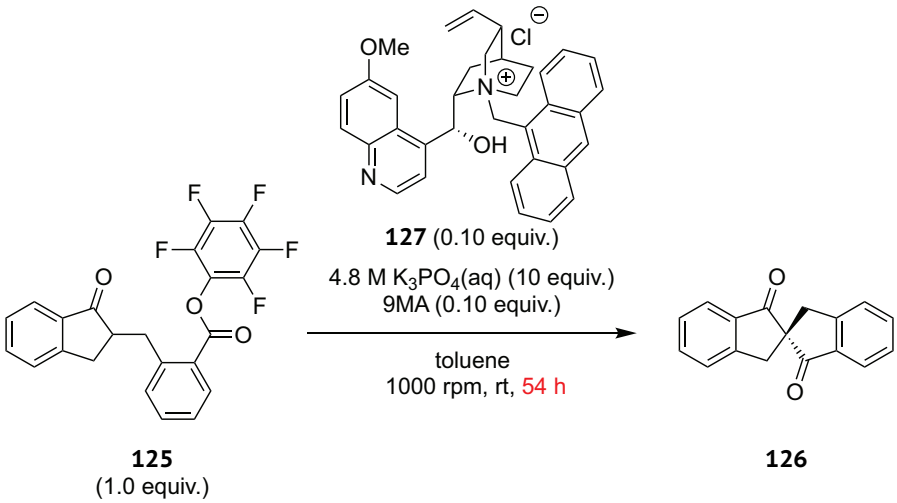



**Scheme 3.6: Initial hypothesis for the cyclisation reaction. A)** Deprotonation of the substrate occurs via an interfacial mechanism to generate the potassium enolate **134**; **B)** metathesis of the potassium enolate **134** to generate the ammonium enolate complex **135**; **C)** cyclisation to generate product **126** and the ammonium phenolate complex **136**; **D)** metathesis to regenerate the ammonium salt **127**; **E)** transport of the insoluble salt **127** to the interface for reaction.

We supposed this was a reasonable hypothesis to base our investigations on, at least initially. The potential for ammonium salt **127** to act as pre-catalyst in this system was a consideration we would look out for experimentally (see 2.4.2).

## 3.5 Preliminary reaction monitoring

To commence our investigations, we examined the reaction for the majority of its duration (Scheme 3.7). Three reactions were carried out simultaneously. The reactions were set up using our standard reaction protocol; the catalyst **127** and aqueous $K_3PO_4$ were pre-stirred together for a set period of time prior to initiation of the reaction by the addition of the substrate **125** as a solution in toluene. The reactions were monitored for a total of 3240 min (54 h) sampling the reaction mixtures every hour over that period.




**Scheme 3.7: Conditions for monitoring the reaction for an extended period of time.** Equivalents are reported with respect to substrate **125**. The reactions were carried out using the standard reaction protocol and monitored every 1 h (60 min) for a total of 54 h (3240 min).

The extracted aliquots were analysed using our HPLC method. The raw data were processed using the R scripts and assay, and the temporal concentration data plotted (Figure 3.8).

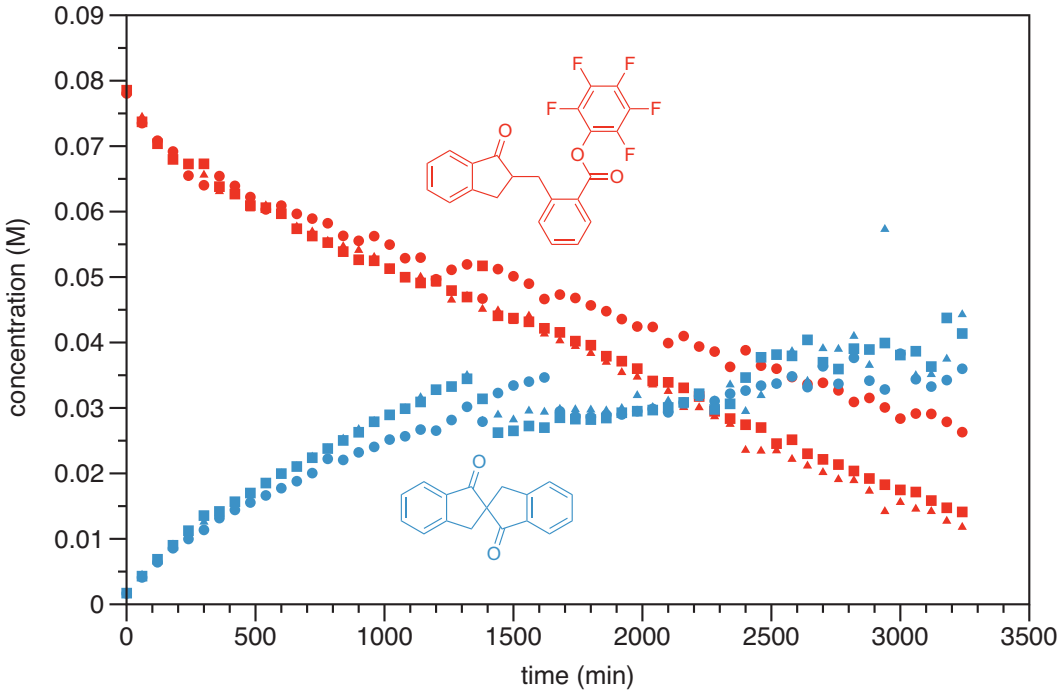



**Figure 3.8: Concentration data for the substrate 125 (red) and product 126 (blue) over time.** Reaction conditions are described in Scheme 3.7. The $x$-axis corresponds to time (in min) following initiation of the reaction. The $y$-axis corresponds to concentration of the analyte in M. The circles, triangles and squares correspond to individual reactions.

During the initial stages of the reaction (within 300 min) we observed good coherence between the three data sets. At higher conversion (approx. 1300 min), the product **126** concentration appeared to drop off. This was attributed to highly enantioenriched product (>99% ee)

crystallising from the reaction mixture; a sample of the solid was isolated and analysed by chiral HPLC (Figure 3.9). Overall, the substrate was steadily converted to product in an unexpectedly pseudo-zeroth order fashion.

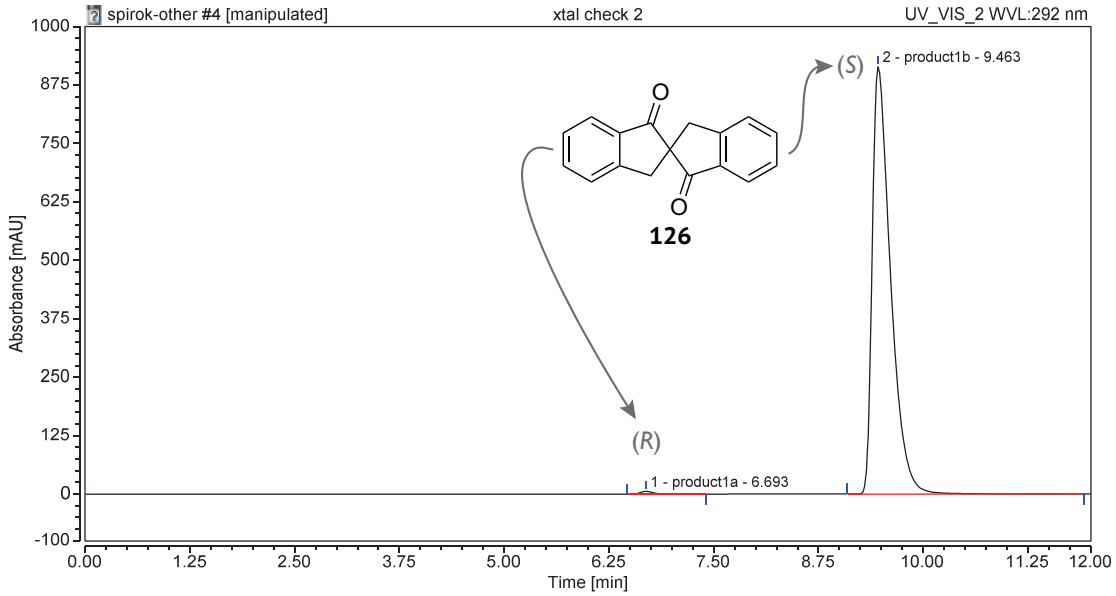



**Figure 3.9: HPLC chromatogram of the isolated solid material indicates it is product 126 with an ee of >99%.** The data is extracted at 292 nm. The $x$-axis represents retention time; the $y$-axis is UV absorption at the extracted wavelength. The peaks correspond to the enantiomers of the product **126**.

Physically, the reaction mixtures were heterogeneous during the pre-stirring protocol (A, Figure 3.10). Within 3 min after the addition of substrate **125** the reaction mixtures turned clear and biphasic (B, Figure 3.10). After 1000 min the reaction mixtures were heavily heterogeneous (C, Figure 3.10). Uncontrolled deposition of solid material occurred at the liquid-air interface. This effect contributed to the variation of product concentration observed in the data.

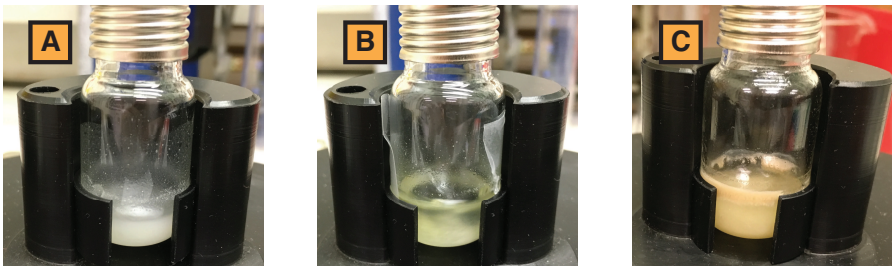



**Figure 3.10: Appearance of the reaction mixture over time.** The photos were taken at the described times with respect to initiation of the reaction (before or after time zero). **A)** At approximately −5 min, **B)** 5 min, and **C)** 1000 min.

The enantiomeric excesses of the substrate **125** and product **126** were determined (Figure 3.11).

We observed an increase in the enantiomeric excess of the substrate **125** over time (A, Figure 3.11). This suggested that discrimination of the substrate enantiomers was occurring via a kinetic resolution. The increase in ee of the substrate over time suggested the catalyst was involved in the deprotonation event, which meant that our initial hypothesis of $K_3PO_4$ being solely involved in deprotonation of the substrate was incorrect (see 3.4). Over time, the product ee slightly decreased from its initial value of approximately 94% (B, Figure 3.11), consistent with the observation that it crystallised as highly enantioenriched material from the reaction mixture. We were presumably sampling the mother liquor of the heterogeneous reaction mixture, with minimal collection of solid material.

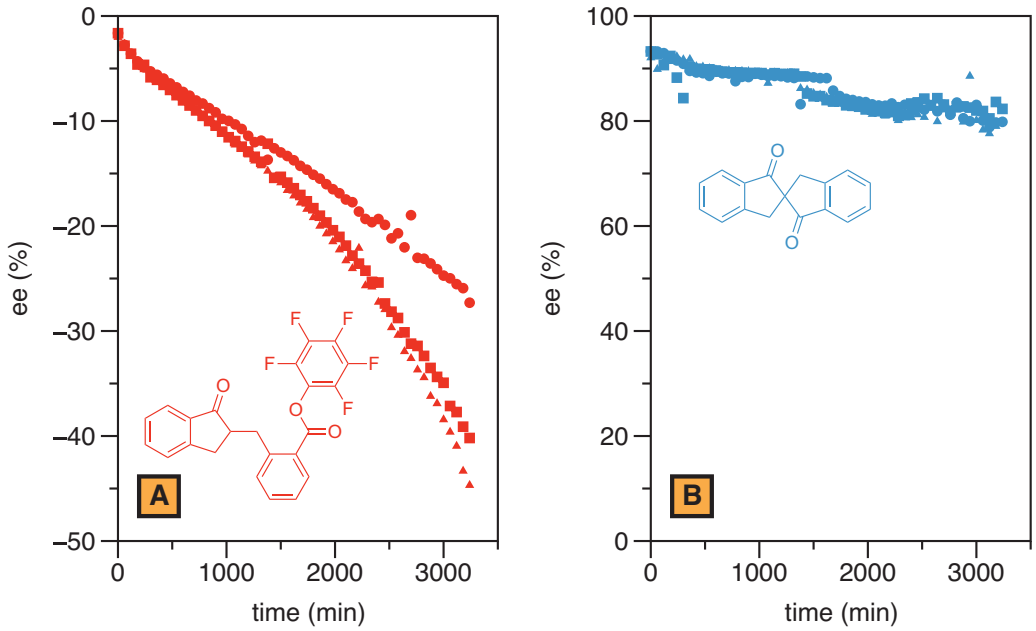


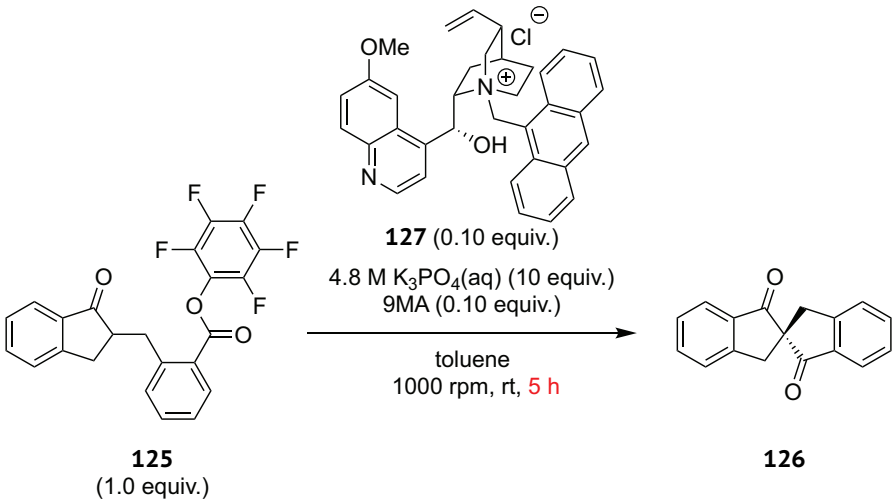

**Figure 3.11: Enantiomeric excesses of the A) substrate 125 and B) product 126 over time.** The $x$-axis in both graphs corresponds to time in min from initiation of the reaction; the $y$-axis corresponds to enantiomeric excess (ee) in %. The circles, triangles and squares correspond to individual reactions within a triplicate set. Complementary conversion data are in Figure 3.8.

The uncontrolled increase in heterogeneity of the reaction mixtures led to variations in the data. This indicated that monitoring the reactions for the majority of their duration would not be a feasible method for the elucidation of the mechanism of our model.

## 3.6 Viability of initial rate studies

Given the variation of the physical reaction mixture at extended reaction times, we thought that initial rate kinetic studies might provide more reliable data due to the simpler, liquid-liquid biphasic nature of the reaction mixtures (i.e. with minimal solids) at lower conversion (up to 5 h, with >20% yield of product **126**).

In order to assess the viability of the method, we carried out a triplicate experiment monitoring the reaction mixtures over 5 h (Scheme 3.8). For this experiment, the initial rates (slopes) for the reactions were taken as the rate of formation of product **126** (in mmol) over time (in min). The mean slopes between the three separate reactions were determined. The data analysed over the first 60 min were then compared to the data analysed over the full 5 h (Figure 3.12). We found the initial rates were comparable within error when analysing the first 60 min (red, Figure 3.12), compared to the whole 5 h (black, Figure 3.12). As such, we elected to monitor the first 60 min of the reaction to carry out further investigations of the model reaction.




**Scheme 3.8: Conditions used to monitor the reactions for 5 h.** Equivalents are reported with respect to substrate **125**. The reactions were carried out using the standard reaction protocol and monitored every 20 min for a total of 300 min (5 h).

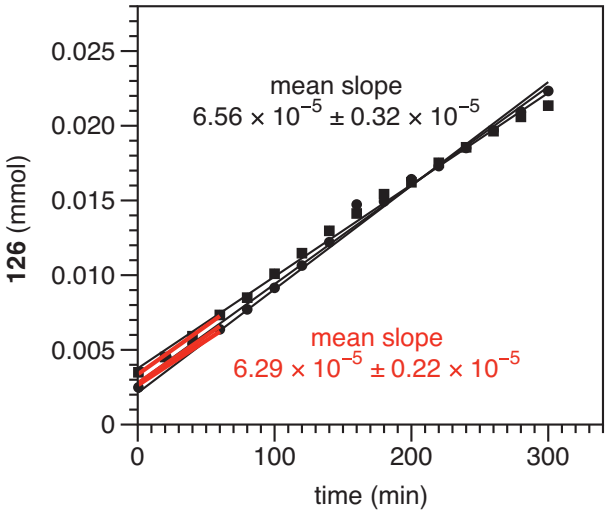



**Figure 3.12: Comparing data analyses over the first 1 h vs 5 h of the reaction.** The $x$-axis corresponds to time in min, and the $y$-axis corresponds to amount of product **126** in mmol. The circles, triangles, and squares correspond to single reactions within the triplicate experiment. The black lines correspond to the linear regression analyses of each reaction to give the rate of formation of product over 5 h; the mean and error of the slopes are indicated by the black text. The respective data analyses over 1 h are indicated by the red slopes and text.

## 3.7 Preliminary investigations

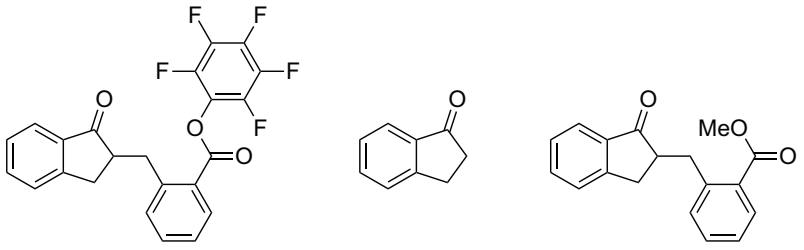
### 3.7.1 Investigating the transport reaction mechanism

The p$K_a$ value of the substrate and reaction rate dependencies on the stirring speed of phase-transfer reaction mixtures may provide an indication of whether the reaction proceeds via an interfacial or an extractive mechanism (see 1.1.2). To evaluate whether an extractive or interfacial rate-limiting transport mechanism was in effect, we attempted to determine the p$K_a$ of the substrate **125**, and evaluate the effect of stirring speed on the rate of the reaction.

All experiments to determine the p$K_a$ of selected species were carried out by AM; all corresponding procedure optimisations were carried out by AM (see 7.2). The p$K_a$ values were determined by NMR titration of the relevant compound against a base with known p$K_a$.

Unfortunately, we were unable to measure the p$K_a$ of the exact substrate **125** due to its propensity for cyclisation once deprotonated under homogeneous conditions at room temperature. As such, we evaluated the p$K_a$ values of 1-indanone **128** (literature p$K_a$ value of 23.0 in

DMSO)[117] and methyl ester **137** using dimsyl sodium (the p$K_a$ of DMSO is 35.1)[118] as the titrant. The p$K_a$ values of 1-indanone and **128** methyl ester **137** were 22.78 ± 0.51 and 21.94 ± 0.84 in DMSO respectively (Figure 3.13; see 7.2). Based on the titration experiments of the evaluated indanones (1-indanone **128** and pseudosubstrate **137**), we estimated the p$K_a$ of the substrate **125** to be approximately 22–23 in DMSO.

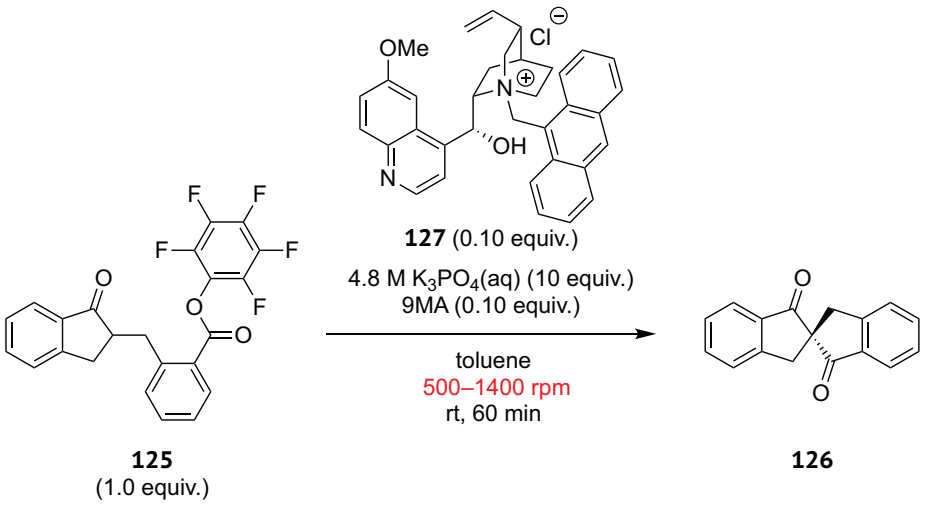



| | **125** | **128** | **137** |
|---|---|---|---|
| **p$K_a$ (DMSO)** | indeterminable | 22.78 ± 0.51 | 21.94 ± 0.84 |

**Figure 3.13: Results of the substrate p$K_a$ experiments.** The p$K_a$ values of the above compounds were determined by titration with dimsyl sodium in DMSO.

The estimated p$K_a$ value of the substrate **125** suggested the reaction was likely proceeding via an interfacial reaction mechanism.[1,15,19] The rate-dependence of the reaction on the stirring speed would also provide an indication of which transport mechanism was in operation—extractive or interfacial.[1,15,17,19]

We thus carried out a series of reactions varying the stirring speed of the reaction from 500 rpm to the maximum rate of the stirrer plates of 1400 rpm (Scheme 3.9). The initial rates ($k_{obs}$) were taken as the rate of formation of product (in M min$^{-1}$). We found a strong rate-dependence on the stirring speed of the reaction—a larger $k_{obs}$ was observed with faster stirring speeds (Figure 3.14).




**Scheme 3.9: Conditions used to evaluate the effect of stirring speed on the reaction.** Equivalents are reported with respect to the substrate **125**.

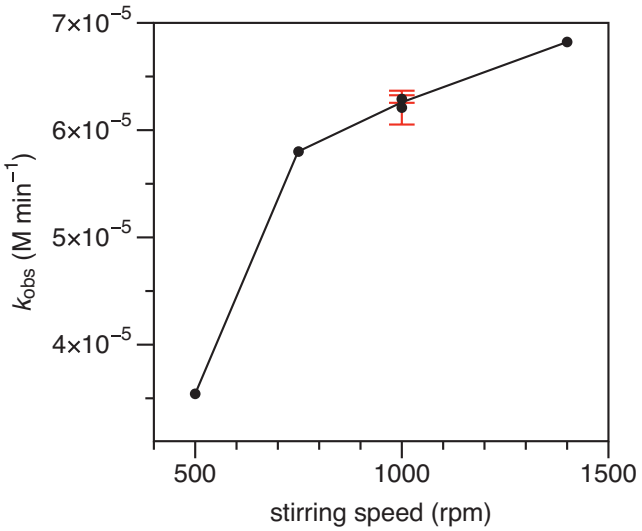


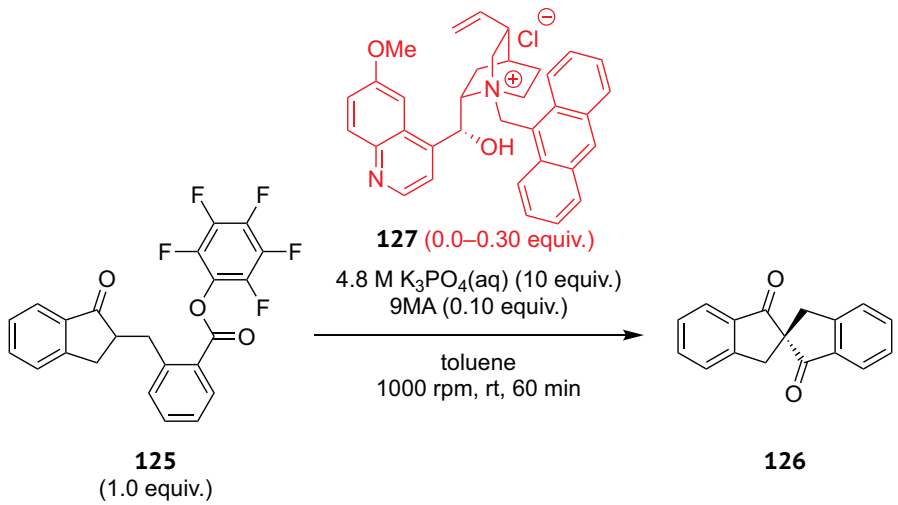

**Figure 3.14: Determining the effect of stirring speed on the rate.** The $x$-axis corresponds to the stirring speed of the reaction with conditions otherwise indicated in Scheme 3.9. The $y$-axis corresponds to the initial rate of formation of product ($k_{obs}$) in in M min$^{-1}$. The line is a guide for the eye.

Given the dependence of the reaction rate on the stirring speed and the estimated p$K_a$ of the starting material **125**, we suspected the reaction was proceeding via an interfacial reaction mechanism.

### 3.7.2 Investigating the catalyst and its effect on the rate

Our next set of experiments using initial rates looked at the effect of the catalyst **127** concentration on the rate of the reaction (Scheme 3.10). We varied the initial catalyst concentration

from 0 to 26 mM, corresponding to catalyst **127** to substrate **125** loadings of 0.0 to 0.30 equiv., then measured the rate of formation of product ($k_{obs}$) in each reaction (Figure 3.15). The experiments for each initial catalyst concentration (0.0–0.30 equiv.) were carried out in duplicate or triplicate; the averages and errors were subsequently determined.




**Scheme 3.10: Conditions used to evaluate the effect of catalyst concentration on the reaction.** Equivalents (equiv.) are reported with respect to the substrate **125**.

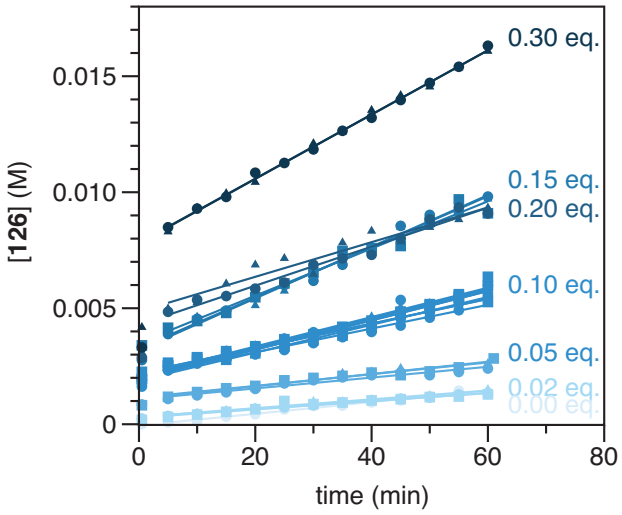



**Figure 3.15: Reactions used to determine the effect of catalyst concentration on the rate.** The $x$-axis corresponds to time in min following initiation of the reaction. The $y$-axis corresponds to the concentration of product **126** in M. The different shades of blue indicate the catalyst loading in equivalents (eq.) with respect to substrate **125** (to 2 dp). Circles, triangles, and squares correspond to individual reactions within the duplicate or triplicate set. The lines are linear regression analyses of each individual reaction and correspond to the extracted initial rates $k_{obs}$ which were used for further analysis.

In each reaction, we observed an initial jump in the generation of product, followed by a flattening out of the rate. Conversion to product over time appeared linear with a non-zero intercept. This burst phase indicated that a fast process occurred before the reaction apparently

settled into the predominant rate-determining regime. For consistent analyses, the data were extracted after excluding the burst phase time point (usually just the 0.5 min aliquot after initiation of the reaction).

We found a strong rate-dependence of the formation of product on the concentration of catalyst; the greater the initial catalyst concentration, the larger the $k_{obs}$ (Figure 3.16). A double logarithmic plot of the initial catalyst concentration (ln $[\mathbf{127}]_0$) against the rate of product formation (ln $k_{obs}$) revealed a catalyst order of 0.79 under our reaction conditions; with a 68% confidence interval of 0.69 to 0.90.

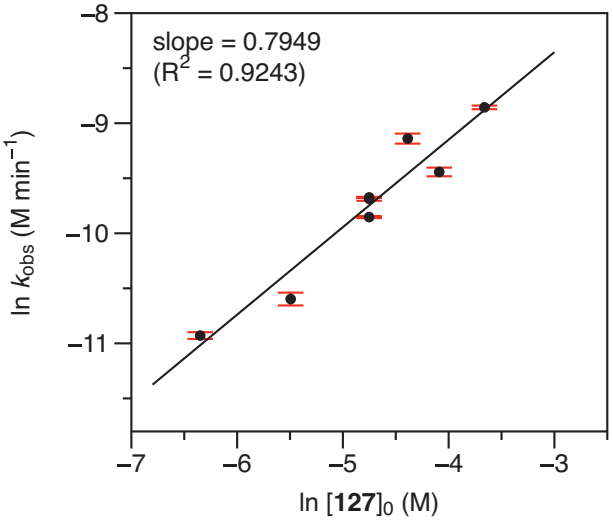



**Figure 3.16: Double logarithmic plot to determine the reaction order with respect to catalyst 127.** The $x$-axis corresponds to the ln of the initial concentration of catalyst **127** (ln [**127**]) in M. The $y$-axis corresponds to the ln of the initial rates (ln $k_{obs}$) in M min$^{-1}$. The line corresponds to linear regression analysis of the whole data set to give the slope and catalyst order of 0.79.

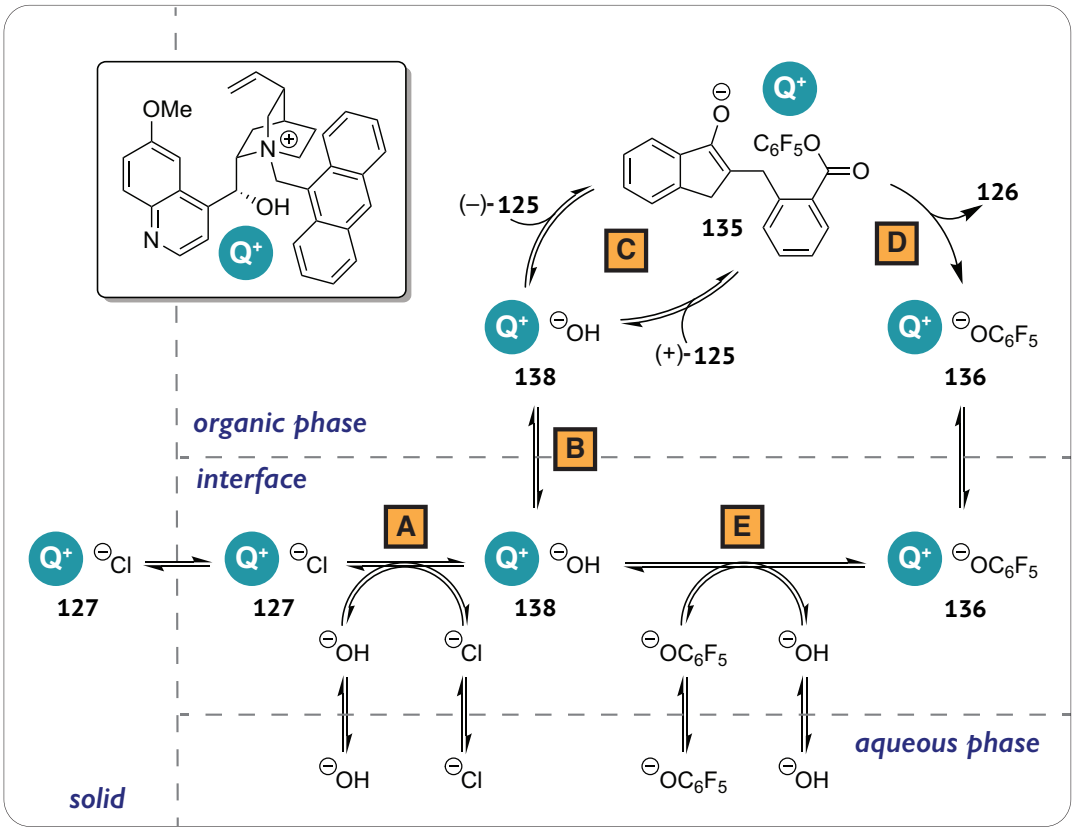
The partial catalyst order was consistent with two different mechanistic features. The first, was that an interfacial mechanism was rate-determining; a partial order with respect to catalyst is characteristic of phase-transfer hydroxide ion-initiated reactions proceeding by an interfacial reaction mechanism.[1,15] The second was that the active catalyst species was monomeric and in equilibrium with an inactive dimer. A catalyst order between 0.5 and 1 may be consistent with this effect.[119] The discussion concerning these two different factors will now be presented.

The interfacial hydroxide ion-initiated phase-transfer reaction proceeds via deprotonation of

the substrate at the interface by hydroxide (analogous to Scheme 1.4).[1,15] Once the substrate anion is generated at the interface, the catalyst then "detaches" it, migrating as an ion pair into the organic phase where the intrinsic reaction takes place. It is interfacial phenomena that contribute to the complex kinetic behaviour indicated by a partial order with respect to catalyst.[15,17]

In our system, the increase in enantioenrichment of the substrate over time, suggested that the catalyst, not exclusively the achiral base, was involved in the substrate deprotonation event. It was thus unlikely that the standard interfacial reaction mechanism was the sole cause for the partial catalyst order.

A further alternative to the hydroxide ion-initiated interfacial reaction mechanism is that an extractive-type process might be occurring (Scheme 3.11); where hydroxide is extracted into the organic phase as an ammonium salt **138**. Consistent with the kinetic resolution of the substrate (see Figure 3.11), the catalyst species differentiates between the two substrate enantiomers and generates the common enolate intermediate **135**. Enantiodetermining cyclisation then takes place in the organic phase before the active hydroxide **138** is regenerated, again, at the interface. The partial order with respect to catalyst may be due to the interfacial phenomena associated with "activating" the ammonium ion by this process.

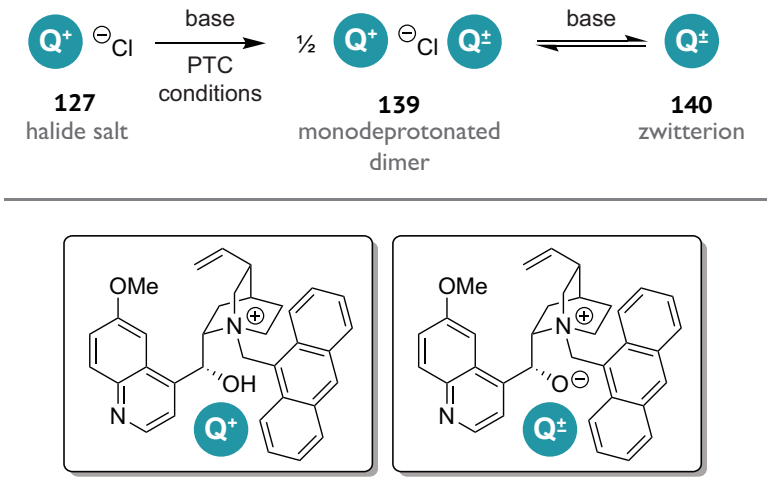



**Scheme 3.11: A hydroxide initiated reaction mechanism.** Key features of the mechanism are: **A)** the formation of the active ammonium hydroxide **138** from the corresponding halide salt **127** at the interface; **B)** extraction of the **138** into the organic phase; **C)** deprotonation of the substrates to form the common enolate intermediate **135**; **D)** cyclisation and formation of the product **126**; and **E)** the formed ammonium phenolate **136** is converted to the active ammonium hydroxide **138**.

If activation of the catalyst proceeded via this type of reaction mechanism, it might give rise to the partial order kinetics that we observed. However, the physical appearance of the reaction mixtures over time suggested this process was unlikely to be occurring. This is because the organosolubility of ammonium salts decreases from halide to hydroxide and from halide to phosphate.[1,16] The ammonium chloride **127** is completely insoluble in the organic solvent; it forms a heterogeneous mixture in the presence of aqueous $K_3PO_4$ and toluene (for example, A in Figure 3.10). On addition of the substrate, the reaction mixture turns clear and biphasic; all solid materials are solubilised. If activation of the catalyst was to form the hydroxide-counterioned species **138**, we expected the reaction mixture to remain heterogeneous.

The second mechanistic feature that might give rise to the partial order with respect to the catalyst was it existed off-cycle as a dimeric species in equilibrium with an active monomer.

This hypothesis was consistent with the observation that cinchona alkaloid-derived ammonium ions may exist as inactive *organosoluble* dimeric species under phase-transfer reaction conditions.[29,86] In our system, the catalyst species involved in this type of process would be the insoluble halide salt **127**, soluble dimer **139** and soluble zwitterion **140** (Scheme 3.12).



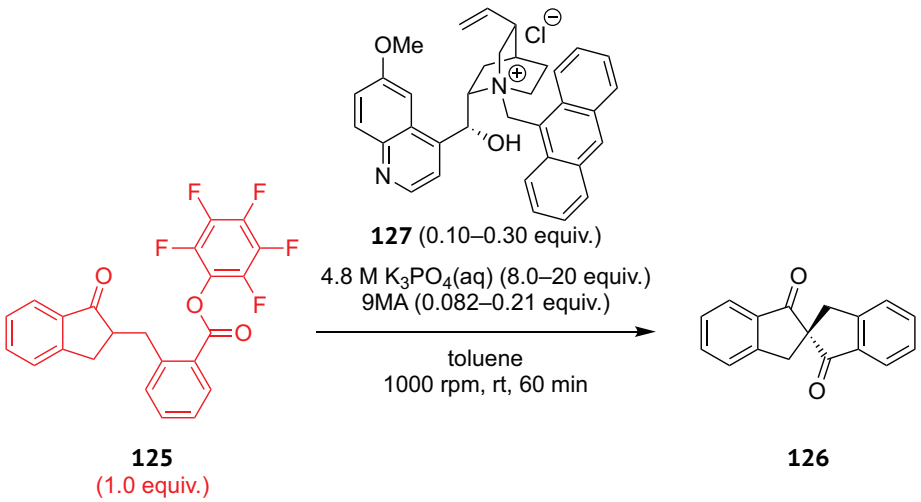

**Scheme 3.12: Formation and equilibrium of a catalyst dimer under phase-transfer reaction conditions.**

To investigate whether the zwitterion might be formed under the reaction conditions, we measured the p$K_a$ of the catalyst **127** in DMSO. The hydroxy group of the catalyst was easily deprotonated under the titration conditions using sodium phenoxide as the base. We found the catalyst had a p$K_a$ of 16.33 ± 0.43 in DMSO, which indicated it was much more acidic than a typical alcohol in DMSO—for example ethanol has a p$K_a$ of 29.8 in DMSO,[118] and phenol is 18.[117]

It was highly likely that the catalyst was deprotonated under the reaction conditions and instead of the ammonium hydroxide **138**, the zwitterion **140** was the active catalyst species. The partial order with respect to catalyst may be due to activation of the ammonium halide **127** to generate the zwitterion **140** via an interfacial process in combination with the presence of an off-cycle inactive dimer **139**.

### 3.7.3 Investigating the order in substrate

To determine the reaction order with respect to substrate **125**, we carried out a series of reactions varying only the initial concentration of substrate **125** ($[\mathbf{125}]_0$) (Scheme 3.13). The reactions were carried out analogously to those used to determine the reaction order with respect to catalyst.




**Scheme 3.13: Conditions used to evaluate the effect of initial substrate 125 concentration on the reaction.** Equivalents (equiv.) are reported with respect to the substrate **125**.

Altering the initial substrate concentration whilst keeping everything else constant consequently changed the catalyst loading and base equivalents in each experiment. However, across all experiments, we did not observe much change in the rate ($k_{\text{obs}}$) (Figure 3.17).

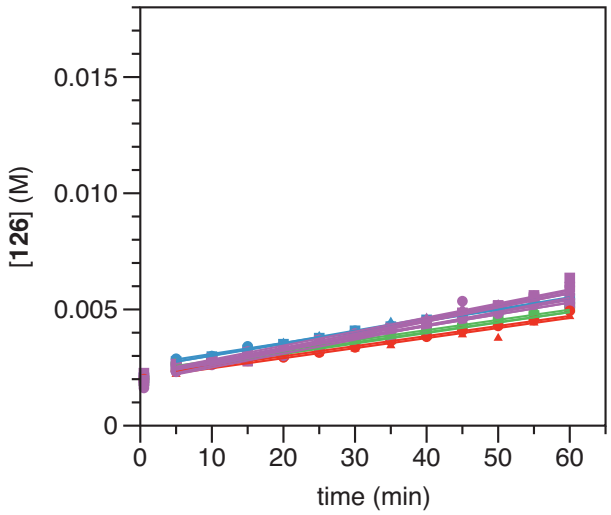



**Figure 3.17: Reactions used to determine the effect of substrate 125 concentration on the rate.** The $x$-axis corresponds to time in min. The $y$-axis corresponds to the concentration of product **126** in M. The different colours indicate different initial substrate **125** concentrations: 0.0412 M (blue), 0.0623 M (green), 0.0827 M (purple), 0.103 M (red). Circles, triangles, and squares correspond to individual reactions within the duplicate or triplicate set. The lines are linear regression analyses of each individual reaction and correspond to the extracted initial rates $k_{obs}$ which were used for further analysis.

Indeed, the double logarithmic plot to determine the reaction order with respect to substrate revealed a value close to zero (Figure 3.18). An order of 0.026 was obtained with a 68% confidence interval of −0.27 to 0.33, indicating the rate-determining step of the reaction was likely to not be affected by the concentration of the substrate.

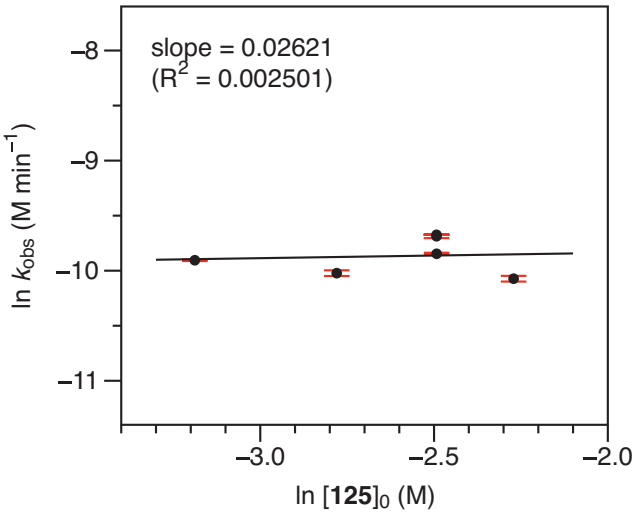


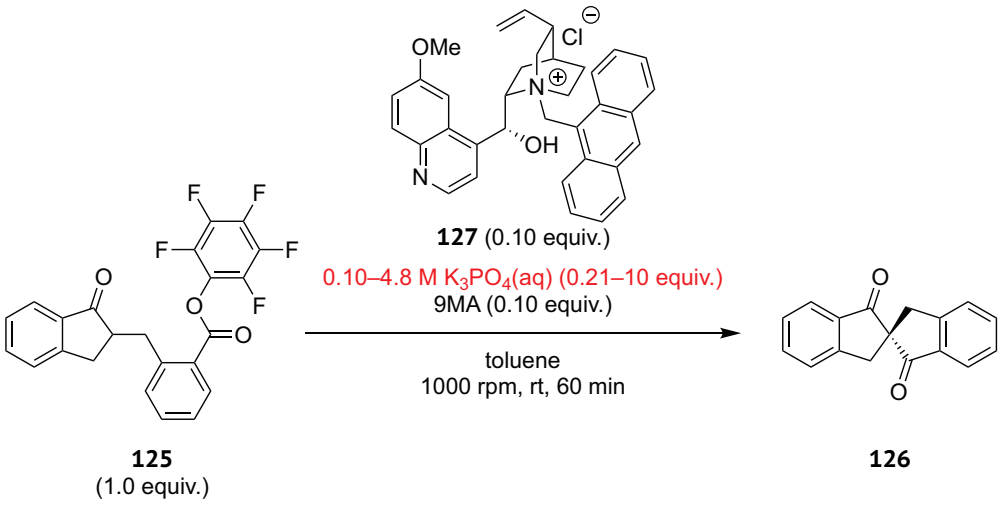

**Figure 3.18: Double logarithmic plot to determine the reaction order with respect to substrate 125.** The $x$-axis corresponds to the natural logarithm of the initial concentration of substrate **125** (ln [**125**]) in M. The $y$-axis corresponds to the natural logarithm of the initial rates (ln $k_{obs}$) in M $min^{-1}$. The line corresponds to linear regression analysis of the whole data set to give the slope and substrate order of 0.026.

### 3.7.4 Investigating the order in base

There were two different methods through which we could investigate the effect of base concentration on the reaction. The first was to maintain a constant amount of aqueous base, while varying the concentration. The second was to use the same concentration and simply vary the volume added to the reaction.

The extractability of ions under phase-transfer catalysis is dependent on the concentration of the aqueous solution.[16] Furthermore, the magnitude and nature of the interfacial region would change when varying the ratio of organic to aqueous solvent. Hence, by changing either the concentration or the volume of aqueous base added, the rate of the reaction might be affected in an unforeseen manner. To gauge the outcomes, we assessed both methods of altering total base concentration in the whole system.

Of the two methods, we first evaluated the order of reaction with respect to $K_3PO_4$ whilst keeping the added aqueous volume constant (at 305 µL) (Scheme 3.14). Again, a double logarithmic plot was constructed to determine the dependence of the rate on the concentration of $K_3PO_4$ (Figure 3.19); the concentration of $K_3PO_4$ was taken as the total amount in both the organic and aqueous solvents combined.




**Scheme 3.14: Conditions used to evaluate the effect of initial base concentration on the reaction (added as constant volume).** Equivalents (equiv.) are reported with respect to the substrate **125**.

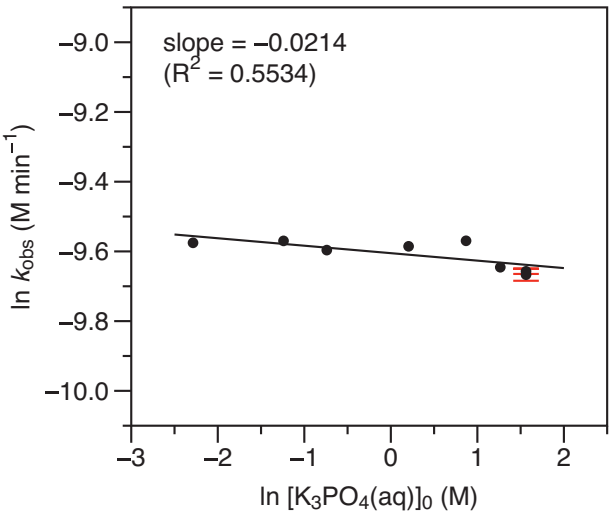
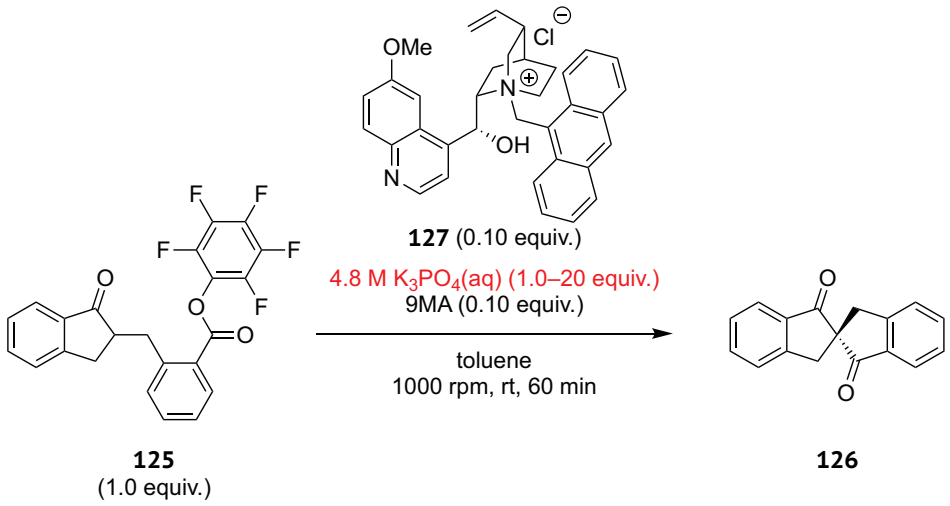



**Figure 3.19: Double logarithmic plot to determine the reaction order with respect to aqueous $K_3PO_4$ concentration.** The $x$-axis corresponds to the ln of the initial concentration of aqueous $K_3PO_4$ (ln [$K_3PO_4$(aq)]) in M. The $y$-axis corresponds to the ln of the initial rates (ln $k_{obs}$) in M min$^{-1}$. The line corresponds to linear regression analysis of the whole data set to give the slope and order of −0.021.

Altering the concentration of aqueous $K_3PO_4$ had little bearing on the observed rate. An order of −0.021 was obtained with a 68% confidence interval of −0.042 to 0.0025. Similar to the order determined with respect to substrate, the rate-dependence of the reaction on $K_3PO_4$(aq) at constant aqueous volume appeared to be negligible.

Next, we evaluated the reaction outcomes when adding different volumes of 4.77 M $K_3PO_4$(aq) (Scheme 3.15). Unexpectedly, we observed a slight inverse partial order with respect to the total $K_3PO_4$ concentration (Figure 3.20).




**Scheme 3.15: Conditions used to evaluate the effect of initial base concentration on the reaction (added with constant aqueous concentration).** Equivalents (equiv.) are reported with respect to the substrate **125**.

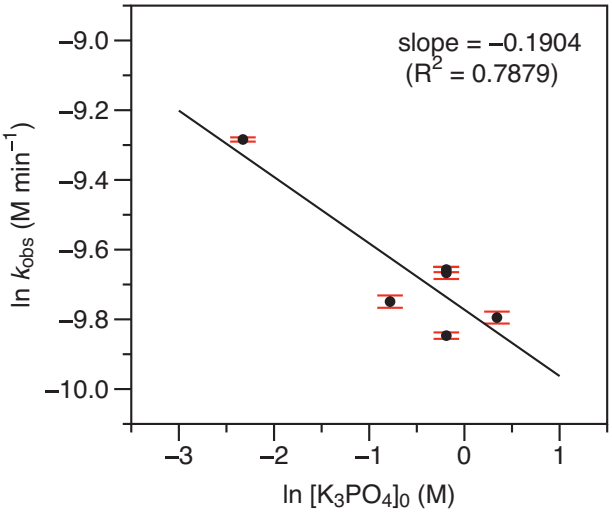


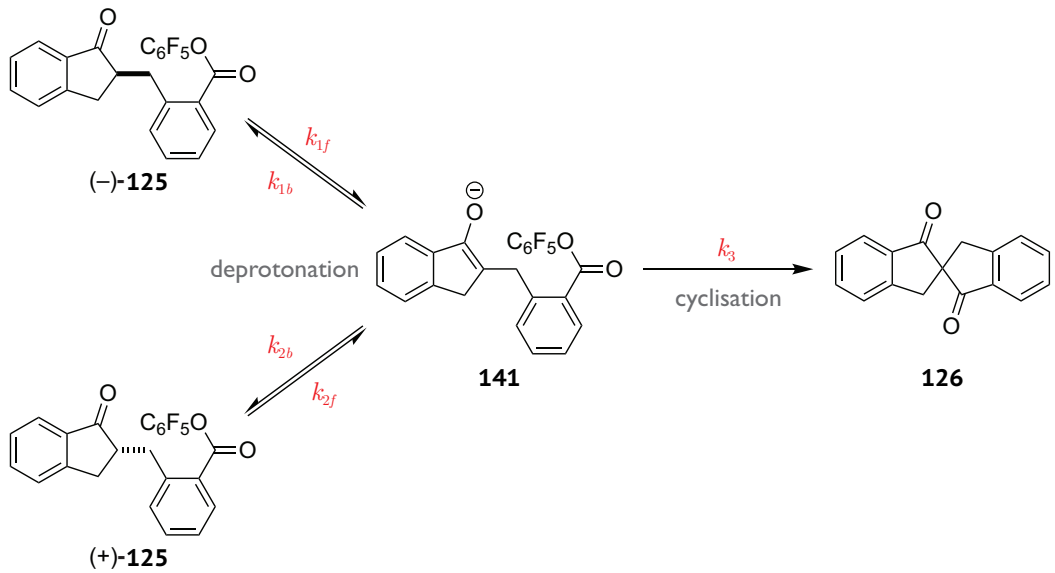

**Figure 3.20: Double logarithmic plot to determine the reaction order with respect to aqueous $K_3PO_4$ concentration.** The $x$-axis corresponds to the ln of the initial concentration of $K_3PO_4$ (ln $[K_3PO_4]$) in the whole system in M. The $y$-axis corresponds to the ln of the initial rates (ln $k_{obs}$) in M min$^{-1}$. The line corresponds to linear regression analysis of the whole data set to give the slope and order of $-0.19$.

An order of $-0.19$ with a 68% confidence interval of $-0.25$ to $-0.13$ was obtained. Because we observed a strong rate-dependence of the reaction on the concentration of the catalyst **127**, we attributed the apparent decrease in the rate to the increase in catalyst dilution in the whole system as more 4.77 M $K_3PO_4$ was added. Alternatively, the partial inverse order indicated that the base $K_3PO_4$ may be involved in other processes than our hypothesis accounted for.

### 3.7.5 Enantioenriched substrates under the reaction conditions

The observation that the substrate was becoming enantioenriched led us to examine the effect of using enantioenriched substrates under the reaction conditions; we wanted to use the substrate enantiomers to probe both the deprotonation and cyclisation events. Before we conducted the experiments practically, we carried out an analysis of the potential outcomes for these experiments.

We worked under the assumptions that formation of enolate **141** was a reversible process and formation of product (combined cyclisation and collapse of the tetrahedral intermediate) was irreversible (Scheme 3.16).



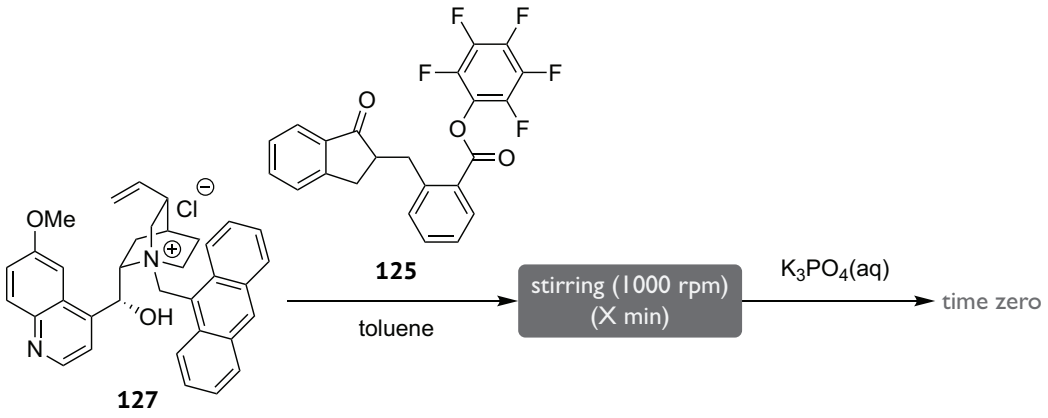

**Scheme 3.16: Simple schematic showing deprotonation of the substrates and cyclisation of the enolate.** The red labels correspond to the rate constants for the associated steps.

Firstly, we expected to see a different rate of consumption of starting material when subjecting the two enantiomers ((−)-**125** and (+)-**125**) to the reaction conditions. This would be consistent with the kinetic resolution. Secondly, we would look for racemisation of the starting material. If racemisation occurred, it would indicate that cyclisation was slow relative to the reprotonation steps ($k_3 << k_{1b}, k_{2b}$). If we did not observe racemisation of the starting materials, it would indicate that either deprotonation was irreversible and cyclisation was slow relative to deprotonation ($k_{1f}, k_{2f} >>> k_{1b}, k_{2b}$; $k_3 << k_{1f}, k_{2f}$), or that cyclisation was fast

relative to reprotonation ($k_3 >> k_{1b}, k_{2b}$).

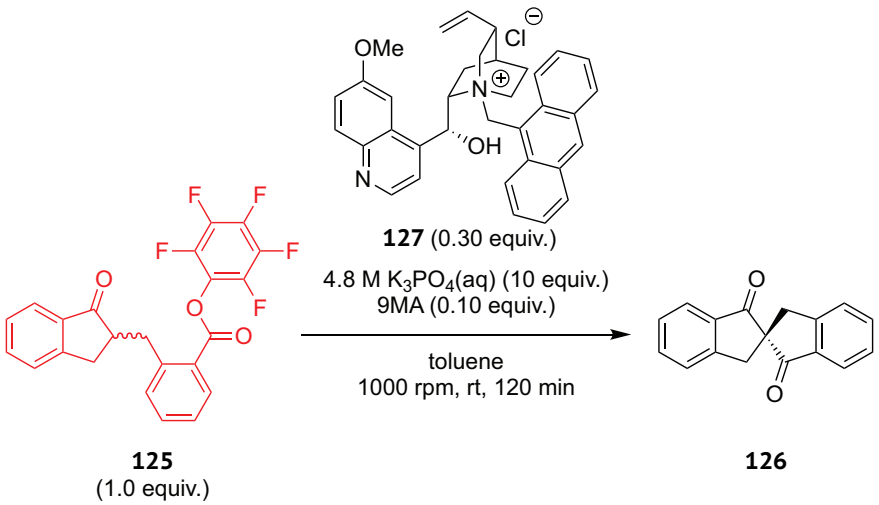
Before we could carry out the desired reactions, we required the substrates (−)-**125** and (+)-**125**. The enantiomers were separated using HPLC with a chiral stationary phase and were obtained with enantiomeric excesses of 98% and 94%, respectively. Unfortunately, the enriched samples were oils at room temperature and we were unable to assign their absolute configurations.

Due to practical limitations, we had to alter our protocol from that which we used as standard (see 7.4.1). Instead of carrying out a pre-stirring protocol (stirring the base with the catalyst prior to the addition of substrate as a solution), the reactions were carried out by initiating the reactivity by the addition of base (see 7.4.2) (Scheme 3.17). Simply put, the relevant substrate and catalyst **127** were stirred for a specified amount of time before the addition of aqueous $K_3PO_4$ at the designated time zero.




**Scheme 3.17: Example schematic of the modified reaction protocol.** General setup of reactions using the modified reaction protocol involved pre-stirring the catalyst with substrate for a specified period of time (X min) before initiating the reaction by the addition of base.

Three reactions were carried out using the modified protocol; the substrate in each reaction was either (−)-**125**, (+)-**125**, or the racemate **125** as a control (Scheme 3.18). To maximise the data collected for the conversion to product, we used a catalyst loading of 0.30 equiv. with respect to the substrate.




**Scheme 3.18: Conditions used to evaluate enantioenriched substrates.** Equivalents are reported with respect to substrate racemic **125**, (−)-**125**, or (+)-**125**. The reactions were carried out using a modified reaction protocol and monitored over 120 min.

Due to the slight variabilities in the amounts of substrate added—a consequence of the manner in which the substrates were isolated and their physical form—we analysed the reactions as normalised data. The total amount of substrate and product were calculated and the conversion to product plots were generated (Figure 3.21).

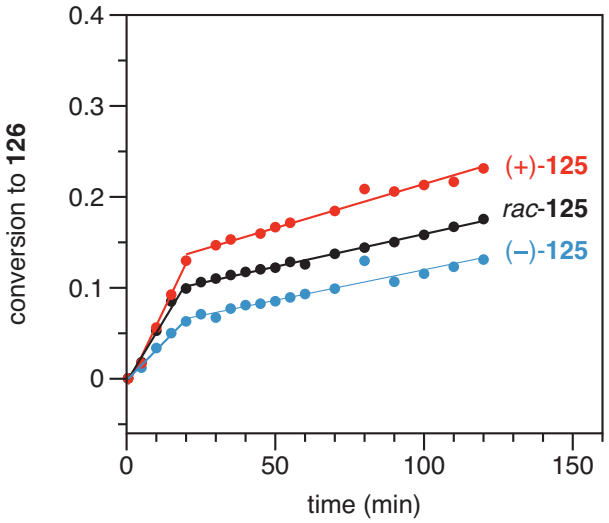



**Figure 3.21: Overlay of reactions investigating the effect of enantioenriched substrates.** The lines correspond to linear regression analyses of each rate-limiting regime within the three experiments. The different colours correspond to differently enantioenriched substrates: racemic **125** (black), (−)-**125** (blue), and (+)-**125** (red).

The first thing we noticed was that the period of the burst phase was extended. Instead of occurring within 0.5 min to $<$ 5 min from initiation of the reaction, it persisted for around 20 min under these reaction conditions. Kinetically, we observed an increase in the rate from

substrate (−)-**125**, to the racemate **125**, and then to the (+)-**125** enriched substrate for the burst phase and, slightly, during the predominant rate-determining regime. The changes in rate that we observed were consistent with the kinetic resolution.

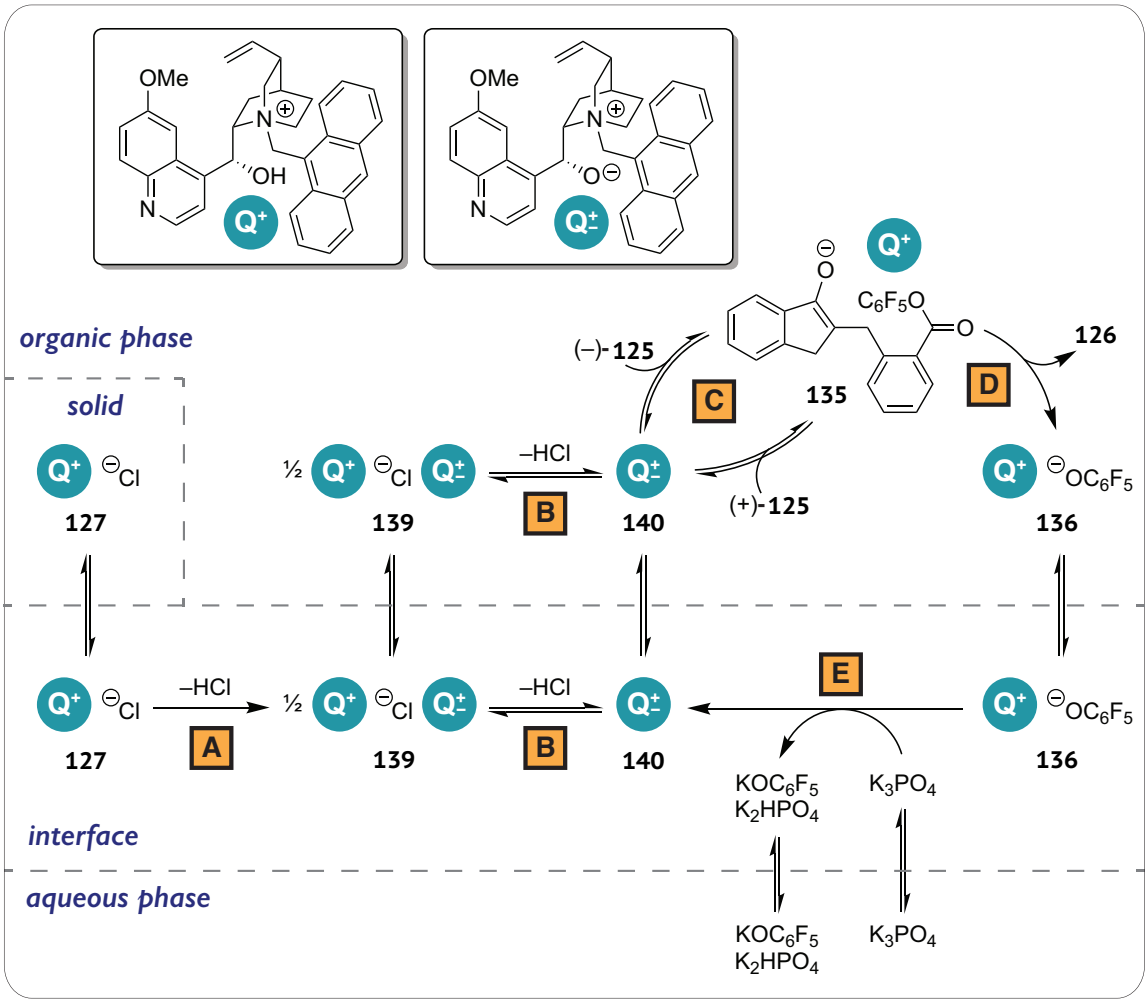
When we examined the enantiomeric excesses of the substrates (−)-**125** and (+)-**125** over the course of the reaction, we observed no racemisation. This suggested that either deprotonation of the substrate was irreversible, or that cyclisation was very fast relative to reprotonation. This new data provided some information as to what was occurring in the reaction, however the ambiguity dictated we change our strategy for approaching the elucidation of the reaction mechanism.

## 3.8 Revising the mechanistic hypothesis

At this stage of the project, we had collected enough information to inform us that our initial hypothesis was incorrect. Several key observations were made that indicated that deprotonation of the substrate did not occur by the mechanism we first proposed. As such, we revised our working hypothesis.

Firstly, the increase in enantioenrichment of the substrate **125** over time, suggested that a catalyst species—not solely the achiral base—was involved in the substrate deprotonation event. This indicated the mechanism was not proceeding via a simple interfacial reaction mechanism (i.e. not Scheme 3.6). Additionally, the p$K_a$ of the catalyst **127** (of 16.33 in DMSO) suggested the zwitterion **140** might be the active catalyst species involved in substrate deprotonation and not ammonium hydroxide **138**. It was unlikely that the ammonium hydroxide **138** would exist persistently in the organic phase.[16] The kinetic resolution of the substrate also dictated that we treat the deprotonation step of the two substrates as distinct elementary steps, rather than treating the racemic mixture equally as in our first hypothesis. Lastly, enantioenriched product is obtained via the coordinated chiral ammonium ion directing the cyclisation event.

Using the information we had garnered, we revised our working hypothesis (Scheme 3.19). The ammonium halide **127** was a pre-catalyst that, under phase-transfer reaction conditions, forms a monodeprotonated dimer **139** in equilibrium with a zwitterionic oxide **140** (A and B, Scheme 3.19). Both dimer **139** and zwitterion **140** may be partitioned between the organic phase and interfacial region. The zwitterion **140** was then able to deprotonate the substrates (−)-**125** and (+)-**125**, differentiating between the two enantiomers (C, Scheme 3.19). The resultant ammonium enolate complex **135** then cyclises stereoselectively to generate enantioenriched product **126** (D, Scheme 3.19). In order to regenerate the active zwitterion, a deprotonation event of the catalyst must be occurring. We hypothesised that the ammonium phenolate complex might be directly deprotonated, liberating potassium 2,3,4,5,6-pentafluorophenolate, potassium hydrogen phosphate, and the active zwitterion (E, Scheme 3.19).



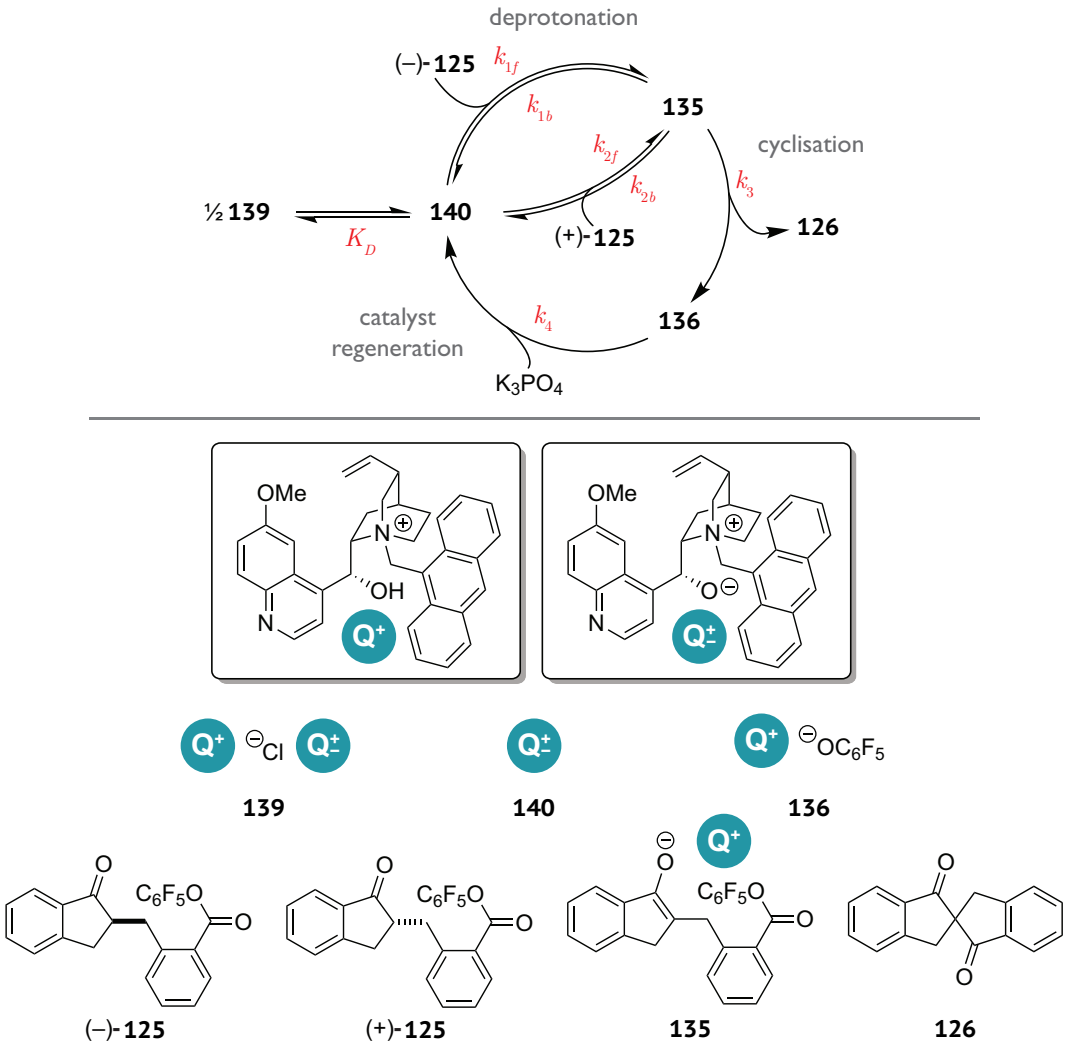

**Scheme 3.19: Revised mechanistic hypothesis.** Key features are: **A)** the formation of the inactive organosoluble dimer **139**; **B)** further deprotonation to form zwitterion **140**; **C)** deprotonation of the substrates (−)-**125** and (+)-**125** by the zwitterion **140**; **D)** formation of product **126**; **E)** regeneration of the active zwitterion **140** from the ammonium phenolate **136**.

## 3.9 Commencing a theoretical approach

To complement the experimental studies, we began a theoretical approach by examining the revised hypothesis as a kinetic model. All of the work in this section was carried out in collaboration with Dr Martin Galpin (MRG). Mathematical treatments of the calculated rate equation for this system, construction of all Mathematica scripts, numerical analyses of all hypotheses, and refining of rate constants for all systems were carried out by MRG.

We thought if we calculated the rate equation for the revised hypothesis (Scheme 3.19), it might provide insight into the direction we should take the project next. To calculate the

rate equation for the reaction—the rate of formation of product **126**— we first simplified our current overall hypothesis (Scheme 3.20). The transport steps were excluded from the kinetic model and were assumed to be incorporated into the corresponding rate constants. Generation of the dimer **139** and zwitterion **140** was via the halide salt **127** in the presence of $K_3PO_4$ under phase-transfer conditions (A and B, Scheme 3.19); because we typically carried out a pre-stirring protocol (see 3.3.1), we presumed the equilibrium (**139** $\rightleftharpoons$ **140**) was established prior to the addition of substrate (as (−)-**125** and (+)-**125**), hence the activation steps were excluded from the theoretical model. At this point in time, we were unconcerned with the byproducts produced during the $K_3PO_4$-mediated regeneration of zwitterion **140**.




**Scheme 3.20: Schematic used to generate the overall rate equation 3.16.** The red labels correspond to the rate or equilibrium constants for the associated steps.

The rate constants in the equations following (equations 3.1 to 3.28) are indicated by the

corresponding elementary steps in Scheme 3.20. The rate of formation of product was given by equation 3.1. Because we were unable to monitor the concentration of intermediate **135**, we required a rate equation in terms of the substrate and catalyst, namely the substrates (−)-**125** and (+)-**125** and the total amount of catalyst in the system ($[\text{cat}]_\text{T}$).

$$\frac{d[\mathbf{126}]}{dt} = k_3[\mathbf{135}] \tag{3.1}$$

To generate the rate equation with respect to substrate, base and catalyst, we required the $[\text{cat}]_\text{T}$ to be solely in terms of the concentration of intermediate **135** ([**135**]). First, we considered the total catalyst concentration in the system, which was given by equation 3.2.

$$[\text{cat}]_\text{T} = 2[\mathbf{139}] + [\mathbf{140}] + [\mathbf{135}] + [\mathbf{136}] \tag{3.2}$$

We then considered the concentrations of dimer **139** and zwitterion **140** in the system, which was dictated by the equilibrium constant $K_D$ (equation 3.3).

$$K_D = \frac{[\mathbf{139}]}{[\mathbf{140}]^2} \tag{3.3}$$

This rearranges to give equation 3.4:

$$[\mathbf{139}] = K_D[\mathbf{140}]^2 \tag{3.4}$$

Applying the steady state approximation to $\frac{d[\mathbf{135}]}{dt}$ we obtained equation 3.5 and thus equations 3.6 and 3.7.

$$\begin{aligned}\frac{d[\mathbf{135}]}{dt} &= k_{1f}[(-)\text{-}\mathbf{125}][\mathbf{140}] + k_{2f}[(+)\text{-}\mathbf{125}][\mathbf{140}] - k_{1b}[\mathbf{135}] - k_{2b}[\mathbf{135}] - k_3[\mathbf{135}] \\ &= (k_{1f}[(-)\text{-}\mathbf{125}] + k_{2f}[(+)\text{-}\mathbf{125}])[\mathbf{140}] - (k_{1b} + k_{2b} + k_3)[\mathbf{135}] \\ &\simeq 0\end{aligned} \tag{3.5}$$

$$\begin{aligned}(k_{1f}[(-)\text{-}\mathbf{125}] + k_{2f}[(+)\text{-}\mathbf{125}])[\mathbf{140}] &= (k_{1b} + k_{2b} + k_3)[\mathbf{135}] \\ [\mathbf{140}] &= \frac{k_{1b} + k_{2b} + k_3}{k_{1f}[(-)\text{-}\mathbf{125}] + k_{2f}[(+)\text{-}\mathbf{125}]}[\mathbf{135}]\end{aligned} \tag{3.6}$$

$$[\mathbf{140}]^2 = \left(\frac{k_{1b} + k_{2b} + k_3}{k_{1f}[(-)\text{-}\mathbf{125}] + k_{2f}[(+)\text{-}\mathbf{125}]}\right)^2 [\mathbf{135}]^2 \tag{3.7}$$

By applying the same approximation to $\frac{d[\mathbf{136}]}{dt}$ we obtain equation 3.8 and thus equation 3.9, where B is representative of a basic species, for example $K_3PO_4$.

$$\begin{aligned}\frac{d[\mathbf{136}]}{dt} &= k_3[\mathbf{135}] - k_4[\mathrm{B}][\mathbf{136}] \\ &\simeq 0\end{aligned} \tag{3.8}$$

$$\begin{aligned}k_3[\mathbf{135}] &= k_4[\mathrm{B}][\mathbf{136}] \\ [\mathbf{136}] &= \frac{k_3}{k_4[\mathrm{B}]}[\mathbf{135}]\end{aligned} \tag{3.9}$$

Substituting equations 3.4, 3.6 and 3.9 back into equation 3.2, we obtain the following expression:

$$[\mathrm{cat}]_\mathrm{T} = 2K_D[\mathbf{140}]^2 + \frac{(k_{1b} + k_{2b} + k_3)}{k_{1f}[(-)\text{-}\mathbf{125}] + k_{2f}[(+)\text{-}\mathbf{125}]}[\mathbf{135}] + [\mathbf{135}] + \frac{k_3}{k_4[\mathrm{B}]}[\mathbf{135}] \tag{3.10}$$

Further substitution of equation 3.7 into equation 3.10 gives:

$$[\text{cat}]_\text{T} = 2K_D \left( \frac{k_{1b} + k_{2b} + k_3}{k_{1f}[(-)\textbf{-125}] + k_{2f}[(+)\textbf{-125}]} \right)^2 [\textbf{135}]^2 + \frac{k_{1b} + k_{2b} + k_3}{k_{1f}[(-)\textbf{-125}] + k_{2f}[(+)\textbf{-125}]}[\textbf{135}] + [\textbf{135}] + \frac{k_3}{k_4[\text{B}]}[\textbf{135}] \quad (3.11)$$

The expression then simplifies to:

$$\begin{aligned} [\text{cat}]_\text{T} &= a[\textbf{135}]^2 + b[\textbf{135}] \\ 0 &= a[\textbf{135}]^2 + b[\textbf{135}] - [\text{cat}]_\text{T} \end{aligned} \quad (3.12)$$

Where the terms $a$ and $b$ are defined below in equations 3.13 and 3.14.

$$a = 2K_D \left( \frac{k_{1b} + k_{2b} + k_3}{k_{1f}[(-)\textbf{-125}] + k_{2f}[(+)\textbf{-125}]} \right)^2 \quad (3.13)$$

$$b = \frac{k_4[\text{B}](k_{1b} + k_{2b} + k_3) + k_4[\text{B}](k_{1f}[(-)\textbf{-125}] + k_{2f}[(+)\textbf{-125}]) + k_3(k_{1f}[(-)\textbf{-125}] + k_{2f}[(+)\textbf{-125}])}{k_4[\text{B}](k_{1f}[(-)\textbf{-125}] + k_{2f}[(+)\textbf{-125}])} \quad (3.14)$$

Equation 3.12 can then be solved using the quadratic formula (taking only the positive solution) and further manipulated to give **[135]** as follows:

$$\begin{aligned} [\textbf{135}] &= \frac{-b + \sqrt{b^2 + 4a[\text{cat}]_\text{T}}}{2a} \\ &= \frac{2[\text{cat}]_\text{T}}{b + \sqrt{b^2 + 4a[\text{cat}]_\text{T}}} \end{aligned} \quad (3.15)$$

Substitution of equation 3.15 into equation 3.1 gives the overall rate equation:

$$\frac{d[\textbf{126}]}{dt} = \frac{2k_3[\text{cat}]_\text{T}}{b + \sqrt{b^2 + 4a[\text{cat}]_\text{T}}} \quad (3.16)$$

To interrogate the rate equation and evaluate potential rate-determining steps, we then re-expressed equation 3.16 to give equation 3.17 as follows:

$$\begin{aligned}\frac{d[\mathbf{126}]}{dt} &= \frac{2k_3[\text{cat}]_\text{T}}{b+\sqrt{b^2+4a[\text{cat}]_\text{T}}} \\ &= \frac{2k_3[\text{cat}]_\text{T}}{b(1+\sqrt{1+(\frac{4a}{b^2})[\text{cat}]_\text{T}})} \\ &= \frac{2(\frac{k_3}{b})[\text{cat}]_\text{T}}{1+\sqrt{1+(\frac{4a}{b^2})[\text{cat}]_\text{T}}}\end{aligned} \tag{3.17}$$

Taking the logarithm of both sides of equation 3.17 provided a function that we could evaluate against experimental data (equation 3.18).

$$\begin{aligned}\frac{d[\mathbf{126}]}{dt} &= \frac{2(\frac{k_3}{b})[\text{cat}]_\text{T}}{1+\sqrt{1+(\frac{4a}{b^2})[\text{cat}]_\text{T}}} \\ \ln\left(\frac{d[\mathbf{126}]}{dt}\right) &= \ln\left(\frac{2(\frac{k_3}{b})\times e^{\ln\,[\text{cat}]_\text{T}}}{1+\sqrt{1+(\frac{4a}{b^2})\times e^{\ln\,[\text{cat}]_\text{T}}}}\right) \\ \ln\,k_\text{obs} &= \ln\left(\frac{2(\frac{k_3}{b})\times e^{\ln\,[\text{cat}]_\text{T}}}{1+\sqrt{1+(\frac{4a}{b^2})\times e^{\ln\,[\text{cat}]_\text{T}}}}\right)\end{aligned} \tag{3.18}$$

By plotting the result of equation 3.17 (equation 3.18) and fitting to data used to determine the reaction order with respect to catalyst **127** i.e. fitting to Figure 3.16 (Figure 3.22) we were able to extract values for $\frac{a}{b^2}$ and $\frac{k_3}{b}$ of approximately 60 $\text{M}^{-1}$ and 0.0096 $\text{min}^{-1}$, respectively.

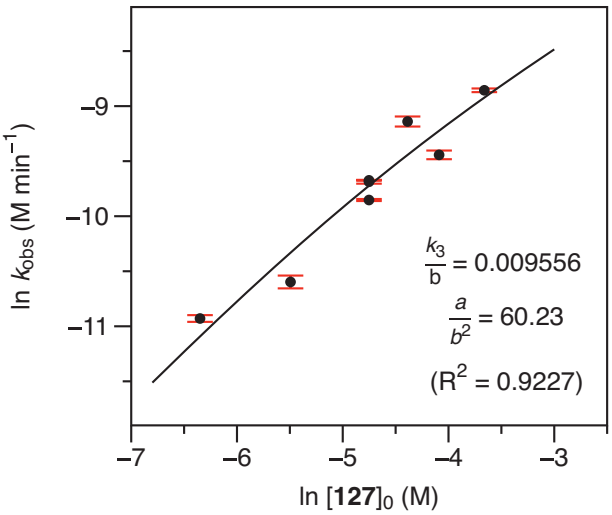



**Figure 3.22: Overlay of fit of equation 3.18 against the catalyst order data.** The line corresponds to the fit obtained. The dots correspond to the catalyst order data. By extracting constants from the fit, values for $\frac{a}{b^2}$ and $\frac{k_3}{b}$ were obtained and are displayed on the graph along with the goodness of fit ($R^2$).

To try and understand the experimental significance of the values calculated, we sought to evaluate the $\frac{a}{b^2}$ term by first looking at its inverse (equation 3.19).

$$\frac{b^2}{a} = \frac{(k_4[\mathrm{B}](k_{1b} + k_{2b} + k_3) + k_4[\mathrm{B}](k_{1f}[(-)\textbf{-125}] + k_{2f}[(+)\textbf{-125}]) + k_3(k_{1f}[(-)\textbf{-125}] + k_{2f}[(+)\textbf{-125}]))^2}{2K_D(k_4[\mathrm{B}])^2(k_{1b} + k_{2b} + k_3)^2} \tag{3.19}$$

Experimentally, the deprotonation event was effectively irreversible suggesting cyclisation was very fast with respect to reprotonation (see 3.7.5). If we assume cyclisation was also fast relative to deprotonation we obtain $(k_{1b} + k_{2b} + k_3) >> (k_{1f}[(-)\textbf{-125}] + k_{2f}[(+)\textbf{-125}])$; we can then ignore $k_4[\mathrm{B}](k_{1f}[(-)\textbf{-125}] + k_{2f}[(+)\textbf{-125}])$ relative to $k_4[\mathrm{B}](k_{1b} + k_{2b} + k_3)$, which gives equation 3.20.

$$\frac{b^2}{a} \simeq \frac{(k_4[\mathrm{B}](k_{1b} + k_{2b} + k_3) + k_3(k_{1f}[(-)\textbf{-125}] + k_{2f}[(+)\textbf{-125}]))^2}{2K_D(k_4[\mathrm{B}])^2(k_{1b} + k_{2b} + k_3)^2} \tag{3.20}$$

Again, consistent with effectively irreversible deprotonation, where cyclisation is fast relative to reprotonation, we assumed that $k_3 >> k_{1b} + k_{2b}$, thus:

$$\frac{b^2}{a} \simeq \frac{(k_4[\mathrm{B}] + k_{1f}[(-)\text{-}\mathbf{125}] + k_{2f}[(+)\text{-}\mathbf{125}])^2}{2K_D(k_4[\mathrm{B}])^2} \tag{3.21}$$

We then end up with two scenarios. The first is where the rate-determining step is deprotonation of the substrate ($(k_{1f}[(-)\text{-}\mathbf{125}] + k_{2f}[(+)\text{-}\mathbf{125}]) << k_4[\mathrm{B}]$). Equation 3.21 then simplifies to give:

$$\frac{b^2}{a} \simeq \frac{1}{2K_D} \tag{3.22}$$

Hence we were able to obtain an expression for $\frac{a}{b^2}$:

$$\frac{a}{b^2} \simeq 2K_D \tag{3.23}$$

The data extracted from Figure 3.22 and the derived equation 3.23 gave a value for $K_D \simeq 30$. This indicated the equilibrium between dimer **139** and zwitterion **140** lies towards the dimer **139**, which was consistent with previous studies.[29,86,88]

In the second scenario, where $k_4[\mathrm{B}] << (k_{1f}[(-)\text{-}\mathbf{125}]+k_{2f}[(+)\text{-}\mathbf{125}])$ and the rate-determining step is regeneration of the active catalyst, we get:

$$\frac{b^2}{a} \simeq \frac{(k_{1f}[(-)\text{-}\mathbf{125}] + k_{2f}[(+)\text{-}\mathbf{125}]))^2}{2K_D(k_4[\mathrm{B}])^2} \tag{3.24}$$

This proved to be too complex to further explore algebraically. We had no clear direction for the further treatment of equation 3.24 within the whole rate equation 3.17 because we had no experimental information about the relative magnitudes of the rates of catalyst regeneration ($k_4$) vs deprotonation ($k_{1f}[(-)\text{-}\mathbf{125}] + k_{2f}[(+)\text{-}\mathbf{125}]$).

We thus continued our examination of the first scenario, where $\frac{a}{b^2} \simeq 2K_D$. By substitut-

ing equation 3.23 into equation 3.17 we obtained a rate of formation of product in the form described by equation 3.25.

$$\begin{aligned}\frac{d[\mathbf{126}]}{dt} &= \frac{2(\frac{k_3}{b})[\text{cat}]_\text{T}}{1+\sqrt{1+(\frac{4a}{b^2})[\text{cat}]_\text{T}}} \\ &= \frac{2(\frac{k_3}{b})[\text{cat}]_\text{T}}{1+\sqrt{1+8K_D[\text{cat}]_\text{T}}}\end{aligned} \tag{3.25}$$

By evaluating the two extreme cases $8K_D[\text{cat}]_\text{T} >> 1$ and $8K_D[\text{cat}]_\text{T} << 1$ we obtained a range for the reaction order with respect to total catalyst ($\text{cat}_\text{T}$). The first, where $8K_D[\text{cat}]_\text{T} >> 1$ gives the result described by equation 3.26. Under these assumptions, the order with respect to catalyst is 0.5.

$$\frac{d[\mathbf{126}]}{dt} = \frac{2(\frac{k_3}{b})}{\sqrt{8K_D}}[\text{cat}]_\text{T}{}^{\frac{1}{2}} \tag{3.26}$$

To evaluate the second outcome, $8K_D[\text{cat}]_\text{T} << 1$, we first considered the denominator of equation 3.25, which could be expanded as a Taylor series:

$$(1+8K_D[\text{cat}]_\text{T})^{\frac{1}{2}} = 1+\frac{1}{2}8K_D[\text{cat}]_\text{T}+... \tag{3.27}$$

Substituting equation 3.27 back into equation 3.25 we obtain equation 3.28, which suggests that under these conditions, the reaction order with respect to total catalyst was 1.

$$
\begin{aligned}
\frac{d[\mathbf{126}]}{dt} &= \frac{2(\frac{k_3}{b})[\text{cat}]_\text{T}}{1+(1+\frac{1}{2}8K_D[\text{cat}]_\text{T}+...)} \\
&= \frac{2(\frac{k_3}{b})[\text{cat}]_\text{T}}{2+4K_D[\text{cat}]_\text{T}+...} \\
&= \frac{(\frac{k_3}{b})[\text{cat}]_\text{T}}{1+2K_D[\text{cat}]_\text{T}+...} \\
&= (\frac{k_3}{b})[\text{cat}]_\text{T}(1+2K_D[\text{cat}]_\text{T}+...)^{-1} \\
&= (\frac{k_3}{b})[\text{cat}]_\text{T}(1-2K_D[\text{cat}]_\text{T}+...) \\
&\simeq (\frac{k_3}{b})[\text{cat}]_\text{T}
\end{aligned}
\tag{3.28}
$$

These results indicated that the reaction order with respect to the catalyst was likely to lie somewhere between 0.5 and 1, which was consistent with the value of 0.79 that we obtained experimentally. However, we were working under the assumption that the regeneration of the active catalyst species was fast relative to the deprotonation steps (i.e. $k_4[\text{B}] >> (k_{1f}[(-)\text{-}\mathbf{125}]+k_{2f}[(+)\text{-}\mathbf{125}])$) and that cyclisation was also very fast relative to deprotonation (i.e. operating under $(k_{1f}+k_{2b}+k_3) >> (k_{1f}[(-)\text{-}\mathbf{125}]+k_{2f}[(+)\text{-}\mathbf{125}])$).

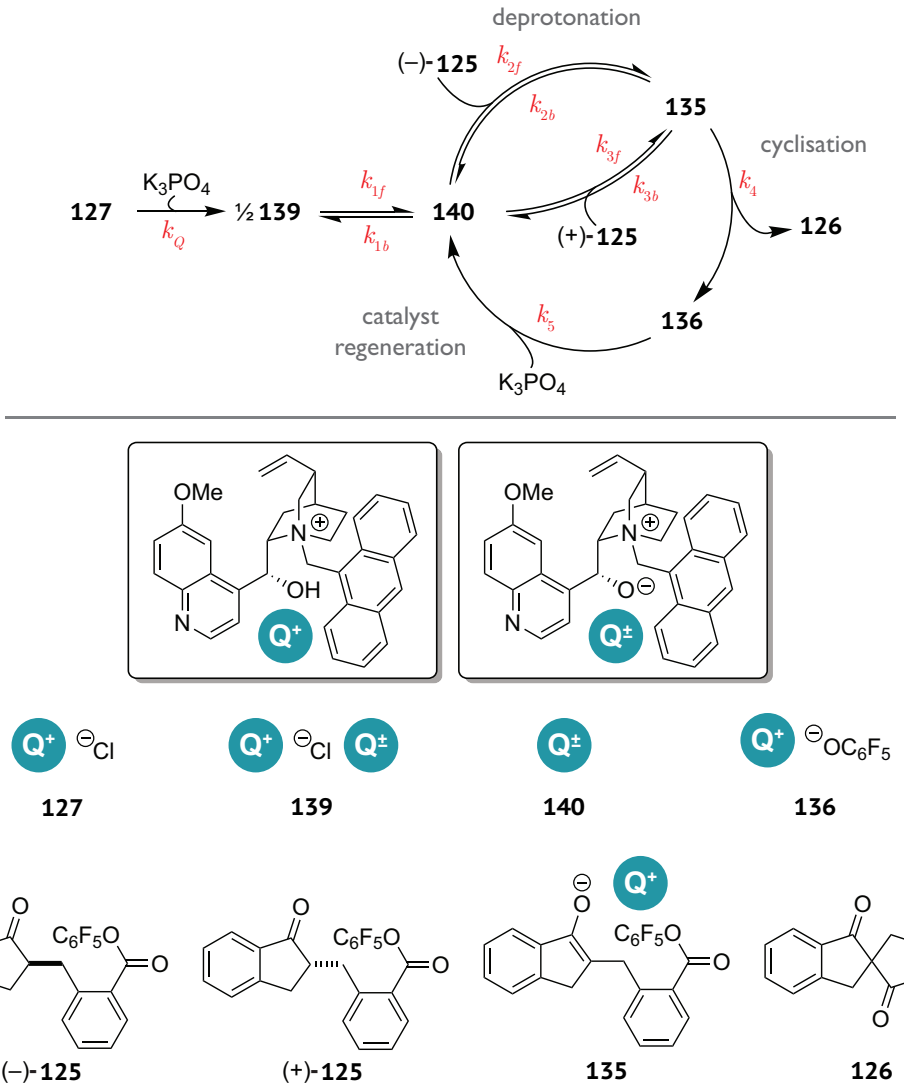
Due to the complexity of our mechanistic hypothesis, we were forced to make a number of assumptions. These included the steady-state approximation and the relative rates of particular steps. The ambiguous results in addition to the non-productive route to obtain equation 3.24, led us to instead begin evaluating the system numerically instead of considering treatments of the derived rate equation (equation 3.17).

### 3.9.1 Numerical evaluation of the mechanistic hypothesis

The new theoretical approach involved calculating the numerical solution of all the differential equations corresponding to each elementary step instead of the integrated solution of the whole rate equation. We thus did not require assumptions such as the steady-state approximation.

This method of analysis also enabled us to include the activation step for the formation of the dimer **139** from the halide salt **127** (as in A, Scheme 3.19).

Hence, a new schematic for the reaction model was created (Scheme 3.21). The rate equations for each elementary step in Scheme 3.21 were then inputted into Mathematica and the whole solution calculated. By varying the parameters (initial concentrations and rate constants) we were able to rapidly explore the effect of different rate-determining steps and initial concentrations on the kinetic behaviour of the reaction according to this particular hypothesis.




**Scheme 3.21: First schematic used to evaluate the reaction system numerically using Mathematica (model 1).** The red labels correspond to the rate constants for the associated steps.

A particular advantage to this approach was that we would be able to fit the generated substrate **125** and product **126** data (for example A, Figure 3.23) to our experimentally acquired

data, whilst visualising the behaviour of otherwise untrackable intermediates (for example B, Figure 3.23).

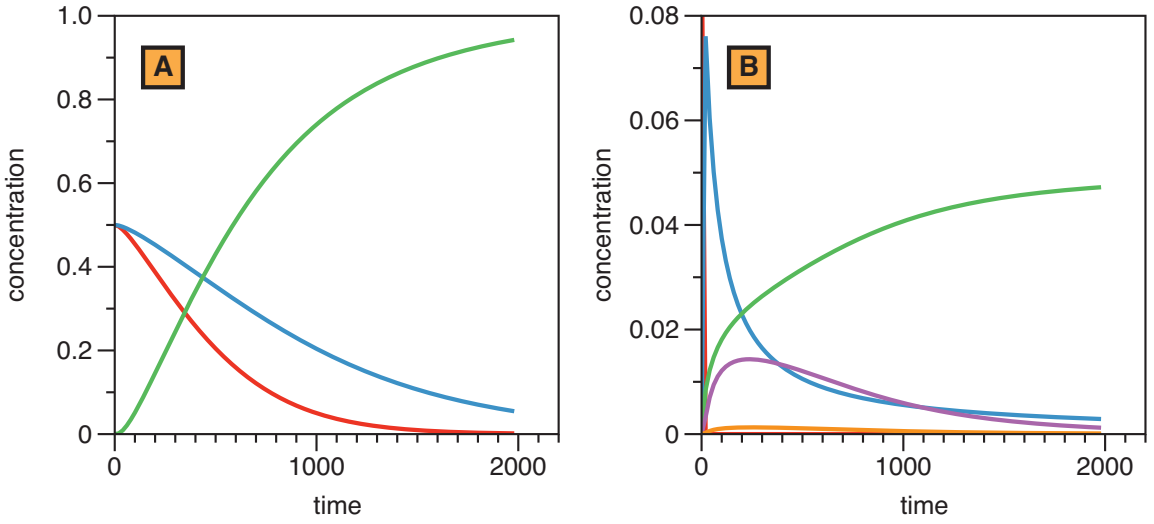


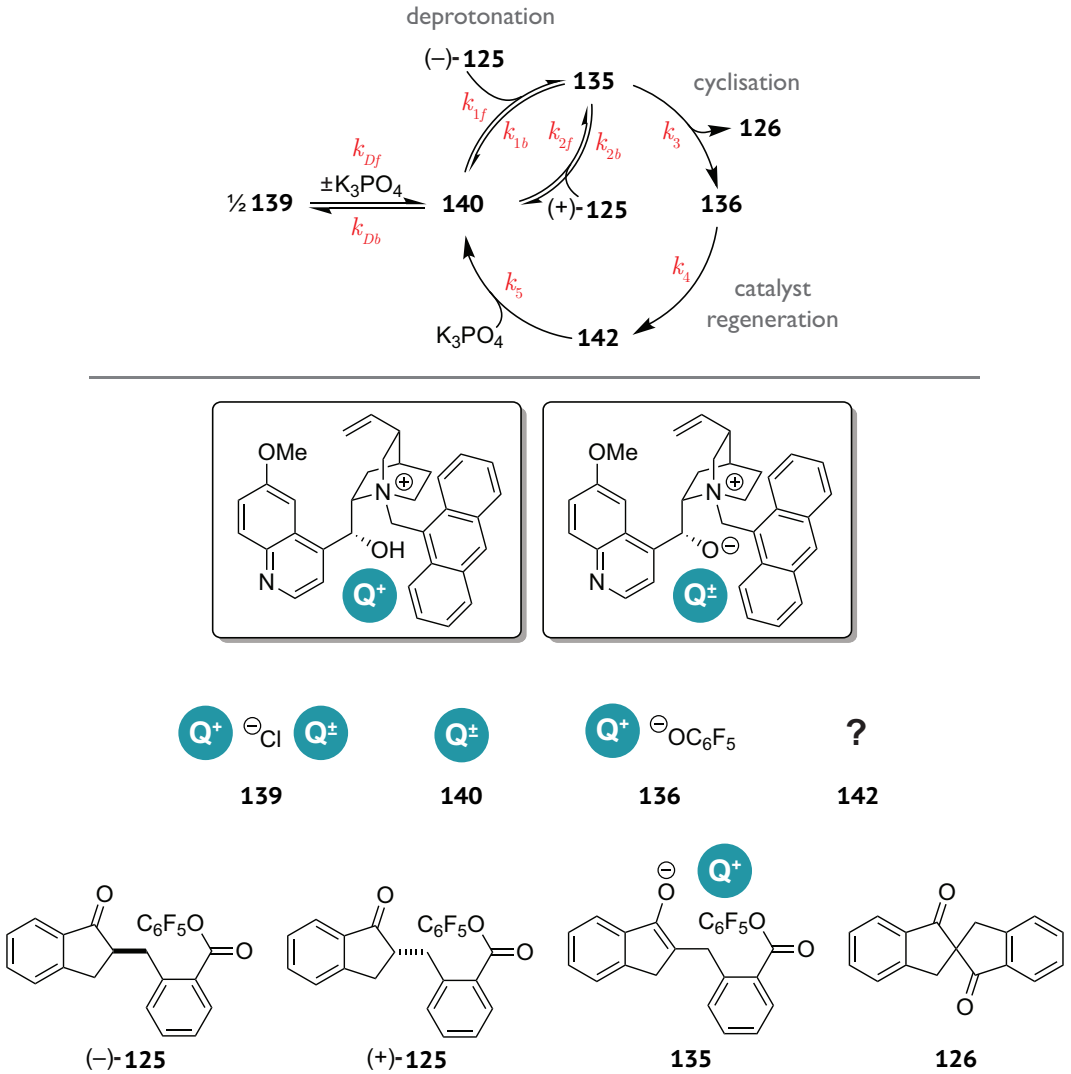

**Figure 3.23: One example solution for the numerical treatment of the rate equations described by Scheme 3.21.** In both graphs, the $x$-axis corresponds to time in arbitrary units, the $y$-axis corresponds to concentration in arbitrary units. In **A**) the red and blue lines correspond to the concentration of the substrate enantiomers over time ((+)-**125** and (−)-**125**, respectively), the green line corresponds to the total concentration of product **126** (both enantiomers) over time; in **B)** the concentration of the species visualised are as follows: **127** (red), **139** (blue), **140** (green), **135** (purple), **136** (orange). The parameters used to generate the whole example were as follows (if unspecified, the parameter was set with a value of zero): $[\mathbf{127}]_0 = 0.1$; $[(+)\text{-}\mathbf{125}]_0 = 0.5$; $[(-)\text{-}\mathbf{125}]_0 = 0.5$; $[K_3PO_4]_0 = 10$; $k_Q = 0.1$; $k_{1f} = 0.09$; $k_{2f} = 0.08$; $k_{3f} = 0.03$; $k_4 = 0.07$; $k_5 = 0.08$.

Whilst evaluating iterations of the numerical model, and upon re-examining the experimental data, we had a revelation. Throughout all practical experiments, we consistently observed an initial jump in the conversion of substrate to product before it settled into a linear rate-limiting regime. This effect was most noticeable when examining the reaction data varying the catalyst concentration (see Figure 3.15). The fast generation of product that occurred initially implied that the rate-determining step was occurring *after* the steps to generate product. This suggested that the deprotonation and cyclisation events were *not* rate-determining in this system.

To explore different mechanistic hypotheses we used different theoretical models (for example, model 2 in 7.22 and 9), each evaluating a series of changes that focused on fitting the model to the experimental data we had acquired thus far. In summary, these changes included how the proposed active catalyst species—zwitterion **140**—was being generated from the pre-catalyst

halide salt **127**, whether or not we included base in the steps to generate active catalyst, and whether another step was potentially present in the regeneration of zwitterion **140** from the ammonium phenolate **136**.

Following the evaluation of a number of different kinetic scenarios, a landmark model (model 4) was subsequently obtained (Scheme 3.22). In this particular iteration, we excluded generation of the zwitterion from the halide salt, which was rationalised by the pre-stirring protocol that we typically carried out prior to initiation of reactions by the addition of substrate (i.e. according to the standard reaction protocol); the distribution of zwitterion and dimer was determined during the pre-stirring period, and we were only examining the reaction on addition of the substrate. We also included an additional step in the regeneration of zwitterion **140** from the phenolate **136**. This was because we observed no significant rate-dependence on the concentration of $K_3PO_4$ experimentally (see 3.7.4); even though $K_3PO_4$ was likely required at some point in order to re-obtain the zwitterion **140**, another process might potentially be rate-limiting that did not involve $K_3PO_4$. The identity of the new proposed intermediate was unknown, but that was unimportant at this point in time. Lastly, because we observed some conversion of substrate **125** to product **126** in the absence of catalyst (see Figure 3.15), we included a background reaction in the updated model (i.e. (+)-**125** + $K_3PO_4 \xrightarrow{k_z}$ **126** and (−)-**125** + $K_3PO_4 \xrightarrow{k_z}$ **126**).




**Scheme 3.22: Schematic used to evaluate the reaction system numerically using Mathematica (model 4).** The red labels correspond to the rate constants for the associated steps.

The theoretical model described by Scheme 3.22 was fitted to a selection of experiments, which generated values for the rate constants of each of the included steps (Entries 1 to 9, Table 3.1). The data suggested that deprotonation of the substrate and subsequent cyclisation were indeed not rate-determining in this particular system. It appeared that the rate-determining step was related to regeneration of the proposed active catalyst species i.e. that described by the rate constant $k_5$ (Entry 9, Table 3.1).

To obtain good agreement between the theoretical and experimental data, we needed to introduce the "catfactor" parameter (Entry 11, Table 3.1). This factor was multiplied by the total concentration of catalyst ($[\text{cat}]_\text{T}$) in the system, given by the known concentration that

we used experimentally. This suggested that only about one third of the catalyst was doing work in the reaction system, with the remainder sequestered in off-cycle processes.

**Table 3.1: Parameters obtained from fitting the theoretical model (model 4 according to Scheme 3.22) to selected experimental data.** Data are reported to three significant figures.

| Entry | Parameter | Value | Event |
|---|---|---|---|
| 1 | $k_{Df}$ | 3.75 $M^{-1}$ $min^{-1}$ | catalyst monomerisation |
| 2 | $k_{Db}$ | 12.7 $min^{-1}$ | catalyst dimerisation |
| 3 | $k_{1f}$ | 30.5 $M^{-1}$ $min^{-1}$ | deprotonation |
| 4 | $k_{1b}$ | 0.00 $min^{-1}$ | reprotonation |
| 5 | $k_{2f}$ | 69.1 $M^{-1}$ $min^{-1}$ | deprotonation |
| 6 | $k_{2b}$ | 0.00 $min^{-1}$ | reprotonation |
| 7 | $k_3$ | 355 $min^{-1}$ | cyclisation |
| 8 | $k_4$ | 160 $min^{-1}$ | unknown |
| 9 | $k_5$ | 0.0189 $M^{-1}$ $min^{-1}$ | catalyst deprotonation |
| 10 | $k_z$ | 0.00350 $M^{-1}$ $min^{-1}$ | background reaction |
| 11 | catfactor | 0.329 | N/A |

Using the values of the parameters in Table 3.1, the known initial concentration of substrate, and the known total concentration of catalyst, we then plotted the whole result against experimental data that was obtained under a variety of conditions (selected examples in Figure 3.24). The shape of the outputted kinetic model was exceptionally sensitive to the total concentration of catalyst ($[cat]_T$) available in the system. Even slight variations in $[cat]_T$ resulted in changes in both the burst phase behaviour and the slope of the linear data.

The model showed reasonable graphical agreement with a number of examples, including the initial burst of reactivity, particularly in experiments evaluating different initial catalyst **127** concentrations (A to C, Figure 3.24). When examining the model against different initial substrate concentrations ($[\mathbf{125}]_0$), we found good agreement with data acquired at lower and moderate $[\mathbf{125}]_0$ (C and D, Figure 3.24), but the model began to overestimate the rate of formation of product at higher $[\mathbf{125}]_0$ (E, Figure 3.24). Another example where the model did not accurately fit the observed experimental behaviour was when we evaluated the rate of formation of product **126** using different stock concentrations of $K_3PO_4$ and varied its total

concentration in the reaction system (for example F, Figure 3.24).

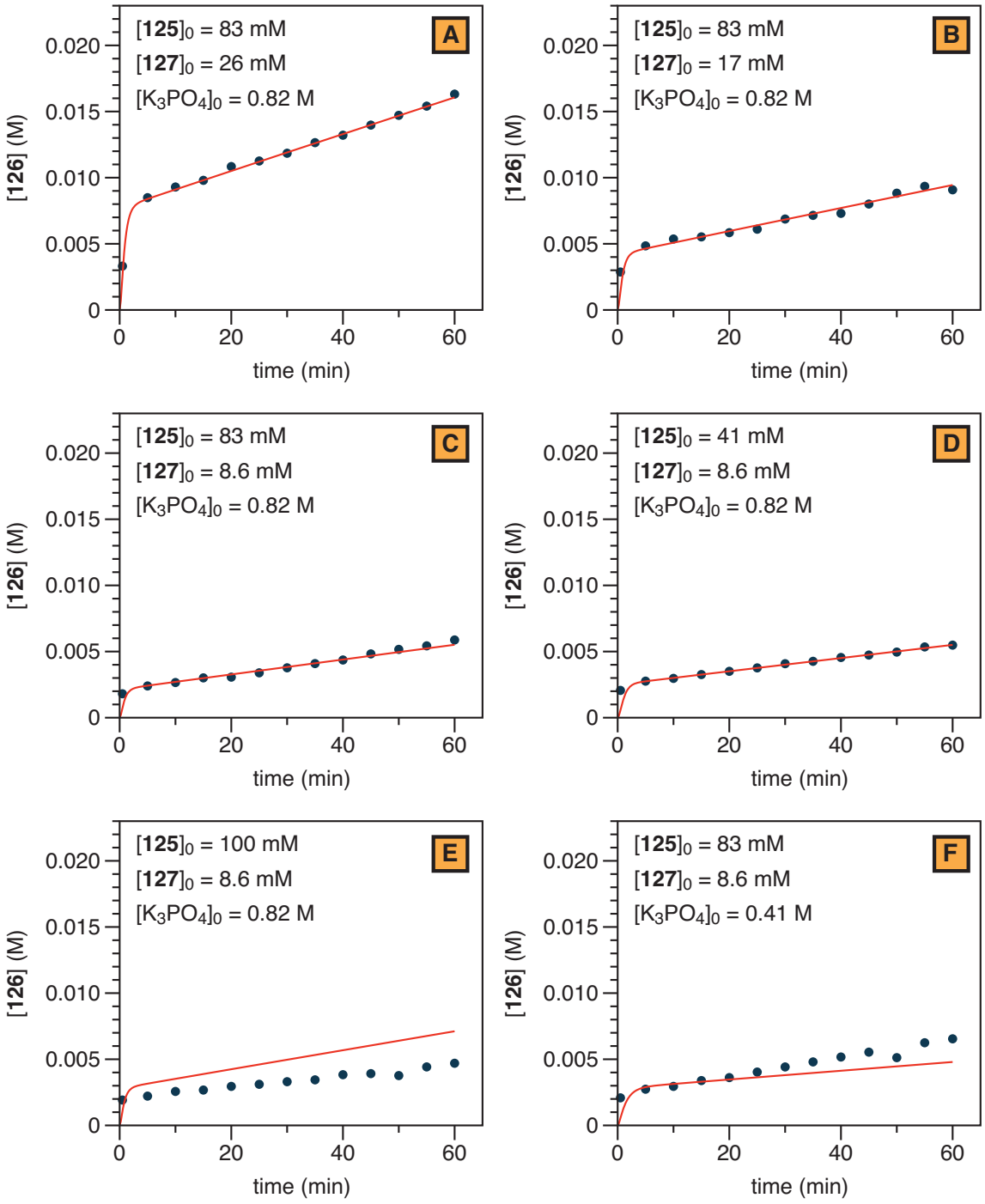



**Figure 3.24: Selected examples of the kinetic model against experimentally acquired results.** Each example corresponds to different initial reaction conditions (to 2 sf), which are indicated on each graph as the total initial concentration in the whole reaction system (both organic and aqueous layers). The data sets have the designated reaction codes (*rxn.code*) as follows: **A)** spirok-12 replicate 1; **B)** spirok-7 replicate 1; **C)** spirok-35 replicate 2; **D)** spirok-16 replicate 3; **E)** spirok-14 replicate 2; **F)** spirok-30b. All examples were carried out according to the standard reaction protocol, with a reaction stirring speed of 1000 rpm, and stock concentrations of $K_3PO_4$ of 4.77 M (except for example **F** which used $K_3PO_4$ with a stock concentration of 2.39 M). In all graphs, the dots correspond to data that was acquired experimentally, and the red lines correspond to the model described by Scheme 3.22 and Table 3.1. The $x$-axes correspond to time following initiation of the reaction, the $y$-axes correspond to the concentration of product **126**.

The overall kinetic model and numerical solution was mostly consistent with the majority of our experimental data. Firstly, the strong dependence of the rate of reaction on the concentration of the catalyst suggested a catalyst species was involved in the rate-determining step (see 3.7.2), which in this case was likely to be regeneration of the active zwitterion **140** from ammonium phenolate **136** by some process. The rate-determining step did not involve the substrate **125** (see 3.7.3), which was again consistent with our model.

Despite introducing an additional step that did not require $K_3PO_4$ to manipulate the ammonium phenolate intermediate **136** (i.e. the unknown event described by $k_4$), the data fitting suggested that this step was fast, with the rate-determining step again including $K_3PO_4$ (i.e. the catalyst deprotonation event described by $k_5$). However, experimentally, we observed negligible dependence of the concentration of $K_3PO_4$ on the rate (see 3.7.4), suggesting that base was not involved in the rate-determining step, which was *inconsistent* with the results obtained from fitting the model to our experimental data.

Further experimental findings that were consistent with the theoretical model included the data obtained when subjecting the enantioenriched substrates to the reaction conditions. The lack of racemisation suggested that deprotonation of the substrate was effectively irreversible (see 3.7.5). Theoretically, we obtained a rate constant for cyclisation that was very large (fast), relative to reprotonation (i.e. 355 $min^{-1}$ for cyclisation vs 0.00 $min^{-1}$ for reprotonation). The difference in rate observed between the two substrate enantiomers (i.e. 30.5 $M^{-1}$ $min^{-1}$ vs 69.1 $M^{-1}$ $min^{-1}$) was consistent with the kinetic resolution of the substrate that we observed, and again, these details were all reflected in the refined kinetic model.

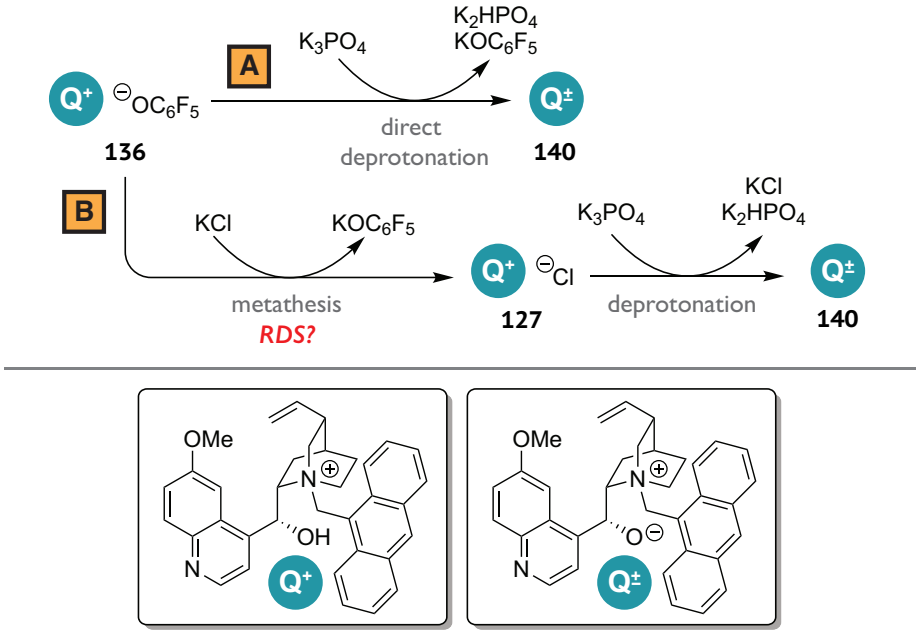
To further explore the scenario where regeneration of the active catalyst was rate-determining, we continued our experimental approach.

## 3.10 Investigating the revised mechanistic hypothesis

We next carried out a series of experiments to examine aspects of our working mechanistic hypothesis. We first wanted to scrutinise our newfound rate-determining step, which was regeneration of the active catalyst **140** following formation of the product **126**.

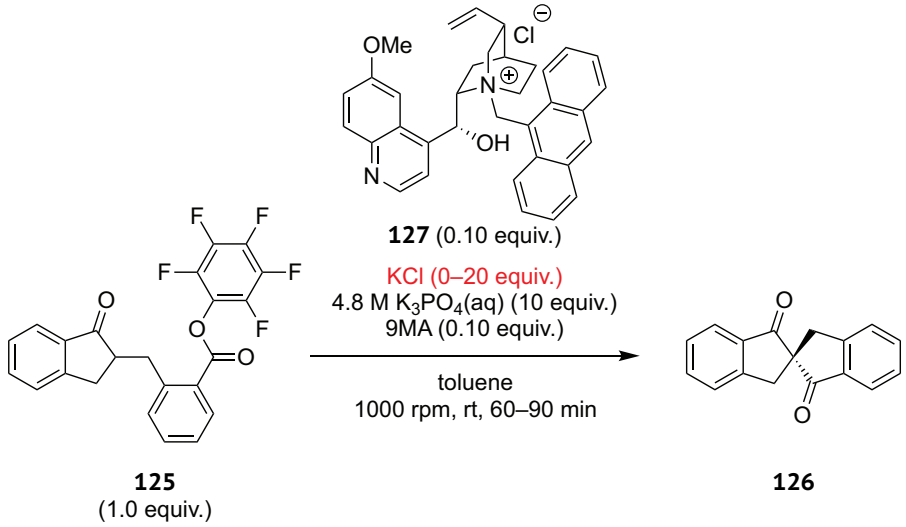
### 3.10.1 The effect of chloride in the system

To investigate regeneration of zwitterion **140** from ammonium phenolate **136**, we first considered potential pathways through which this process might proceed (Scheme 3.23). Despite the results from the theoretical model and because we experimentally observed negligible dependence of the reaction rate on the concentration of base ($K_3PO_4$), we hypothesised there might be an additional metathesis step that liberated the ammonium phenolate **136** prior to deprotonation of the cinchona alkaloid to regenerate the zwitterion **140** (Scheme 3.23) (path B, Scheme 3.23). This species might also represent the unknown intermediate in our latest model (see Scheme 3.22).




**Scheme 3.23: Potential for the proposed rate-determining step—regeneration of zwitterion 140—to proceed via different routes. A)** Direct deprotonation of phenolate **136** or; **B)** metathesis to regenerate halide **127** before deprotonation to give zwitterion **140**.

The most feasible salt available to undergo metathesis with the ammonium phenolate **136** was KCl, which might be present following generation of the zwitterion from the halide salt **127** and $K_3PO_4$. As such, we carried out the reaction with added KCl to gauge its effect on the rate of formation of product ($k_{obs}$) (Scheme 3.24).




**Scheme 3.24: Conditions used to evaluate the effect of added KCl.** Equivalents (equiv.) are reported with respect to substrate **125**.

The data showed little change in the observed rate with different amounts of KCl added (from 0 to 20 equiv. with respect to substrate) (A, Figure 3.25). The slope comparing the linear relationship of the $k_{obs}$ to [KCl] was minuscule ($-7.5 \times 10^{-7}$). Similarly, the double logarithmic plot to determine the reaction order with respect to the KCl gave a value that was effectively zero (0.0043) (B , Figure 3.25).

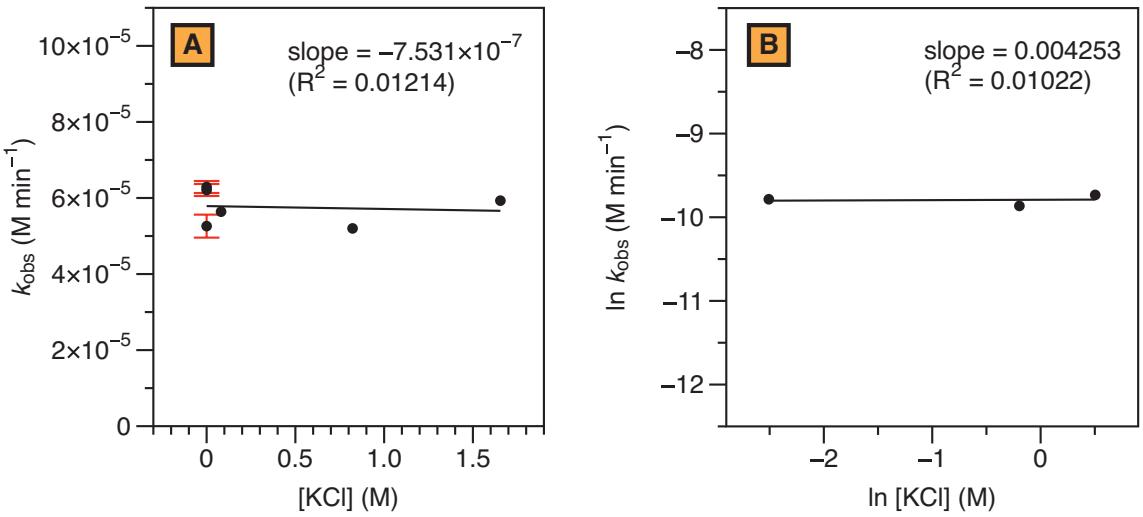



**Figure 3.25: Plots to evaluate the effect of added KCl on the rate of the reaction. A)** The $x$-axis corresponds to the concentration of KCl in the whole reaction system ([KCl]); the $y$-axis corresponds to the observed rate of formation of product ($k_{obs}$). **B)** Double logarithmic plot to determine the reaction order with respect to KCl. The $x$-axis corresponds to the natural logarithm of the concentration of KCl in the whole reaction system (ln [KCl]); the $y$-axis corresponds to the natural logarithm of the observed rate of formation of product (ln $k_{obs}$). The lines in both graphs are linear regression analyses of the corresponding data; the line in **B** corresponds to the obtained reaction order with respect to KCl of 0.0043.

Overall, the results suggested that either a metathesis step was not occurring, that the metathesis step was present and not rate-determining, or that it was present but had reached the maximum mass transfer of chloride allowed by the system and hence additional KCl had no effect. Given the lack of solubility of the ammonium halide salt **127** and the lack of effect of added KCl, it was likely that a metathesis step was not occurring, and was hence not rate-determining. We turned our attention back to the deprotonation of the ammonium phenolate **136** as being rate-determining.

### 3.10.2 Revisiting the order in base

The results of the KCl experiments led us to re-examine the effect of base in the system. The hypothesised rate-determining step in our model was deprotonation of ammonium phenolate **136** by base ($K_3PO_4$) to give the active zwitterion **140**. This was consistent with the strong dependence of the rate on the concentration of the catalyst (see 3.7.2). Previously, we found negligible dependence of the concentration of $K_3PO_4$ on the rate (see 3.7.4), which inconsis-

tently suggested that base was not involved in the rate-determining step.

However, if regeneration of the active catalyst was occurring in a first order manner with respect to the catalyst, then we were always operating under conditions where the total catalyst was saturated with base; the total amount of base (0.50–20 equiv. with respect to substrate) was always in excess of the catalyst (0.10 equiv. with respect to substrate). We thus examined the reaction at reduced base loadings (0.030–3.0 equiv. with respect to substrate), and at intermediate points within our existing data set (Figure 3.20), and combined the data with that obtained previously to obtain a better picture of the effect of $K_3PO_4$ in the system (Figure 3.26).

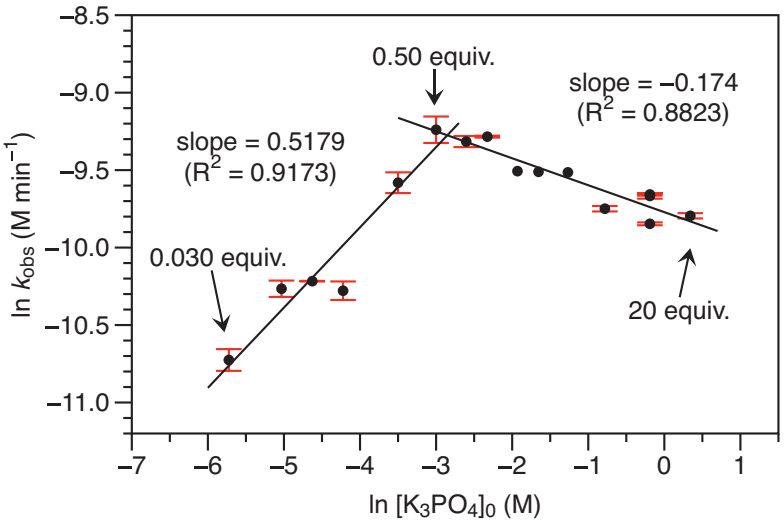



**Figure 3.26: Updated rate-dependence of the reaction on the concentration of $K_3PO_4$.** A double logarithmic plot to determine the order of the reaction with respect to the total concentration of $K_3PO_4$. The $x$-axis corresponds to the natural logarithm of the concentration of $K_3PO_4$ in the total reaction system (ln [$K_3PO_4$]); the $y$-axis corresponds to the natural logarithm of the rate of formation of product (ln $k_{obs}$). The lines are linear regression analyses of the two apparent regimes. Landmark equivalents (equiv. of $K_3PO_4$ with respect to substrate **125**) are indicated on the graph.

Gratifyingly, we found that reduced loadings of $K_3PO_4$ with respect to substrate, which corresponded roughly to stoichiometric loadings with respect to added catalyst **127**, exhibited a positive effect on the initial rates. The order with respect to $K_3PO_4$ at these lower loadings (0.030–0.50 equiv. with respect to substrate) was 0.52 with a 68% confidence interval of 0.429 to 0.607. Again, at higher total $K_3PO_4$ concentrations (0.50–20 equiv. with respect to substrate), we observed a partial negative order of −0.17 with a 68% confidence interval of −0.197

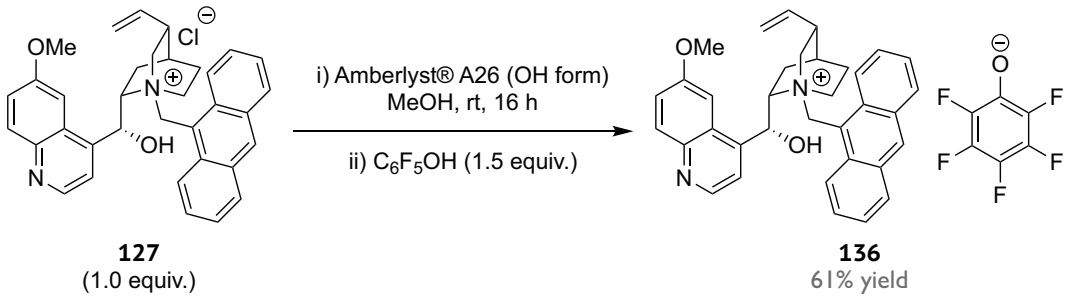
to −0.152. The attribution of the inverse order remained the same: that increased dilution of the catalyst in the total system at higher volumes of added $K_3PO_4$ resulted in a decrease in the rate. Under the standard reaction conditions, the system is saturated by $K_3PO_4$.

These experimental findings were consistent with our current working hypothesis: the rate-determining step following the burst phase was regeneration of the active catalyst species, which occurred via deprotonation of the ammonium phenolate **136** in a process mediated by base.

### 3.10.3 Ammonium phenolate as a mechanistic probe

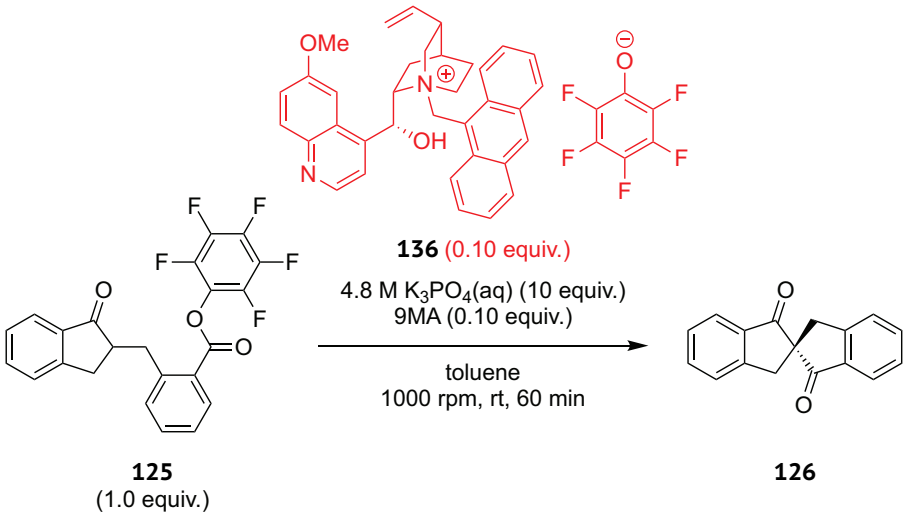
Again, the burst phase and apparent lack of the zero intercept for the reaction suggested that the rate-determining step was occurring after product formation. If we could potentially initiate the reaction *from* the proposed rate-determining step, we expected to observe a comparable rate to the linear portion of the rate of formation of product, but with an intercept of zero. To experimentally examine this, we required access to the ammonium phenolate **136**, which was the substrate in our proposed rate-determining step.

The synthesis and application of cinchona alkaloid-derived ammonium catalysts bearing phenoxide counterions is well known.[75] Using procedures adapted from the literature,[80] we synthesised the ammonium phenolate **136** from the corresponding chloride **127** using an ion-exchange resin and 2,3,4,5,6-pentafluorophenol (Scheme 3.25).




**Scheme 3.25: Synthesis of ammonium phenolate 136**. Equivalents (equiv.) are reported with respect to the starting material **127**.

With access to the phenolate **136**, we next wanted to evaluate its effect on the kinetic behaviour in the conversion of substrate **125** to product **126**. We first needed to consider what reaction conditions we would use. Our standard reaction conditions involved pre-stirring the catalyst (usually halide salt **127**) with base ($K_3PO_4$) prior to initiating the reaction by the addition of substrate **125** as a solution (see 3.3.1 and 7.4.1). In the case of phenolate **136**, pre-stirring with $K_3PO_4$ prior to initiation of the reaction by the addition of substrate would potentially generate a pool of active zwitterion **140** and we would just observe the same rate behaviour as before. As such, we carried out a triplicate set of reactions evaluating the phenolate **136** as the starting catalyst, using the modified reaction protocol, i.e. initiating the reaction by the addition of $K_3PO_4$ (Scheme 3.26).




**Scheme 3.26: Conditions used to evaluate the effect of starting catalyst 136 on the reaction.** Equivalents (equiv.) are reported with respect to the substrate **125**.

Excitingly, the reaction effected by ammonium phenolate **136** exhibited the behaviour that we had predicted. We completely eliminated the burst phase and the initial rate of formation of product gave an intercept of zero (Figure 3.27). The triplicate experiment showed good coherence between the three reactions.

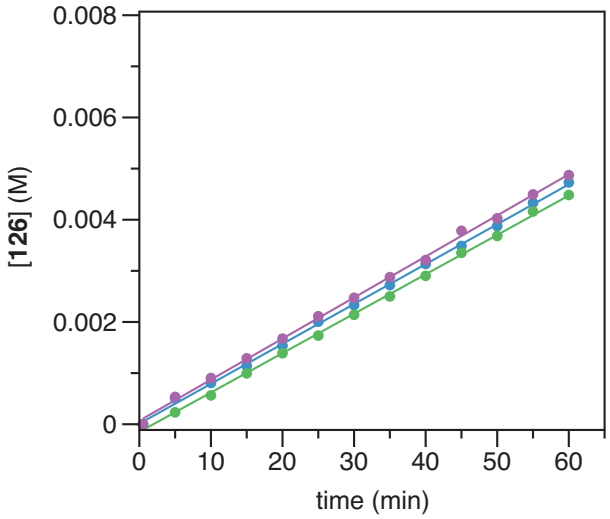



**Figure 3.27: Triplicate experiment to evaluate catalyst 136 under the reaction conditions with no pre-stirring.** The colours indicate different individual reactions within the triplicate set. The lines are linear regression analyses of the corresponding set.

Unlike the ammonium chloride **127**, the ammonium phenolate **136** exhibited remarkable solubility in the organic solvent; catalyst **136** was completely soluble in toluene during set up and under the reaction conditions (initially at 8.6 mM). Suddenly, we could rationalise the change in the physical reaction over time when deploying ammonium halide **127** as the initial catalyst.

The following schematic depicts the change in physical appearance of the reaction mixtures in comparison to the change in rate when carrying out the reaction using the halide catalyst **127** (Figure 3.28). During the pre-stirring phase (−30 to 0 min), the reaction mixtures were heterogeneous and polyphasic. After initiating the reaction at the designated time zero, we observed a burst phase and rapid formation of product, before the reactions settled into a rate-limiting regime, designated as the "normal phase." During the normal phase, and within the time scale for the reaction (usually 60 min), the reaction mixtures were clear and biphasic—all solid material that was previously present was solubilised. We attributed the change in rate at the start of the normal phase and the concurrent change to fully solubilised reaction mixtures to the major catalyst species being the soluble ammonium phenolate **136**; the changes in rate and heterogeneity of the reaction mixtures were correlated with sequestration of the bulk of

the catalyst as the ammonium phenolate **136** at the rate-determining step.

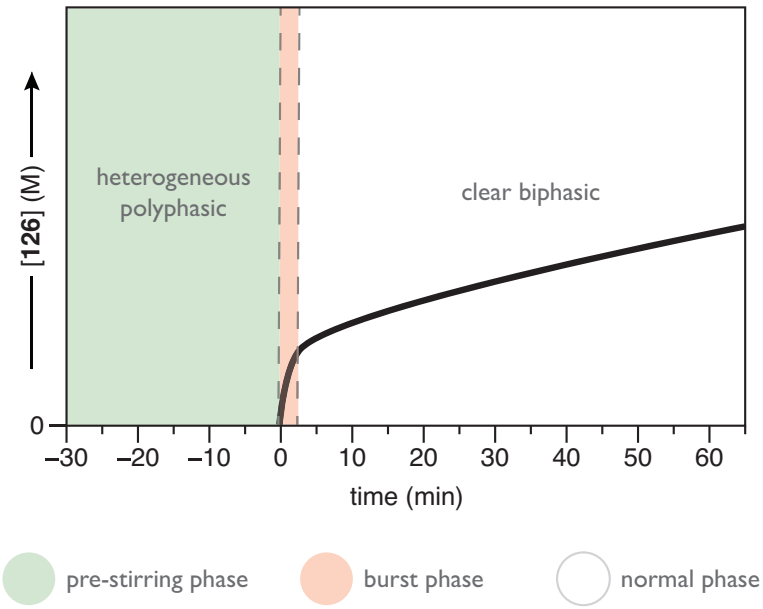



**Figure 3.28: Schematic depicting the general change in rate observed with the appearance of the reaction mixtures.** The green area corresponds to the pre-stirring phase of the reaction protocol. On addition of substrate at time zero, the burst phase occurs (red area), before the reaction mixture turns clear and biphasic during the normal phase of the reaction (white area).

Our current hypothesis regarding the burst phase was that it was due to a pool of active zwitterion **140** being formed during the pre-stirring protocol. The catalyst existed as an equilibrium mixture of dimer (soluble), zwitterion (soluble), and halide salt (insoluble). On addition of substrate **125** as a solution at time zero, all of the catalyst as the zwitterion **140** rapidly gave product before getting "stuck" as the ammonium phenolate **136** at the rate-determining step. The observation of the physical reaction mixtures were consistent with this hypothesis.

We attempted to reproduce the burst phase behaviour exhibited by the chloride catalyst **127**, but starting from the ammonium phenolate **136**. We thought that pre-stirring phenolate **136** as per the standard reaction protocol would similarly generate a pool of active zwitterion **140**. Then, on addition of substrate at time zero, product would be produced rapidly, consuming all of the zwitterion **140** and giving the burst phase behaviour. However, we found that pre-stirring the phenolate **136** using our standard reaction protocol did not introduce a burst phase (Figure 3.29). We hypothesised that the pre-stirring time might have been insufficient to pre-

form a pool of the zwitterion **140**. However, when we extended the pre-stirring time, this also did not produce the expected burst phase.

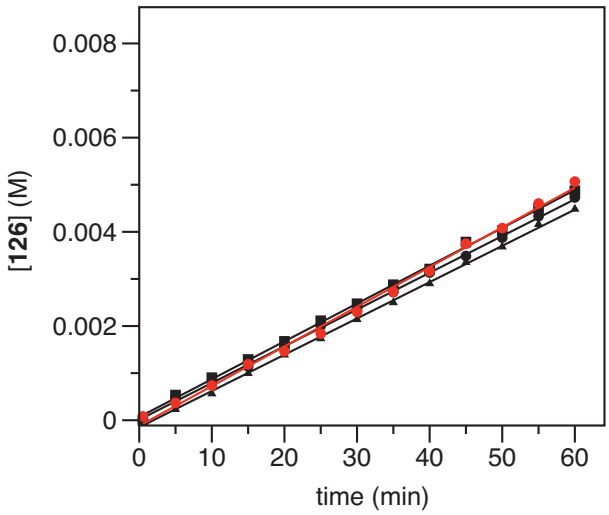
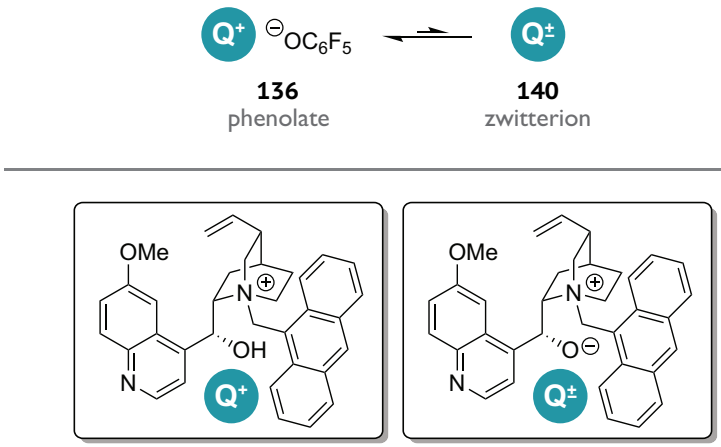



**Figure 3.29: Overlay of the reactions deploying catalyst 136 and using different reaction protocols.** The black data set are the same triplicate data depicted in Figure 3.27 and correspond to reaction carried out using the modified reaction protocol (no pre-stirring); the red data set corresponds to data collected using the standard reaction protocol (pre-stirring). The lines are from linear regression analyses of each data set to give the corresponding $k_{obs}$.

One explanation for the lack of burst phase behaviour when deploying phenolate **136** using the standard reaction protocol was that it was highly favourable for the catalyst to exist as the organophilic phenolate **136** (Scheme 3.27). In the absence of substrate, formation of the zwitterion **140** was non-productive, and the equilibrium lies in favour of phenolate **136**. Thus, pre-stirring the catalyst **136** with base does not generate a pool of zwitterion **140** and we do not observe a burst phase upon addition of substrate **125** on initiation of the reaction. An experiment to further investigate this possibility would be to give the catalyst the option to generate the ammonium phenolate **136** by starting with the halide **127** and commencing the reaction (using the standard reaction protocol with pre-stirring) with added 2,3,4,5,6-pentafluorophenolate. This particular experiment will be explored at a later point. Overall, these results suggested that formation of zwitterion **140** from phenolate **136** was reversible, which was not accounted for in our previous mechanistic hypothesis.




**Scheme 3.27: Equilibrium between zwitterion 140 and ammonium phenolate 136.**

When we compared the data generated using ammonium phenolate **136** to that we obtained with the halide catalyst **127**, we found the initial rate for the reaction was slightly faster than that for the corresponding reaction using the starting halide salt **127** ($7.85 \times 10^{-5} \pm 0.14 \times 10^{-5}$ M min$^{-1}$ vs $5.92 \times 10^{-5} \pm 0.48 \times 10^{-5}$ M min$^{-1}$) (Figure 3.30). The origin for the change in rate during the normal phase of both reactions remained unclear at the time, but we suspected it was due to the presence of chloride in the system.

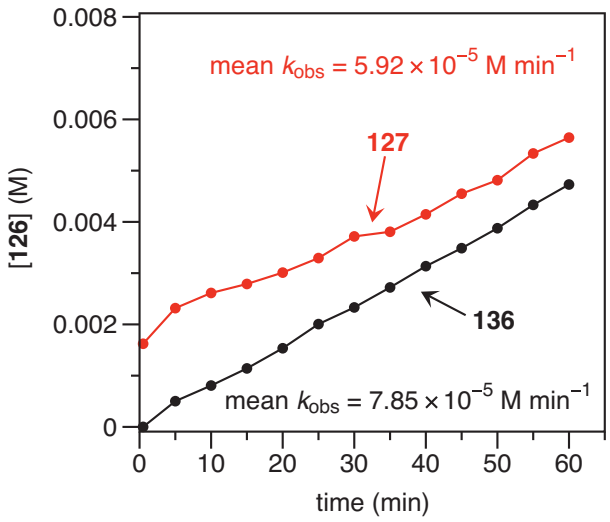
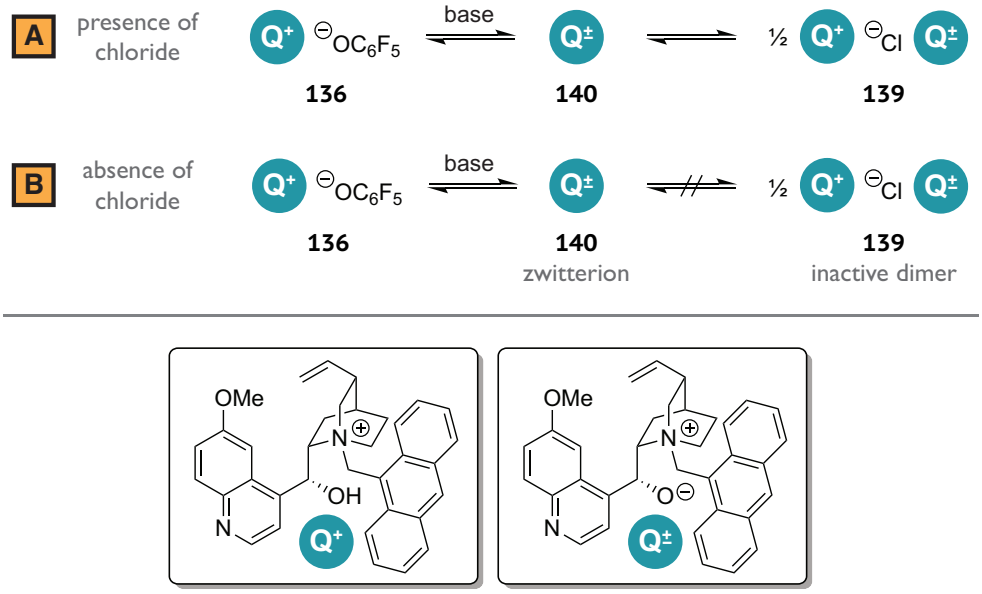


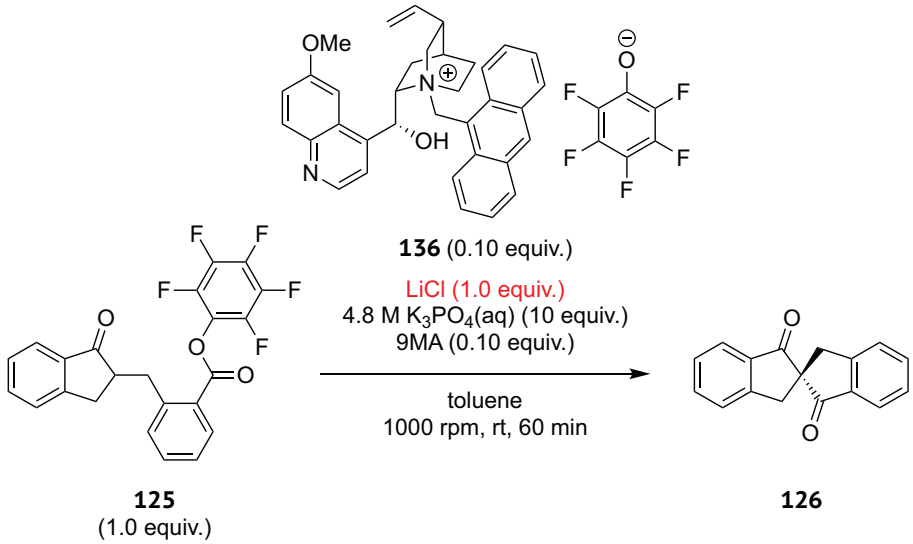

**Figure 3.30: Selected experiments showing the change in the burst phase when using catalyst 136 (red) vs catalyst 127 (black).** The lines are guides for the eye. The displayed rates are the mean values and errors of the corresponding whole replicate sets, $n$, where for **136**, $n = 3$, and for **127**, $n = 9$.

We hypothesised that added chloride might enable formation of the off-cycle dimer **139** in systems starting from catalyst **136** (A, Scheme 3.28). The system using catalyst **136** has no chloride, hence formation of the inactive dimer bearing a chloride counterion was not possible (B, Scheme 3.28).




**Scheme 3.28: Potential for catalyst intermediates to exist in equilibrium. A)** In the presence of chloride, formation of the off-cycle inactive dimer **139** is possible resulting in sequestration of a portion of the total available catalyst; **B)** in the absence of chloride, formation of the chloride-counterioned dimer **139** is not possible, thus more active catalyst is available.

To investigate the potential for chloride to decrease the rate, we carried out a reaction using added LiCl (Scheme 3.29). The results from the pre-stirring experiments using **136** and its solubility in toluene suggested it was highly organophilic. We also suspected an equilibrium existed between the phenolate **136** and zwitterion **140** in the organic phase and that it lay heavily towards the phenolate **136**. Lithium chloride was selected because it is more organosoluble than KCl,[120] thus potentially more able to interact with **136** in the organic phase.




**Scheme 3.29: Conditions evaluating the effect of chloride in the reaction system starting from phenolate catalyst 136.** Equivalents (equiv.) are reported with respect to substrate **125**. The reaction was carried out using the standard reaction protocol (see 7.4.1).

When we carried out the reaction with added LiCl, we found the rate of the reaction decreased from approximately $7.85 \times 10^{-5}$ M min$^{-1}$ to $5.46 \times 10^{-5}$ M min$^{-1}$ (Figure 3.31), which was more consistent with the rate exhibited by the ammonium halide **127** ($5.92 \times 10^{-5}$ M min$^{-1}$). Again, despite pre-stirring, we were not able to re-introduce the burst phase, which strongly suggested that once the ammonium phenolate **136** was formed, any equilibria between it and the zwitterion lay heavily towards the phenolate **136**. If the zwitterion was formed it was in negligible quantities over the pre-stirring period and any formation was non-productive due to the absence of substrate **125**.

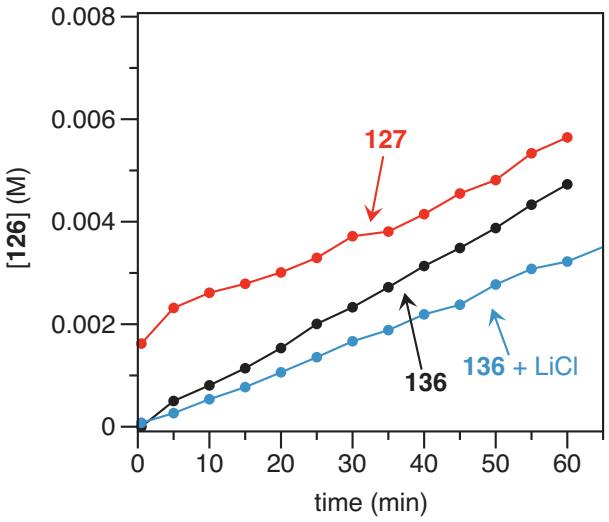
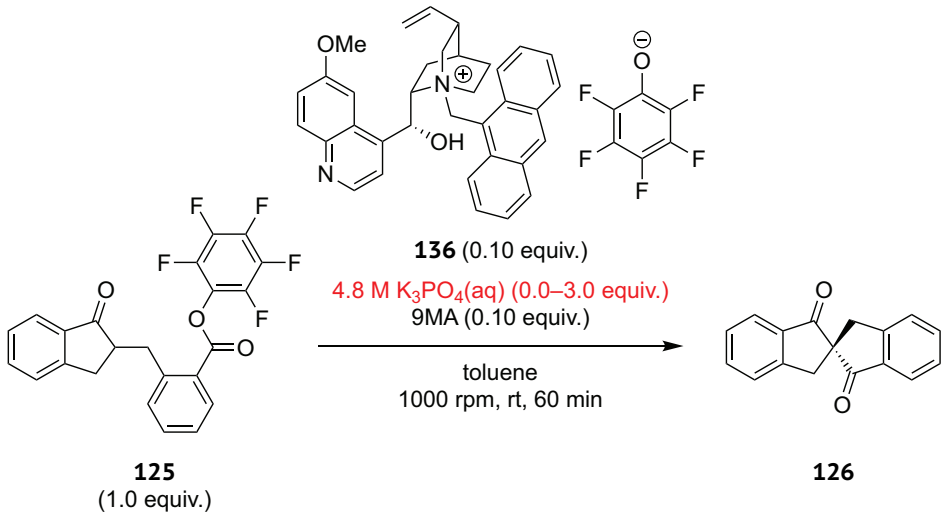



**Figure 3.31: Overlay of results highlighting the effect of chloride on the reaction system.** The red data correspond to reactions carried out using halide salt **127** as the initial catalyst. The black data correspond to reactions carried out using ammonium phenolate **136** as the initial catalyst. The blue data correspond to reactions carried out using ammonium phenolate **136** as the initial catalyst in the presence of LiCl. The lines are guides for the eye.

According to our current hypothesis, when using the phenolate **136** as the starting catalyst, we were commencing the reaction from the rate-determining step. This was a process proposed to be mediated by base ($K_3PO_4$). As such, we expected to observe a strong rate-dependence of the reaction on the concentration of base when subjecting phenolate **136** to the reaction conditions and varying the amount of $K_3PO_4$ that was added (Scheme 3.30).




**Scheme 3.30: Conditions evaluating the effect of $K_3PO_4$ on the reaction with phenolate 136 as the starting catalyst.** Equivalents (equiv.) are reported with respect to substrate **125**.

Indeed, when we examined the effect of base under these new conditions, a clear positive dependence of the rate of reaction on the amount of base was observed (A, Figure 3.32).

Interestingly, we obtained a comparable order with respect to base under these conditions (0.45 ± 0.049) (B, Figure 3.32) compared to the ammonium chloride catalyst at low base loadings (0.52 ± 0.08) (Figure 3.26).

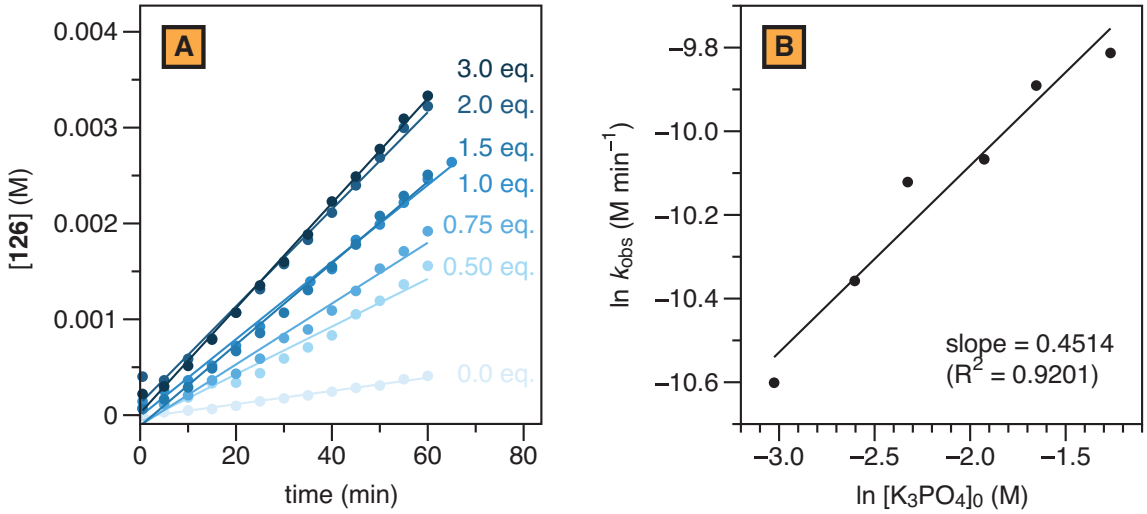



**Figure 3.32: Data showing the effect of base on the rate of formation of product in systems starting with catalyst 136. A)** Change in concentration of product **126** over time in all experiments used to determine the effect of added base. The different colours indicate the amount of base that was added to the reaction initially in equivalents (eq.) with respect to substrate **125**. **B)** Double logarithmic plot of total base concentration (ln $[K_3PO_4]_0$) against initial rate (ln $k_{obs}$) to give the order with respect to base of 0.45.

Again, the data were consistent with our proposed hypothesis. We had evidence to support the proposed rate-determining step in our reaction system. However, we had little information as to what was occurring during the burst phase.

## 3.11 Investigating the burst phase

In reactions directly comparing the standard and modified protocols, we observed a change only in the length of the burst phase, with comparable rates of reaction following this initial period (Figure 3.33). Our current hypothesis was that whilst pre-stirring (standard reaction protocol), a pool of the active zwitterion was being formed, and that on addition of substrate, was quickly consumed as product was rapidly generated. Under the modified reaction conditions—when initiating the reaction with base—we did not have a pool of active zwitterion, hence it was formed in addition to product being formed.

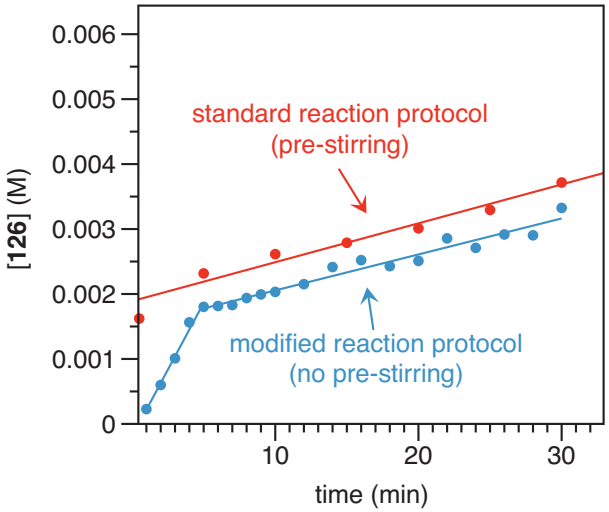


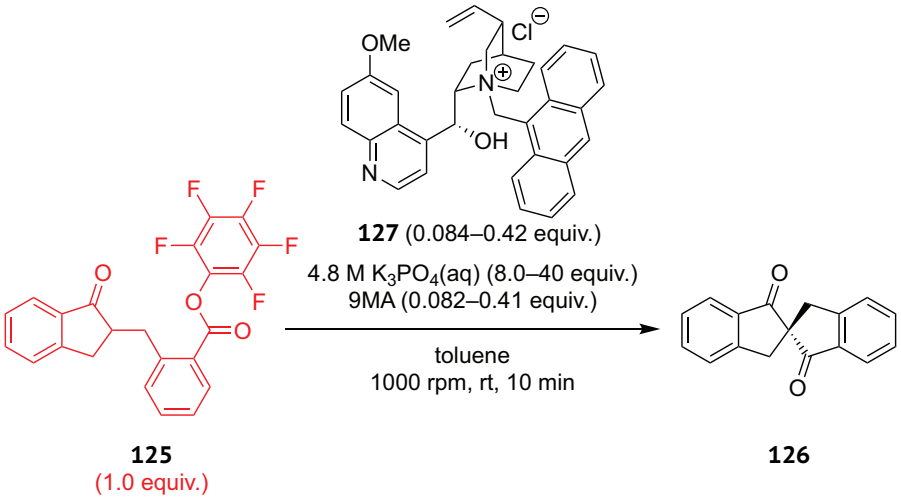

**Figure 3.33: Comparing the rate behaviour for formation of product 126 when carrying out the standard reaction protocol (red) vs the modified reaction protocol (blue).** The standard reaction protocol involves pre-stirring the catalyst with base prior to initiation of the reaction with substrate, the modified reaction protocol involves initiation of the reaction by the addition of base. The lines are linear regression analyses of the corresponding data sets.

Under the standard reaction conditions—initiating the reaction by the addition of substrate after pre-stirring the catalyst with base—the burst phase occurred in << 5 min after initiation and usually within 0.5 min. Under the modified reaction conditions, i.e. initiating the reaction by the addition of base, the burst phase occurred over 5 to 20 min, depending on how much catalyst was used in the reaction (0.10 to 0.30 equiv.). To further investigate the burst phase, we carried out a series of reactions using the modified reaction protocol to ensure we obtained a sufficient amount of data during this initial period.

Whilst it was likely catalyst activation steps were occurring during the burst phase under the modified reaction conditions, we had little experimental information as to what the rate-determining step was. To experimentally explore what might be rate-determining during the burst phase, we first turned our attention to the effect of substrate **125** concentration.

To investigate the role of substrate during the burst phase, we carried out a series of reactions using the modified reaction protocol (see 7.4.2) and varied only the initial substrate **125** concentration (Scheme 3.31). The reactions were monitored for 10 min only following the addition of base to initiate the reactions. Data analyses were carried out only on the burst phase of

each reaction, i.e. before the change in rate was observed, which was usually within 5 min from initiation.




**Scheme 3.31: Conditions evaluating the effect of substrate 125 concentration on the initial rate observed during the burst phase.** Equivalents (equiv.) are reported with respect to substrate **125**. The reactions were carried out using the modified reaction protocol (see 7.4.2) and were monitored for the first 10 min only.

We obtained a small partial negative order with respect to substrate of −0.10 (Figure 3.34), with a 68% confidence interval of −0.13 to −0.074. The small inverse partial order was close to zero, and suggested that the substrate had little effect on the rate of reaction during the burst phase.

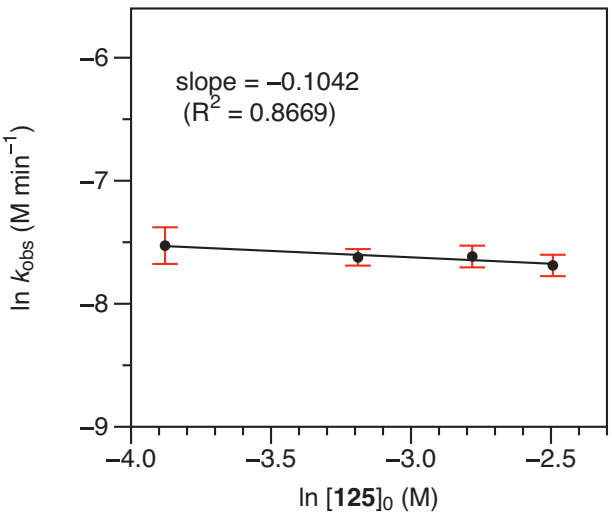



**Figure 3.34: Investigating the effect of substrate on the burst phase.** Double logarithmic plot of initial substrate **125** concentration (ln $[\mathbf{125}]_0$) against observed rate (ln $k_{obs}$) to give the reaction order with respect to substrate **125** of −0.10 under the modified reaction protocol (observing the burst phase during the first 5 min of the reaction).

Previous work by Yufit and Zinovyev found initial burst phase kinetics in solid-liquid phase-

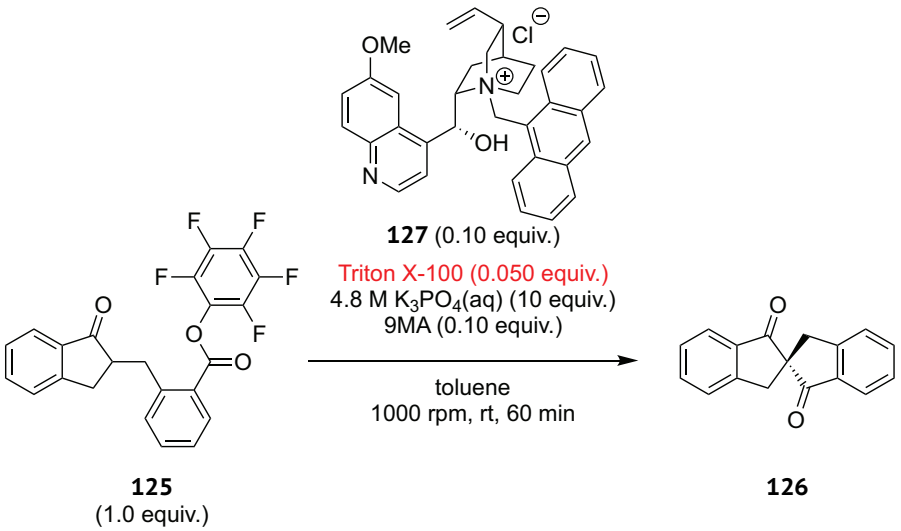
transfer reaction systems.[121,122] The system involved the $S_N2$ reaction of solid KBr with an alkyl mesylate in the presence of an achiral tetraalkyl ammonium salt as the phase-transfer catalyst. The initial burst phase kinetic behaviour was attributed to rapid adsorption and reaction on the surface of the solid KBr. Once the surface of the KBr was contaminated, the number of active sites on the surface was reduced. The change in rate to the "normal phase" of the reaction was obtained when a steady-state was achieved; where the active sites were being occupied and released at the same rate.

During the burst phase of their reaction, the reaction was first order with respect to substrate, and zeroth order during the normal phase.[122] These reaction orders were consistent with their proposed hypothesis that during the burst phase, the intrinsic reaction was dominant and during the steady-state regime, the physical process of surface renewal was rate-limiting.

We hypothesised that the solid-liquid-liquid nature of the reaction mixture and the burst in the formation of product might have been related to the presence of an emulsion that increased the rate. If, in our reaction system, the burst phase was a result of an interfacial or emulsion process, then adding surfactant to the reaction mixtures might perpetuate the burst phase and we would obtain an overall increase in the rate of the reaction.

The use of surfactants to assist enantioselective phase-transfer reactions is known.[123,124] Previous work by Jew and co-workers found addition of a non-ionic surfactant increased both the yield and enantioselectivity of the phase-transfer catalysed epoxidation of *trans*-chalcone.[124] They proposed this was due to the increased interaction of the catalyst with the substrates.

To investigate whether the burst phase was a result of an interfacial process, we carried out the reaction using the modified reaction protocol, with added surfactant: Triton X-100 (Scheme 3.32). This surfactant was previously shown in the literature to increase the rate of reactions effected by cinchona alkaloid-derived phase-transfer catalysts.[123,124]




**Scheme 3.32: Conditions evaluating the effect of added surfactant Triton X-100.** Equivalents (equiv.) are reported with respect to substrate **125**. The reaction was set up according to the modified reaction protocol (see 7.4.2).

When we carried out the reaction with added surfactant, we observed no change in the burst phase when comparing the results to an appropriate control (Figure 3.35). The burst phase rate and duration was identical to the reaction in the absence of surfactant. However, we observed a slight increase in the rate during the normal phase relative to the reaction without added surfactant.

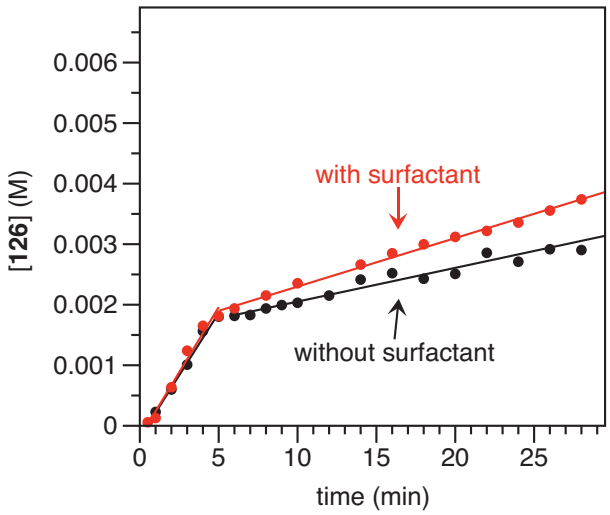


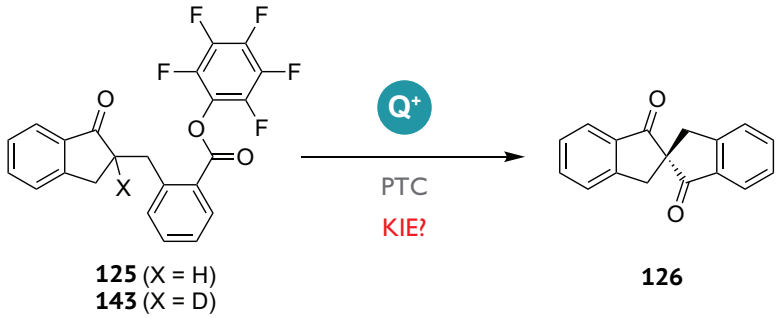

**Figure 3.35: Overlay of results comparing the rate of formation of product over time using the modified reaction protocol with or without added surfactant.** The $x$-axis corresponds to time following initiation of the reaction by the addition of base; the $y$-axis corresponds to concentration of product **126** in the reaction mixture. The red data corresponds to the reaction carried out with added Triton X-100, and the black data corresponds to the control reaction which was carried out analogously in the absence of Triton X-100. The lines are linear regression analyses of the rate-limiting regimes, the slopes of which gave the observed rates in both data sets (see Figure 7.36).

The result suggested that the burst phase was *not* due to an emulsion- or interfacial-promoted process. It was probable that the rate-limiting regime in the burst phase was related to an intrinsic process, potentially deprotonation of the catalyst scaffold to generate the zwitterion **140**.

Whilst the results did not provide much insight into what was occurring in the burst phase, they suggested the rate-limiting regime in the normal phase was indeed via an interfacial process. The increase in the rate was presumably correlated to an increase in the area of the interfacial region, which promoted the interfacial rate-determining step.

## 3.12 Isotope effects

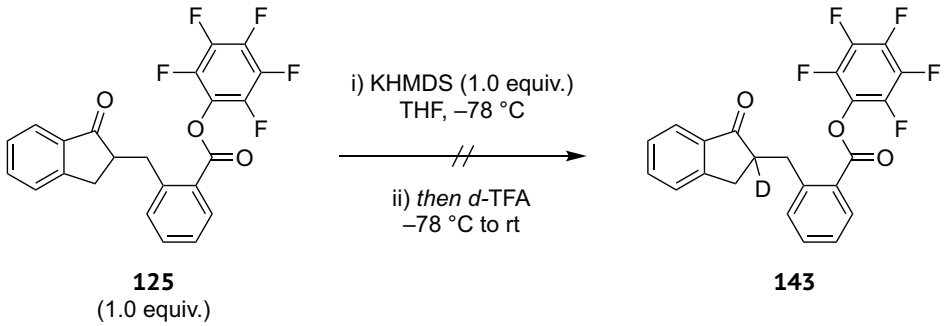
To further explore the reaction system, we looked to evaluate isotope effects by subjecting an $\alpha$-deuterated substrate **143** to the reaction conditions (Scheme 3.33). By comparing the rate of reaction of $\alpha$-deuterated substrate **143** to substrate **125**—i.e. evaluating the ratio of rates between the hydrogenated substrate against the deuterated substrate to obtain the kinetic isotope effect (KIE)—we might obtain further information as to what the rate-determining step in this system might be.




**Scheme 3.33: Ideal substrate and experiment to evaluate isotope effects in the PTC reaction system.** Q+ corresponds to the chiral quaternary ammonium ion catalyst.

We first required access to $\alpha$-deuterated substrate **143**. Ideally, we would deprotonate the substrate **125** and quench the formed enolate with a source of deuterium e.g. $CF_3CO_2D$ (*d*-TFA).

Unfortunately, attempts to synthesise the deuterated substrate **143** via this strategy did not give the desired result (Scheme 3.34); instead, the result was cyclisation to give product **126** (confirmed by TLC). A repeat reaction was carried out to evaluate whether cyclisation occurred before the addition of *d*-TFA and warming the reaction mixture to rt. It appeared that in the presence of base, even at −78 °C, cyclisation occurred. In our hands, attempts to deprotonate the substrate under homogenous conditions resulted in formation of the cyclised product **126**. Therefore, to obtain $\alpha$-deuterated material, we required a different strategy.



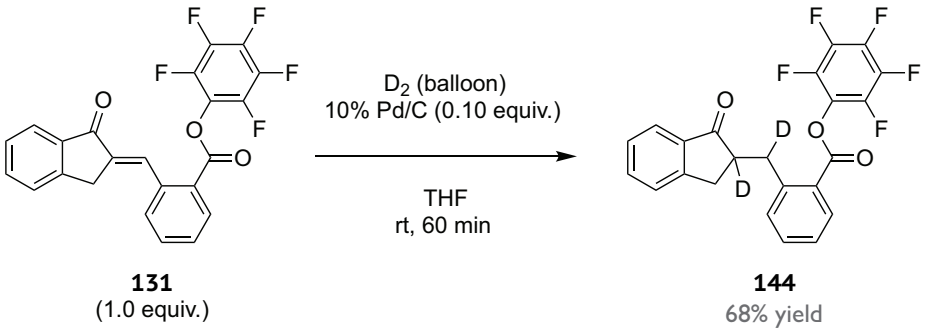

**125**
(1.0 equiv.)

**143**

**Scheme 3.34: Attempt to obtain $\alpha$-deuterated substrate 143.** Equivalents (equiv.) are reported with respect to substrate **125**.

The model substrate in this project was synthesised in the final step via hydrogenation of the corresponding unsaturated intermediate **131** (C, Scheme 3.3). To obtain the $\alpha$-deuterated substrate we thought we could use analogous conditions; i.e. using $D_2$ instead of $H_2$ in the reduction of intermediate **131**.

Synthesis of the deuterated substrate via this route, and all optimisation required, was carried out by AM. After modification of the previous reaction conditions, we were able to obtain the deuterated substrate **144** as a 1:1 mixture of diastereomers in 68% yield with 60% deuteration at the position alpha to the ketone and 40% (total) at beta (Scheme 3.35).




**131**
(1.0 equiv.)

**144**
68% yield

**Scheme 3.35: Reaction to obtain $\alpha$-deuterated substrate 144.** Equivalents (equiv.) are reported with respect to substrate **131**. The product **144** was obtained in 68% yield with 60% deuterium at alpha and 40% (total) at beta.

As expected, the diastereomeric mixture of **144** behaved identically to substrate **125** under our HPLC conditions (Figure 3.36); we therefore treated it analogously for the purposes of our assay (both by HPLC and calculations of amounts in reaction mixtures).

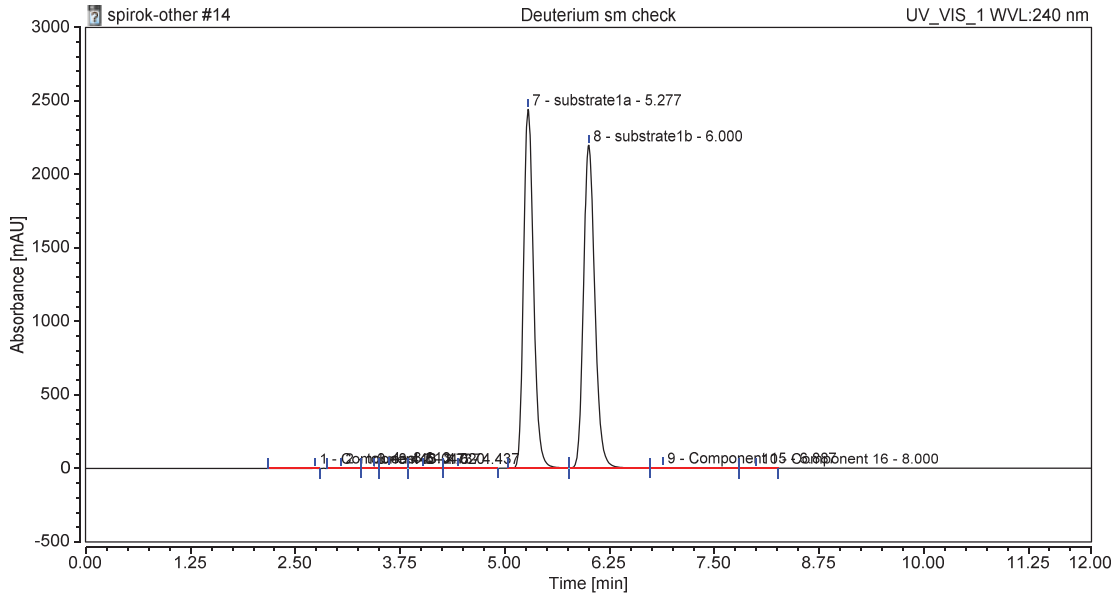
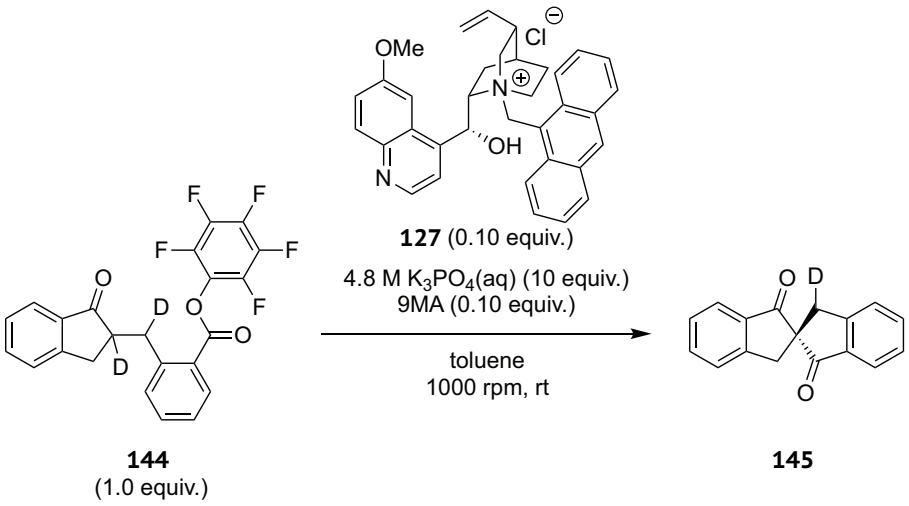



**Figure 3.36: HPLC chromatogram of $\alpha$-deuterated substrate 144.** Only two peaks were observed, which corresponded to the stereoisomers arising from the stereogenic centre alpha to the ketone with the same retention times as the enantiomers of substrate **125** (compare to Figure 3.3). The diastereomers arising from the stereogenic centre beta to the ketone co-eluted with the aforementioned isomers. The $x$-axis represents retention time; the $y$-axis is UV absorption at the extracted wavelength of 240 nm.

We next subjected deuterated substrate **144** to the reaction conditions using the standard reaction protocol (Scheme 3.36). When we plotted the total concentration of product over time, we found that compared to the hydrogenated system, the reaction exhibited a change in

the burst phase, and a slight decrease in the overall observed rate (Figure 3.37). Taking the mean rates of reaction from both hydrogenated and deuterated systems of $6.21 \times 10^{-5}$ M min$^{-1}$ and $4.15 \times 10^{-5}$ M min$^{-1}$, respectively, we obtained a KIE value of 1.50.




**Scheme 3.36: Conditions evaluating the effect of deuterated substrate 144.** Equivalents (equiv.) are reported with respect to substrate **144**. The amount of $\beta$-deuteration in the substrate **144** was 40% and in the product **145** was 20%.

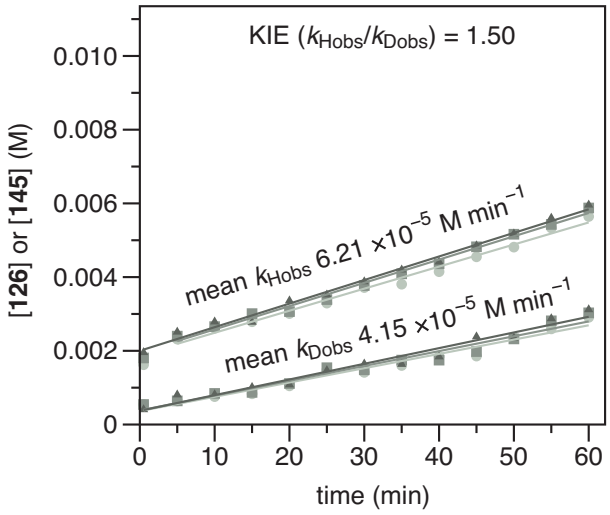



**Figure 3.37: Overlay of data obtained from the hydrogenated and deuterated reaction systems using the standard reaction protocol.** The $x$-axis corresponds to time following initiation of the reactions; the $y$-axis corresponds to the concentration of product—either **126** or **145**—depending on which substrate was used. The light grey circles, grey squares, and dark grey triangles correspond to individual reactions within the two triplicate sets. The lines correspond to linear regression analyses of each reaction and are indicated by the location and colour of the line. The mean rates of reaction obtained for the hydrogenated ($k_{\mathrm{Hobs}}$) and deuterated ($k_{\mathrm{Dobs}}$) systems are indicated on the graphs. The calculated KIE based on these mean rates was 1.50 (to 3 sf).

The ee of the product mixture exhibited unusual kinetic behaviour over the period that we monitored the reaction (A, Figure 3.38). Across the triplicate experiments using substrate **144**,

the quaternary stereocenter of the product **145** showed an increase in ee over time, however the overall ee was less than that obtained with the hydrogenated system (B, Figure 3.38).

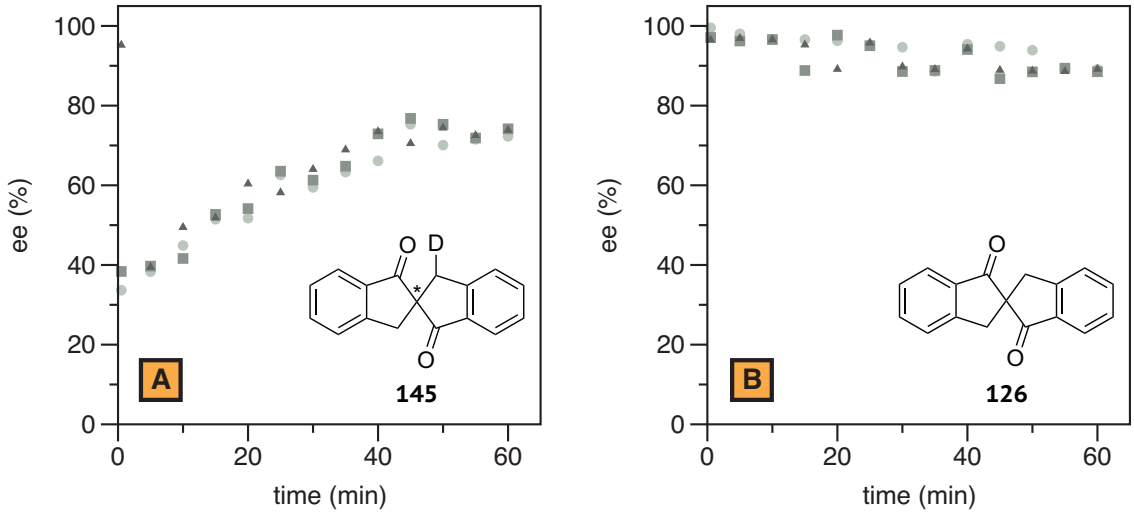



**Figure 3.38: Enantiomeric excess of the product over time in the A) deuterated and B) hydrogenated systems.** The $x$-axes correspond to time following initiation of the reactions; the $y$-axes correspond to ee of the products shown in each graph. The light grey circles, grey squares, and dark grey triangles correspond to individual reactions within the triplicate set. Complementary conversion data are shown in Figure 3.37. The shapes and colours correspond to analogous data sets.

The exact distribution of all stereoisomers was not known due to co-elution of the isomers by HPLC with respect to the stereogenic centre beta to the carbonyls, and thus, interpretation of the ee results must be with caution. Tentatively, it appeared the additional deuterium present at the beta position interfered with the interaction of the catalyst scaffold, which decreased the overall ee of the product mixture. The change in ee over time suggested that the interaction of the formed enolate with the catalyst scaffold was changing over time.

To further investigate the diastereoisomerism of the product, we subjected substrate **144** to the reaction conditions for 48 h to obtain more product for isolation. This experiment was carried out by AM. The 40% deuteration of the beta position of substrate **144** was fully retained in the isolated product, which was obtained as a 1:1 mixture of diastereomers (by $^{1}$H-NMR spectroscopy).

When we subjected deuterated substrate **144** to the reaction conditions using the modified reaction protocol, again we found a change in the burst phase and an overall decrease in the

observed rate. As the reactions carried out using the modified protocol were single experiments, we were only able to obtain approximate KIE values for the two rate-limiting regimes that were evident: for the burst phase, we observed a KIE of approximately 2.3, and for the normal phase, a KIE of approximately 2.4. Again, as the modified reactions were carried out as single experiments, the KIE value of 2.4 obtained for the normal phase of the reaction remained comparable to the value of 1.5 that we obtained when evaluating the reaction using the standard reaction protocol.

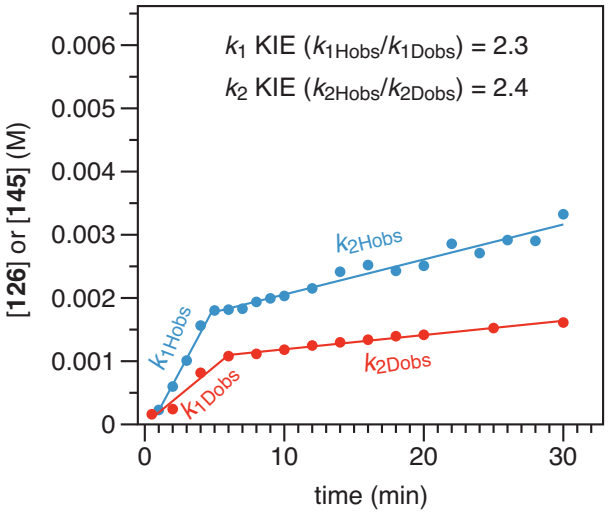
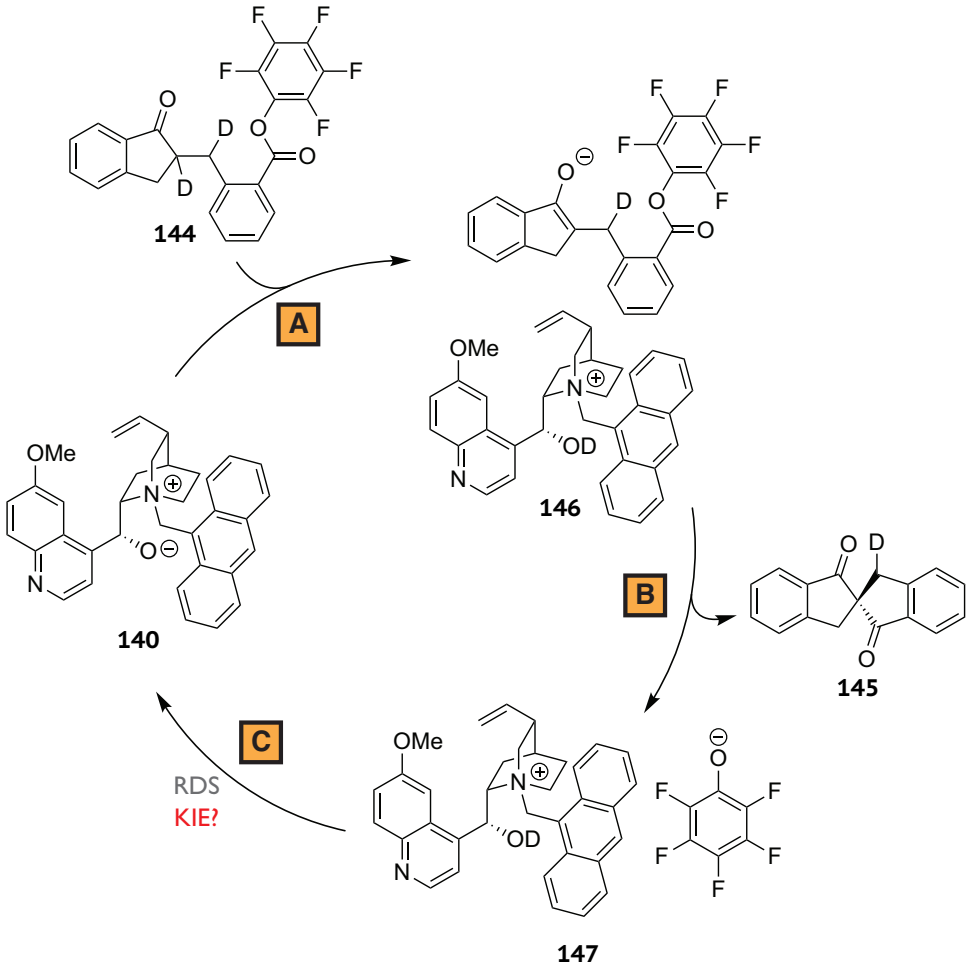



**Figure 3.39: Overlay of data obtained from the hydrogenated and deuterated reaction systems using the modified reaction protocol.** The $x$-axis corresponds to time following initiation of the reactions; the $y$-axis corresponds to the concentration of product—either **126** or **145**—depending on which substrate was used. The blue data correspond to the hydrogenated system and the red data correspond to the deuterated system. The lines are linear regression analyses of the burst (i.e. $k_1$) and normal (i.e. $k_2$) phases of the reaction and correspond to the rates obtained for those regimes. The following values were obtained: $k_{1Hobs} = 4.1 \times 10^{-4}$ M min$^{-1}$; $k_{2Hobs} = 5.5 \times 10^{-5}$ M min$^{-1}$; $k_{1Dobs} = 1.8 \times 10^{-4}$ M min$^{-1}$; $k_{2Dobs} = 2.3 \times 10^{-5}$ M min$^{-1}$.

The observed isotope effect values of 1.5, 2.3, and 2.4 were complicated by the 60% α-deuteration (as opposed to >95%). This meant that if deprotonation was rate-determining in this system, we might be observing values that were lower in magnitude than would be expected given a primary kinetic isotope effect. Alternatively, we were observing equilibrium isotope effects preceding the rate determining step in our system, which resulted in an overall diminished rate with the deuterated substrate.

Another hypothesis for the origin of the KIE involved deuteration of the catalyst scaffold. In the

process of deprotonating the substrate **144**, the catalyst would be deuterated (A, Scheme 3.37). Cyclisation of the ammonium enolate intermediate **146** would occur to generate the product **145** and the deuterated ammonium phenolate **147** (B, Scheme 3.37). The KIE that we were observing may have been a result of deprotonation of the deuterated catalyst intermediate **147** in the proposed rate-determining step (C, Scheme 3.37); the smaller than expected primary KIE effect (i.e. 1.5 vs 4 to 6) may be due to some exchange of O−D for O−H under the reaction conditions.




**Scheme 3.37: The potential for deuteration of the catalyst scaffold during the reaction. A)** Deprotonation of substrate **144** to generate the deuterated ammonium enolate complex **146**; **B)** cyclisation to generate product **145** and deuterated ammonium phenolate **147**; **C)** deprotonation of deuterated ammonium phenolate **147** to regenerate the zwitterion **140** in a proposed rate-determining step (RDS).

However, we expected that exchange of O−D for O−H would occur rapidly and completely under the biphasic reaction conditions. To fully investigate the potential of catalyst deuteration

to influence the obtained KIE we would need to synthesise deuterated ammonium phenolate **147**, evaluate it under the reaction conditions, compare it to an appropriate hydrogenated system then determine the KIE. These experiments remain the subject of future work.

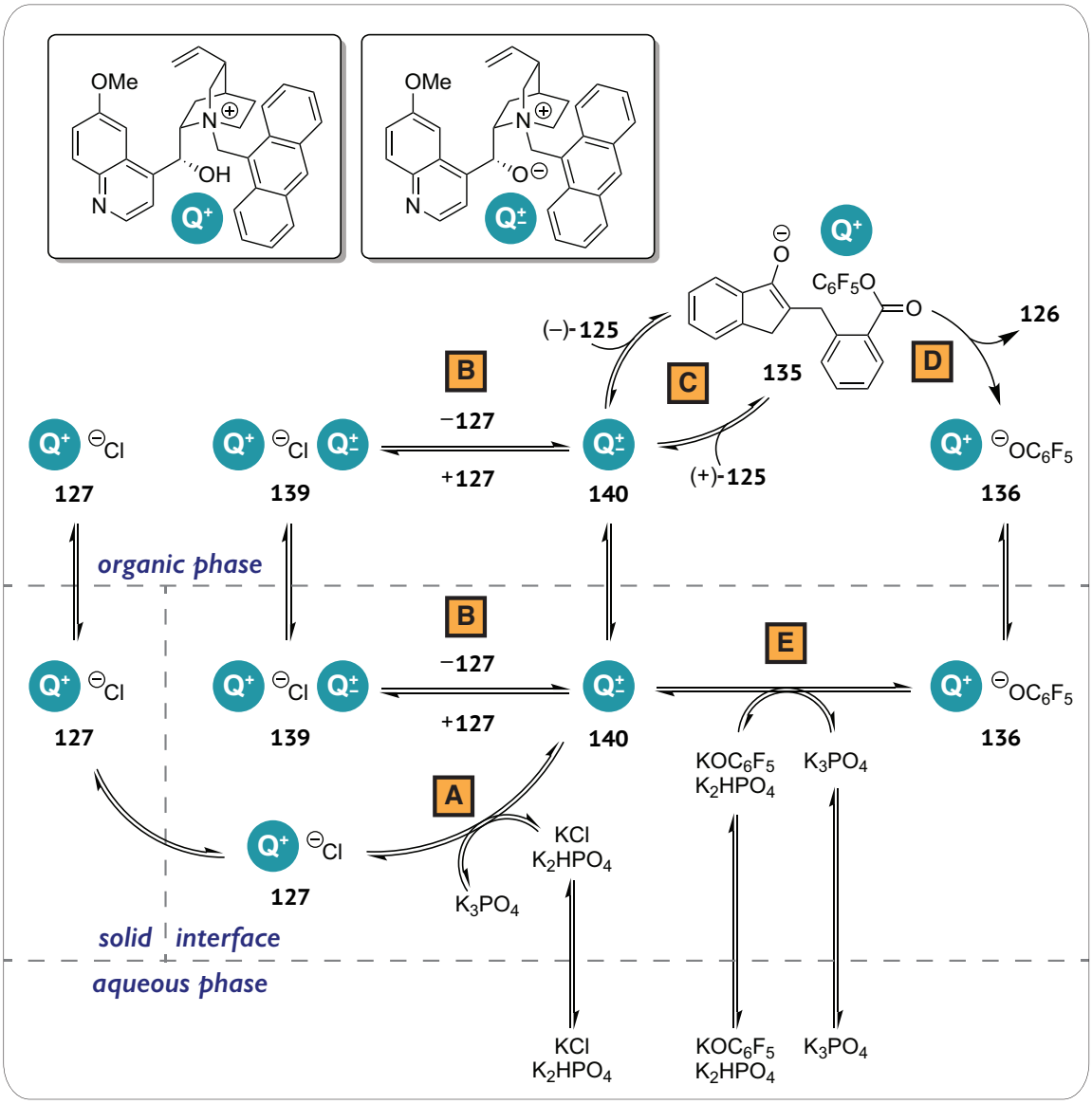
Despite these speculations, a definitive explanation for the origin of the KIE when subjecting $\alpha$-deuterated substrate **144** to the reaction conditions remained elusive at this time. The diastereomeric mixture of the substrate made for challenging analysis of results; there was potential for the contribution of small secondary isotope effects, both normal and inverse, based on the 40% deuteration of the beta position of the substrate.

## 3.13 Further revision of the mechanistic hypothesis

The latest results indicated the majority of our working hypothesis was consistent with what we observed experimentally. It was likely that during the pre-stirring protocol, we were generating a highly active species: zwitterion **140**. On addition of the substrates (−)-**125** and (+)-**125** as a racemic mixture, the zwitterion was quickly turned over facilitating generation of product **126** and **136**. Once the product was generated and the pool of zwitterion consumed, the reaction effectively reached a steady state, where the majority of the catalyst was sequestered as ammonium phenolate **136**. Turn over from this species to the zwitterion **140** was the proposed rate-determining step. Any equilibria between the zwitterion **140**, the dimer **139** and the phenolate **136** lay heavily towards phenolate **136** and the presence of chloride facilitated sequestration of some of the catalyst (possibly as inactive dimer **139** with another equivalent of halide salt **127**).

Further examination of the hypothesis revealed that formation of the zwitterion likely did not proceed via the dimer as was depicted in Scheme 3.19 and Scheme 3.20. A more plausible mechanism was that deprotonation of the halide salt **127** occurred to generate the zwitterion **140**, which *then* formed the inactive dimer **139**.

Our developing mechanistic hypothesis now first involved formation of the zwitterion **140** from halide salt **127** (A, Scheme 3.38). The zwitterion was in equilibrium with the halide salt **127** and the inactive dimer **139** (B, Scheme 3.38). On addition of the substrate (a racemic mixture of (−)-**125** and (+)-**125**), deprotonation to form the ammonium enolate **135** occurred (C, Scheme 3.38). Next, was cyclisation to give the product **126** and ammonium phenolate **136** (D, Scheme 3.38). The rate-determining step was regeneration of the zwitterion **140** from ammonium phenolate **136** in a process mediated by base (E, Scheme 3.38).

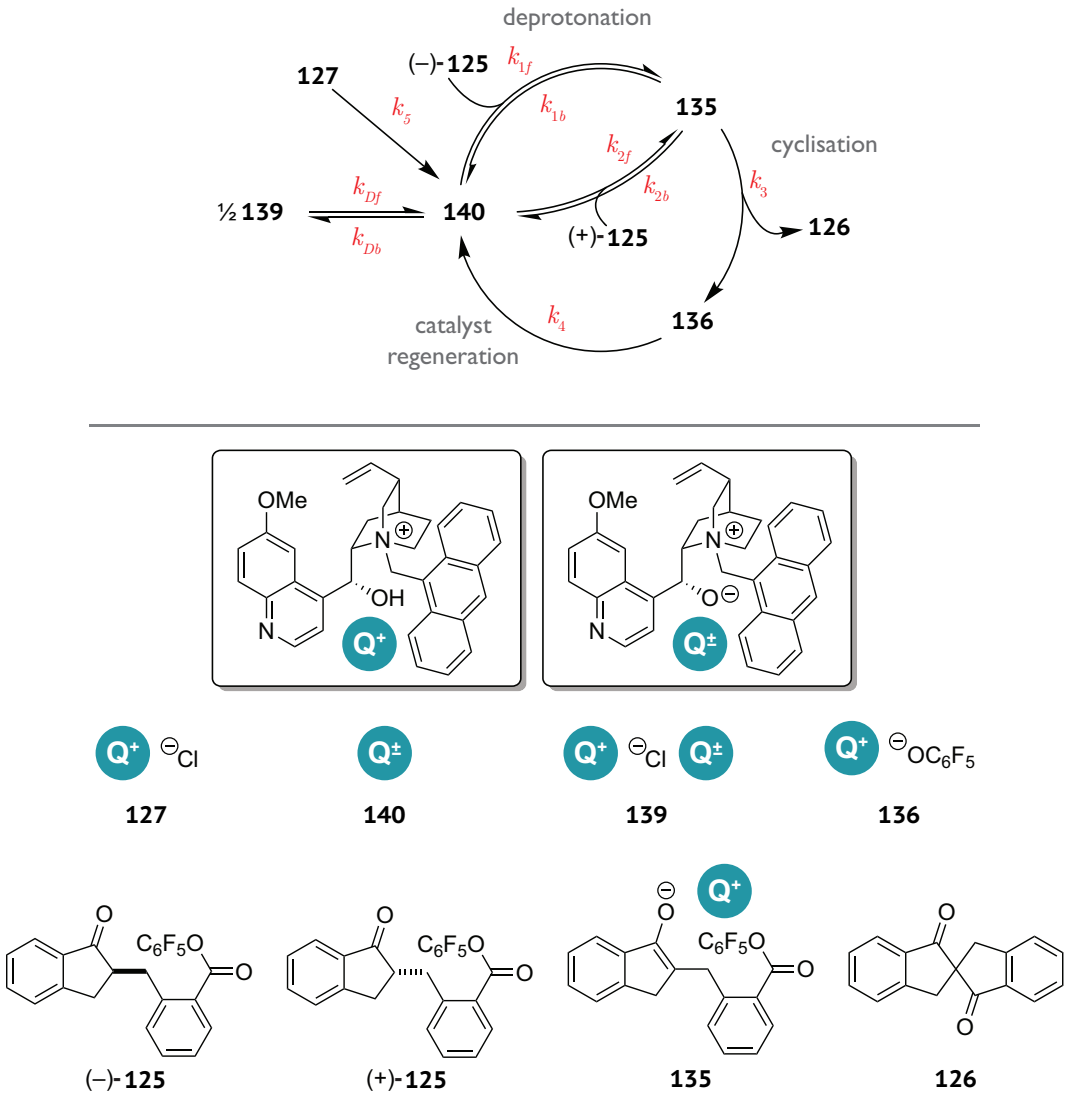



**Scheme 3.38: Developing mechanistic hypothesis. A)** Generation of the active zwitterion **140** from halide salt **127** in a process mediated by $K_3PO_4$; **B)** equilibrium between zwitterion **140** and inactive dimer **139**; **C)** deprotonation of substrates (−)-**125** and (+)-**125** to generate the common ammonium enolate complex **135**; **D)** cyclisation to generate product **126**; **E)** $K_3PO_4$-mediated regeneration of the active zwitterion **140** from ammonium phenolate **136**.

### 3.13.1 Refining the theoretical model

Throughout the acquisition of additional experimental data, we concurrently evaluated working iterations of the theoretical model. One significant change arose from the results obtained when deploying phenolate **136** as the initial catalyst. If, in the theoretical model (described by Scheme 3.22), we started the catalytic cycle from **136**, applying the correction factor of approximately 0.3 (catfactor) resulted in vast underestimations of the observed rates. To try and rationalise this disparity when commencing the reaction from different points in the catalytic cycle, we needed to alter the initial steps in the theoretical model.

We thus amended the model to reflect our latest hypothesis and experimental protocols (according to Scheme 3.39). This involved introducing steps that reflected what might be occurring during the pre-stirring period. The catalyst, under phase-transfer reaction conditions in the absence of substrate, was distributed from the halide salt **127** to the zwitterion **140** and dimer **139**. On the addition of substrate at the designated time, the reaction was initiated and conversion to product occurred. The catalytic cycle was closed by a single step: formation of the active zwitterion **140** directly from the ammonium phenolate **136**. For the moment, the dimerisation of the catalyst was described analogously to that previously (see Scheme 3.22).




**Scheme 3.39: Schematic used to evaluate the reaction system numerically using Mathematica (model 5).** The red labels correspond to the rate constants for the associated steps.

The exact role of the base in the reaction was not yet fully understood. It was likely required in the formation of active zwitterion **140** from the halide salt **127**, and regeneration of **140** from the ammonium phenolate **136**. However, the half-order value obtained experimentally (see 3.10.2 and Figure 3.32) suggested that additional steps may be necessary in these particular processes. In the developing theoretical model, we removed it from the calculations for simplification and better fitting of the model output to the experimental data.

By fitting the model to a selection of experiments, we were able to extract rate constants for the proposed steps (Table 3.2). Again, deprotonation of the substrate and subsequent cyclisation were not rate-determining. Equilibrium between the zwitterion **140** and dimer **139** lay heavily

toward the dimer. The rate-determining steps involved deprotonation of the catalyst, either from halide salt **127** or the ammonium phenolate **136**.

**Table 3.2: Parameters obtained from fitting the theoretical model (model 5 according to Scheme 3.39) to selected experimental data.** Data are reported to three significant figures.

| Entry | Parameter | Value | Event |
|---|---|---|---|
| 1 | $k_{Df}$ | 0.200 $M^{-1}$ $min^{-1}$ | catalyst monomerisation |
| 2 | $k_{Db}$ | 20.0 $min^{-1}$ | catalyst dimerisation |
| 3 | $k_{1f}$ | 30.5 $M^{-1}$ $min^{-1}$ | deprotonation |
| 4 | $k_{1b}$ | 0.00 $min^{-1}$ | reprotonation |
| 5 | $k_{2f}$ | 55.8 $M^{-1}$ $min^{-1}$ | deprotonation |
| 6 | $k_{2b}$ | 0.00 $min^{-1}$ | reprotonation |
| 7 | $k_3$ | 355 $min^{-1}$ | cyclisation |
| 8 | $k_4$ | 0.00455 $min^{-1}$ | catalyst regeneration |
| 9 | $k_5$ | 0.00424 $min^{-1}$ | catalyst deprotonation |
| 10 | $k_z$ | 0.000350 $M^{-1}$ $min^{-1}$ | background reaction |

Using the latest model, we were able to visualise the distribution of all proposed catalyst species during the pre-stirring period and during the reaction of substrate **125** (for example in A, Figure 3.40). At the very start of the pre-stirring protocol, all of the catalyst was present as the halide salt **127**. As the pre-stirring continued, the catalyst existed as the halide salt **127**, and increasingly as the zwitterion **140** and dimer **139**. On addition of the substrate **125**, the catalyst zwitterion **140** was rapidly converted, and the ammonium phenolate **136** concentration increased. Interestingly, consumption of the halide **127** continued as the reaction progressed. Throughout all processes, the concentration of ammonium enolate **135** was negligible.

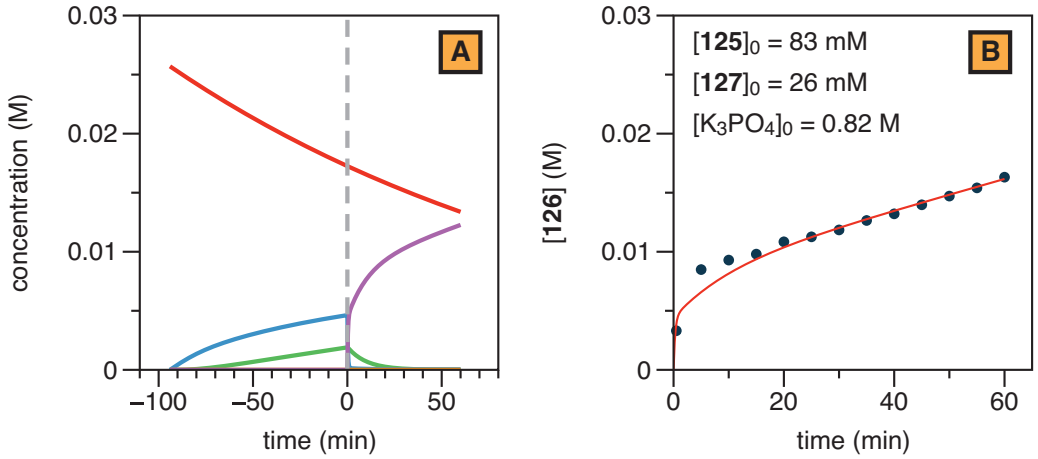



**Figure 3.40: Example of the model output for one experiment (spirok-12 replicate 1).** In both graphs, the $x$-axes correspond to time before and after initiation of the reaction at 0 min, the $y$-axes correspond to concentration. All lines correspond to the output from the theoretical model. **A)** The data correspond to the concentration of catalyst species as follows: halide salt **127** (red), dimer **139** (green), zwitterion **140** (blue), ammonium enolate **135** (orange), and ammonium phenolate **136** (purple). **B)** The data correspond to the concentration of product **126** over time, both experimentally (dots) and theoretically (red line); the initial reaction conditions are detailed on the graph.

Practically, we carried out the pre-stirring protocol over a period of 30 min interspersed with regular treatments of the catalyst mixture in an ultrasound bath. To compensate, the theoretical pre-stirring period was set to be 94 min, which resulted in good agreement between the output and a number of the experimental results (for example in B, Figure 3.40).

The latest model (model 5) showed reasonable graphical agreement with a number of different experiments (Figure 3.41). The rates of formation of product—observed as a result of the changes in initial total catalyst concentration commencing from halide salt **127**—were well predicted (B in Figure 3.40, and A and B, Figure 3.41). Low initial substrate concentration was similarly in good agreement (C, Figure 3.41). However, once again, the model over-predicted the rate when examining the reaction at higher initial substrate concentrations (D, Figure 3.41).

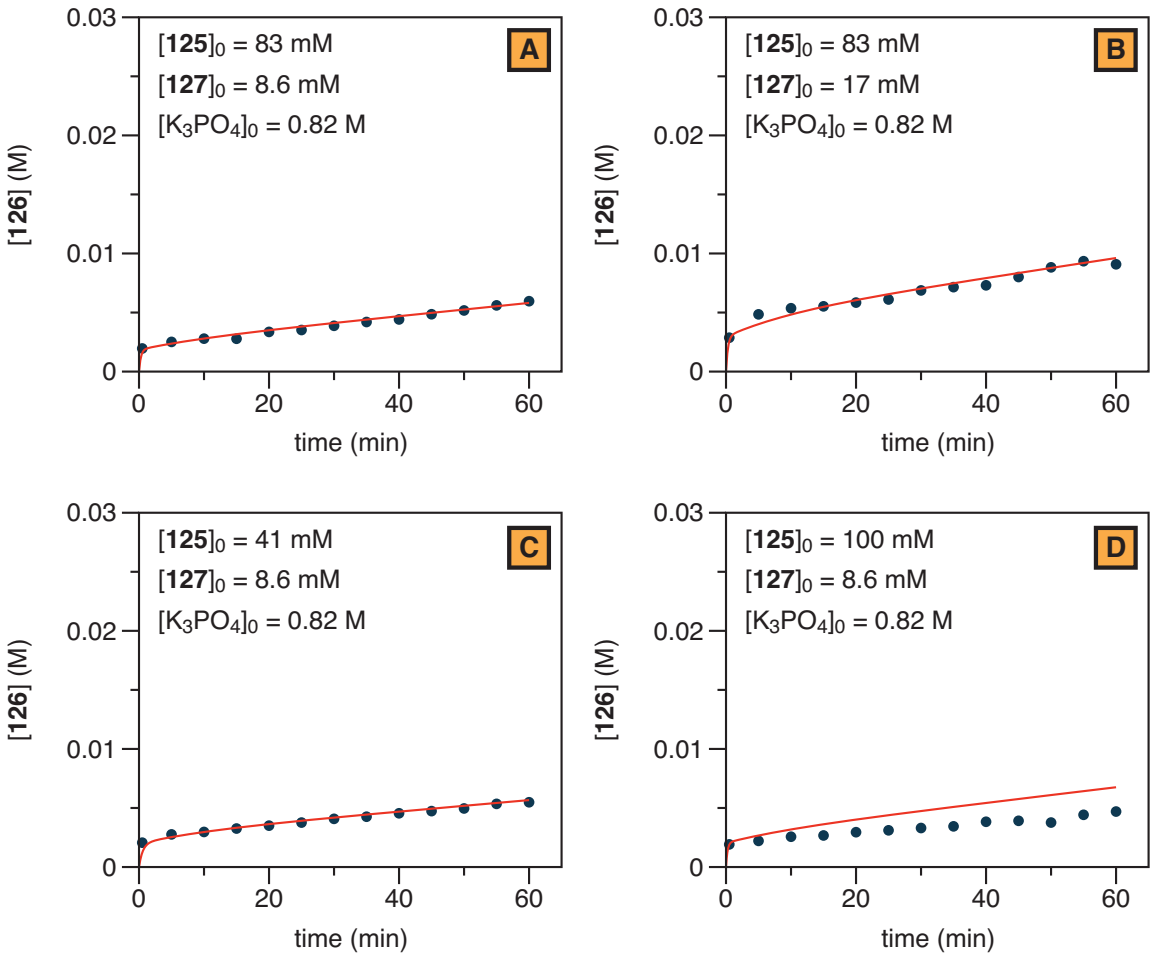



**Figure 3.41: Selected examples of model 5 (described by Scheme 3.39 and Table 3.2) against experimentally acquired results.** Each example corresponds to different initial reaction conditions (to 2 sf), which are indicated on each graph as the total initial concentration in the whole reaction system (both organic and aqueous layers). The data sets have the designated reaction codes (*rxn.code*) as follows: **A)** spirok-35 replicate 3; **B)** spirok-7 replicate 1; **C)** spirok-16 replicate 3; **D)** spirok-14 replicate 2. All examples were carried out according to the standard reaction protocol, with a reaction stirring speed of 1000 rpm, and stock concentrations of $K_3PO_4$(aq) of 4.77 M. In all graphs, the dots correspond to data that was acquired experimentally, and the red lines correspond to the model described by Scheme 3.39 and Table 3.2. The $x$-axes correspond to time following initiation of the reaction, the $y$-axes correspond to the concentration of product **126**.

We could also remove the pre-stirring period, commence the reaction using all of the initial catalyst as the ammonium phenolate **136**, and evaluate the result (Figure 3.42). The burst phase in both theoretical and experimental data was absent, with good graphical overlay between the two results, albeit with a slight underestimation by the model at increasing time.

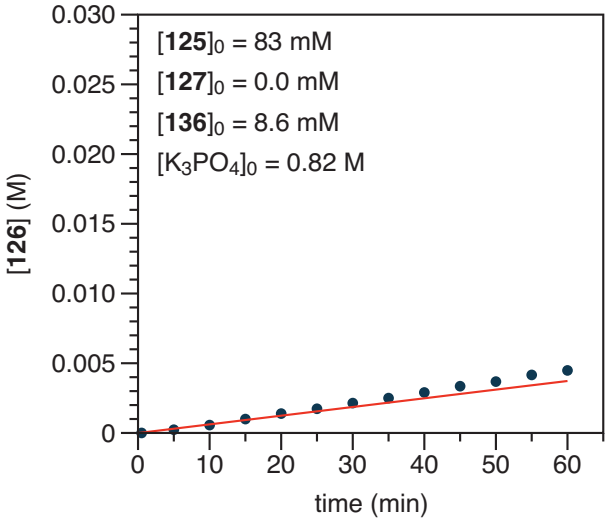



**Figure 3.42: Comparing the model (model 5 according to Scheme 3.39 and Table 3.2) output when commencing the reaction from ammonium phenolate 136.** The initial reaction conditions are indicated on the graph (to 2 sf); the values are of the total initial concentration in the whole reaction system (both organic and aqueous layers). The data are from the reaction code: spirok-41 replicate 1. The example was carried out according to the modified reaction protocol, with a stirring speed of 1000 rpm, and a stock concentration of $K_3PO_4$(aq) of 4.77 M. The dots correspond to data that was acquired experimentally, the red line corresponds to the model output. The $x$-axis corresponds to time following initiation of the reaction, the $y$-axis corresponds to the concentration of product **126**.

The latest theoretical pre-stirring model was producing adequate results. As such, we began finalising the overall model considering the hypothesis revisions we had devised thus far, in addition to *all* of the experimental data we had acquired. To do this there were several key results we needed to re-examine and with which the model must fit.

The first result that we wanted to address was the role of base in the reaction system. Because base species ($K_3PO_4$, $K_2HPO_4$, etc) were not included in the previous model (model 5, described by Scheme 3.39), comparison of the output of that model to the any of the reactions that evaluated the effect of initial $K_3PO_4$(aq) concentration (i.e. results described in 3.7.4, 3.10.2 and Figure 3.32) was a meaningless exercise. Before reintroducing base into the kinetic model, we needed to consider the origin of the half-order value that we obtained experimentally.

We hypothesised that the rate-determining steps in our reaction involved either generation or regeneration of an active catalyst species in a process that was mediated by base, in this case, $K_3PO_4$. Thus far, when including $K_3PO_4$ in our calculations, we had all catalyst salt

deprotonation steps as direct processes (for example **127** + $K_3PO_4$ $\longrightarrow$ **140**, without even considering the other byproducts: KCl and $K_2HPO_4$). Chemically, there are multiple ions that must coordinate and dissociate to give intermediate species. A half-order value with respect to base may be explained by a two-step process with the limiting factor involving a disassociated species. The derivation will be described below.

Consider the transformation below, where $A$ corresponds to an intermediate, for example **136**, and $B$ corresponds to the base (equation 3.29); $C$, $E$, and $F$ correspond to the products $K_2HPO_4$, $KOC_6F_5$, and **140**, respectively.

$$A + B \longrightarrow C + E + F \tag{3.29}$$

The mechanism proceeds via two steps described by equations 3.30 and 3.31. The equilibrium constant for equation 3.30 is $K$ and the rate constant for the second step, equation 3.31 is $k$. In this scenario, the process in equation 3.30 is fast, and equation 3.31, described by the rate constant $k$ is slow and rate-determining.

$$A + B \overset{K}{\rightleftharpoons} C + D \tag{3.30}$$

$$D \overset{k}{\longrightarrow} E + F \tag{3.31}$$

The overall rate may be described by equation 3.32:

$$\text{rate} = k[D] \tag{3.32}$$

However, the equilibrium in equation 3.30 gives:

$$K = \frac{[C][D]}{[A][B]} \tag{3.33}$$

But:

$$[C] = [D] \tag{3.34}$$

Hence:

$$\begin{aligned} K &= \frac{[D]^2}{[A][B]} \\ D &= \sqrt{K[A][B]} \end{aligned} \tag{3.35}$$

Therefore using equation 3.35 and 3.32:

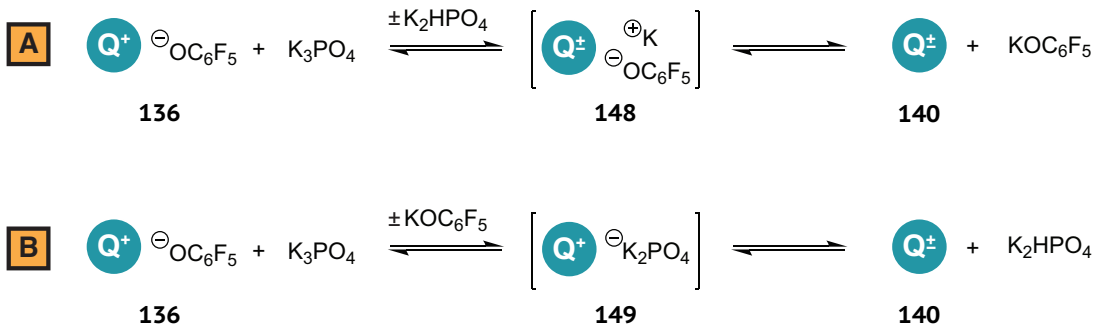
$$\text{rate} = k\sqrt{K}[A]^{\frac{1}{2}}[B]^{\frac{1}{2}} \tag{3.36}$$

Thus, in the overall system described by 3.29, the reaction order with respect to both $A$ and $B$ are expected to be 0.5 (equation 3.36).

Considering the general processes described by equations 3.30 to 3.31, we applied them to the appropriate steps within our reaction: formation of zwitterion **140**, which occurred during the pre-stirring protocol or the burst phase of the reaction, and regeneration of the zwitterion from the ammonium phenolate.

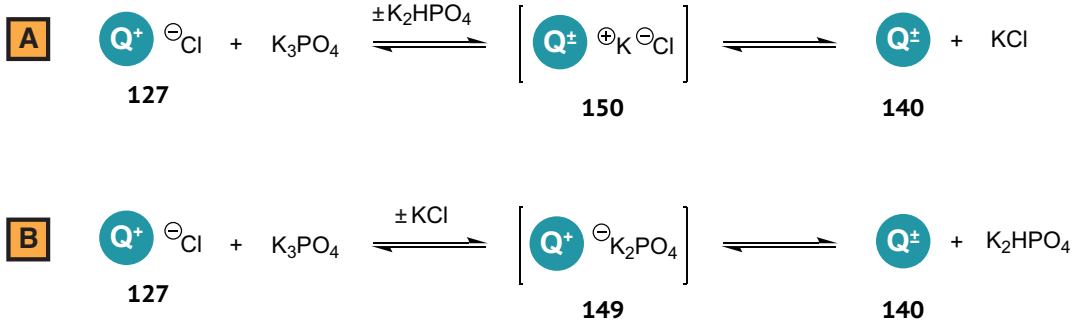
As the presumed rate-determining transformation, we first examined the two-step process occurring in the reaction of ammonium phenolate **136** with $K_3PO_4$ (Scheme 3.40). One potential pathway involved the deprotonation of ammonium phenolate **136** to form com-

plex **148**, followed by slow dissociation to generate zwitterion **140** and potassium 2,3,4,5,6-pentafluorophenolate (A, Scheme 3.40). Another involved metathesis of the phenoxide counterion with dipotassium phosphate liberating $KOC_6F_5$, followed by deprotonation of the ammonium scaffold as **149** to generate zwitterion **140** and $K_2HPO_4$ (B, Scheme 3.40).




**Scheme 3.40: Potential pathways for the rate-determining regeneration of zwitterion 140 from ammonium phenolate 136. A)** Pathway proceeds via deprotonation of the catalyst scaffold to generate intermediate **148** followed by dissociation of the salt to generate zwitterion **140** and $KOC_6F_5$. **B)** Pathway proceeds via metathesis to generate base-coordinated intermediate **149** followed by deprotonation of the scaffold to give zwitterion **140** and dibasic potassium phosphate.

In the initial formation of zwitterion **140** from the halide salt **127**, analogous steps were considered (Scheme 3.41). These included either formation of the zwitterion-KCl salt **150** first, followed by dissociation (A, Scheme 3.41) or coordination of the phosphate to give **149** before deprotonation occurred (B, Scheme 3.41).

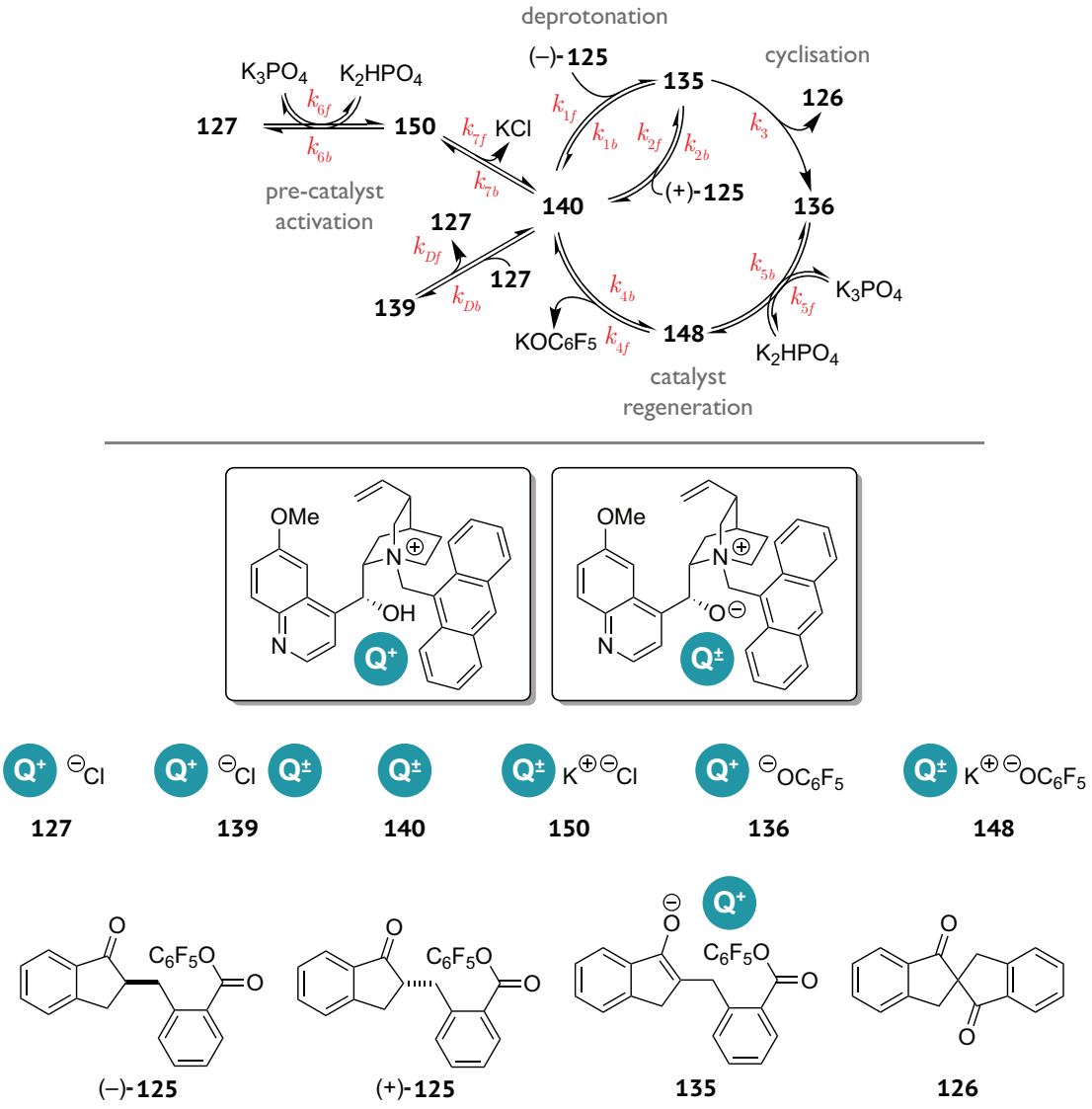



**Scheme 3.41: Potential pathways for the generation of zwitterion 140 from halide salt 127.** Both **A** and **B** proceed via the analogous intermediates described in Scheme 3.40, however commencing from halide salt **127**.

Because we observed negligible effect of added KCl on the reaction (see 3.10.1), and given the remarkable acidity of the secondary alcohol on the catalyst scaffold (p$K_a$ 16.3 in DMSO), deprotonation of the catalyst might be preferable to metathesis. Hence, we operated under

the assumption that pathway A in both scenarios (Scheme 3.40 and Scheme 3.41) was in operation.

When updating the working theoretical kinetic model, the different potential pathways (A and B in both Scheme 3.40 and Scheme 3.41) were mostly interchangeable. However, for consistency, only pathway A will be depicted. The model was thus constructed according to Scheme 3.42, with the included options of the pre-stirring protocol and/or commencing the reaction using **136** as the initial catalyst species. In an attempt to fully describe the reaction, the concentration of byproducts and basic species (e.g. $K_3PO_4$, $K_2HPO_4$, KCl etc) were now included in the numerical evaluation.




**Scheme 3.42: Schematic used to evaluate the reaction system numerically using Mathematica (model 6).** The red labels correspond to the rate constants for the associated steps.

We were particularly interested in how the catalyst was being transformed during the pre-reaction protocol, if present, the burst phase, and during the reaction itself. As such, fitting of the model to the practical data was carried out with an emphasis on experiments that provided more kinetic data during catalyst activation or regeneration steps. These experiments were those that used the modified reaction protocol, hence providing more data for the catalyst activation steps, and those that commenced the reaction from the ammonium phenolate catalyst **136**.

Following fitting of the model to the experimental data, a set of rate constants for each of the described steps in Scheme 3.42 was obtained (Table 3.3). The results indicated that the rate-determining step in the system was the second process in the overall regeneration of zwitterion **140** from ammonium phenolate **136** (Entry 8, Table 3.3).

**Table 3.3: Parameters obtained from fitting the theoretical model (model 6 according to Scheme 3.42) to selected experimental data.** Data are reported to three significant figures.

| Entry | Parameter | Value | Event |
|---|---|---|---|
| 1 | $k_{Df}$ | $2.15 \times 10^{-4}$ min$^{-1}$ | catalyst monomerisation |
| 2 | $k_{Db}$ | $1.50 \times 10^{5}$ M$^{-1}$ min$^{-1}$ | catalyst dimerisation |
| 3 | $k_{1f}$ | 700 M$^{-1}$ min$^{-1}$ | deprotonation |
| 4 | $k_{1b}$ | 0.00 min$^{-1}$ | reprotonation |
| 5 | $k_{2f}$ | 1400 M$^{-1}$ min$^{-1}$ | deprotonation |
| 6 | $k_{2b}$ | 0.00 min$^{-1}$ | reprotonation |
| 7 | $k_{3}$ | 355 min$^{-1}$ | cyclisation |
| 8 | $k_{4f}$ | 0.0150 min$^{-1}$ | dissociation |
| 9 | $k_{4b}$ | 100 M$^{-1}$ min$^{-1}$ | association |
| 10 | $k_{5f}$ | 1.00 M$^{-1}$ min$^{-1}$ | catalyst deprotonation |
| 11 | $k_{5b}$ | 100 M$^{-1}$ min$^{-1}$ | catalyst reprotonation |
| 12 | $k_{6f}$ | 0.800 M$^{-1}$ min$^{-1}$ | catalyst deprotonation |
| 13 | $k_{6b}$ | 0.00 M$^{-1}$ min$^{-1}$ | catalyst reprotonation |
| 14 | $k_{7f}$ | 0.800 min$^{-1}$ | dissociation |
| 15 | $k_{7b}$ | 0.00 M$^{-1}$ min$^{-1}$ | association |
| 16 | $k_{z}$ | $3.00 \times 10^{-5}$ M$^{-1}$ min$^{-1}$ | background reaction |

According to the model, the change in the distribution of catalyst species over time depended heavily on how the reaction was set up (for example, Figure 3.43, Figure 3.44, and Figure 3.45).

During the pre-stirring period, if present, the catalyst mixture rapidly equilibrated from **127** to a mixture of dimer **139** and zwitterion **140** via the intermediate species **150** (A, Figure 3.43). Following addition of the substrate **125** (at time zero), the catalyst was predominantly sequestered as dimer **139** and the pentafluorophenolate-bound species **136** and **148** (B, Figure 3.43). The theoretical pre-stirring period was set to be 50 min in duration, which was slightly longer than the actual 30 min (with sonication intervals) that was used practically.

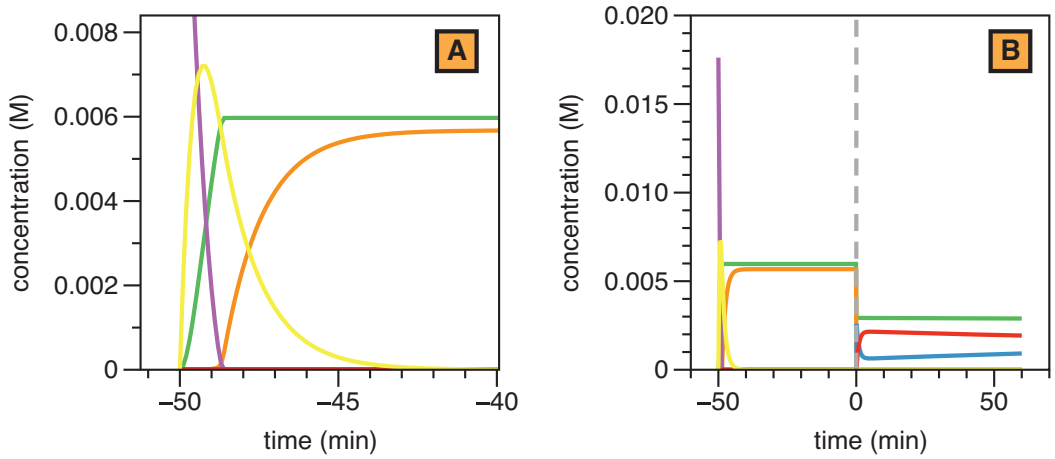



**Figure 3.43: Example of the model output for catalyst species concentrations for one experiment using the standard reaction protocol (spirok-35 replicate 1).** In both graphs, the $x$-axes correspond to time before and after initiation of the reaction at 0 min, the $y$-axes correspond to concentration. The coloured lines correspond to the catalyst species as follows: halide salt **127** (purple), KCl-bound intermediate **150** (yellow), zwitterion **140** (orange), dimer **139** (green), ammonium phenolate **136** (blue), and phenolate-bound intermediate **148** (red). The concentration of ammonium enolate **135** was negligible at all times and is not shown. **A)** Zoomed-in region highlighting initial reaction of **127**. **B)** Distribution of relevant catalyst species over the full duration of the simulation. The grey dotted line indicates time zero and initiation of the model reaction by the addition of substrate **125** as a solution. The protocol was modelled according to the standard reaction protocol. The reaction conditions following time zero were as follows (to 2 sf): substrate **125** (83 mM), $[\text{cat}]_\text{T}$ (8.6 mM), $K_3PO_4$ (0.82 M).

If we initiated the reaction by the addition of $K_3PO_4$, i.e. without pre-stirring the catalyst **127** with $K_3PO_4$, conversion of **127** proceeded to give a mixture of **139**, **136** and **148**, again, via intermediate **150** (Figure 3.44). The concentrations of zwitterion **140** and ammonium enolate **135** remained negligible throughout the reaction.

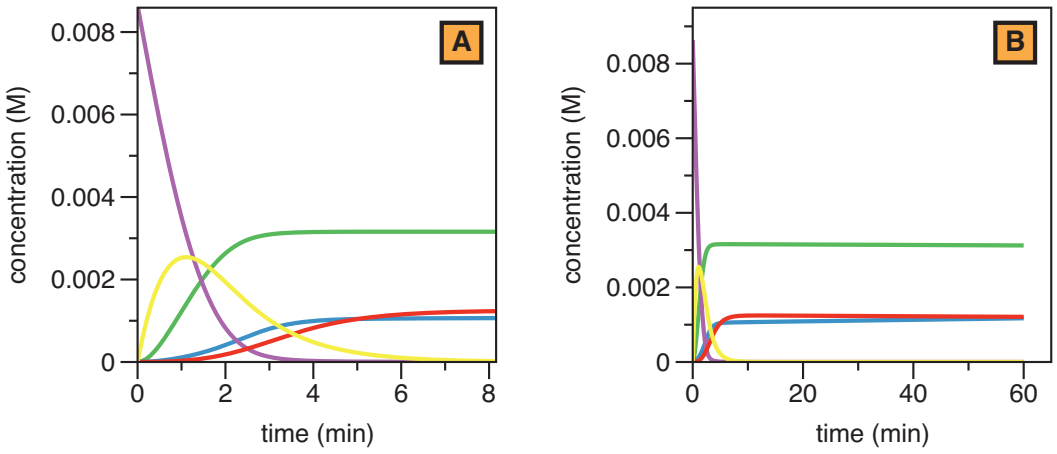



**Figure 3.44: Example of the model output for catalyst species concentrations for one experiment using the modified reaction protocol (spirok-36 replicate 1).** In both graphs, the $x$-axes correspond to time following initiation of the reaction at 0 min, the $y$-axes correspond to concentration. The coloured lines correspond to the catalyst species as follows: halide salt **127** (purple), KCl-bound intermediate **150** (yellow), dimer **139** (green), ammonium phenolate **136** (blue), and phenolate-bound intermediate **148** (red). The concentrations of ammonium enolate **135** and zwitterion **140** were negligible at all times and are not shown. **A)** Zoomed-in region highlighting initial reaction of **127**. **B)** Distribution of relevant catalyst species over the full duration of the simulation. Time zero and initiation of the model reaction was by the addition of $K_3PO_4$(aq). The protocol was modelled according to the modified reaction protocol. The reaction conditions following time zero were as follows (to 2 sf): substrate **125** (83 mM), $[cat]_T$ (8.6 mM), $K_3PO_4$ (0.82 M).

Additionally, we could commence the reaction with $[cat]_T$ initially as ammonium phenolate **136**, with or without pre-stirring with $K_3PO_4$(aq) and subsequently examine the catalyst behaviour (Figure 3.45). In the absence of any chloride sources, the catalyst system was much simpler with the concentrations of dimer **139**, the halide **127**, and intermediate **150** at zero throughout the reaction. As reactive intermediates, the concentrations of zwitterion **140** and ammonium enolate **135** were negligible at all times. No change in the catalyst behaviour was observed when introducing a pre-stirring period, which correlated well with our experimental finding that pre-stirring **136** with $K_3PO_4$(aq) made no difference to the observed rate behaviour.

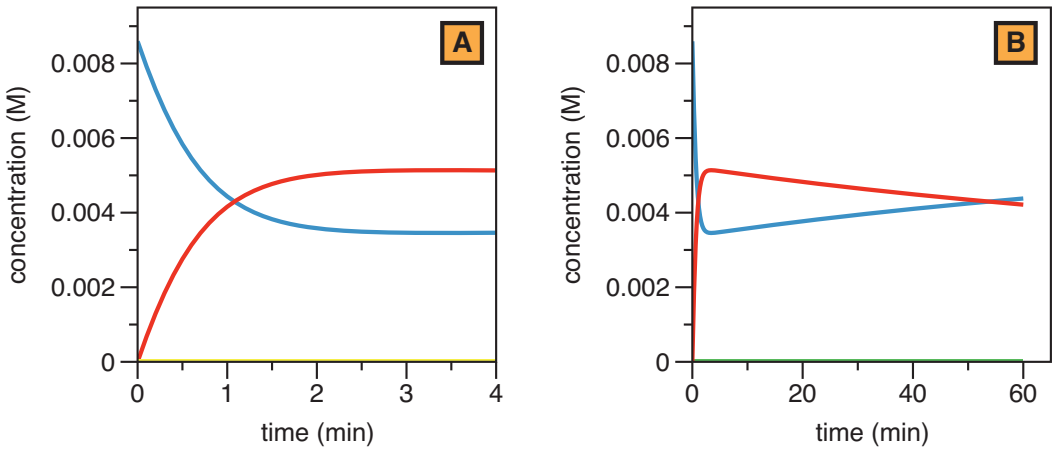



**Figure 3.45: Example of the model output for catalyst species concentrations for one experiment (spirok-41 replicate 1).** In both graphs, the $x$-axes correspond to time following initiation of the reaction at 0 min, the $y$-axes correspond to concentration. The coloured lines correspond to the catalyst species as follows: ammonium phenolate **136** (blue), and phenolate-bound intermediate **148** (red). The concentrations of dimer **139**, halide salt **127**, and intermediate **150** were zero at all times and are not shown. The concentrations of ammonium enolate **135** and zwitterion **140** were negligible at all times and are not shown. **A)** Zoomed-in region highlighting initial reaction of **136**. **B)** Distribution of relevant catalyst species over the full duration of the simulation. Time zero and initiation of the model reaction was by the addition of $K_3PO_4$(aq). The protocol was modelled according to the modified reaction protocol. The reaction conditions following time zero were as follows (to 2 sf): substrate **125** (82 mM), $[cat]_T$ initially as **136** (8.6 mM), $K_3PO_4$ (0.82 M).

The model output exhibited excellent agreement with a large selection of different experimental data that we had collected (for example, Figure 3.46, Figure 3.47, and Figure 3.48). Even for the extended reactions (Figure 3.46); this was before the reaction mixtures became uncontrollably and excessively heterogeneous—i.e. beyond ~1500 min—causing variations in the product concentration measurements (A, Figure 3.46). Another example with extended monitoring was when we removed the pre-stirring protocol and commenced the reaction using all initial $[cat]_T$ as **136** (B, Figure 3.46).

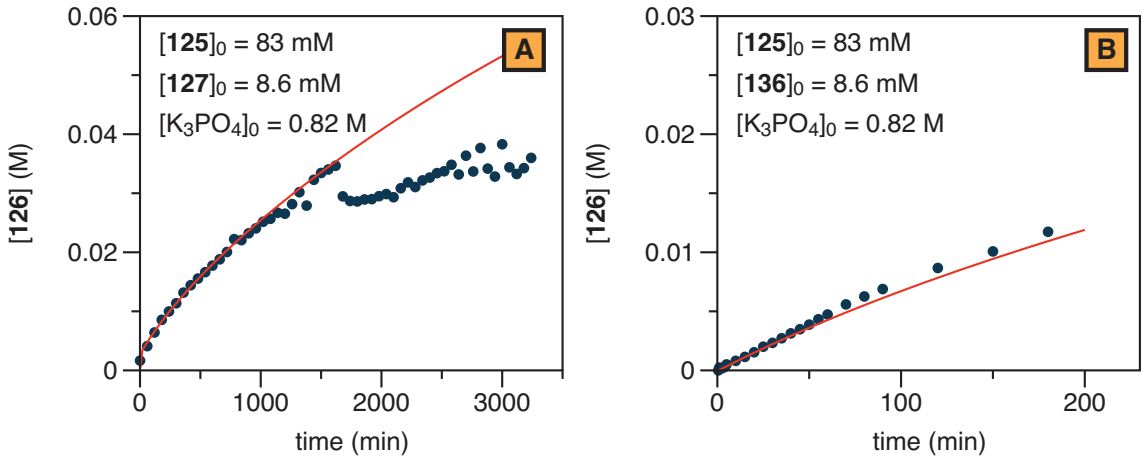



**Figure 3.46: Examples of the output of model (described by Scheme 3.42 and Table 3.3) against data acquired over extended reaction times.** Each example corresponds to different initial reaction conditions (to 2 sf), which are indicated on each graph as the total initial concentration in the whole reaction system (both organic and aqueous layers). The data are from the designated reaction codes (*rxn.code*) as follows and are of the first replicate of the set: **A)** spirok-6; and **B)** spirok-40. Example **A** was carried out using the standard reaction protocol, example **B** used the modified protocol. Both examples used a reaction stirring speed of 1000 rpm and stock concentrations of $K_3PO_4$ of 4.77 M. In both graphs, the dots correspond to data that was acquired experimentally, and the red lines correspond to the model described by Scheme 3.42 and Table 3.3. The $x$-axes correspond to time following initiation of the reaction, the $y$-axes correspond to the concentration of product **126**.

We could extend the burst phase in the simulation simply by removing the pre-stirring period and initiating the reaction by the addition of $K_3PO_4$ (Figure 3.47). Again, good agreement with the experimental data was observed across all of these examples (for example A, Figure 3.47), including when we varied the initial substrate concentration (for example B, Figure 3.47).

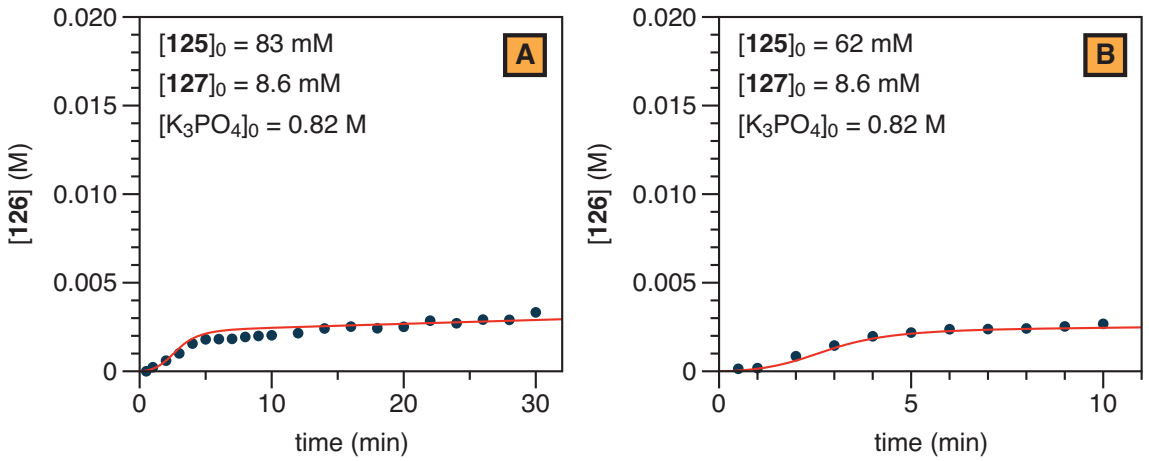



**Figure 3.47: Examples of the output of model (described by Scheme 3.42 and Table 3.3) against data acquired using the modified reaction protocol.** Each example corresponds to different initial reaction conditions (to 2 sf), which are indicated on each graph as the total initial concentration in the whole reaction system (both organic and aqueous layers). The data are from the designated reaction codes (*rxn.code*) as follows and are of the first replicate of the set: **A)** spirok-36; and **B)** spirok-76. Both examples used a reaction stirring speed of 1000 rpm and stock concentrations of $K_3PO_4$ of 4.77 M. In both graphs, the dots correspond to data that was acquired experimentally, and the red lines correspond to the model described by Scheme 3.42 and Table 3.3. The $x$-axes correspond to time following initiation of the reaction, the $y$-axes correspond to the concentration of product **126**.

The model continued to agree with the experimental data at different 4.77 M $K_3PO_4$(aq) loadings when using **136** as the initial catalyst (Figure 3.48). The predicted reaction order of 0.5 with respect to $K_3PO_4$ (see equations 3.29 to 3.36) was well reflected in the graphical outputs of the model (for example A to D, Figure 3.48), and the predicted reaction order for $K_3PO_4$ using catalyst **136** of 0.43 (Figure 3.49). The value of 0.43 also correlated with the 0.45 value that was obtained experimentally from practical reactions (see Figure 3.32).

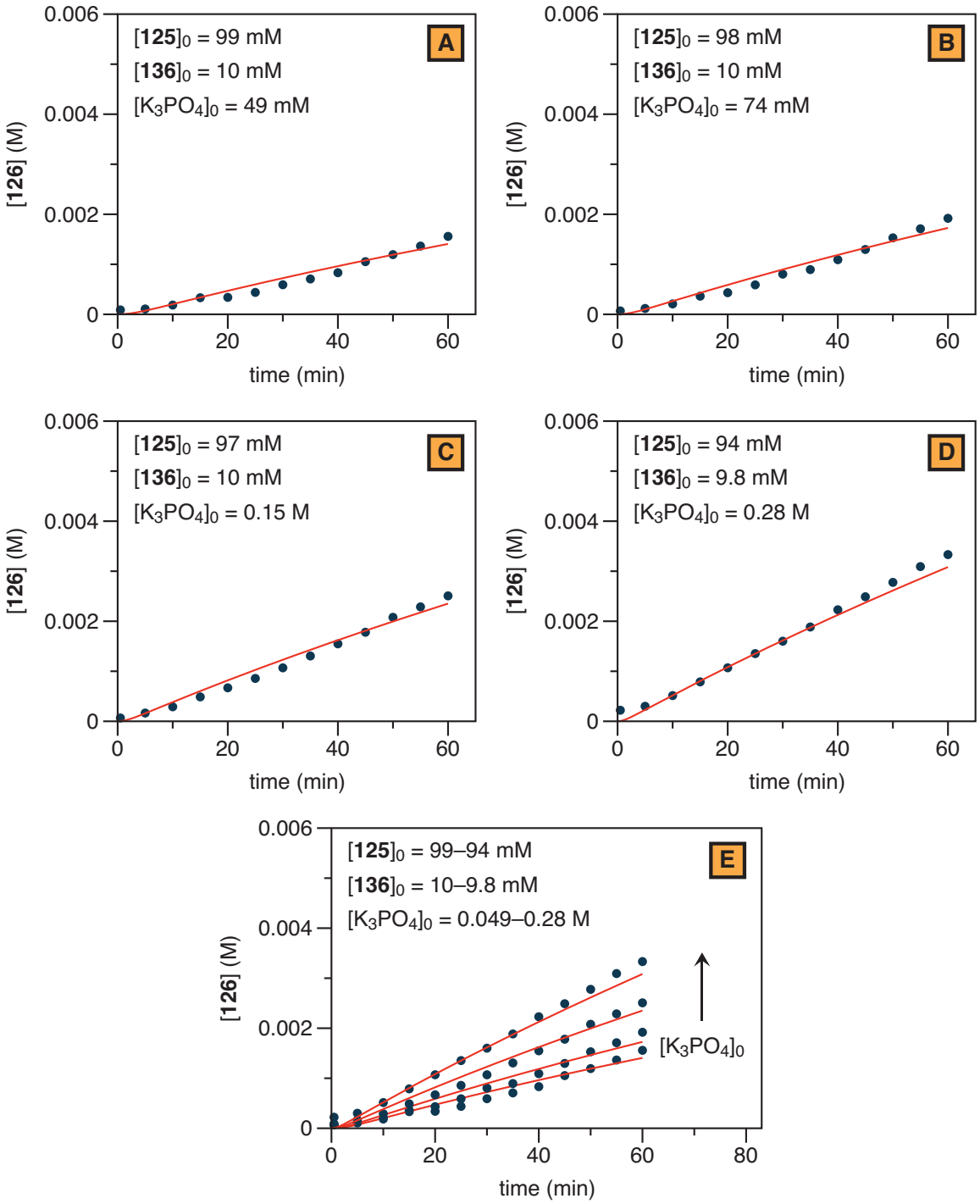



**Figure 3.48: Examples of the output of model (described by Scheme 3.42 and Table 3.3) against data acquired using the modified reaction protocol with initial $[\mathbf{cat}]_T$ as 136, and at different $K_3PO_4$(aq) loadings.** Each example corresponds to different initial reaction conditions (to 2 sf), which are indicated on each graph as the total initial concentration in the whole reaction system (both organic and aqueous layers). The data are from the designated reaction codes (*rxn.code*) as follows and are of the first replicate of the set: **A)** spirok-47; **B)** spirok-49; **C)** spirok-51; **D)** spirok-52. **E)** Overlay of data from **A** to **D** to show the trend of increasing rate with increasing $[K_3PO_4]_0$. All examples used a reaction stirring speed of 1000 rpm and stock concentrations of $K_3PO_4$ of 4.77 M. In all graphs, the dots correspond to data that was acquired experimentally, and the red lines correspond to the model described by Scheme 3.42 and Table 3.3. The $x$-axes correspond to time following initiation of the reaction, the $y$-axes correspond to the concentration of product **126**.

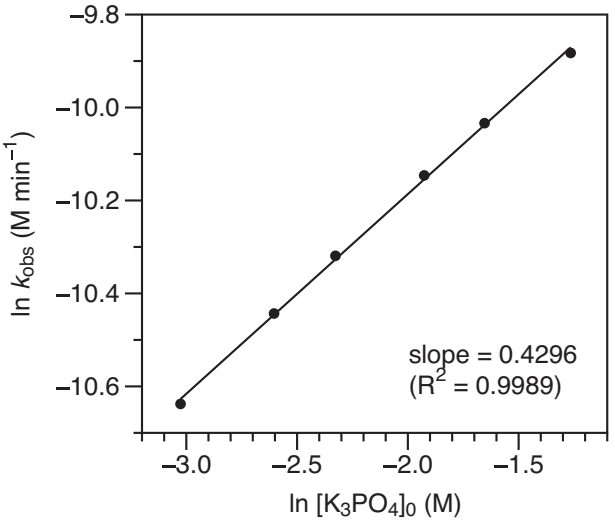



**Figure 3.49: Double logarithmic plot of total base concentration (ln $[\mathbf{K_3PO_4}]_0$) against the simulated initial rate (ln $k_{\mathbf{obs}}$) to give the theoretical order with respect to base of 0.43 (when commencing the reaction using $[\mathbf{cat}]_\mathbf{T}$ as 136 and using the modified reaction protocol).** The data were obtained by taking the natural logarithm of the $k_{\text{obs}}$ (obtained between 20 and 50 min) from the graphically reproduced output of the model described by Scheme 3.42 and Table 3.3. Reaction conditions inputted into the model were from the corresponding experimental data sets (see 7.16). The line is the result of linear regression analysis of the data set. The 68% confidence interval for the slope and order was 0.42 to 0.44 (to 2 sf).

The results obtained from the simulation of the standard reaction protocol with initial $[\text{cat}]_\text{T}$ as **127** at different concentrations exhibited variable outcomes when compared to the experimental data (Figure 3.50). The burst phase in each example was well predicted, as was the behaviour in the normal phase of reactions carried out with lower $[\mathbf{127}]_0$ (<10 mM) (for example A and B, Figure 3.50). However, the model began to underestimate the rate of formation of product **126** over time at higher $[\mathbf{127}]_0$ (>10 mM) (C and D, Figure 3.50).

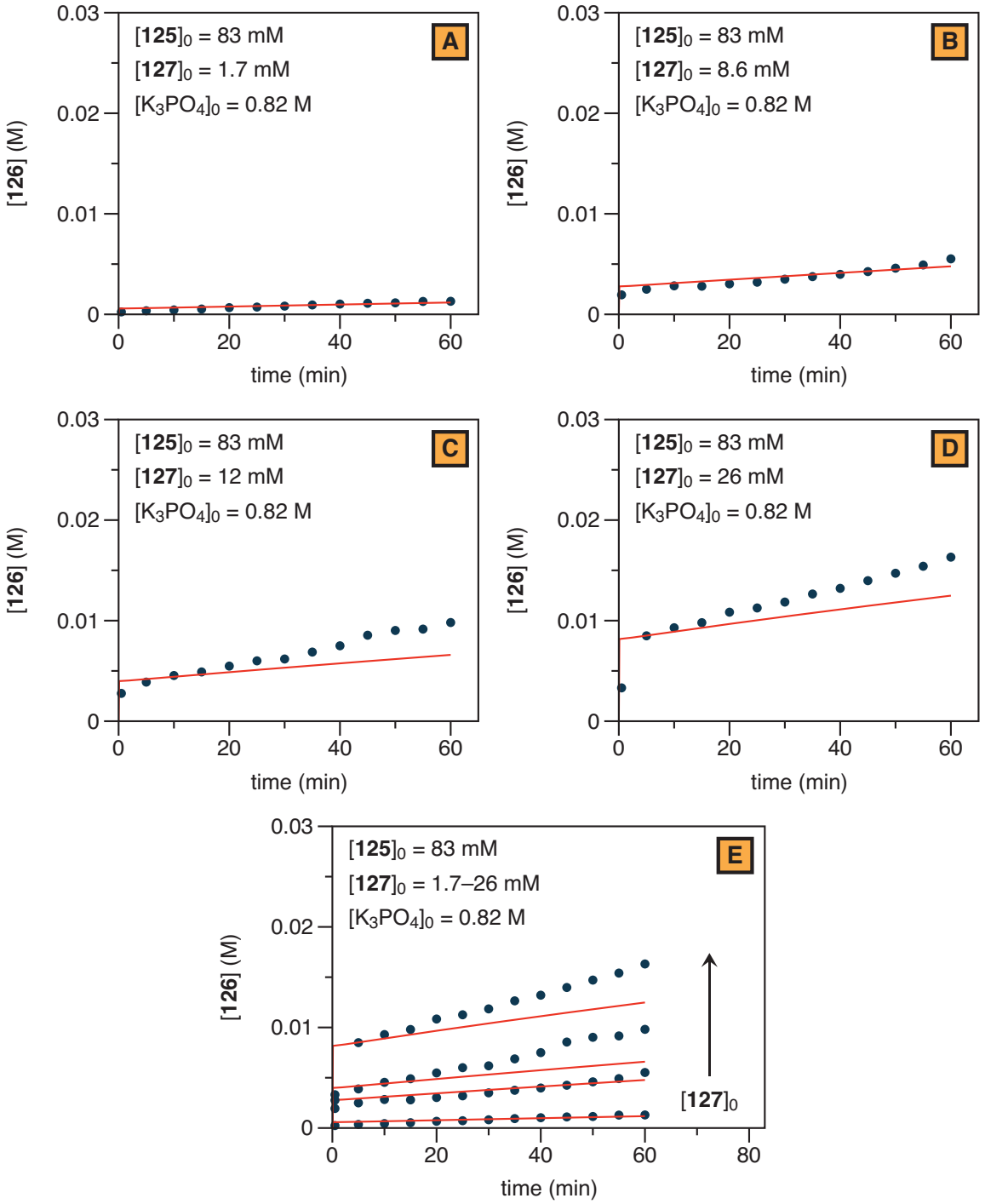



**Figure 3.50: Examples of the output of model (described by Scheme 3.42 and Table 3.3) against data acquired using the standard reaction protocol with initial $[\mathbf{cat}]_\mathbf{T}$ as 127.** Each example corresponds to different initial reaction conditions (to 2 sf), which are indicated on each graph as the total initial concentration in the whole reaction system (both organic and aqueous layers). The data are from the designated reaction codes (*rxn.code*) as follows and are of the first replicate of the set: **A)** spirok-11; **B)** spirok-8; **C)** spirok-9; **D)** spirok-12. **E)** Overlay of data from **A** to **D** to show the trend of increasing rate with increasing $[\mathbf{127}]_0$. All examples used a reaction stirring speed of 1000 rpm and stock concentrations of $K_3PO_4$ of 4.77 M. In all graphs, the dots correspond to data that was acquired experimentally, and the red lines correspond to the model described by Scheme 3.42 and Table 3.3. The $x$-axes correspond to time following initiation of the reaction, the $y$-axes correspond to the concentration of product **126**.

The model output for the reaction order with respect to halide salt **127** under the standard reaction conditions was evaluated (Figure 3.51). We varied $[\mathbf{127}]_0$ within the model and simulated the rate of formation of product. The double logarithmic plot of the results revealed a predicted order with respect to **127** under the standard reaction conditions was 0.73 with a 68% confidence interval of 0.72 to 0.74. These values were in reasonable agreement with our practically obtained value of 0.79 (see 3.7.2).

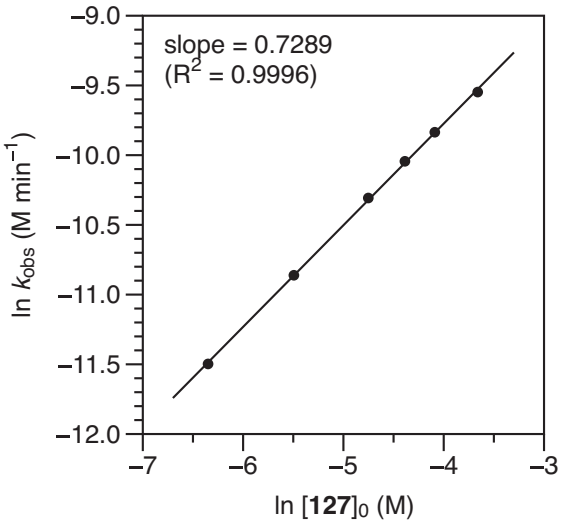



**Figure 3.51: Double logarithmic plot of initial halide salt concentration (ln $[\mathbf{127}]_0$) against the simulated initial rate (ln $k_{\mathbf{obs}}$) to give the theoretical order with respect to 127 of 0.73 (when commencing the reaction using $[\mathbf{cat}]_{\mathbf{T}}$ initially as 127 and using the standard reaction protocol).** The data were obtained by taking the natural logarithm of the $k_{\text{obs}}$ (obtained between 20 and 50 min) from the graphically reproduced output of the model described by Scheme 3.42 and Table 3.3. Reaction conditions inputted into the model were from the corresponding experimental data sets (see 3.7.2). The line is the result of linear regression analysis of the data set. The 68% confidence interval for the slope and order was 0.72 to 0.74 (to 2 sf).

Whilst the model was in good agreement with the majority of the experimental data, there were a selection of results that were not reproducible by the simulation. These were in addition to the results obtained when using higher $[\mathbf{127}]_0$. The model vastly underestimated the rate at reduced base loadings (e.g. $[K_3PO_4]_0 < 100$ mM) when using halide salt **127** and the standard reaction protocol (A, Figure 3.52). At $[K_3PO_4]_0 = 0.46$ M, the model continued to underestimate the rate (B, Figure 3.52); this trend was observed in results obtained from reaction conditions using up to $[K_3PO_4]_0 = 0.82$ M.

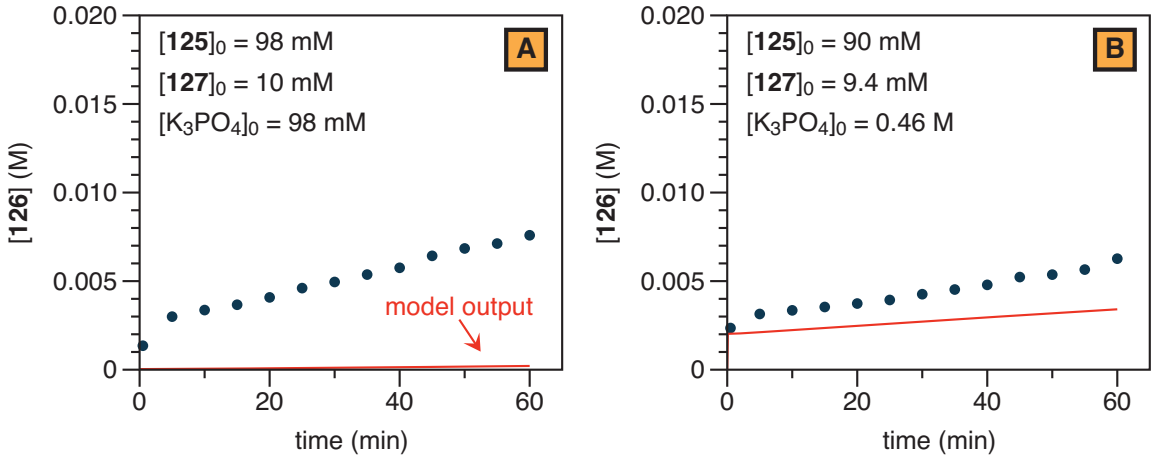



**Figure 3.52: Examples of the output of model (described by Scheme 3.42 and Table 3.3) against data acquired using the standard reaction protocol with initial $[\mathbf{cat}]_\mathbf{T}$ as 127 and at different $\mathbf{K_3PO_4}$(aq) loadings.** Each example corresponds to different initial reaction conditions (to 2 sf), which are indicated on each graph as the total initial concentration in the whole reaction system (both organic and aqueous layers). The data are from the designated reaction codes (*rxn.code*) as follows and are of the first replicate of the set: **A)** spirok-21; and **B)** spirok-22. Both examples used a reaction stirring speed of 1000 rpm and stock concentrations of $K_3PO_4$ of 4.77 M. In both graphs, the dots correspond to data that was acquired experimentally, and the red lines correspond to the model described by Scheme 3.42 and Table 3.3. The $x$-axes correspond to time following initiation of the reaction, the $y$-axes correspond to the concentration of product **126**.

Another aspect that we were unable to completely explain using the kinetic model was related to the KIE experiments. Lowering the relative rates of substrate deprotonation to that expected for deuterium-labelled analogues (i.e. by factors of 4–6) did not reproduce the graphical kinetic behaviour we observed experimentally. Additionally, the change in the burst phase was not mimicked and the overall simulated KIE for the system was 1.002 (vs 1.5 obtained experimentally). However, our experimental systems were not operating with a purely α-deuterium-labelled analogue. The results were complicated by additional labelling at the beta position, and the potential distribution of diastereomers. As such, the precise origin of the experimentally acquired KIE remained somewhat elusive and is the subject of future work.

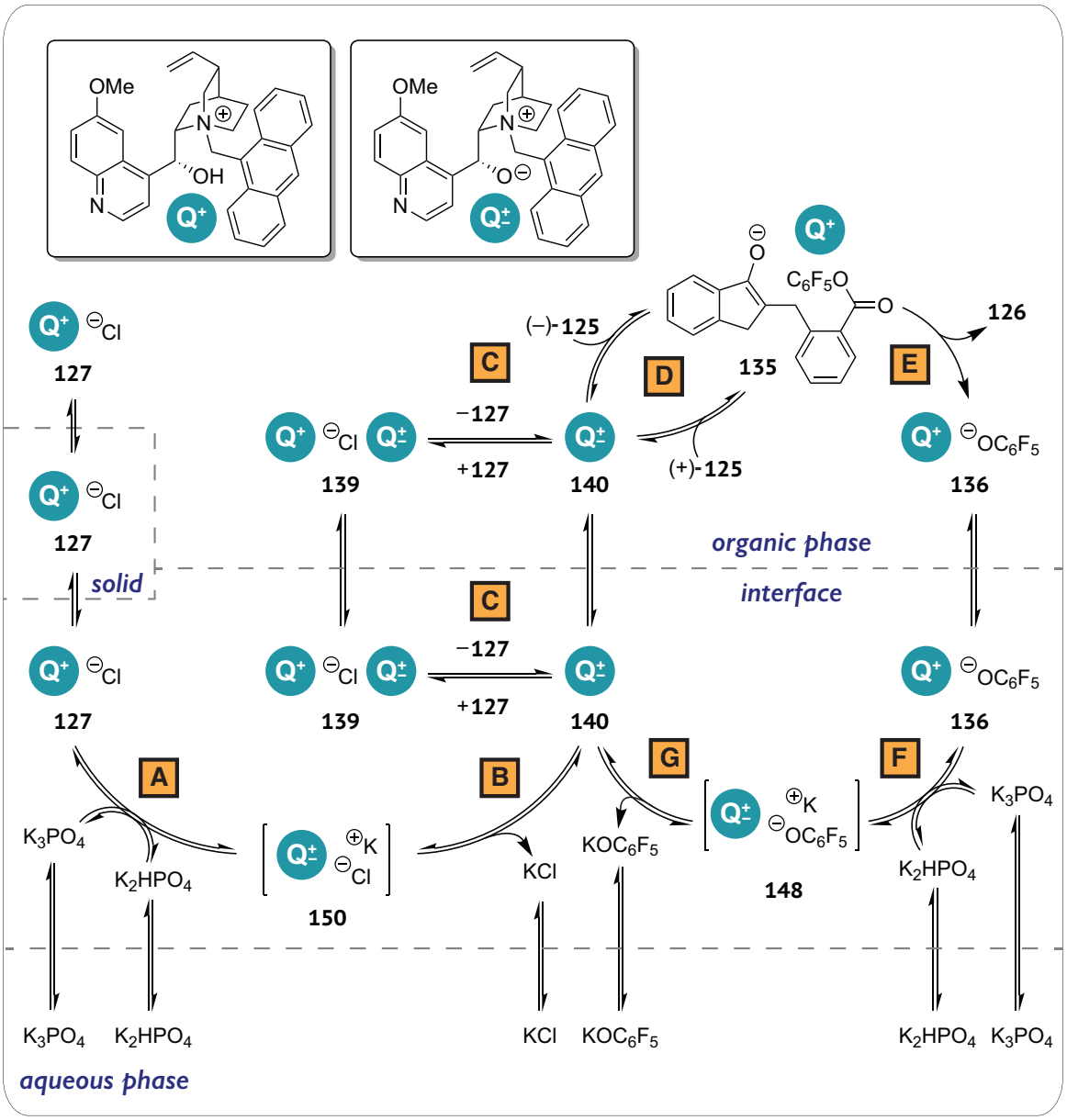
The kinetic model provided good theoretical suggestions for the origins of the burst phase when carrying out the reaction using either the standard or modified reaction protocols. The burst phase that was observed during the standard reaction protocol (i.e. initiating the reaction by the addition of substrate **125**) was simply due to the pool of zwitterion that was formed during the pre-stirring period. When initiating the reaction of substrate **125** to product **126** by the

addition of $K_3PO_4$(aq) (i.e. according to the modified reaction protocol), a complex series of steps occurred concurrently. These included generation of the zwitterion **140** via intermediate **150**, reaction of the zwitterion with substrates (−)-**125** and (+)-**125** to generate product **126**, dimerisation to form **139**, and sequestration of the catalyst as pentafluorophenolate-bound **136** and **148**.

Generally, the model was consistent with the experimental observations. The changes in rate behaviour observed when examining the differences in the standard vs modified reaction protocols were in excellent agreement. The modelled distribution of catalyst species over time provided visual and chemical rationales for the observed rate behaviour. When we simulated selected reaction orders with respect to either **127** or $K_3PO_4$ under various conditions, we obtained values that were similar in magnitude to those obtained experimentally. Exceptions included the results obtained with higher $[\mathbf{127}]_0$, the evaluation of different $K_3PO_4$ loadings when commencing the reaction using halide **127**, and the results of the KIE experiments.

### 3.13.2 Final mechanistic hypothesis

The culmination of the practical and theoretical experiments thus far was our final hypothesis for the reaction system (Scheme 3.43). Commencing the reaction from the halide salt **127** under phase-transfer reaction conditions proceeded to give the catalyst species zwitterion **140** and dimer **139**, via intermediate **150** (A to C, Scheme 3.43). Addition of the substrates, (−)-**125** and (+)-**125**, results in deprotonation events with different rates to give common intermediate **135** (D, Scheme 3.43). Next, cyclisation to give product **126** and ammonium phenolate **136** rapidly occurs (E, Scheme 3.43). Zwitterion **140** regeneration from **136** proceeds as a two-step process mediated by $K_3PO_4$ (F and G, Scheme 3.43). The rate-limiting factor in our proposed mechanism was regeneration of the active zwitterion **140** from ammonium phenolate **136** via **148** in a process mediated by $K_3PO_4$.




**Scheme 3.43: Final hypothesis for the spirocyclisation reaction model. A)** Following transport of halide **127** to the interfacial region, the reaction with $K_3PO_4$ proceeds to generate intermediate **150**; **B)** further reaction of **150** results in the formation of zwitterion **140**; **C)** sequestration of the catalyst as monodeprotonated dimer **139** occurs as the reaction between zwitterion **140** and halide salt **127**; **D)** in the presence of substrates (−)-**125** and (+)-**125**, deprotonation gives common intermediate **135**; **E)** subsequent cyclisation generates product **126** and ammonium phenolate **136**; **F)** subsequent active catalyst regeneration proceeds firstly via intermediate **148**; and **G)** dissociation of the intermediate **148** regenerates zwitterion **140**.

Overall, we had a good picture of what was occurring in the reaction model. Still, there remained aspects of the system that we wanted to investigate.

## 3.14 Final investigations

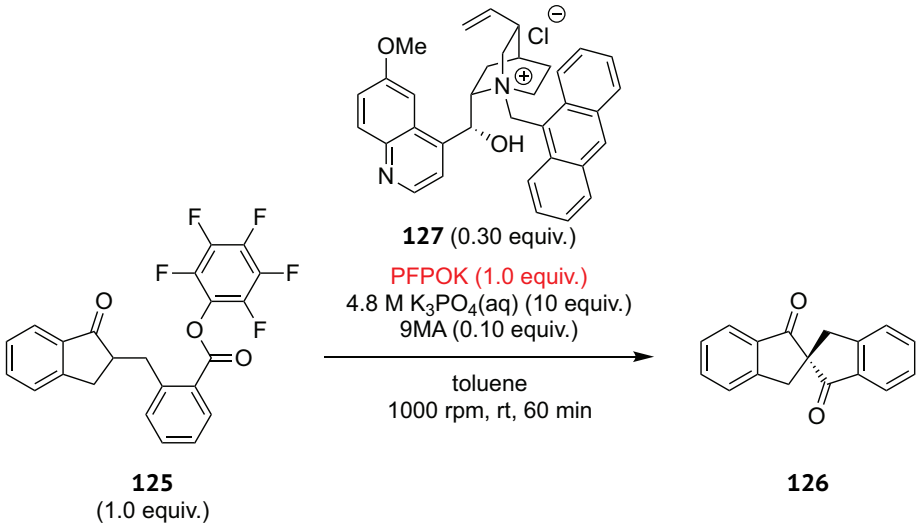
There were two aspects of the reaction that we had not yet addressed. The first was to evaluate the effect of 2,3,4,5,6-pentafluorophenolate on the reaction. The second was to increase the overall rate of reaction—without compromising enantioenrichment of the product **126**—based on our current understanding of the rate-determining step.

### 3.14.1 Investigating the effect of 2,3,4,5,6-pentafluorophenolate on the reaction

We wanted to evaluate the effect of 2,3,4,5,6-pentafluorophenolate on the mechanism due to the fact it was consistently being produced in the reaction. A quantity of the phenolate would be sequestered in the form of ammonium phenolate **136**, however, the fate of the remainder was unknown.

Over the course of our study, we did not observe 2,3,4,5,6-pentafluorophenol by HPLC. The p$K_a$ of 2,3,4,5,6-pentafluorophenol is 7.6 in DMSO (measured) and 5.5 in $H_2O$.[125] As such, we suspected it was sequestered in the aqueous phase as potassium 2,3,4,5,6-pentafluorophenolate, and was not extracted during execution of the sampling protocol, or that it was removed via our method for quenching reaction mixture aliquots.

To investigate the effect of 2,3,4,5,6-pentafluorophenolate on the reaction we first carried out the reaction under the standard reaction conditions, but with added potassium 2,3,4,5,6-pentafluorophenolate (PFPOK) (Scheme 3.44). The catalyst **127** (0.30 equiv. with respect to substrate), PFPOK (1.0 equiv.), $K_3PO_4$(aq) (10 equiv.), and toluene were stirred (1000 rpm), interspersed with regular treatments in an ultrasound bath, prior to the addition of substrate **125** as a solution in toluene at time zero. The increased catalyst loading (compared to 0.10 equiv.) was used to obtain more data over the observed time period.




**Scheme 3.44: Conditions used to evaluate the effect of added PFPOK.** Equivalents (equiv.) are reported with respect to substrate **125**.

We found, that under these conditions, the burst phase was eliminated and the kinetics obtained were analogous to the reaction effected by the phenolate catalyst **136** (Figure 3.53). This suggested that formation of the ammonium phenolate **136** was favourable and allowed the reaction of substrate **125** to commence from the proposed rate-determining step.

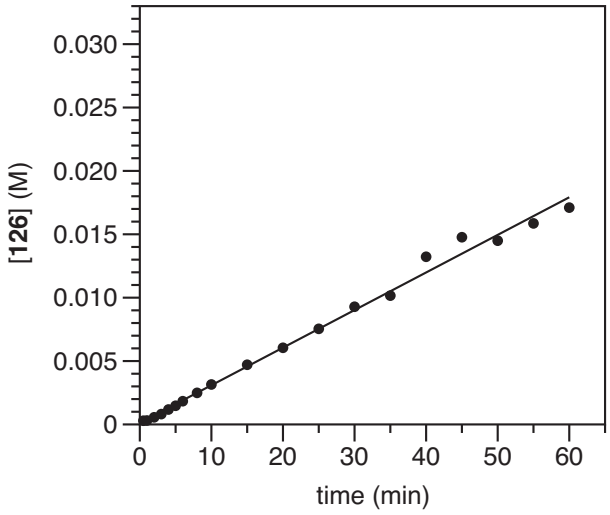



**Figure 3.53: Rate behaviour of the reaction with added PFPOK.** The $x$-axis corresponds to time following initiation of the reaction; the $y$-axis corresponds to the concentration of product **126**. The line is obtained from linear regression analysis of the data set.

We next evaluated the effect of PFPOK on the reaction when using the modified reaction protocol. The PFPOK was added to the catalyst, before toluene was added, followed by substrate **125** as a solution in toluene. The mixture was stirred for approximately 5 min before

$K_3PO_4$ was added at the designated time zero.

To our surprise, the reaction exhibited an initial burst phase, with an apparent non-zero intercept (Figure 3.54). Typically, when monitoring the formation of product **126** under the modified reaction conditions, we obtained an intercept of zero, with a burst phase that occurred over 5 to 20 min (for example in Figure 3.33). Despite the low p$K_a$ of the conjugate acid, it appeared the added PFPOK might have been able to deprotonate the substrate—either directly or via the zwitterion **140**—to effect formation of product in the presence of catalyst and the absence of $K_3PO_4$.

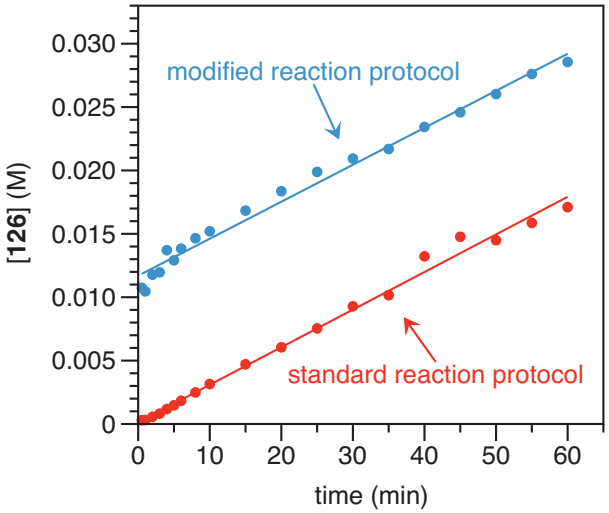



**Figure 3.54: Overlay of the rate behaviour of the reaction with added PFPOK using the standard (red) or modified (blue) reaction protocols.** The $x$-axis corresponds to time following initiation of the reaction; the $y$-axis corresponds to the concentration of product **126**. The lines are obtained from linear regression analyses of the data sets.

To further evaluate whether this scenario might be in operation, we carried out a reaction under the modified reaction protocol, where addition of $K_3PO_4$(aq) was delayed (Scheme 3.45). Indeed, we found conversion to the product was obtained prior to the addition of $K_3PO_4$(aq) (Figure 3.55). In the absence of $K_3PO_4$, conversion to product reached a plateau at around 20 min after the addition of substrate **125**. Further addition of $K_3PO_4$(aq) recommenced conversion of the substrate to product.




**Scheme 3.45: General order of events when carrying out the reaction with added PFPOK and without $K_3PO_4$ initially.** Equivalents (equiv.) are reported with respect to substrate **125**.

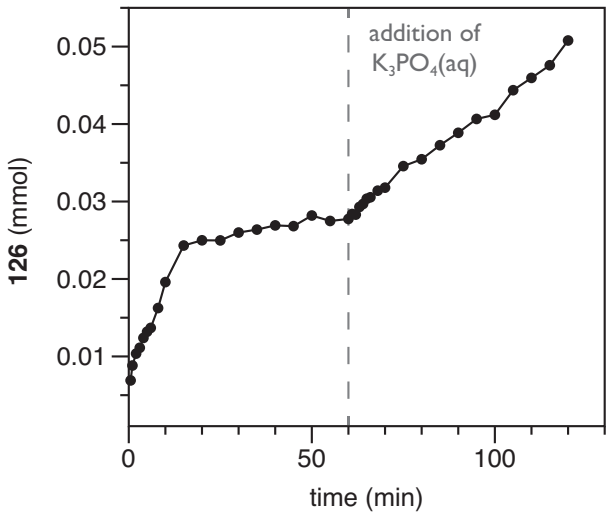



**Figure 3.55: Formation of product 126 observed when carrying out the protocol described in Scheme 3.45.** The $x$-axis corresponds to time following initiation of the reaction; the $y$-axis corresponds to the amount of product **126**. The black line is a guide for the eye. The dashed line indicates the time when $K_3PO_4$(aq) was added to the reaction mixture.

We suspected that PFPOK was facilitating formation of product **126** in the absence of $K_3PO_4$ by forming the zwitterion **140** from the halide salt **127**. The formed zwitterion would then be able to deprotonate the substrate **125** leading to cyclisation and product **126** formation. This supposition was based on three pieces of experimental data. Firstly, the enantiomeric excess of the substrate increased as it was being consumed prior to the addition of $K_3PO_4$ (A, Figure 3.56). This suggested a chiral species was deprotonating the substrate, not PFPOK. Secondly, if PFPOK were carrying out deprotonation of the substrate, we expected to obtain racemic product. However, enantiomeric excess of the product remained comparable to the normal reaction (carried out in the presence of $K_3PO_4$ and absence of added PFPOK) (B, Figure 3.56). Lastly, prior to the addition of $K_3PO_4$, the point of plateau was just under 0.03 mmol, which corresponded well to the initial amount of halide **127** of 0.045 mmol. Again, if PFPOK (1.0 equiv. with respect to substrate) was deprotonating the substrate to generate

product, we would have expected far more than 0.03 mmol of product to have formed prior to the addition of $K_3PO_4$.

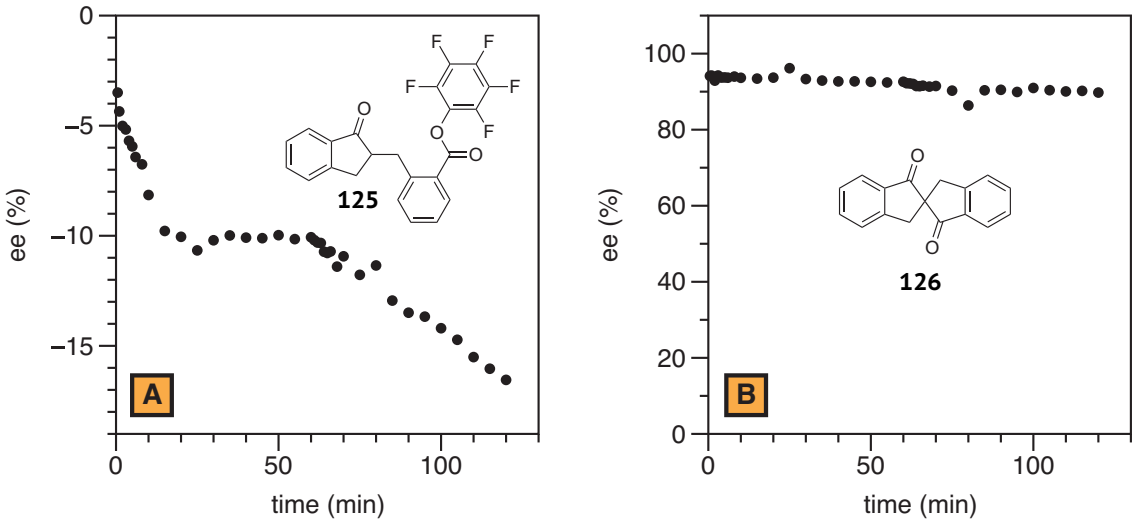



**Figure 3.56: Enantiomeric excesses of A) substrate 125 and B) product 126 over time for the reaction detailed in Scheme 3.45.** The $x$-axes correspond to time following initiation of the reaction; the $y$-axes correspond to enantiomeric excess of the pictured analyte. The corresponding product **126** conversion data are shown in Figure 3.55.

The initial stages of these reactions were not carried out under biphasic conditions; water was not present for PFPOK to migrate into. The lack of aqueous phase may have augmented the action of PFPOK in the organic phase and the results may not have been truly representative of what PFPOK would do under the regular reaction conditions. Additionally, the lack of appearance of PFPOH by HPLC even during the organic only reaction (absence of an aqueous phase) suggested we were removing any PFPOK during the quench of the extracted reaction aliquots.

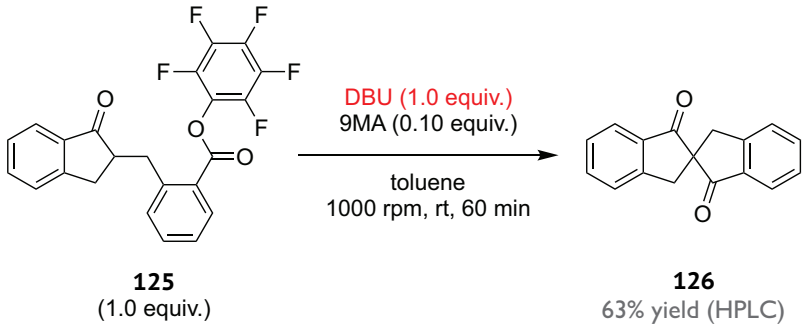
Nonetheless, the data suggested the 2,3,4,5,6-pentafluorophenate that was liberated in the reaction might not be as benign as was suggested by the p$K_a$ of the conjugate acid. Addition of PFPOK in the reaction mixture likely facilitated formation of ammonium phenolate **136**. Furthermore, PFPOK may have a role in generating product, most likely by deprotonating the ammonium salt **127** to form productive quantities of the active zwitterion **140**.

### 3.14.2 Evaluating bases as additives in the reaction

The overall reaction for complete consumption of the substrate to generate product was slow; it took over 54 h to reach completion (see 3.5). To try and speed up the reaction, we would need to address the rate-determining step. At the time, we were still operating under the assumption that the rate-determining step during the normal phase of the reaction was deprotonation of the phenolate **136** to regenerate the active zwitterion **140**. The phenolate **136** was highly organophilic, which made it likely that the interfacial process to deprotonate it was disfavoured. It made sense then, that we should evaluate organosoluble bases of appropriate p$K_a$ to try and speed up the reaction.

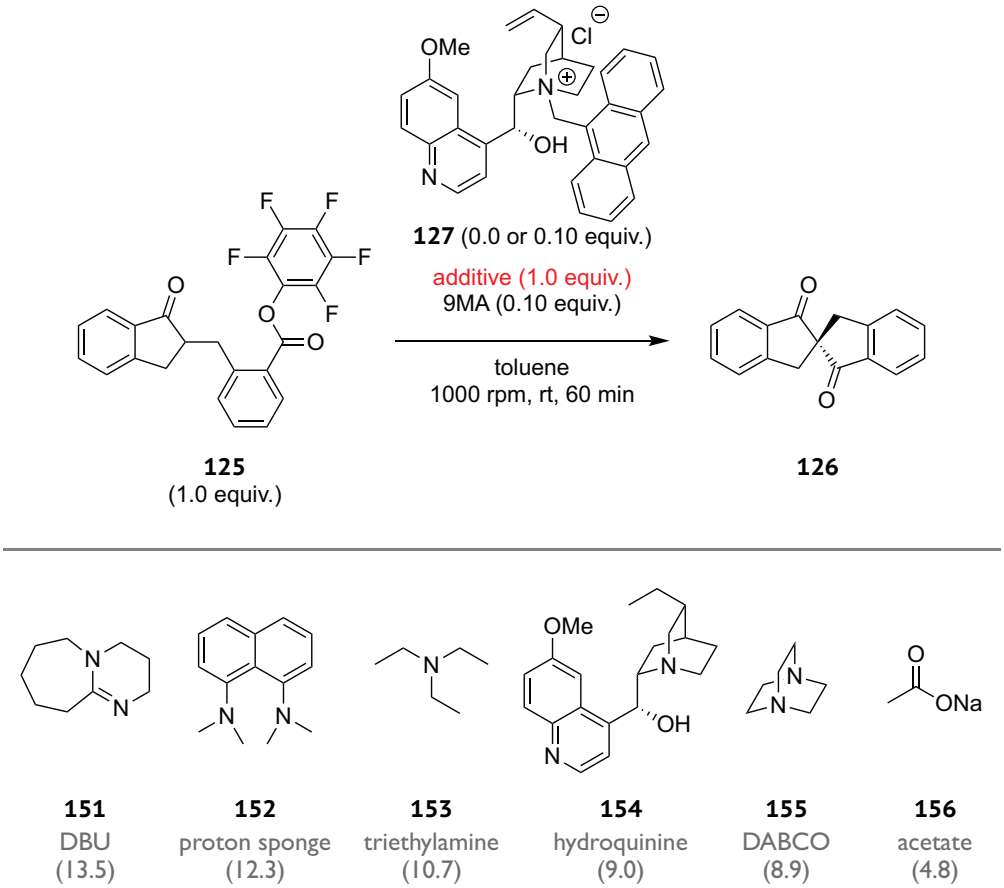
Deprotonation of the substrate **125** led to facile cyclisation under homogenous conditions. Therefore, it was essential that we evaluate bases of appropriate p$K_a$ i.e. those that *would not* deprotonate the substrate (p$K_a$ of 22 to 23 in DMSO) but *would* deprotonate the catalyst (p$K_a$ 16.3 in DMSO). If we used an overly basic species, we risked generating racemic product instead of the desired enantioenriched material.

We first evaluated DBU under control conditions to give an indication of what bases we might apply in the screen (Scheme 3.46). The protonated form of DBU has a p$K_a$ of about 13.5 in $H_2O$,[126] and a p$K_a$ of 13.9 in DMSO,[127] which we thought was an appropriate starting point. The reaction was carried out in the absence of aqueous $K_3PO_4$ and catalyst **127**. After 60 min, a value for the product yield was calculated. Racemic product was obtained in 63% yield, which was much greater than the catalysed reaction in the absence of DBU: 7% yield after 60 min with a catalyst loading of 0.10 equiv. in the presence of 10 equiv. of $K_3PO_4$(aq). Given the significant reactivity of DBU with the substrate **125**, we decided to evaluate bases with protonated p$K_a$ values of less than 13.5 in $H_2O$.




**Scheme 3.46: Conditions evaluating the background reaction in the presence of DBU.** Equivalents (equiv.) are reported with respect to substrate **125**.

The additives that were evaluated in the reaction are detailed in Scheme 3.47. The reactions were carried out with the additives (1.0 equiv. with respect to substrate **125**), and with and without catalyst **127**, and all were in the absence of any aqueous phase and $K_3PO_4$. The results and conditions are summarised in Table 3.4.




**Scheme 3.47: Conditions evaluating the effect of additives (with and without catalyst 127).** Equivalents (equiv.) are reported with respect to substrate **125**. The results are summarised in Table 3.4. The p$K_a$ value of the protonated additives are indicated in brackets (to 1 dp), and were obtained from the following references: DBU,[126] proton sponge,[128] triethylamine,[129] hydroquinine,[130] DABCO,[131] and acetate.[132]

**Table 3.4: Summary of results from reactions carried out according to Scheme 3.47.**

| Entry | Additive (1.0 equiv.) | p$K_a$[a] (in $H_2O$) | 127 Loading (equiv.) | Yield of 126[b] (%) | ee of 126 (%) |
|---|---|---|---|---|---|
| 1 | N/A | N/A | 0.10 | 6–7 | 87–94 |
| 2 | DBU **151** | 13.5 | 0 | 63 | 0 |
| 3 | proton sponge **152** | 12.3 | 0 | 2 | 0 |
| 4 | triethylamine **153** | 10.7 | 0 | 0 | 0 |
| 5 | hydroquinine **154** | 9.0 | 0 | 5 | 5 |
| 6 | DABCO **155** | 8.9 | 0 | 1 | 0 |
| 7 | sodium acetate **156** | 4.8 | 0 | 0 | 0 |
| 8 | proton sponge **152** | 12.3 | 0.10 | 15 | <1 |
| 9 | triethylamine **153** | 10.7 | 0.10 | 1 | 35 |
| 10 | hydroquinine **154** | 9.0 | 0.10 | 29 | 85 |
| 11 | DABCO **155** | 8.9 | 0.10 | 8 | 83 |
| 12 | sodium acetate **156** | 4.8 | 0.10 | 1 | 65 |

[a]to 1 dp; [b]Yields were either estimated by HPLC (as the ratio of the signal integrals corresponding to the product to the total areas of substrates and products combined), or determined using the typical method with the internal standard and assay, and are given to the nearest whole percent.

For reference, the reaction carried out in the absence of additives and in the presence of catalyst **127** (0.10 equiv.) and 4.8 M $K_3PO_4$(aq) (10 equiv.) gave product **126** in 6–7% yield and 87–94% ee after 60 min (Entry 1, Table 3.4). DBU (p$K_a$ 13.5 in $H_2O$), as described earlier, was an ineffectual additive, which resulted in significant formation of racemic product **126** in the absence of catalyst **127** (Entry 2, Table 3.4). Decreasing the p$K_a$ of the additives mostly resulted in negligible yields of product **126** in the absence of catalyst **127** (Entries 3 to 7, Table 3.4). The reaction with added hydroquinine **154** without catalyst **127** resulted in generation of the product in 5% yield with 5% ee; some ee was expected given the presence of a chiral base (Entry 5, Table 3.4). Interestingly, both hydroquinine **154** and catalyst **127** were required to obtain increased yields of product **126** with only slightly reduced enantiomeric excess relative to the normal reaction (comparing Entries 1 and 10, Table 3.4). All other additives (proton sponge, triethylamine, DABCO, and sodium acetate) gave less desirable results, with either increased yield but racemic product, or very low yield and moderate to good ee (Entries 8, 9, 11, and 12, Table 3.4).

Whilst hydroquinine **154** was evaluated predominantly out of curiosity—the additional equiva-

lent of a chiral source with the same pseudoenantiomerism as the catalyst **127** was not exactly conducive to enantioselective catalysis—it proved to give the most interesting results. It appeared the addition of both hydroquinine **154** and catalyst **127** was necessary to obtain an increase in the yield with comparable ee compared to the parent reaction. As an initial result, it provided direction on how this system might be improved further, for example, by decreasing the amount of additive to a catalytic loading, then carrying out the reaction under standard biphasic reaction conditions in the presence of $K_3PO_4$(aq). Alas, the scope and application of this finding is the subject of future work.

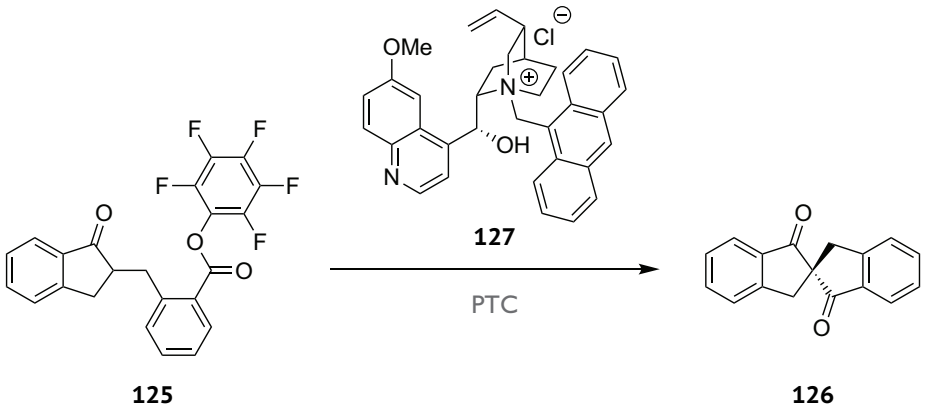
However, we had discovered that introducing mildly basic additives in phase-transfer systems may improve the rates of otherwise slow reactions. The potential of introducing other mildly basic additives in phase-transfer reactions, and the investigation of their precise effects, remains an exciting prospect.

## 3.15 Availability of data

All of the kinetic data that was acquired and generated over the course of this project is available as electronic supporting information. The raw and processed data for every practical experimental reaction are located in the folder: "spirok-reaction-data". Reference of each experiment is by the designated reaction code (*rxn.code*, for example "spirok-27"). The R workspace that was used to process the raw data are also made available (in folder "R-kinetics"). All working theoretical models are given as .nb files that were used in Mathematica (in folder "spirok-mathm-files") and additionally as .txt files. The final model output (from model 6) for every reaction is provided (in folder "spirok-model-output").

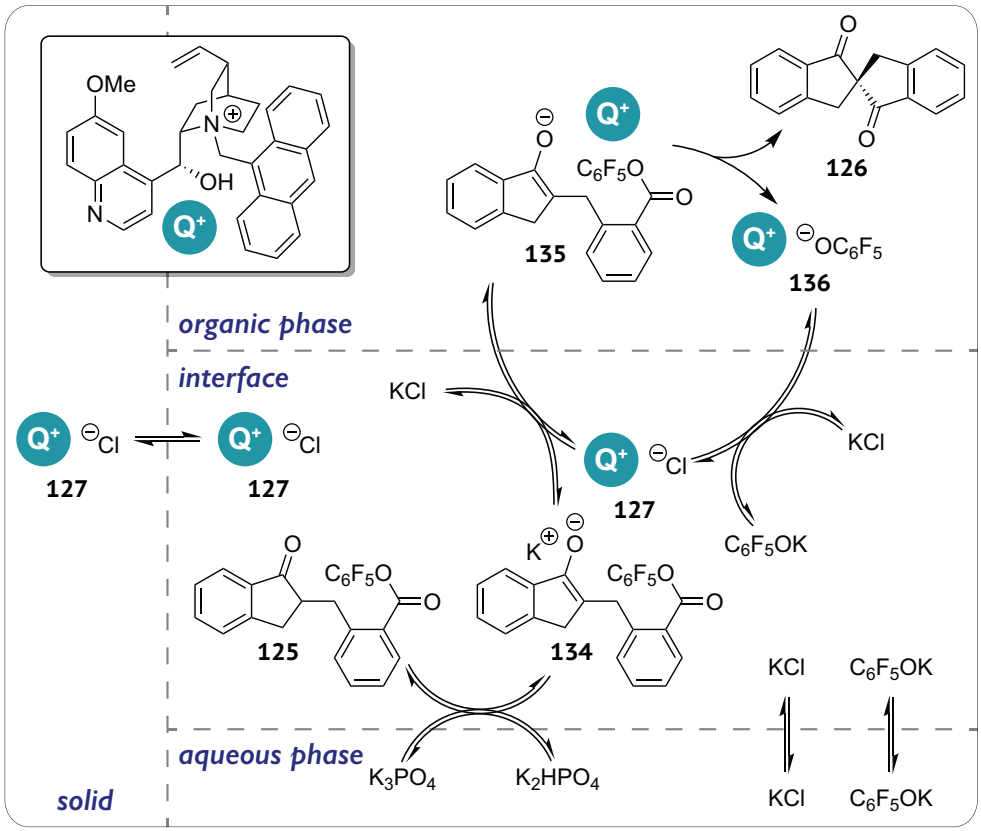
## 3.16 Summary and conclusions of the project

This chapter described the kinetic and mechanistic study of a reaction model: intramolecular *C*-acylation to give spirobiindanone (Scheme 3.48). We began with the thorough consideration of chemicals, equipment, and procedures that we might utilise throughout the duration of the study before all required materials were sourced. We developed a reliable assay for quantifying reaction mixtures over time, and implemented strict protocols for carrying out reactions. The result of the considerable pre-planning was that we immediately obtained reliable, reproducible results when examining reactions over times less than 1500 min.




**Scheme 3.48: Selected asymmetric PTC reaction model for study.**

Our initial hypothesis for the reaction was that it proceeded via a classical interfacial reaction mechanism (Scheme 3.49). Preliminary investigations indicated that this hypothesis was incorrect.




**Scheme 3.49: Initial hypothesis for the cyclisation reaction.**

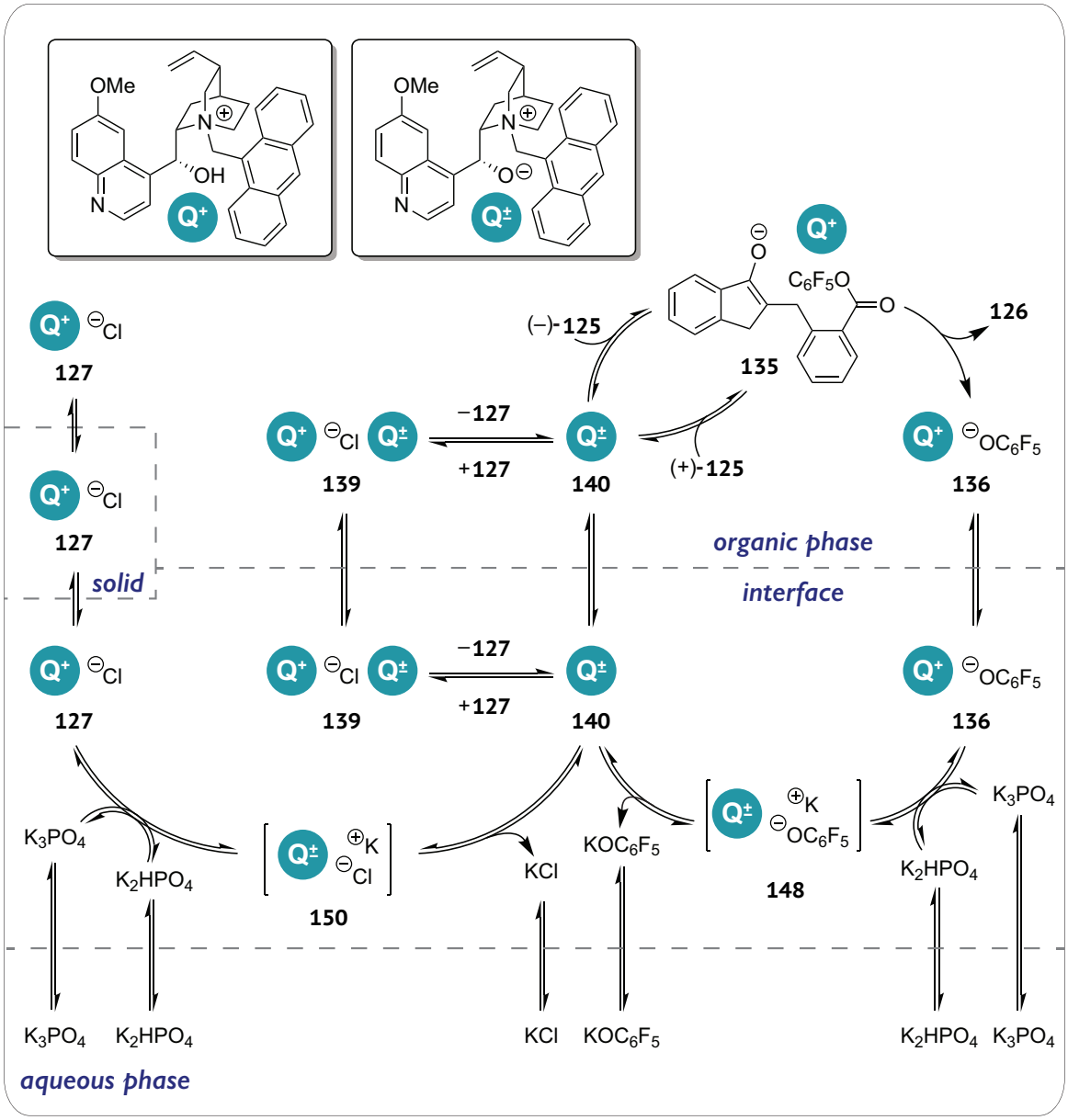
A key finding when examining the reaction for the majority of its duration was the significant kinetic resolution of the substrate **125**. This information indicated a catalyst species was responsible for not only directing facial selectivity of the cyclisation step, but also deprotonation and activation of the substrate. We proposed the active catalyst species responsible was ammonium oxide zwitterion **140**, which was consistent with p$K_a$ data and previous findings.

The rate-determining step in our reaction system was identified to be regeneration of the active zwitterion from the in situ-generated ammonium phenolate **136**. This step was independent to the concentration of substrate or the substrate enolate. By deploying ammonium phenolate **136** as the initial catalyst, we verified the expected kinetic behaviour when commencing the reaction from the rate-determining step. The distribution of catalyst species highly dictated the outcomes of the kinetic behaviour of the reactions.

Throughout the practical experimental investigations, we constructed and evaluated theoretical models of our developing hypotheses. We found the rate-determining step was likely part

of a two-step process via an ammonium salt complex **148**. We had obtained good theoretical evidence for the existence of previously undisclosed catalyst intermediates **150** and **148**. However, additional studies to verify the identities of the proposed intermediates remain the subject of future work.

The end result was good comprehension of the reaction mechanism for our selected model system. Our final hypothesis for the reaction was thus constructed (Scheme 3.50).




**Scheme 3.50: Final hypothesis for the spirocyclisation reaction model.**

We commenced this project with the perspective that it would be a simple reaction model to study. Our experience was that it was highly convoluted with subtle aspects contributing

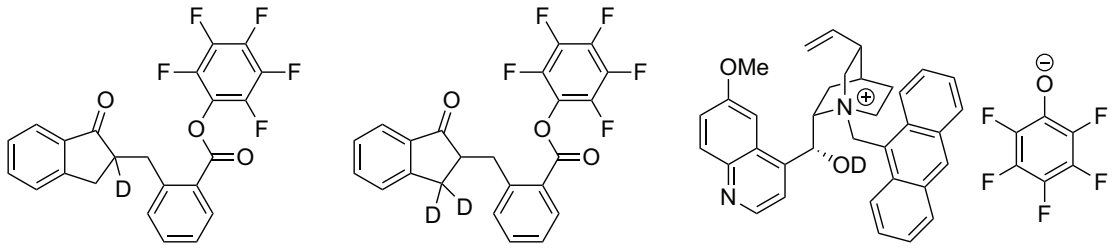
to the rate behaviour that we observed. Ultimately, a combination of both theoretical and practical experimental approaches were required to deconvolute the mechanism of the reaction in question.

## 3.17 Future work

Several aspects of this project remain unexplored. These include investigating the role of chloride in the reaction system, the origin of the isotope effect values, the reaction order with respect to ammonium phenolate **136**, the nature of the proposed catalyst intermediates, and the effects of additives to improve catalytic efficiency.

To further explore the role of chloride in the reaction, a number of control experiments have yet to be carried out. We found that added KCl in the reaction with ammonium halide catalyst **127** had no effect, yet the reaction with ammonium phenolate **136** and added LiCl exhibited a diminished rate. Thus, evaluation of reactions with added LiCl and KCl with either ammonium halide **127** or phenolate **136** catalysts are required.

The KIE values that we obtained when subjecting the mixed substrate **144** to the cyclisation reaction conditions were complicated by both the deuteration pattern of the substrate, and the relatively low deuterium incorporation. Ideally we would access the singly α-deuterated and the doubly β-deuterated substrates, **143** and **157** (Scheme 3.51), via alternative synthetic routes. The capacity for the catalyst scaffold to be deuterated under the reaction conditions was a potential contributing factor to the observed isotope effects, which requires synthesis of the corresponding intermediate—the catalyst bearing the O−D group **147**—and evaluation of the material under adequate reaction conditions. By subjecting these substrates to the reaction conditions, and analysing the acquired kinetic data, we might conclusively obtain isotope effect values, and ascertain the origin of the effects.




**143** α-deuterated substrate

**157** β-deuterated substrate

**147** deuterated catalyst scaffold

**Scheme 3.51: Deuterated materials for further investigation into the observed isotope effects**.

The mathematical treatment to determine the reaction order with respect to $K_3PO_4$ in the rate-determining step also predicts an order with respect to ammonium phenolate **136** of 0.5 (see equation 3.36). These experiments are ongoing and will provide evidence for or against the proposed two-step process to regenerate zwitterion **140** from ammonium phenolate **136** (see Scheme 3.38).

Additional investigations include the synthesis and characterisation of the proposed dimer **139** and zwitterion **140**. Previous work by Hughes and co-workers isolated material that was characterised as the corresponding dimer in their system.[29] Reproducing their result with the ammonium halide catalyst **127** would be an adequate starting point.

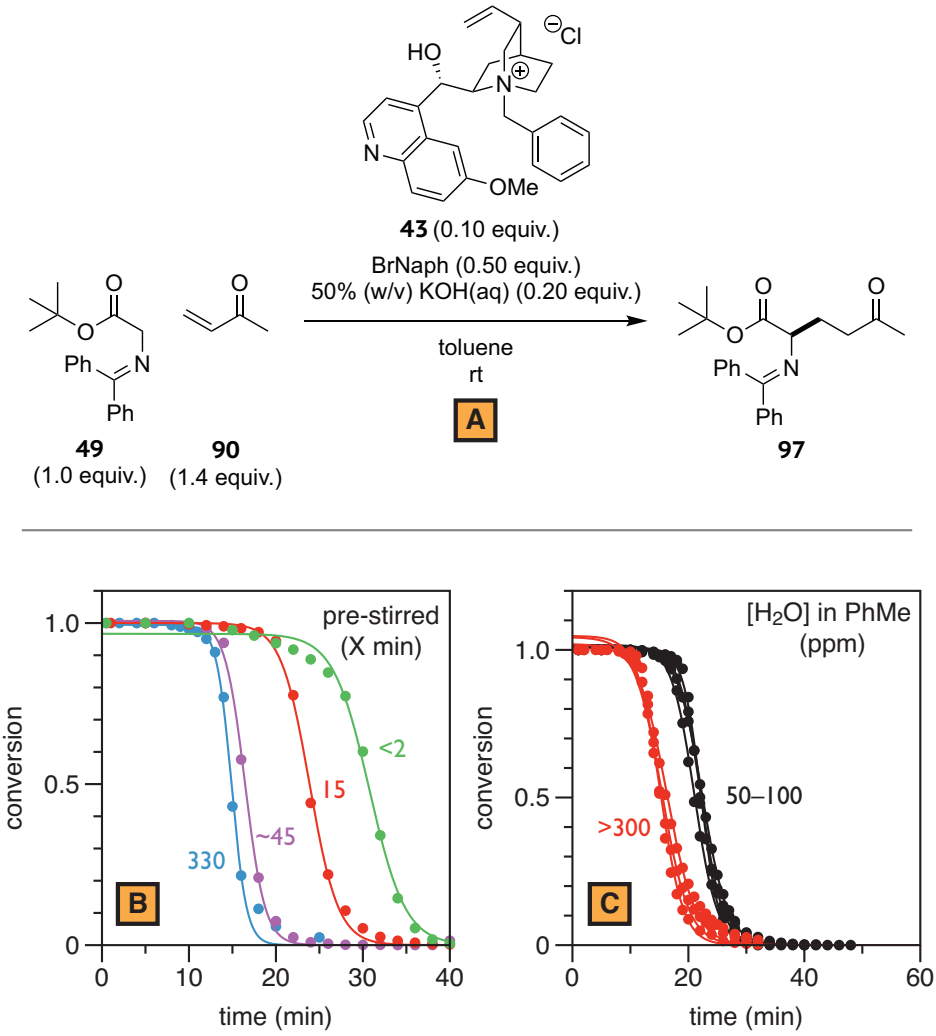
There is scope for further exploration of the effects of hydroquinine or quinine as an additive in the reaction. Reducing the quantity of additive to a catalytic loading might be viable for improving the rate of the reaction without compromising the enantioselectivity. Rationalising the source of the catalytic improvement might be interesting, with additional consequences to enantioselective phase-transfer catalysis effected by cinchona alkaloid-derived catalysts in general.

These are examples of studies that are ongoing work in this particular project. Further work would be to apply the methods and approaches developed in this thesis, both theoretical and experimental, to elucidate other interesting asymmetric phase-transfer reaction models.

# 4. Summary and Conclusions

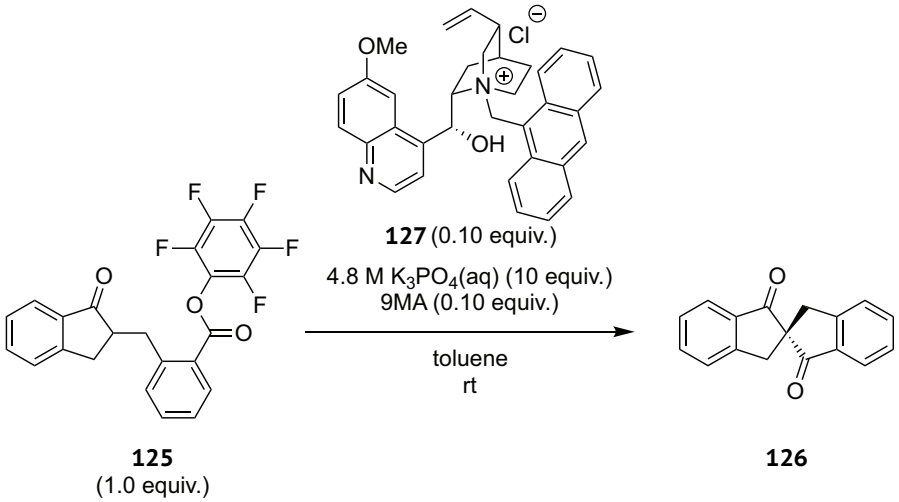
This thesis has described the development of practical methods for scrutinising asymmetric phase-transfer catalysis and the application of those methods in the mechanistic elucidation of an intramolecular *C*-acylation reaction model.

Chapter 2 focused on developing practical methods that enabled the interrogation of asymmetric phase-transfer catalysis. A bimolecular model reaction was carefully selected (A, Scheme 4.1), which facilitated the development of methods whilst exhibiting interesting kinetic behaviour. Obtaining kinetically reproducible results initially presented a series of challenges, which were each addressed by controlling many practical aspects of the reaction, e.g. the time the reaction mixture was stirred before initiation (B, Scheme 4.1) and the water content of the organic solvent (C, Scheme 4.1). Ultimately, the reaction mechanism of the selected bimolecular system remained elusive and we sought to examine an intramolecular reaction in its place.



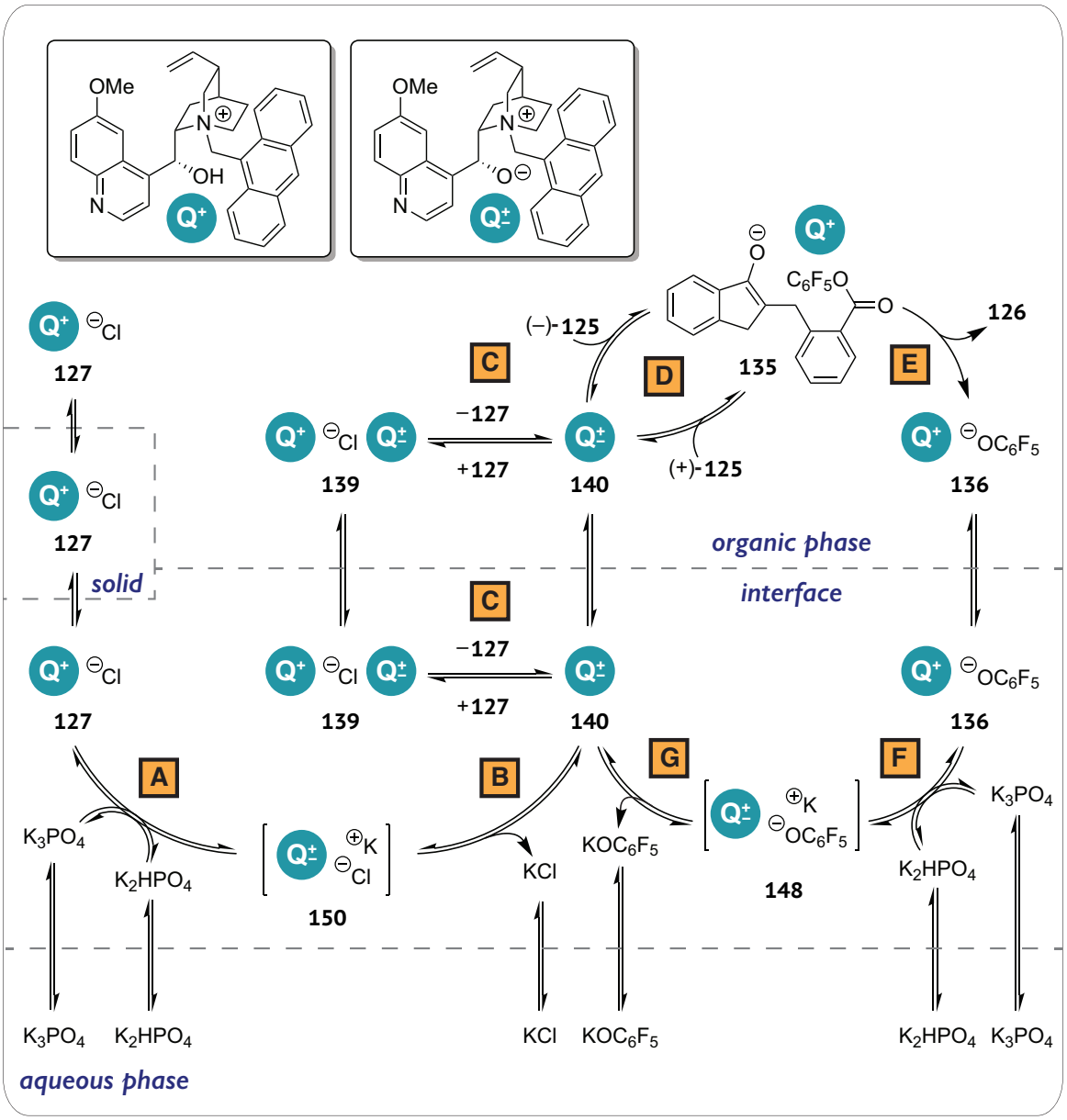

**Scheme 4.1: Bimolecular reaction model and examples of kinetic outcomes.**

The model reaction that we chose to study in detail was the intramolecular phase-transfer catalysed cyclisation reaction to give spirobiindanone (Scheme 4.2), which was the subject of Chapter 3. The investigative study relied on both practical experimental results and theoretical approaches.




**Scheme 4.2: Selected model reaction for study.**

The reaction mechanism, which was initially thought to be simple, was found to be subtly complex (Scheme 4.3). The ammonium halide salt **127** deployed as the catalyst in the reaction was likely a pre-catalyst, that under phase-transfer reaction conditions, generated the corresponding organosoluble zwitterion **140**, which was proposed to be the active catalyst species (A to B, Scheme 4.3). The zwitterion **140** was in equilibrium with the inactive dimer **139** (C, Scheme 4.3). The rate-determining processes in the reaction did not involve the substrate (e.g. D and E, Scheme 4.3), and were proposed to be from catalyst regeneration or activation steps (A to B and F to G, Scheme 4.3). Overall, our final hypothesis was consistent with the majority of both practical and theoretical experimental results. Using the understanding we had gleaned from the mechanistic hypothesis, we were able to commence work aimed at improving the catalytic efficiency of the model system.




**Scheme 4.3: Final hypothesis for the spirocyclisation reaction model.**

To conclude, despite the breadth and scope of enantioselective phase-transfer catalysis as a technique in organic chemistry, there is relatively little understanding of the mechanisms behind the catalysis; particularly when deploying cinchona alkaloid-derived ammonium salts as catalysts. This may be due to the challenge of obtaining reproducible results when attempting kinetic analysis of such systems, or the complexity of potential outcomes. We found that, indeed, studying enantioselective phase-transfer catalysis was initially, a formidable exercise. However, we were able to develop methods to scrutinise catalytic systems and use them to deconvolute the mechanism of our selected model reaction.

# 5. General Experimental Details

## 5.1 General information relevant to material syntheses and characterisation

### 5.1.1 Naming and numbering

Compounds have been named according to IUPAC recommendations or with commonly used names where appropriate. For ease of assignment, the atomic numbering system is arbitrarily designated, and does not correspond to IUPAC names.

### 5.1.2 Reaction conditions, solvents, and reagents

Where specified, "anhydrous" conditions corresponds to reactions carried out using oven-dried glassware under an inert atmosphere (nitrogen or argon), unless otherwise specified. Room temperature (rt) refers to 20–22 °C. Reflux conditions were obtained using a Drysyn® heating block of appropriate size equipped with a contact thermometer.

Anhydrous solvents were obtained by purification through activated alumina prior to use,[133] or dehydration using molecular sieves.[134] Unless specified, all solvents and reagents were used as supplied. "Petrol" corresponds to the fractions of petroleum boiling between 40 °C and 60 °C.

### 5.1.3 Chromatography

Thin layer chromatography (TLC) was carried out on Merck Kieselgel 60, $F_{254}$ 0.25 mm pre-coated aluminium plates. Visualisation was achieved by UV light ($\lambda_{max}$ = 254 nm) and/or by staining with potassium permanganate solution. Flash column chromatography was performed

using silica gel 60 (0.043–0.063 nm, VWR) using nitrogen head pressure.[135]

### 5.1.4 Nuclear magnetic resonance (NMR) spectroscopy

NMR spectra were recorded on either a Bruker AVIIIHD 500, Bruker AVII 500 with 13C cryoprobe, Bruker AVIIIHD 600 with Prodigy broadband cryoprobe, or Bruker AVIII 700 with 1H/13C/15N TCI cryoprobe. Chemical shifts in $^{1}$H-NMR spectra are reported in ppm with signal splitting: for example, singlet (s), doublet (d), doublet of doublets (dd), doublet of doublet of doublets (ddd), multiplet (m), doublet of doublet of multiplets (ddm), etc. Coupling constants ($J$) are reported to the nearest 0.5 Hz. $^{19}$F-NMR spectra were referenced externally to $CFCl_3$ (0 ppm). Spectra were assigned using additional data acquired by COSY, HSQC, HMBC, and/or NOESY.

### 5.1.5 HPLC

Analytical HPLC was carried out on a Thermo UltiMate 3000 HPLC system comprising of a Thermo LPG-3400A pump, WPS-3000SL autosampler, TCC-3000SD column compartment, and an appropriate Daicel Chiralpak column (0.46 cm (⌀) × 25 cm) and guard column (0.4 cm (⌀) × 1 cm). Wavelengths are reported in nm, analyte retention times are reported in min and solvent flow rates are reported in mL min$^{-1}$.

### 5.1.6 Infrared spectroscopy

Infrared (IR) spectra were recorded on a Bruker Tensor 27 FTIR spectrometer equipped with a diamond ATR module. Absorption maxima ($\nu_{max}$) are quoted in wavenumbers (cm$^{-1}$).

### 5.1.7 Mass spectrometry

Low-resolution mass spectrometry (LRMS) was carried out on a Micro Mass LCT Premier spectrometer under conditions of electrospray ionization (ESI). High-resolution mass (HRMS) spectra were recorded on a Bruker MicroTOF under conditions of electrospray ionization (ESI).

### 5.1.8 Polarimetry

Optical rotations were recorded on a Schmidt-Haensch Unipol L2000 polarimeter. Values are quoted in $^\circ$ mL g$^{-1}$ dm$^{-1}$. Concentrations ($c$) are reported in g/100 mL and temperatures in °C.

### 5.1.9 Melting points

Melting points were measured using Reichert melting point apparatus and are uncorrected.

## 5.2 General information relevant to the kinetic studies in project 1 (additions)

All kinetic experiments were carried out at ambient room temperature (rt) which was maintained at 20–22 °C. Unless otherwise stated, no precautions were made to subject the reaction mixtures to inert atmospheres.

All kinetic reactions were carried out in non-rounded 7 mL screw-cap vials ($\varnothing = 1.5$ cm). Stirrer bars that were deployed as single use only, were obtained from Fisher Scientific (8 mm × 3 mm; 11818892). Vial holders used in the reactions were specifically fabricated to fit the dimensions of the reaction vials. Liquid volumes were handled using automatic pipettes, gas-tight syringes, or volumetric flasks of appropriate capacity.

Non-synthesised materials that were used in the kinetic studies were obtained as follows: catalyst **43** was obtained from TCI (B1684 Lot IFJ2G-CE) and was used without further purification; methyl vinyl ketone (MVK) (99%; contains 0.5% hydroquinone and 0.1% acetic acid as stabilizer; 269549) was obtained from Sigma-Aldrich and was used without further purification—MVK was stored at −20 °C and allowed to warm to rt before use; 1-bromonaphthalene (BrNaph) (97%; B73104) was obtained from Sigma-Aldrich, was distilled prior to use and was stored in the dark; 50% (w/v) KOH(aq) was prepared as a 500 mL batch (using a 500 mL volumetric flask), and was stored in ∼20 mL containers under argon.

## 5.3 General information relevant to the kinetic studies in project 2 (spirok)

All kinetic experiments were carried out at ambient room temperature (rt) which was maintained at 20–22 °C. Unless otherwise stated, no precautions were made to subject the reaction mixtures to inert atmospheres.

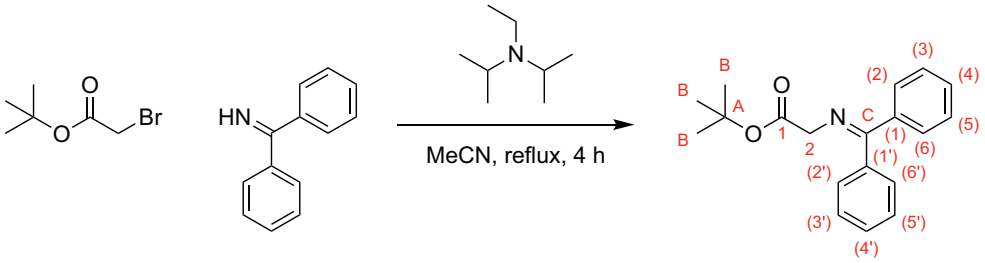
Unless otherwise stated, all kinetic reactions were carried out in rounded 10 mL magnetic screw-cap vials (Precision Thread Headspace Vial 46 mm × 22.5 mm, clear glass; 11506114), obtained from Fisher Scientific. Stirrer bars were deployed as single use only, and were obtained from Fisher Scientific (12 mm × 3 mm; 11587572), unless otherwise specified. Vial holders used in the reactions were specifically fabricated to fit the dimensions of the reaction vials. Liquid volumes were handled using automatic pipettes and volumetric flasks of appropriate capacity.

Non-synthesised materials that were used in the kinetic studies were obtained as follows: 9-methylanthracene (9MA) (analytical standard; 45793) was obtained from Sigma-Aldrich, and used without further purification; saturated aqueous $K_3PO_4$ was prepared as a single batch and was titrated to 4.77 M.

# 6. Project 1: Experimental

## 6.1 Material syntheses and characterisation

### 6.1.1 *tert*-Butyl-2-((diphenylmethylene)amino)acetate (49)




**158** **159** **49**

Literature procedure.[136] A solution of *tert*-butyl 2-bromoacetate **158** (11 mL, 72 mmol, 1.0 equiv.), benzophenoneimine **159** (12 mL, 72 mmol, 1.0 equiv.), and diisopropylethyl amine (12.5 mL, 72 mmol, 1.0 equiv.) in acetonitrile (80 mL) was heated at reflux for 4 h. The now dark yellow solution was allowed to cool, then carefully concentrated under reduced pressure until solid material just started to precipitate. Diethyl ether (150 mL) was added and the mixture was washed with water (80 mL) to give a clear biphasic mixture. The aqueous layer was extracted with diethyl ether (2 × 200 mL). The combined organic fractions were dried ($Na_2SO_4$) and partially concentrated under reduced pressure until solid material just started to precipitate. The solution was allowed to stand at rt overnight to give *the title compound* as fine colourless needles. The crystals were isolated via filtration, washed with minimal diethyl ether, and dried *in vacuo*. The crystallisation process was repeated with the mother liquor to produce *the title compound* with a total yield of 11 g, 52%;

mp 111–112 °C;

$\nu_{max}$ (neat) 2977, 1735, 1624, 1367, 1147, 694;

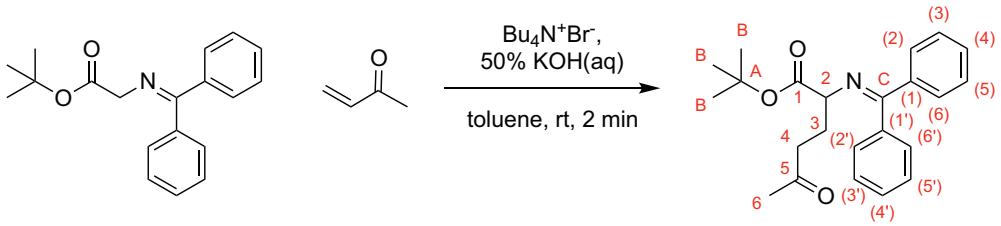
$^{1}$H-NMR: $\delta$ (500 MHz, $CDCl_3$) 7.70–7.68 (m, 2 H, *H(2)* and *H(6)*), 7.51–7.46 (m, 3 H, *H(3′)*, *H(4′)*, and *H(5′)*), 7.44–7.40 (m, 1 H, *H(4)*), 7.37–7.34 (m, 2 H, *H(3)* and *H(5)*), 7.22–7.20 (m, 2 H, *H(2′)* and *H(6′)*), 4.15 (s, 2 H, *H2*), 1.49 (s, 9 H, *HB*);

$^{13}$C{$^{1}$H}-NMR: $\delta$ (126 MHz, $CDCl_3$) 171.5 (*CC*), 169.9 (*C1*), 139.4 (*C(1)*), 136.2 (*C(1′)*), 130.4 (*C(4)*), 128.8 (*C(2)* and *C(6)*), 128.7 (*C(4′)*), 128.6 (*C(3′)* and *C(5′)*), 128.0 (*C(3)* and *C(5)*), 127.7 (*C(2′)* and *C(6′)*), 81.1 (*CA*), 56.3 (*C2*), 28.1 (*CB*);

LRMS (ESI) 296.2 ($[M+H]^+$).

Data in accordance with the literature.[136–138]

### 6.1.2 Racemic *tert*-butyl 2-((diphenylmethylene)amino)-5-oxohexanoate (97)




**49** **90** **97**

A clear, colourless solution of **49** (0.50 g, 1.7 mmol, 1.0 equiv.) and $Bu_4N^+Br^-$ (0.055 g, 0.17 mmol, 0.10 equiv.) in toluene (8.5 mL) was vigorously stirred at rt before 50% (w/v) KOH (0.38 mL, 3.4 mmol, 2.0 equiv.) was added. Methyl vinyl ketone (0.20 mL, 2.5 mmol, 1.5 equiv.) was added to the now yellow solution, which resulted in the mixture turning briefly colourless. The mixture was stirred at rt for a further 2 min before it was poured over water (20 mL). The aqueous layer was extracted with diethyl ether (2 × 30 mL). The combined organic fractions were dried ($MgSO_4$) and concentrated under reduced pressure. The crude product was purified by flash chromatography on silica gel (5–15% (v/v) ethyl acetate/petrol) to give *the title compound* as a colourless oil (0.52 g, 87%);

$\nu_{max}$ (neat) 2977, 2934, 1731, 1624, 1446, 1368, 1316, 1288, 1254, 1150, 848, 782, 698;

$^{1}$H-NMR: $\delta$ (500 MHz, $CDCl_3$) 7.67–7.65 (m, 2 H, *H(2)* and *H(6)*), 7.48–7.44 (m, 3 H, *H(3′)*,

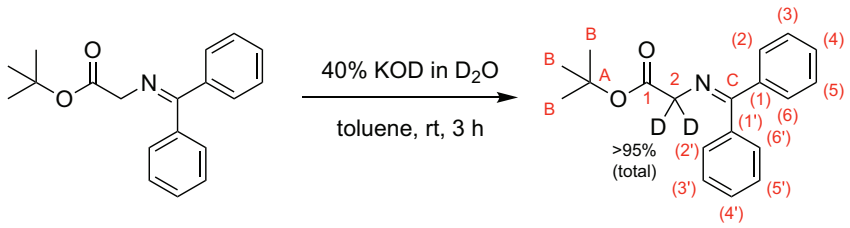
*H(4′)*, and *H(5′)*), 7.42–7.39 (m, 1 H, *H(4)*), 7.36–7.33 (m, 2 H, *H(3)* and *H(5)*), 7.20–7.17 (m, 2 H, *H(2′)* and *H(6′)*), 3.99–3.97 (m, 1 H, *H2*), 2.60–2.47 (m, 2 H, *H4*), 2.19–2.15 (m, 2 H, *H3*), 2.14 (s, 3 H, *H6*), 1.46 (s, 9 H, *HB*);

$^{13}C\{^{1}H\}$-NMR: $\delta$ (126 MHz, $CDCl_3$) 208.3 (*C5*), 171.0 (*CC*), 170.5 (*C1*), 139.5 (*C(1)*), 136.5 (*C(1′)*), 130.3 (*C(4)*), 128.8 (*C(2)* and *C(6)*), 128.6 (*C(4′)*), 128.5 (*C(3′)* and *C(5′)*), 128.0 (*C(3)* and *C(5)*), 127.7 (*C(2′)* and *C(6′)*), 81.1 (*CA*), 64.7 (*C2*), 39.9 (*C4*), 29.9 (*C6*), 28.1 (*CB*), 27.7 (*C3*);

LRMS (ESI) 366.2 ($[M+H]^+$).

Data in accordance with the literature.[103]

### 6.1.3 *tert*-Butyl 2-((diphenylmethylene)amino)acetate-$d_2$ (116)




**49** **116**

Imine **49** (1.0 g, 3.4 mmol, 1.0 equiv.) was dissolved in anhydrous toluene (20 mL) in a dried flask under argon. A solution of 40% KOD in $D_2O$ (3.0 mL, 34 mmol, 10 equiv.) was added and the biphasic mixture was stirred under argon for 3 h before $D_2O$ (10 mL) was added. The mixture was opened to the air and the aqueous layer was extracted with anhydrous diethyl ether (2 × 20 mL). The combined organic fractions were dried ($Na_2SO_4$) and concentrated under reduced pressure to give a colourless solid. Recrystallisation of the crude material from diethyl ether gave *the title compound* as fine colourless needles (0.32 g, 32%);

mp 111–113 °C;

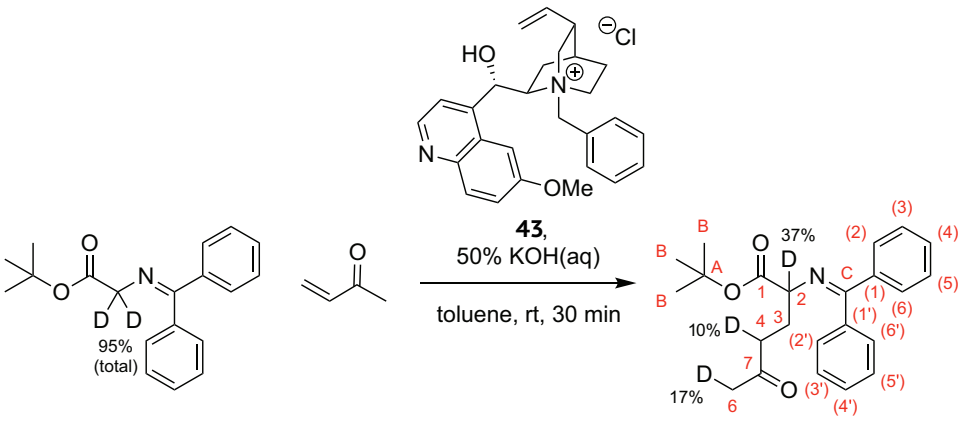
$\nu_{max}$ (neat) 2978, 1736, 1625, 1315, 1273, 1257, 1163, 1109, 695;

$^{1}$H-NMR: $\delta$ (500 MHz, $CDCl_3$) 7.70–7.68 (m, 2.0 H, *H(2)* and *H(6)*), 7.50–7.46 (m, 3.0 H, *H(3′)*, *H(4′)*, and *H(5′)*), 7.43–7.40 (m, 1.0 H, *H(4)*), 7.37–7.34 (m, 2.0 H, *H(3)* and *H(5)*), 7.22–7.20 (m, 2.0 H, *H(2′)* and *H(6′)*), 4.13–4.12 (m, 0.047 H, *H2*), 1.49 (s, 9 H, *HB*);

$^{13}$C{$^{1}$H}-NMR: $\delta$ (126 MHz, $CDCl_3$) 171.6 (*CC*), 169.8 (*C1*), 139.4 (*C(1)*), 136.2 (*C(1′)*), 130.4 (*(4)*), 128.8 (*C(2)* and *C(6)*), 128.7 (*C(4′)*), 128.6 (*C(3′)* and *C(5′)*), 128.0 (*C(3)* and *C(5)*), 127.7 (*C(2′)* and *C(6′)*), 81.0 (*CA*), 56.3–55.4 (m, *C2*), 28.1 (*CB*);

HRMS (ESI) 298.17664 ([M+H]$^{+}$), calcd. for $C_{19}H_{20}D_2NO_2^{+}$ 298.17706.

### 6.1.4 *tert*-Butyl 2-((diphenylmethylene)amino)-5-oxohexanoate-2,4,6-$d_n$ (117)




**116** **90** **117**

A sample of *the title compound* was isolated following execution of the protocol described in 6.11. The reaction mixture was directly purified by flash chromatography on silica gel (5–15% (v/v) ethyl acetate/petrol) to give *the title compound* as a colourless oil (50 mg, 82% yield);

$\nu_{max}$ (neat) 2977, 2933, 1716, 1623, 1446, 1367, 1315, 1288, 1255, 1150, 1095, 847, 782, 697;

$^{1}$H-NMR: $\delta$ (500 MHz, $CDCl_3$) 7.67–7.65 (m, 2.0 H, *H(2)* and *H(6)*), 7.48–7.44 (m, 3.0 H, *H(3′)*, *H(4′)*, and *H(5′)*), 7.42–7.39 (m, 1.0 H, *H(4)*), 7.36–7.33 (m, 2.0 H, *H(3)* and *H(5)*),

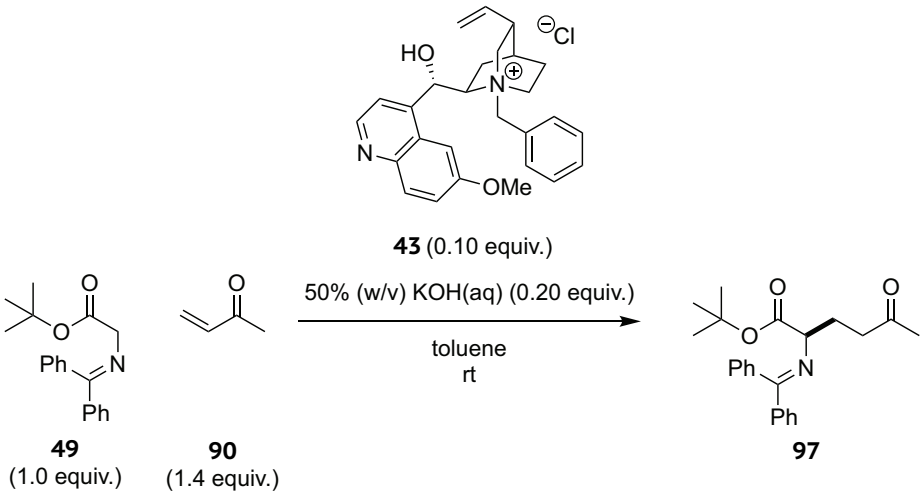
7.20–7.17 (m, 2.0 H, *H(2′)* and *H(6′)*), 3.99–3.97 (m, 0.63 H, *H2*), 2.60–2.47 (m, 1.8 H, *H4*), 2.19–2.12 (m, 4.5 H, *H3* and *H6*), 1.46 (s, 9.0 H, *HB*);

$^{13}C\{^{1}H\}$-NMR: $\delta$ (126 MHz, $CDCl_3$) 208.4, 208.3, 208.3, 171.0, 171.0, 170.5, 139.5, 136.5, 130.3, 128.8, 128.6, 128.5, 128.0, 127.7, 81.2, 64.7, 39.9, 39.8, 29.9, 29.8, 29.7, 29.5, 28.1, 27.7, 27.7, 27.6, 27.6 (due to the complexity of the acquired spectrum, all peaks have been reported and are unassigned);

LRMS (ESI) 389 ($[M+Na]^+$ as $C_{23}H_{26}DNNaO_3^+$).

## 6.2 Preliminary kinetic results

### 6.2.1 Conditions and protocols




Equivalents (equiv.) are reported with respect to substrate **49**.

A mixture of substrate **49** (50 mg. 0.17 mmol, 1.0 equiv.), catalyst **43**, (7.6 mg, 0.017 mmol, 0.10 equiv.), and 50% (w/v) KOH(aq) (3.8 µL, 0.034 mmol, 0.20 equiv.) in toluene (1.7 mL) was vigorously stirred before the addition of methyl vinyl ketone **90** (MVK) (20 µL, 0.24 mmol, 1.4 equiv.). Initiation of the reaction and the designated time zero was upon addition of MVK.

The reactions were sampled over time by extracting aliquots (1 µL) from the reaction mixtures,

which were then filtered through a short plug of silica gel, eluting 30% (v/v) 2-propanol/hexane (∼1.6 mL by syringe) under a stream of nitrogen. The filtrate was directly analysed by HPLC (ChiralPak® IC, 1.000 mL $min^{-1}$, 20% (v/v) 2-propanol/hexane, 25 °C). An example of an acquired chromatogram is shown below (Figure 6.1).

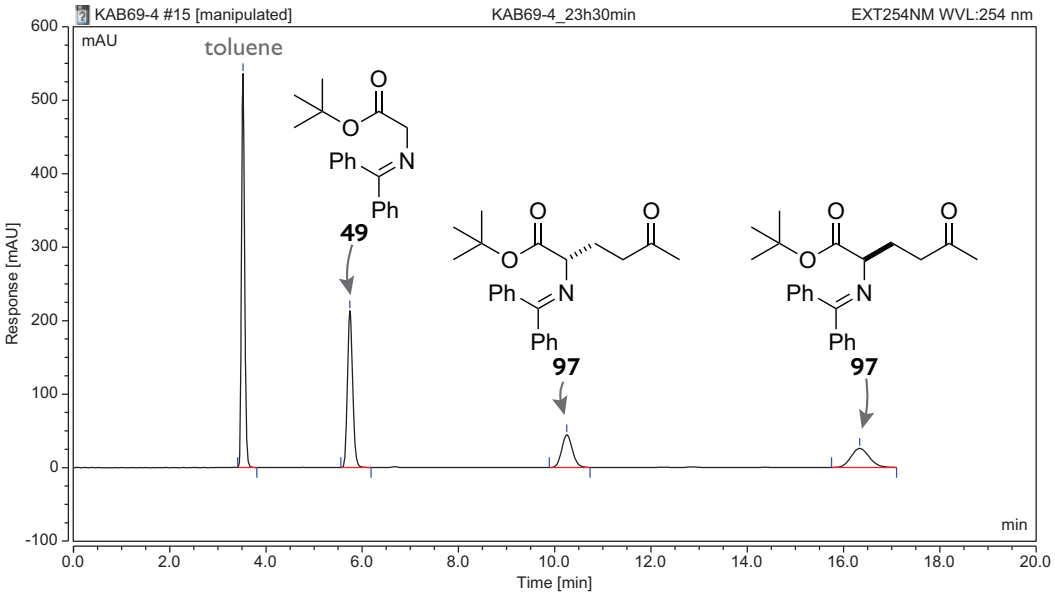



**Figure 6.1: Example chromatogram obtained from an extracted and processed reaction aliquot.** The $x$-axis represents retention time, and the $y$-axis UV absorption at the extracted wavelength (254 nm). Peak identities are indicated on the chromatogram. Depiction of stereochemistry is arbitrary.

### 6.2.2 Graphical results

To qualitatively gauge conversion of the substrate **49** to product **97** (both enantiomers) in both reactions, the ratios of the signal integrals corresponding to the analytes were taken and plotted in DataGraph (Figure 6.2 and Figure 6.3). In both graphs, the amount of substrate **49** is represented by the red data, the total amount of product **97** is depicted by the blue data. The $x$-axis in both graphs corresponds to the time following initiation of the reaction, the $y$-axes correspond to the ratio of signals corresponding to the substrate **49** and product **97** by HPLC. The lines are guides for the eye.

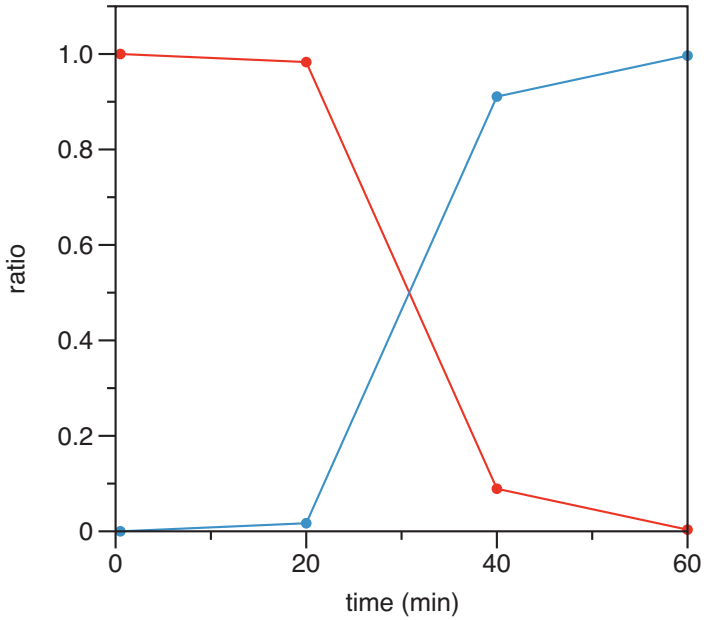



**Figure 6.2: Results obtained from the first reaction.**

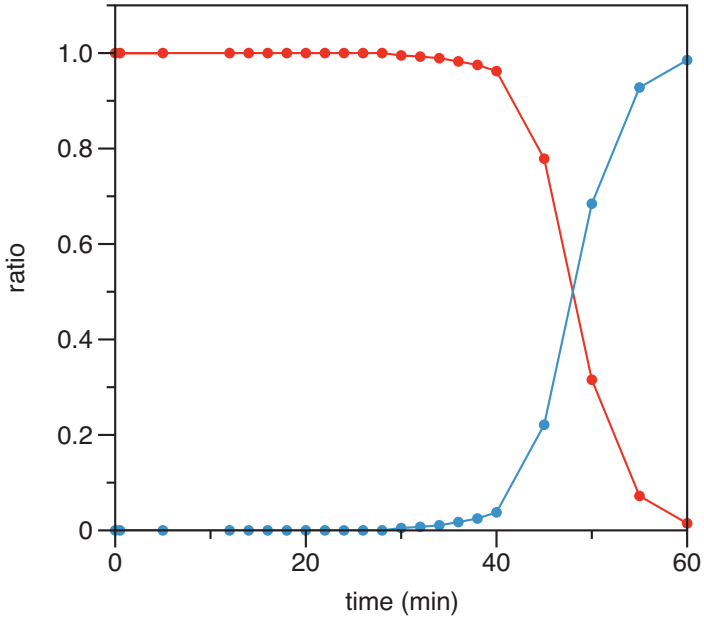



**Figure 6.3: Results obtained from the repeated reaction.**

## 6.3 Quantitative HPLC assay

### 6.3.1 Sample preparations

Solutions of the internal standard 1-bromonaphthalene **115** (BrNaph), substrate **49**, and racemic product **97** were made up in toluene (added 1.0 mL) (see Table 6.1 for full details). An

aliquot (100 µL) was extracted from each sample and diluted with 30% (v/v) 2-propanol/hexane then analysed by HPLC. An example chromatogram is shown below in Figure 6.4. One standard curve was constructed for the substrate **49**, and the product **97** enantiomers using BrNaph **115** as the internal standard, and in the presence of toluene.

**Table 6.1: Quantities of internal standard 115, substrate 49, and racemic product 97 added to each sample used to construct the standard curves.** Descriptions are of the amounts added to each sample before the addition of toluene (1.0 mL) and dissolution of material, and *not* the amounts added to the 30% (v/v) 2-propanol/hexane solutions.

| **Entry** | **115 (mg)** | **115 (mmol)** | **49 (mg)** | **49 (mmol)** | **97 (mg)** | **97 (mmol)** |
|---|---|---|---|---|---|---|
| 1 | 10.4 | 0.0502 | 0.0 | 0.0 | 34.5 | 0.0982 |
| 2 | 9.8 | 0.047 | 2.2 | 0.0074 | 29.3 | 0.08337 |
| 3 | 10.0 | 0.0483 | 2.8 | 0.0095 | 29.3 | 0.0834 |
| 4 | 10.2 | 0.0493 | 4.8 | 0.016 | 21.2 | 0.0603 |
| 5 | 10.2 | 0.0493 | 5.2 | 0.018 | 21.2 | 0.0603 |
| 6 | 10.1 | 0.0488 | 5.6 | 0.019 | 20.8 | 0.0592 |
| 7 | 10.2 | 0.0493 | 8.7 | 0.029 | 11.2 | 0.0319 |
| 8 | 10.3 | 0.0497 | 10.2 | 0.0345 | 10.9 | 0.0310 |
| 9 | 9.9 | 0.048 | 10.9 | 0.0369 | 9.6 | 0.027 |
| 10 | 9.0 | 0.044 | 17.7 | 0.0599 | 3.0 | 0.0085 |
| 11 | 10.1 | 0.0488 | 19.4 | 0.0657 | 6.1 | 0.017 |
| 12 | 10.1 | 0.0488 | 19.9 | 0.0674 | 4.8 | 0.014 |
| 13 | 11.2 | 0.0541 | 31.5 | 0.107 | 1.5 | 0.0043 |
| 14 | 10.4 | 0.0502 | 32.1 | 0.109 | 2.0 | 0.0057 |
| 15 | 10.5 | 0.0507 | 35.2 | 0.119 | 0.0 | 0.0 |

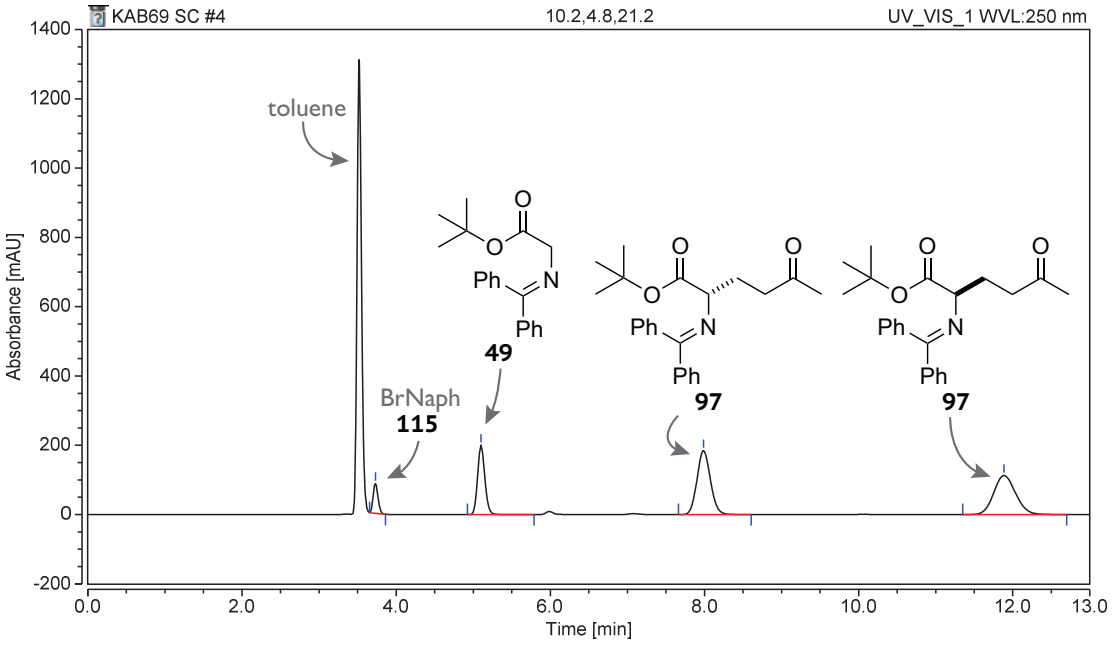



**Figure 6.4: Example HPLC-UV chromatogram of one sample.** The data are extracted at 250 nm. The $x$-axis represents retention time; the $y$-axis is UV absorption at the extracted wavelength. In this sample, the analytes eluted in the following order with their retention times in brackets: BrNaph (3.73 min); **49** (5.10 min); **97** enantiomer 1 (7.99 min); and **97** enantiomer 2 (11.88 min). Peak identities are indicated on the chromatogram. Compound **97** structures are depicted with arbitrary stereochemistry.

### 6.3.2 Standard curves

Three curves were generated, one for each analyte: substrate **49**, product **97** enantiomer 1 (early retention time), and product **97** enantiomer 2 (late retention time) (Figure 6.5). The standard curves were constructed by taking known mole ratios of the analyte (either substrate **49** or 50% of racemic product **97**) against the amount of internal standard BrNaph **115** and plotting the values against the signal integral ratios of the analyte against the signal integral corresponding to the internal standard BrNaph **115**. The data used to construct the curves are detailed in Table 6.2.

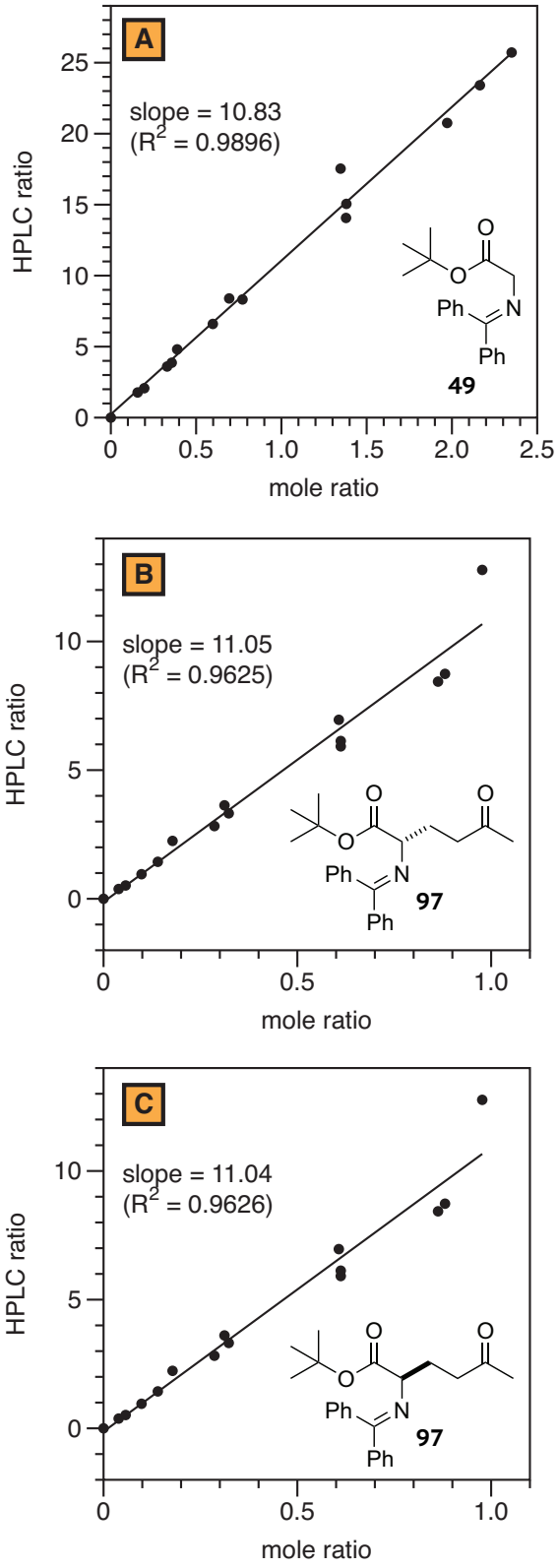



**Figure 6.5: Standard curves for the analytes: A) substrate 49; B) product 97 enantiomer 1; and C) product 97 enantiomer 2.** The calibration factors (slopes) were obtained via linear regression analysis of the data obtained when comparing the mole and HPLC ratios of the analyte to internal standard. The goodness of fit ($R^2$) is indicated on each graph. Stereochemical configuration of the displayed compounds are arbitrary. See Table 6.2 for full details.

**Table 6.2: Data used to construct the standard curves in Figure 6.5.** "Ent-1" and "ent-2" refer to the enantiomers of product **97** that elute early and late by HPLC, respectively; "HPLC int." refers to the signal integral obtained for the corresponding analyte. All data are reported to three dp.

| Entry | 49:115 (mole ratio) | 97 ent-1:115 (mole ratio) | 97 ent-2:115 (mole ratio) | 115 (HPLC int.) | 49 (HPLC int.) | 97 ent-1 (HPLC int.) | 97 ent-2 (HPLC int.) | 49:115 (HPLC ratio) | 97 ent-1:115 (HPLC ratio) | 97 ent-2:115 (HPLC ratio) |
|---|---|---|---|---|---|---|---|---|---|---|
| 1 | 0.000 | 0.977 | 0.977 | 4.388 | 0.000 | 56.070 | 56.002 | 0.000 | 12.779 | 12.764 |
| 2 | 0.157 | 0.881 | 0.881 | 6.084 | 10.770 | 53.180 | 53.111 | 1.770 | 8.740 | 8.729 |
| 3 | 0.196 | 0.863 | 0.863 | 6.899 | 14.291 | 58.219 | 58.176 | 2.071 | 8.439 | 8.433 |
| 4 | 0.330 | 0.612 | 0.612 | 6.049 | 21.769 | 37.085 | 37.057 | 3.599 | 6.131 | 6.126 |
| 5 | 0.357 | 0.612 | 0.612 | 5.678 | 21.957 | 33.627 | 33.596 | 3.867 | 5.923 | 5.917 |
| 6 | 0.389 | 0.607 | 0.607 | 4.904 | 23.581 | 34.112 | 34.152 | 4.808 | 6.955 | 6.964 |
| 7 | 0.598 | 0.323 | 0.323 | 5.106 | 33.691 | 16.953 | 16.935 | 6.598 | 3.320 | 3.317 |
| 8 | 0.694 | 0.312 | 0.312 | 5.465 | 45.869 | 19.840 | 19.724 | 8.394 | 3.631 | 3.609 |
| 9 | 0.772 | 0.286 | 0.286 | 6.188 | 51.503 | 17.477 | 17.456 | 8.324 | 2.825 | 2.821 |
| 10 | 1.379 | 0.098 | 0.098 | 6.016 | 84.612 | 5.743 | 5.739 | 14.064 | 0.955 | 0.954 |
| 11 | 1.347 | 0.178 | 0.178 | 4.857 | 85.182 | 10.922 | 10.853 | 17.537 | 2.249 | 2.234 |
| 12 | 1.381 | 0.140 | 0.140 | 6.458 | 97.214 | 9.277 | 9.269 | 15.053 | 1.437 | 1.435 |
| 13 | 1.972 | 0.039 | 0.039 | 7.651 | 158.781 | 2.906 | 2.897 | 20.754 | 0.380 | 0.379 |
| 14 | 2.164 | 0.057 | 0.057 | 6.505 | 152.276 | 3.365 | 3.361 | 23.410 | 0.517 | 0.517 |
| 15 | 2.350 | 0.000 | 0.000 | 5.878 | 151.157 | 0.000 | 0.000 | 25.717 | 0.000 | 0.000 |

### 6.3.3 Standard curve application

The aliquots sampled from reaction mixtures (see 6.4.1) were analysed by HPLC (20 µL; ChiralPak® IC, 1.000 mL $min^{-1}$, 30% (v/v) 2-propanol/hexane, 25 °C; 250 nm) and the signal integrals of the standard BrNaph **115** (retention time 3.7 min), the substrate **49** (retention time 5.1 min), and product **97** enantiomers (retention times 8.0 and 11.9 min) were obtained.

The HPLC data were saved as .csv files and processed using the relevant R scripts (see 6.4.3 and 8.2). In summary, the scripts calculated the amount (mmol) of each component in the reaction mixture at that point in time, and where relevant, the concentration of the material in the reaction mixture. The general equations that were used to carry out the calculations are described below (in equations 6.1 to 6.3). The calibration factors for each analyte were obtained from the slopes of the standard curves (in Figure 6.5).

Substrate **49**:

$$\text{mol}_a = \frac{\text{int-}a \times \text{mol-}s}{10.83 \times \text{int-}s} \tag{6.1}$$

Where $\text{mol}_a$ is the amount of substrate **49** in mmol in the reaction mixture, int-$a$ is the HPLC signal integral of substrate **49** at 250 nm, mol-$s$ is the amount of standard BrNaph **115** present in the reaction mixture in mmol, 10.83 is the calibration factor for **49**, and int-$s$ is the HPLC signal integral of standard **115** at 250 nm.

Product **97** enantiomer 1 (with retention time of 8.0 min):

$$\text{mol}_b = \frac{\text{int-}b \times \text{mol-}s}{11.05 \times \text{int-}s} \tag{6.2}$$

Where $\text{mol}_b$ is the amount of product **97** enantiomer 1 in mmol in the reaction mixture, int-$b$

is the HPLC signal integral of product **97** enantiomer 1 at 250 nm, mol-$s$ is the amount of standard BrNaph **115** present in the reaction mixture in mmol, 11.05 is the calibration factor for product **97** enantiomer 1, and int-$s$ is the HPLC signal integral of standard **115** at 250 nm.

Product **97** enantiomer 2 (with retention time of 11.9 min):

$$\text{mol}_c = \frac{\text{int-}c \times \text{mol-}s}{11.04 \times \text{int-}s} \tag{6.3}$$

Where $\text{mol}_c$ is the amount of product **97** enantiomer 2 in mmol in the reaction mixture, int-$c$ is the HPLC signal integral of product **97** enantiomer 2 at 250 nm, mol-$s$ is the amount of standard BrNaph **115** present in the reaction mixture in mmol, 11.04 is the calibration factor for product **97** enantiomer 2, and int-$s$ is the HPLC signal integral of standard **115** at 250 nm.

## 6.4 General protocols

### 6.4.1 Sampling protocol

Unless otherwise stated, the reactions were monitored by sampling and analysis as follows: the reaction vial caps were removed 3 s prior to extracting an aliquot. Aliquots (1.50 µL) were sampled directly from the reaction mixtures at the designated times (following initiation of the reaction), without ceasing stirring or disturbing the stirrer bar. The reaction vessels were immediately resealed. The aliquots were immediately quenched by passing through a small plug of silica ($\varnothing$ = 6 mm, $l$ = 3–5 mm), eluting with 30% (v/v) 2-propanol/hexane (∼1.6 mL by syringe) under a stream of nitrogen. The silica plug was dried with a stream of nitrogen prior to elution of the next sample. The aliquots were analysed by HPLC and the contents quantified using the standard curves via processing using the appropriate R scripts.

### 6.4.2 HPLC data collection

The HPLC data from each aliquot was collected and processed at 250 nm using the instrument conditions as follows: ChiralPak® IC, 1.000 mL $min^{-1}$, 30% (v/v) 2-propanol/hexane, 25 °C. The signal integrals of the internal standard, substrate **49**, and product **97** enantiomers were extracted from the acquired chromatograms and subjected to post-reaction processing.

### 6.4.3 Approach for data processing

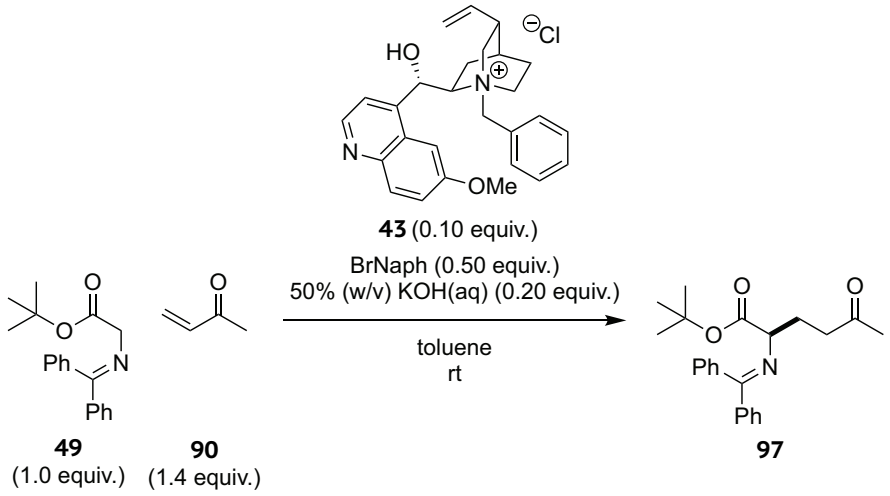
Post-reaction data processing was carried out using a series of R scripts. For full expansions of the R scripts see 8.2. This approach enabled the rapid, consistent, repetitive processing of data. The R scripts processed the HPLC data for each analyte (as .csv data), applied the calibration factors as was determined from the standard curves and calculated the amount present in the reaction mixture (in mmol). The general approach for applying the R scripts was analogous to the method described for project 2 (see 7.4.4).

For the experiments carried out using protocols 1–5, the data were processed as normalised conversion (relative ratio of mmol of substrate **49** to mmol of product **97**). For the data obtained using protocol 6, and the experiments directed at determining the reaction order with respect to substrate **49**, the concentration of the analytes were determined and the data processed as such. The total reaction volume was corrected by considering the volume removed from the reaction mixtures during the sampling protocol. Further details relevant to each applied protocol are described in the relevant sections.

The data were represented graphically (using DataGraph) before further processing. To quantify the processed data, a function was fitted and the values for the parameters extracted. Depending on the shape of the data, either the autocatalytic model was applied (see section 2.2.3) or a that for a first order reaction (see section 2.4.2).

## 6.5 Results obtained using protocol 1

### 6.5.1 General information and conditions




Three reactions (triplicate set) were carried out using the protocol described below. Equivalents are described with respect to the substrate **49**.

The substrate **49** (50 mg, 0.17 mmol, 1.0 equiv.), catalyst **43** (7.6 mg, 0.017 mmol, 0.10 equiv.) and a stirrer bar were added to a 7 mL vial. Toluene (1.7 mL) was introduced by washing down the sides of the vial, before the sequential addition of 1-bromonaphthalene **115** (15 µL, 0.11 mmol, 0.63 equiv.) and 50% (w/v) KOH(aq) (3.8 µL, 0.034 mmol, 0.20 equiv.). The mixture was stirred at ∼1000 rpm before methyl vinyl ketone (20 µL, 0.24 mmol, 1.4 equiv.) was added to initiate the reaction at the designated time zero.

### 6.5.2 Graphical results

Results of the triplicate set are depicted below (Figure 6.6, Figure 6.7, and Figure 6.8). In each graph, the $x$-axis corresponds to time following initiation of the reaction by the addition of MVK; the $y$-axis corresponds to conversion as a ratio of the total amount (in mol) of substrate **49** and product **97**; the red data corresponds to the substrate **49**; the blue data analogously corresponds to the relative amount of product **97**. The red lines in each graph correspond

to the fitting of equation 2.1, the extracted values for the parameters $k_1$ and $k_2$ and their goodness of fit ($R^2$) are displayed on the appropriate graph. In all cases, the initial value for the concentration of substrate $[\mathbf{49}]_0$ as described in the equation 2.1 was initially set to the unitless value of 1.0.

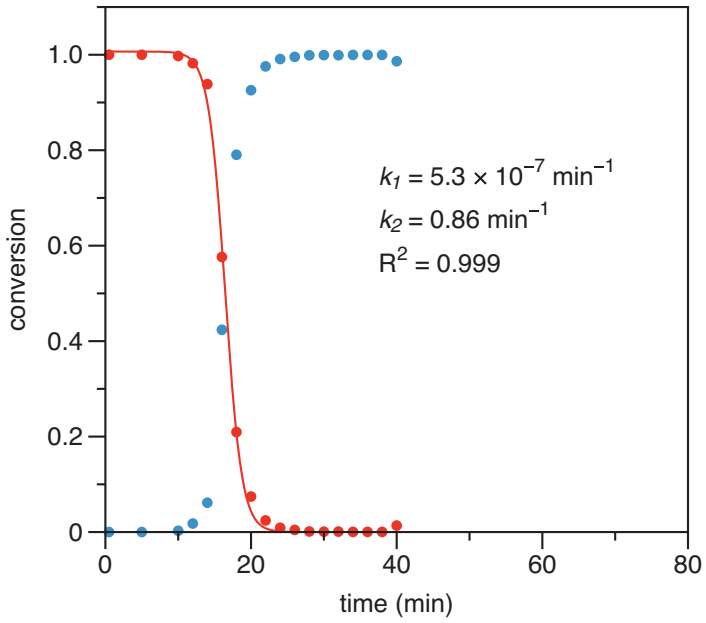



**Figure 6.6: Results obtained from the first reaction.**

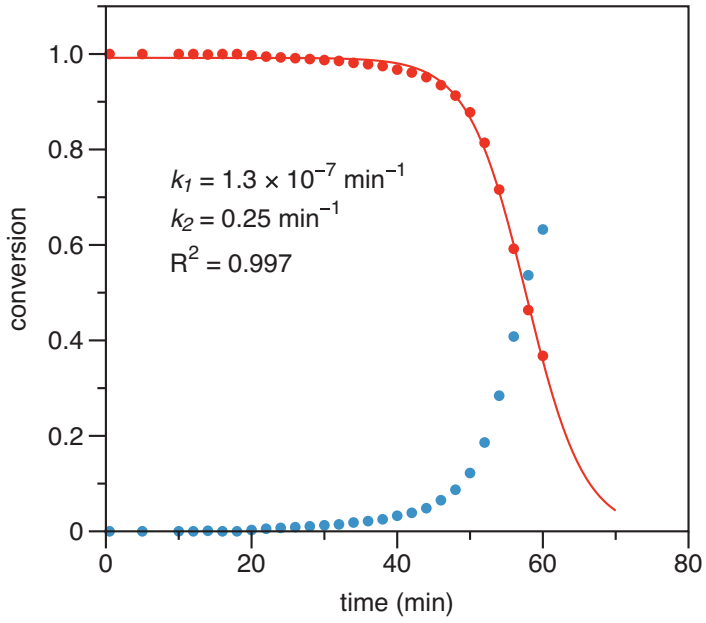



**Figure 6.7: Results obtained from the second reaction.**

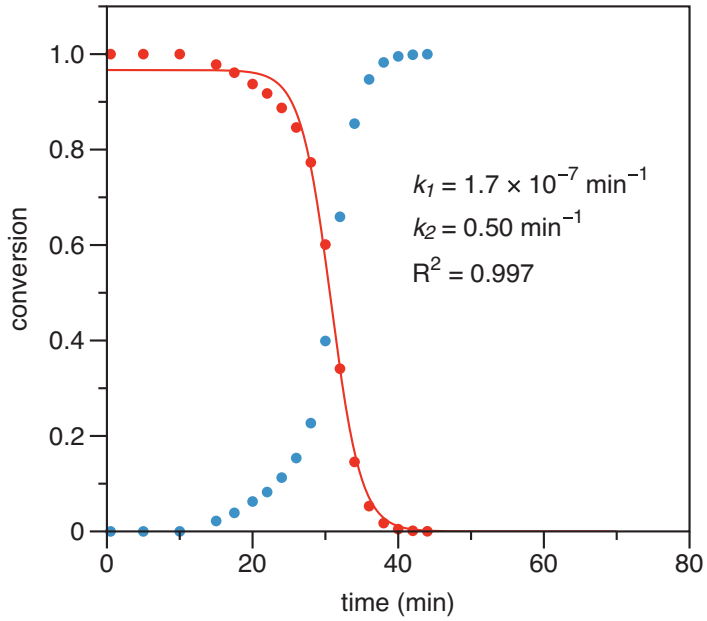
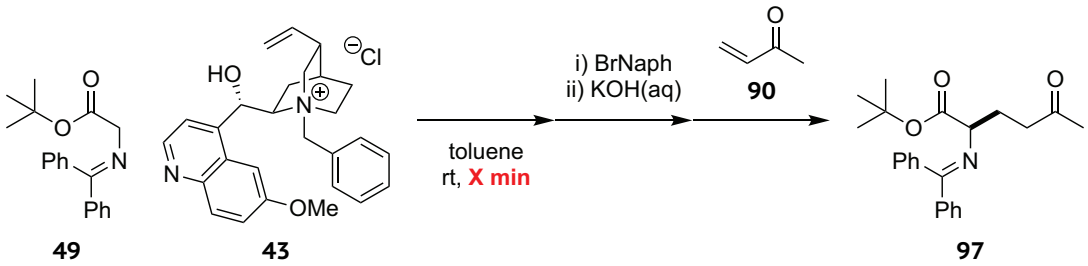



**Figure 6.8: Results obtained from the third reaction.**

## 6.6 Effect of pre-stirring the catalyst and substrate

### 6.6.1 General information and conditions




A series of single reactions were carried out to evaluate the kinetic effects of pre-stirring catalyst **43** and substrate **49**. The reactions varied the duration of pre-stirring (designated by X min) in the protocol described below. Pre-stirring times for the reactions were <2 min, 15 min, ~45 min, or 330 min.

The substrate **49** (50 mg. 0.17 mmol, 1.0 equiv.), catalyst **43** (7.6 mg, 0.017 mmol, 0.10 equiv.) and a stirrer bar were added to a 7 mL vial. Toluene (1.7 mL) was introduced by washing down the sides of the vial, and the mixture immediately stirred at ~1000 rpm for X min. Without ceasing stirring or disturbing the stirrer bar, 1-bromonaphthalene **115** (15 µL,

0.11 mmol, 0.63 equiv.), 50% (w/v) KOH(aq) (3.8 µL, 0.034 mmol, 0.20 equiv.), and methyl vinyl ketone **90** (MVK) (20 µL, 0.24 mmol, 1.4 equiv.) were sequentially added. Initiation of the reaction and time zero was designated by the addition of MVK.

### 6.6.2 Graphical results

The result of the whole experiment is depicted below (Figure 6.9). For clarity only substrate conversion data are depicted. The data are colour-coded for reference, with pre-stirring times indicated on the graph.

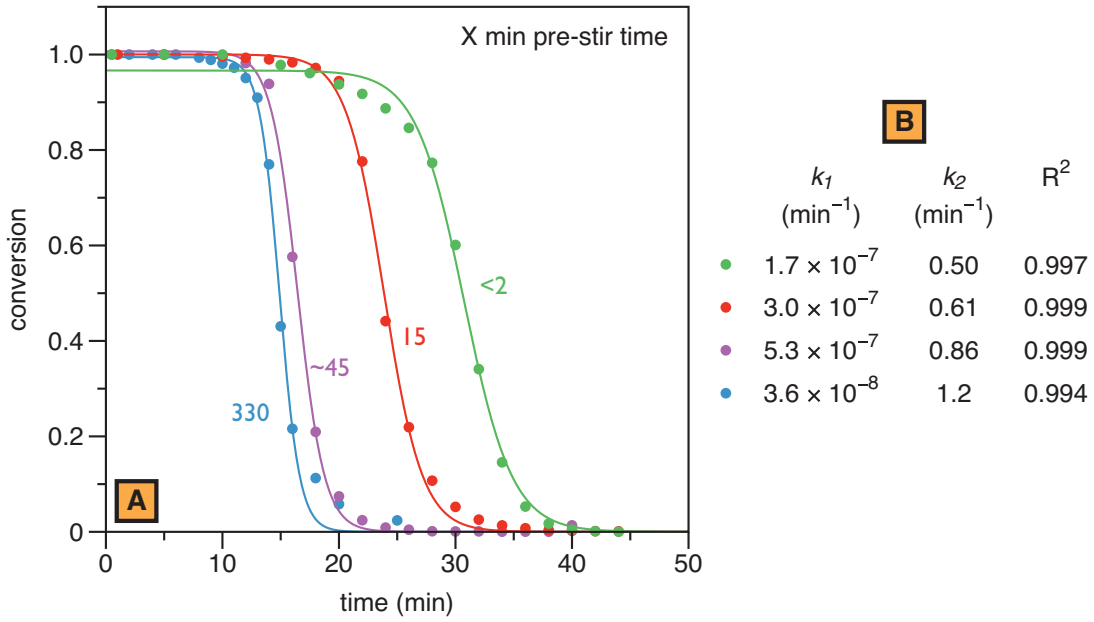
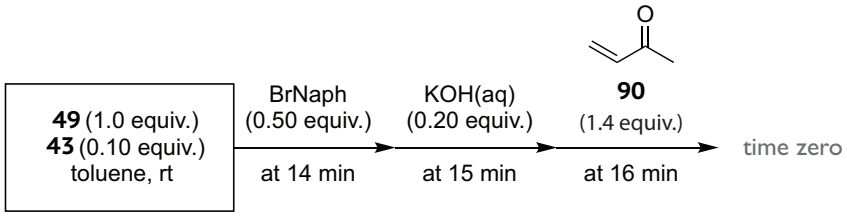



**Figure 6.9: Summary of data obtained when varying the substrate 49 and catalyst 43 pre-stir time. A)** Overlay of kinetic data obtained when varying the pre-stir time: <2 min (green data), 15 min (red data), ~45 min (purple data), and 330 min (blue data). The lines correspond to the fitting of equation 2.1 to the appropriately coloured data set. The $x$-axis corresponds to time following initiation of the reaction by the addition of MVK, the $y$-axis corresponds to conversion of substrate as a ratio of the total amount (in mol) of substrate **49** and product **97**. **B)** Values obtained following fitting of equation 2.1 to each data set. In all cases, the initial value for the concentration of substrate $[\mathbf{49}]_0$ as described in equation 2.1 was initially set to the unitless value of 1.0.

## 6.7 Results obtained using protocol 2

### 6.7.1 General information and conditions

Three reactions (triplicate set) were carried out using the protocol described below. Equivalents are described with respect to the substrate **49**.




The substrate **49** (50 mg. 0.17 mmol, 1.0 equiv.), catalyst **43** (7.6 mg, 0.017 mmol, 0.10 equiv.) and a stirrer bar were added to a 7 mL vial. Toluene (1.7 mL) was introduced by washing down the sides of the vial, and the mixture immediately stirred at ∼1000 rpm and a timer was started. After 14 min, without ceasing stirring or disturbing the stirrer bar, 1-bromonaphthalene **115** (15 µL, 0.11 mmol, 0.63 equiv.) was added. At 15 min, 50% (w/v) KOH(aq) (3.8 µL, 0.034 mmol, 0.20 equiv.) was added. At 16 min methyl vinyl ketone **90** (MVK) (20 µL, 0.24 mmol, 1.4 equiv.) was added. Initiation of the reaction and time zero was designated by the addition of MVK.

### 6.7.2 Graphical results

Results of the triplicate set are depicted below (Figure 6.10, Figure 6.11, and Figure 6.12). In each graph, the $x$-axis corresponds to time following initiation of the reaction by the addition of MVK; the $y$-axis corresponds to conversion as a ratio of the total amount (in mol) of substrate **49** and product **97**; the red data corresponds to the substrate **49**; the blue data analogously corresponds to the relative amount of product **97**. The red lines in each graph correspond to the fitting of equation 2.1, the extracted values for the parameters $k_1$ and $k_2$ and their goodness of fit ($R^2$) are displayed on the appropriate graph. In all cases, the initial value for

the concentration of substrate $[\mathbf{49}]_0$ as described in the equation 2.1 was initially set to the unitless value of 1.0.

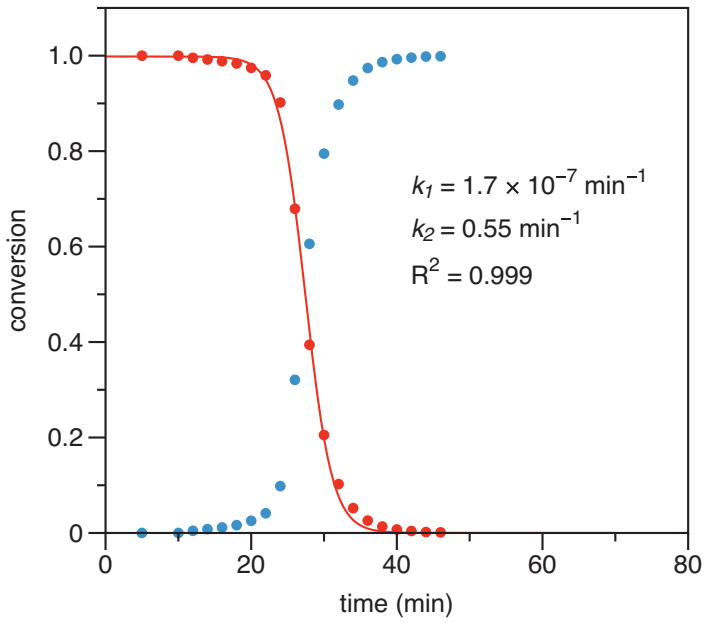



**Figure 6.10: Results obtained from the first reaction.**

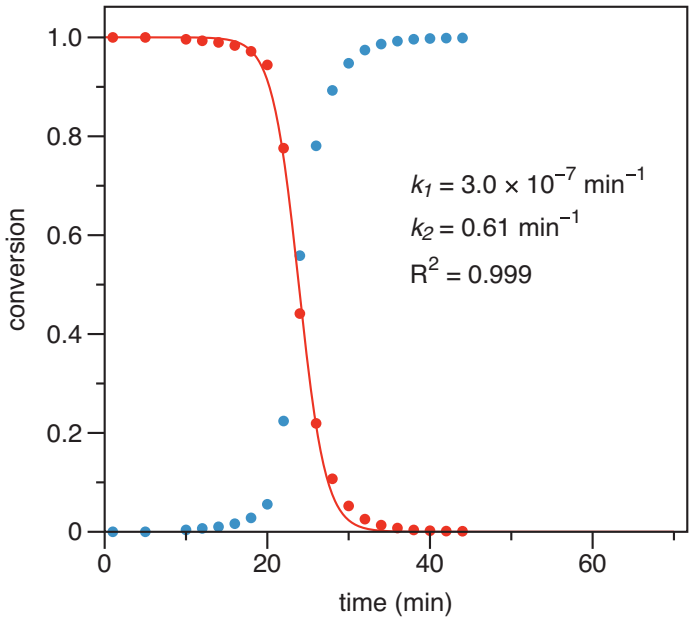



**Figure 6.11: Results obtained from the second reaction.**

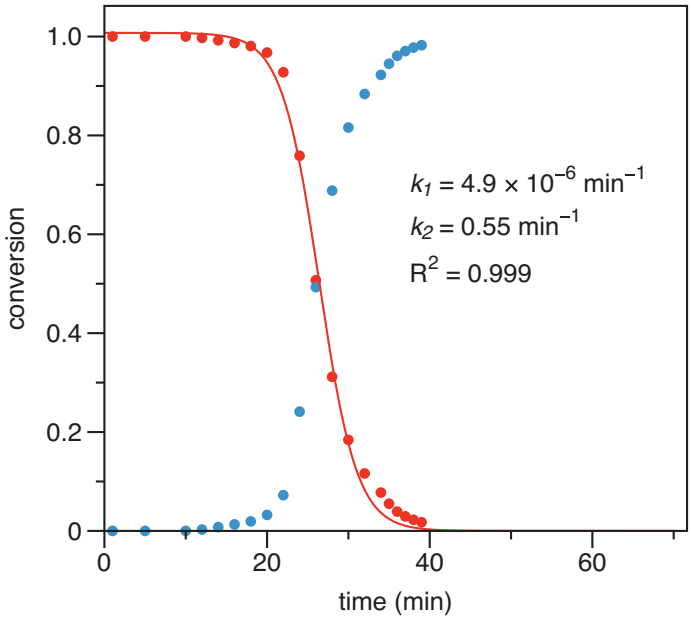
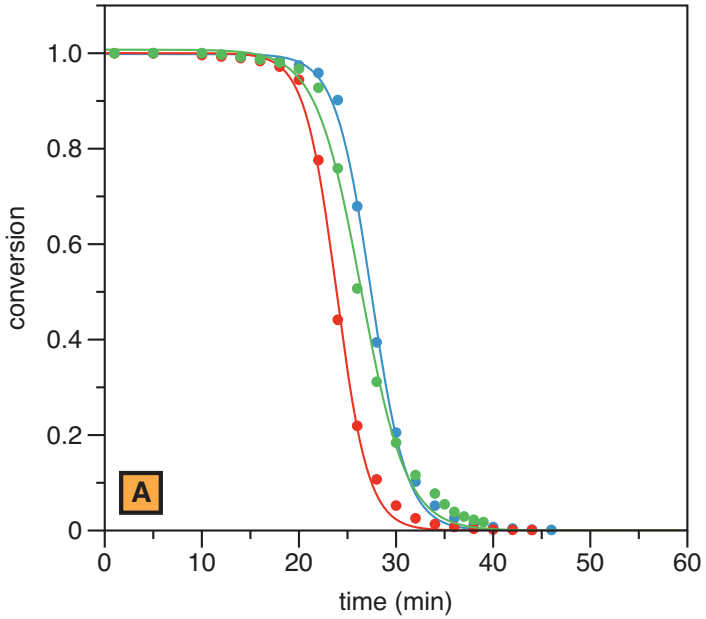



**Figure 6.12: Results obtained from the third reaction.**

A summary of the whole experiment is depicted below (Figure 6.13). For clarity only substrate conversion data are depicted. The data are colour-coded for reference.




B

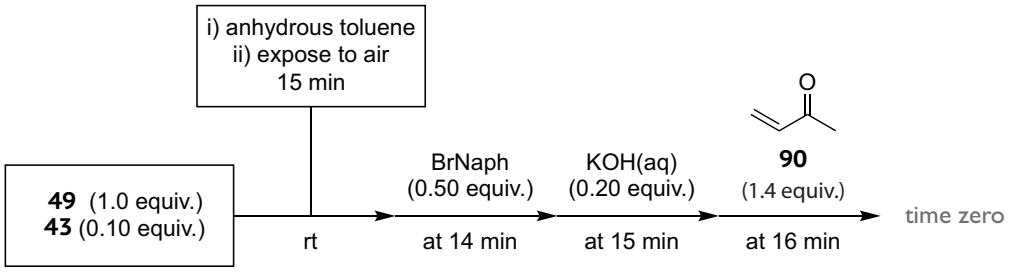
| $k_1$ (min$^{-1}$) | $k_2$ (min$^{-1}$) | R$^2$ |
|---|---|---|
| 4.9 × 10$^{-6}$ | 0.43 | 0.999 |
| 3.0 × 10$^{-7}$ | 0.61 | 0.999 |
| 1.7 × 10$^{-7}$ | 0.55 | 0.999 |

**Figure 6.13: Data obtained from the triplicate set carried out according to protocol 2. A)** Overlay of kinetic data obtained; the different colours correspond to individual reactions within the set. The lines correspond to the fitting of equation 2.1 to the appropriately coloured data set. The $x$-axis corresponds to time following initiation of the reaction by the addition of MVK, the $y$-axis corresponds to conversion of substrate as a ratio of the total amount (in mol) of substrate **49** and product **97**. **B)** Values obtained following fitting of equation 2.1 to each data set. In all cases, the initial value for the concentration of substrate $[\mathbf{49}]_0$ as described in the equation 2.1 was initially set to the unitless value of 1.0.

## 6.8 Results obtained using protocol 3

### 6.8.1 General information and conditions

A set of four reactions were carried out using the protocol described below. Equivalents are described with respect to the substrate **49**. Stirring speeds were calibrated using a stroboscope. The same stirrer bar was used between reactions following cleaning with water and acetone.




Anhydrous toluene (7 mL) was filtered through dried alumina into a 7 mL vial. The vial was opened to the air for 15 min before toluene (1.7 mL) was added to substrate **49** (50 mg. 0.17 mmol, 1.0 equiv.), catalyst **43** (7.6 mg, 0.017 mmol, 0.10 equiv.), and a stirrer bar in another 7 mL vial, which was fitted in a holder that was specifically designed to consistently place the vial centrally on the stirrer plate (Figure 6.14). The vial was attached so that the bottom did not touch the surface of the holder. The toluene was introduced by washing down the sides of the reaction vial. The mixture was immediately stirred at ∼1000 rpm and a timer was started. After 14 min, without ceasing stirring or disturbing the stirrer bar, 1-bromonaphthalene **115** (15 µL, 0.11 mmol, 0.63 equiv.) was added. At 15 min, 50% (w/v) KOH(aq) (3.8 µL, 0.034 mmol, 0.20 equiv.) was added. At 16 min methyl vinyl ketone **90** (MVK) (20 µL, 0.24 mmol, 1.4 equiv.) was added. Initiation of the reaction and time zero was designated by the addition of MVK.

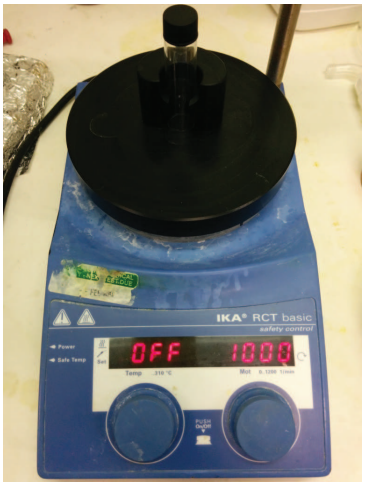



**Figure 6.14: Vial holder fitted onto a stirrer plate holding an empty vial.**

### 6.8.2 Graphical results

Results of the reaction set are depicted below (Figure 6.15, Figure 6.16, Figure 6.17 and Figure 6.18). In each graph, the $x$-axis corresponds to time following initiation of the reaction by the addition of MVK; the $y$-axis corresponds to conversion as a ratio of the total amount (in mol) of substrate **49** and product **97**; the red data corresponds to the substrate **49**; the blue data analogously corresponds to the relative amount of product **97**. The red lines in each graph correspond to the fitting of equation 2.1, the extracted values for the parameters $k_1$ and $k_2$ and their goodness of fit ($R^2$) are displayed on the appropriate graph. In all cases, the initial value for the concentration of substrate $[\mathbf{49}]_0$ as described in the equation 2.1 was initially set to the unitless value of 1.0.

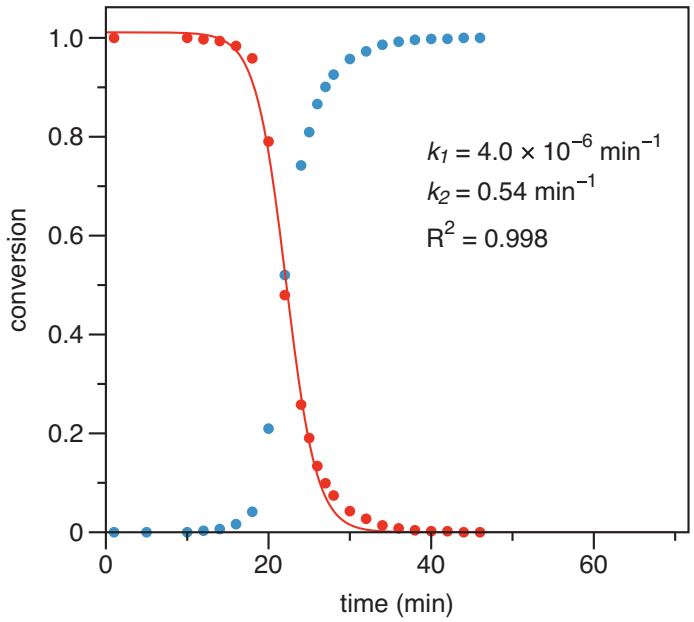



**Figure 6.15: Results obtained from the first reaction.**

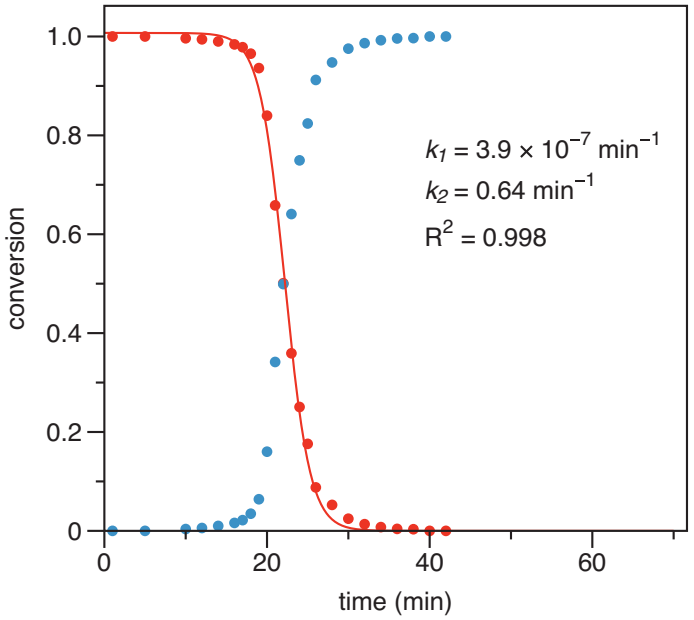



**Figure 6.16: Results obtained from the second reaction.**

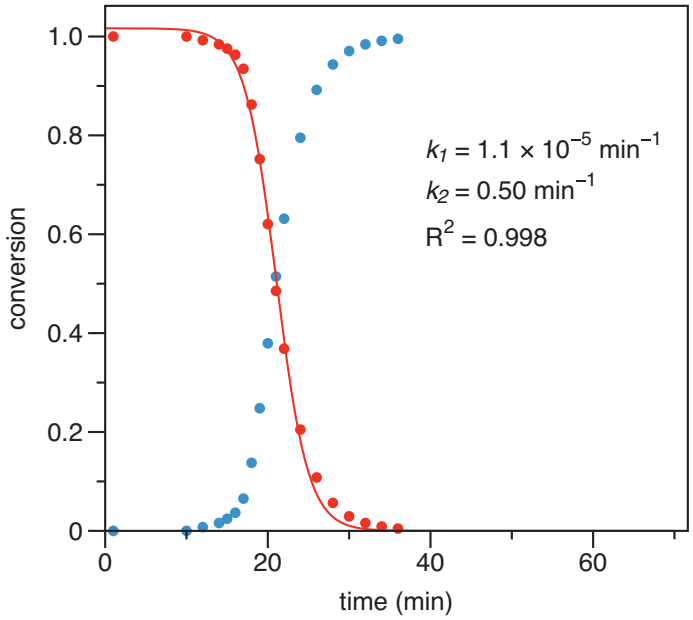



**Figure 6.17: Results obtained from the third reaction.**

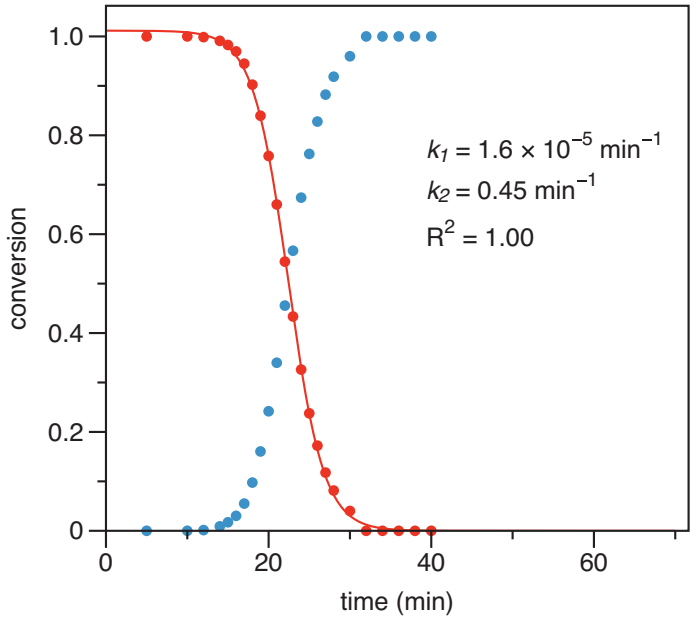



**Figure 6.18: Results obtained from the fourth reaction.**

A summary of the whole experiment is depicted below (Figure 6.19). For clarity only substrate conversion data are depicted. The data are colour-coded for reference. The average values for the extracted parameters, $k_1$ and $k_2$, were $7.9 \times 10^{-6} \pm 6 \times 10^{-6}$ min$^{-1}$ and $0.53 \pm 0.07$ min$^{-1}$, respectively.

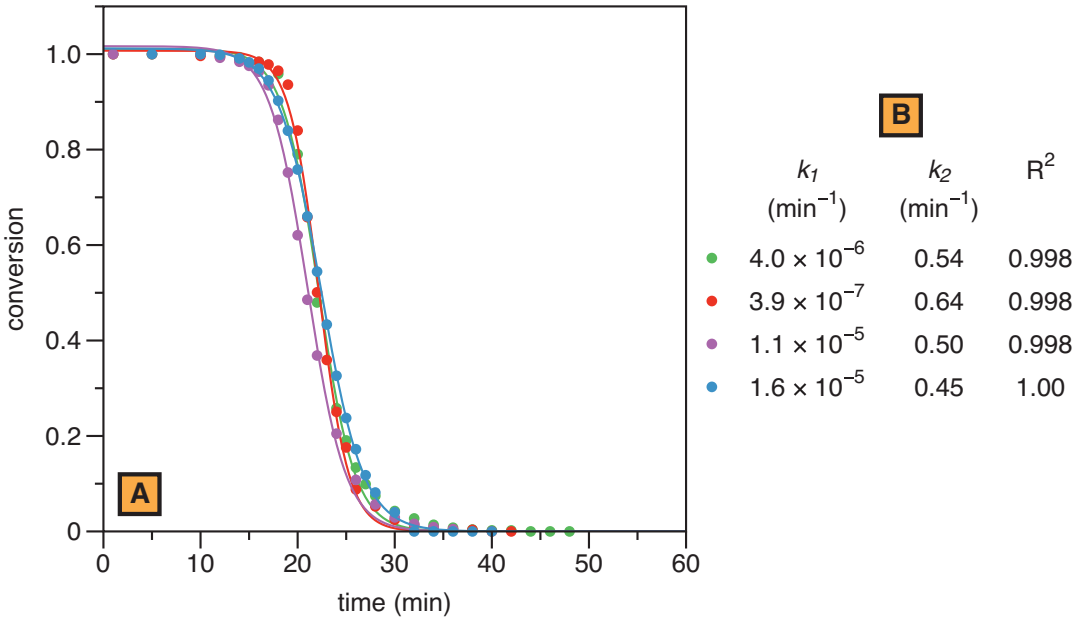
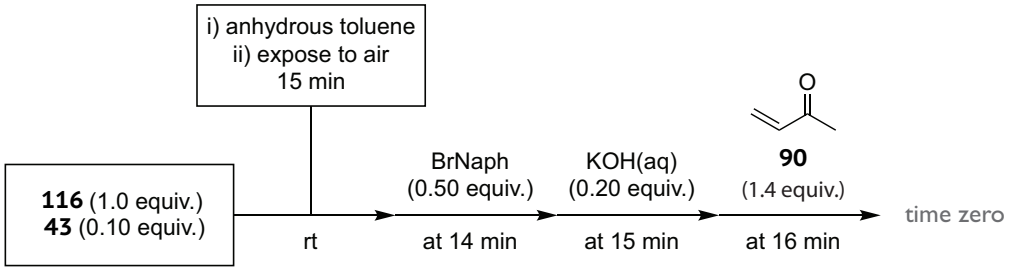



**Figure 6.19: Data obtained from the reaction set carried out according to protocol 3. A)** Overlay of kinetic data obtained; the different colours correspond to individual reactions within the set. The lines correspond to the fitting of equation 2.1 to the appropriately coloured data set. The $x$-axis corresponds to time following initiation of the reaction by the addition of MVK, the $y$-axis corresponds to conversion of substrate as a ratio of the total amount (in mol) of substrate **49** and product **97**. **B)** Values obtained following fitting of equation 2.1 to each data set. In all cases, the initial value for the concentration of substrate $[\mathbf{49}]_0$ as described in equation 2.1 was initially set to the unitless value of 1.0.

## 6.9 Initial results obtained using deuterated substrate

### 6.9.1 General information and conditions

A set of three reactions were carried out using the protocol described in section 6.8 (protocol 3) but with substrate **116**. Equivalents are described with respect to the substrate **116**. Stirring speeds were calibrated using a stroboscope. The same stirrer bar was used between reactions following cleaning with water and acetone.



Initial conditions were as follows: substrate **116** (50.3 mg, 0.169 mmol, 1.00 equiv.), catalyst **43** (7.6 mg, 0.017 mmol, 0.10 equiv.), toluene (1.7 mL), 1-bromonaphthalene **115** (BrNaph) (15 µL, 0.11 mmol, 0.63 equiv.), 50% (w/v) KOH(aq) (3.8 µL, 0.034 mmol, 0.20 equiv.), and methyl vinyl ketone **90** (MVK) (20 µL, 0.24 mmol, 1.4 equiv.).

### 6.9.2 Graphical results

Results of the reaction set are depicted below (Figure 6.20, Figure 6.21, and Figure 6.22). In each graph, the $x$-axis corresponds to time following initiation of the reaction by the addition of MVK; the $y$-axis corresponds to conversion as a ratio of the total amount (in mol) of substrate **116** and product **117**; the red data corresponds to the substrate **116**; the blue data analogously corresponds to the relative amount of product **117**. The red lines in each graph correspond to the fitting of equation 2.1, the extracted values for the parameters $k_1$ and $k_2$ and their goodness of fit ($R^2$) are displayed on the appropriate graph. In all cases, the initial value for the concentration of substrate $[\mathbf{116}]_0$ as described in the equation 2.1 was initially set to the unitless value of 1.0.

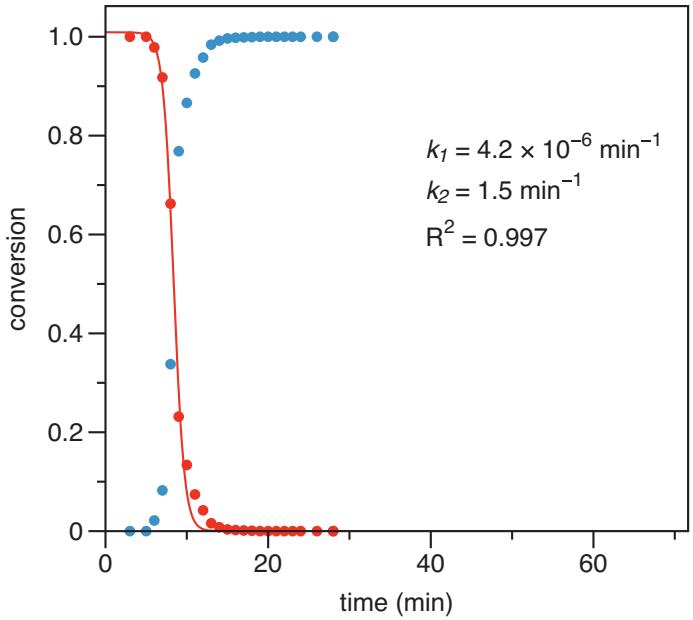



**Figure 6.20: Results obtained from the first reaction.**

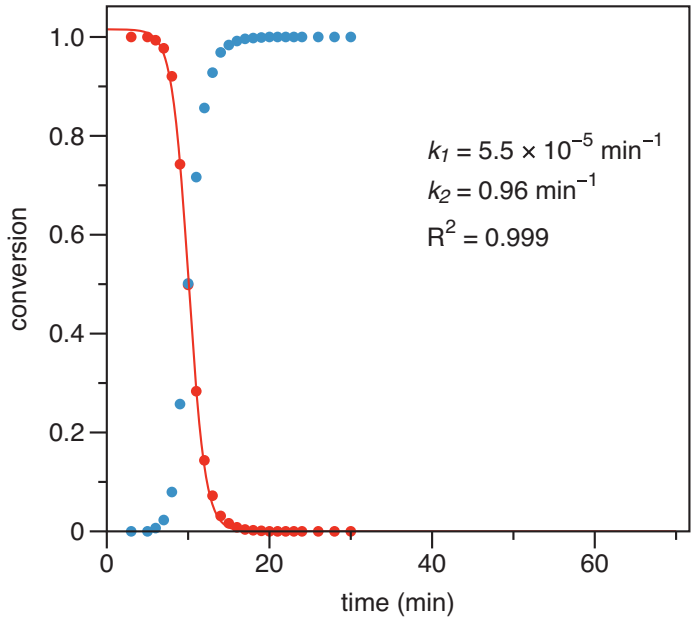



**Figure 6.21: Results obtained from the second reaction.**

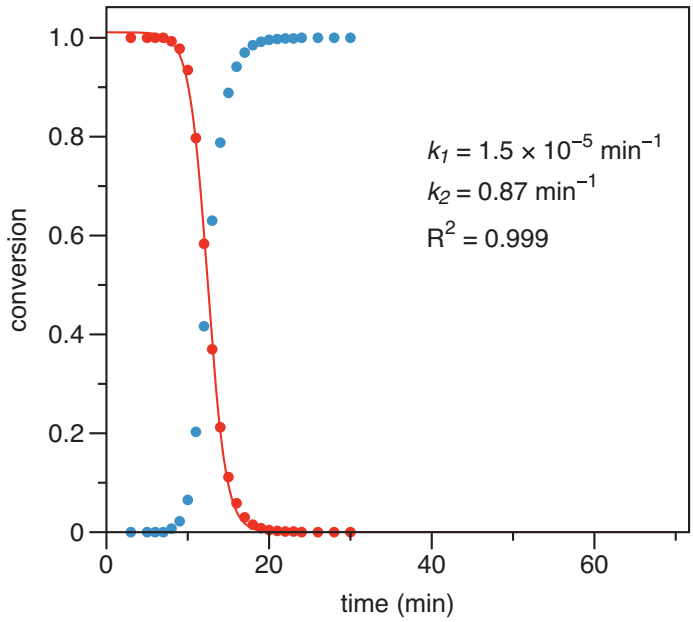
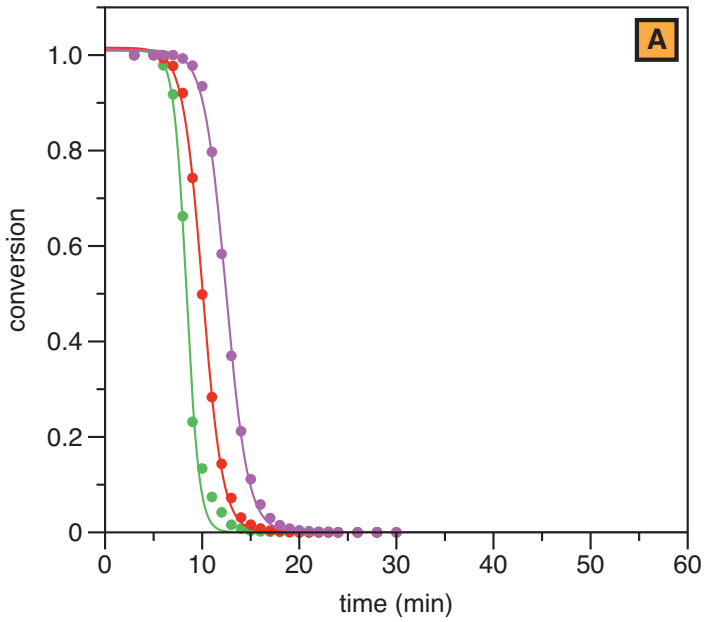



**Figure 6.22: Results obtained from the third reaction.**

A summary of the whole experiment is depicted below (Figure 6.23). For clarity only substrate conversion data are depicted. The data are colour-coded for reference.




B

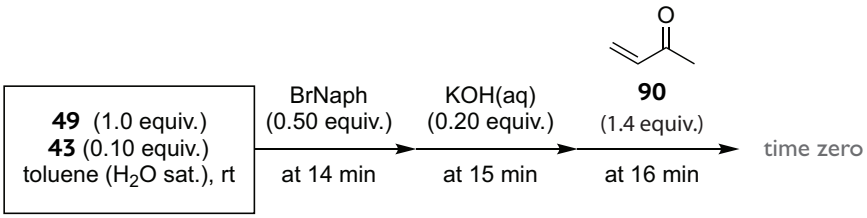
| | $k_1$ ($min^{-1}$) | $k_2$ ($min^{-1}$) | $R^2$ |
|---|---|---|---|
| ● | $4.2 \times 10^{-6}$ | 1.5 | 0.997 |
| ● | $5.5 \times 10^{-5}$ | 0.96 | 0.999 |
| ● | $1.5 \times 10^{-5}$ | 0.87 | 0.999 |

**Figure 6.23: Data obtained from the reaction set carried out using deuterated substrate 116 and carried out according to protocol 3. A)** Overlay of kinetic data obtained; the different colours correspond to individual reactions within the set. The lines correspond to the fitting of equation 2.1 to the appropriately coloured data set. The $x$-axis corresponds to time following initiation of the reaction by the addition of MVK, the $y$-axis corresponds to conversion of substrate as a ratio of the total amount (in mol) of substrate **116** and product **117**. **B)** Values obtained following fitting of equation 2.1 to each data set. In all cases, the initial value for the concentration of substrate $[\mathbf{116}]_0$ as described in equation 2.1 was initially set to the unitless value of 1.0.

## 6.10 Results obtained using protocol 4

### 6.10.1 General information and conditions

A set of three reactions were carried out using the protocol described below. Equivalents are described with respect to the substrate **49**. Stirring speeds were calibrated using a stroboscope. The same stirrer bar was used between reactions following cleaning with water and acetone. Toluene used in the reactions was stored over water (approximately 30 mL of water per 1000 mL of toluene; titrated to >300 ppm), shaken and allowed to settle for 5 min before use.



The substrate **49** (50 mg. 0.17 mmol, 1.0 equiv.), catalyst **43** (7.6 mg, 0.017 mmol, 0.10 equiv.) and a stirrer bar were added to a 7 mL vial. The vial was set in a holder that was specifically designed to consistently place the vial centrally on the stirrer plate (Figure 6.14). The vial was attached so that the bottom did not touch the surface of the holder. Toluene (1.7 mL) was introduced to the vial by washing down the sides, and the mixture immediately stirred at ∼1000 rpm and a timer was started. After 14 min, without ceasing stirring or disturbing the stirrer bar, 1-bromonaphthalene **115** (15 µL, 0.11 mmol, 0.63 equiv.) was added. At 15 min, 50% (w/v) KOH(aq) (3.8 µL, 0.034 mmol, 0.20 equiv.) was added. At 16 min methyl vinyl ketone **90** (MVK) (20 µL, 0.24 mmol, 1.4 equiv.) was added. Initiation of the reaction and time zero was designated by the addition of MVK.

### 6.10.2 Graphical results

Results of the reaction set are depicted below (Figure 6.24, Figure 6.25, and Figure 6.26). In each graph, the $x$-axis corresponds to time following initiation of the reaction by the addition of MVK; the $y$-axis corresponds to conversion as a ratio of the total amount (in mol) of substrate **49** and product **97**; the red data corresponds to the substrate **49**; the blue data analogously corresponds to the relative amount of product **97**. The red lines in each graph correspond to the fitting of equation 2.1, the extracted values for the parameters $k_1$ and $k_2$ and their goodness of fit ($R^2$) are displayed on the appropriate graph. In all cases, the initial value for the concentration of substrate $[\mathbf{49}]_0$ as described in the equation 2.1 was initially set to the unitless value of 1.0.

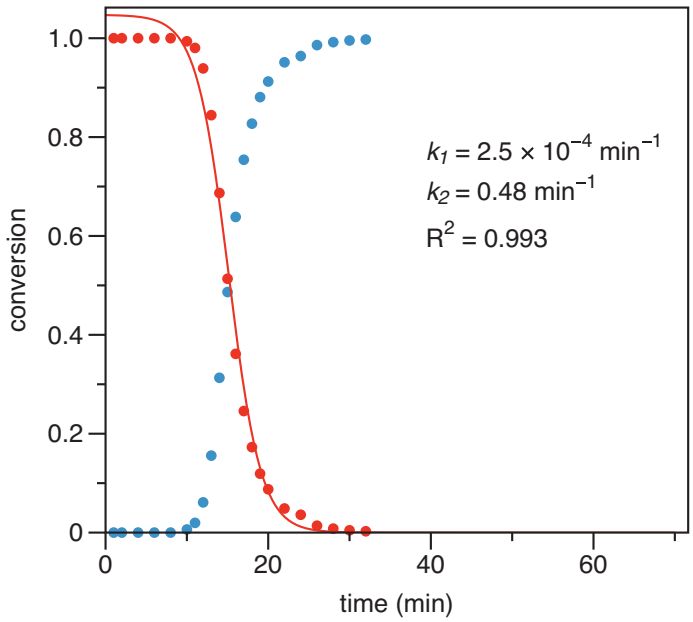



**Figure 6.24: Results obtained from the first reaction.**

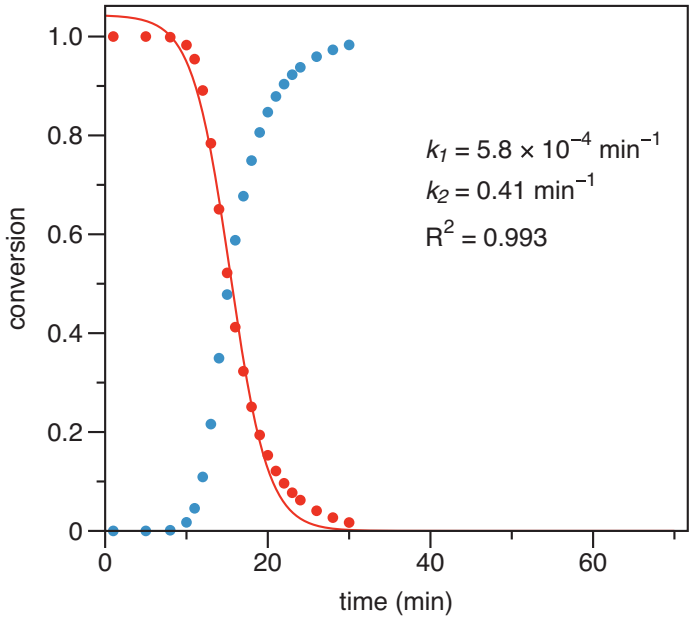



**Figure 6.25: Results obtained from the second reaction.**

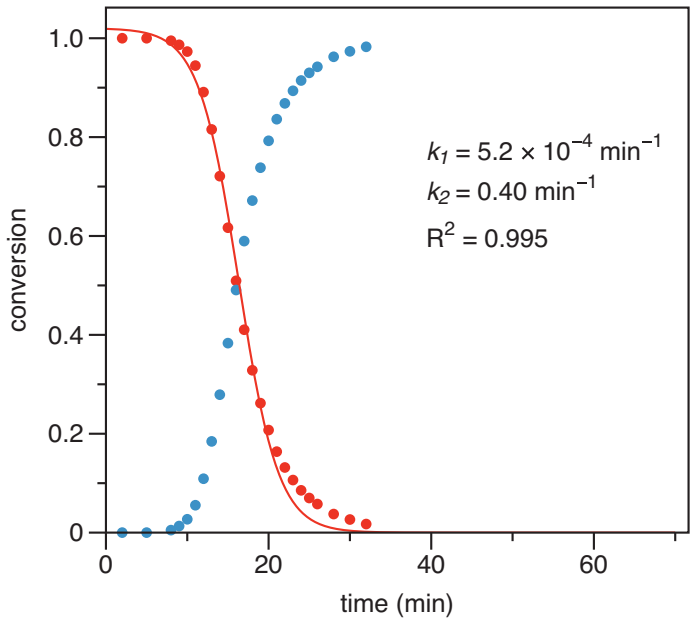
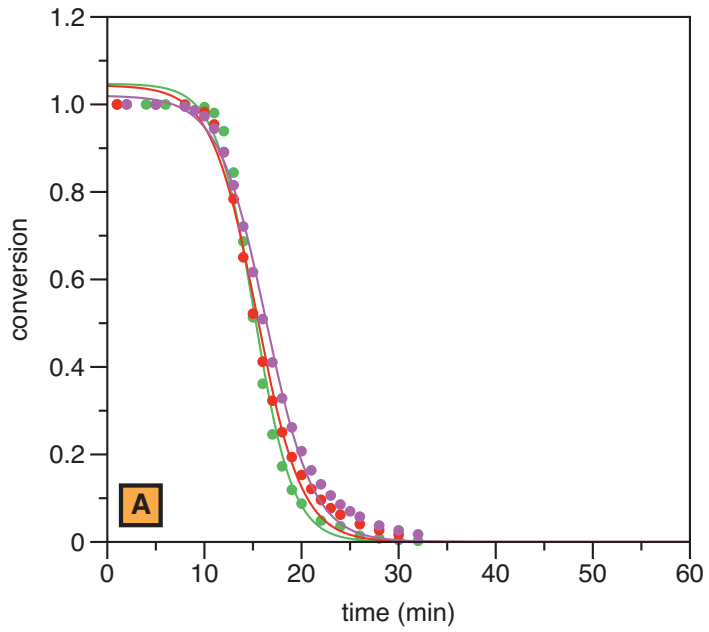



**Figure 6.26: Results obtained from the third reaction.**

A summary of the whole experiment is depicted below (Figure 6.27). For clarity only substrate conversion data are depicted. The data are colour-coded for reference. The average values for the extracted parameters, $k_1$ and $k_2$, were $4.5 \times 10^{-4} \pm 1 \times 10^{-4}$ min$^{-1}$ and $4.3 \pm 0.04$ min$^{-1}$, respectively.




B

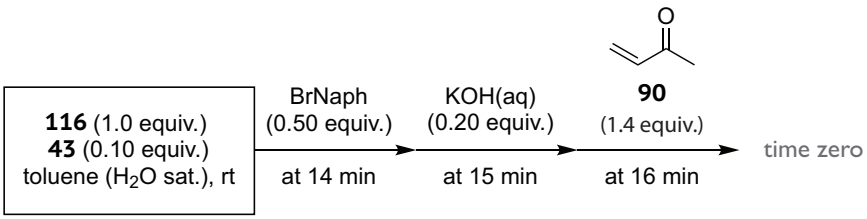
| | $k_1$ ($min^{-1}$) | $k_2$ ($min^{-1}$) | $R^2$ |
|---|---|---|---|
| ● | $2.5 \times 10^{-4}$ | 0.48 | 0.993 |
| ● | $5.8 \times 10^{-4}$ | 0.41 | 0.993 |
| ● | $5.2 \times 10^{-4}$ | 0.40 | 0.995 |

**Figure 6.27: Data obtained from the reaction set carried out according to protocol 4. A)** Overlay of kinetic data obtained; the different colours correspond to individual reactions within the set. The lines correspond to the fitting of equation 2.1 to the appropriately coloured data set. The $x$-axis corresponds to time following initiation of the reaction by the addition of MVK, the $y$-axis corresponds to conversion of substrate as a ratio of the total amount (in mol) of substrate **49** and product **97**. **B)** Values obtained following fitting of equation 2.1 to each data set. In all cases, the initial value for the concentration of substrate $[\mathbf{49}]_0$ as described in equation 2.1 was initially set to the unitless value of 1.0.

## 6.11 Evaluating the effect of deuterated substrate

### 6.11.1 General information and conditions

A set of three reactions were carried out using the protocol described in section 6.10 (protocol 4) but with substrate **116**. Equivalents are described with respect to the substrate **116**. Stirring speeds were calibrated using a stroboscope. The same stirrer bar was used between reactions following cleaning with water and acetone. Toluene used in the reactions was stored over water (approximately 30 mL of water per 1000 mL of toluene; titrated to >300 ppm), shaken and allowed to settle for 5 min before use.



Initial conditions were as follows: substrate **116** (50.3 mg, 0.169 mmol, 1.00 equiv.), catalyst **43** (7.6 mg, 0.017 mmol, 0.10 equiv.), toluene (1.7 mL), 1-bromonaphthalene **115** (BrNaph) (15 µL, 0.11 mmol, 0.63 equiv.), 50% (w/v) KOH(aq) (3.8 µL, 0.034 mmol, 0.20 equiv.), and methyl vinyl ketone **90** (MVK) (20 µL, 0.24 mmol, 1.4 equiv.).

### 6.11.2 Graphical results

Results of the reaction set are depicted below (Figure 6.28, Figure 6.29, and Figure 6.30). In each graph, the $x$-axis corresponds to time following initiation of the reaction by the addition of MVK; the $y$-axis corresponds to conversion as a ratio of the total amount (in mol) of substrate **116** and product **117**; the red data corresponds to the substrate **116**; the blue data analogously corresponds to the relative amount of product **117**. The red lines in each graph correspond to the fitting of equation 2.1, the extracted values for the parameters $k_1$ and $k_2$ and their goodness of fit ($R^2$) are displayed on the appropriate graph. In all cases, the initial value for the concentration of substrate $[\mathbf{116}]_0$ as described in the equation 2.1 was initially set to the unitless value of 1.0.

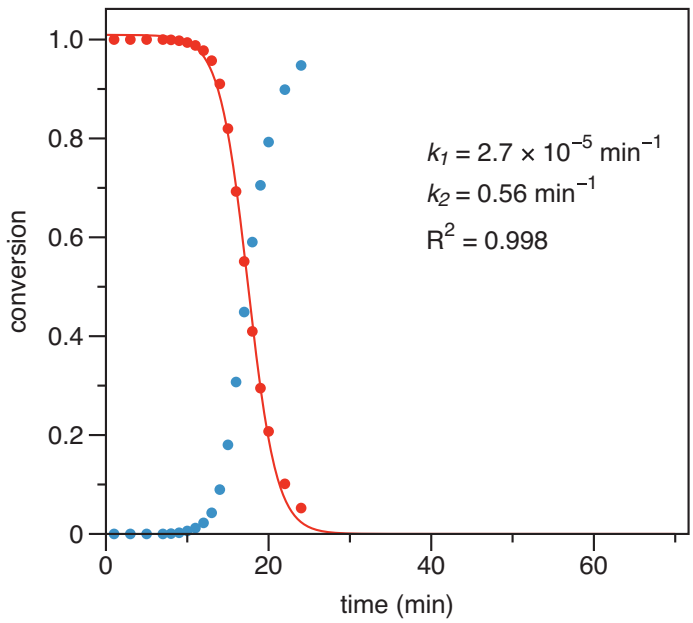



**Figure 6.28: Results obtained from the first reaction.**

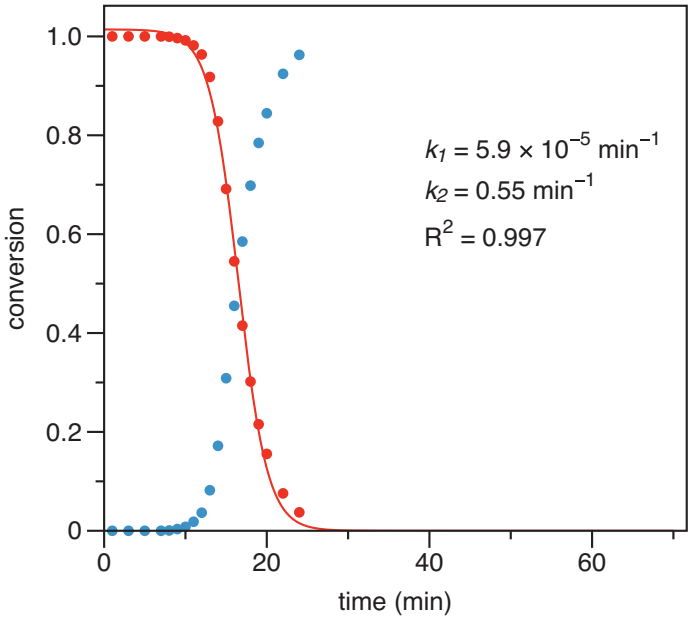



**Figure 6.29: Results obtained from the second reaction.**

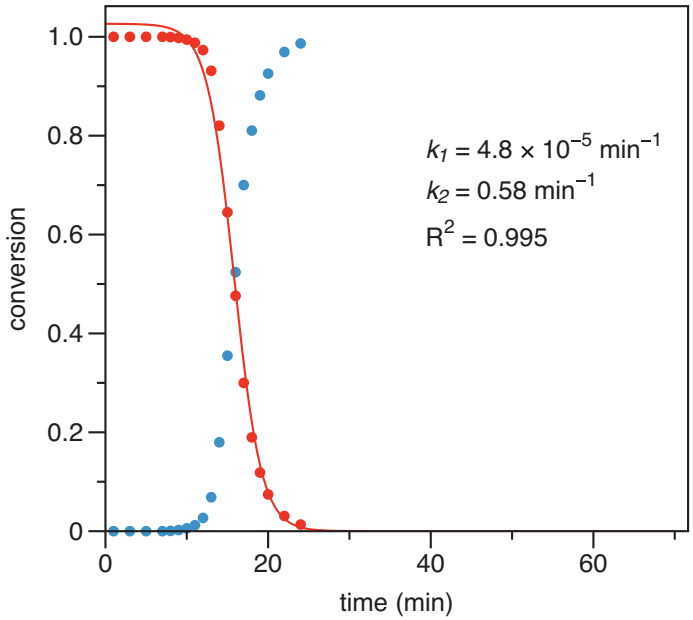



**Figure 6.30: Results obtained from the third reaction.**

A summary of the whole experiment is depicted below (Figure 6.31). For clarity only substrate conversion data are depicted. The data are colour-coded for reference. The average values for the extracted parameters, $k_1$ and $k_2$, were $4.5 \times 10^{-5} \pm 1 \times 10^{-5}$ min$^{-1}$ and $0.56 \pm 0.01$ min$^{-1}$, respectively.

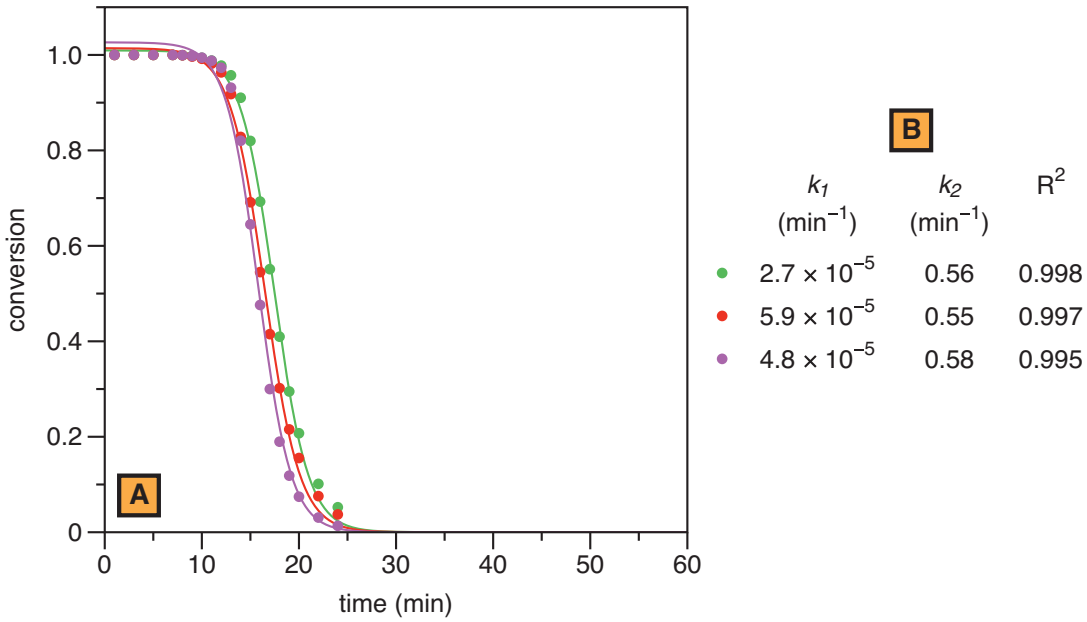



**Figure 6.31: Data obtained from the reaction set carried using deuterated substrate 116 and carried out according to protocol 4. A)** Overlay of kinetic data obtained; the different colours correspond to individual reactions within the set. The lines correspond to the fitting of equation 2.1 to the appropriately coloured data set. The $x$-axis corresponds to time following initiation of the reaction by the addition of MVK, the $y$-axis corresponds to conversion of substrate as a ratio of the total amount (in mol) of substrate **116** and product **117**. **B)** Values obtained following fitting of equation 2.1 to each data set. In all cases, the initial value for the concentration of substrate $[\mathbf{116}]_0$ as described in equation 2.1 was initially set to the unitless value of 1.0.

The data collected from the current experiment were compared to that obtained previously using protocol 4 (section 6.10) i.e. analogous experiment using non-deuterated substrate **49** (Figure 6.32). The outcome revealed only subtle differences in the rate behaviour of each experiment, thus an alternative method for representing the data was devised.

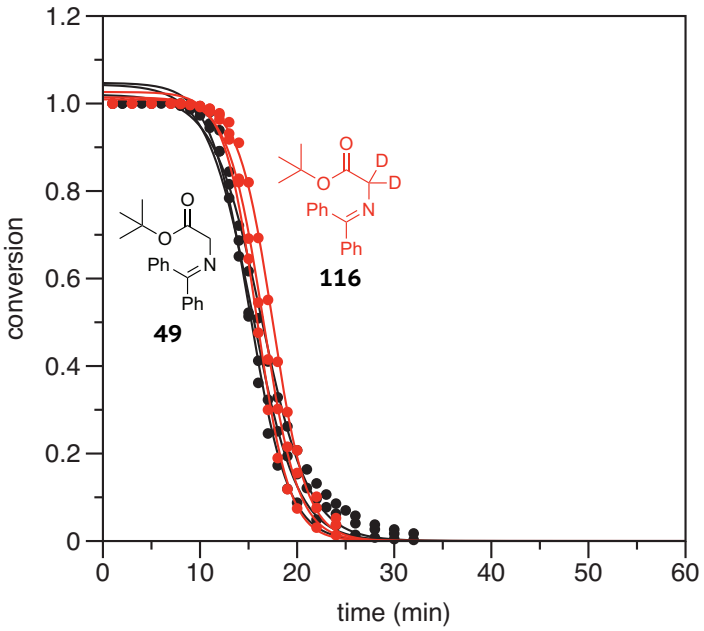



**Figure 6.32: Overlay of results obtained when subjecting substrate 49 (black data) or deuterated substrate 116 (red data) to protocol 4.** The overlays are of the data described in Figure 6.27 and Figure 6.31. The initial substrates used are indicated on the graph. The lines correspond to the fitting of equation 2.1 to each reaction. The $x$-axis corresponds to time following initiation of the reaction by the addition of MVK, the $y$-axis corresponds to conversion of substrate as a ratio of the total amount (in mol) of substrate and product.

Graphical deconvolution of the data was attempted by taking the extracted rate parameters from the experiments, substituting them into the autocatalytic function, and plotting the result (Figure 6.33). The KIE values for each parameter were calculated based on the same extracted parameters, $k_1$ and $k_2$ to give 10 and 0.76 respectively.

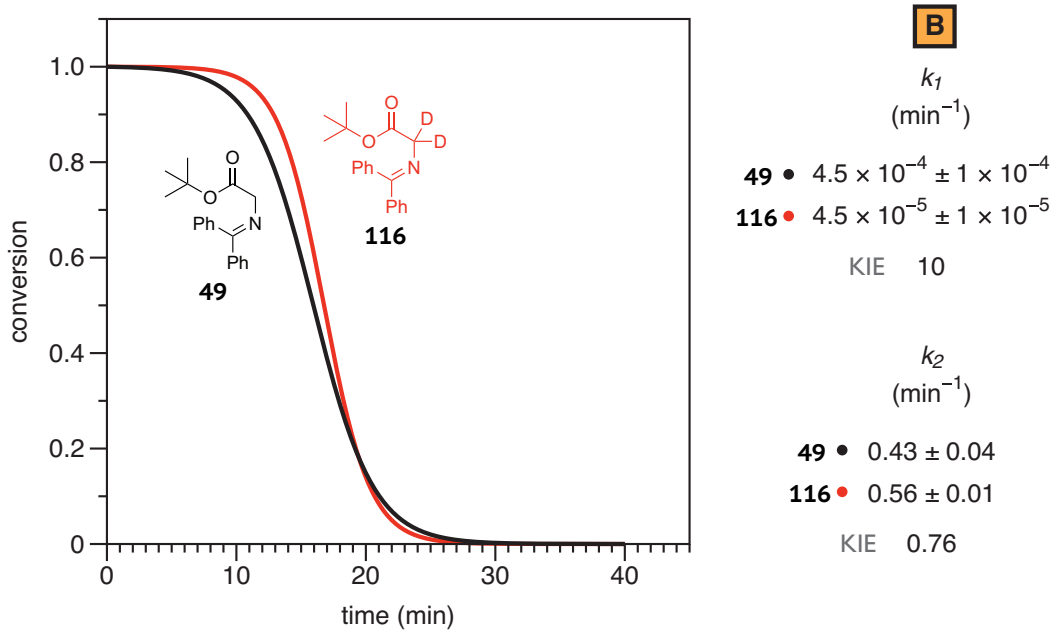
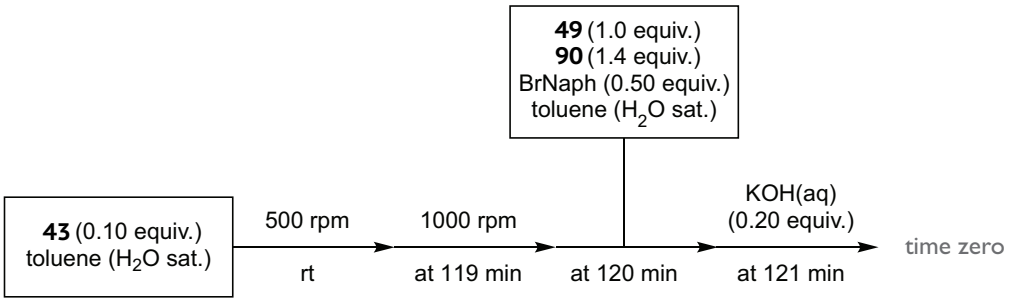



**Figure 6.33: Overlay of data comparing the kinetic behaviour of reactions using isotopically labelled substrates 49 (black) and 116 (red). A)** Comparing the graphical kinetic behaviour of results obtained using substrates **49** (black) and **116** (red). The $x$-axis corresponds to time following initiation of the reactions, the $y$-axis corresponds to conversion of the appropriate substrate (**49** or **116**) based on the ratio of the amount (in mol) of substrate to the combined amount of substrate and product. The lines are the result of inputting the parameters detailed in **B** into equation 2.1, and plotting the respective result. The data are colour-coded. **B)** Average values for the parameters $k_1$ and $k_2$ obtained from fitting the respective kinetic data to the model described by equation 2.1 and the KIE values associated with each parameter.

## 6.12 Illuminating a rate-determining step

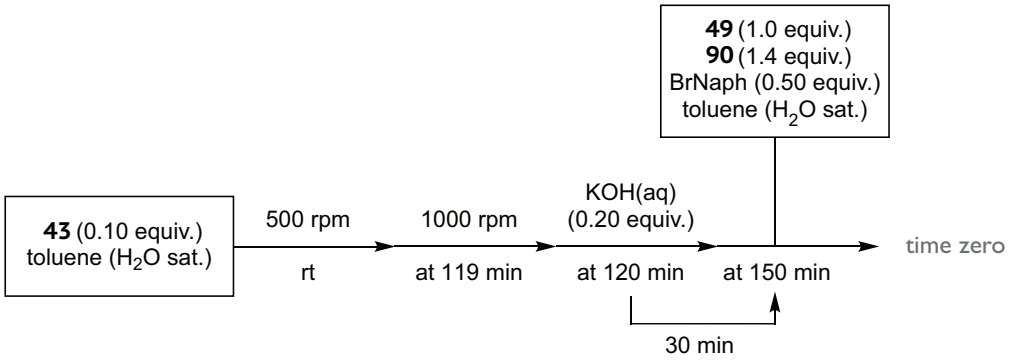
### 6.12.1 General information and conditions

Two single reactions—a test and a control—were carried out using the protocols described below. The whole experiment was carried out to determine the effect of pre-catalyst activation on the observed rate behaviour of the reaction. Equivalents are described with respect to the substrate **49**. Stirring speeds were calibrated using a stroboscope. The same stirrer bar was used between reactions following cleaning with water and acetone. Toluene used in the reactions was stored over water (approximately 30 mL of water per 1000 mL of toluene; titrated to >300 ppm), shaken and allowed to settle for 5 min before use.




**Scheme 6.1: Schematic for the pre-stirring experiment control reaction.**

**Control reaction protocol:** The catalyst **43** (7.6 mg, 0.017 mmol, 0.10 equiv.) and stirrer bar were added to a 7 mL vial before toluene (0.70 mL) was added by washing down the sides of the vial. The vial was set in a holder that was specifically designed to consistently place the vial centrally on the stirrer plate (Figure 6.14). The vial was attached so that the bottom did not touch the surface of the holder. The mixture was immediately stirred at 50 rpm before the stirring rate was gradually ramped up to 500 rpm over 1 min and a timer started. Substrate **49** (50 mg. 0.17 mmol, 1.0 equiv.) was added to a separate 7 mL vial before toluene (1.0 mL) was added and the substrate dissolved. After the catalyst **43** had been stirring for 1 h 45 min, 1-bromonaphthalene **115** (15 µL, 0.11 mmol, 0.63 equiv.) and methyl vinyl ketone **90** (MVK) (20 µL, 0.24 mmol, 1.4 equiv.) were added to the solution of substrate **49**. After the catalyst had been stirring for 1 h 59 min, the stirring rate was ramped up to 1000 rpm. At 2 h 0 min, the substrate solution was added in one portion. The mixture was stirred for 1 min before 50% (w/v) KOH(aq) (3.8 µL, 0.034 mmol, 0.20 equiv.) was added. Initiation of the reaction and time zero was designated by the addition of KOH(aq).




**Scheme 6.2: Schematic for the pre-stirring experiment test reaction.**

**Test reaction protocol:** The catalyst **43** (7.6 mg, 0.017 mmol, 0.10 equiv.) and stirrer bar were added to a 7 mL vial before toluene (0.70 mL) was added by washing down the sides of the vial. The vial was set in a holder that was specifically designed to consistently place the vial centrally on the stirrer plate (Figure 6.14). The vial was attached so that the bottom did not touch the surface of the holder. The mixture was immediately stirred at 50 rpm before the stirring rate was gradually ramped up to 500 rpm over 1 min and a timer started. Substrate **49** (50 mg. 0.17 mmol, 1.0 equiv.) was added to a separate 7 mL vial before toluene (1.0 mL) was added and the substrate dissolved. After the catalyst **43** had been stirring for 1 h 59 min, the stirring rate was ramped up to 1000 rpm. At 2 h 0 min, 50% (w/v) KOH(aq) (3.8 µL, 0.034 mmol, 0.20 equiv.) was added. After the catalyst **43** had been stirring for 2 h 15 min, 1-bromonaphthalene **115** (15 µL, 0.11 mmol, 0.63 equiv.) and methyl vinyl ketone **90** (MVK) (20 µL, 0.24 mmol, 1.4 equiv.) were added to the solution of substrate **49**. After the catalyst **43** had been stirring for 2 h 30 min, the substrate solution was added in one portion. Initiation of the reaction and time zero was designated by the addition of the substrate solution.

### 6.12.2 Graphical results

Results of the control (Figure 6.34) and test (Figure 6.35) reactions are depicted below. In each graph, the $x$-axis corresponds to time following initiation of the reaction; the $y$-axis corresponds to conversion as a ratio of the total amount (in mol) of substrate **49** and product **97**; the red data corresponds to the substrate **49**; the blue data analogously corresponds to the relative amount of product **97**. The lines are guides for the eye.

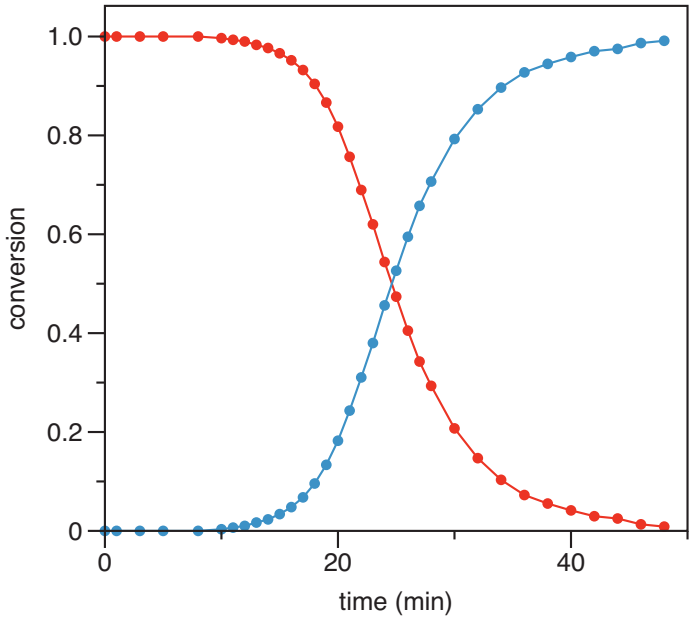



**Figure 6.34: Results obtained from the control reaction.**

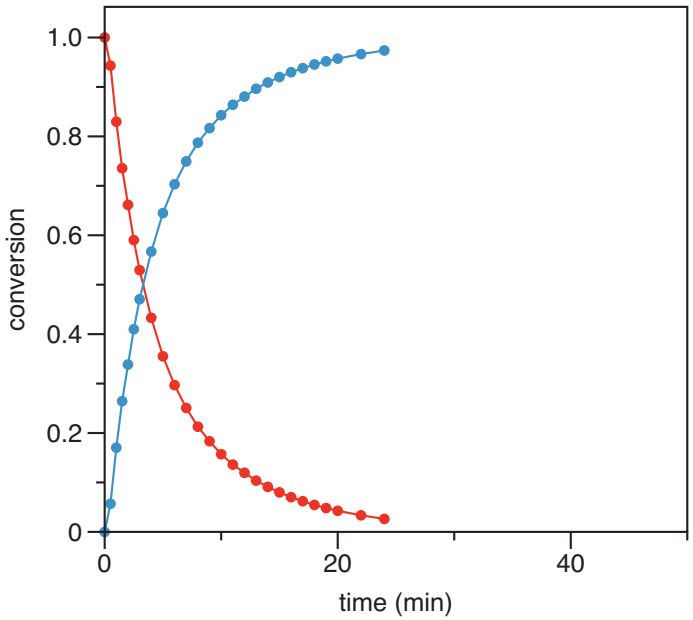



**Figure 6.35: Results obtained from the test reaction.**

A summary of the whole experiment is depicted below (Figure 6.36). For clarity only substrate conversion data are depicted. The data are colour-coded for reference.

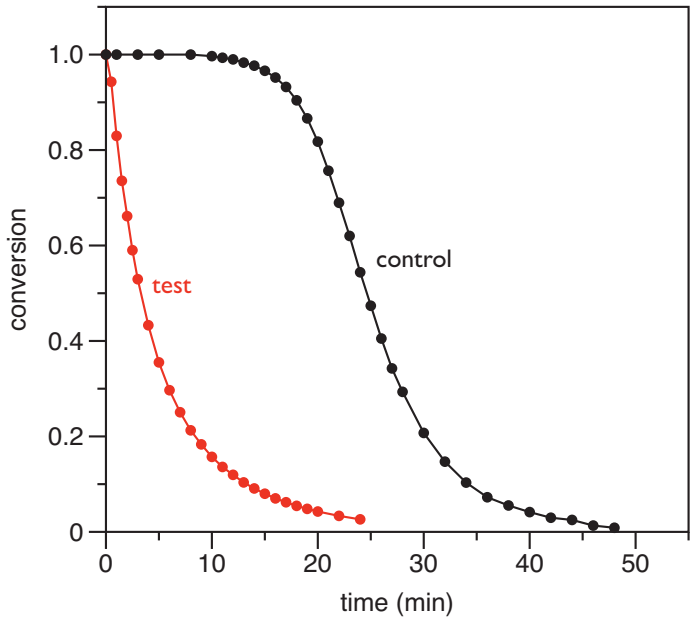


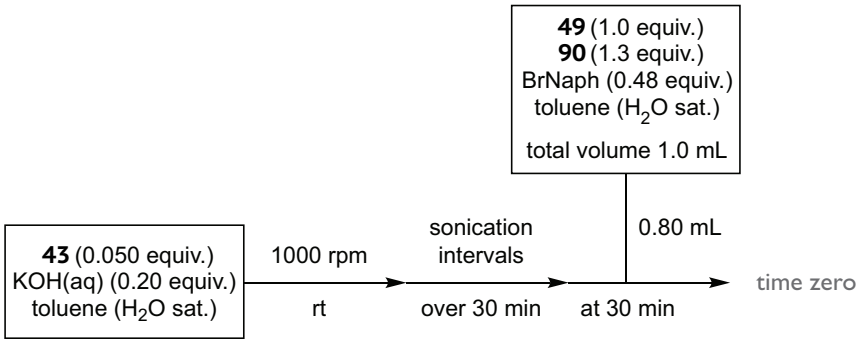

**Figure 6.36: Evaluating the potential for catalyst activation by pre-stirring halide salt 43 with base prior to initiation of the reaction (red data); carried out with an appropriate control (black data).** The red data correspond to the test protocol described above; the black data correspond to the control protocol described above. The $x$-axis corresponds to time following initiation of the reactions at the designated time zeros, the $y$-axis corresponds to conversion on substrate **49** taken as a ratio of the total amount (in mol) of substrate **49** and product **97**. The lines are guides for the eye.

## 6.13 Results obtained using protocol 5

### 6.13.1 General information and conditions

A set of four reactions were carried out using the protocol described below. Equivalents are described with respect to the substrate **49**. Stirring speeds were calibrated using a stroboscope. Unused reaction vials and stirrer bars were deployed for each reaction. Toluene used in the reactions was stored over water (approximately 30 mL of water per 1000 mL of toluene; titrated to >300 ppm), shaken and allowed to settle for 5 min before use. All liquid volumes were handled using volumetric flasks or automatic pipettes of appropriate capacity (either 0.50–5.00 µL, 1.0–10.0 µL, 10–100 µL, or 0.100–1.000 mL). Solid material was weighed out to the nearest 0.1 mg. Quantities of BrNaph and MVK that were used in the reactions were verified by weighing the distributed volume to the nearest 0.1 mg. The vial holder that was used in all reactions was installed with insulation inserted between the holder and the stirrer plate. The

ambient temperature was verified before carrying out each reaction, which was set as 20–22 °C (rt). Treatment of mixtures in an ultrasound bath first entailed removing the vial from the holder perpendicularly without ceasing stirring, immersing the vial up to the solvent level in the ultrasound bath for no more than 3 s, then re-fitting the vial to the holder on the stirrer plate. Stirring was maintained with a consistent shearing motion.




A **substrate solution** was prepared as follows: methyl vinyl ketone **90** (19.2–19.8 mg, 0.274–0.282 mmol), 1-bromonaphthalene **115** (BrNaph) (20.9–21.1 mg, 0.101–0.102 mmol), and substrate **49** (62.7 mg. 0.2122 mmol) were added to a 1.0 mL volumetric flask before toluene (∼0.9 mL) was added. The mixture was treated briefly in an ultrasound bath to dissolve all material before the flask was topped up to 1.0 mL with toluene. The solution was prepared within 10 min of being added to the reaction mixture and thoroughly mixed before use.

The catalyst **43** (3.8 mg, 0.0084 mmol, 0.062 equiv.) and a stirrer bar were added to a 7 mL vial. The vial was set in a holder that was specifically designed to consistently place the vial centrally on the stirrer plate (Figure 6.14). The vial was attached so that the bottom did not touch the surface of the holder. Toluene (900 µL) was introduced to the vial by washing down the sides, and the mixture immediately stirred at ∼200 rpm and a timer was started. After 1 min, 50% (w/v) KOH(aq) (3.8 µL, 0.034 mmol, 0.20 equiv.) was added and the stirring speed adjusted to 1000 rpm. After an additional 5 min (6 min total), the vial was treated in an ultrasound bath. The vial was then stirred for a further 10 min (16 min total) before being treated in an ultrasound bath. The vial was then stirred for a further 10 min

(26 min total) before being treated in an ultrasound bath. After an additional 5 min (31 min total), the **substrate solution** (800 µL) was added in one portion to initiate the reaction at the designated time zero. The added amount of substrate solution corresponded to the initial reaction conditions as follows: substrate **49** (0.170 mmol, 1.00 equiv.), MVK **90** (0.219–0.226 mmol, 1.29–1.33 equiv.), BrNaph **115** (0.0807–0.0815 mmol, 0.475–0.480 equiv.).

### 6.13.2 Graphical results

Results of the reaction set are depicted below (Figure 6.37, Figure 6.38, Figure 6.39, and Figure 6.40). In each graph, the $x$-axis corresponds to time following initiation of the reaction by the addition of the substrate solution; the $y$-axis corresponds to concentration; the red data corresponds to the substrate **49**; the blue data analogously corresponds to the relative amount of product **97**. The red lines in each graph correspond to the fitting of equation 2.2, and the extracted values for the parameter $k$ and its goodness of fit ($R^2$) are displayed on the appropriate graph.

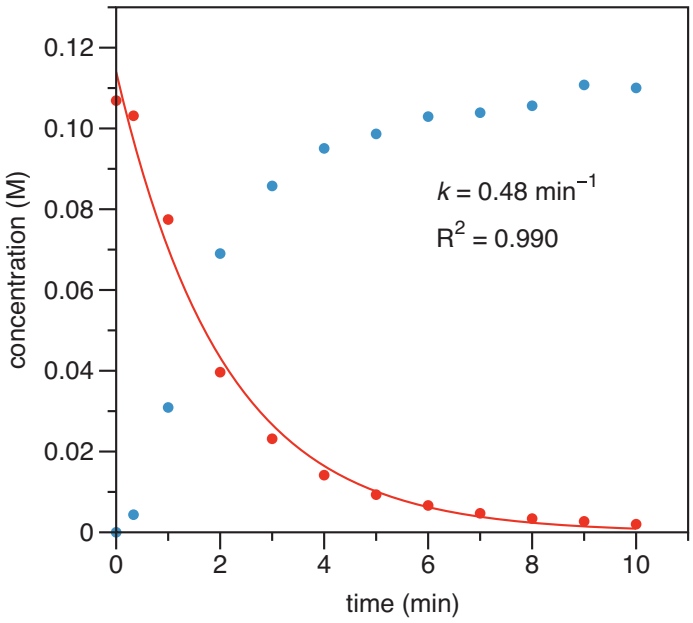



**Figure 6.37: Results obtained from the first reaction.**

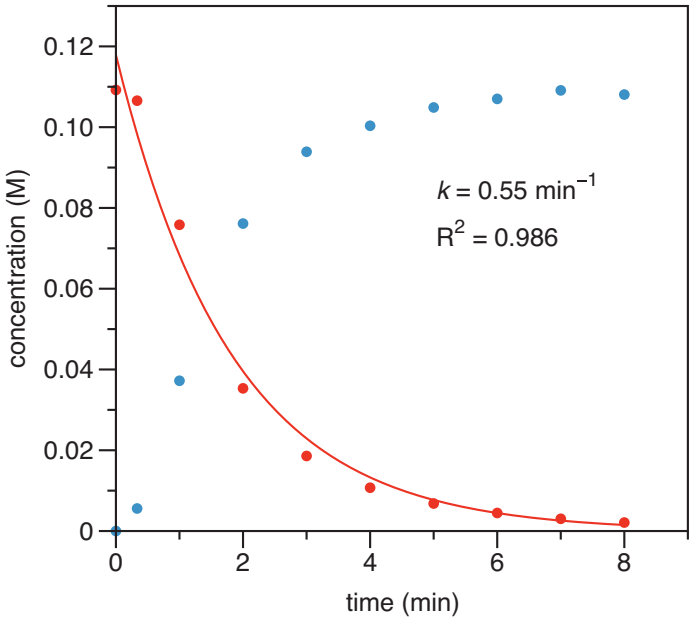



**Figure 6.38: Results obtained from the second reaction.**

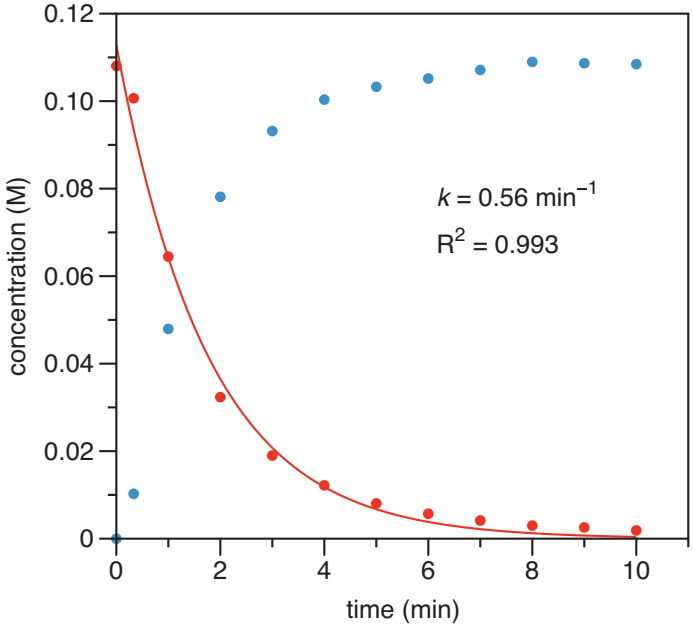



**Figure 6.39: Results obtained from the third reaction.**

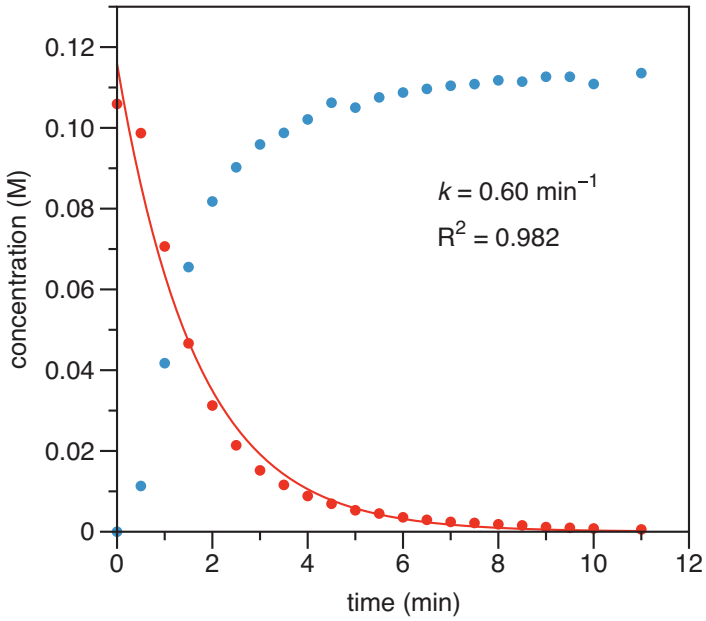



**Figure 6.40: Results obtained from the fourth reaction.**

A summary of the whole experiment is depicted below (Figure 6.41). For clarity only substrate conversion data are depicted. The data are colour-coded for reference. The average value of the extracted parameter, $k$, was $0.55 \pm 0.04$ min$^{-1}$.

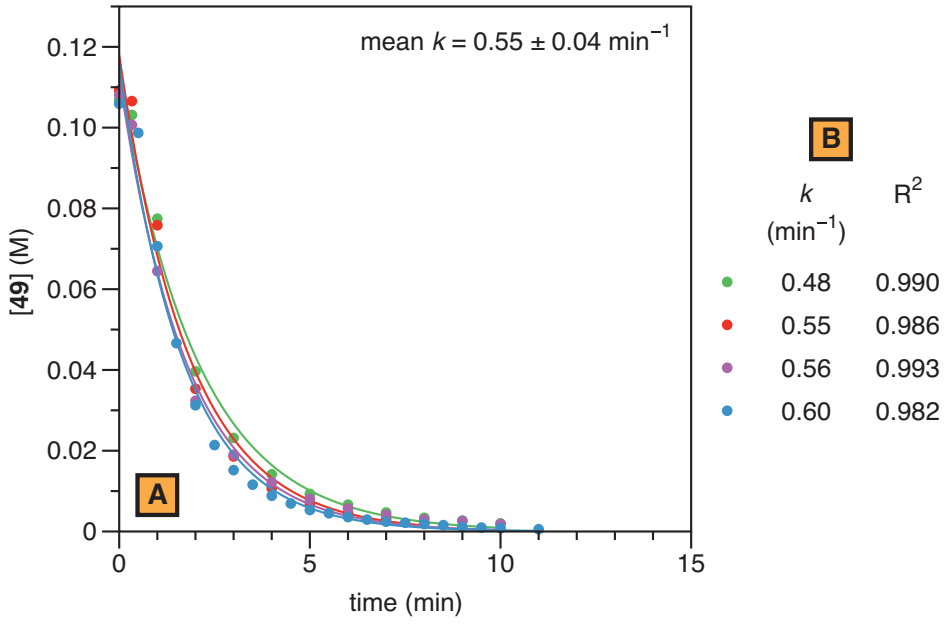



**Figure 6.41: Data acquired using protocol 5. A)** Overlay of concentration data obtained from the four reactions. The $x$-axis corresponds to time following initiation of the reaction by the addition of the substrates to the reaction mixture, the $y$-axis corresponds to the concentration of substrate **49**. The different colours correspond to each of the four reactions. The coloured lines correspond to fitting of the function described by equation 2.2 corresponding to the appropriately coloured data set. **B)** Values obtained following fitting of equation 2.2 to each data set, which follows the same colour convention as in **A**.

## 6.14 Evaluating the reaction order with respect to the substrate

### 6.14.1 General information and conditions

A series of reactions were carried out using a modified version of protocol 5 (see 6.13); the reactions varied only by the amount of substrate **49** that was used in the reaction. Each experiment was carried out as single reactions within a triplicate or as a set of four reactions. Equivalents (equiv.) are reported with respect to the amount of substrate **49**. The numbered entries across the three tables—Table 6.3, Table 6.4, and Table 6.5—correspond to data from the same reactions.

The conditions for the reactions were as follows: catalyst **43** (3.8 mg, 0.0084 mmol, 0.032–0.071 equiv.), toluene (900 µL), 50% (w/v) KOH(aq) (3.8 µL, 0.034 mmol, 0.13–0.28 equiv.). For details of the added quantities of substrate **49**, methyl vinyl ketone (MVK) **90**, and 1-bromonaphthalene (BrNaph) **115**, see Table 6.3 and Table 6.4.

**Table 6.3: Quantities of added substrate 49, MVK 90, and BrNaph 115 to the substrate solution used in each reaction.** Corresponding quantities added to each reaction are in Table 6.4.

| Entry | 49 (mg) | 49 (mmol) | 90 (mg) | 90 (mmol) | 115 (mg) | 115 (mmol) |
|---|---|---|---|---|---|---|
| 1 | 43.9 | 0.149 | 19.3 | 0.275 | 21.2 | 0.102 |
| 2 | 43.9 | 0.149 | 19.7 | 0.281 | 21.3 | 0.103 |
| 3 | 43.9 | 0.149 | 19.5 | 0.278 | 21.5 | 0.104 |
| 4 | 49.8 | 0.169 | 19.8 | 0.282 | 21.5 | 0.104 |
| 5 | 49.8 | 0.169 | 20.4 | 0.291 | 21.7 | 0.105 |
| 6 | 49.8 | 0.169 | 19.6 | 0.280 | 21.7 | 0.105 |
| 7 | 55.7 | 0.189 | 19.7 | 0.281 | 21.3 | 0.103 |
| 8 | 55.7 | 0.189 | 20.4 | 0.291 | 21.7 | 0.105 |
| 9 | 55.7 | 0.189 | 19.7 | 0.281 | 21.3 | 0.103 |
| 10 | 70.9 | 0.240 | 20.0 | 0.285 | 21.3 | 0.103 |
| 11 | 70.9 | 0.240 | 19.7 | 0.281 | 21.4 | 0.103 |
| 12 | 70.9 | 0.240 | 19.7 | 0.281 | 21.7 | 0.105 |
| 13 | 79.0 | 0.267 | 19.9 | 0.284 | 21.0 | 0.101 |
| 14 | 79.0 | 0.267 | 20.2 | 0.288 | 21.3 | 0.103 |
| 15 | 79.0 | 0.267 | 19.5 | 0.278 | 21.2 | 0.102 |
| 16 | 96.9 | 0.328 | 19.3 | 0.275 | 21.5 | 0.104 |
| 17 | 96.9 | 0.328 | 19.8 | 0.282 | 22.3 | 0.108 |
| 18 | 96.9 | 0.328 | 19.7 | 0.281 | 20.9 | 0.101 |
| 19 | 96.9 | 0.328 | 19.5 | 0.278 | 21.6 | 0.104 |

**Table 6.4: Final initial quantities of substrate 49, MVK 90, and BrNaph 115 used in each reaction.** Corresponding quantities added to each **substrate solution** are in Table 6.3.

| Entry | 49 (mmol) | 49 (equiv.) | 90 (mmol) | 90 (equiv.) | 115 (mmol) | 115 (equiv.) |
|---|---|---|---|---|---|---|
| 1 | 0.119 | 1.00 | 0.220 | 1.85 | 0.0819 | 0.689 |
| 2 | 0.119 | 1.00 | 0.225 | 1.89 | 0.0823 | 0.692 |
| 3 | 0.119 | 1.00 | 0.223 | 1.87 | 0.0831 | 0.699 |
| 4 | 0.135 | 1.00 | 0.226 | 1.68 | 0.0831 | 0.616 |
| 5 | 0.135 | 1.00 | 0.233 | 1.73 | 0.0838 | 0.622 |
| 6 | 0.135 | 1.00 | 0.224 | 1.66 | 0.0838 | 0.622 |
| 7 | 0.151 | 1.00 | 0.225 | 1.49 | 0.0823 | 0.545 |
| 8 | 0.151 | 1.00 | 0.233 | 1.54 | 0.0838 | 0.556 |
| 9 | 0.151 | 1.00 | 0.225 | 1.49 | 0.0823 | 0.545 |
| 10 | 0.192 | 1.00 | 0.228 | 1.19 | 0.0823 | 0.429 |
| 11 | 0.192 | 1.00 | 0.225 | 1.17 | 0.0827 | 0.431 |
| 12 | 0.192 | 1.00 | 0.225 | 1.17 | 0.0838 | 0.437 |
| 13 | 0.214 | 1.00 | 0.227 | 1.06 | 0.0811 | 0.379 |
| 14 | 0.214 | 1.00 | 0.231 | 1.08 | 0.0823 | 0.385 |
| 15 | 0.214 | 1.00 | 0.223 | 1.04 | 0.0819 | 0.383 |
| 16 | 0.262 | 1.00 | 0.220 | 0.839 | 0.0831 | 0.317 |
| 17 | 0.262 | 1.00 | 0.226 | 0.861 | 0.0862 | 0.328 |
| 18 | 0.262 | 1.00 | 0.225 | 0.857 | 0.0807 | 0.308 |
| 19 | 0.262 | 1.00 | 0.223 | 0.848 | 0.0835 | 0.318 |

### 6.14.2 Graphical results

Results of each reaction set are summarised below (Figure 6.42, Figure 6.43, Figure 6.44, Figure 6.45, Figure 6.46, and Figure 6.47). For clarity only substrate conversion data are depicted. The data are colour-coded for reference. In each graph, the $x$-axis corresponds to time following initiation of the reaction by the addition of the substrates to the reaction mixture, the $y$-axis corresponds to the concentration of substrate **49**. The coloured lines correspond to fitting of the function described by equation 2.2 corresponding to the appropriately coloured data set. Values obtained following fitting of equation 2.2 to each data set, which follows the same colour convention, are indicated on each figure.

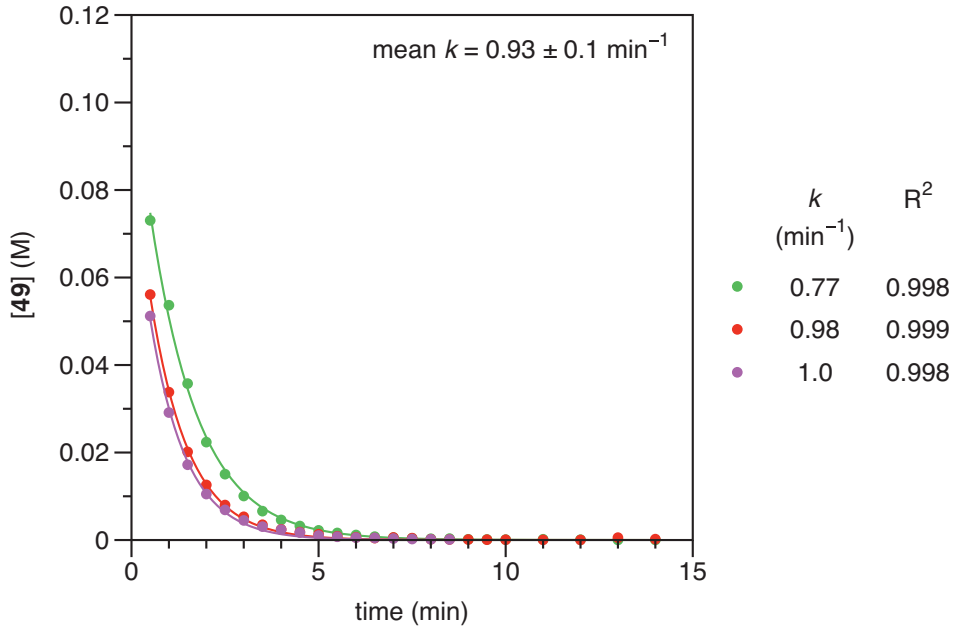



**Figure 6.42: Results obtained from the initial substrate 49 concentration of 0.0698 M.**

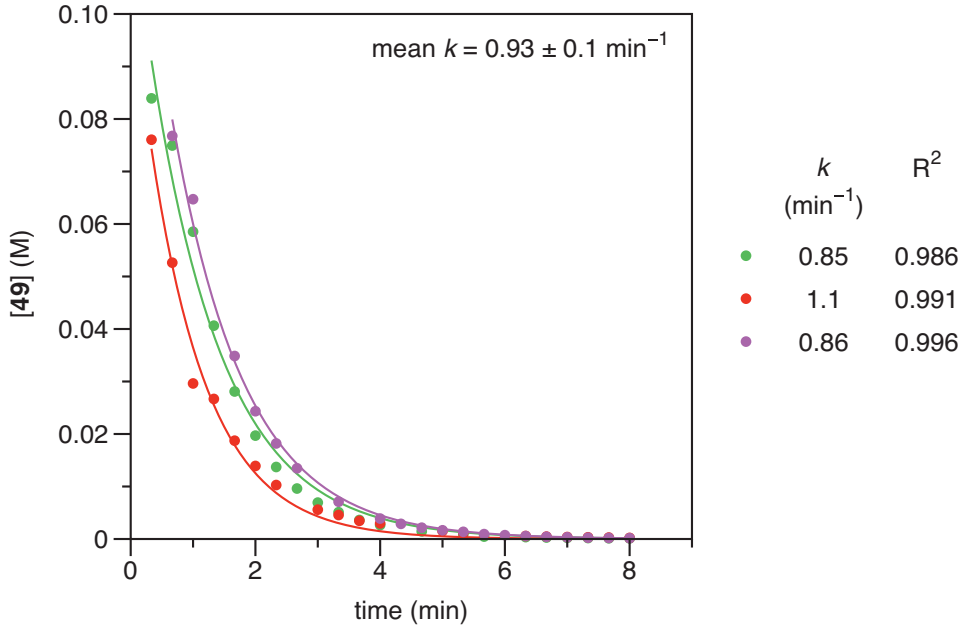



**Figure 6.43: Results obtained from the initial substrate 49 concentration of 0.0792 M.**

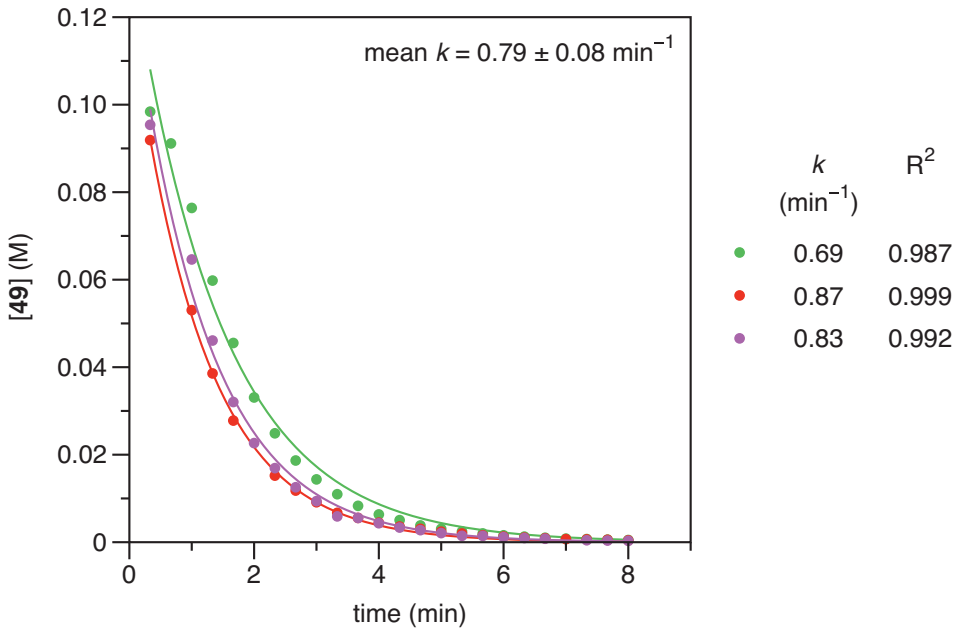



**Figure 6.44: Results obtained from the initial substrate 49 concentration of 0.0885 M.**

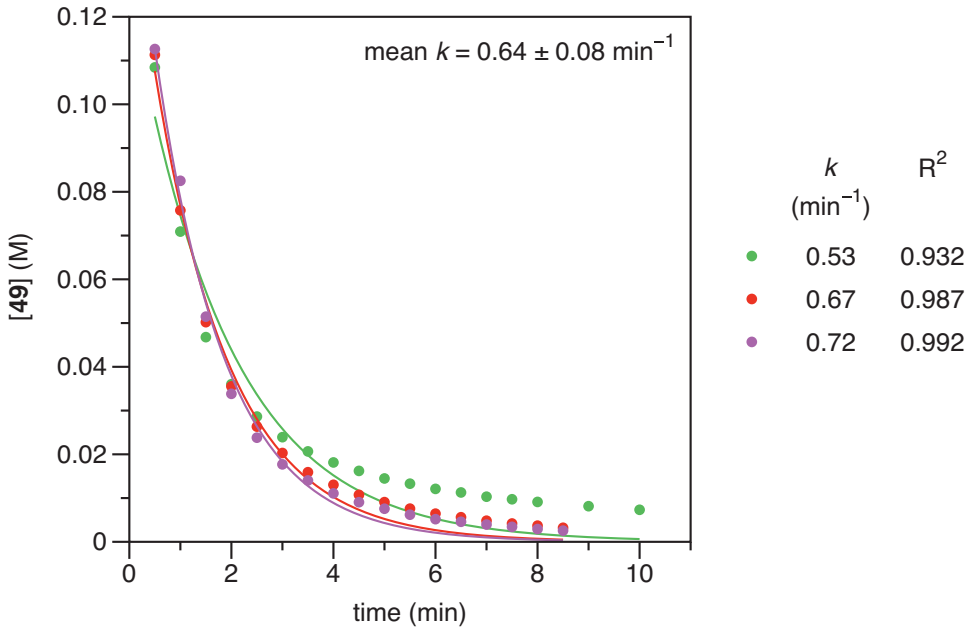



**Figure 6.45: Results obtained from the initial substrate 49 concentration of 0.113 M.**

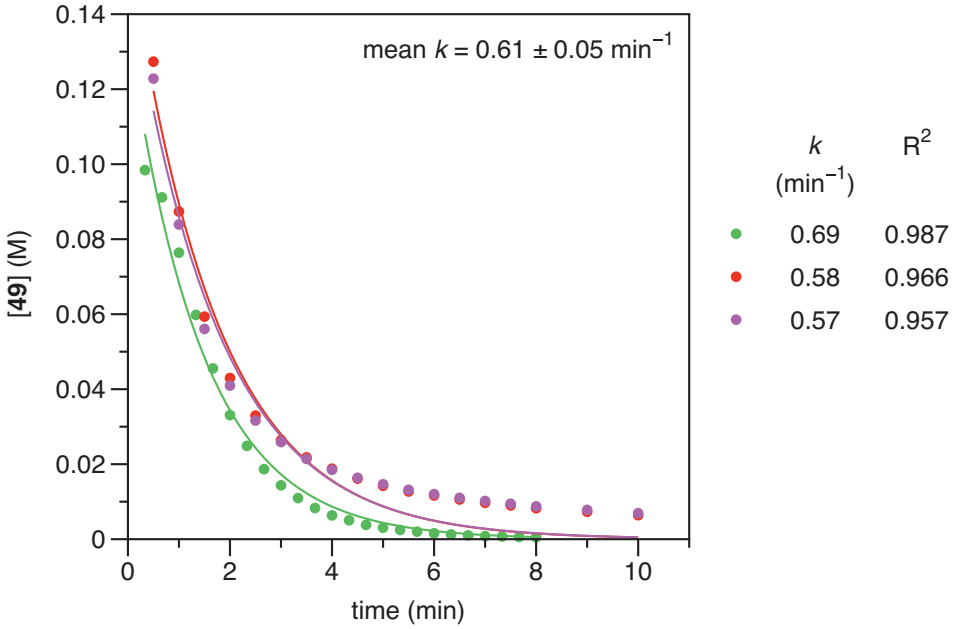



**Figure 6.46: Results obtained from the initial substrate 49 concentration of 0.126 M.**

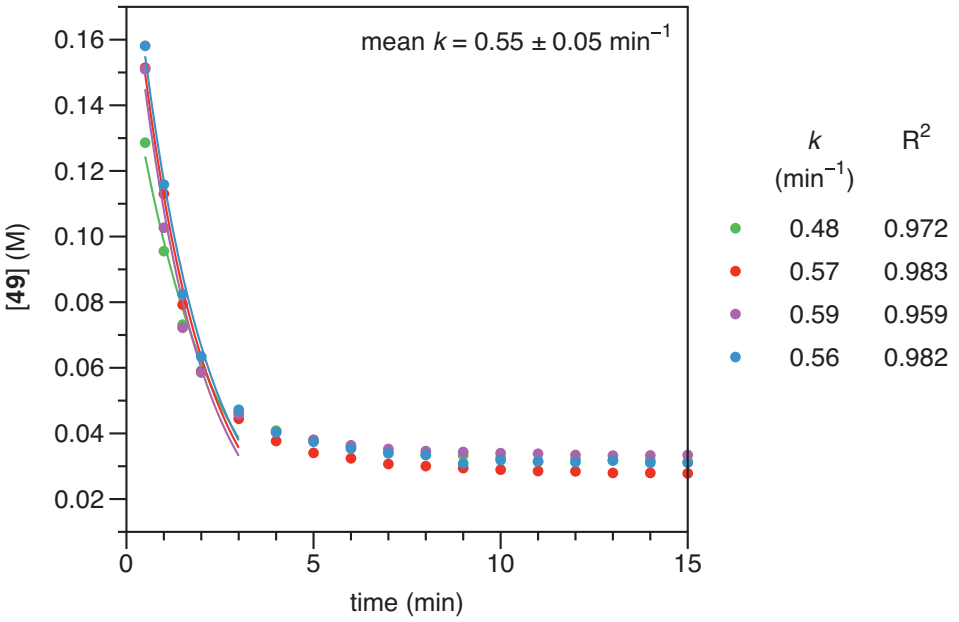



**Figure 6.47: Results obtained from the initial substrate 49 concentration of 0.154 M.**

Following analysis of each reaction to obtain values for the $k$ parameter (from fitting the data to equation 2.2), the mean natural logarithm values and error for each set was calculated. The data are summarised in Table 6.5.

**Table 6.5: Summary of results investigating the order in substrate 49.** Equivalents (equiv.) are reported with respect to substrate **49**.

| Entry | 49[a] (mg) | $[49]_0$[b] (M) | ln $[49]_0$[c] (M) | 43 loading[d] (equiv.) | KOH[e] (equiv.) | $k$[f] $min^{-1}$ | ln $k$[g] $min^{-1}$ | mean ln $k$[h] $min^{-1}$ | SD[i] $min^{-1}$ |
|---|---|---|---|---|---|---|---|---|---|
| 1 | 43.9 | 0.0698 | −2.66 | 0.071 | 0.28 | 0.772 | −0.258 | | |
| 2 | 43.9 | 0.0698 | −2.66 | 0.071 | 0.28 | 0.981 | −0.0191 | −0.080 | 0.1 |
| 3 | 43.9 | 0.0698 | −2.66 | 0.071 | 0.28 | 1.04 | 0.037 | | |
| 4 | 49.8 | 0.0792 | −2.54 | 0.063 | 0.25 | 0.855 | −0.157 | | |
| 5 | 49.8 | 0.0792 | −2.54 | 0.063 | 0.25 | 1.07 | 0.0663 | −0.080 | 0.1 |
| 6 | 49.8 | 0.0792 | −2.54 | 0.063 | 0.25 | 0.860 | −0.150 | | |
| 7 | 55.7 | 0.0885 | −2.42 | 0.056 | 0.22 | 0.688 | −0.375 | | |
| 8 | 55.7 | 0.0885 | −2.42 | 0.056 | 0.22 | 0.867 | −0.143 | −0.24 | 0.1 |
| 9 | 55.7 | 0.0885 | −2.42 | 0.056 | 0.22 | 0.826 | −0.192 | | |
| 10 | 70.9 | 0.113 | −2.18 | 0.044 | 0.18 | 0.530 | −0.634 | | |
| 11 | 70.9 | 0.113 | −2.18 | 0.044 | 0.18 | 0.672 | −0.397 | −0.45 | 0.1 |
| 12 | 70.9 | 0.113 | −2.18 | 0.044 | 0.18 | 0.726 | −0.320 | | |
| 13 | 79.0 | 0.126 | −2.07 | 0.040 | 0.16 | 0.688 | −0.375 | | |
| 14 | 79.0 | 0.126 | −2.07 | 0.040 | 0.16 | 0.581 | −0.543 | −0.49 | 0.08 |
| 15 | 79.0 | 0.126 | −2.07 | 0.040 | 0.16 | 0.571 | −0.561 | | |
| 16 | 96.9 | 0.154 | −1.87 | 0.032 | 0.13 | 0.468 | −0.760 | | |
| 17 | 96.9 | 0.154 | −1.87 | 0.032 | 0.13 | 0.574 | −0.555 | −0.60 | 0.09 |
| 18 | 96.9 | 0.154 | −1.87 | 0.032 | 0.13 | 0.590 | −0.528 | | |
| 19 | 96.9 | 0.154 | −1.87 | 0.032 | 0.13 | 0.564 | −0.573 | | |

[a]Amount of **49** added to the pre-reaction **substrate solution**; [b]initial concentration of substrate **49** in the reaction mixtures; [c]natural logarithm of the initial concentration of substrate **49** in the reaction mixtures; [d]catalyst **43** loading in each reaction, with respect to substrate **49**; [e]KOH loading in each reaction, with respect to substrate **49**; [f]extracted parameter for the rate of consumption of substrate **49**, according to equation 2.2; [g]natural logarithm of the extracted parameter for the rate of consumption of substrate **49**; [h]average (to 2 sf) of all replicate extracted parameters (natural logarithm) corresponding to the consumption of substrate **49**; [i]standard deviation (to 1 sf) of the parameters corresponding to the consumption of substrate **49** of the specified data set replicates.

A double logarithmic plot of initial concentration of substrate **49** (ln $[49]_0$) against the observed rate (ln $k$) was constructed to give a reaction order with respect to substrate of −0.73 (Figure 6.48), with a 68% confidence interval of −0.81 to −0.66.

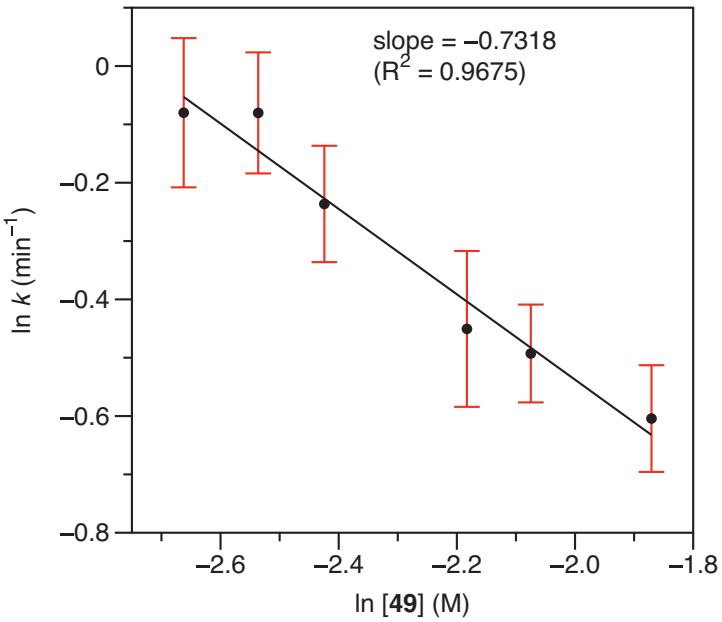
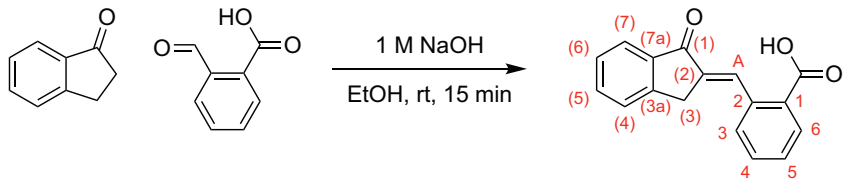



**Figure 6.48: Double logarithmic plot to evaluate the rate-dependence on the concentration of substrate 49.** The $x$-axis corresponds to the natural logarithm of the initial concentration of substrate **49** in M, the $y$-axis corresponds to the natural logarithm of the extracted $k$ value from each reaction set in $\mathrm{min}^{-1}$. The line is linear regression analysis of the data, which gave a slope of $-0.73$ with an $R^2$ value of 0.968.

# 7. Project 2: Experimental

## 7.1 Material syntheses and characterisation

### 7.1.1 2-((1-Oxo-1,3-dihydro-2*H*-inden-2-ylidene)methyl)benzoic acid (130)




**128** **129** **130**

Carried out by BFR.[115] 1-Indanone **128** (24.0 g, 114 mmol, 1.00 equiv.) and 2-carboxybenzaldehyde **129** (17.0 g, 114 mmol, 1.00 equiv.) were dissolved in EtOH (272 mL). A solution of 1 M NaOH(aq) (204 mL, 240 mmol, 2.10 equiv.) was added. The reaction mixture was stirred for 15 min at rt before cold water (75 mL) was added. The mixture was extracted with TBME (150 mL) and the organic layers were discarded. The aqueous layer was acidified with 10 M $H_2SO_4$. The resulting precipitate was isolated by filtration, washed with water (100 mL), then dried in a vacuum oven (40 °C, 10 mbar) overnight. The crude material was used without further purification (26.0 g, 87%);

$\nu_{max}$ (neat) 2634, 1681, 1263, 736;

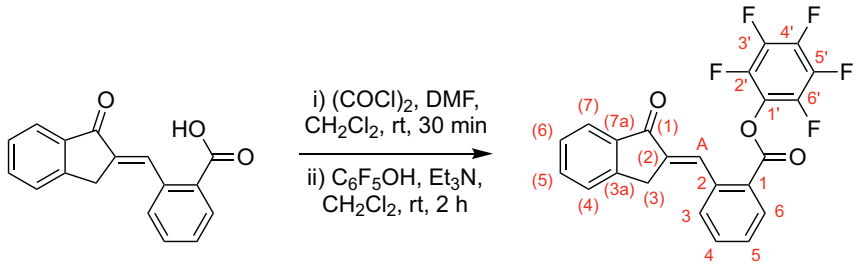
$^1$H-NMR: $\delta$ (500 MHz; DMSO-$d_6$) 13.21 (brs, 1 H, $CO_2H$), 8.15 (brt, $J$ = 2.0 Hz, 1 H, *HA*), 7.94 (dd, $J$ = 8.0, 1.5 Hz, 1 H, *H6*), 7.88 (brd, $J$ = 8.0 Hz, 1 H, *H3*), 7.81 (dm, $J$ = 7.5 Hz, 1 H, *H(7)*), 7.72 (ddd, $J$ = 7.5, 7.5, 1.0 Hz, 1 H, *H(5)*), 7.70–7.67 (m, 1 H, *H4*), 7.65 (dm, $J$ = 7.5 Hz, 1 H, *H(4)*), 7.55 (ddd, $J$ = 7.5, 7.5, 1.0 Hz, 1 H, *H5*), 7.51–7.48 (m, 1 H, *H(6)*), 4.02 (d, $J$ = 2.0 Hz, 2 H, *H(3)*);

$^{13}$C{$^1$H}-NMR: $\delta$ (126 MHz; DMSO-$d_6$) 193.7 (*C(1)*), 168.7 ($CO_2$H), 150.8 (*C(3a)*), 137.8 (*C(7a)*), 136.5 (*C(2)*), 135.8 (*C2*), 135.4 (*C(5)*), 132.8 (*C1*), 132.8 (*CA*), 132.3 (*C4*), 130.9

(*C6*), 130.3 (*C3*), 129.6 (*C5*), 128.2 (*C(6)*), 127.2 (*C(4)*), 124.1 (*C(7)*), 31.5 (*C(3)*);

HRMS (ESI) 265.08598 ([M+H]$^+$), calcd. for $C_{17}H_{13}O_3^+$ 265.08592.

### 7.1.2 Perfluorophenyl 2-((1-oxo-1,3-dihydro-2*H*-inden-2-ylidene)methyl)benzoate (131)




**130** **131**

Carried out by BFR under anhydrous conditions.[115] Compound **130** (42.0 g, 159 mmol, 1.00 equiv.) was suspended in a solution of $CH_2Cl_2$ (420 mL) and DMF (1.00 mL). Oxalyl chloride (20.4 mL, 238 mmol, 1.50 equiv.) was added dropwise. After evolution of gas had ceased (30 min), pentafluorophenol (32.2 g, 175 mmol, 1.10 equiv.) and $Et_3N$ (48.7 mL, 350 mmol, 2.20 equiv.) were added. The mixture was stirred for 2 h before water (320 mL) and $CH_2Cl_2$ (175 mL) were added. The layers were separated and the organic layer was washed with 6 M aqueous HCl (225 mL) and brine (320 mL). The solvent was evaporated at atmospheric pressure. The residue was purified by crystallisation from iPrOAc (300 mL, 60 °C → 25 °C at −0.1 °C min$^{-1}$, then stirred at 25 °C for 6 h) to give *the title compound* as a tan solid (34.0 g, 50%);

mp 124–126 °C (decomp.);

$\nu_{max}$ (neat) 3054, 1758, 1701, 1637, 1518, 1468, 1324, 1296, 1265, 1232, 1208, 1184, 1145, 1127, 1089, 1030;

$^1$H-NMR: $\delta$ (500 MHz; $CDCl_3$) 8.31 (ddd, $J$ = 8.0, 1.5, 0.5 Hz, 1 H, *H6*), 8.26–8.24 (m, 1 H, *HA*), 7.94 (dddt, $J$ = 8.0, 0.5, 0.5, 0.5 Hz, *H(7)*), 7.79–7.73 (m, 2 H, *H4* and *H3*), 7.61–7.58

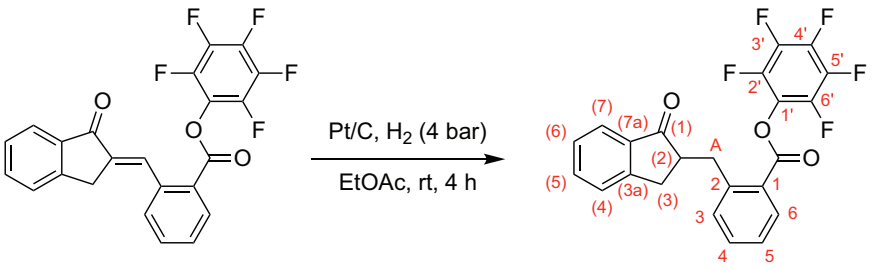
(m, 2 H, *H(5)* and *H5*), 7.51 (dddt, $J$ = 7.5, 1.0, 1.0 1.0 Hz, *H(4)*), 7.44 (dddt, $J$ = 8.0, 7.5, 1.0, 1.0 Hz, 1 H, *H(6)*), 3.92–3.91 (m, 2 H, *H(3)*);

$^{19}$F-NMR: $\delta$ (471 MHz; $CDCl_3$) −152.1 (m, 2 F, *F2′* and *F6′*), −157.6 (m, 1 F, *F4′*), −162.1 (m, 2 F, *F3′* and *F5′*);

$^{13}$C{$^{1}$H,$^{19}$F}-NMR: $\delta$ (126 MHz; $CDCl_3$) 193.4 (*C(1)*), 162.2 (*C*$O_2$*C*$_6$*F*$_5$), 149.7 (*C(3a)*), 141.3 (*C2′* and *C6′*), 139.6 (*C4′*), 138.8 (*C2*), 138.1 (*C(7a)*), 137.9 (*C3′* and *C5′*), 137.4 (*C(2)*), 134.8 (*C(5)*), 133.9 (*C4*), 132.3 (*CA*), 132.1 (*C6*), 130.1 (*C3*), 128.9 (*C5*), 127.8 (*C(6)*), 126.9 (*C1*), 126.2 (*C(4)*), 125.1 (*C1′*), 124.7 (*C(7)*), 31.2 (*C(3)*);

HRMS (ESI) 431.06976 ([M+H]$^+$), calcd. for $C_{23}H_{12}O_3F_5^+$ 431.07011.

### 7.1.3 Perfluorophenyl 2-((1-oxo-2,3-dihydro-1*H*-inden-2-yl)methyl)benzoate (125)




**131** **125**

Carried out by BFR according to a modified literature procedure.[114,115] **5 g scale:** A stirred suspension of JM1R163 (1% Pt/C, 2.5 g, 50 wt%) and **131** (5.0 g, 12 mmol, 1.0 equiv.) in EtOAc (150 mL) in a miniclave was pressurised to 3 bar with $N_2$ and the pressure vented three times. The vessel was then pressurised to 3 bar with $H_2$ and vented twice. Finally, the vessel was pressurised to 3 bar with $H_2$ and the reaction mixture stirred for 2.5 h. The reaction was sampled by venting the $H_2$ atmosphere and taking an aliquot with a needle through a sidearm to find that the starting material had all been consumed (by reverse phase HPLC analysis). The suspension was filtered through Celite® and the solvent was evaporated under reduced pressure to afford crude **125** (5 g, 99%). The residue was combined with the residue from the

20 g reaction for purification. **20 g scale:** A stirred suspension of JM1R163 (1% Pt/C, 10 g, 50 wt%) and **131** (20 g, 48 mmol, 1.0 equiv.) in EtOAc (600 mL) in an autoclave was pressurised to 4 bar with $N_2$ and the pressure vented four times. The vessel was then pressurised to 4 bar with $H_2$ and vented twice. Finally, the vessel was pressurised to 4 bar with $H_2$ and the reaction mixture stirred for 4 h. The reaction was sampled by venting the $H_2$ atmosphere and taking an aliquot with a needle through a sidearm to find that the starting material had all been consumed (by reverse phase HPLC analysis). The suspension was filtered through Celite® and the solvent was evaporated under reduced pressure to afford crude **125** (20.4 g, quant.). The residue was combined with the residue from the 5 g reaction for purification. The combined crude material was purified first by flash chromatography on silica gel, eluting with 10% (v/v) ethyl acetate/petrol, before recrystallisation from 2-propanol (200 mL, 60 °C → rt) to give *the title compound* as clear crystals (18.0 g, 71% overall).

mp 83–88 °C;

$\nu_{max}$ (neat) 2928, 1759, 1712, 1602, 1519, 1488, 1466, 1320, 1288, 1273, 1227, 1145, 1115, 1030;

$^1$H-NMR: $\delta$ (500 MHz; $CDCl_3$) 8.26 (ddd, $J$ = 8.0, 1.5, 0.5 Hz, 1 H, *H6*), 7.79 (ddddd, $J$ = 7.5, 1.0, 0.5, 0.5, 0.5 Hz, 1 H, *H(7)*), 7.63 (ddd, $J$ = 7.5, 7.5, 1.5 Hz, 1 H, *H4*), 7.59 (ddd, $J$ = 7.5, 7.5, 1.0 Hz, 1 H, *H(5)*), 7.49 (ddd, $J$ = 7.5, 1.5, 0.5 Hz, 1 H, *H3*), 7.47–7.42 (m, 2 H, *H5* and *H(4)*), 7.39 (ddddd, $J$ = 8.0, 7.0, 1.0, 1.0, 1.0 Hz, 1 H, *H(6)*), 3.79 (dd, $J$ = 13.0, 5.0 Hz, 1 H, *HA*), 3.22 (ddddd, $J$ = 17.0, 7.5, 0.5, 0.5, 0.5 Hz, 1 H, *H(3)*), 3.20–3.09 (m, 2 H, *HA* and *H(2)*), 2.91 (ddm, $J$ = 17.0, 4.0 Hz, 1 H, *H(3)*);

$^{19}$F-NMR: $\delta$ (471 MHz; $CDCl_3$) −152.4 (m, 2 F, *F2′* and *F6′*), −157.9 (m, 1 F, *F4′*), −162.2 (m, 2 F, *F3′* and *F5′*);

$^{13}$C{$^1$H,$^{19}$F}-NMR: $\delta$ (126 MHz; $CDCl_3$) 207.2 (*C(1)*), 162.9 ($CO_2C_6F_5$), 153.3 (*C(3a)*), 143.8 (*C2*), 141.4 (*C2′* and *C6′*), 139.5 (*C4′*), 138.0 (*C3′* and *C5′*), 136.4 (*C(7a)*), 134.8 (*C(5)*), 134.0

(*C4*), 132.2 (*C3*), 132.1 (*C6*), 127.5 (*C(6)*), 127.0 (*C5*), 126.5 (*C(4)*), 126.2 (*C1*), 125.3 (*C1′*), 124.1 (*C(7)*), 48.5 (*C(2)*), 35.0 (*CA*), 32.3 (*C(3)*);

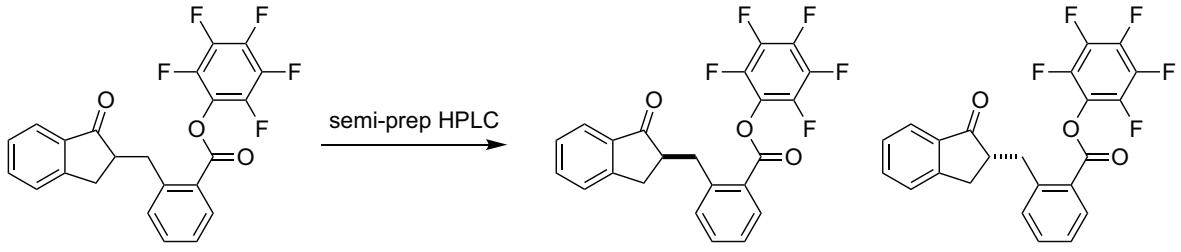
$^{1}$H-NMR: $\delta$ (600 MHz; toluene-$d_8$) 8.05 (dd, $J$ = 8.0, 1.5 Hz, 1 H, *H6*), 7.66 (d, $J$ = 7.0 Hz, 1 H, *H(7)*), 7.12–7.09 (m, 1 H, *H4*), 7.10–7.08 (m, 1 H, *H(5)*), 7.04 (dd, $J$ = 8.0, 1.0 Hz, 1 H, *H3*), 6.96–6.94 (m, 1 H, *H5*), 6.94–6.91 (m, 2 H, *H(4)* and *H(6)*), 3.76 (dd, $J$ = 14.0, 5.0 Hz, 1 H, *HA*), 2.92 (dd, $J$ = 14.0, 9.0 Hz, 1 H, *HA*), 2.76 (dddd, $J$ = 9.0, 8.0, 5.0, 5.0 Hz, 1 H, *H(2)*), 2.66 (dd, $J$ = 17.0, 8.0 Hz, 1 H, *H(3)*), 2.49 (dd, $J$ = 17.0, 5.0 Hz, 1 H, *H(3)*);

$^{19}$F-NMR: $\delta$ (471 MHz; toluene-$d_8$) −153.8 (m, 2 F, *F2′* and *F6′*), −158.4 (m, 1 F, *F4′*), −163.0 (m, 2 F, *F3′* and *F5′*);

$^{13}$C{$^{1}$H,$^{19}$F}-NMR: $\delta$ (126 MHz; toluene-$d_8$) 205.0 (*C(1)*), 162.6 (*C*$O_2C_6F_5$), 152.6 (*C(3a)*), 144.1 (*C2*), 141.3 (*C2′* and *C6′*), 139.2 (*C4′*), 137.7 (*C3′* and *C5′*), 136.7 (*C(7a)*), 133.9 (*C(5)*), 133.4 (*C4*), 132.0 (*C3*), 131.6 (*C6*), 127.1 (*C(6)*), 126.4 (*C5*), 126.21 (*C1*), 126.11 (*C(4)*), 125.2 (*C1′*), 123.7 (*C(7)*), 48.3 (*C(2)*), 34.7 (*CA*), 32.0 (*C(3)*);

HRMS (ESI) 455.06750 ([M+Na]$^+$), calcd. for $C_{23}H_{13}F_5O_3Na^+$ 455.06771;

### 7.1.4 (−)- and (+)-Perfluorophenyl 2-((1-oxo-2,3-dihydro-1*H*-inden-2-yl) methyl)benzoate ((−)-125 and (+)-125)




**125** **(–)-125** **(+)-125**

A saturated solution of racemic **125** in 50% (v/v) 2-propanol/hexane was prepared. The solution was allowed to flocculate and once the solid had settled to the bottom, the upper layers of solvent were removed and subjected to semi-preparative HPLC (YMC Chiral Amylose-

SA, 5.0 mL $min^{-1}$, 10% (v/v) 2-propanol/hexane, 25 °C, monitoring at 287 nm). The peaks corresponding to elution of both enantiomers were collected separately and concentrated under reduced pressure to give *the title compounds* as colourless oils.

**(−)-125:** 98% ee, HPLC retention 5.283–5.297 min (ChiralPak® IA, 1.1 mL $min^{-1}$, 30% (v/v) 2-propanol/hexane, 25 °C); $[\alpha]_D^{25}$ −63.6 (*c* 0.19, $CHCl_3$).

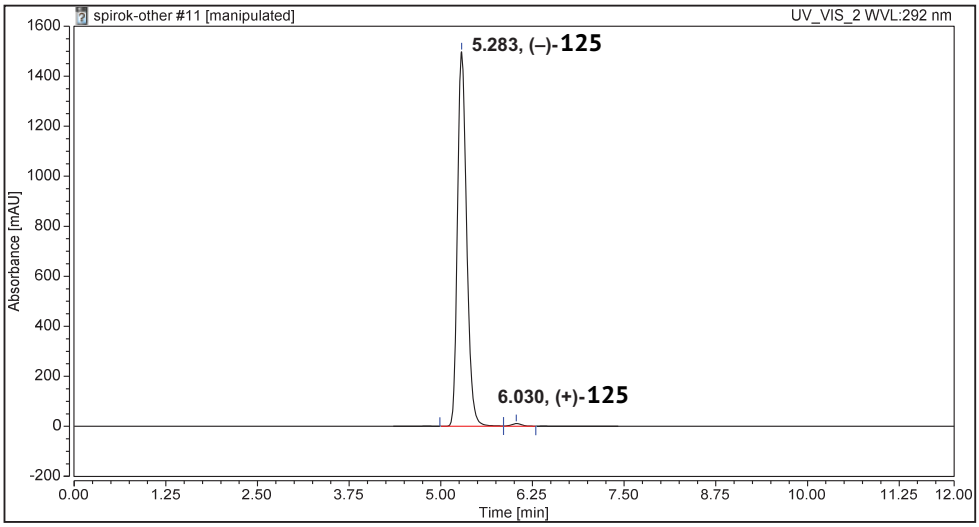



**Figure 7.1: HPLC chromatogram of isolated (−)-125.** The major enantiomer was obtained with 98% ee.

**(+)-125:** 94% ee, HPLC retention 6.017–6.020 min (ChiralPak® IA, 1.1 mL $min^{-1}$, 30% (v/v) 2-propanol/hexane, 25 °C); $[\alpha]_D^{25}$ +54.5 (*c* 0.61, $CHCl_3$).

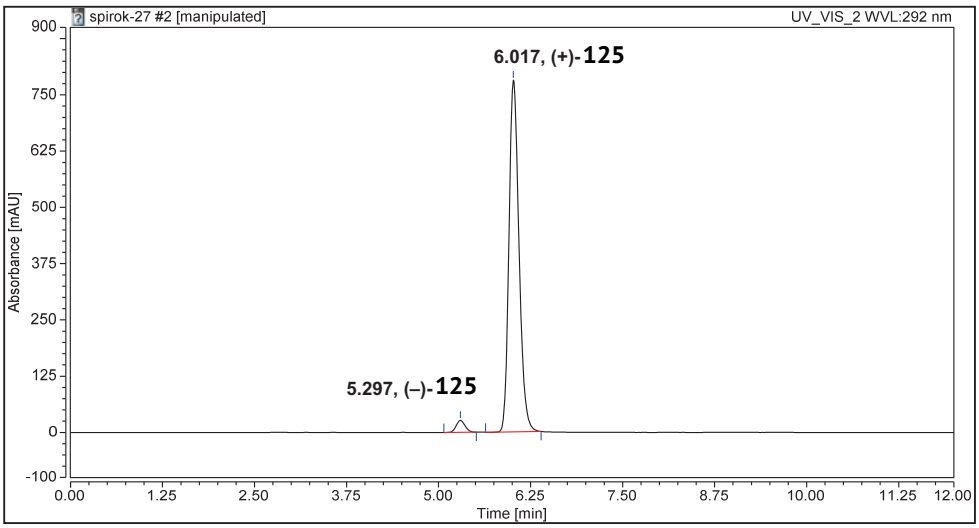
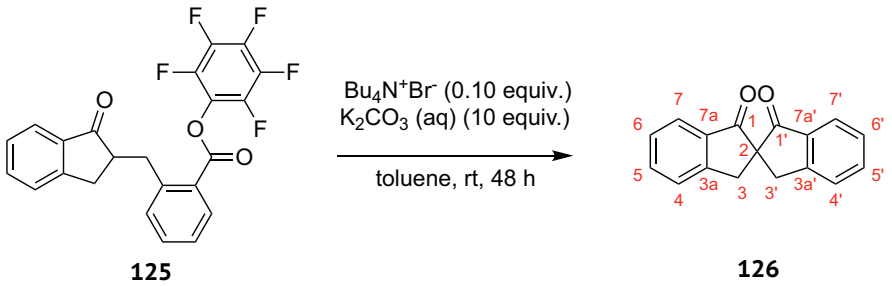



**Figure 7.2: HPLC chromatogram of isolated (+)-125.** The major enantiomer was obtained with 94% ee.

### 7.1.5 Racemic 2,2′-spirobi[indene]-1,1′(3*H*,3′*H*)-dione (126)




**125** **126**

Carried out by BFR. Substrate **125** (120 mg, 0.28 mmol, 1.0 equiv.) and $Bu_4N^+Br^-$ (8.9 mg, 0.028 mmol, 0.10 equiv.) were dissolved in toluene (3.2 mL) before the addition 50% $K_2CO_3$ (w/w) (0.40 mL, 0.29 mmol, 10 equiv.). The resulting mixture was stirred for 48 h at rt before the reaction mixture was quenched with water (5.0 mL). The aqueous layer was extracted with $CH_2Cl_2$ (3 × 5 mL). The combined organic fractions were dried ($MgSO_4$) and concentrated under reduced pressure. The crude product was purified by flash chromatography on silica gel eluting with 15% (v/v) ethyl acetate/petrol to give *the title compound* as a colourless solid (65 mg, 95% yield);

mp 170–172 °C;

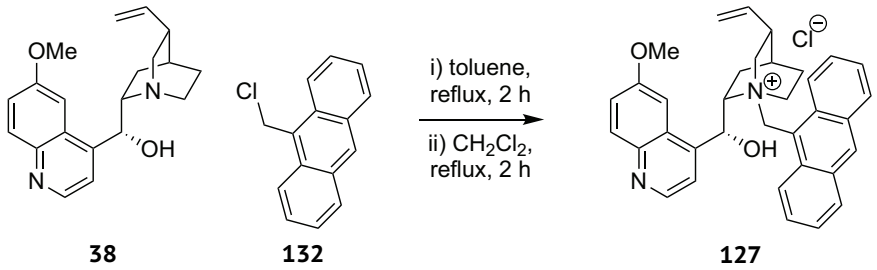
$\nu_{max}$ (neat) 2917, 1720, 1696, 1605, 1586, 1463, 1429, 1325, 1273, 1209, 1186, 1154, 1137, 1038, 1027;

$^1$H-NMR: $\delta$ (500 MHz; $CDCl_3$) 7.79 (dm, $J$ = 7.5 Hz, 2 H, *H7* and *H7′*), 7.68 (ddd, $J$ = 7.5, 7.5, 1.0 Hz, 2 H, *H5* and *H5′*), 7.59 (ddddd, $J$ = 7.5, 0.5, 0.5, 0.5, 0.5 Hz, 2 H, *H4* and *H4′*), 7.44 (ddm, $J$ = 7.5, 7,5 Hz, 2 H, *H6* and *H6′*), 3.76 (d, $J$ = 17.0 Hz, 2 H, *H3* and *H3′*), 3.22 (d, $J$ = 17.0 Hz, 2 H, *H3* and *H3′*);

$^{13}$C{$^1$H}-NMR: $\delta$ (126 MHz; $CDCl_3$) 202.7 (*C1* and *C1′*), 153.8 (*C3a* and *C3a′*), 135.5 (*C7a* and *C7a′*), 135.3 (*C5* and *C5′*), 127.8 (*C6* and *C6′*), 126.4 (*C4* and *C4′*), 124.9 (*C7* and *C7′*), 65.4 (*C2*), 38.1 (*C3* and *C3′*);

LRMS (ESI) 249 ([M+H]$^+$).

### 7.1.6 (1*S*,2*R*,4*S*,5*R*)-1-(Anthracen-9-ylmethyl)-2-((*R*)-hydroxy(6-methoxyquinolin-4-yl)methyl)-5-vinylquinuclidin-1-ium chloride (127)



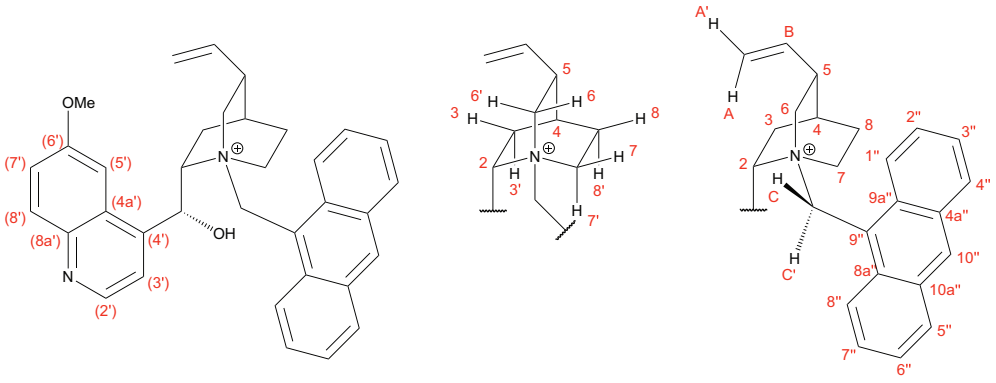

**38** **132** **127**

Carried out by BFR according to a literature procedure.[139] Quinine (14.0 g, 43.1 mmol, 1.00 equiv.) was suspended in toluene (280 mL). 9-(Chloromethyl)anthracene **132**[115] (9.98 g, 44.0 mmol, 1.02 equiv.) was added and the mixture was heated at reflux for 2.0 h. The mixture was cooled to rt, poured onto $Et_2O$ (700 mL), and the suspension filtered. The precipitate was washed with $Et_2O$ (140 mL) and dried *in vacuo*. The residue was collected in $CH_2Cl_2$ (700 mL) and the resulting suspension heated to reflux for 2.0 h. The mixture was cooled to −15 °C and $Et_2O$ (140 mL) was added at this temperature. The precipitate was isolated by filtration and dried *in vacuo* to give *the title compound* as a light yellow solid (8.2 g, 37%);

mp 148–150 °C;

$\nu_{max}$ (neat) 3088, 2363, 2210, 1751, 1622, 1509, 1473, 1450, 1431, 1363, 1259, 1240, 1227, 1031;

$[\alpha]_D^{25}$ −420.0 (*c* 0.80, $CHCl_3$);



$^{1}$H-NMR: $\delta$ (500 MHz; DMSO-$d_6$) 8.96 (s, 1 H, *H10″*), 8.92 (d, $J$ = 9.0 Hz, 1 H, *H1″*), 8.86 (d, $J$ = 4.5 Hz, 1 H, *H(2′)*), 8.83 (d, $J$ = 9.0 Hz, 1 H, *H8″*), 8.27–8.25 (m, 2 H, *H5″* and *H4″*), 8.05 (d, $J$ = 9.0 Hz, 1 H, *H(8′)*), 7.88 (d, $J$ = 4.5 Hz, 1 H, *H(3′)*), 7.79–7.71 (m, 2 H, *H2″* and *H7″*), 7.71 (d, $J$ = 2.5 Hz, 1 H, *H(5′)*), 7.67–7.62 (m, 2 H, *H6″* and *H3″*), 7.53–7.50 (m, 2 H, O*H* and *H(7′)*), 7.04–7.03 (m, 1 H, C*H*OH), 6.67 (d, $J$ = 14.5 Hz, 1 H, *HC′*), 5.71 (ddd, $J$ = 17.5, 10.5, 7.0 Hz, 1 H, *HB*), 5.66 (d, $J$ = 14.5 Hz, 1 H, *HC*), 4.97–4.94 (m, 1 H, *HA′*), 4.94–4.90 (m, 1 H, *HA*), 4.62–4.58 (m, 2 H, *H2* and *H7′*), 4.05 (s, 3 H, OC*H*$_3$), 3.84–3.79 (m, 1 H, *H6′*), 3.01–2.96 (m, 1 H, *H6*), 2.87–2.81 (m, 1 H, *H7*), 2.40–2.35 (m, 1 H, *H5*), 2.28–2.24 (m, 1 H, *H3′*), 2.19–2.12 (m, 1 H, *H8′*), 1.89–1.87 (m, 1 H, *H4*), 1.62–1.56 (m, 1 H, *H8*), 1.52–1.46 (m, 1 H, *H3*);

$^{13}$C{$^{1}$H}-NMR: $\delta$ (126 MHz; DMSO-$d_6$) 157.7 (*C(6′)*), 148.0 (*C(2′)*), 145.0 (*C(4′)*), 144.3 (*C(8a′)*), 138.4 (*CB*), 133.6 (*C8a″*), 133.4 (*C9a″*), 132.5 (*C10″*), 131.8 (*C(8′)*), 131.7 (*C4a″*), 131.5 (*C10a″*), 130.2 (*C5″*), 129.9 (*C4″*), 128.13 (*C7″* or *C2″*), 128.10 (*C7″* or *C2″*), 126.01 (*C(4a′)*), 125.98 (*C1″* or *C3″*), 125.95 (*C1″* or *C3″*), 125.9 (*C6″*), 125.1 (*C8″*), 122.3 (*C(7′)*), 121.0 (*C(3′)*), 119.5 (*C9″*), 117.1 (*CA*), 103.1 (*C(5′)*), 69.6 (*C2*), 64.3 (*C*HOH), 60.1 (*C6*), 56.5 (*CC*), 55.9 (*C*OCH$_3$), 52.3 (*C7*), 37.9 (*C5*), 25.9 (*C4*), 25.1 (*C8*), 21.1 (*C3*);

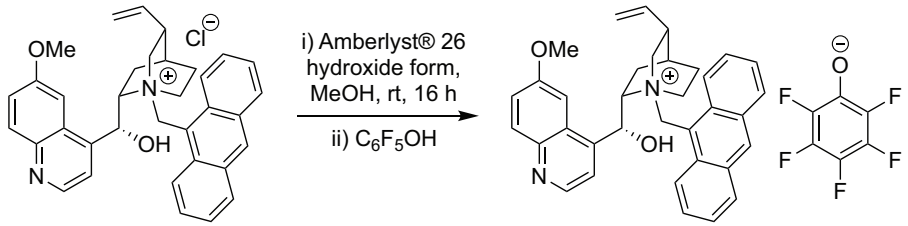
$^{1}$H-NMR: $\delta$ (500 MHz; CD$_3$OD) 8.89 (s, 1 H, *H10″*), 8.85 (d, $J$ = 4.5 Hz, 1 H, *H(2′)*), 8.69 (d, $J$ = 9.0 Hz, 1 H, *H1″*), 8.61 (d, $J$ = 9.0 Hz, 1 H, *H8″*), 8.28–8.23 (m, 2 H, *H5″* and *H4″*), 8.09 (d, $J$ = 9.0 Hz, 1 H, *H(8′)*), 8.03 (d, $J$ = 4.5 Hz, 1 H, *H(3′)*), 7.85–7.70 (m, 2 H, *H2″* and *H7″*), 7.73 (d, $J$ = 2.5 Hz, 1 H, *H(5′)*), 7.67–7.63 (m, 2 H, *H6″* and *H3″*), 7.58 (dd, $J$ = 9.0, 2.5 Hz, 1 H, *H(7′)*), 7.13–7.12 (m, 1 H, C*H*OH), 6.66 (d, $J$ = 14.0 Hz, 1 H, *HC′*), 5.80 (d, $J$ = 14.0 Hz, 1 H, *HC*), 5.77–5.70 (m, 1 H, *HB*), 5.01–5.01 (m, 1 H, *HA′*), 4.99–4.97 (m, 1 H, *HA*), 4.76–4.70 (m, 1 H, *H7′*), 4.44–4.40 (m, 1 H, *H2*), 4.11 (s, 3 H, OC*H*$_3$), 3.77–3.72 (m, 1 H, *H6′*), 3.23–3.18 (m, 1 H, *H6*), 3.00–2.94 (m, 1 H, *H7*), 2.46–2.40 (m, 2 H, *H5* and *H3′*), 2.31–2.45 (m, 1 H, *H8′*), 1.98–1.96 (m, 1 H, *H4*), 1.70–1.60 (m, 2 H, *H8* and *H3*);

$^{13}C\{^{1}H\}$-NMR: $\delta$ (126 MHz; $CD_3OD$) 160.1 (*C(6′)*), 148.3 (*C(2′)*), 146.3 (*C(4′)*), 144.9 (*C(8a′)*), 138.6 (*CB*), 134.6 (*C8a″* or *C9a″*), 134.6 (*C8a″* or *C9a″*), 133.9 (*C10″*), 133.1 (*C4a″*), 133.0 (*C10a″*), 131.9 (*C(8′)*), 131.3 (*C4″* or *C5″*), 131.1(*C4″* or *C5″*), 129.5 (*C2″* or *C7″*), 129.3 (*C2″* or *C7″*), 127.5 (*C(4a′)*), 126.6 (*C3″*), 126.6 (*C6″*), 125.2 (*C1″*), 124.8 (*C8″*), 123.4 (*C(7′)*), 121.8 (*C(3′)*), 119.0 (*C9″*), 117.7 (*CA*), 102.8 (*C(5′)*), 71.0 (*C2*), 66.7 (*C*HOH), 63.1 (*C6*), 57.6 (*CC*), 56.4 ($COCH_3$), 54.1 (*C7*), 39.7 (*C5*), 27.4 (*C4*), 26.3 (*C8*), 22.5 (*C3*);

LRMS (ESI) 515 ($[M-Cl]^+$).

Data in accordance with the literature.[139]

### 7.1.7 (1*S*,2*R*,4*S*,5*R*)-1-(Anthracen-9-ylmethyl)-2-((*R*)-hydroxy(6-methoxyquinolin-4-yl)methyl)-5-vinylquinuclidin-1-ium 2,3,4,5,6-pentafluorophenolate (136)



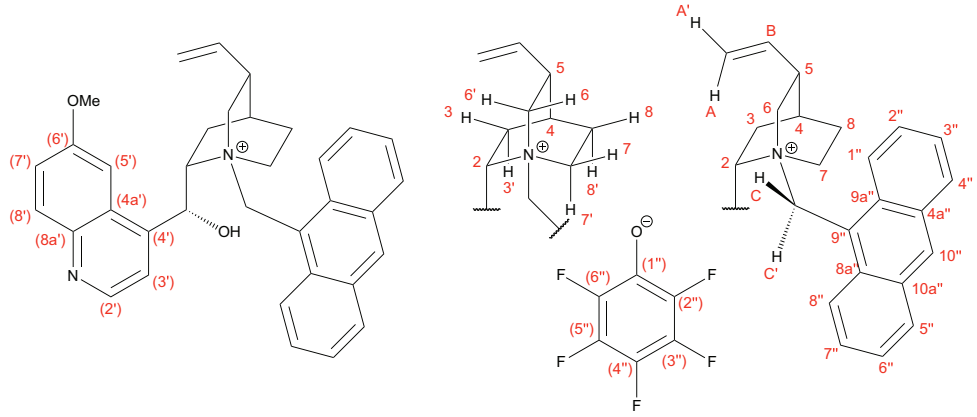

**127** **136**

Modified literature procedure.[80] Compound **127** (0.30 g, 0.55 mmol, 1.0 equiv.) was dissolved in anhydrous methanol (6.0 mL) before Amberlyst®26 (hydroxide form) (1.5 g) was added. The mixture was stirred at rt for 16 h before the resin was removed by vacuum filtration. Pentafluorophenol (0.15 g, 0.84 mmol, 1.5 equiv.) was added to the filtrate. The solution was azeotroped with benzene three times. The resulting solid was dissolved in $Et_2O$ (∼5 mL). Pentane (∼3 mL) was added. The resulting precipitate was isolated by vacuum filtration and dried *in vacuo* to give *the title compound* as a pale yellow solid (0.23 g, 61%);

mp 124–127 °C;

$\nu_{max}$ (neat) 2953, 1496, 1003, 982, 744;

$[\alpha]_D^{25}$ −361 (*c* 0.86, $CHCl_3$);




$^1$H-NMR: $\delta$ (700 MHz; $CD_3OD$) 8.90–8.90 (m, 1 H, *H10″*), 8.85 (d, $J$ = 4.5 Hz, 1 H, *H(2′)*), 8.64 (dm, $J$ = 9.0 Hz, 1 H, *H1″*), 8.58 (dm, $J$ = 9.0 Hz, 1 H, *H8″*), 8.27–8.25 (m, 2 H, *H4″* and *H5″*), 8.10 (d, $J$ = 9.0 Hz, 1 H, *H(8′)*), 8.03 (dd, $J$ = 4.5, 1.0 Hz, 1 H, *H(3′)*), 7.83–7.79 (m, 2 H, *H2″* and *H7″*), 7.70 (d, $J$ = 2.5 Hz, 1 H, *H(5′)*), 7.67–7.64 (m, 2 H, *H3″* and *H6″*), 7.60 (dd, $J$ = 9.0, 2.5 Hz, 1 H, *H(7′)*), 7.10–7.09 (m, 1 H, C*H*OH), 6.63 (d, $J$ = 14.0 Hz, 1 H, *HC′*), 5.79 (d, $J$ = 14.0 Hz, 1 H, *HC*), 5.73 (ddd, $J$ = 17.0, 10.5, 7.5 Hz, 1 H, *HB*), 5.01 (ddd, $J$ = 10.5, 1.0, 1.0 Hz, 1 H, *HA′*), 5.00 (ddd, $J$ = 17.0, 1.0, 1.0 Hz, 1 H, *HA*), 4.74 (dddd, 11.5, 11.5, 3.0, 3.0 Hz, 1 H, *H7′*), 4.39–4.36 (m, 1 H, *H2*), 4.12 (s, 3 H, COC*H*$_3$), 3.71 (ddd, $J$ = 12.5, 6.0, 3.0 Hz, 1 H, *H6′*), 3.22 (dd, $J$ = 12.5, 11.0 Hz, 1 H, *H6*), 2.98 (dddd, $J$ = 11.5, 11.5, 6.0, 1.5 Hz, 1 H, *H7*), 2.46–2.41 (m, 2 H, *H5* and *H3′*), 2.30–2.25 (m, 1 H, *H8′*), 1.99–1.96 (m, 1 H, *H4*), 1.69–1.64 (m, 1 H, *H8*), 1.64–1.59 (m, 1 H, *H3*);

$^{19}$F-NMR: $\delta$ (471 MHz; $CD_3OD$) −168.3 (m, 2 F, *F(2″)* and *F(6″)*), −171.3 (m, 2 F, *F(3″)* and *F(5″)*), −183.3 (m, 1 F, *F(4″)*);

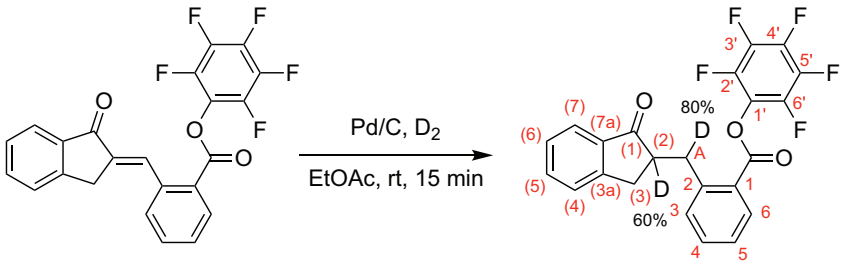
$^{13}$C{$^1$H,$^{19}$F}-NMR: $\delta$ (126 MHz; $CD_3OD$) 158.7 (*C(6′)*), 146.9 (*C(2′)*), 144.8 (*C(4′)*), 143.4 (*C(8a′)*), 140.0 (*C(2″)* and *C(6″)*), 139.7 (*C(1″)*), 138.1 (*C(3″)* and *C(5″)*), 137.2 (*CB*), 133.22 (*C8a″* or *C9a″*), 133.19 (*C8a″* or *C9a″*), 132.5 (*C10″*), 131.7 (*C4a″*), 131.6 (*C10a″*), 130.7 (*C(4″)*), 130.6 (*C(8′)*), 130.0 (*C5″*), 129.7 (*C4″*), 128.2 (*C2″* or *C7″*), 127.9 (*C2″* or *C7″*), 126.1 (*C(4a′)*), 125.24 (*C3″*), 125.18 (*C6″*), 123.6 (*C1″*), 123.3 (*C8″*), 121.9 (*C(7′)*), 120.3

(*C(3′)*), 117.5 (*C9″*), 116.2 (*CA*), 101.3 (*C(5′)*), 69.6 (*C2*), 65.3 (*C*HOH), 61.8 (*C6*), 56.1 (*CC*), 54.9 (*C*$H_3$), 52.7 (*C7*), 38.3 (*C5*), 26.0 (*C4*), 24.9 (*C8*), 21.1 (*C3*);

HRMS (ESI) 515.26936 ([M−$C_6F_5O$]$^+$), calcd. for $C_{35}H_{35}O_2N_2^+$ 515.26930;

HRMS (ESI) 182.98728 ([M−$C_{35}H_{35}N_2O_2$]$^-$), calcd. for $C_6F_5O^-$ 182.98748.

### 7.1.8 Perfluorophenyl 2-((1-oxo-2,3-dihydro-1*H*-inden-2-yl-2-*d*)methyl-*d*)benzoate (144)




**131** **144**

Carried out by AM according to a modified procedure under anhydrous conditions.[114,115] A stirred suspension of **131** (0.590 g, 1.37 mmol, 1.00 equiv.) and 10% Pd/C (59 mg, 10 wt%) in ethyl acetate (70 mL) was sparged with $D_2$ (1 balloon). After 15 min, the flask was evacuated and refilled with $D_2$ (balloon pressure). The reaction was monitored by TLC (approx. 15 min). *Note: prolonged reaction times could lead to the undesired, over-reduced product.* The reaction mixture was filtered through Celite® eluting with $CH_2Cl_2$. The filtrate was concentrated *in vacuo* and purified by flash chromatography on silica gel eluting with 10% (v/v) ethyl acetate/petrol to give *the title compound* as a white solid (0.44 g, 74%);

mp 87–89 °C;

$\nu_{max}$ (neat) 2160, 2025, 1978, 1757, 1702, 1518, 1486, 1475, 1465, 1447, 1436, 1320, 1295, 1262, 1234, 1029, 1000, 794, 726, 708, 622;

$^1$H-NMR: $\delta$ (500 MHz; $CDCl_3$) 8.23 (dd, $J$ = 8.0, 1.5 Hz, 1.0 H, *H6*), 7.78 (d, $J$ = 7.5 Hz, 1.0 H, *H(7)*), 7.65–7.62 (m, 1.0 H, *H4*), 7.59 (ddd, $J$ = 7.5, 7.5, 1.0 Hz, 1.0 H, *H(5)*), 7.49

(dm, $J$ = 8.0 Hz, 1.0 H, *H3*), 7.47–7.42 (m, 2.0 H, *H5* and *H(4)*), 7.38 (ddm, $J$ = 7.5, 7.5 Hz, 1.0 H, *H(6)*), 3.82–3.76 (m, 0.54 H, *HA*), 3.25–3.06 (m, 2.1 H, *H(3)*, *HA* and *H(2)*), 2.94–2.89 (m, 1.0 H, *H(3)*);

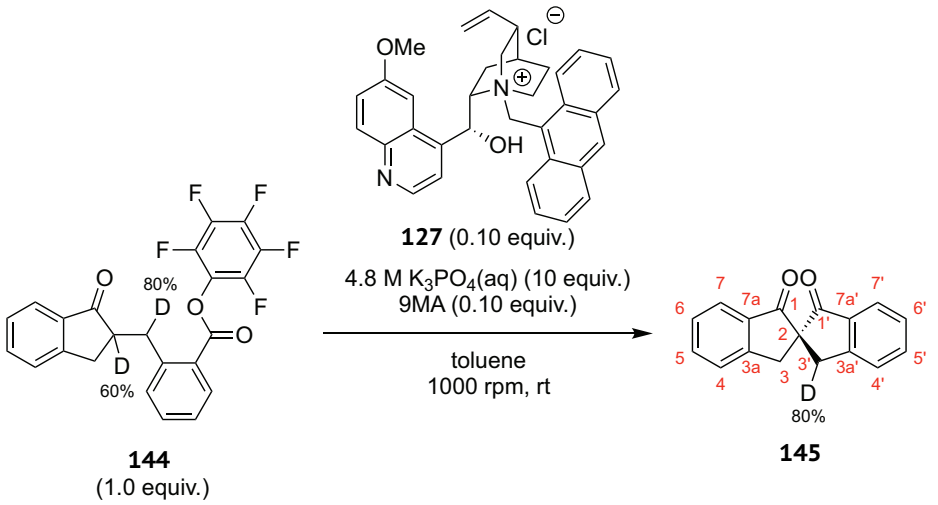
$^{19}$F-NMR: $\delta$ (471 MHz; $CDCl_3$) −152.4 (m, 2 F, *F2′* and *F6′*), −158.0 (m, 1 F, *F4′*), −162.3 (m, 2 F, *F3′* and *F5′*);

$^{13}C\{^1H\}$-NMR: $\delta$ (126 MHz; $CDCl_3$) 207.2, 207.2, 207.2, 162.9, 153.3, 153.3, 143.8, 143.8, 143.7, 142.5, 142.4, 142.4, 142.4, 142.3, 140.5, 140.5, 140.4, 140.4, 140.4, 140.3, 139.1, 139.1, 139.1, 139.0, 139.0, 139.0, 138.9, 138.9, 138.9, 138.9, 138.8, 138.6, 138.6, 138.5, 138.4, 137.1, 137.0, 136.9, 136.8, 136.4, 136.4, 134.8, 134.0, 132.2, 132.2, 132.1, 127.5, 127.0, 126.5, 126.5, 126.1, 125.4, 125.3, 125.3, 125.2, 124.0, 48.5, 48.4, 48.4, 48.4, 48.2, 48.1, 48.0, 47.8, 35.1, 35.0, 34.9, 34.7, 34.6, 32.3, 32.3, 32.3, 32.2 (due to the complexity of the acquired spectrum, all peaks have been reported and are unassigned);

$^1$H-NMR: $\delta$ (500 MHz; toluene-$d_8$) 8.05 (dd, $J$ = 8.0, 1.0 Hz, 1.0 H, *H6*), 7.68 (d, $J$ = 8.0 Hz, 1.0 H, *H(7)*), 3.77–3.72 (m, 0.55 H, *HA*), 2.93–2.89 (m, 0.58 H, *HA*), 2.78–2.73 (m, 0.40 H, *H(2)*), 2.64–2.62 (m, 1.0 H, *H(3)*), 2.51–2.46 (m, 1.0 H, *H(3)*) (due to obscuration of the signals corresponding to the *H4*, *H(5)*, *H3* and *H5*, *H(4)*, and *H(6)* environments by residual toluene, these chemical shifts have been omitted);

HRMS (ESI) 435.09744 ($[M+H]^+$), calcd. for $C_{23}H_{12}D_2F_5O_3^+$ 435.09832.

### 7.1.9 2,2′-Spirobi[indene]-1,1′(3*H*,3′*H*)-dione-3-*d* (145)




Isolation of *the title compound* as an analytical sample was carried out by AM following execution of the protocol described in 7.19. The reaction was carried out without sampling, and with a reaction time of 48 h. The reaction mixture was quenched with water (5.0 mL). The aqueous layer was extracted with $CH_2Cl_2$ (3 × 5 mL). The combined organic fractions were dried ($MgSO_4$) and concentrated under reduced pressure. The crude product was purified by flash chromatography on silica gel (15% ethyl acetate/petrol) to give *the title compound* in a 1:1 mixture of diastereomers as a colourless solid (35 mg, 95%);

mp 185–195 °C;

$\nu_{max}$ (neat) 2922, 2852, 2361, 2341, 2197, 1718, 1692, 1637, 1604, 1586, 1473, 1461, 1266, 1208, 1027, 933, 784, 764, 746, 671;

$^1$H-NMR: $\delta$ (500 MHz; $CDCl_3$) 7.79 (dm, $J$ = 7.5 Hz, 2.0 H, *H7* and *H7′*), 7.68 (ddd, $J$ = 7.5, 7.5, 1.5 Hz, 2.0 H, *H5* and *H5′*), 7.59 (dm, $J$ = 7.5 Hz, 2.0 H, *H4* and *H4′*), 7.44 (ddm, $J$ = 7.5, 7.5 Hz, 2.0 H, *H6* and *H6′*), 3.75 (d, $J$ = 17.0 Hz, 1.6 H, *H3* and *H3′*), 3.22 (d, $J$ = 17.0 Hz, 1.6 H, *H3* and *H3′*);

$^{13}$C{$^1$H}-NMR: $\delta$ (126 MHz; $CDCl_3$) 202.8, 202.7, 153.9, 153.9, 153.8, 135.5, 135.5, 135.5, 135.5, 135.3, 127.8, 127.8, 127.8, 126.4, 126.4, 126.4, 124.9, 65.4, 65.3, 65.3, 38.1, 38.1, 38.0,

38.0, 37.9, 37.8, 37.8, 37.6, 37.6, 29.7 (due to the complexity of the acquired spectrum, all peaks have been reported and are unassigned);

HRMS (ESI) 250.09714 ([M+H]$^+$), calcd. for $C_{17}H_{12}DO_2^+$ 250.09728.

## 7.2 Determination of p$K_a$ values

### 7.2.1 General information

All of the work in this section was carried out by AM. In summary, the p$K_a$ values of selected compounds were determined in deuterated DMSO using NMR spectroscopy and titration with a base with known p$K_a$. Titrations were carried out under an inert atmosphere.

### 7.2.2 General equations

The relationship between the protonated compound of interest, e.g. HA, and the base ($B^-$) is given by equation 7.1.

$$[HA] + [B^-] \overset{K}{\rightleftharpoons} [A^-] + [HB] \tag{7.1}$$

Where $K$ is given by:

$$\begin{aligned} K &= \frac{[A^-][HB]}{[HA][B^-]} \\ &= \frac{[A^-]^2}{[HA]^2} \\ &= \frac{[HB]^2}{[B^-]^2} \end{aligned} \tag{7.2}$$

Subsequently using the relationships described by equations 7.3 to 7.6, $K$ may be described by equation 7.7.

$$\mathrm{HA} \overset{K_{\mathrm{HA}}}{\rightleftharpoons} \mathrm{H^+} + \mathrm{A^-} \tag{7.3}$$

$$K_{\mathrm{HA}} = \frac{[\mathrm{H^+}][\mathrm{A^-}]}{[\mathrm{HA}]} \tag{7.4}$$

$$\mathrm{B^-} + \mathrm{H^+} \overset{K_{\mathrm{B}}}{\rightleftharpoons} \mathrm{HB} \tag{7.5}$$

$$K_{\mathrm{B}} = \frac{[\mathrm{HB}]}{[\mathrm{B^-}][\mathrm{H^+}]} \tag{7.6}$$

$$\begin{aligned} K &= K_{\mathrm{HA}} \times K_{\mathrm{B}} \\ &= \frac{K_{\mathrm{HA}}}{K_{\mathrm{HB}}} \end{aligned} \tag{7.7}$$

If proton exchange is fast by NMR spectroscopy, the observed chemical shift ($\delta_{\mathrm{obs}}$) is the weighted average of the protonated and free base forms. This may be represented by equation 7.8, where $c_1$ and $c_2$ correspond to the mole fractions of the free base and protonated forms, respectively, and $\delta_1$ and $\delta_2$ are their corresponding chemical shifts. All chemical shift values are in ppm.

$$\delta_{\mathrm{obs}} = c_1\delta_1 + c_2\delta_2 \tag{7.8}$$

Because:

$$c_2 = 1 - c_1 \tag{7.9}$$

Equation 7.8 may be rewritten to give equation 7.10:

$$\delta_{\text{obs}} = c_1\delta_1 + (1 - c_1)\delta_2 \tag{7.10}$$

The mole fractions for the free base (equation 7.11) and protonated (equation 7.12) forms can thus be calculated and are proportional to [$A^-$] and [HA], respectively.

$$c_1 = \frac{\delta_{\text{obs}} - \delta_2}{\delta_1 - \delta_2} \tag{7.11}$$

$$c_2 = 1 - \frac{\delta_{\text{obs}} - \delta_2}{\delta_1 - \delta_2} \tag{7.12}$$

Using the results obtained from equation 7.2, $K$ may now be given by equation 7.13.

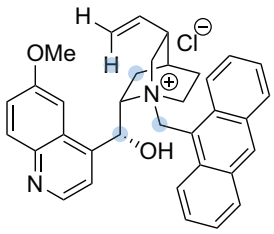
$$K = \frac{{c_2}^2}{{c_1}^2} \tag{7.13}$$

By rearranging 7.7, using the known p$K_a$ value of the base ($-\log K_{\text{HB}}$), and equation 7.13, the p$K_a$ of the HA species may be determined (equation 7.14).

$$\begin{aligned} K_{\text{HA}} &= K_{\text{HB}} \times K \\ -\log K_{\text{HA}} &= -\log K_{\text{HB}} - \log K \\ \text{p}K_a &= -\log K_{\text{HB}} - \log\left(\frac{{c_2}^2}{{c_1}^2}\right) \end{aligned} \tag{7.14}$$

### 7.2.3 Estimation of p$K_a$ values in DMSO

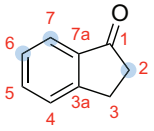
**(1*S*,2*R*,4*S*,5*R*)-1-(Anthracen-9-ylmethyl)-2-((*R*)-hydroxy(6-methoxyquinolin-4-yl) methyl)-5-vinylquinuclidin-1-ium chloride (127)**




p$K_a$ (DMSO)
16.33 ± 0.43

Titration of ammonium halide **127** was carried out with sodium phenoxide (protonated p$K_a$ of 18.0 in DMSO).[117] Analysis was carried out using $^1$H-NMR spectroscopy. The chemical shifts corresponding to the *HA*, C*H*OH, *HC*, *HC′*, *H3*, and *H3′* environments were evaluated (see 7.1.6, and highlighted in blue in the figure above). The experiment was repeated a total of two times. The calculated p$K_a$ value of 16.33 ± 0.43 was obtained.

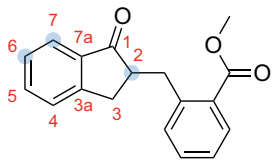
**2,3-Dihydro-1*H*-inden-1-one (128)**




p$K_a$ (DMSO)
22.78 ± 0.51

Titration of 2,3-dihydro-1*H*-inden-1-one (1-indanone) **128** was carried out with dimsyl sodium (protonated p$K_a$ of 35.1 in DMSO).[118] Analysis was carried out using $^{13}$C{$^1$H}-NMR spectroscopy. The chemical shifts corresponding to the *C2*, *C6*, and *C7* environments were evaluated (highlighted in blue in the figure above). The experiment was repeated a total of two times. The calculated p$K_a$ value of 23.78 ± 0.51 was obtained, which was in accordance with the literature.[117]

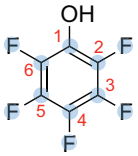
**Methyl 2-((1-oxo-2,3-dihydro-1*H*-inden-2-yl)methyl)benzoate (137)**




p$K_a$ (DMSO)
21.94± 0.84

Titration of methyl ester **137**[115] was carried out with dimsyl sodium (protonated p$K_a$ of 35.1 in DMSO).[118] Analysis was carried out using $^{13}C\{^1H\}$-NMR spectroscopy. The chemical shifts corresponding to the *C2*, *C6*, and *C7* environments were evaluated (highlighted in blue in the figure above). The experiment was repeated a total of two times. The calculated p$K_a$ value of 21.94 ± 0.84 was obtained.

**2,3,4,5,6-Pentafluorophenol**




p$K_a$ (DMSO)
7.54 ± 0.14

Titration of 2,3,4,5,6-pentafluorophenol was carried out with triethylamine (protonated p$K_a$ 9.0 in DMSO).[140] Analyses were carried out using $^{13}C\{^1H\}$-NMR and $^{19}F$-NMR spectroscopy. The chemical shifts corresponding to the *C1*, *C2* and *C6*, *C3* and *C5*, *C4*, *F2* and *F6*, *F3* and *F5*, and *F4* environments were evaluated (highlighted in blue in the figure above). The experiment was repeated a total of two times. The calculated p$K_a$ value of 7.54 ± 0.14 was obtained.

## 7.3 Quantitative HPLC assay

### 7.3.1 General sample preparations

Solutions of the internal standard 9-methylanthracene **133** (9MA), solvent toluene, racemic substrate **125** and racemic product **126** were diluted with 50 %(v/v) 2-propanol/hexane then analysed using HPLC. An example chromatogram is shown below in Figure 7.3; the absolute configuration of **126** was known from previous work.[114] Three standard curves were constructed for the enantiomers of **125** and **126** using 9-methylanthracene (9MA) **133** as the internal standard, and in the presence of toluene.

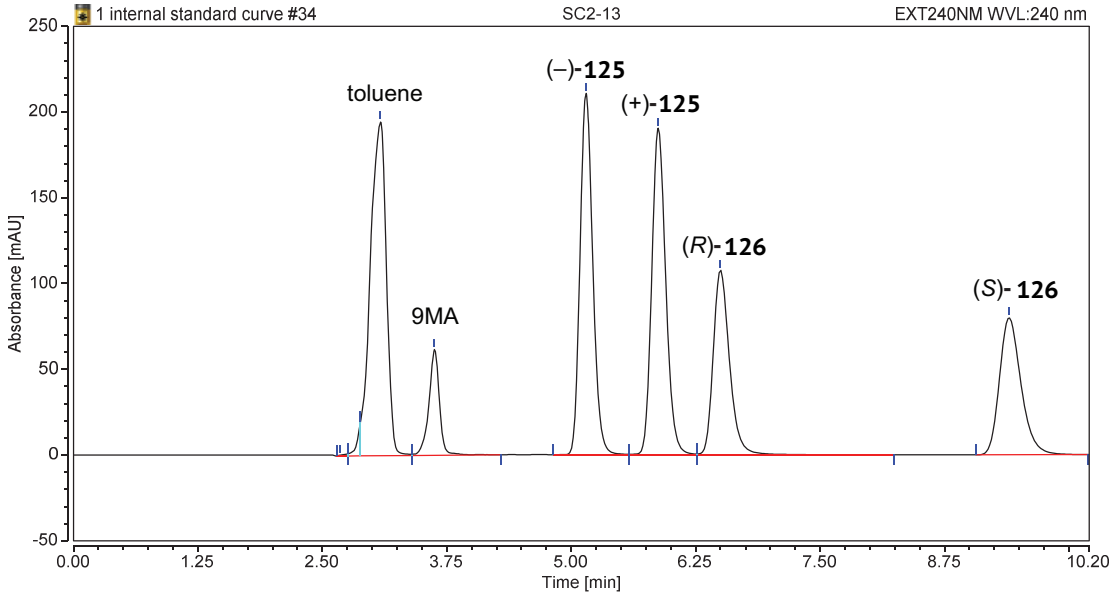



**Figure 7.3: Example HPLC-UV chromatogram of one sample.** The data are extracted at 240 nm. The $x$-axis represents retention time; the $y$-axis is UV absorption at the extracted wavelength. In this sample, the analytes eluted in the following order with their retention times in brackets: 9MA (3.63 min); (−)-**125** (5.15 min); (+)-**125** (5.87 min); (*R*)-**126** (6.50 min); and (*S*)-**126** (9.40 min).

The amounts of **125** and **126** measured against **133** were evaluated at concentrations in range of the amounts that would be sampled under real reaction conditions. These different concentrations were made up with an emphasis on high substrate concentrations against low product concentrations for initial rate kinetic analyses. Each standard curve was constructed by comparing the mole ratio of the analyte against the corresponding signal integrals. Each curve consisted initially of 21 samples. Linear regression analyses were carried out on the plots.

Points outside 1.5 $\sigma$ were removed and the curves were re-fit. The slopes of each analyte were obtained from their corresponding curve to give the calibration factor (m).

Three standard curves were constructed for all four compounds: (−)-**125**, (+)-**125**, (*R*)-**126**, and (*S*)-**126**. All curves used a common stock solution of 9MA **133** that was prepared as follows: **133** (248.4 mg, 1.292 mmol) was dissolved in 2-propanol in a 500 mL volumetric flask to give a standard solution of 2.584 mM. All samples contained 3.80 µL of the 9MA **133** standard stock solution.

The composition of each sample was calculated such that the final solvent volume was 1.603 mL, consisting of 1.600 mL 50% (v/v) solution of 2-propanol/hexane in addition to 3.00 uL of toluene. Stock solutions of **125** and **126** were made up in 2-propanol, and amounts were added across the conversion of substrate to product that would occur under reaction conditions. Additional 2-propanol was added to give a 2-propanol volume of 0.800 mL. Hexane (0.800 mL) and toluene (3.00 µL) were added to each sample.

### 7.3.2 Preparation and HPLC analysis of internal standard curve samples

#### Internal standard curve 1 (ISC1) sample preparation

A stock solution of **125** (15.2 mg, 0.0352 mmol) was made up with 2-propanol in a 100 mL volumetric flask to give a concentration of 0.352 mM; amounts added to sample vials were in the range of 465 µL–0 µL. A stock solution of **126** (19.1 mg, 0.0769 mmol) was made up with 2-propanol in a 100 mL volumetric flask to give a concentration of 0.769 mM; amounts added to sample vials were in the range of 0 µL–213 µL. A total of 21 samples were prepared.

#### Internal standard curve 2 (ISC2) sample preparation

A stock solution of **125** (12.9 mg, 0.0298 mmol) was made up with 2-propanol in a 100 mL volumetric flask to give a concentration of 0.298 mM; amounts added to sample vials were in

the range of 548 µL–0 µL. A stock solution of **126** (19.3 mg, 0.0777 mmol) was made up with 2-propanol in a 100 mL volumetric flask to give a concentration of 0.777 mM; amounts added to sample vials were in the range of 0 µL–211 µL. A total of 21 samples were prepared.

**Internal standard curve 3 (ISC3) sample preparation**

A stock solution of **125** (13.6 mg, 0.0315 mmol) was made up with 2-propanol in a 100 mL volumetric flask to give a concentration of 0.315 mM; amounts added to sample vials were in the range of 520 µL–0 µL. A stock solution of **126** (18.2 mg, 0.0733 mmol) was made up with 2-propanol in a 100 mL volumetric flask to give a concentration of 0.733 mM; amounts added to sample vials were in the range of 0 µL–223 µL. A total of 21 samples were prepared.

All samples were analysed by HPLC-UV at 200–400 nm (ChiralPak® IA, 1.100 mL $min^{-1}$, 30% (v/v) 2-propanol/hexane, 25 °C).

### 7.3.3 Overlay of the standard curve triplicates

The HPLC and stock volume data (as .csv files) were processed using the following R scripts, which bulk-generated the compound values integral ratios and mole ratios for plotting:

```
project <- "spirok"
"~/functions/global/compound-properties.R"
volume <- 1.603
"~/functions/sc/sc-format.R"
"~/functions/sc/sc-process.R"
"~/functions/sc/sc-export-crd.R"
```

The input files required to execute the above scripts were saved in the following locations:

```
"~/data/input/sc/spirok/"
"~/data/raw/sc/spirok/hplc/
```

The exported data were obtained in the following location:

```
"~/data/processed/sc/spirok/"
```

Using the exported data, the following plots were constructed:

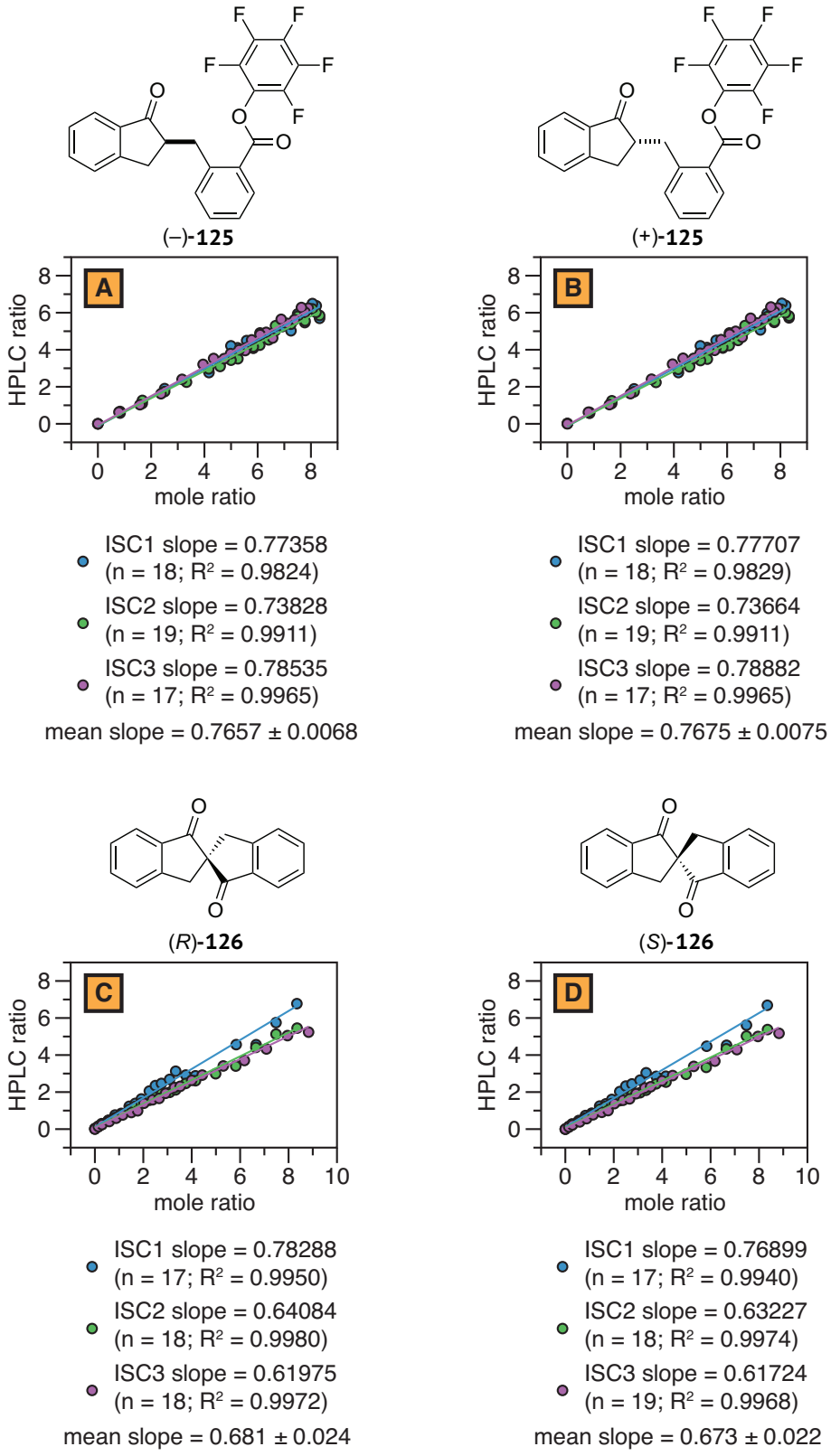



**Figure 7.4: Standard curves for the analytes: A) (−)-125; B) (+)-125; C) (*R*)-126; and D) (*S*)-126.** The curves were constructed by plotting the mole ratio of the analytes to the standard 9MA **133** against the ratios of their corresponding HPLC signal integrals to the HPLC signal integral of 9MA **133**. Outliers beyond $1.5\,\sigma$ were removed and linear regression analyses were carried out on the plots. The mean slopes were calculated to give the calibration factors for assaying each analyte.

### 7.3.4 General standard curve application

The aliquots sampled from reaction mixtures (see 7.4.3) were analysed by HPLC (injection volume 50 µL; ChiralPak® IA, 1.100 mL $min^{-1}$, 30% (v/v) 2-propanol/hexane, 25 °C) and the signal integrals of the standard 9MA **133** (retention time 3.6 min at 240 nm), the substrates (−)-**125** (retention time 5.2 min, at 240 nm and 292 nm) and (+)-**125** (retention time 5.9 min, at 240 nm and 292 nm), and the products (*R*)-**126** (retention time 6.5 min, at 240 nm and 292 nm) and (*S*)-**126** (retention time 9.4 min, at 240 nm and 292 nm) were obtained.

The HPLC data were saved as .csv files and processed using the relevant R scripts (see 7.4.4). In summary, the scripts calculated the amount (mmol) of each component in the reaction mixture at that point in time, in addition to the concentration of the material in the reaction mixture. The general equations that were used to carry out the calculations are described below. The calibration factors for each analyte were obtained from the standard curves (in Figure 7.4).

Substrate (−)-**125**:

$$\text{mol}_a = \frac{\text{int-}a_{240} \times \text{mol-}s}{0.7657 \times \text{int-}s_{240}} \tag{7.15}$$

Where $\text{mol}_a$ is the amount of (−)-**125** in mmol in the reaction mixture, int-$a_{240}$ is the HPLC signal integral of (−)-**125** at 240 nm, mol-$s$ is the amount of standard **133** present in the reaction mixture in mmol, 0.7657 is the calibration factor for (−)-**125**, and int-$s_{240}$ is the HPLC signal integral of standard **133** at 240 nm.

Substrate (+)-**125**:

$$\text{mol}_b = \frac{\text{int-}b_{292} \times \text{int-}a_{240} \times \text{mol-}s}{0.7675 \times \text{int-}a_{292} \times \text{int-}s_{240}} \tag{7.16}$$

Where $\text{mol}_b$ is the amount of (+)-**125** in mmol in the reaction mixture, int-$b_{292}$ is the HPLC signal integral of (+)-**125** at 292 nm, int-$a_{240}$ is the HPLC signal integral of (−)-**125** at 240 nm, mol-$s$ is the amount of standard **133** present in the reaction mixture in mmol, 0.7675 is the calibration factor for (+)-**125**, int-$a_{292}$ is the HPLC signal integral of (−)-**125** at 292 nm, and int-$s_{240}$ is the HPLC signal integral of standard **133** at 240 nm.

Product (*R*)-**126**:

$$\text{mol}_c = \frac{\text{int-}c_{292} \times \text{int-}d_{240} \times \text{mol-}s}{0.681 \times \text{int-}d_{292} \times \text{int-}s_{240}} \tag{7.17}$$

Where $\text{mol}_c$ is the amount of (*R*)-**126** in mmol in the reaction mixture, int-$c_{292}$ is the HPLC signal integral of (*R*)-**126** at 292 nm, int-$d_{240}$ is the HPLC signal integral of (*S*)-**126** at 240 nm, mol-$s$ is the amount of standard **133** present in the reaction mixture in mmol, 0.681 is the calibration factor for (*R*)-**126**, int-$d_{292}$ is the HPLC signal integral of (*S*)-**126** at 292 nm, and int-$s_{240}$ is the HPLC signal integral of standard **133** at 240 nm.

Product (*S*)-**126**:

$$\text{mol}_d = \frac{\text{int-}d_{240} \times \text{mol-}s}{0.673 \times \text{int-}s_{240}} \tag{7.18}$$

Where $\text{mol}_d$ is the amount of (*S*)-**126** in mmol in the reaction mixture, int-$d_{240}$ is the HPLC signal integral of (*S*)-**126** at 240 nm, mol-$s$ is the amount of standard **133** present in the reaction mixture in mmol, 0.673 is the calibration factor for (*S*)-**126**, and int-$s_{240}$ is the HPLC signal integral of standard **133** at 240 nm.

In summary, the script calculates the ratio of (+)-**125** to (−)-**125** at 292 nm, and multiplies the result by the signal integral of (−)-**125** at 240 nm to extrapolate the integral of (+)-**125** at 240 nm. Similarly, the ratio of (*S*)-**126** to (*R*)-**126** at 292 nm is multiplied by the signal integral of (*S*)-**126** at 240 nm to obtain the extrapolated integral of (*R*)-**126** at 240 nm.

Concentration values for each component were calculated using the mmol data ($mol_a$, $mol_b$, $mol_c$ and $mol_d$) and the known total volume of the reaction mixture. Corrections were made considering the amount of solvent removed via sample aliquots.

## 7.4 Reaction protocols

We used strict protocols to set up and carry out reactions, and to sample reaction mixtures over time for HPLC analyses. The types of protocols and the general method for data analysis will be described below.

### 7.4.1 Standard reaction protocol

Unless otherwise stated, the standard reaction protocol was carried out as follows: *the appropriate amount of catalyst* was added to the reaction vial before a stirrer bar was added. The reaction vials were set in the custom moulds before toluene (560 µL) was added and the mixture stirred at 200 rpm. *The appropriate amount of* $K_3PO_4$ was added and the stirring adjusted to 1000 rpm. The vial was stirred for 5 min before being treated in an ultrasound bath for 3 s. The vial was stirred for a further 10 min before treating in an ultrasound bath for 3 s. The vial was stirred for a further 10 min (25 min total) before treating in an ultrasound bath for 3 s. The vial was stirred for a further 4 min (total of 29 min) before the stirring speed was adjusted to *the appropriate value*. At precisely 30 min, the **substrate solution** (900 µL) was added to initiate the reaction at the designated time zero.

The **substrate solution** was prepared as follows: *the appropriate amount of substrate* ***125*** and *the appropriate amount of standard* ***133*** were dissolved in a volumetric flask *of appropriate volume* and made up with toluene. For single reactions, the *appropriate volume* was 1.0 mL. For duplicate reactions, the *appropriate volume* was 2.0 mL. For triplicate reactions, the *appropriate volume* was 3.0 mL. The same substrate solution was used for each set (e.g. single, duplicate,

or triplicate sets).

For reactions run in duplicate, or triplicate, the procedures were carried out with a 2.0 min stagger.

### 7.4.2 Modified reaction protocol

Unless otherwise stated, the modified reaction protocol was carried out as follows: *the appropriate amount of catalyst* was added to the reaction vial before a stirrer bar was added. The reaction vials were set in the custom moulds before toluene (560 µL) was added. The vial was treated in an ultrasound bath for 5 s. The mixture stirred at 200 rpm before the **substrate solution** (900 µL) was added. The mixture was stirred at 1000 rpm for *the appropriate time* before *the appropriate amount of* $K_3PO_4$ was added to initiate the reaction at the designated time zero.

The **substrate solutions** were prepared analogously to those prepared in the standard reaction protocol.

### 7.4.3 Sampling protocol

Unless otherwise stated, the reactions were monitored by sampling and analysis as follows: the reaction vial caps were removed 5 s prior to extracting an aliquot. Aliquots (2.00 µL) were sampled directly from the reaction mixtures at the designated times (following initiation of the reaction), without ceasing stirring or disturbing the stirrer bar. The reaction vessels were immediately resealed. The aliquots were immediately quenched by passing through a small plug of silica ($\varnothing$ = 6 mm, $l$ = 3–5 mm), eluting with 50% (v/v) 2-propanol/hexane (∼1.6 mL by syringe) under a stream of nitrogen. The silica plug was dried with a stream of nitrogen prior to elution of the next sample. The aliquots were analysed by HPLC (50 µL; ChiralPak®IA, 1.100 mL $min^{-1}$, 30% (v/v) 2-propanol/hexane, 25 °C) and the reaction mixture components

quantified using the standard curves via processing using R and the appropriate scripts (see 7.3.4 and 7.4.4).

### 7.4.4 Data processing and analysis

Post-reaction data processing was carried out using a series of R scripts. For full expansions of the R scripts see Chapter 8. This approach enabled the rapid, consistent, repetitive processing of data. Each set of reactions was given a designated code (*rxn.code*). The reaction data were first saved as specific files in the corresponding *rxn.code* input folder. For example, one input file—user-input3.R—for the experiment designated "spirok-9" is described below:

```
#Reaction code spirok-9

which_protocol <- 1
#0 = n/a, 1 = srp, 2 = mrp, 3 = misc

which_rep <- 3

base_added <- 305
#in uL

base_conc <- 4.77
#in M

catalyst_added <- 12.1
#in mg

catalyst_MW <- 551.13
#in g/mol

catalyst_code <- "QN-Anth"

limiting <- "substrate1"

solvent <- 0.56
#in mL

stock_volume <- 3
#in mL #volume of the volumetric flask containing the stock solutions

stock_added <- 0.9
#in mL # how much of the stock solution is added to the rxn

stock.amount.standard <- 9.7
#amount (mg) of standard in the stock solution

stock.amount.substrate1 <- 210.1
#amount (mg) of substrate1 in the stock solution
```

The input files were strictly saved in the designated location for that particular *rxn.code*. For example, the above input file for spirok-9 was saved with the following naming convention in the following location:

```
"~/data/input/rxn/spirok/spirok-9/user-input3.R"
```

In addition to the input files, the HPLC integral data were required. These were imported into the corresponding folder, again named after the *rxn.code*. Again, the locations and naming conventions for the HPLC files were strict, for example, the file related to the above input file for spirok-9 had the corresponding HPLC data extracted at 240 nm, which was saved in the following location:

```
"~/data/raw/rxn/spirok/hplc/spirok-9/240-hplc-data3.csv"
```

The file contained HPLC data in .csv format:

| time | standard | substrate1a | substrate1b | product1a | product1b |
|---|---|---|---|---|---|
| 0.5 | 18.42760256 | 64.35748664 | 60.96297366 | 0.18147399 | 4.725079075 |
| 5 | 16.12744006 | 59.04634031 | 55.73486906 | 0.489059372 | 5.075346239 |
| 10 | 18.08578213 | 62.34558384 | 58.5290456 | 0.539865306 | 5.905890586 |
| 15 | 17.95928594 | 61.80401951 | 57.80166884 | 0.650188335 | 6.445584961 |
| 20 | 17.82967611 | 64.27401546 | 59.89795069 | 0.697900518 | 7.284144861 |
| 25 | 16.08494511 | 57.85118859 | 53.49523002 | 0.649335361 | 7.277699124 |
| 30 | 16.90555661 | 60.39303993 | 55.69694069 | 0.774180107 | 8.117654095 |
| 35 | 18.39228709 | 65.78897866 | 60.32983028 | 0.891570466 | 9.57988532 |
| 40 | 18.85310078 | 63.16567356 | 57.57144305 | 0.918422414 | 9.981858759 |
| 45 | 19.55495725 | 65.22488572 | 59.09191122 | 0.93210506 | 10.9991466 |
| 50 | 18.30014079 | 64.58881099 | 58.38643257 | 0.940806155 | 11.30856804 |
| 55 | 20.70330913 | 72.78441973 | 65.17703295 | 1.110983936 | 13.96736051 |
| 60 | 18.56184066 | 60.94366543 | 54.55711722 | 0.994176465 | 11.99093873 |

The project code and number of replicates were then specified explicitly in the main R script, again, using spirok-9 as an example:

```
# REACTION DATA PROCESSING
project <- "spirok"  #additions, snark or spirok
rxn.code <- "spirok-9"
replicates <- 3   # a minimum of 2 replicates for snark and spirok projects
```

Lastly, the following lines of script were initiated to process all data simultaneously. In summary, the scripts generally applied the HPLC assay as detailed in 7.3.4.

```
data.types <- c("hplc.ratios.240e","conv","mmol","M", "ee")
source(file="functions/spirok/spirok-rxn-conditions.R")
source(file="functions/spirok/wavelength-extrapolation-240-292.R")
source(file="functions/spirok/spirok-rxn-process.R")
source(file="functions/spirok/spirok-rxn-export.R")
```

Following execution of the above lines, the reaction data were obtained in .csv format which enabled analysis, plotting, and manipulation. The data were exported to the relevant "processed" folder, for example:

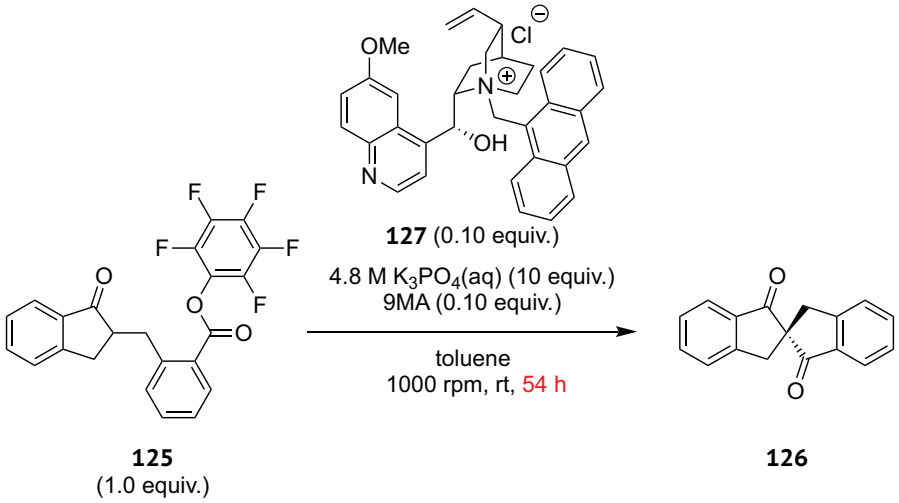
```
"~/data/processed/rxn/spirok/spirok-9/"
```

The contents of the folders included temporal concentration, mmol, and ee data, in addition to the initial reaction conditions for the entire set. An example of the exported concentration data for the same spirok-9 reaction is below. In the interest of space, the headings have been removed and the data manually truncated to 5 decimal spaces:

| A | B | C | D | E | F | G |
|---|---|---|---|---|---|---|
| 0.5 | 0.07616 | 0.03916 | 0.03700 | 0.00340 | 0.00013 | 0.00327 |
| 5 | 0.07972 | 0.04110 | 0.03863 | 0.00416 | 0.00014 | 0.00402 |
| 10 | 0.07507 | 0.03874 | 0.03633 | 0.00445 | 0.00027 | 0.00418 |
| 15 | 0.07474 | 0.03872 | 0.03603 | 0.00480 | 0.00020 | 0.00460 |
| 20 | 0.07825 | 0.04060 | 0.03764 | 0.00547 | 0.00024 | 0.00524 |
| 25 | 0.07779 | 0.04055 | 0.03723 | 0.00607 | 0.00026 | 0.00581 |
| 30 | 0.07744 | 0.04033 | 0.03711 | 0.00653 | 0.00036 | 0.00617 |
| 35 | 0.07708 | 0.04043 | 0.03665 | 0.00747 | 0.00077 | 0.00670 |
| 40 | 0.07226 | 0.03791 | 0.03435 | 0.00759 | 0.00077 | 0.00682 |
| 45 | 0.07178 | 0.03778 | 0.03399 | 0.00768 | 0.00043 | 0.00725 |
| 50 | 0.07606 | 0.04002 | 0.03604 | 0.00872 | 0.00075 | 0.00798 |
| 55 | 0.07549 | 0.03991 | 0.03558 | 0.00969 | 0.00097 | 0.00872 |
| 60 | 0.07037 | 0.03732 | 0.03306 | 0.00909 | 0.00074 | 0.00836 |

The data array above consists of data in seven columns (for this example, manually labelled A to G), which correspond to A) time (in min), B) total concentration of substrate **125** (in M), C) concentration of (−)-**125** (in M), D) concentration of (+)-**125** (in M), E) total concentration of product **126** (in M), F) concentration of (*R*)-**126** (in M), and G) concentration of (*S*)-**126** (in M). Further analyses of the data were carried out in R, Microsoft® Excel, or DataGraph.

## 7.5 Evaluating the extended reaction




### 7.5.1 General information and conditions

Three reactions were carried out using the standard reaction protocol (see 7.4.1); the *rxn.code* for this experiment was designated "spirok-6". The conditions will be described for one vial only: catalyst **127** (8.4 mg, 0.015 mmol, 0.10 equiv.), $K_3PO_4$(aq) (4.77 M; 305 µL, 1.46 mmol, 10.0 equiv.), stirring speed 1000 rpm.

**Substrate solution:** substrate **125** (210.0 mg, 0.486 mmol), standard **133** (9.6 mg, 0.050 mmol) in 3.00 mL; corresponding to an added amount of **125** (63.0 mg, 0.146 mmol, 1.00 equiv.), **133** (2.9 mg, 0.015 mmol, 0.10 equiv.) per vial.

The reactions were sampled using the sampling protocol (see 7.4.3) and analysed according to the method described in 7.4.4. Aliquots were extracted at 0.5 min per sample, then at 60 min, then at 60 min intervals for a total of 3240 min.

### 7.5.2 Data processing and analysis

The physical appearances of the reaction mixtures were observed over time (Figure 7.5). The raw HPLC data were collected at 240 nm and 292 nm and were processed according to the methods detailed in 7.3.4 and 7.4.4. The plots of total substrate **125** and product **126** concen-

tration over time were generated (Figure 7.6). The enantiomeric excess of the substrate **125** and product **126** were calculated and plotted against time (Figure 7.7 and Figure 7.8).

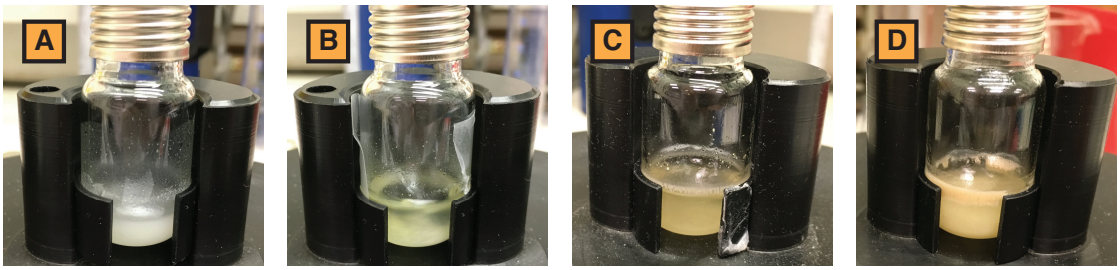



**Figure 7.5: Appearance of the reaction mixture over time.** The photos were taken at the described times with respect to initiation of the reaction (before or after time zero): At approximately **A)** −5 min; **B)** 5 min; **C)** 180 min and; **D)** 1000 min.

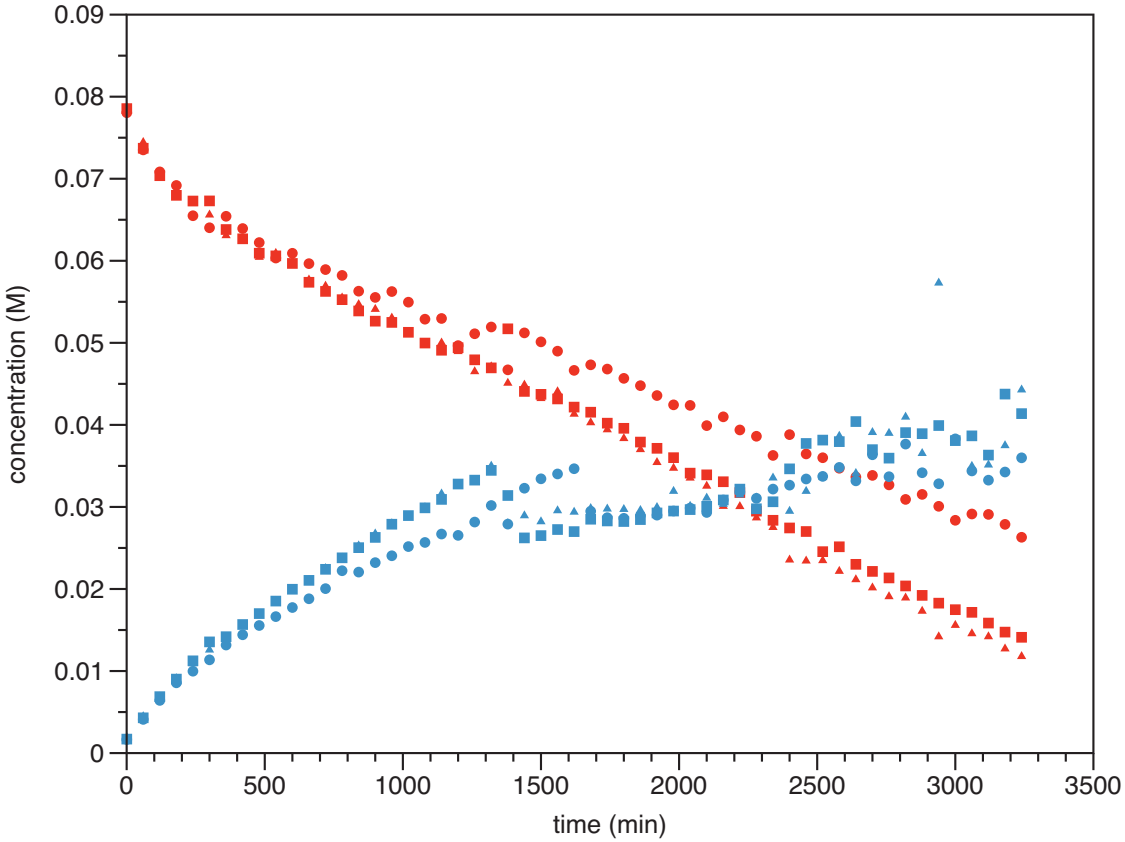



**Figure 7.6: Concentration of substrate 125 (red) and product 126 (blue) over time.** Circles, triangles and squares correspond to the triplicate runs.

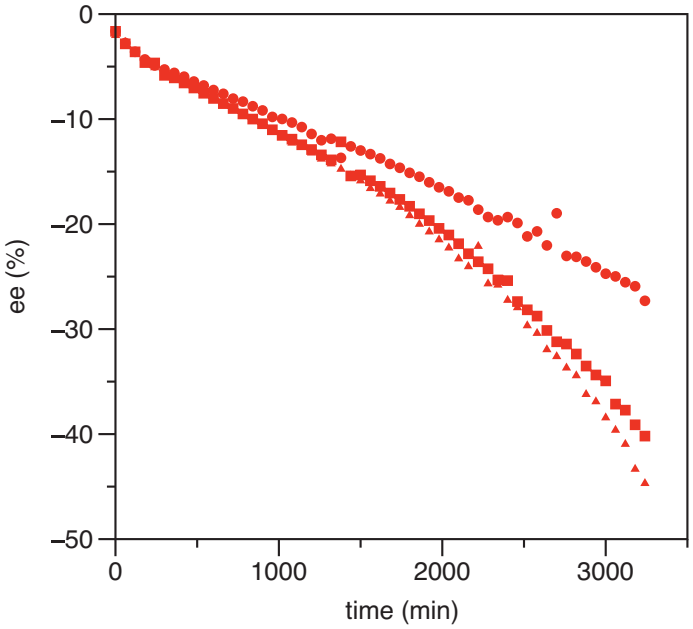



**Figure 7.7: Enantiomeric excess (ee) of substrate 125 over time in min.** Circles, triangles and squares correspond to the triplicate runs.

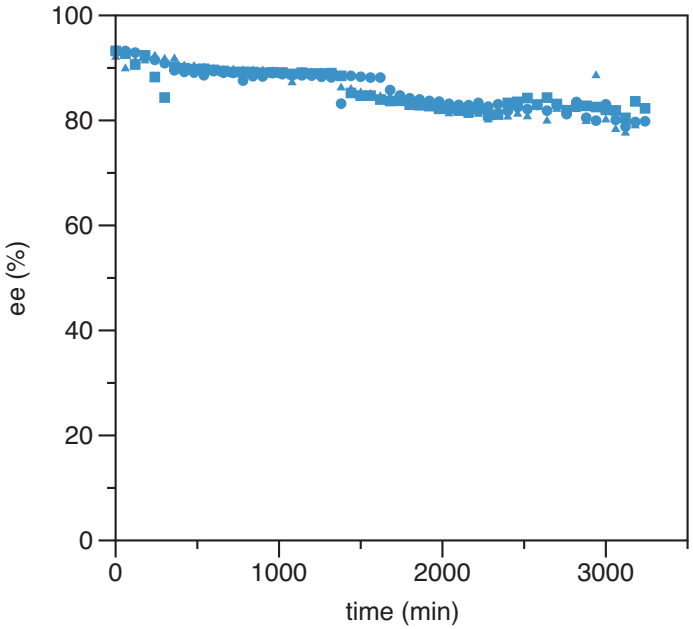
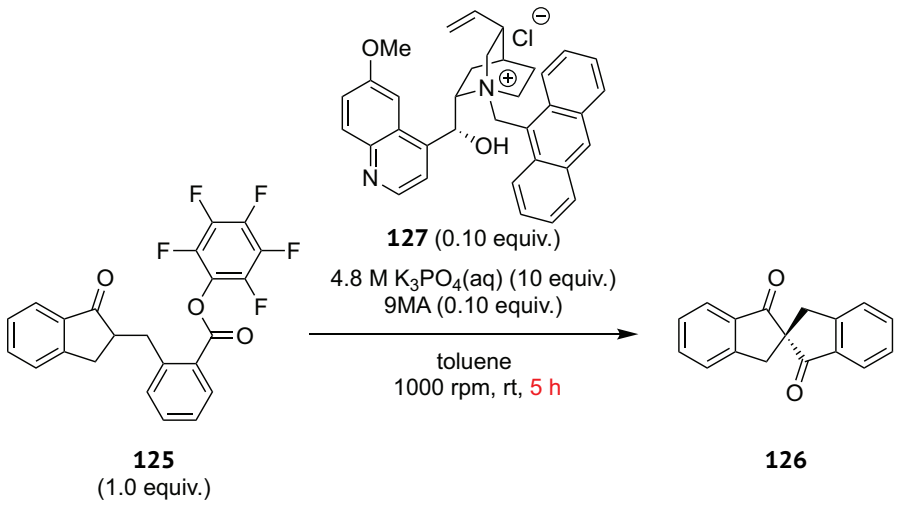



**Figure 7.8: Enantiomeric excess (ee) of product 126 over time in min.** Circles, triangles and squares correspond to the triplicate runs.

## 7.6 Viability of initial rate kinetic studies




### 7.6.1 General information and conditions

Three reactions were carried out using the standard reaction protocol (see 7.4.1); the *rxn.code* for this experiment was designated "spirok-5". The conditions will be described for one vial only: catalyst **127** (8.4 mg, 0.015 mmol, 0.10 equiv.), $K_3PO_4$(aq) (4.77 M; 305 µL, 1.46 mmol, 10.0 equiv.), stirring speed 1000 rpm.

**Substrate solution:** substrate **125** (210.0 mg, 0.486 mmol), standard **133** (9.6 mg, 0.050 mmol) in 3.00 mL; corresponding to an added amount of **125** (63.0 mg, 0.146 mmol, 1.00 equiv.), **133** (2.9 mg, 0.015 mmol, 0.10 equiv.) per vial.

The reactions were sampled using the sampling protocol (see 7.4.3) and analysed according to the method described in 7.4.4. Aliquots were extracted at 0.5 min per sample, then at 20 min, then at 20 min intervals for a total of 300 min.

### 7.6.2 Data processing and analysis

The raw HPLC data were collected at 240 nm and 292 nm and were processed according to the methods detailed in 7.3.4 and 7.4.4. The data were first compared to the full reaction (see 7.5), which showed good agreement (Figure 7.9).

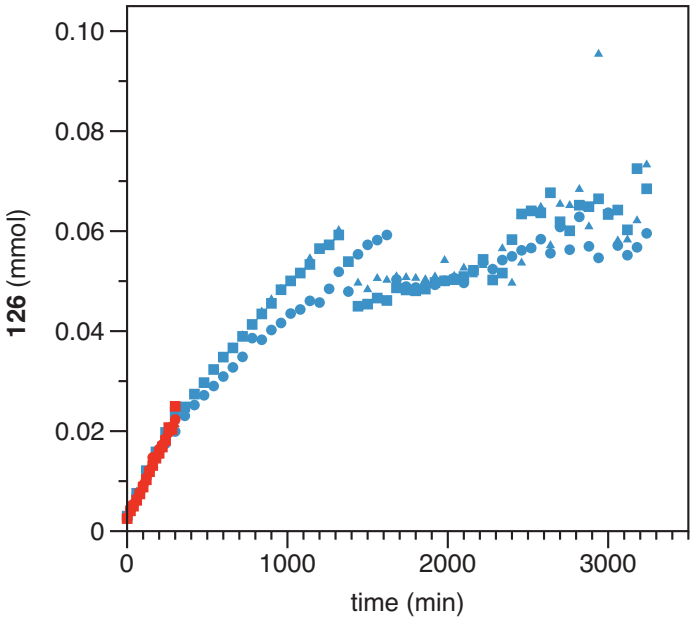



**Figure 7.9: Overlay of reaction data obtained over 5 h (300 min) (red) vs 54 h (3240 min)(blue).** The red data were obtained in this experiment to monitor the reaction over 5 h only; the blue data were obtained previously (see 7.5). Circles, triangles, and squares correspond to individual reactions within the triplicate sets.

The triplicate plots for formation of product **126** over time were generated for analyses (Figure 7.10). Linear regression analysis of the rate of total product formation gave the slopes as the initial rate ($k_{obs}$); the data were analysed over the first 1 h of the reaction (red) or over the full 5 h.

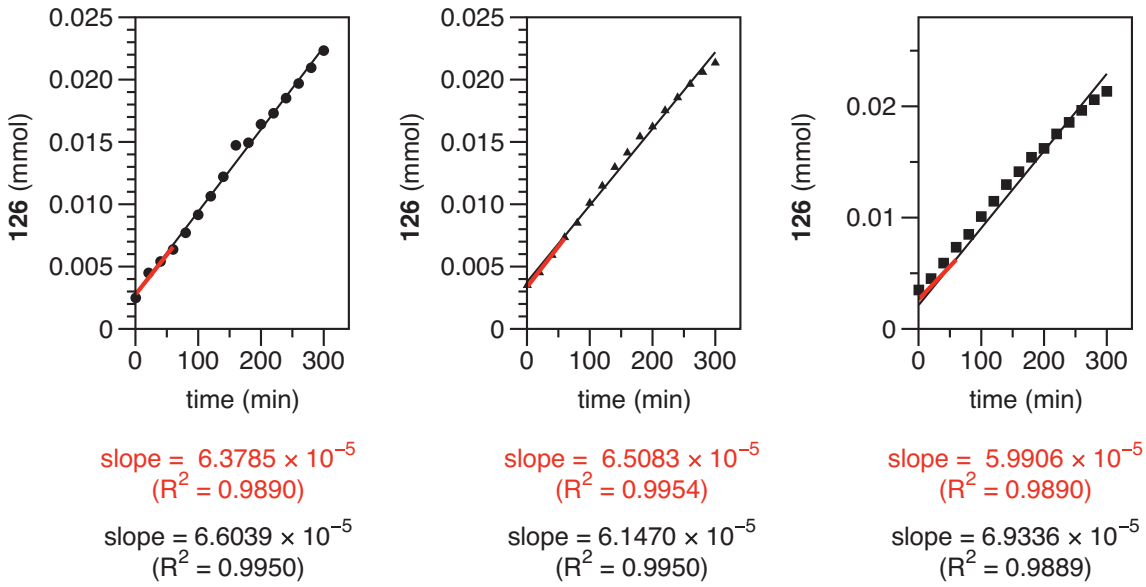



**Figure 7.10: Three reactions evaluating the reaction over the first 5 h.** Circles, triangles, and squares correspond to individual reactions within the triplicate set. The lines are linear regression analyses to give the slope, which corresponds to the initial rate over the first 1 h (red) or for the full 5 h (black) of the reaction.

The averages and the error of the slopes and were then calculated for the whole triplicate experiment (Figure 7.11). Comparable rates (mean slope) were observed when analysing the 1 h vs the full 5 h.

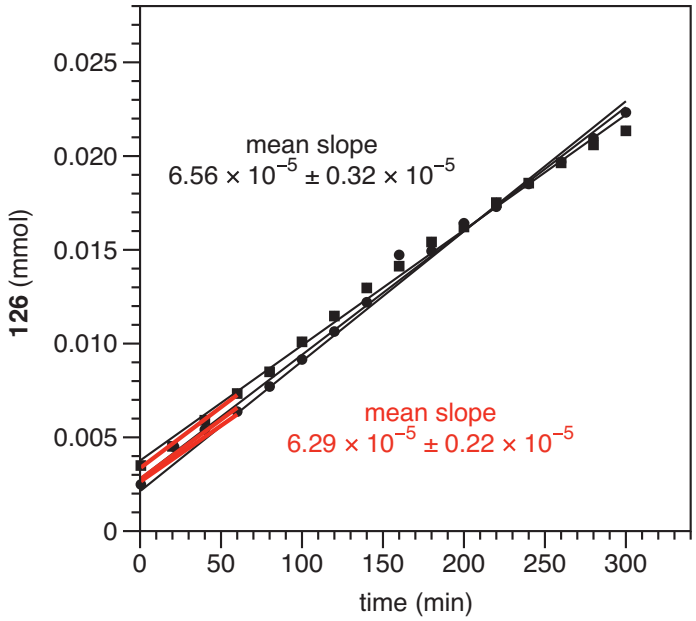
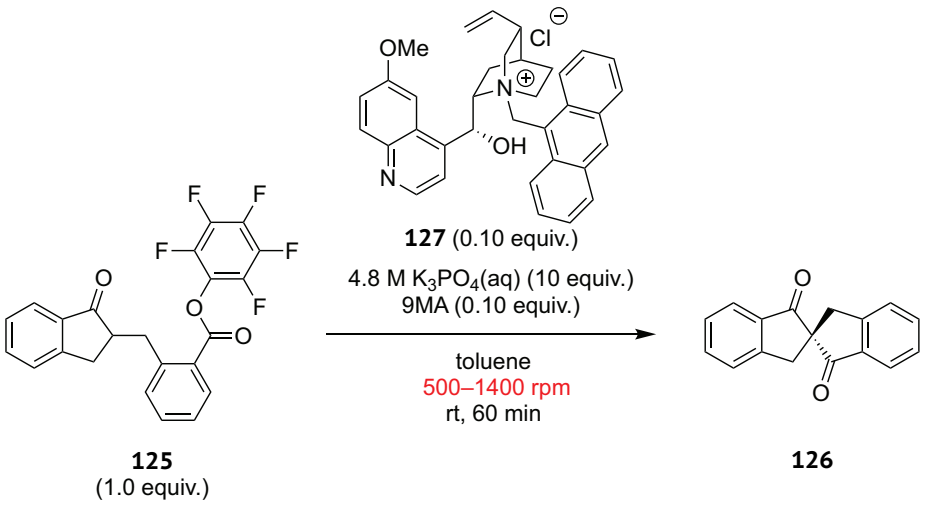



**Figure 7.11: Overlay of the triplicate set to compare the rates over 1 h vs 5 h.** Circles, triangles, and squares correspond to individual reactions within the triplicate set. The lines are linear regression analyses to give the slope, which corresponds to the initial rate over the first 1 h (red) or for the full 5 h (black) of the reaction.

## 7.7 Evaluating the effect of stirring speed



### 7.7.1 General information and conditions

A series of reactions were carried out using the standard reaction protocol (see 7.4.1). The reactions varied only by the stirring speed of the reaction. Each reaction was carried out as a single experiment, or as a set of triplicate reactions. The equivalents (equiv.) are reported with respect to the amount of substrate **125**. All reactions were sampled using the sampling protocol (see 7.4.3) and analysed according to the method described in 7.4.4. Aliquots were extracted at 0.5 min per sample, then at 5.0 min, then at 5.0 min intervals for a total of 60 min.

The single experiments were carried out using the following conditions and the same substrate solution made up as follows: catalyst **127** (8.4 mg, 0.015 mmol, 0.10 equiv.), $K_3PO_4$(aq) (4.77 M; 305 µL, 1.46 mmol, 10.0 equiv.). **Substrate solution:** substrate **125** (210.0 mg, 0.486 mmol), standard **133** (9.6 mg, 0.0499 mmol) in 3.0 mL; corresponding to an added amount of **125** (63.0 mg, 0.146 mmol, 1.00 equiv.), **133** (2.9 mg, 0.0151 mmol, 0.104 equiv.) per vial.

The reactions carried out in triplicate used the following conditions, described for one replicate only: catalyst **127** (8.4 mg, 0.015 mmol, 0.10 equiv.), $K_3PO_4$(aq) (4.77 M; 305 µL, 1.46 mmol, 10.0 equiv.). **Substrate solution:** substrate **125** (210.0 mg, 0.486 mmol), standard **133** (9.6 mg, 0.0499 mmol) in 3.0 mL; corresponding to an added amount of **125** (63.0 mg, 0.146 mmol, 1.00 equiv.), **133** (2.9 mg, 0.0151 mmol, 0.104 equiv.) per vial.

### 7.7.2 Data processing and analysis

The raw HPLC data were collected at 240 nm and 292 nm and were processed according to the methods detailed in 7.3.4 and 7.4.4. The processed data were analysed using linear regression analysis of the rate of total product formation to give the initial rate ($k_{obs}$). The $k_{obs}$ or mean

$k_{obs}$ of each set was then plotted against the stirring speed of the corresponding reaction to give a positive dependence of the $k_{obs}$ on the stirring speed (Figure 7.12). The mean slope and error for each triplicate was calculated. The data are summarised in Table 7.1.

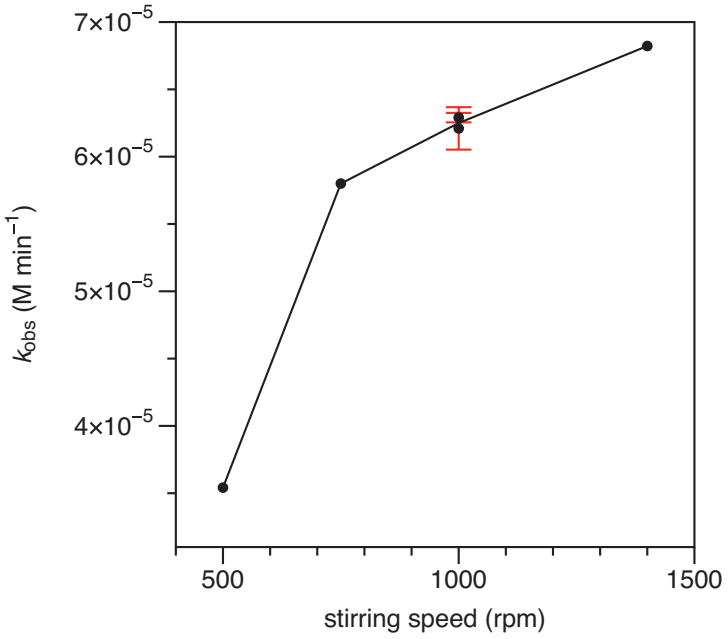


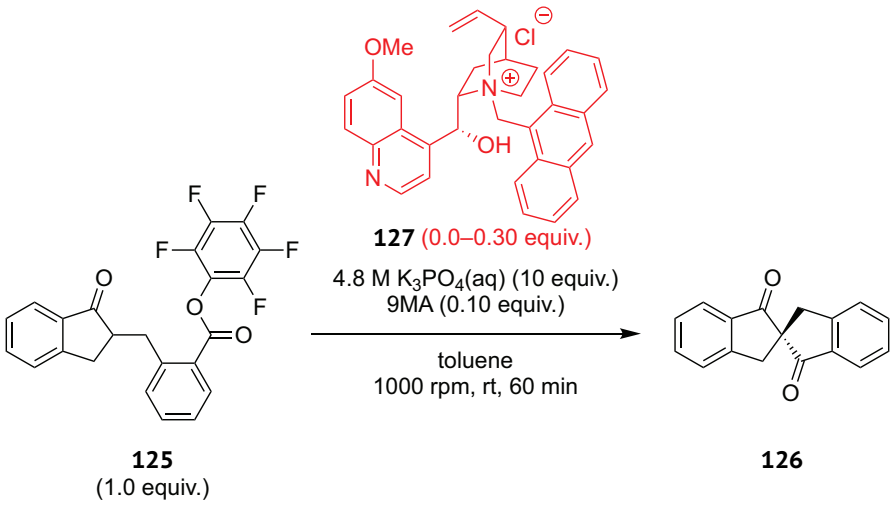

**Figure 7.12: Comparison of initial rate $k_{obs}$ with different reaction stirring speeds.** The line is a guide for the eye.

**Table 7.1: Summary of experiments investigating the effect of stirring speed.**

| Entry | *rxn.code*[a] | Replicate (#) | stirring speed[b] (rpm) | $k_{obs}$[c] (M min$^{-1}$) | mean $k_{obs}$[d] (M min$^{-1}$) | SD[e] (M min$^{-1}$) |
|---|---|---|---|---|---|---|
| 1 | spirok-28a | 1 | 500 | $3.541\times10^{-5}$ | $3.541\times10^{-5}$ | N/A |
| 2 | spirok-28b | 1 | 750 | $5.800\times10^{-5}$ | $5.800\times10^{-5}$ | N/A |
| 3 | spirok-18 | 1 | 1000 | $6.280\times10^{-5}$ | | |
| 4 | spirok-18 | 2 | 1000 | $6.250\times10^{-5}$ | $6.2887\times10^{-5}$ | $0.0035\times10^{-5}$ |
| 5 | spirok-18 | 3 | 1000 | $6.335\times10^{-5}$ | | |
| 6 | spirok-35 | 1 | 1000 | $5.987\times10^{-5}$ | | |
| 7 | spirok-35 | 2 | 1000 | $6.314\times10^{-5}$ | $6.210\times10^{-5}$ | $0.016\times10^{-5}$ |
| 8 | spirok-35 | 3 | 1000 | $6.328\times10^{-5}$ | | |
| 9 | spirok-28c | 1 | 1400 | $6.822\times10^{-5}$ | $6.822\times10^{-5}$ | N/A |

[a]*rxn.code* corresponds to the set of experiments used to obtain the data; [b]reaction stirring speed; [c]the observed initial rate in M min$^{-1}$ of each reaction (to 4 sf); [d]average $k_{obs}$ for reactions carried out in triplicate (to 4 sf or within the range of the standard deviation); [e]standard deviation (to 2 sf) of the corresponding $k_{obs}$, where appropriate.

## 7.8 Evaluating the reaction order with respect to the ammonium chloride catalyst




### 7.8.1 General information and conditions

A series of reactions were carried out using the standard reaction protocol (see 7.4.1). The reactions varied only by the amount of catalyst **127** that was used in the reaction. Each experiment was carried out as a single reaction, in duplicate or triplicate. All reactions were carried out with a reaction stirring speed of 1000 rpm. The equivalents (equiv.) are reported with respect to the amount of substrate **125**. All reactions were sampled using the sampling protocol (see 7.4.3). In each reaction, aliquots were extracted at 0.50 min after time zero, then at 5.0 min, then at 5.0 min intervals for a total of 60 min.

The single experiment was carried out using the following conditions: catalyst **127** (0 mg, 0 mmol, 0 equiv.), $K_3PO_4$(aq) (4.77 M; 305 µL, 1.46 mmol, 10.0 equiv.). **Substrate solution:** substrate **125** (70.0 mg, 0.162 mmol), standard **133** (3.2 mg, 0.017 mmol) in 1.0 mL; corresponding to an added amount of **125** (63.0 mg, 0.146 mmol, 1.00 equiv.), **133** (2.9 mg, 0.015 mmol, 0.10 equiv.) per reaction vial.

The reactions carried out in duplicate used the following conditions, described for one replicate only: catalyst **127** (1.7–12.1 mg, 0.0031–0.0220 mmol, 0.02–0.15 equiv.; amounts detailed

in Table 7.2), $K_3PO_4$(aq) (4.77 M; 305 µL, 1.46 mmol, 10.0 equiv.). **Substrate solution:** substrate **125** (140.0 mg, 0.324 mmol), standard **133** (6.4 mg, 0.033 mmol) in 2.0 mL; corresponding to an added amount of **125** (63.0 mg, 0.146 mmol, 1.00 equiv.), **133** (2.9 mg, 0.0151 mmol, 0.104 equiv.) per reaction vial.

The reactions carried out in triplicate used the following conditions, described for one replicate only: catalyst **127** (16.3–25.0 mg, 0.0296–0.0454 mmol, 0.20–0.31 equiv.; amounts detailed in Table 7.2), $K_3PO_4$(aq) (4.77 M; 305 µL, 1.46 mmol, 10.0 equiv.). **Substrate solution:** substrate **125** (210.0 mg, 0.486 mmol), standard **133** (9.6 mg, 0.0499 mmol) in 3.0 mL; corresponding to an added amount of **125** (63.0 mg, 0.146 mmol, 1.00 equiv.), **133** (2.9 mg, 0.0151 mmol, 0.104 equiv.) per reaction vial.

### 7.8.2 Data processing and analysis

The raw HPLC data were collected at 240 nm and 292 nm and were processed according to the methods detailed in 7.3.4 and 7.4.4. The plots of total substrate **125** and product **126** concentration over time were generated (Figure 7.13). The processed data were analysed using linear regression analysis of the rate of total product formation to give the initial rate ($k_{obs}$) (Figure 7.14). The mean slope and error for each triplicate or duplicate was calculated. The data are summarised in Table 7.2.

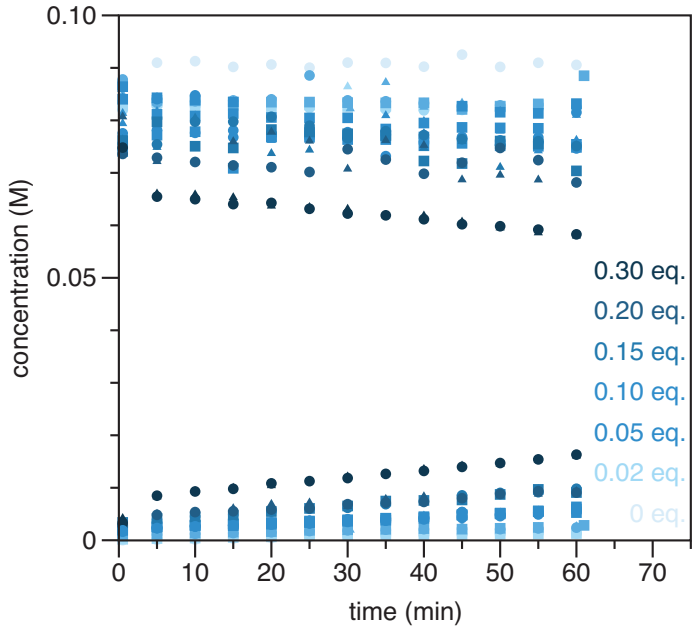



**Figure 7.13: Overlay of all reactions investigating the order in catalyst 127.** The upper dots (above 0.05 M) correspond to the total substrate concentration ((−)-**125** and (+)-**125**) over time, the lower dots (below 0.05 M) correspond to the product concentration ((*R*)-**126** and (*S*)-**126**) over time. The colours correspond to the different initial catalyst concentrations; percentages indicate loading of catalyst **127** with respect to substrate **125** in equivalents (eq.). Circles, triangles and squares correspond to single, duplicate, or triplicate runs.

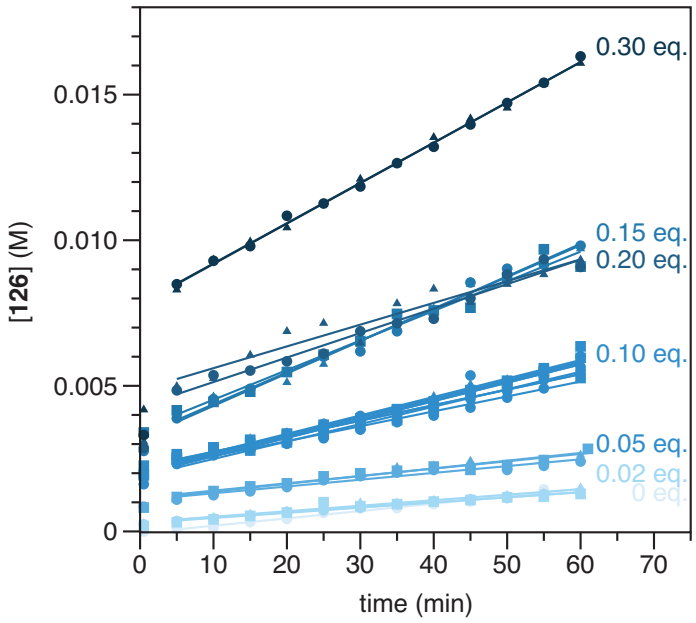



**Figure 7.14: Overlay of product 126 concentration over time for all reactions investigating the effect of catalyst 127 concentration.** The lines correspond to linear regression analysis of each replicate. The colours correspond to the different initial catalyst concentrations; the numbers indicate loading of catalyst **127** with respect to substrate **125** in equivalents (eq.). Circles, triangles and squares correspond to single, duplicate, or triplicate runs.

A double logarithmic plot of initial concentration of catalyst **127** (ln $[\mathbf{127}]_0$) against the ob-

served rate (ln $k_{obs}$) was constructed to give a reaction order with respect to catalyst of 0.79 (Figure 7.15), with a 68% confidence interval of 0.69 to 0.90.

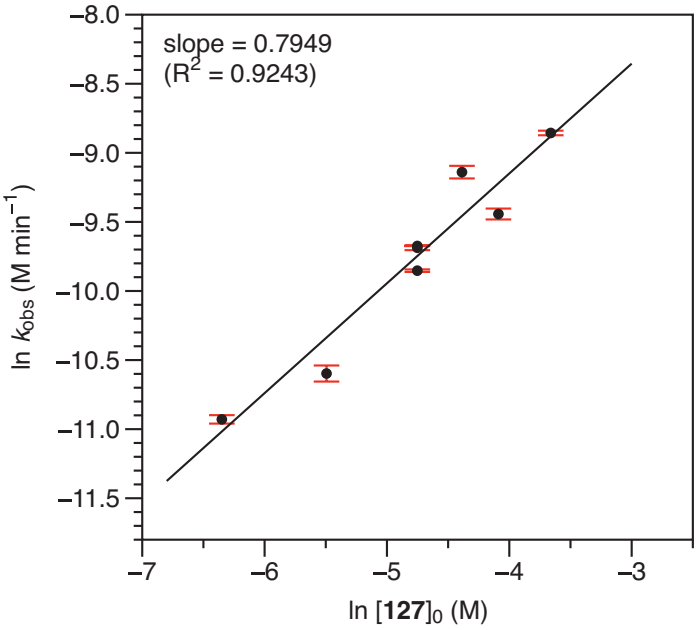


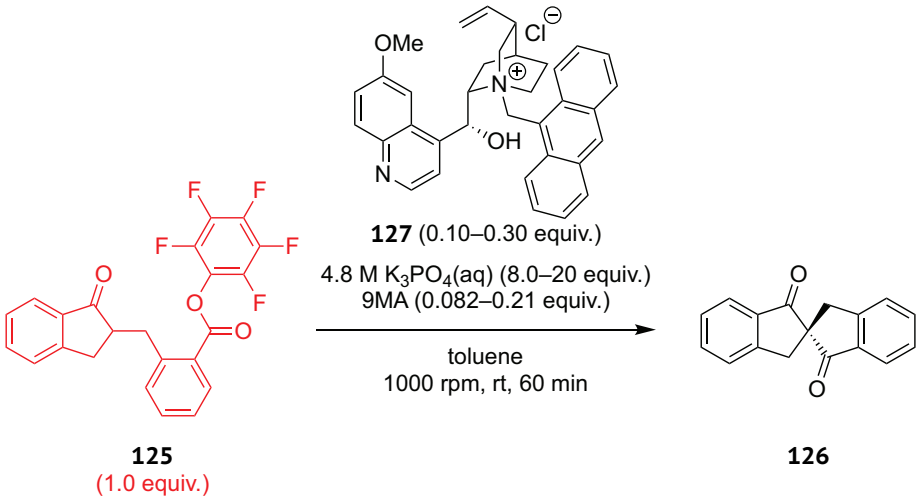

**Figure 7.15: Double logarithmic plot to determine the reaction order with respect to catalyst 127.** The line corresponds to linear regression analysis of the whole data set to give the slope and catalyst order of 0.79.

**Table 7.2: Summary of results investigating the order in catalyst 127.** The slopes to give the $k_{obs}$ were obtained by linear regression analysis of each whole data set.

| Entry | *rxn.code*[a] | Replicate (#) | 127 loading[b] | $[127]_0$[c] (mM) | ln $[127]_0$[d] (M) | ln $k_{obs}$[e] (M min$^{-1}$) | mean ln $k_{obs}$[f] (M min$^{-1}$) | SD[g] (M min$^{-1}$) |
|---|---|---|---|---|---|---|---|---|
| 1 | spirok-45 | 1 | 0.0 equiv. | 0.000 | 0.000 | −10.59 | −10.59 | N/A |
| 2 | spirok-11 | 1 | 0.020 equiv. | 1.750 | −6.348 | −10.94 | | |
| 3 | spirok-11 | 2 | 0.020 equiv. | 1.750 | −6.348 | −10.87 | −10.929 | 0.043 |
| 4 | spirok-11 | 3 | 0.020 equiv. | 1.750 | −6.348 | −10.98 | | |
| 5 | spirok-10 | 1 | 0.050 equiv. | 4.118 | −5.492 | −10.67 | | |
| 6 | spirok-10 | 2 | 0.050 equiv. | 4.118 | −5.492 | −10.54 | −10.597 | 0.053 |
| 7 | spirok-10 | 3 | 0.050 equiv. | 4.118 | −5.492 | −10.58 | | |
| 8 | spirok-8 | 1 | 0.10 equiv. | 8.647 | −4.751 | −9.880 | | |
| 9 | spirok-8 | 2 | 0.10 equiv. | 8.647 | −4.751 | −9.842 | −9.853 | 0.020 |
| 10 | spirok-8 | 3 | 0.10 equiv. | 8.647 | −4.751 | −9.836 | | |
| 11 | spirok-18 | 1 | 0.10 equiv. | 8.647 | −4.751 | −9.675 | | |
| 12 | spirok-18 | 2 | 0.10 equiv. | 8.647 | −4.751 | −9.680 | −9.6571 | 0.0075 |
| 13 | spirok-18 | 3 | 0.10 equiv. | 8.647 | −4.751 | −9.667 | | |
| 14 | spirok-35 | 1 | 0.10 equiv. | 8.647 | −4.751 | −9.723 | | |
| 15 | spirok-35 | 2 | 0.10 equiv. | 8.647 | −4.751 | −9.670 | −9.687 | 0.026 |
| 16 | spirok-35 | 3 | 0.10 equiv. | 8.647 | −4.751 | −9.668 | | |
| 17 | spirok-9 | 1 | 0.15 equiv. | 12.46 | −4.386 | −9.122 | | |
| 18 | spirok-9 | 2 | 0.15 equiv. | 12.46 | −4.386 | −9.103 | −9.140 | 0.039 |
| 19 | spirok-9 | 3 | 0.15 equiv. | 12.46 | −4.386 | −9.193 | | |
| 20 | spirok-7 | 1 | 0.20 equiv. | 16.79 | −4.087 | −9.384 | −9.443 | 0.059 |
| 21 | spirok-7 | 2 | 0.20 equiv. | 16.79 | −4.087 | −9.502 | | |
| 22 | spirok-12 | 1 | 0.30 equiv. | 25.73 | −3.660 | −8.857 | −8.85623 | 0.00090 |
| 23 | spirok-12 | 2 | 0.30 equiv. | 25.73 | −3.660 | −8.855 | | |

[a]*rxn.code* corresponds to the set of experiments used to obtain the data; [b]loading of catalyst **127** with respect to substrate **125** (to 2 sf); [c]initial concentration of catalyst **127** using the combined volumes of the aqueous and organic layers (to 4 sf); [d]natural logarithm of the initial concentration of catalyst **127** using the combined volumes of the aqueous and organic layers (to 4 sf); [e]natural logarithm of the initial rate of the formation of total product **126** (both enantiomers) (to 4 sf); [f]mean of all replicate initial rates (as the natural logarithms) corresponding to the formation of total product **126** (both enantiomers); [g]standard deviation (to 2 sf) of the initial rates (as the natural logarithms) corresponding to the formation of total product **126** (both enantiomers) of the specified data set replicates.

## 7.9 Evaluating the reaction order with respect to the substrate




### 7.9.1 General information and conditions

A series of reactions were carried out using the standard reaction protocol (see 7.4.1). The reactions varied only by the amount of substrate **125** that was used in the reaction. Each experiment was carried out as duplicate or triplicate reactions. All reactions were carried out with a reaction stirring speed of 1000 rpm. The equivalents (equiv.) are reported with respect to the amount of substrate **125**. All reactions were sampled using the sampling protocol (see 7.4.3). In each reaction, aliquots were extracted at 0.50 min after time zero, then at 5.0 min, then at 5.0 min intervals for a total of 60 min.

The reaction carried out in duplicate used the following conditions: catalyst **127** (8.4 mg, 0.015 mmol, 0.084 equiv.), $K_3PO_4$(aq) (4.77 M; 305 µL, 1.46 mmol, 8.00 equiv.). **Substrate solution:** substrate **125** (262.5 mg, 0.607 mmol), standard **133** (9.6 mg, 0.050 mmol) in 3.0 mL; corresponding to an added amount of **125** (78.8 mg, 0.182 mmol, 1.00 equiv.), **133** (2.9 mg, 0.015 mmol, 0.082 equiv.) per reaction vial.

The reactions carried out in triplicate used the following conditions, described for one replicate only: catalyst **127** (8.4 mg, 0.015 mmol, 0.084–0.21 equiv.), $K_3PO_4$(aq) (4.77 M; 305 µL, 1.46 mmol, 10–20 equiv.). **Substrate solution:** substrate **125** (104.9–210.0 mg, 0.243–

0.486 mmol), standard **133** (9.6 mg, 0.050 mmol) in 3.0 mL; corresponding to an added amount of **125** (31.5–63.0 mg, 0.0728–0.146 mmol, 1.00 equiv.), **133** (2.9 mg, 0.015 mmol, 0.21–0.10 equiv.) per reaction vial.

Full details of amounts are described in Table 7.3.

### 7.9.2 Data processing and analysis

The raw HPLC data were collected at 240 nm and 292 nm and were processed according to the methods detailed in 7.3.4 and 7.4.4. The plots of total substrate **125** and product **126** concentration over time were generated (Figure 7.16). The data were analysed using linear regression analysis of the rate of total product formation to give the initial rate ($k_{obs}$) (Figure 7.17). The mean slope and error for each triplicate or duplicate was calculated. The data are summarised in Table 7.3.

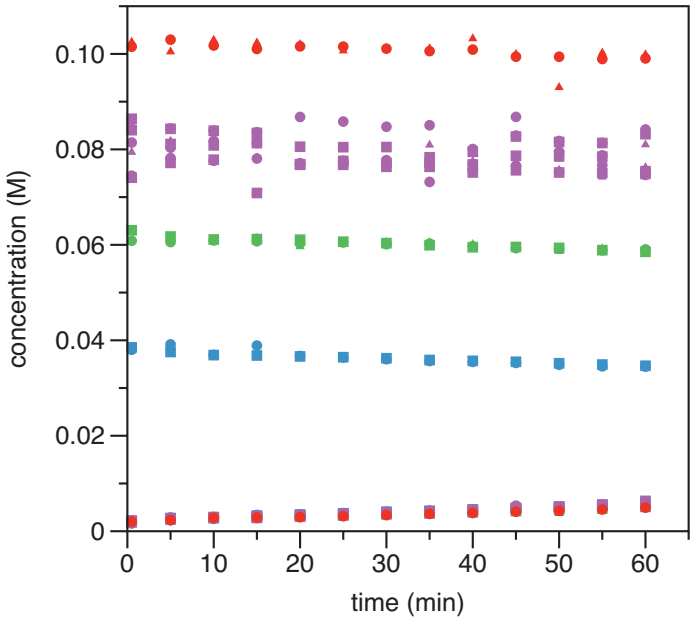



**Figure 7.16: Overlay of all reactions investigating the order in substrate 125.** The upper dots (above 0.02 M) correspond to the total substrate concentration ((−)-**125** and (+)-**125**) over time, the lower dots (below 0.02 M) correspond to the product concentration ((*R*)-**126** and (*S*)-**126**) over time. The colours correspond to the different initial substrate **125** concentrations: 0.0412 M (blue), 0.0623 M (green), 0.0827 M (purple), 0.103 M (red). Circles, triangles and squares correspond to duplicate or triplicate runs.

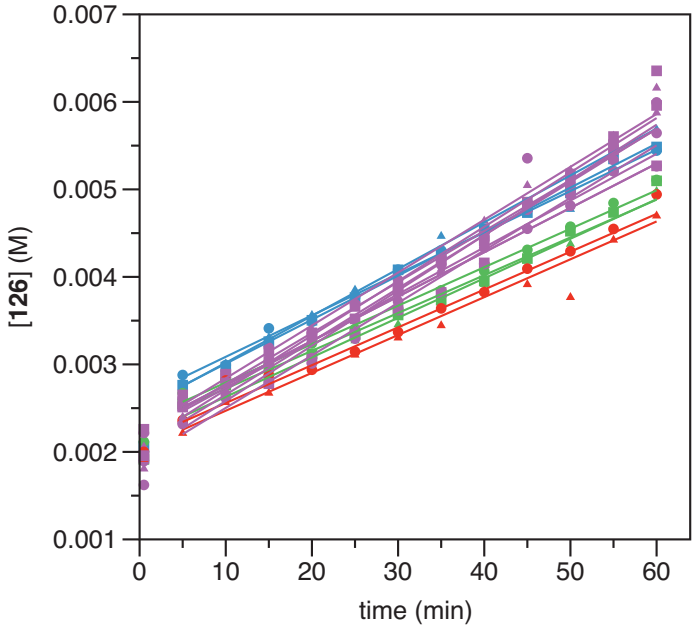



**Figure 7.17: Overlay of product 126 concentration over time for all reactions investigating the effect of substrate 125 concentration.** The lines correspond to linear regression analysis of each reaction. The colours correspond to the different initial substrate **125** concentrations: 0.0412 M (blue), 0.0623 M (green), 0.0827 M (purple), 0.103 M (red). Circles, triangles and squares correspond to duplicate or triplicate runs.

A double logarithmic plot of initial concentration of substrate **125** (ln $[\mathbf{125}]_0$) against the observed rate (ln $k_{obs}$) was constructed to give a reaction order with respect to substrate of 0.026 (Figure 7.35), with a 68% confidence interval of −0.27 to 0.33.

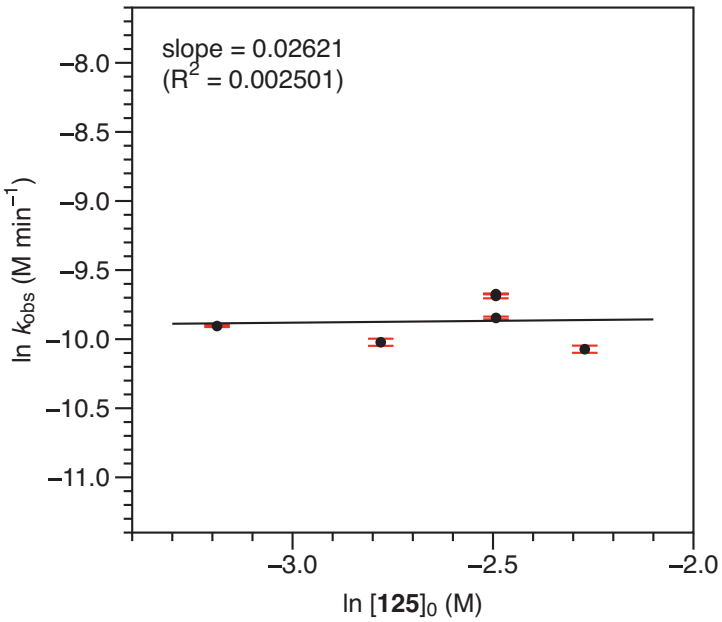


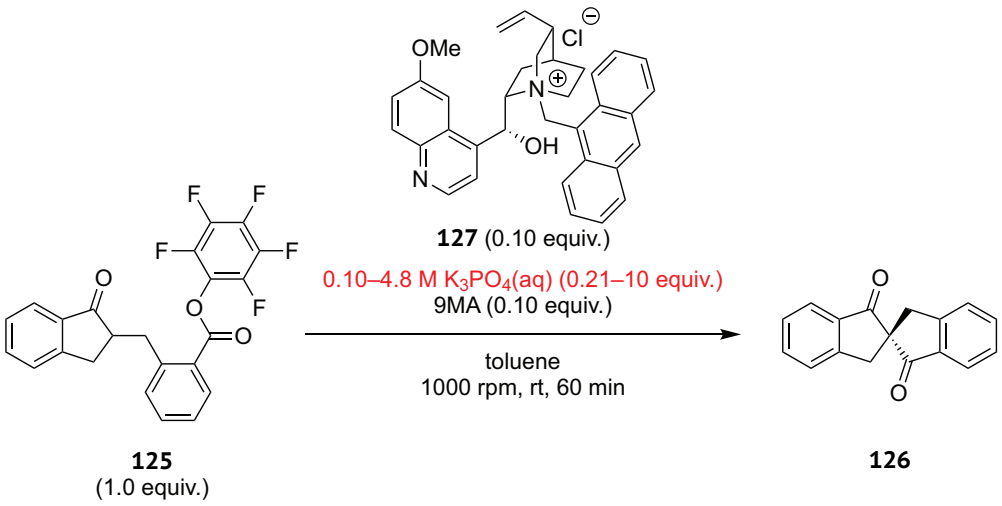

**Figure 7.18: Double logarithmic plot to determine the reaction order with respect to substrate 125.** The line corresponds to linear regression analysis of the whole data set to give the slope and substrate order of 0.026.

**Table 7.3: Summary of results investigating the order in substrate 125.** Specific details of the reaction conditions are described. The slopes to give the $k_{obs}$ were obtained by linear regression analysis of each whole data set and the ln $k_{obs}$ calculated.

| **Entry** | ***rxn.code*[a]** | **Replicate** (#) | **[125]$_0$[b]** (M) | **ln [125]$_0$[c]** (M) | **127 loading[d]** | **$K_3PO_4$[e]** (equiv.) | **ln $k_{obs}$[f]** (M min$^{-1}$) | **mean ln $k_{obs}$[g]** (M min$^{-1}$) | **SD[h]** (M min$^{-1}$) |
|---|---|---|---|---|---|---|---|---|---|
| 1 | spirok-16 | 1 | 0.04124 | −2.780 | 0.21 equiv. | 20 equiv. | −9.947 | | |
| 2 | spirok-16 | 2 | 0.04124 | −2.780 | 0.21 equiv. | 20 equiv. | −9.871 | −9.905 | 0.031 |
| 3 | spirok-16 | 3 | 0.04124 | −2.780 | 0.21 equiv. | 20 equiv. | −9.897 | | |
| 4 | spirok-15 | 1 | 0.06204 | −3.188 | 0.14 equiv. | 13 equiv. | −10.03 | | |
| 5 | spirok-15 | 2 | 0.06204 | −3.188 | 0.14 equiv. | 13 equiv. | −10.03 | −10.0225 | 0.0073 |
| 6 | spirok-15 | 3 | 0.06204 | −3.188 | 0.14 equiv. | 13 equiv. | −10.01 | | |
| 7 | spirok-8 | 1 | 0.08270 | −2.493 | 0.10 equiv. | 10 equiv. | −9.880 | | |
| 8 | spirok-8 | 2 | 0.08270 | −2.493 | 0.10 equiv. | 10 equiv. | −9.842 | −9.853 | 0.020 |
| 9 | spirok-8 | 3 | 0.08270 | −2.493 | 0.10 equiv. | 10 equiv. | −9.836 | | |
| 10 | spirok-18 | 1 | 0.08270 | −2.493 | 0.10 equiv. | 10 equiv. | −9.675 | | |
| 11 | spirok-18 | 2 | 0.08270 | −2.493 | 0.10 equiv. | 10 equiv. | −9.680 | −9.6571 | 0.0075 |
| 12 | spirok-18 | 3 | 0.08270 | −2.493 | 0.10 equiv. | 10 equiv. | −9.667 | | |
| 13 | spirok-35 | 1 | 0.08270 | −2.493 | 0.10 equiv. | 10 equiv. | −9.723 | | |
| 14 | spirok-35 | 2 | 0.08270 | −2.493 | 0.10 equiv. | 10 equiv. | −9.670 | −9.687 | 0.026 |
| 15 | spirok-35 | 3 | 0.08270 | −2.493 | 0.10 equiv. | 10 equiv. | −9.668 | | |
| 16 | spirok-14 | 1 | 0.1032 | −2.271 | 0.084 equiv. | 8.0 equiv. | −10.05 | −10.073 | 0.026 |
| 17 | spirok-14 | 2 | 0.1032 | −2.271 | 0.084 equiv. | 8.0 equiv. | −10.10 | | |

[a]*rxn.code* corresponds to the set of experiments used to obtain the data; [b]initial substrate **125** concentration using the combined volumes of the aqueous and organic layers (to 4 sf); [c]natural logarithm of the initial substrate **125** concentration using the combined volumes of the aqueous and organic layers (to 4 sf); [d]initial loading of catalyst **127** with respect to substrate **125** (to 2 sf); [e]initial equivalents of $K_3PO_4$ with respect to substrate **125** (to 2 sf); [f]natural logarithm of the initial rate of formation of total product **126** (both enantiomers) (to 4 sf); [g]mean of natural logarithm of the initial rate of formation of total product **126** (both enantiomers) of all replicates; [h]standard deviation (to 2 sf) of the initial rates corresponding to the formation of total product **126** (both enantiomers) of the specified data set replicates.

## 7.10 Evaluating the reaction order with respect to $K_3PO_4$ at constant volume




### 7.10.1 General information and conditions

A series of reactions were carried out using the standard reaction protocol (see 7.4.1). The reactions varied only by the concentration of aqueous $K_3PO_4$ that was used in the reaction. Each experiment was carried out as a single reaction or in triplicate. All reactions were carried out with a reaction stirring speed of 1000 rpm. The equivalents (equiv.) are reported with respect to the amount of substrate **125**. All reactions were sampled using the sampling protocol (see 7.4.3). In each reaction, aliquots were extracted at 0.50 min after time zero, then at regular intervals for a specified time. The data for analysis corresponds to the first 60 min of the reaction, however aliquots were extracted over 360 min for substoichiometric amounts of base to gauge the effect on overall conversion to product (see Figure 7.19).

The single experiments were carried out using the conditions and two batches of substrate solution made up as follows: catalyst **127** (8.4 mg, 0.015 mmol, 0.10 equiv.), $K_3PO_4$(aq) (0.101–3.54 M; 305 µL, 0.0310–1.08 mmol, 0.212–7.41 equiv.). **Substrate solutions:** substrate **125** (210.0 mg, 0.486 mmol), standard **133** (9.6 mg, 0.0499 mmol) in 3.0 mL, twice; corresponding to an added amount of **125** (63.0 mg, 0.146 mmol, 1.00 equiv.), **133** (2.9 mg, 0.0151 mmol, 0.104 equiv.) per reaction vial.

The reactions carried out in triplicate used the following conditions, described for one replicate only: catalyst **127** (8.4 mg, 0.015 mmol, 0.10 equiv.), $K_3PO_4$(aq) (4.77 M; 305 µL, 1.46 mmol, 10.0 equiv.). **Substrate solution:** substrate **125** (210.0 mg, 0.486 mmol), standard **133** (9.6 mg, 0.0499 mmol) in 3.0 mL; corresponding to an added amount of **125** (63.0 mg, 0.146 mmol, 1.00 equiv.), **133** (2.9 mg, 0.0151 mmol, 0.104 equiv.) per vial.

Full details of amounts are described in Table 7.4.

### 7.10.2 Data processing and analysis

The raw HPLC data were collected at 240 nm and 292 nm and were processed according to the methods detailed in 7.3.4 and 7.4.4. The plots of total substrate **125** and product **126** concentration over time were generated for each data set. The processed data were analysed using linear regression analysis of the rate of total product formation to give the initial rate ($k_{obs}$). The mean slope and error for each triplicate was calculated. The data are summarised in Table 7.4.

Reactions carried out with substoichiometric amounts of $K_3PO_4$ appeared to seize after approximately 250 min (reaction completion time is in excess of 3240 min), suggesting stoichiometric or excess amounts of base were required for the reaction to proceed completely. An example of the seized behaviour is in Figure 7.19.

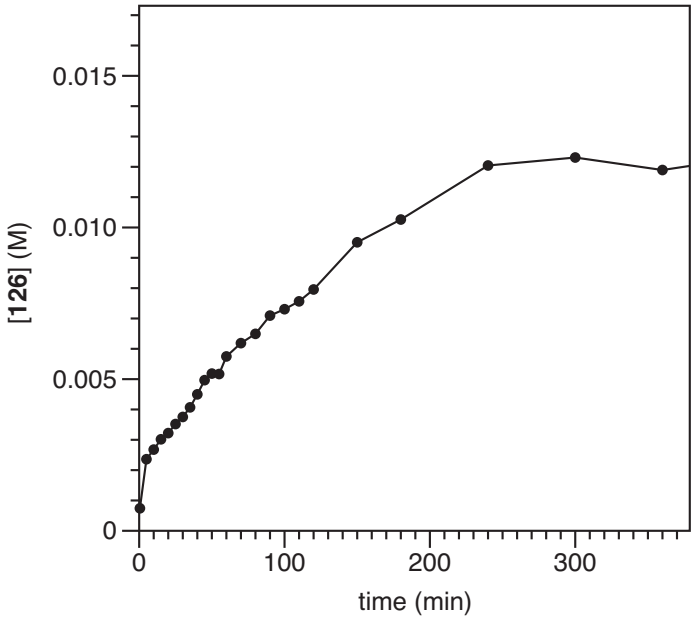



**Figure 7.19: Extended monitoring formation of product 126 using a substoichiometric amount of $K_3PO_4$.** Reaction conditions: catalyst **127** (8.4 mg, 0.015 mmol, 0.10 equiv.), $K_3PO_4$ (0.101 M; 305 µL, 0.0310 mmol, 0.212 equiv.) **125** (63.0 mg, 0.146 mmol, 1.00 equiv.), **133** (2.9 mg, 0.015 mmol, 0.10 equiv.), and standard reaction protocol. The line is a guide for the eye.

A double logarithmic plot of initial concentration of $K_3PO_4$ in the total reaction volume ($\ln [K_3PO_4]_0$) against the observed rate ($\ln k_{obs}$) was constructed to give a reaction order with respect to $K_3PO_4$ of $-0.020$ (Figure 7.20), with a 68% confidence interval of $-0.042$ to 0.0025.

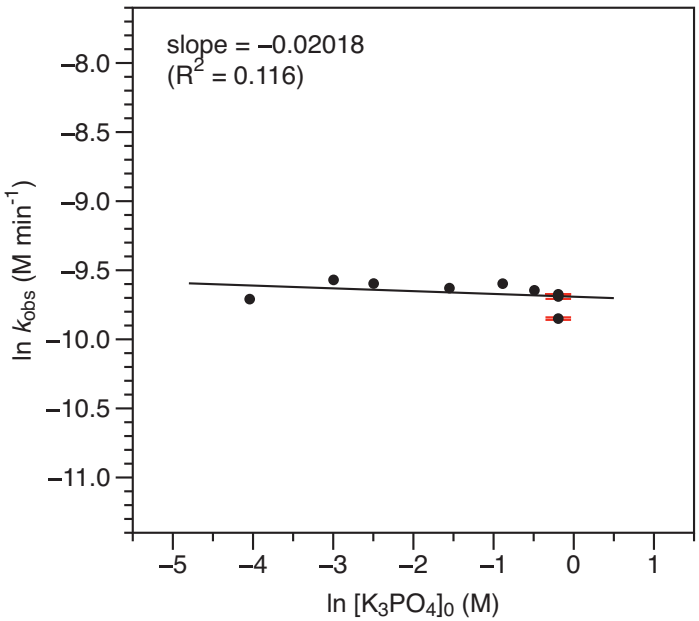


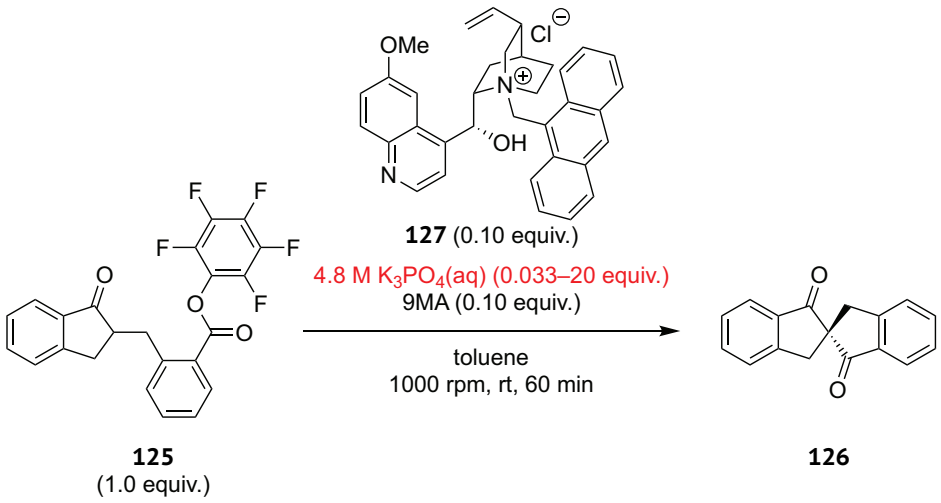

**Figure 7.20: Double logarithmic plot to determine the reaction order with respect to $K_3PO_4$ at constant aqueous volume.** The data are further summarised in Table 7.4.

**Table 7.4: Summary of results investigating the order in $K_3PO_4$ at constant volume.** The slopes to give the $k_{obs}$ were obtained by linear regression analysis of each data set.

| Entry | *rxn.code*[a] | Replicate (#) | $K_3PO_4$[b] (equiv.) | $[K_3PO_4(aq)]_0$[c] (M) | $[K_3PO_4]_0$[d] (M) | ln $[K_3PO_4]_0$[e] (M) | ln $k_{obs}$[f] (M $min^{-1}$) | mean ln $k_{obs}$[g] (M $min^{-1}$) | SD[h] (M $min^{-1}$) |
|---|---|---|---|---|---|---|---|---|---|
| 1 | spirok-31a | 1 | 0.21 equiv. | 0.102 | 0.0176 | −4.042 | −9.709 | −9.709 | N/A |
| 2 | spirok-31b | 1 | 0.61 equiv. | 0.289 | 0.0500 | −3.00 | −9.570 | −9.570 | N/A |
| 3 | spirok-31c | 1 | 1.0 equiv. | 0.477 | 0.0824 | −2.50 | −9.596 | −9.596 | N/A |
| 5 | spirok-30a | 1 | 2.6 equiv. | 1.23 | 0.212 | −1.55 | −9.629 | −9.629 | N/A |
| 6 | spirok-30b | 1 | 5.0 equiv. | 2.39 | 0.412 | −0.886 | −9.597 | −9.597 | N/A |
| 7 | spirok-30c | 1 | 7.4 equiv. | 3.54 | 0.612 | −0.491 | −9.709 | −9.709 | N/A |
| 8 | spirok-8 | 1 | 10 equiv. | 4.77 | 0.824 | −0.193 | −9.880 | | |
| 9 | spirok-8 | 2 | 10 equiv. | 4.77 | 0.824 | −0.193 | −9.842 | −9.853 | 0.020 |
| 10 | spirok-8 | 3 | 10 equiv. | 4.77 | 0.824 | −0.193 | −9.836 | | |
| 11 | spirok-18 | 1 | 10 equiv. | 4.77 | 0.824 | −0.193 | −9.675 | | |
| 12 | spirok-18 | 2 | 10 equiv. | 4.77 | 0.824 | −0.193 | −9.680 | −9.6571 | 0.0075 |
| 13 | spirok-18 | 3 | 10 equiv. | 4.77 | 0.824 | −0.193 | −9.667 | | |
| 14 | spirok-35 | 1 | 10 equiv. | 4.77 | 0.824 | −0.193 | −9.723 | | |
| 15 | spirok-35 | 2 | 10 equiv. | 4.77 | 0.824 | −0.193 | −9.670 | −9.687 | 0.026 |
| 16 | spirok-35 | 3 | 10 equiv. | 4.77 | 0.824 | −0.193 | −9.668 | | |

[a]*rxn.code* corresponds to the set of experiments used to obtain the data; [b]equivalents of $K_3PO_4$ used in the reaction with respect to substrate **125** (to 2 sf); [c]initial aqueous concentration of $K_3PO_4$; [d]initial concentration of $K_3PO_4$ using the combined volumes of the aqueous and organic layers; [e]natural logarithm of the initial concentration of $K_3PO_4$ using the combined volumes of the aqueous and organic layers (to 3 sf); [f]initial rate for the formation of total product **126** (both enantiomers) (to 4 sf); [g]mean of all replicate initial rates corresponding to the formation of total product **126** (both enantiomers) (to 4 sf or within the range of the standard deviation); [h]standard deviation (to 2 sf) of the initial rates corresponding to the formation of total product **126** (both enantiomers) of the specified data set replicates.

## 7.11 Evaluating the reaction order with respect to $K_3PO_4$ at constant aqueous concentration




### 7.11.1 General information and conditions

A series of reactions were carried out using the standard reaction protocol (see 7.4.1). The reactions varied only by the volume of aqueous $K_3PO_4$ (4.77 M) that was used in the reaction. Each experiment was carried out as a single reaction or in triplicate. All reactions were carried out with a reaction stirring speed of 1000 rpm. The equivalents (equiv.) are reported with respect to the amount of substrate **125**. All reactions were sampled using the sampling protocol (see 7.4.3). In each reaction, aliquots were extracted at 0.50 min after time zero, then at 5.0 min, then at 5.0 min intervals for a total of 60 min.

The single experiments were carried out using the conditions and the same substrate solution made up as follows: catalyst **127** (8.4 mg, 0.015 mmol, 0.10 equiv.), $K_3PO_4$(aq) (4.77 M; 45.8–91.6 µL, 0.218–0.437 mmol, 1.50–3.00 equiv.). **Substrate solution:** substrate **125** (210.0 mg, 0.486 mmol), standard **133** (9.6 mg, 0.0499 mmol) in 3.0 mL; corresponding to an added amount of **125** (63.0 mg, 0.146 mmol, 1.00 equiv.), **133** (2.9 mg, 0.015 mmol, 0.10 equiv.) per vial.

The reactions carried out in triplicate used the following conditions, described for one repli-

cate only: catalyst **127** (8.4 mg, 0.015 mmol, 0.10 equiv.), $K_3PO_4$(aq) (4.77 M; 1.00–611 µL, 0.00477–2.91 mmol, 0.0327–20.0 equiv.). **Substrate solution:** substrate **125** (210.0 mg, 0.486 mmol), standard **133** (9.6 mg, 0.050 mmol) in 3.0 mL; corresponding to an added amount of **125** (63.0 mg, 0.146 mmol, 1.00 equiv.), **133** (2.9 mg, 0.015 mmol, 0.10 equiv.) per vial.

Full details of amounts are described in Table 7.5.

**Table 7.5: Additional conditions investigating the reaction order with respect to 4.77 M $K_3PO_4$(aq).** Details are reported for added $K_3PO_4$ amounts of 0 to 23.0 µL. The details are continued in Table 7.6. Equivalents (equiv.) are reported with respect to substrate **125**.

| Entry | *rxn.code*[a] | Replicate (#) | $K_3PO_4$[b] (µL) | $K_3PO_4$[c] (equiv.) | $[K_3PO_4]_0$[d] (M) | ln $[K_3PO_4]_0$[e] (M) |
|---|---|---|---|---|---|---|
| 1 | spirok-46 | 1 | 0 | 0 | 0 | N/A |
| 2 | spirok-64 | 1 | 1.00 | 0.0327 | 0.00326 | −5.72 |
| 3 | spirok-64 | 2 | 1.00 | 0.0327 | 0.00326 | −5.72 |
| 4 | spirok-64 | 3 | 1.00 | 0.0327 | 0.00326 | −5.72 |
| 5 | spirok-65 | 1 | 2.00 | 0.0655 | 0.00652 | −5.03 |
| 6 | spirok-65 | 2 | 2.00 | 0.0655 | 0.00652 | −5.03 |
| 7 | spirok-65 | 3 | 2.00 | 0.0655 | 0.00652 | −5.03 |
| 8 | spirok-66 | 1 | 3.00 | 0.0982 | 0.00978 | −4.63 |
| 9 | spirok-66 | 2 | 3.00 | 0.0982 | 0.00978 | −4.63 |
| 10 | spirok-66 | 3 | 3.00 | 0.0982 | 0.00978 | −4.63 |
| 11 | spirok-67 | 1 | 4.50 | 0.147 | 0.015 | −4.22 |
| 12 | spirok-67 | 2 | 4.50 | 0.147 | 0.015 | −4.22 |
| 13 | spirok-67 | 3 | 4.50 | 0.147 | 0.015 | −4.22 |
| 14 | spirok-68 | 1 | 9.3 | 0.30 | 0.030 | −3.50 |
| 15 | spirok-68 | 2 | 9.3 | 0.30 | 0.030 | −3.50 |
| 16 | spirok-68 | 3 | 9.3 | 0.30 | 0.030 | −3.50 |
| 17 | spirok-53 | 1 | 15.4 | 0.504 | 0.0498 | −3.00 |
| 18 | spirok-53 | 2 | 15.4 | 0.504 | 0.0498 | −3.00 |
| 19 | spirok-53 | 3 | 15.4 | 0.504 | 0.0498 | −3.00 |
| 20 | spirok-54 | 1 | 23.0 | 0.753 | 0.0740 | −2.60 |
| 21 | spirok-54 | 2 | 23.0 | 0.753 | 0.0740 | −2.60 |
| 22 | spirok-54 | 3 | 23.0 | 0.753 | 0.0740 | −2.60 |

[a] *rxn.code* corresponds to the set of experiments used to obtain the data; [b] volume of aqueous $K_3PO_4$ (4.77 M) used in the reaction; [c] equivalents of $K_3PO_4$ used in the reaction with respect to substrate **125**; [d] initial concentration of $K_3PO_4$ using the combined volumes of the aqueous and organic layers; [e] natural logarithm of the initial concentration of $K_3PO_4$ using the combined volumes of the aqueous and organic layers.

**Table 7.6: Continued conditions investigating the reaction order with respect to 4.77 M $K_3PO_4$(aq).** Details are reported for added $K_3PO_4$ amounts of 30.5 to 611 µL. These details are continued from Table 7.5. Equivalents (equiv.) are reported with respect to substrate **125**

| Entry | *rxn.code*[a] | Replicate (#) | $K_3PO_4$[b] (µL) | $K_3PO_4$[c] (equiv.) | $[K_3PO_4]_0$[d] (M) | ln $[K_3PO_4]_0$[e] (M) |
|---|---|---|---|---|---|---|
| 23 | spirok-21 | 1 | 30.5 | 1.00 | 0.0976 | −2.33 |
| 24 | spirok-21 | 2 | 30.5 | 1.00 | 0.0976 | −2.33 |
| 25 | spirok-21 | 3 | 30.5 | 1.00 | 0.0976 | −2.33 |
| 26 | spirok-55a | 1 | 45.8 | 1.50 | 0.145 | −1.93 |
| 27 | spirok-55b | 1 | 61.0 | 2.00 | 0.191 | −1.65 |
| 28 | spirok-55c | 1 | 91.6 | 3.00 | 0.282 | −1.27 |
| 29 | spirok-22 | 1 | 155 | 5.07 | 0.458 | −0.781 |
| 30 | spirok-22 | 2 | 155 | 5.07 | 0.458 | −0.781 |
| 31 | spirok-22 | 3 | 155 | 5.07 | 0.458 | −0.781 |
| 32 | spirok-8 | 1 | 305 | 10.0 | 0.827 | −0.190 |
| 33 | spirok-8 | 2 | 305 | 10.0 | 0.827 | −0.190 |
| 34 | spirok-8 | 3 | 305 | 10.0 | 0.827 | −0.190 |
| 35 | spirok-18 | 1 | 305 | 10.0 | 0.827 | −0.190 |
| 36 | spirok-18 | 2 | 305 | 10.0 | 0.827 | −0.190 |
| 37 | spirok-18 | 3 | 305 | 10.0 | 0.827 | −0.190 |
| 38 | spirok-35 | 1 | 305 | 10.0 | 0.827 | −0.190 |
| 39 | spirok-35 | 2 | 305 | 10.0 | 0.827 | −0.190 |
| 40 | spirok-35 | 3 | 305 | 10.0 | 0.827 | −0.190 |
| 41 | spirok-23 | 1 | 611 | 20.0 | 1.41 | 0.342 |
| 42 | spirok-23 | 2 | 611 | 20.0 | 1.41 | 0.342 |
| 43 | spirok-23 | 3 | 611 | 20.0 | 1.41 | 0.342 |

[a]*rxn.code* corresponds to the set of experiments used to obtain the data; [b]volume of aqueous $K_3PO_4$ (4.77 M) used in the reaction; [c]equivalents of $K_3PO_4$ used in the reaction with respect to substrate **125**; [d]initial concentration of $K_3PO_4$ using the combined volumes of the aqueous and organic layers; [e]natural logarithm of the initial concentration of $K_3PO_4$ using the combined volumes of the aqueous and organic layers.

### 7.11.2 Data processing and analysis

The raw HPLC data were collected at 240 nm and 292 nm and were processed according to the method detailed in 7.3.4. The plots of total substrate **125** and product **126** concentration over time were generated for each data set. The processed data were analysed using linear regression analysis of the rate of total product formation to give the initial rate ($k_{obs}$). The mean slope and error for each triplicate was calculated. The data are summarised in Table 7.7 and Table 7.8.

A double logarithmic plot of initial concentration of $K_3PO_4$ in the total reaction volume (ln $[K_3PO_4]_0$) against the observed rate (ln $k_{obs}$) was constructed to give reaction orders with respect to $K_3PO_4$ (Figure 7.21). Two different orders were obtained from the plot; at low total $[K_3PO_4]_0$ (0.0033–0.050 M, 0.033–0.50 equiv.) an order of 0.52, with a 68% confidence interval of 0.43 to 0.61 was obtained, whilst at higher total $[K_3PO_4]_0$ (0.050–1.41 M, 0.50–20 equiv.) an order of −0.17, with a 68% confidence interval of −0.20 to −0.15 was obtained.

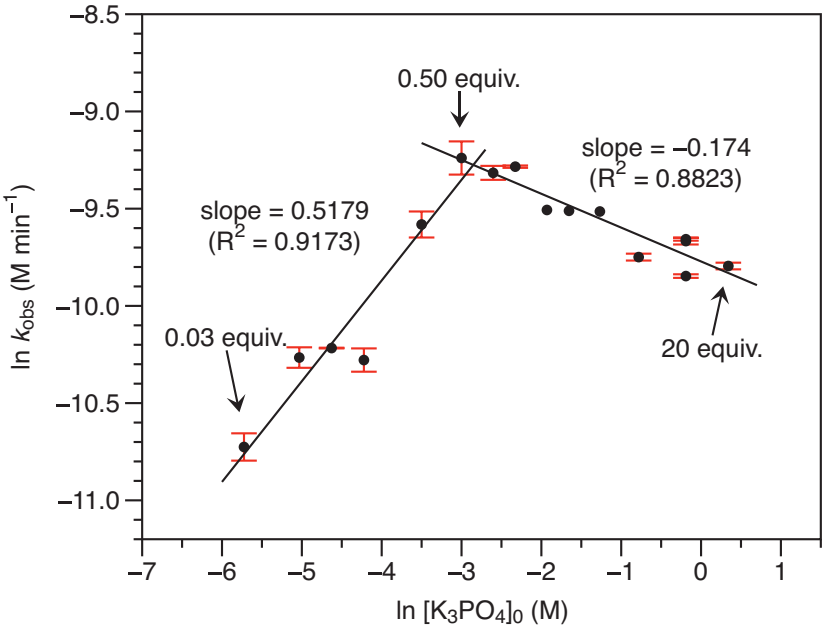



**Figure 7.21: Double logarithmic plot to determine the reaction order with respect to $K_3PO_4$ at constant aqueous concentration.** The data are further summarised in Table 7.7 and Table 7.8. Two regimes where observed in the plot. The lines are the slopes from linear regression analyses of the appropriate regime, which gave the reaction orders with respect to $K_3PO_4$ at low concentration and high concentration of 0.52 and −0.17, respectively.

**Table 7.7: Summary of results investigating the reaction order with respect to 4.77 M $K_3PO_4$(aq).** The slopes to give the $k_{obs}$ were obtained by linear regression analysis of each whole data set. The data are reported for ln $[K_3PO_4]_0$ concentrations of −5.72 to −2.33 and are continued in Table 7.8.

| Entry | *rxn.code*[a] | Replicate (#) | ln $[K_3PO_4]_0$[b] (M) | ln $k_{obs}$[c] (M min$^{-1}$) | mean ln $k_{obs}$[d] (M min$^{-1}$) | SD[e] (M min$^{-1}$) |
|---|---|---|---|---|---|---|
| 1 | spirok-46 | 1 | N/A | −10.22653 | −10.22653 | N/A |
| 2 | spirok-64 | 1 | −5.72 | −10.65 | | |
| 3 | spirok-64 | 2 | −5.72 | −10.82 | −10.725 | 0.069 |
| 4 | spirok-64 | 3 | −5.72 | −10.71 | | |
| 5 | spirok-65 | 1 | −5.03 | −10.20 | | |
| 6 | spirok-65 | 2 | −5.03 | −10.27 | −10.266 | 0.053 |
| 7 | spirok-65 | 3 | −5.03 | −10.33 | | |
| 8 | spirok-66 | 1 | −4.63 | −10.22 | | |
| 9 | spirok-66 | 2 | −4.63 | −10.22 | −10.2169 | 0.0018 |
| 10 | spirok-66 | 3 | −4.63 | −10.21 | | |
| 11 | spirok-67 | 1 | −4.22 | −10.36 | | |
| 12 | spirok-67 | 2 | −4.22 | −10.24 | −10.279 | 0.060 |
| 13 | spirok-67 | 3 | −4.22 | −10.23 | | |
| 14 | spirok-68 | 1 | −3.50 | −9.676 | | |
| 15 | spirok-68 | 2 | −3.50 | −9.527 | −9.581 | 0.067 |
| 16 | spirok-68 | 3 | −3.50 | −9.542 | | |
| 17 | spirok-53 | 1 | −3.00 | −9.581 | | |
| 18 | spirok-53 | 2 | −3.00 | −9.310 | −9.41 | 0.12 |
| 19 | spirok-53 | 3 | −3.00 | −9.346 | | |
| 20 | spirok-54 | 1 | −2.60 | −9.451 | | |
| 21 | spirok-54 | 2 | −2.60 | −9.461 | −9.423 | 0.046 |
| 22 | spirok-54 | 3 | −2.60 | −9.358 | | |
| 23 | spirok-21 | 1 | −2.33 | −9.368 | | |
| 24 | spirok-21 | 2 | −2.33 | −9.382 | −9.3708 | 0.0080 |
| 25 | spirok-21 | 3 | −2.33 | −9.363 | | |

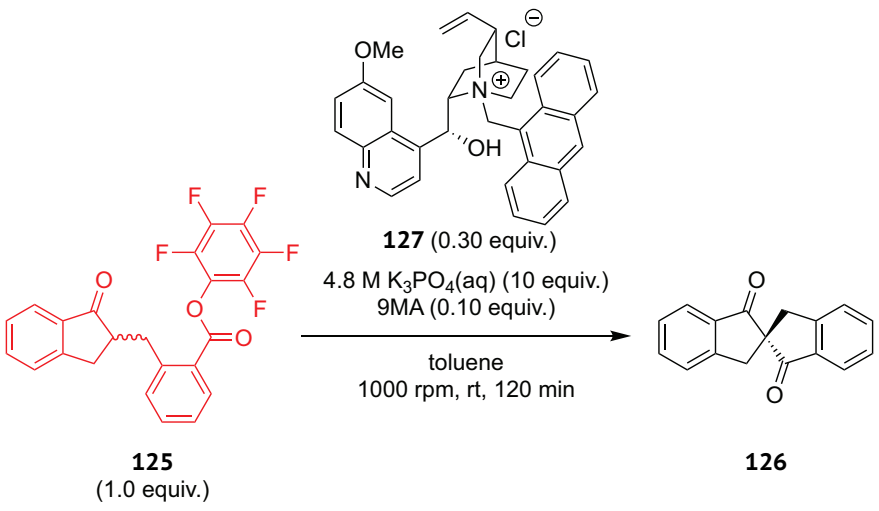
[a] *rxn.code* corresponds to the set of experiments used to obtain the data; [b] natural logarithm of the initial concentration of $K_3PO_4$ using the combined volumes of the aqueous and organic layers; [c] initial rate for the formation of total product **126** (both enantiomers) (to 4 sf); [d] mean of all replicate initial rates corresponding to the formation of total product **126** (both enantiomers); [e] standard deviation (to 2 sf) of the initial rates corresponding to the formation of total product **126** (both enantiomers) of the specified data set replicates.

**Table 7.8: Continued summary of results investigating the reaction order with respect to 4.77 M $K_3PO_4$(aq).** The slopes to give the $k_{obs}$ were obtained by linear regression analysis of each whole data set. The data are reported for ln $[K_3PO_4]_0$ concentrations of −1.93 to 0.342 and are continued from Table 7.7.

| Entry | *rxn.code*[a] | Replicate (#) | ln $[K_3PO_4]_0$[b] (M) | ln $k_{obs}$[c] (M min$^{-1}$) | mean ln $k_{obs}$[d] (M min$^{-1}$) | SD[e] (M min$^{-1}$) |
|---|---|---|---|---|---|---|
| 26 | spirok-55a | 1 | −1.93 | −9.587 | −9.59 | N/A |
| 27 | spirok-55b | 1 | −1.65 | −9.547 | −9.55 | N/A |
| 28 | spirok-55c | 1 | −1.27 | −9.532 | −9.53 | N/A |
| 29 | spirok-22 | 1 | −0.781 | −9.815 | | |
| 30 | spirok-22 | 2 | −0.781 | −9.756 | −9.762 | 0.041 |
| 31 | spirok-22 | 3 | −0.781 | −9.716 | | |
| 32 | spirok-8 | 1 | −0.190 | −9.880 | | |
| 33 | spirok-8 | 2 | −0.190 | −9.842 | −9.853 | 0.020 |
| 34 | spirok-8 | 3 | −0.190 | −9.836 | | |
| 35 | spirok-18 | 1 | −0.190 | −9.675 | | |
| 36 | spirok-18 | 2 | −0.190 | −9.680 | −9.6571 | 0.0075 |
| 37 | spirok-18 | 3 | −0.190 | −9.667 | | |
| 38 | spirok-35 | 1 | −0.190 | −9.723 | | |
| 39 | spirok-35 | 2 | −0.190 | −9.670 | −9.687 | 0.026 |
| 40 | spirok-35 | 3 | −0.190 | −9.668 | | |
| 41 | spirok-23 | 1 | 0.342 | −9.807 | | |
| 42 | spirok-23 | 2 | 0.342 | −9.788 | −9.806 | 0.014 |
| 43 | spirok-23 | 3 | 0.342 | −9.823 | | |

[a]*rxn.code* corresponds to the set of experiments used to obtain the data; [b]natural logarithm of the initial concentration of $K_3PO_4$ using the combined volumes of the aqueous and organic layers; [c]initial rate for the formation of total product **126** (both enantiomers) (to 4 sf); [d]mean of all replicate initial rates corresponding to the formation of total product **126** (both enantiomers); [e]standard deviation (to 2 sf) of the initial rates corresponding to the formation of total product **126** (both enantiomers) of the specified data set replicates.

## 7.12 Evaluating the effect of enantioenriched substrates



### 7.12.1 General information

Three reactions were carried out using a version of the modified reaction protocol (see 7.4.2). The reactions varied by the enantioenrichment of substrate used: either racemic **125**, (−)-**125** (98% ee), or (+)-**125** (94% ee). Each experiment was carried out as a single reaction. All reactions were carried out with a reaction stirring speed of 1000 rpm. The equivalents (equiv.) are reported with respect to the amount of substrate **125**. All reactions were sampled using the sampling protocol (see 7.4.3). In each reaction, aliquots were extracted at 0.50 min after time zero, then at regular intervals for a total of 120 min.

The reactions were performed in 7 mL screw cap vials ($\varnothing$ = 1.5 cm), using short stirrer bars (11818892, 8 × 3 mm obtained from Fisher Scientific).

### 7.12.2 Reaction protocol and conditions

Compound **125**, (−)-**125**, or (+)-**125** (50 mg, 0.12 mmol, 1.0 equiv.) was added to a vial, before **133** (2.2 mg, 0.011 mmol, 0.10 equiv.), **127** (19.1 mg, 0.0347 mmol, 0.300 equiv.), and a stirrer bar were added. Toluene (2 × 580 µL) was introduced by washing down the sides of the vial. The mixture was stirred at 1000 rpm (stroboscope) for 15 min, before $K_3PO_4$ (4.77 M; 242 µL, 1.15 mmol, 9.87 equiv.) was added to initiate the reaction at the designated time zero.

### 7.12.3 Data processing and analysis

The raw HPLC data were collected at 240 nm and 292 nm and were processed according to the methods detailed in 7.3.4 and 7.4.4. Concentration data were unobtainable due to the unknown total reaction volume. Due to the variations in the mmol data acquired (Figure 7.22), presumably due to the physical nature of the enantioenriched samples, analyses were performed

on the normalised conversion data (taken as mmol of substrate over the total mmol of substrate and product). The plots of conversion over time were generated (Figure 7.23). The slopes of the two rate-determining regimes ($k_{1\text{obs}}$ and $k_{2\text{obs}}$) were obtained by linear regression analysis of the data; the results were comparable due to the zeroth order dependence of the $k_{\text{obs}}$ on the concentration of substrate **125** (see 7.9).

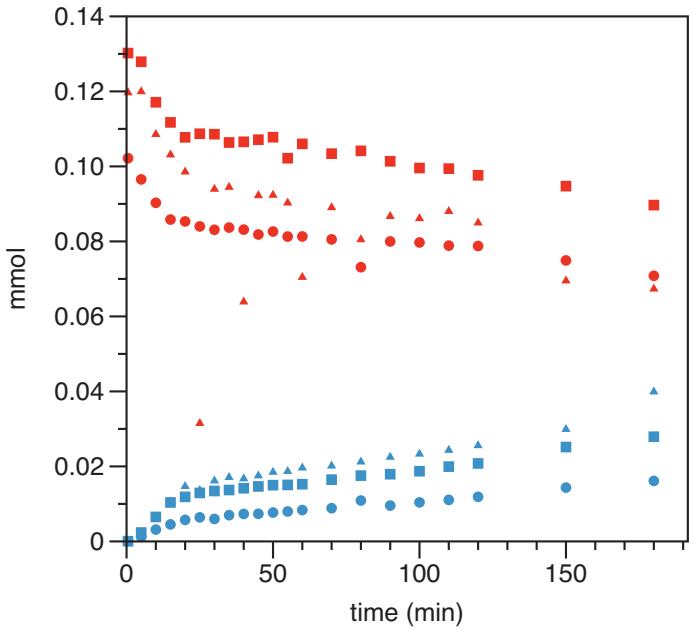



**Figure 7.22: Data obtained when subjecting the substrates to the modified reaction conditions. Substrate is in red and product 126 is in blue.** The substrate in each reaction (red) was either racemic **125** (squares), (−)-**125** (circles), and (+)-**125** (triangles).

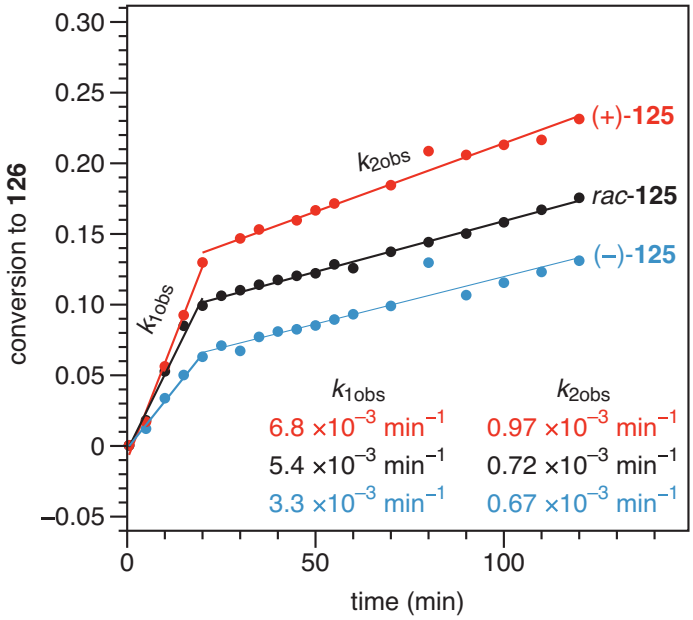
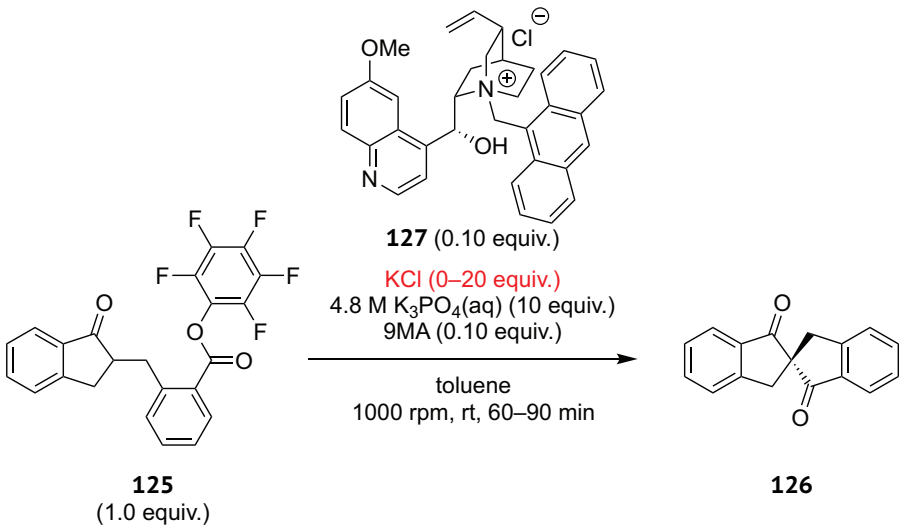



**Figure 7.23: Conversion to product 126 data when subjecting racemic 125 (black), (−)-125 (blue), and (+)-125 (red) to the reaction conditions.** The $k_{1obs}$ and $k_{2obs}$ values were obtained by linear regression analyses of both rate-limiting regimes in each data set. The measured values are depicted on the graph and are colour-coded.

## 7.13 Evaluating the effect of added KCl




### 7.13.1 General information and conditions

A series of reactions were carried out using a variation of the standard reaction protocol (see 7.4.1). The reactions varied only by the amount of solid KCl that was added to the reaction. Each experiment was carried out as single experiments. All reactions were carried out with a

reaction stirring speed of 1000 rpm. The equivalents (equiv.) are reported with respect to the amount of substrate **125**. All reactions were sampled using the sampling protocol (see 7.4.3). In each reaction, aliquots were extracted at 0.50 min after time zero, then at 5.0 min, then at 5.0 min intervals for a total of 60 min.

Solid KCl was added to the reaction vial following the addition of catalyst **127** but prior to the addition of toluene. The single experiments were carried out using the conditions and the same substrate solution made up as follows: catalyst **127** (8.4 mg, 0.015 mmol, 0.10 equiv.), KCl (10.7–217 mg, 0.144–2.92 mmol, 0.98–20 equiv.), $K_3PO_4$(aq) (4.77 M; 305 µL, 1.45 mmol, 9.98 equiv.). **Substrate solution:** substrate **125** (210.0 mg, 0.486 mmol), standard **133** (9.6 mg, 0.050 mmol) in 3.0 mL; corresponding to an added amount of **125** (63.0 mg, 0.146 mmol, 1.00 equiv.), **133** (2.9 mg, 0.0151 mmol, 0.104 equiv.) per vial.

The reactions carried out in triplicate used the following conditions, described for one replicate only: catalyst **127** (8.4 mg, 0.015 mmol, 0.10 equiv.), $K_3PO_4$(aq) (4.77 M; 305 µL, 1.46 mmol, 10.0 equiv.). **Substrate solution:** substrate **125** (210.0 mg, 0.486 mmol), standard **133** (9.6 mg, 0.050 mmol) in 3.0 mL; corresponding to an added amount of **125** (63.0 mg, 0.146 mmol, 1.00 equiv.), **133** (2.9 mg, 0.015 mmol, 0.10 equiv.) per reaction vial.

Full details of amounts are described in Table 7.9.

### 7.13.2 Data processing and analysis

The raw HPLC data were collected at 240 nm and 292 nm and were processed according to the methods detailed in 7.3.4 and 7.4.4. The plots of total substrate **125** and product **126** concentration over time were generated. The processed data were analysed using linear regression analysis of the rate of total product formation to give the initial rate ($k_{obs}$). The data are summarised in Table 7.9.

A plot of initial KCl concentration ($[KCl]_0$) against the observed rate ($k_{obs}$) was constructed

to give an indication of the effect of added KCl on the rate of the reaction (Figure 7.24). A double logarithmic plot of initial concentration of KCl (ln $[KCl]_0$) against the observed rate (ln $k_{obs}$) was constructed to give a reaction order with respect to KCl of 0.0043 (Figure 7.25), with a 68% confidence interval of −0.073 to 0.081.

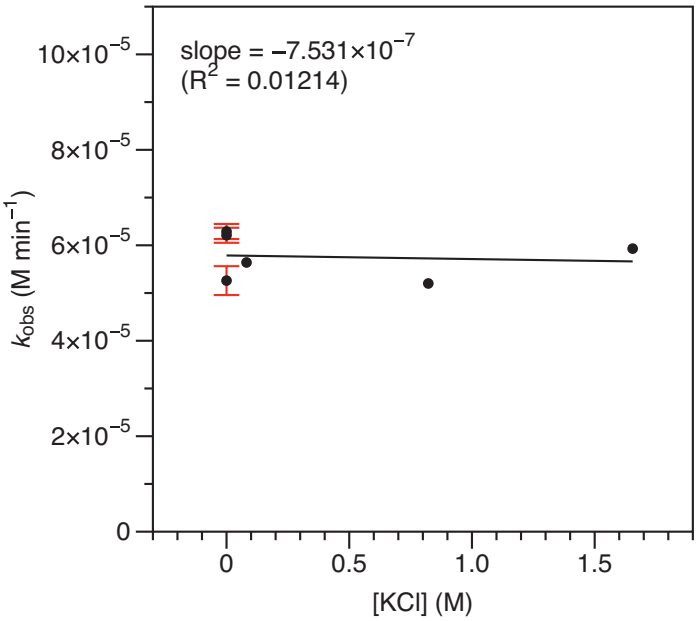



**Figure 7.24: Plot to determine the effect of added KCl on the observed reaction rate ($k_{obs}$).** The volume contribution of solid KCl was considered to be negligible.

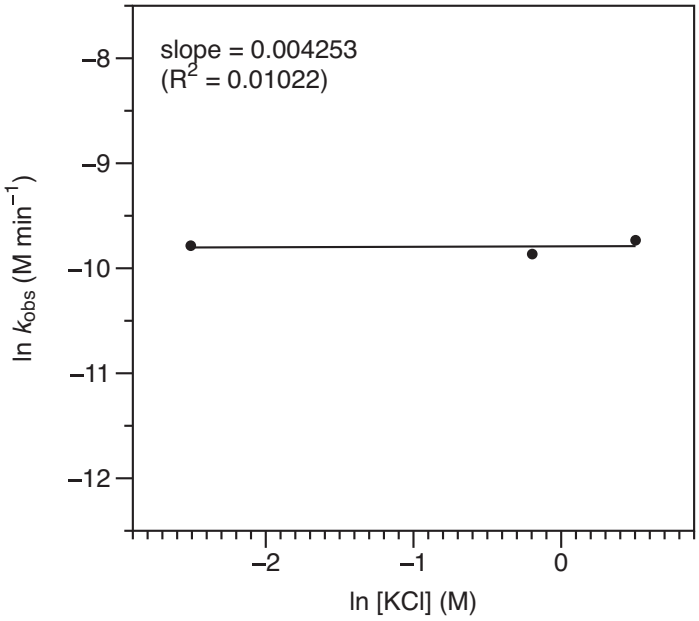


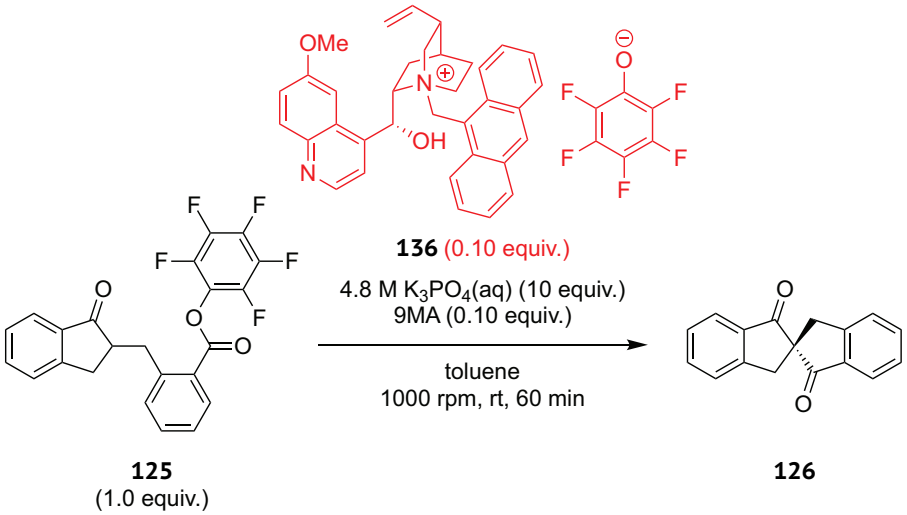

**Figure 7.25: Double logarithmic plot to determine the reaction order with respect to added KCl.** The volume contribution of solid KCl was considered to be negligible.

**Table 7.9: Summary of results investigating the effect of added KCl.** The volume contribution of solid KCl was considered to be negligible. The slopes to give the $k_{obs}$ were obtained by linear regression analysis of each whole data set.

| Entry | *rxn.code*[a] | Replicate (#) | KCl[b] (mg) | $[KCl]_0$[c] (M) | ln $[KCl]_0$[d] (M) | KCl[e] (equiv.) | ln $k_{obs}$[f] ($M\ min^{-1}$) | mean ln $k_{obs}$[g] ($M\ min^{-1}$) | SD[h] ($M\ min^{-1}$) |
|---|---|---|---|---|---|---|---|---|---|
| 7 | spirok-8 | 1 | 0 | 0 | 0 | 0 | −9.880 | | |
| 8 | spirok-8 | 2 | 0 | 0 | 0 | 0 | −9.842 | −9.853 | 0.020 |
| 9 | spirok-8 | 3 | 0 | 0 | 0 | 0 | −9.836 | | |
| 10 | spirok-18 | 1 | 0 | 0 | 0 | 0 | −9.675 | | |
| 11 | spirok-18 | 2 | 0 | 0 | 0 | 0 | −9.680 | −9.6571 | 0.0075 |
| 12 | spirok-18 | 3 | 0 | 0 | 0 | 0 | −9.667 | | |
| 13 | spirok-35 | 1 | 0 | 0 | 0 | 0 | −9.723 | | |
| 14 | spirok-35 | 2 | 0 | 0 | 0 | 0 | −9.670 | −9.687 | 0.026 |
| 15 | spirok-35 | 3 | 0 | 0 | 0 | 0 | −9.668 | | |
| 16 | spirok-32a | 1 | 10.7 | 0.0814 | −2.51 | 0.985 | −9.7850 | −9.7850 | N/A |
| 16 | spirok-32b | 1 | 108.0 | 0.822 | −0.196 | 9.94 | −9.8649 | −9.8649 | N/A |
| 16 | spirok-32c | 1 | 217 | 1.65 | 0.504 | 20.0 | −9.7332 | −9.7332 | N/A |

[a]*rxn.code* corresponds to the set of experiments used to obtain the data; [b]amount of KCl added to the reaction in mg; [c]initial concentration of KCl using the combined volumes of the aqueous and organic layers (contribution of solid KCl was considered to be negligible); [d]natural logarithm of the initial concentration of KCl using the combined volumes of the aqueous and organic layers; [e]equivalents of KCl added with respect to substrate **125**; [f]natural logarithm of the initial rate for the formation of total product **126** (both enantiomers) (to 4 sf); [g]mean of all replicate initial rates corresponding to the formation of total product **126** (both enantiomers); [h]standard deviation (to 2 sf) of the initial rates corresponding to the formation of total product **126** (both enantiomers) of the specified data set replicates.

## 7.14 Evaluating the ammonium phenolate catalyst



### 7.14.1 General information and conditions

A series of reactions were carried out using the modified reaction protocol (see 7.4.2). Each reaction was carried out independently to give one triplicate experiment set. All reactions were carried out with a reaction stirring speed of 1000 rpm. The equivalents (equiv.) are reported with respect to the amount of substrate **125**. All reactions were sampled using the sampling protocol (see 7.4.3). In each reaction, aliquots were extracted at 0.50 min after time zero, then at 5.0 min, then at 5.0 min intervals for a total of 60 min.

The reactions used the following conditions: catalyst **136** (10.6 mg, 0.015 mmol, 0.10 equiv.), $K_3PO_4$(aq) (4.77 M; 305 µL, 1.46 mmol, 10.0 equiv.). **Substrate solution:** substrate **125** (70.0 mg, 0.162 mmol), standard **133** (3.2 mg, 0.0166 mmol) in 1.0 mL; corresponding to an added amount of **125** (63.0 mg, 0.146 mmol, 1.00 equiv.), **133** (2.9 mg, 0.0151 mmol, 0.104 equiv.) per reaction.

Additionally, two reactions were carried out using versions of the standard reaction protocol (see 7.4.1) to investigate the effect of pre-stirring on **136** as the starting catalyst. The conditions were analogous to those described above. One reaction was carried out strictly according to the standard reaction protocol, the second, was stirred for an additional 2 h at 1000 rpm before initiation by the addition of substrate **125** (purple data in Figure 7.29).

### 7.14.2 Data processing and analysis

The raw HPLC data were collected at 240 nm and 292 nm and were processed according to the method detailed in 7.3.4. The plots of total substrate **125** and product **126** concentration over time were generated for each data set (Figure 7.26). The processed data were analysed using linear regression analysis of the rate of total product formation to give the initial rate ($k_{obs}$) (Figure 7.27). The mean slope and error for the triplicate was calculated. The data are

summarised in Table 7.10; data acquired using the catalyst **127** under analogous conditions are provided for comparison (Figure 7.28). To evaluate the general rate effects exhibited by different starting catalysts under different reaction protocols, an overlay of selected data sets was constructed (Figure 7.29).

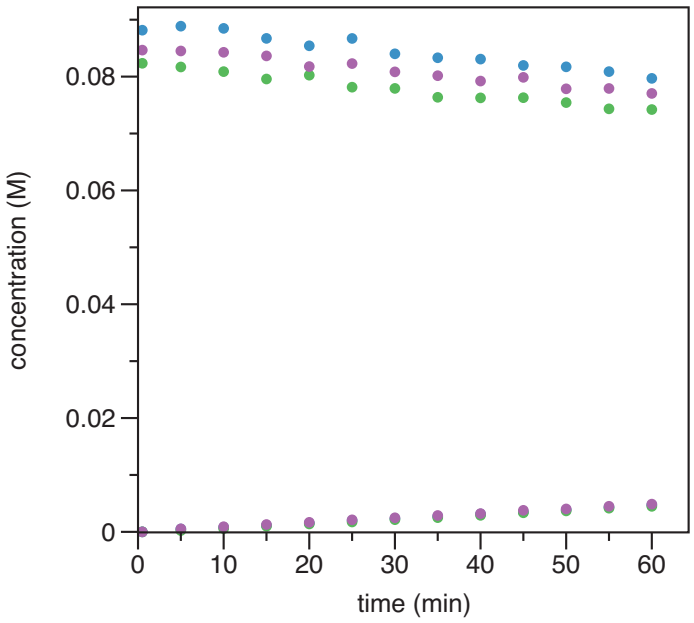



**Figure 7.26: Full results obtained when evaluating the effect of starting catalyst 136 using the modified reaction protocol.** The upper dots (above 0.02 M) correspond to the total substrate concentration ((−)-**125** and (+)-**125**) over time, the lower dots (below 0.02 M) correspond to the product concentration ((*R*)-**126** and (*S*)-**126**) over time. The colours correspond to the different individual reactions within the triplicate set.

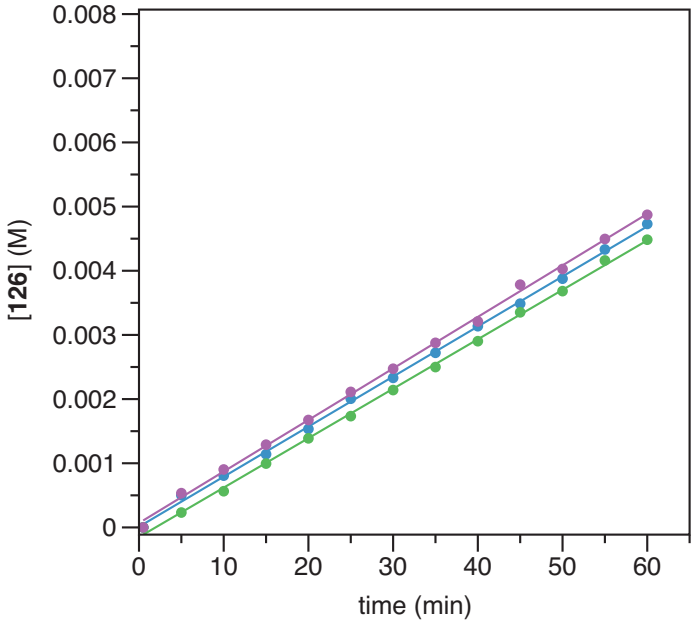



**Figure 7.27: Overlay of product 126 concentration over time for all reactions investigating the effect of starting catalyst 136 using the modified reaction protocol.** The lines correspond to linear regression analysis of each reaction. The colours correspond to the different individual reactions within the triplicate set.

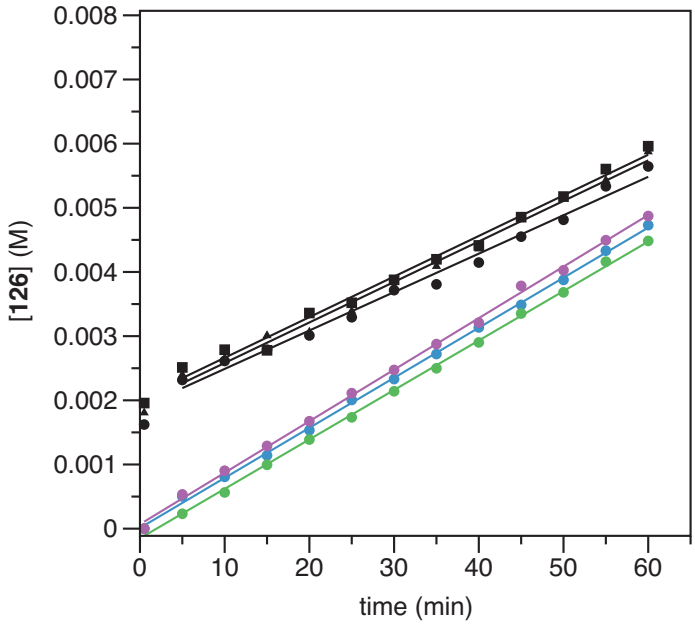



**Figure 7.28: Comparison of triplicate data obtained when using the chloride catalyst 127 (black data) compared to the triplicate data obtained when using the phenolate catalyst 136 (blue, green, and purple data).** The lines are linear regression analyses of the corresponding data sets. The average slopes of the two data sets were as follows: $6.21\times10^{-5}$ M min$^{-1}$ for catalyst **127** (black data), and $7.71\times10^{-5}$ M min$^{-1}$ for catalyst **136** (coloured data).

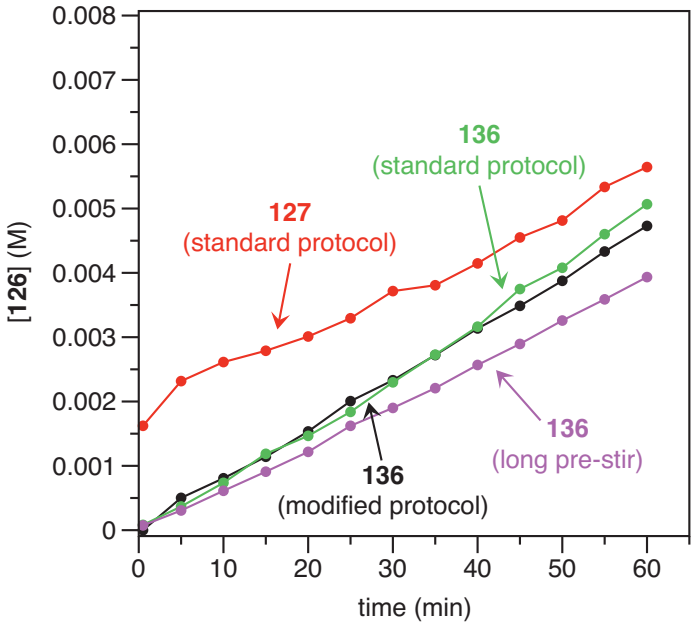


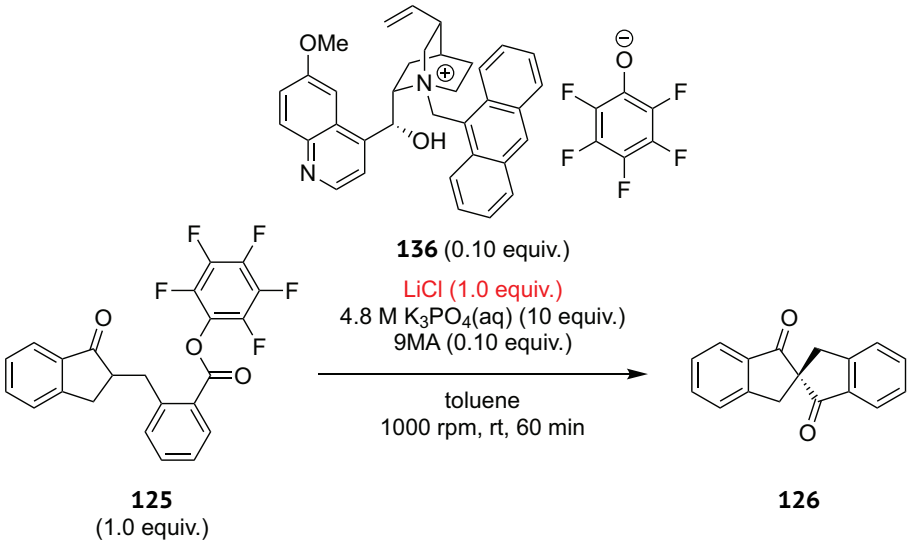

**Figure 7.29: Examples of rate behaviour exhibited when using different starting catalysts (either 127 or 136) and reaction protocols used (either standard, modified, or with extended pre-stirring).** The reaction sets corresponding to the displayed data are as follows: catalyst **127** with the standard reaction protocol (red data), catalyst **136** with the standard reaction protocol (green data), catalyst **136** with the modified reaction protocol (black data), catalyst **136** with the extended standard reaction protocol (purple data). The data sets selected were from the following reaction codes (*rxn.code*): spirok-35 replicate 1 (red data), spirok-44 (green data), spirok-40 replicate 1 (black data), spirok-63 (purple data). The lines are guides for the eye.

**Table 7.10: Summary of data comparing kinetic behaviour of reaction when using either catalyst 127 or catalyst 136.** The slopes to give the $k_{obs}$ were obtained by linear regression analysis of each whole data set.

| Entry | *rxn.code*[a] | Replicate (#) | catalyst[b] | $k_{obs}$[c] (M min$^{-1}$) | mean $k_{obs}$[d] (M min$^{-1}$) | SD[e] (M min$^{-1}$) | ln $k_{obs}$[f] (M min$^{-1}$) | mean ln $k_{obs}$[g] (M min$^{-1}$) | SD[h] (M min$^{-1}$) |
|---|---|---|---|---|---|---|---|---|---|
| 1 | spirok-35 | 1 | **127** | $5.987 \times 10^{-5}$ | | | −9.723 | | |
| 2 | spirok-35 | 2 | **127** | $6.314 \times 10^{-5}$ | $6.21 \times 10^{-5}$ | $0.16 \times 10^{-5}$ | −9.670 | −9.687 | 0.026 |
| 3 | spirok-35 | 3 | **127** | $6.328 \times 10^{-5}$ | | | −9.668 | | |
| 4 | spirok-40 | 1 | **136** | $7.775 \times 10^{-5}$ | | | −9.462 | | |
| 5 | spirok-41 | 2 | **136** | $7.706 \times 10^{-5}$ | $7.708 \times 10^{-5}$ | $0.055 \times 10^{-5}$ | −9.471 | -9.4707 | 0.0071 |
| 6 | spirok-42 | 3 | **136** | $7.641 \times 10^{-5}$ | | | −9.480 | | |
| 7 | spirok-44 | 1 | **136** | $8.427 \times 10^{-5}$ | $8.427 \times 10^{-5}$ | N/A | −9.381 | −9.381 | N/A |
| 8 | spirok-63 | 1 | **136** | $6.550 \times 10^{-5}$ | $6.550 \times 10^{-5}$ | N/A | −9.633 | −9.633 | N/A |

[a]*rxn.code* corresponds to the set of experiments used to obtain the data; [b]identity of the catalyst used in the reaction; [c]initial rate for the formation of total product **126** (both enantiomers); [d]mean of the observed initial rate for the formation of product **126** (both enantiomers); [e]standard deviation (to 2 sf) of the initial rates corresponding to the formation of total product **126** (both enantiomers) of the specified data set replicates; [f]natural logarithm of the observed initial rate for the formation of product **126** (both enantiomers) (to 4 sf); [g]mean of the natural logarithm of the observed initial rate for the formation of product **126** (both enantiomers); [h]standard deviation (to 2 sf) of the logarithms of the initial rates corresponding to the formation of total product **126** (both enantiomers) of the specified data set replicates.

## 7.15 Evaluating the effect of LiCl with the ammonium phenolate catalyst




### 7.15.1 General information and conditions

Due to the increased organosolubility of catalyst **136** and given the lack of effect when deploying KCl as an additive previously (see 3.10.1), LiCl was selected as a more organosoluble source of chloride for this experiment. A reaction was carried out using a variation of the standard reaction protocol (see 7.4.1) using conditions described below. The result was then compared to results obtained previously under control conditions, i.e. in the absence of LiCl with catalyst **127** or **136**. The experiment was carried out as a single reaction with a stirring speed of 1000 rpm. The equivalents (equiv.) are reported with respect to the amount of substrate **125**. The reaction was sampled using the sampling protocol (see 7.4.3).

Solid LiCl was added following the addition of catalyst **136** but prior to the addition of toluene. The single experiment was carried out using the conditions and substrate solution made up as follows: catalyst **136** (10.6 mg, 0.015 mmol, 0.10 equiv.), LiCl (6.2 mg, 0.15 mmol, 1.0 equiv.), $K_3PO_4$(aq) (4.77 M; 305 µL, 1.45 mmol, 9.98 equiv.). **Substrate solution:** substrate **125** (70.0 mg, 0.162 mmol), standard **133** (3.2 mg, 0.017 mmol) in 1.0 mL; corresponding to an added amount of **125** (63.0 mg, 0.146 mmol, 1.00 equiv.), and **133** (2.9 mg, 0.15 mmol,

0.10 equiv.).

### 7.15.2 Data processing and analysis

The raw HPLC data were collected at 240 nm and 292 nm and were processed according to the methods detailed in 7.3.4 and 7.4.4. The plot of total product **126** concentration over time was generated and compared to the previously obtained results. The processed data were analysed using linear regression analysis of the rate of total product formation to give the initial rate ($k_{obs}$) (Figure 7.30). The reaction with catalyst **136** carried out in the presence of LiCl (blue data) showed a decrease in rate compared to the corresponding reaction carried out in the absence of LiCl (black data), and showed a rate comparable to the reaction carried out with the chloride catalyst **127** (red data).

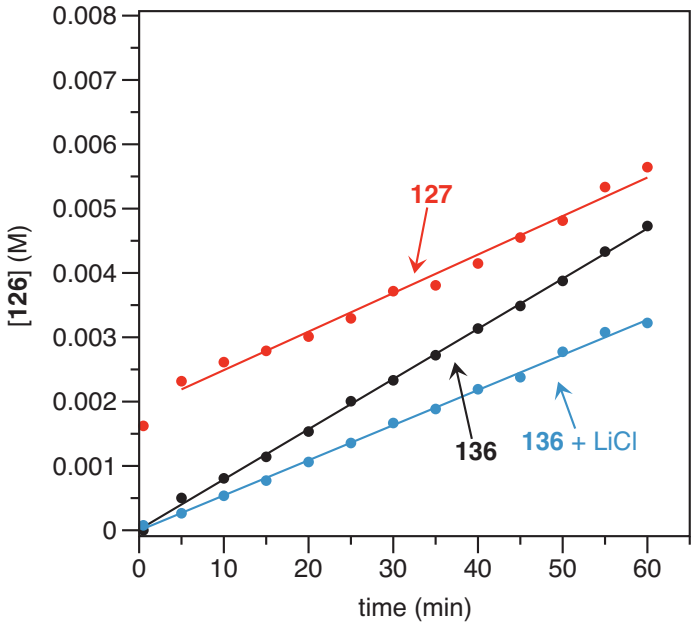
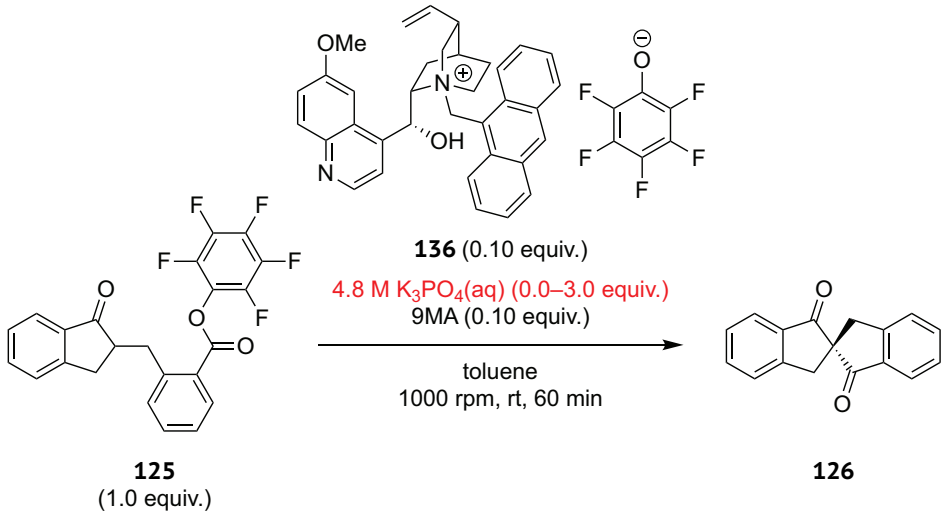



**Figure 7.30: Evaluating the effect of chloride in the reaction system.** The $x$-axis corresponds to time in min following initiation of the reaction. The $y$-axis corresponds to the concentration of product **126** in M. The red data corresponds to the analogous reaction carried out in the absence of added chloride and with catalyst **127** and is provided for comparison. The black data corresponds to the analogous reaction carried out in the absence of added chloride with catalyst **136** and is provided for comparison. The blue data corresponds to the presently described reaction: added LiCl in the system starting from catalyst **136**. The lines are linear regression analysis of the corresponding coloured data sets, to give the slopes as the initial rates ($k_{obs}$) as follows: $5.99 \times 10^{-5}$ M min$^{-1}$ (red), $7.80 \times 10^{-5}$ M min$^{-1}$ (black), and $5.46 \times 10^{-5}$ M min$^{-1}$ (blue).

## 7.16 Evaluating the effect of base with the ammonium phenolate catalyst




### 7.16.1 General information and conditions

A series of reactions were carried out using the modified reaction protocol (see 7.4.2). The reactions varied only by the volume of aqueous $K_3PO_4$ (4.77 M) that was used in the reaction. Each experiment was carried out as single reactions. All reactions were carried out with a reaction stirring speed of 1000 rpm. The equivalents (equiv.) are reported with respect to the amount of substrate **125**. All reactions were sampled using the sampling protocol (see 7.4.3). In each reaction, aliquots were extracted at 0.50 min after time zero, then at 5.0 min, then at 5.0 min intervals for a total of 60 min.

The reactions used the following conditions: catalyst **136** (10.6 mg, 0.015 mmol, 0.10 equiv.), $K_3PO_4$(aq) (4.77 M; 15.0–91.8 µL, 0.0716–0.438 mmol, 0.490–3.00 equiv.). **Substrate solution:** substrate **125** (70.0 mg, 0.162 mmol), standard **133** (3.2 mg, 0.0166 mmol) in 1.0 mL; corresponding to an added amount of **125** (63.0 mg, 0.146 mmol, 1.00 equiv.), **133** (2.9 mg, 0.015 mmol, 0.10 equiv.) per reaction.

### 7.16.2 Data processing and analysis

The raw HPLC data were collected at 240 nm and 292 nm and were processed according to the methods detailed in 7.3.4 and 7.4.4. The plots of total product **126** concentration over time were generated for each data set; the processed data were analysed using linear regression analysis of the rate of total product formation to give the initial rate ($k_{obs}$) (Figure 7.31). The data are summarised in Figure 7.31 and Table 7.11.

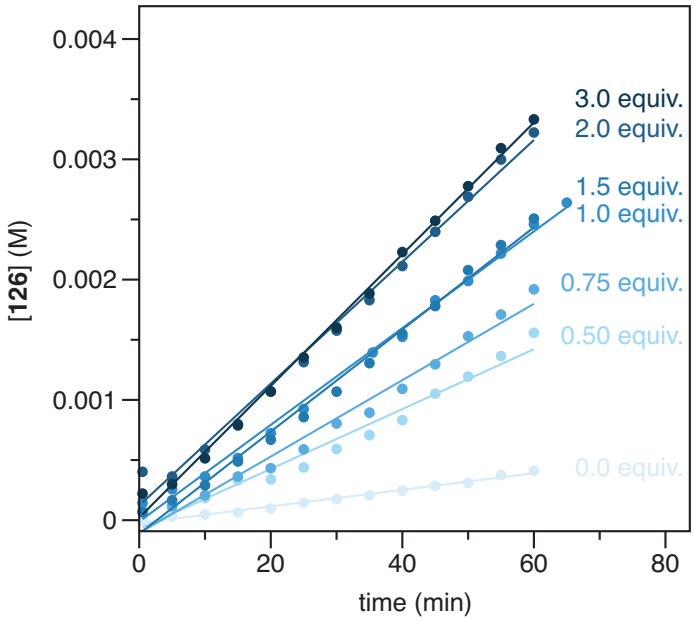



**Figure 7.31: Overlay of product 126 concentration over time for all reactions investigating the effect of $K_3PO_4$ concentration on the reaction effected by starting catalyst 136.** The lines correspond to linear regression analysis of each replicate. The colours correspond to the different initial $K_3PO_4$ concentrations; equivalents (equiv.) with respect to substrate **125** are indicated on the graph.

A double logarithmic plot of initial concentration of $K_3PO_4$ in the total reaction volume (ln $[K_3PO_4]_0$) against the observed rate (ln $k_{obs}$) was constructed to give a reaction order with respect to $K_3PO_4$ of 0.45 (Figure 7.32), with a 68% confidence interval of 0.384 to 0.518.

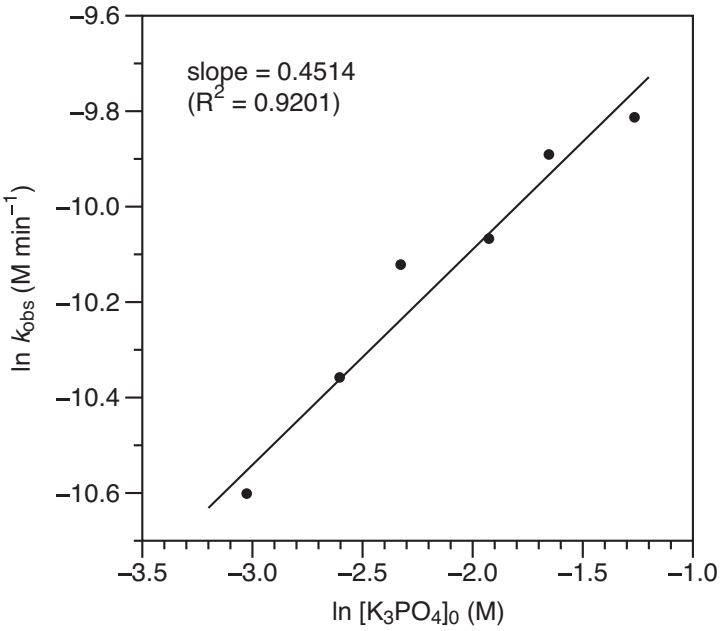


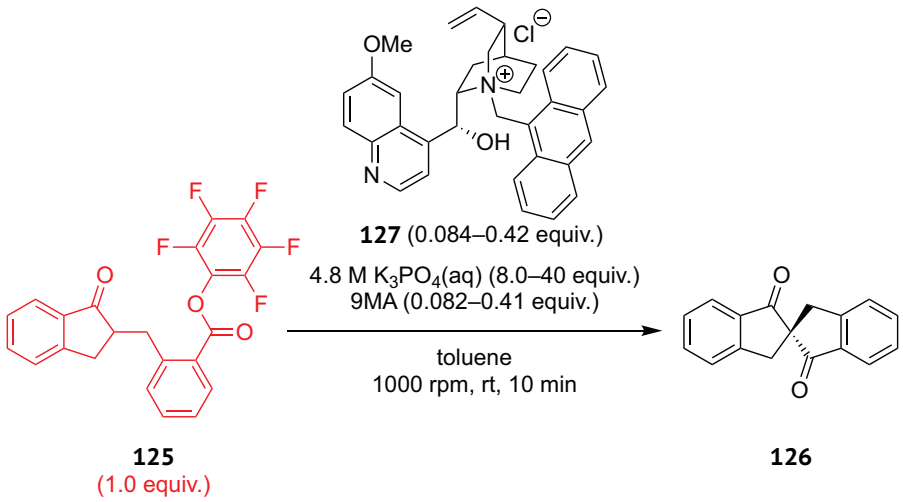

**Figure 7.32: Double logarithmic plot to determine the reaction order with respect to $K_3PO_4$ in reaction systems starting with catalyst 136.** The line corresponds to linear regression analysis of the whole data set to give the slope and $K_3PO_4$ order of 0.45.

**Table 7.11: Summary of results investigating the order in $K_3PO_4$ when using catalyst 136.** The slopes to give the $k_{obs}$ were obtained by linear regression analysis of each whole data set.

| Entry | *rxn.code*[a] | $K_3PO_4$[b] (µL) | $K_3PO_4$[c] (equiv.) | $[K_3PO_4]_0$[d] (M) | ln $[K_3PO_4]_0$[e] (M) | ln $k_{obs}$[f] (M min$^{-1}$) |
|---|---|---|---|---|---|---|
| 1 | spirok-47 | 15.0 | 0.490 | 0.0485 | −3.03 | −10.60 |
| 1 | spirok-49 | 23.0 | 0.752 | 0.0740 | −2.60 | −10.36 |
| 1 | spirok-48 | 30.5 | 1.00 | 0.0976 | −2.33 | −10.12 |
| 1 | spirok-51 | 46.0 | 1.50 | 0.146 | −1.93 | −10.07 |
| 1 | spirok-50 | 61.0 | 1.99 | 0.191 | −1.65 | −9.891 |
| 1 | spirok-52 | 91.8 | 3.00 | 0.282 | −1.27 | −9.813 |

[a] *rxn.code* corresponds to the set of experiments used to obtain the data; [b] volume of aqueous $K_3PO_4$ (4.77 M) used in the reaction; [c] equivalents of $K_3PO_4$ used in the reaction with respect to substrate **125**; [d] initial concentration of $K_3PO_4$ using the combined volumes of the aqueous and organic layers; [e] natural logarithm of the initial concentration of $K_3PO_4$ using the combined volumes of the aqueous and organic layers; [f] initial rate for the formation of total product **126** (both enantiomers)(given to 4 sf).

## 7.17 Reaction order with respect to substrate during the burst phase




### 7.17.1 General information and conditions

A series of reactions were carried out using the modified reaction protocol (see 7.4.2). The reactions varied only by the amount of substrate **125** that was used in the reaction. Each experiment was carried out as triplicate reactions. All reactions were carried out with a reaction stirring speed of 1000 rpm. The equivalents (equiv.) are reported with respect to the amount of substrate **125**. All reactions were sampled using the sampling protocol (see 7.4.3). In each reaction, aliquots were extracted at 0.50 min after time zero, then at 1.0 min, then at 1.0 min intervals for a total of 10 min.

The reactions used the following conditions, described for one replicate only: catalyst **127** (8.4 mg, 0.015 mmol, 0.42–0.10 equiv.), $K_3PO_4$(aq) (4.77 M; 305 µL, 1.46 mmol, 40–10 equiv.). **Substrate solution:** substrate **125** (52.6–209.3 mg, 0.122–0.484 mmol), standard **133** (9.6 mg, 0.050 mmol) in 3.0 mL; corresponding to an added amount of **125** (15.8–62.8 mg, 0.0365–0.145 mmol, 1.00 equiv.), **133** (2.9 mg, 0.015 mmol, 0.41–0.10 equiv.) per reaction vial.

Full details of amounts are described in Table 7.12.

### 7.17.2 Data processing and analysis

The raw HPLC data were collected at 240 nm and 292 nm and were processed according to the methods detailed in 7.3.4 and 7.4.4. The plots of total substrate **125** and product **126** concentration over time were generated (Figure 7.33). The data were analysed using linear regression analysis of the rate of total product formation during the burst phase only (0.5 to 4.0 min following initiation of the reaction) to give the initial rate ($k_{obs}$) (Figure 7.34). The mean slope and error for each triplicate was calculated. The data are summarised in Table 7.12.

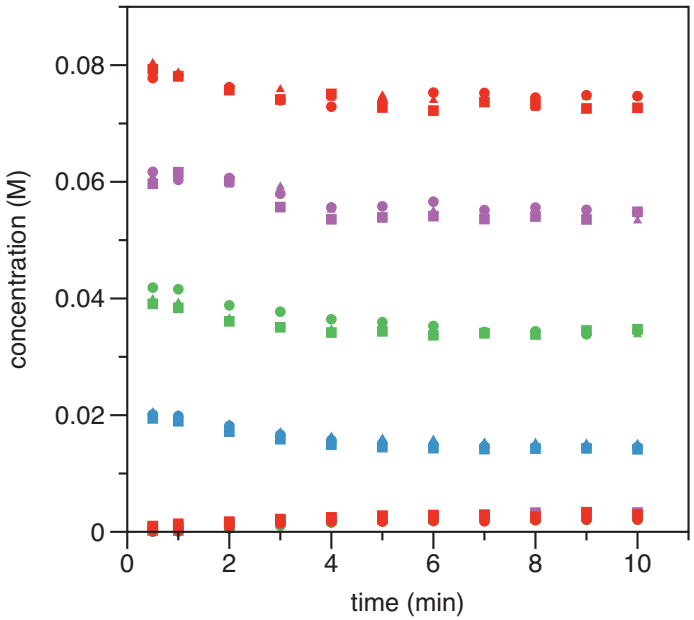



**Figure 7.33: Overlay of all reactions investigating the order in substrate 125 under modified reaction conditions and during the burst phase.** The upper dots (above 0.01 M) correspond to the total substrate concentration ((−)-**125** and (+)-**125**) over time, the lower dots (below 0.01 M) correspond to the product concentration ((*R*)-**126** and (*S*)-**126**) over time. The colours correspond to the different initial substrate **125** concentrations: 0.0207 M (blue), 0.0412 M (green), 0.0620 M (purple), 0.0823 M (red). Circles, triangles and squares correspond to triplicate runs.

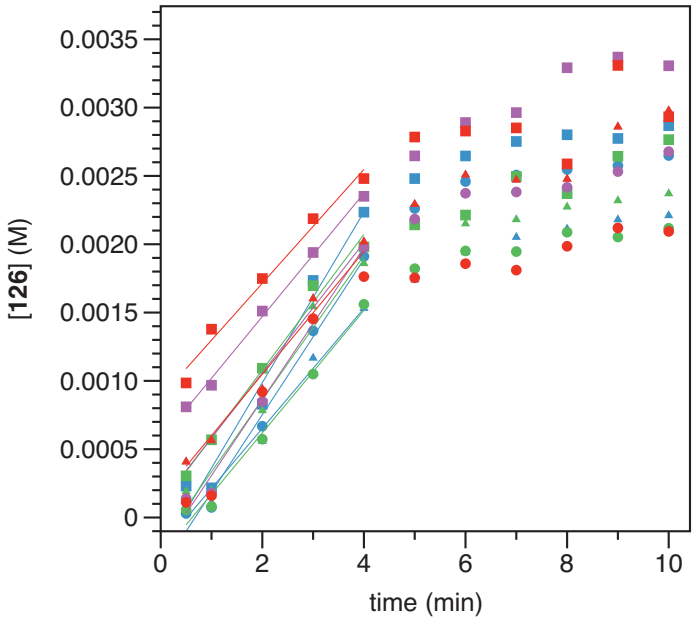



**Figure 7.34: Overlay of product 126 concentration over time for all reactions investigating the effect of substrate 125 concentration under modified reaction conditions and during the burst phase.** The lines correspond to linear regression analysis of the first 4.0 min of each reaction. The colours correspond to the different initial substrate **125** concentrations: 0.0207 M (blue), 0.0412 M (green), 0.0620 M (purple), 0.0823 M (red). Circles, triangles and squares correspond to triplicate runs.

A double logarithmic plot of initial concentration of substrate **125** (ln $[\mathbf{125}]_0$) against the observed rate (ln $k_{obs}$) was constructed to give a reaction order with respect to substrate of −0.10 (Figure 7.35), with a 68% confidence interval of −0.13 to −0.074.

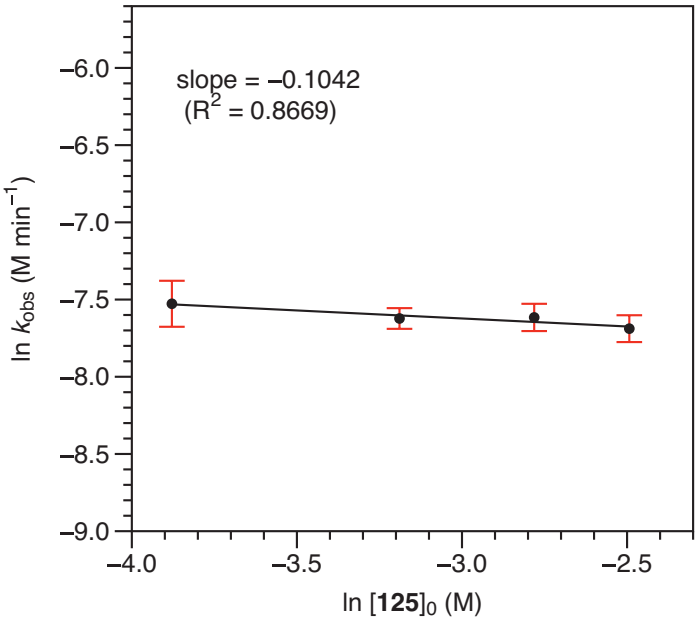


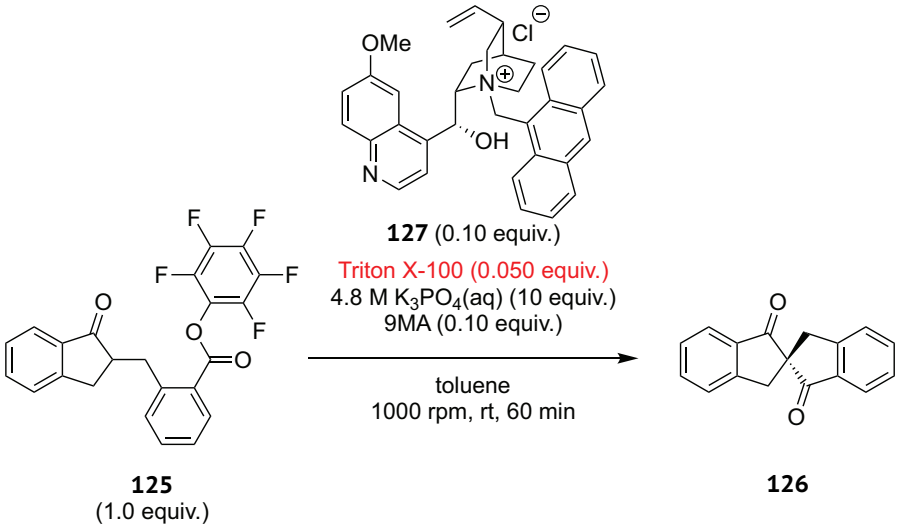

**Figure 7.35: Double logarithmic plot to determine the reaction order with respect to substrate 125 under modified reaction conditions and during the burst phase.** The line corresponds to linear regression analysis of the whole data set to give the slope and substrate order of −0.10.

**Table 7.12: Summary of results investigating the order in substrate 125 under modified reaction conditions and during the burst phase.** Specific details of the reaction conditions are described. The slopes to give the $k_{obs}$ were obtained by linear regression analysis of the first 4 min of each data set before the ln $k_{obs}$ was calculated.

| Entry | *rxn.code*[a] | Replicate (#) | $[125]_0$[b] (M) | ln $[125]_0$[c] (M) | 127 loading[d] | $K_3PO_4$ loading[e] | ln $k_{obs}$[f] (M min$^{-1}$) | mean ln $k_{obs}$[g] (M min$^{-1}$) | SD[h] (M min$^{-1}$) |
|---|---|---|---|---|---|---|---|---|---|
| 1 | spirok-74 | 1 | 0.0207 | −3.88 | 0.42 equiv. | 40 equiv. | −7.472 | | |
| 2 | spirok-74 | 2 | 0.0207 | −3.88 | 0.42 equiv. | 40 equiv. | −7.731 | −7.53 | 0.15 |
| 3 | spirok-74 | 3 | 0.0207 | −3.88 | 0.42 equiv. | 40 equiv. | −7.379 | | |
| 4 | spirok-75 | 1 | 0.0412 | −3.19 | 0.21 equiv. | 21 equiv. | −7.711 | | |
| 5 | spirok-75 | 2 | 0.0412 | −3.19 | 0.21 equiv. | 21 equiv. | −7.548 | −7.623 | 0.067 |
| 6 | spirok-75 | 3 | 0.0412 | −3.19 | 0.21 equiv. | 21 equiv. | −7.609 | | |
| 7 | spirok-76 | 1 | 0.0620 | −2.78 | 0.14 equiv. | 14 equiv. | −7.495 | | |
| 8 | spirok-76 | 2 | 0.0620 | −2.78 | 0.14 equiv. | 14 equiv. | −7.649 | −7.616 | 0.088 |
| 9 | spirok-76 | 3 | 0.0620 | −2.78 | 0.14 equiv. | 14 equiv. | −7.704 | | |
| 10 | spirok-77 | 1 | 0.0823 | −2.49 | 0.10 equiv. | 10 equiv. | −7.574 | | |
| 11 | spirok-77 | 2 | 0.0823 | −2.49 | 0.10 equiv. | 10 equiv. | −7.708 | −7.688 | 0.087 |
| 12 | spirok-77 | 3 | 0.0823 | −2.49 | 0.10 equiv. | 10 equiv. | −7.784 | | |

[a]*rxn.code* corresponds to the set of experiments used to obtain the data; [b]initial substrate **125** concentration using the combined volumes of the aqueous and organic layers; [c]natural logarithm of the initial substrate **125** concentration using the combined volumes of the aqueous and organic layers; [d]initial loading of catalyst **127** with respect to substrate **125** (to 2 sf); [e]initial equivalents of $K_3PO_4$ with respect to substrate **125** (to 2 sf); [f]natural logarithm of the initial rate of formation of total product **126** (both enantiomers); [g]mean of natural logarithm of the initial rate of formation of total product **126** (both enantiomers) of all replicates; [h]standard deviation (to 2 sf) of the initial rates corresponding to the formation of total product **126** (both enantiomers) of the specified data set replicates.

## 7.18 Evaluating the effect of added surfactant




### 7.18.1 General information and conditions

A reaction was carried out using a variation of the modified reaction protocol (see 7.4.2) using conditions described below. The result was then compared to that obtained previously under control conditions, i.e. in the absence of surfactant. The experiment was carried out as a single reaction with a stirring speed of 1000 rpm. The equivalents (equiv.) are reported with respect to the amount of substrate **125**. The reaction was sampled using the sampling protocol (see 7.4.3). For reference, the reaction codes (*rxn.code*) corresponding to the test (with Triton X-100) and control (without Triton X-100) reactions were spirok-70 and spirok-36, respectively.

Triton X-100 was introduced following the addition of catalyst **127** and toluene to the reaction vial. The single experiment was carried out using the conditions and substrate solution made up as follows: catalyst **127** (8.4 mg, 0.015 mmol, 0.10 equiv.), Triton X-100 (4.40 µL, 0.00729 mmol, 0.05 equiv.), $K_3PO_4$(aq) (4.77 M; 305 µL, 1.45 mmol, 9.98 equiv.). **Substrate solution:** substrate **125** (70.0 mg, 0.162 mmol), standard **133** (3.2 mg, 0.017 mmol) in 1.0 mL; corresponding to an added amount of **125** (63.0 mg, 0.146 mmol, 1.00 equiv.), and **133** (2.9 mg, 0.15 mmol, 0.10 equiv.).

### 7.18.2 Data processing and analysis

The raw HPLC data were collected at 240 nm and 292 nm and were processed according to the methods detailed in 7.3.4 and 7.4.4. The plot of total product **126** concentration over time was generated and compared to the previously obtained results (Figure 7.36). The processed data were analysed using linear regression analyses of the two rate-determining regimes to obtain the slopes, which corresponded to the observed rates for each regime ($k_{1obs}$ and $k_{2obs}$). When observing the burst phase (first regime described by $k_{1obs}$), the reaction carried out in the presence of Triton X-100 (red data) showed no appreciable difference to the reaction carried out in the absence of Triton X-100 (blue data). A slight increase in the observed rate of the normal regime ($k_{2obs}$) was exhibited in the reaction carried out in the presence of Triton X-100.

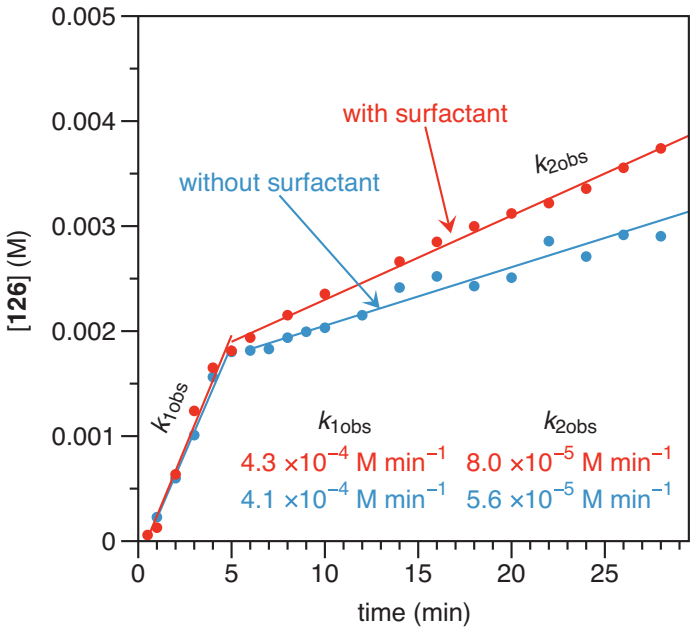
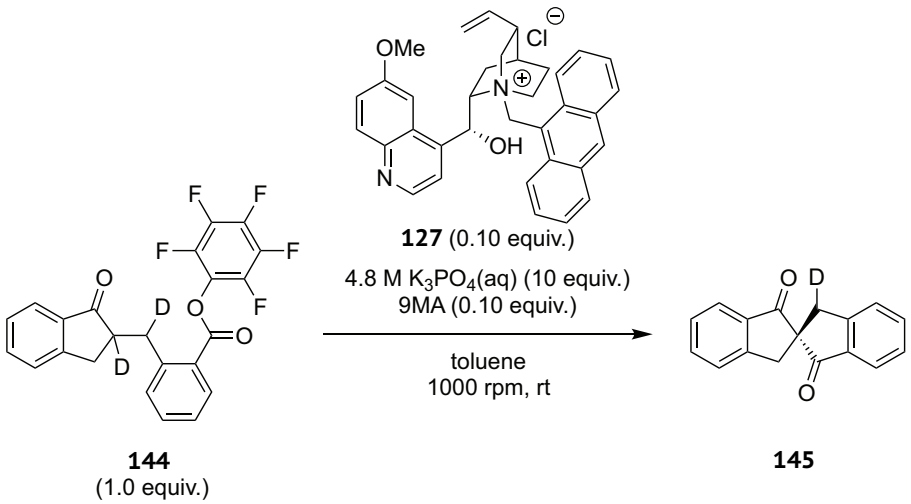



**Figure 7.36: Evaluating the effect of added surfactant (Triton X-100) to the burst phase in reactions carried out using the modified reaction protocol.** The observed rates for each rate-limiting regime ($k_{1obs}$ and $k_{2obs}$) are described on the graph and are colour-coded. Blue data corresponds to the reaction in the absence of surfactant, red data corresponds to the reaction carried out with surfactant.

## 7.19 Evaluating the effect of deuterated substrate




### 7.19.1 General information

A series of reactions were carried out using either the standard reaction protocol (see 7.4.1) or the modified reaction protocol (see 7.4.2). The reactions varied by the identity of the substrate used—either substrate **125** or deuterated substrate **144**—and the protocol employed. All reactions were carried out with a reaction stirring speed of 1000 rpm. The equivalents (equiv.) are reported with respect to the amount of substrate, **125** or **144**. Aliquots were extracted from the reactions over time and analysed according to the sampling protocol (see 7.4.3). Reactions carried out using the standard reaction protocol were carried out as triplicate experiments. Those carried out according to the modified reaction protocol were conducted as single experiments. The whole experiment will be described by dividing into sections according to the protocol that was employed.

### 7.19.2 Reactions carried out using the standard reaction protocol

The reaction codes (*rxn.code*) for these experiments were designated "spirok-35" and "spirok-38" for the reactions that used substrates **125** and **144**, respectively.

### Conditions

The reactions were carried out in triplicate and used the following conditions, described for one replicate only: catalyst **127** (8.4 mg, 0.015 mmol, 0.10 equiv.), $K_3PO_4$(aq) (4.77 M; 305 µL, 1.46 mmol, 10.0 equiv.). **Substrate solution:** substrate **125** (210.0 mg, 0.486 mmol) or deuterated substrate **144** (210.4 mg, 0.486 mmol), standard **133** (9.6 mg, 0.0499 mmol) in 3.0 mL; corresponding to an added amount of **125** (63.0 mg, 0.146 mmol, 1.00 equiv.) or **144** (63.1 mg, 0.146 mmol, 1.00 equiv.), **133** (2.9 mg, 0.0151 mmol, 0.104 equiv.) per reaction vial.

### Data processing and analysis

The reaction system that gave product **145** from deuterated substrate **144** behaved identically to the non-deuterated system by HPLC. As such, the raw HPLC data were collected at 240 nm and 292 nm and were processed according to the method detailed in 7.3.4. The plots of total product concentration over time were generated (Figure 7.37). The processed data were analysed using linear regression analysis of the rate of total product formation to give the initial rates ($k_{obs}$). The mean slope and error for each triplicate was calculated. The data are summarised in Table 7.13.

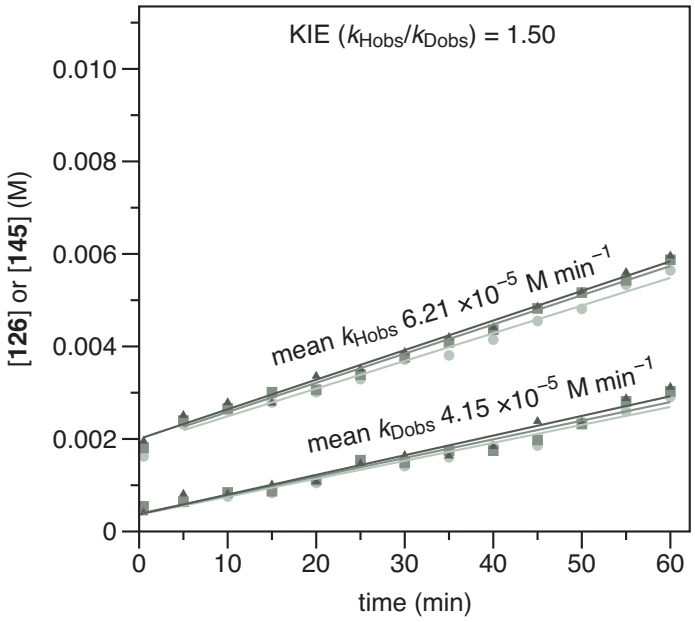



**Figure 7.37: Overlay of data obtained from the hydrogenated and deuterated reaction systems using the standard reaction protocol.** The light grey circles, grey squares, and dark grey triangles correspond to individual reactions within the two triplicate sets. The lines correspond to linear regression analyses of each reaction and are indicated by the location and colour of the line. The mean rates of reaction obtained for the hydrogenated ($k_{\mathrm{Hobs}}$) and deuterated ($k_{\mathrm{Dobs}}$) systems are indicated on the graphs. The calculated KIE based on these mean rates was 1.50 to 3 sf.

**Table 7.13: Summary of results evaluating the reaction using either substrate 125 or deuterated substrate 144 under the standard reaction protocol.** Product in these reactions corresponds to either **126** or **145**, depending on which substrate was deployed.

| **Entry** | ***rxn.code*[a]** | **Replicate (#)** | **substrate** | $k_{obs}$[b] (M min$^{-1}$) | **mean** $k_{obs}$[c] (M min$^{-1}$) | **SD**[d] (M min$^{-1}$) | **ln** $k_{obs}$[e] (M min$^{-1}$) | **mean ln** $k_{obs}$[f] (M min$^{-1}$) | **SD**[g] (M min$^{-1}$) |
|---|---|---|---|---|---|---|---|---|---|
| 1 | spirok-35 | 1 | **125** | $5.987 \times 10^{-5}$ | | | -9.723 | | |
| 2 | spirok-35 | 2 | **125** | $6.314 \times 10^{-5}$ | $6.210 \times 10^{-5}$ | $0.16 \times 10^{-5}$ | -9.670 | -9.687 | 0.026 |
| 3 | spirok-35 | 3 | **125** | $6.328 \times 10^{-5}$ | | | -9.668 | | |
| 4 | spirok-38 | 1 | **144** | $4.022 \times 10^{-5}$ | | | -10.12 | | |
| 5 | spirok-38 | 2 | **144** | $4.153 \times 10^{-5}$ | $4.146 \times 10^{-5}$ | $0.098 \times 10^{-5}$ | -10.09 | -10.09 | 0.024 |
| 6 | spirok-38 | 3 | **144** | $4.263 \times 10^{-5}$ | | | -10.06 | | |

[a]*rxn.code* corresponds to the set of experiments used to obtain the data; [b]the observed initial rate in M min$^{-1}$ of each reaction corresponding to the formation of total product; [c]mean of all replicate initial rates corresponding to the formation of total product; [d]standard deviation (to 2 sf) of the corresponding $k_{obs}$; [e]natural logarithm of the initial rate of the formation of total product (to 4 sf); [f]mean of all replicate initial rates (as the natural logarithms) corresponding to the formation of total product; [g]standard deviation (to 2 sf) of the initial rates (as the natural logarithms) corresponding to the formation of total product.

The temporal ee plots of the products **126** and **145** were generated (Figure 7.38 and Figure 7.39).

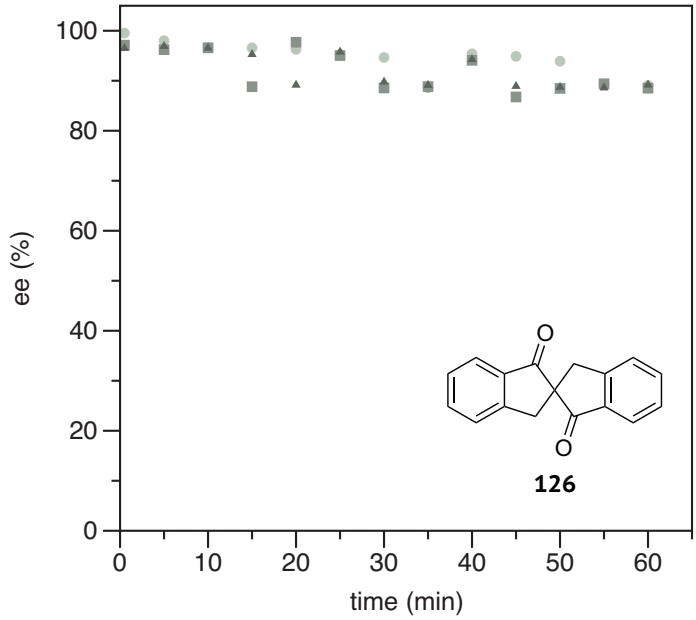



**Figure 7.38: Enantiomeric excess of the product 126 over time.** The reaction was commenced from substrate **125** and carried out using the standard reaction protocol. The light grey circles, grey squares, and dark grey triangles correspond to individual reactions within the triplicate set.

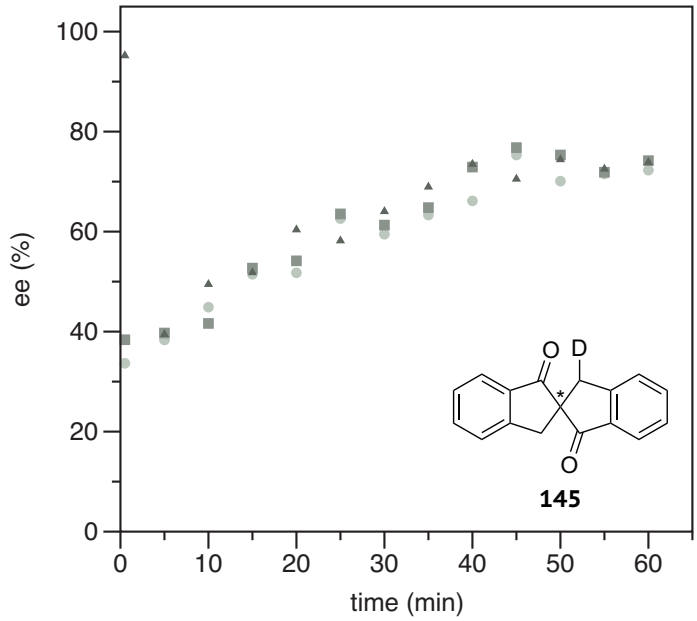



**Figure 7.39: Enantiomeric excess of the deuterated product 145 over time.** The reaction was commenced from substrate **144** and carried out using the standard reaction protocol. The light grey circles, grey squares, and dark grey triangles correspond to individual reactions within the triplicate set.

### 7.19.3 Reactions carried out using the modified reaction protocol

The reaction codes (*rxn.code*) for these experiments were designated "spirok-36" and "spirok-39" for the reactions that used substrates **125** and **144**, respectively.

#### Conditions

The reactions were carried out as single experiments and used the following conditions, described for one replicate only: catalyst **127** (8.4 mg, 0.015 mmol, 0.10 equiv.), $K_3PO_4$(aq) (4.77 M; 305 µL, 1.46 mmol, 10.0 equiv.). **Substrate solution:** substrate **125** (70.0 mg, 0.162 mmol) or deuterated substrate **144** (70.1 mg, 0.162 mmol), standard **133** (3.2 mg, 0.017 mmol) in 1.0 mL; corresponding to an added amount of **125** (63.0 mg, 0.146 mmol, 1.00 equiv.) or **144** (63.1 mg, 0.146 mmol, 1.00 equiv.), **133** (2.9 mg, 0.0151 mmol, 0.104 equiv.) per reaction vial.

#### Data processing and analysis

The raw HPLC data were collected at 240 nm and 292 nm and were processed according to the method detailed in 7.3.4. The plots of total product concentration over time were generated (Figure 7.40). The processed data were analysed using linear regression analyses of the two rate-determining regimes to obtain the slopes, which corresponded to the observed rates for each regime ($k_{1\mathrm{Hobs}}$ or $k_{1\mathrm{Dobs}}$ and $k_{2\mathrm{Hobs}}$ or $k_{2\mathrm{Dobs}}$).

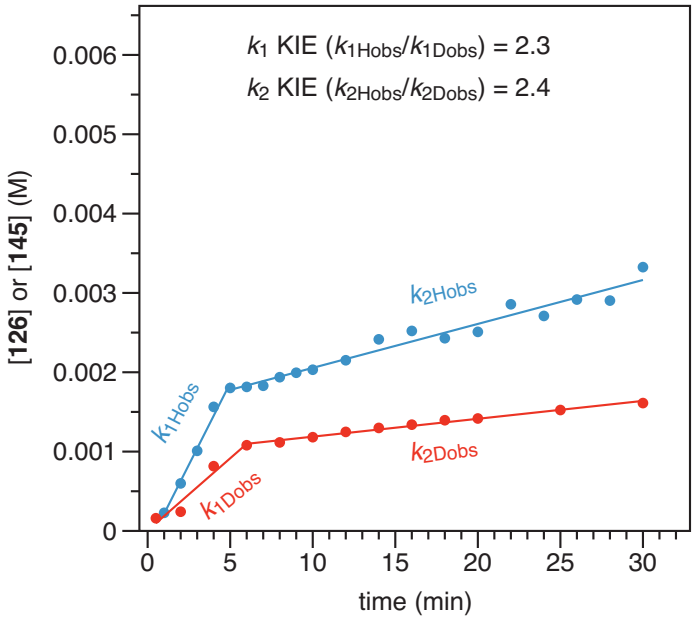
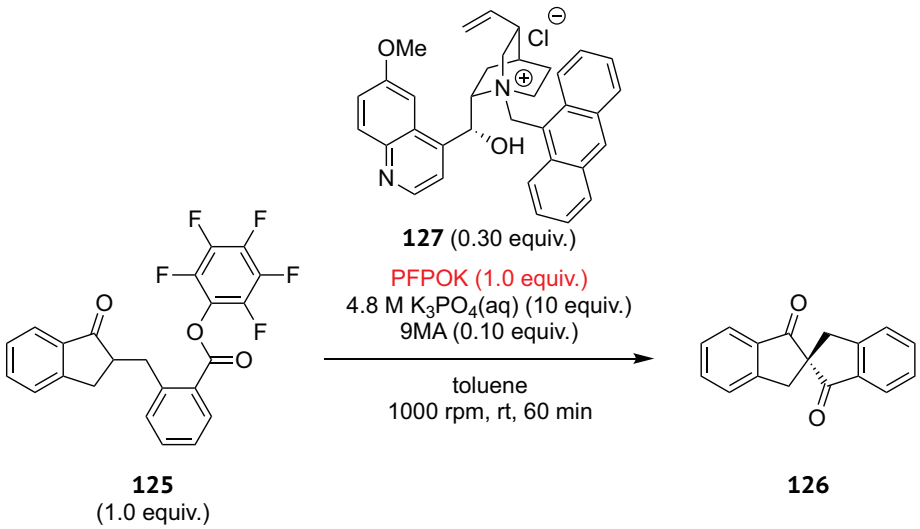



**Figure 7.40: Overlay of data obtained from the hydrogenated (blue data) and deuterated (red data) reaction systems using the modified reaction protocol.** The lines are linear regression analyses of the data in the different regimes, which gave the slopes as follows (to 3 sf): $k_{1Hobs}$: $4.11 \times 10^{-4}$ M min$^{-1}$; $k_{2Hobs}$: $5.54 \times 10^{-5}$ M min$^{-1}$; $k_{1Dobs}$: $1.82 \times 10^{-4}$ M min$^{-1}$; $k_{2Dobs}$: $2.25 \times 10^{-5}$ M min$^{-1}$. The calculated KIE values were thus obtained: KIE $k_1$: 2.3, KIE $k_2$: 2.4.

## 7.20 Evaluating the effect of added 2,3,4,5,6-pentafluorophenolate




### 7.20.1 General information

A series of experiments were carried out to evaluate the effect of added potassium 2,3,4,5,6-pentafluorophenolate (PFPOK) on the reaction. The experiments were carried out according to

either the standard reaction protocol (see 7.4.1), the modified reaction protocol (see 7.4.2), or an additional protocol that delayed the addition of $K_3PO_4$(aq). The designated reaction codes (*rxn.code*) for the three reactions were: "spirok-71", "spirok-72", and "spirok-73", respectively. Each experiment was carried out as a single reaction. All reactions were carried out with a reaction stirring speed of 1000 rpm. The equivalents (equiv.) are reported with respect to the amount of substrate **125**. All reactions were sampled using the sampling protocol (see 7.4.3).

### 7.20.2 Standard and modified protocol reactions

#### Conditions

The reactions carried out according to the standard and modified reaction protocols used the conditions below (described for one reaction only). Solid PFPOK was added to the reaction vial following the addition of catalyst **127** but prior to the addition of toluene. PFPOK (32.5 mg, 0.147 mmol, 1.00 equiv.), catalyst **127** (25.0 mg, 0.0454 mmol, 0.311 equiv.), $K_3PO_4$(aq) (4.77 M; 305 µL, 1.46 mmol, 10.0 equiv.). **Substrate solution:** substrate **125** (70.0 mg, 0.162 mmol), standard **133** (3.2 mg, 0.017 mmol) in 1.0 mL; corresponding to an added amount of **125** (63.0 mg, 0.146 mmol, 1.00 equiv.), **133** (2.9 mg, 0.015 mmol, 0.10 equiv.) per reaction.

#### Data processing and analysis

The raw HPLC data were collected at 240 nm and 292 nm and were processed according to the methods detailed in 7.3.4 and 7.4.4. The plots of product **126** concentration over time were generated and overlaid (Figure 7.41). The processed data were analysed using linear regression analysis of the rate of total product formation to give the initial rates ($k_{obs}$) for the two reactions.

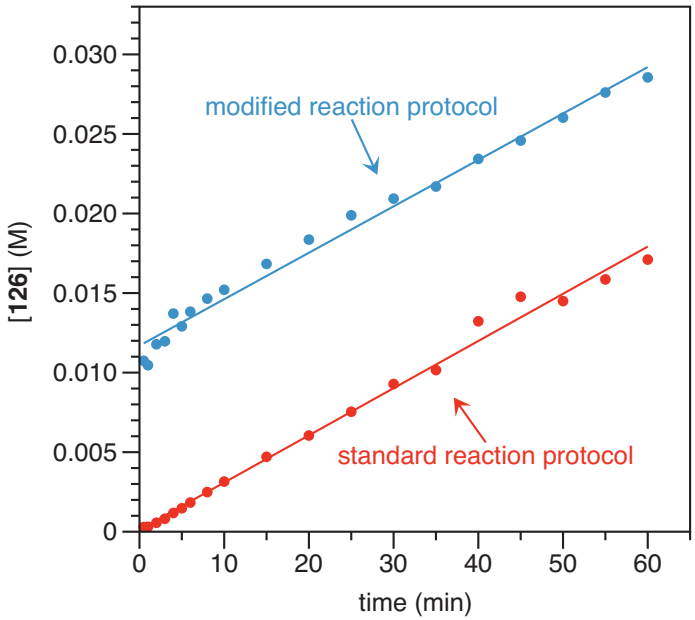



**Figure 7.41: Data comparing the kinetic behaviour of reactions with added PFPOK carried out using the standard (red data) or modified (blue data) reaction protocols.** The lines are linear regression analyses of the corresponding data of the same colour to give the $k_{obs}$ as follows (to 3 sf): standard reaction protocol, 2.97 M $min^{-1}$ (red); modified reaction protocol, 2.92 M $min^{-1}$ (blue).

### 7.20.3 Delayed addition of $K_3PO_4$ reaction conditions

#### Conditions

The reaction was set up according to a version of the modified reaction protocol. Monitoring of the reaction commenced from the addition of the substrate solution. After 60 min, $K_3PO_4$(aq) was added and monitoring continued. Solid PFPOK was added to the reaction vial following the addition of catalyst **127** but prior to the addition of toluene. The reaction conditions were as follows: PFPOK (32.5 mg, 0.147 mmol, 1.00 equiv.), catalyst **127** (25.0 mg, 0.0454 mmol, 0.311 equiv.), $K_3PO_4$(aq) (4.77 M; 305 µL, 1.46 mmol, 10.0 equiv.). **Substrate solution:** substrate **125** (70.0 mg, 0.162 mmol), standard **133** (3.2 mg, 0.017 mmol) in 1.0 mL; corresponding to an added amount of **125** (63.0 mg, 0.146 mmol, 1.00 equiv.), **133** (2.9 mg, 0.015 mmol, 0.10 equiv.) per reaction.

**Data processing and analysis**

The raw HPLC data were collected at 240 nm and 292 nm and were processed according to the methods detailed in 7.3.4 and 7.4.4. The plot of product **126** amounts over time was generated (Figure 7.42). Addition of $K_3PO_4$(aq) occurred at the 60 min time point.

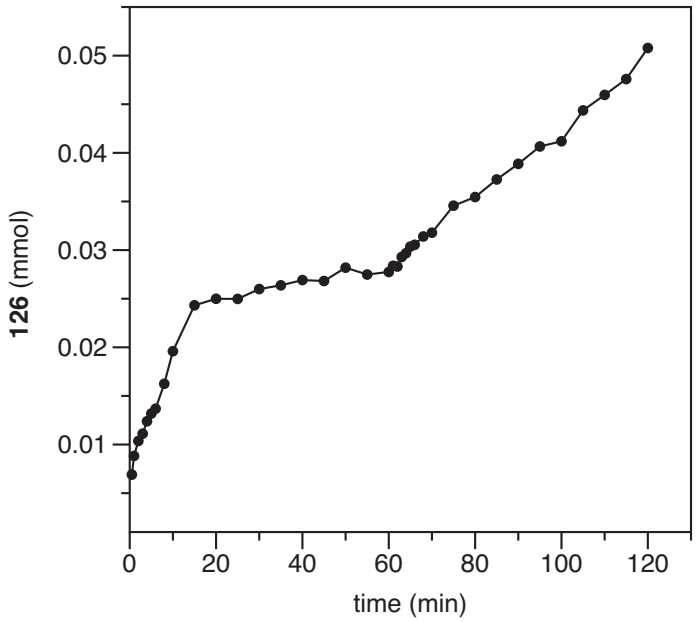



**Figure 7.42: Evaluating the kinetic behaviour when commencing the reaction with added PFPOK in the absence of $K_3PO_4$(aq).** Addition of $K_3PO_4$(aq) occurred at the 60 min time point. The line is a guide for the eye.

The temporal ee plots of the substrate **125** and product **126** were additionally generated (Figure 7.43 and Figure 7.44).

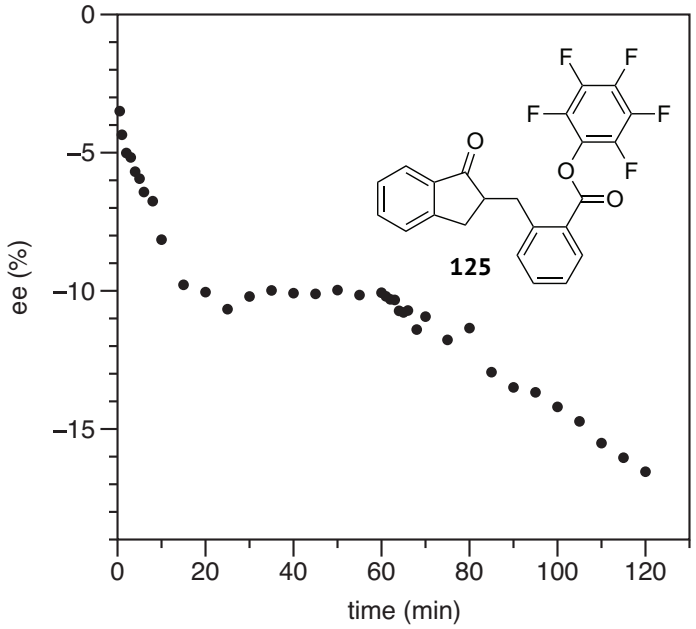



**Figure 7.43: Enantiomeric excess (ee) of the substrate 125 over time when commencing the reaction with added PFPOK in the absence of $K_3PO_4$(aq).** Addition of $K_3PO_4$(aq) occurred at the 60 min time point.

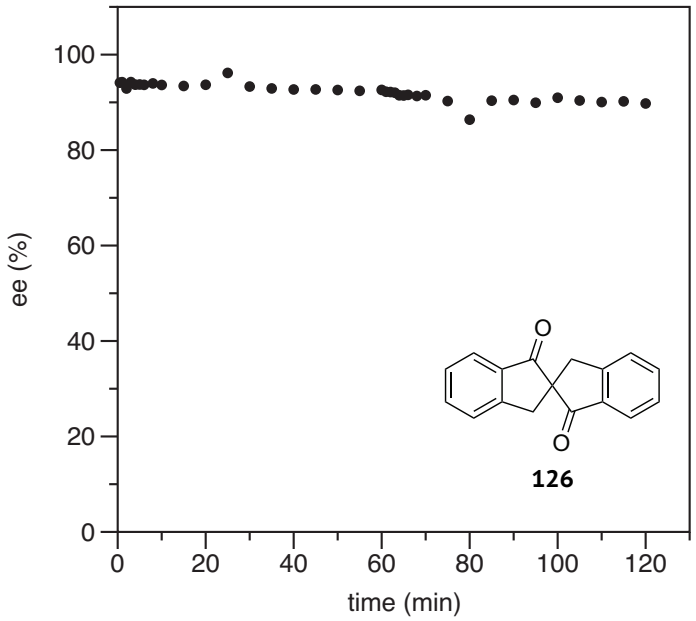
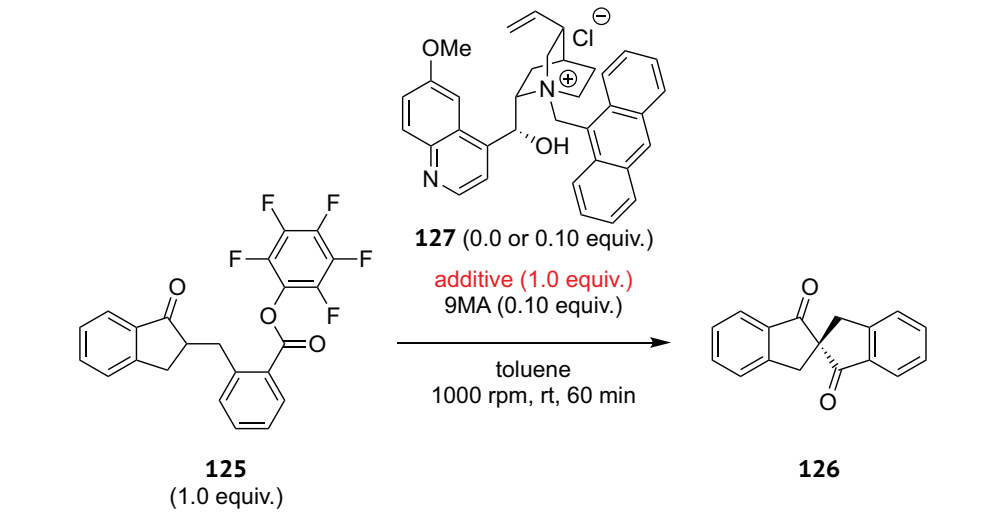
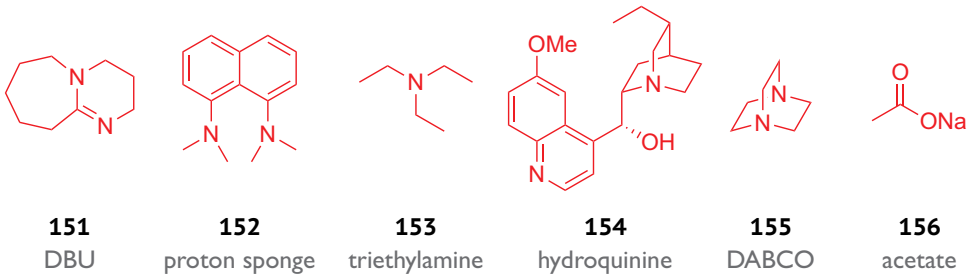



**Figure 7.44: Enantiomeric excess (ee) of the product 126 over time when commencing the reaction with added PFPOK in the absence of $K_3PO_4$(aq).** Addition of $K_3PO_4$(aq) occurred at the 60 min time point.

## 7.21 Evaluating the effect of bases as additives




### 7.21.1 General information

A series of experiments were carried out to evaluate the effect of additives on the reaction carried out in the absence of $K_3PO_4$(aq). The experiments were carried out according to the protocols described below (7.21.2). Each experiment was carried out as a single reaction. All reactions were carried out with a reaction stirring speed of 1000 rpm. The equivalents (equiv.) are reported with respect to the amount of substrate **125**.

### 7.21.2 Experimental protocols

An experiment evaluating the background reaction with 1,8-diazabicyclo[5.4.0]undec-7-ene (DBU) was carried out using the protocol described below.

A substrate solution was prepared as follows: substrate **125** (70 mg, 0.162 mmol), and standard

9MA **133** (3.2 mg, 0.017 mmol) were dissolved in toluene made up to 1.0 mL in a volumetric flask.

A solution of DBU (22.0 µL, 0.147 mmol, 1.00 equiv.) and toluene (538 µL) was stirred at 1000 rpm for 2 min before the addition of the substrate solution (900 µL) at the designated time zero. Final initial amounts of the substrate solution contents in the reaction were as follows: substrate **125** (63.0 mg, 0.146 mmol, 1.00 equiv.), and standard 9MA **133** (2.9 mg, 0.015 mmol, 0.10 equiv.). After 60 min, an aliquot was extracted from the reaction mixture and analysed by HPLC according to the sampling protocol (see 7.4.3).

The ratios of the product **126** were compared to the standard peak giving a calculated yield of product **126** of approximately 63%. The approximation was due to significant unknown byproduct formation, which resulted in incomplete baseline-peak-baseline resolution of the analyte peaks of interest. The peak corresponding to the internal standard was completely unhindered.

Screening of further additives was carried out according to the protocol described below. The following reactions were carried out in non-rounded 7 mL screw-cap vials ($\varnothing$ = 1.5 cm) and with unused magnetic stirrer bars (8 mm × 3 mm).

A substrate solution was prepared as follows: substrate **125** (350 mg, 0.810 mmol), and standard 9MA **133** (16.0 mg, 0.0832 mmol) were dissolved in toluene made up to 5.0 mL in a volumetric flask.

Where relevant, the catalyst **127** (4.0 mg, 0.0073 mmol, 0.10 equiv.) was added to the reaction vial before the additive (see Table 7.14) was introduced. Toluene (280 µL) was added to each vial and the resulting mixtures stirred at 1000 rpm before addition of the substrate solution (450 µL). Initiation of the reactions was by the addition of the substrate solution at the designated time zero. Final initial amounts of the substrate solution contents in each reaction were as follows: substrate **125** (32 mg, 0.073 mmol, 1.0 equiv.), and standard 9MA **133**

(1.4 mg, 0.0075 mmol, 0.10 equiv.). After approximately 60 min, an aliquot was extracted from each reaction mixture and analysed by HPLC according to the sampling protocol (see 7.4.3). Full details of the quantities of additives and the inclusion of catalyst **127** are described in Table 7.14.

**Table 7.14: Conditions for the additives used in the evaluation.** Data are quoted to two significant figures.

| Entry | Additive | Quantity | mmol | equiv. | 127 Loading (equiv.) |
|---|---|---|---|---|---|
| 1 | proton sponge **152** | 16 mg | 0.075 | 1.0 | 0.00 |
| 2 | proton sponge **152** | 16 mg | 0.075 | 1.0 | 0.10 |
| 3 | triethylamine **153** | 10 µL | 0.072 | 0.99 | 0.00 |
| 4 | triethylamine **153** | 10 µL | 0.072 | 0.99 | 0.10 |
| 5 | hydroquinine **154** | 24 mg | 0.074 | 1.0 | 0.00 |
| 6 | hydroquinine **154** | 24 mg | 0.074 | 1.0 | 0.10 |
| 7 | DABCO **155** | 8.2 mg | 0.073 | 1.0 | 0.00 |
| 8 | DABCO **155** | 8.2 mg | 0.073 | 1.0 | 0.10 |
| 9 | sodium acetate **156** | 6.0 mg | 0.073 | 1.0 | 0.00 |
| 10 | sodium acetate **156** | 6.0 mg | 0.073 | 1.0 | 0.10 |

### 7.21.3 Summary of data

Where appropriate, the ratios of the product **126** were compared to the standard peak giving a calculated yield of product **126**. If obscuration of the peak corresponding to the internal standard occurred, the yield of the reaction was estimated by the ratio of the product peaks to the total area of the substrate and product peaks combined (from chromatograms extracted at 240 nm). The data are summarised in Table 7.15.

**Table 7.15: Summary of results evaluating the effect of additives on the reaction of substrate 125 to product 126.** The reactions were carried out for 60 min and were in the absence of $K_3PO_4$(aq) (except for Entry 1). Equivalents (equiv.) are reported with respect to substrate **125**.

| Entry | Additive (1 equiv.)[c] | 127 Loading[a] (equiv.) | 126 Yield (%) | ee[b] (%) |
|---|---|---|---|---|
| 1[d] | N/A | 0.1 | 6–7[e] | 87–94 |
| 2 | DBU | 0 | 63[e] | 0 |
| 3 | proton sponge **152** | 0 | 2[f] | 0 |
| 4 | triethylamine **153** | 0 | 0[e] | 0 |
| 5 | hydroquinine **154** | 0 | 5[f] | 5 |
| 6 | DABCO **155** | 0 | 1[e] | 0 |
| 7 | sodium acetate **156** | 0 | 0[e] | 0 |
| 8 | proton sponge **152** | 0.1 | 15[f] | <1 |
| 9 | triethylamine **153** | 0.1 | 1[e] | 35 |
| 10 | hydroquinine **154** | 0.1 | 29[f] | 85 |
| 11 | DABCO **155** | 0.1 | 8[e] | 83 |
| 12 | sodium acetate **156** | 0.1 | 1[e] | 65 |

[a]to 1 sf; [b]to the nearest whole percent; [c]to 1 sf; [d]for reference, from analogous PTC reaction conditions for this system in the presence of 4.77 M $K_3PO_4$(aq) (10 equiv.); [e]calculated using the internal standard as reference; [f]estimated based on the ratio of the product peaks to the total area of the substrate and product peaks combined (from chromatograms extracted at 240 nm).

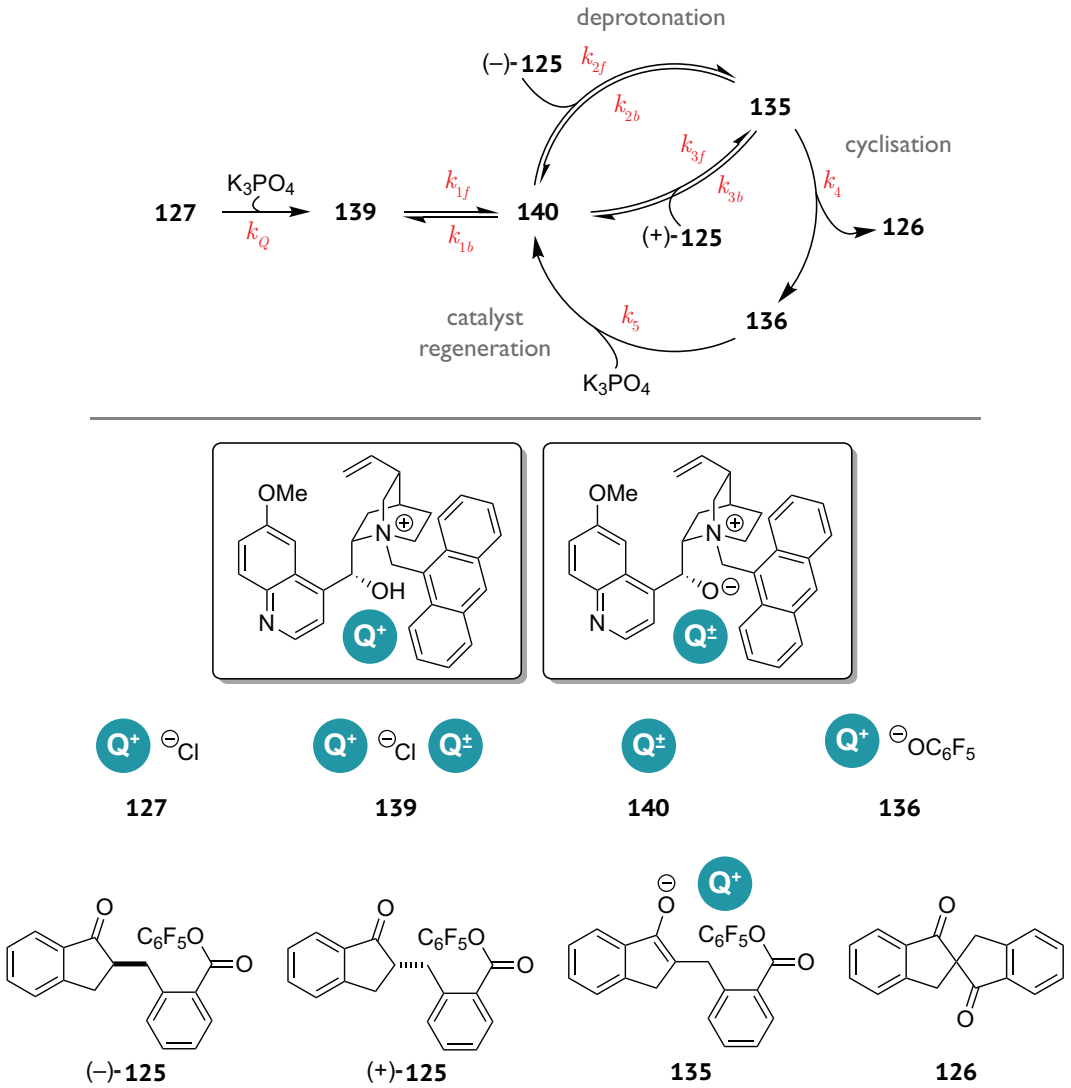
## 7.22 Theoretical kinetics

### 7.22.1 General information

All of the work carried out in this section was in collaboration with MRG, who constructed all of the Mathematica environments and carried out all data fitting. The output from model 6 for every reaction is available as electronic supporting information.

### 7.22.2 Model 1

The model was based on the system described by Scheme 7.1.




**Scheme 7.1: System used to evaluate model 1.** The red text corresponds to the rate constant for the associated step.

The differential rate equations for each step in Scheme 7.1 are described by equations 7.19 to 7.27. The solution for the whole system was evaluated numerically using Mathematica (see 9.2). Iterations of different initial reaction conditions and rate constants were subsequently evaluated.

$$\frac{d[\mathbf{127}]}{dt} = k_Q[\mathbf{127}][\mathrm{K_3PO_4}] \tag{7.19}$$

$$\frac{d[\mathrm{K_3PO_4}]}{dt} = -k_Q[\mathbf{127}][\mathrm{K_3PO_4}] - k_5[\mathbf{136}][\mathrm{K_3PO_4}] \tag{7.20}$$

$$\frac{d[\mathbf{139}]}{dt} = k_Q[\mathbf{127}][\mathrm{K_3PO_4}] - 2k_{1f}[\mathbf{139}]^2 + 2k_{1b}[\mathbf{140}] \tag{7.21}$$

$$\frac{d[\mathbf{140}]}{dt} = k_{1f}[\mathbf{139}]^2 - k_{1b}[\mathbf{140}] - k_{2f}[\mathbf{140}][(-)\text{-}\mathbf{125}] + k_{2b}[\mathbf{135}] - k_{3f}[\mathbf{140}][(+)\text{-}\mathbf{125}] + k_{3b}[\mathbf{135}] + k_5[\mathbf{136}][\mathrm{K_3PO_4}] \tag{7.22}$$

$$\frac{d[(-)\text{-}\mathbf{125}]}{dt} = -k_{2f}[\mathbf{140}][(-)\text{-}\mathbf{125}] + k_{2b}[\mathbf{135}] \tag{7.23}$$

$$\frac{d[(+)\text{-}\mathbf{125}]}{dt} = -k_{3f}[\mathbf{140}][(+)\text{-}\mathbf{125}] + k_{3b}[\mathbf{135}] \tag{7.24}$$

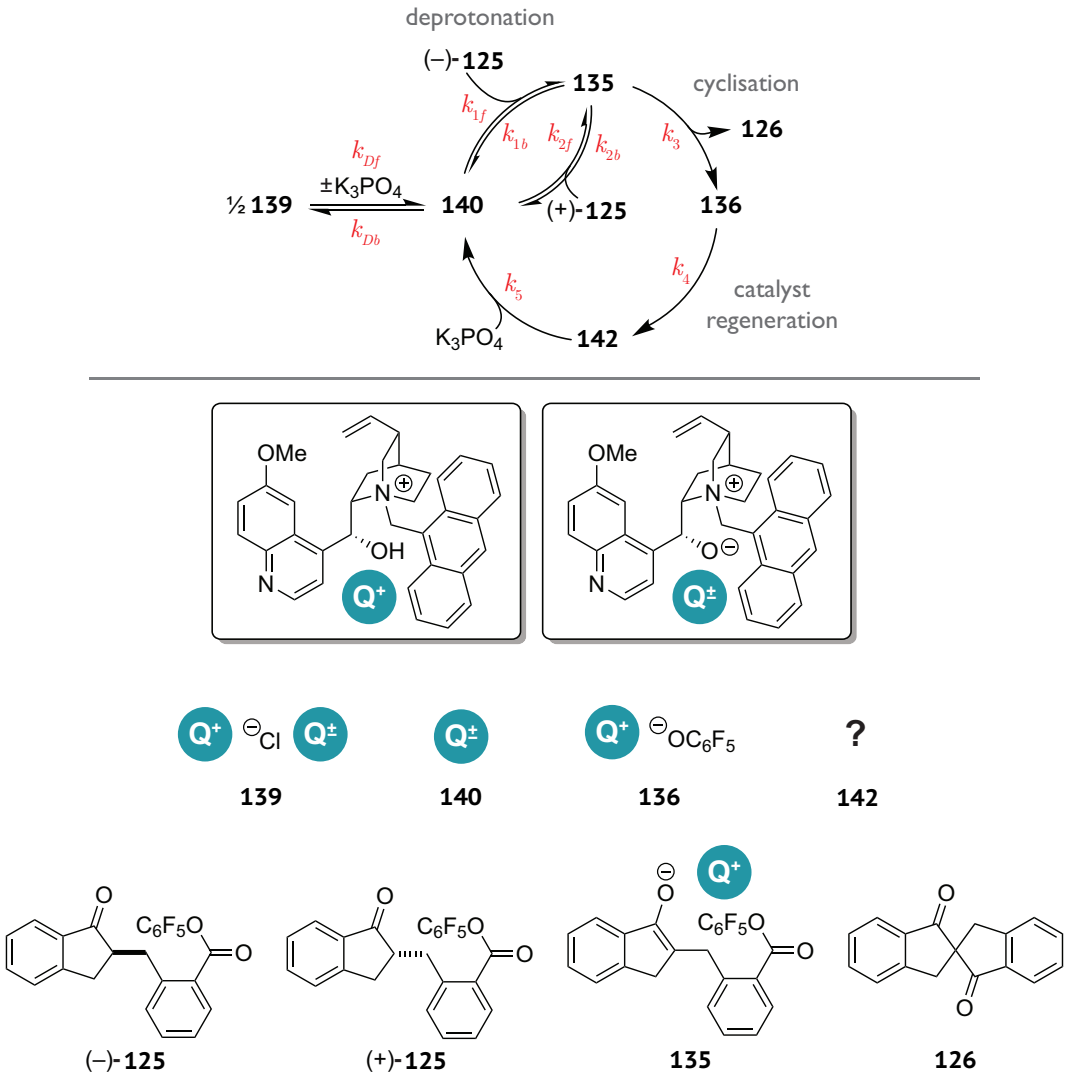
$$\frac{d[\mathbf{135}]}{dt} = k_{2f}[\mathbf{140}][(-)\text{-}\mathbf{125}] - k_{2b}[\mathbf{135}] + k_{3f}[\mathbf{140}][(+)\text{-}\mathbf{125}] - k_{3b}[\mathbf{135}] - k_4[\mathbf{135}] \tag{7.25}$$

$$\frac{d[\mathbf{136}]}{dt} = k_4[\mathbf{135}] - k_5[\mathbf{136}][\mathrm{K_3PO_4}] \tag{7.26}$$

$$\frac{d[\mathbf{126}]}{dt} = k_4[\mathbf{135}] \tag{7.27}$$

### 7.22.3 Model 2

The model was based on the system described by Scheme 7.2.




**Scheme 7.2: System used to evaluate model 2.** The red text corresponds to the rate constant for the associated step.

The corresponding differential rate equations for each step in Scheme 7.2 are described by equations 7.28 to 7.36. The solution for the whole system was evaluated numerically. Fitting of the data was carried out against selected experimental results. Initial total catalyst concentration was set to be species **139**, with a catfactor value of 0.1429 (to 4 sf).

$$\frac{d[\mathbf{139}]}{dt} = -0.5k_{Df}[\mathbf{139}][\mathrm{K_3PO_4}] + 0.5k_{Db}[\mathbf{140}]^2 \tag{7.28}$$

$$\frac{d[\mathbf{140}]}{dt} = k_{Df}[\mathbf{139}][\mathrm{K_3PO_4}] - k_{Db}[\mathbf{140}]^2 - k_{1f}[\mathbf{140}][(-)\text{-}\mathbf{125}] + k_{1b}[\mathbf{135}] \\ - k_{2f}[\mathbf{140}][(+)\text{-}\mathbf{125}] + k_{2b}[\mathbf{135}] + k_5[\mathbf{142}][\mathrm{K_3PO_4}] \quad (7.29)$$

$$\frac{d[(-)\text{-}\mathbf{125}]}{dt} = -k_{1f}[\mathbf{140}][(-)\text{-}\mathbf{125}] + k_{1b}[\mathbf{135}] \quad (7.30)$$

$$\frac{d[(+)\text{-}\mathbf{125}]}{dt} = -k_{2f}[\mathbf{140}][(+)\text{-}\mathbf{125}] + k_{2b}[\mathbf{135}] \quad (7.31)$$

$$\frac{d[\mathbf{135}]}{dt} = k_{1f}[\mathbf{140}][(-)\text{-}\mathbf{125}] - k_{1b}[\mathbf{135}] + k_{2f}[\mathbf{140}][(+)\text{-}\mathbf{125}] - k_{2b}[\mathbf{135}] - k_3[\mathbf{135}] \quad (7.32)$$

$$\frac{d[\mathbf{136}]}{dt} = k_3[\mathbf{135}] - k_4[\mathbf{136}] \quad (7.33)$$

$$\frac{d[\mathbf{142}]}{dt} = k_4[\mathbf{136}] - k_5[\mathbf{142}][\mathrm{K_3PO_4}] \quad (7.34)$$

$$\frac{d[\mathbf{126}]}{dt} = k_3[\mathbf{135}] \quad (7.35)$$

$$\frac{d[\mathrm{K_3PO_4}]}{dt} = -k_5[\mathbf{127}][\mathrm{K_3PO_4}] + k_{Db}[\mathbf{140}]^2 \quad (7.36)$$

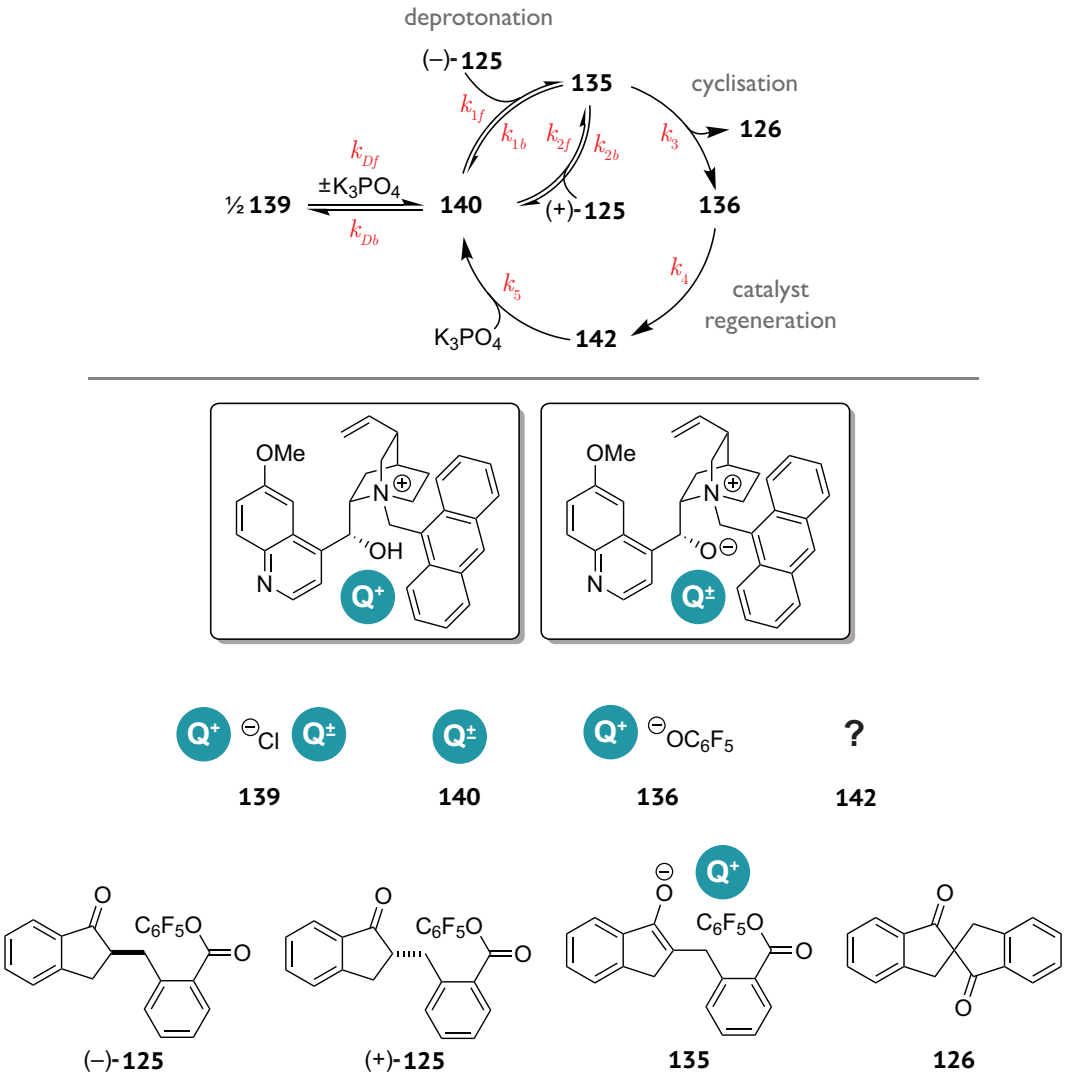
The parameters for each of the steps described by Scheme 7.2 were obtained (Table 7.16).

**Table 7.16: Parameters obtained from fitting model 2 to experimental data.** Data are reported to 4 significant figures.

| Entry | Parameter | Value |
|---|---|---|
| 1 | $k_{Df}$ | 3.452 $M^{-1}$ $min^{-1}$ |
| 2 | $k_{Db}$ | 0.000 $min^{-1}$ |
| 3 | $k_{1f}$ | 33.96 $M^{-1}$ $min^{-1}$ |
| 4 | $k_{1b}$ | 0.000 $min^{-1}$ |
| 5 | $k_{2f}$ | 89.54 $M^{-1}$ $min^{-1}$ |
| 6 | $k_{2b}$ | 0.000 $min^{-1}$ |
| 7 | $k_3$ | 443.4 $min^{-1}$ |
| 8 | $k_4$ | 0.02081 $min^{-1}$ |
| 9 | $k_5$ | 118.0 $M^{-1}$ $min^{-1}$ |
| 10 | catfactor | 0.1429 |

### 7.22.4 Model 3

The model was based on the system described by Scheme 7.3.




**Scheme 7.3: System used to evaluate model 3.** The red text corresponds to the rate constant for the associated step.

The corresponding differential rate equations for each step in Scheme 7.3 are described by equations 7.37 to 7.45. The solution for the whole system was evaluated numerically. Fitting of the data was carried out against selected experimental results. Initial total catalyst concentration was set to be species **139**, with a catfactor value of 0.1646 (to 4 sf).

$$\frac{d[\mathbf{139}]}{dt} = -0.5k_{Df}[\mathbf{139}][\mathrm{K_3PO_4}] + 0.5k_{Db}[\mathbf{140}]^2 \tag{7.37}$$

$$\frac{d[\mathbf{140}]}{dt} = k_{Df}[\mathbf{139}][\mathrm{K_3PO_4}] - k_{Db}[\mathbf{140}]^2 - k_{1f}[\mathbf{140}][(-)\text{-}\mathbf{125}] + k_{1b}[\mathbf{135}] - k_{2f}[\mathbf{140}][(+)\text{-}\mathbf{125}] + k_{2b}[\mathbf{135}] + k_5[\mathbf{142}][\mathrm{K_3PO_4}] \quad (7.38)$$

$$\frac{d[(-)\text{-}\mathbf{125}]}{dt} = -k_{1f}[\mathbf{140}][(-)\text{-}\mathbf{125}] + k_{1b}[\mathbf{135}] \quad (7.39)$$

$$\frac{d[(+)\text{-}\mathbf{125}]}{dt} = -k_{2f}[\mathbf{140}][(+)\text{-}\mathbf{125}] + k_{2b}[\mathbf{135}] \quad (7.40)$$

$$\frac{d[\mathbf{135}]}{dt} = k_{1f}[\mathbf{140}][(-)\text{-}\mathbf{125}] - k_{1b}[\mathbf{135}] + k_{2f}[\mathbf{140}][(+)\text{-}\mathbf{125}] - k_{2b}[\mathbf{135}] - k_3[\mathbf{135}] \quad (7.41)$$

$$\frac{d[\mathbf{136}]}{dt} = k_3[\mathbf{135}] - k_4[\mathbf{136}] \quad (7.42)$$

$$\frac{d[\mathbf{142}]}{dt} = k_4[\mathbf{136}] - k_5[\mathbf{142}][\mathrm{K_3PO_4}] \quad (7.43)$$

$$\frac{d[\mathbf{126}]}{dt} = k_3[\mathbf{135}] \quad (7.44)$$

$$\frac{d[\mathrm{K_3PO_4}]}{dt} = -k_5[\mathbf{127}][\mathrm{K_3PO_4}] + k_{Db}[\mathbf{140}]^2 \quad (7.45)$$

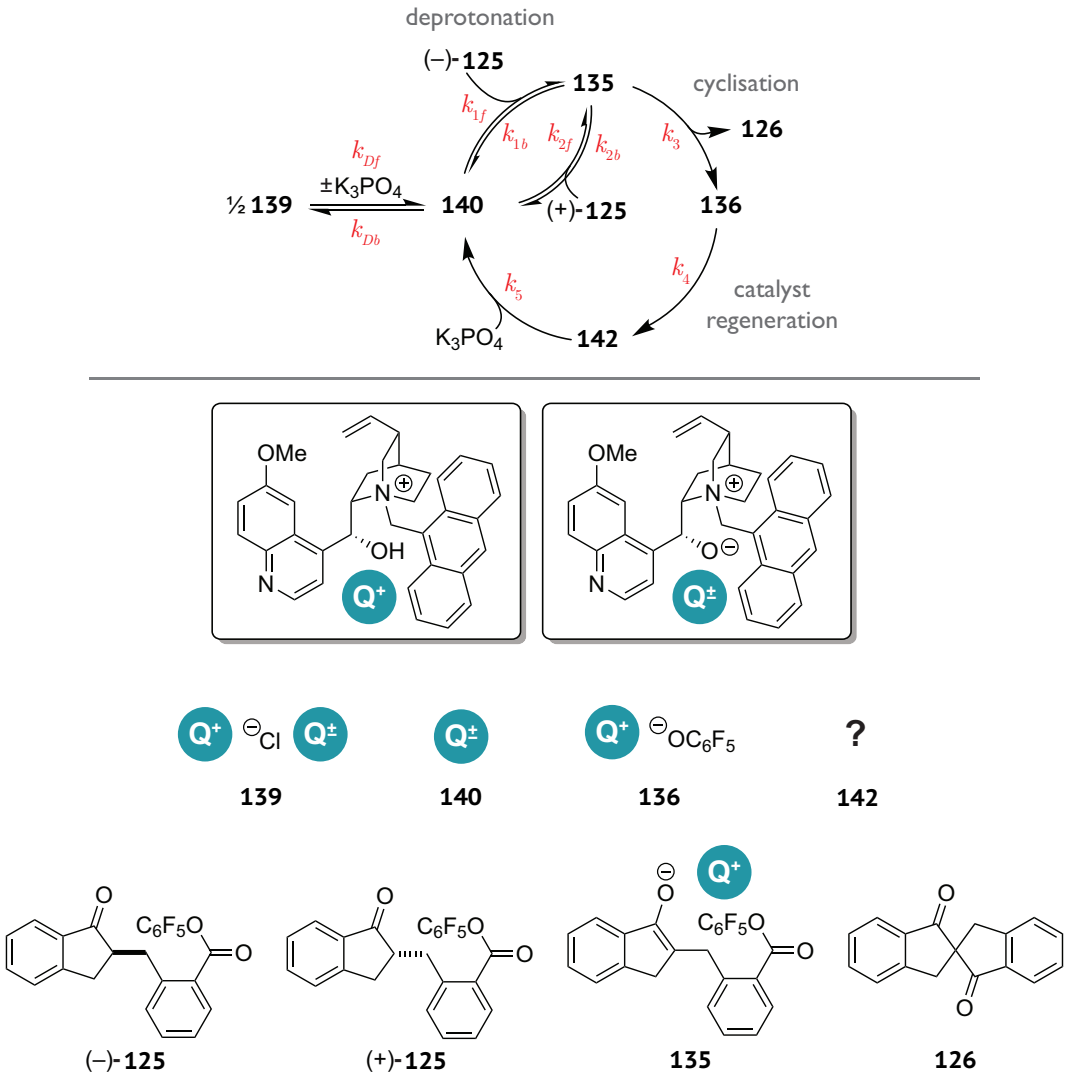
The parameters for each of the steps described by Scheme 7.3 were obtained (Table 7.17).

**Table 7.17: Parameters obtained from fitting model 3 to experimental data.** Data are reported to 4 significant figures.

| Entry | Parameter | Value |
|---|---|---|
| 1 | $k_{Df}$ | 4.214 $M^{-1}$ $min^{-1}$ |
| 2 | $k_{Db}$ | 0.000 $min^{-1}$ |
| 3 | $k_{1f}$ | 9.667 $M^{-1}$ $min^{-1}$ |
| 4 | $k_{1b}$ | 0.000 $min^{-1}$ |
| 5 | $k_{2f}$ | 19.81 $M^{-1}$ $min^{-1}$ |
| 6 | $k_{2b}$ | 0.000 $min^{-1}$ |
| 7 | $k_3$ | 97.67 $min^{-1}$ |
| 8 | $k_4$ | 0.01684 $min^{-1}$ |
| 9 | $k_5$ | 12.65 $M^{-1}$ $min^{-1}$ |
| 10 | catfactor | 0.1646 |

### 7.22.5 Model 4

The model was based on the system described by Scheme 7.4, with the included background reactions: (+)-**125** + $K_3PO_4$ $\xrightarrow{k_z}$ **126** and (−)-**125** + $K_3PO_4$ $\xrightarrow{k_z}$ **126**.




**Scheme 7.4: System used to evaluate model 4.** The red text corresponds to the rate constant for the associated step.

The corresponding differential rate equations for each step in Scheme 7.4 are described by equations 7.46 to 7.54. The solution for the whole system was evaluated numerically. Fitting of the data was carried out against selected experimental results. Initial total catalyst concentration was set to be species **139**, with a catfactor value of 0.3291 (to 4 sf).

$$\frac{d[\mathbf{139}]}{dt} = -0.5k_{Df}[\mathbf{139}][\mathrm{K_3PO_4}] + 0.5k_{Db}[\mathbf{140}]^2 \tag{7.46}$$

$$\frac{d[\mathbf{140}]}{dt} = k_{Df}[\mathbf{139}][\mathrm{K_3PO_4}] - k_{Db}[\mathbf{140}]^2 - k_{1f}[\mathbf{140}][(-)\text{-}\mathbf{125}] + k_{1b}[\mathbf{135}] \\ - k_{2f}[\mathbf{140}][(+)\text{-}\mathbf{125}] + k_{2b}[\mathbf{135}] + k_5[\mathbf{142}][\mathrm{K_3PO_4}] \quad (7.47)$$

$$\frac{d[(-)\text{-}\mathbf{125}]}{dt} = -k_{1f}[\mathbf{140}][(-)\text{-}\mathbf{125}] + k_{1b}[\mathbf{135}] - k_z[(-)\text{-}\mathbf{125}][\mathrm{K_3PO_4}] \quad (7.48)$$

$$\frac{d[(+)\text{-}\mathbf{125}]}{dt} = -k_{2f}[\mathbf{140}][(+)\text{-}\mathbf{125}] + k_{2b}[\mathbf{135}] - k_z[(+)\text{-}\mathbf{125}][\mathrm{K_3PO_4}] \quad (7.49)$$

$$\frac{d[\mathbf{135}]}{dt} = k_{1f}[\mathbf{140}][(-)\text{-}\mathbf{125}] - k_{1b}[\mathbf{135}] + k_{2f}[\mathbf{140}][(+)\text{-}\mathbf{125}] - k_{2b}[\mathbf{135}] - k_3[\mathbf{135}] \quad (7.50)$$

$$\frac{d[\mathbf{136}]}{dt} = k_3[\mathbf{135}] - k_4[\mathbf{136}] \quad (7.51)$$

$$\frac{d[\mathbf{142}]}{dt} = k_4[\mathbf{136}] - k_5[\mathbf{142}][\mathrm{K_3PO_4}] \quad (7.52)$$

$$\frac{d[\mathbf{126}]}{dt} = k_3[\mathbf{135}] + k_z([(-)\text{-}\mathbf{125}][\mathrm{K_3PO_4}] + [(+)\text{-}\mathbf{125}][\mathrm{K_3PO_4}]) \quad (7.53)$$

$$\frac{d[\mathrm{K_3PO_4}]}{dt} = -k_5[\mathbf{127}][\mathrm{K_3PO_4}] - k_{Df}[\mathbf{139}][\mathrm{K_3PO_4}] + k_{Db}[\mathbf{140}]^2$$
$$- k_z[(-)\text{-}\mathbf{125}][\mathrm{K_3PO_4}] - k_z[(+)\text{-}\mathbf{125}][\mathrm{K_3PO_4}] \quad (7.54)$$

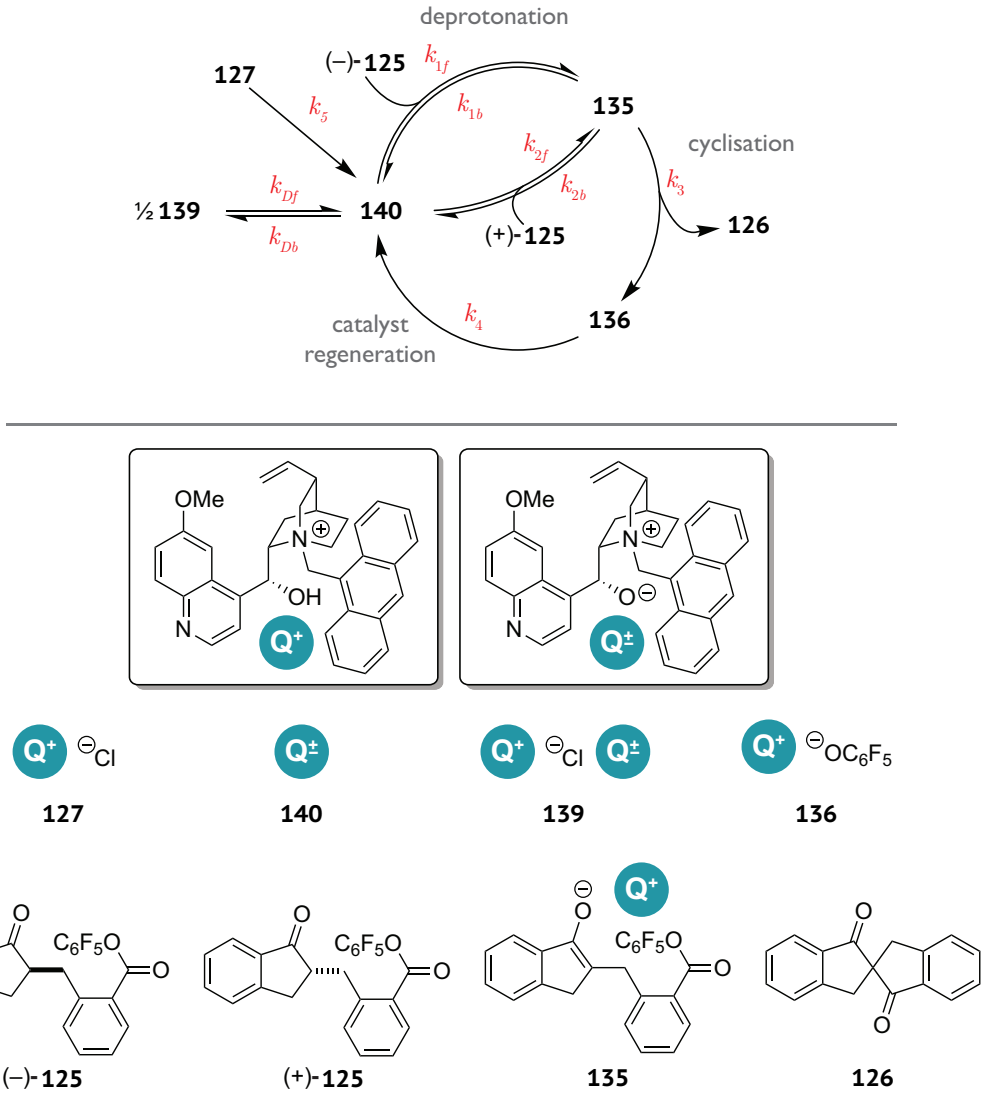
The parameters for each of the steps described by Scheme 7.4 were obtained (Table 7.18).

**Table 7.18: Parameters obtained from fitting model 4 to experimental data.** Data are reported to 4 significant figures.

| Entry | Parameter | Value |
|---|---|---|
| 1 | $k_{Df}$ | 3.746 $M^{-1}$ $min^{-1}$ |
| 2 | $k_{Db}$ | 12.70 $min^{-1}$ |
| 3 | $k_{1f}$ | 30.53 $M^{-1}$ $min^{-1}$ |
| 4 | $k_{1b}$ | 0.000 $min^{-1}$ |
| 5 | $k_{2f}$ | 69.07 $M^{-1}$ $min^{-1}$ |
| 6 | $k_{2b}$ | 0.000 $min^{-1}$ |
| 7 | $k_3$ | 354.6 $min^{-1}$ |
| 8 | $k_4$ | 159.7 $min^{-1}$ |
| 9 | $k_5$ | 0.01886 $M^{-1}$ $min^{-1}$ |
| 10 | $k_z$ | 0.0003500 $M^{-1}$ $min^{-1}$ |
| 11 | catfactor | 0.3291 |

### 7.22.6 Model 5

The model was based on the system described by Scheme 7.5, with the included background reactions: (+)-**125** + $\mathrm{K_3PO_4}$ $\xrightarrow{k_z}$ **126** and (−)-**125** + $\mathrm{K_3PO_4}$ $\xrightarrow{k_z}$ **126**. Pre-stirring was an optional regime and included the relevant steps only (i.e. in the absence of substrates (−)-**125** or (+)-**125**). The catalytic cycle was commenced from either **127** or **136** as appropriate.




**Scheme 7.5: System used to evaluate model 5.** The red text corresponds to the rate constant for the associated step.

The corresponding differential rate equations for each step in Scheme 7.5 and the two regimes (pre-stirring and normal) are described by equations 7.55 to 7.69. The solution for the whole system was evaluated numerically. Fitting of the data was carried out against selected experimental results. The change in concentration of base was considered to be negligible (i.e. $\frac{d[K_3PO_4]}{dt} = 0$). If pre-stirring was carried out, the model evaluated the normal reaction (i.e. that in the presence of substrates (−)-**125** and (+)-**125**) using initial conditions dictated by the results of the pre-stirring protocol. The background reactions were included as follows: (+)-**125** + $K_3PO_4 \xrightarrow{k_z}$ **126** and (−)-**125** + $K_3PO_4 \xrightarrow{k_z}$ **126**.

**Pre-stirring reaction**

$$\frac{d[\mathrm{K_3PO_4}]}{dt} = 0 \tag{7.55}$$

$$\frac{d[\mathbf{139}]}{dt} = -0.5k_{Df}[\mathbf{139}] + 0.5k_{Db}[\mathbf{140}]^2 \tag{7.56}$$

$$\frac{d[\mathbf{140}]}{dt} = k_{Df}[\mathbf{139}] - k_{Db}[\mathbf{140}]^2 + k_5[\mathbf{127}] \tag{7.57}$$

$$\frac{d[\mathbf{140}]}{dt} = k_{Df}[\mathbf{139}] - k_{Db}[\mathbf{140}]^2 + k_5[\mathbf{127}] \tag{7.58}$$

$$[\mathrm{cat}]_\mathrm{T} = 2[\mathbf{139}] + [\mathbf{140}] + [\mathbf{127}] \tag{7.59}$$

**Normal reaction**

$$\frac{d[\mathrm{K_3PO_4}]}{dt} = 0 \tag{7.60}$$

$$\frac{d[\mathbf{139}]}{dt} = -0.5k_{Df}[\mathbf{139}] + 0.5k_{Db}[\mathbf{140}]^2 \tag{7.61}$$

$$\begin{aligned}\frac{d[\mathbf{140}]}{dt} = k_{Df}[\mathbf{139}] - k_{Db}[\mathbf{140}]^2 - k_{1f}[\mathbf{140}][(-)\text{-}\mathbf{125}] + k_{1b}[\mathbf{135}] \\ - k_{2f}[\mathbf{140}][(+)\text{-}\mathbf{125}] + k_{2b}[\mathbf{135}] + k_4[\mathbf{136}] + k_5[\mathbf{127}]\end{aligned} \tag{7.62}$$

$$\frac{d[(-)\textbf{-125}]}{dt} = -k_{1f}[\textbf{140}][(-)\textbf{-125}] + k_{1b}[\textbf{135}] - k_z[(-)\textbf{-125}][\mathrm{K_3PO_4}] \tag{7.63}$$

$$\frac{d[(+)\textbf{-125}]}{dt} = -k_{2f}[\textbf{140}][(+)\textbf{-125}] + k_{2b}[\textbf{135}] - k_z[(+)\textbf{-125}][\mathrm{K_3PO_4}] \tag{7.64}$$

$$\frac{d[\textbf{135}]}{dt} = k_{1f}[\textbf{140}][(-)\textbf{-125}] - k_{1b}[\textbf{135}] + k_{2f}[\textbf{140}][(+)\textbf{-125}] - k_{2b}[\textbf{135}] - k_3[\textbf{135}] \tag{7.65}$$

$$\frac{d[\textbf{136}]}{dt} = k_3[\textbf{135}] - k_4[\textbf{136}] \tag{7.66}$$

$$\frac{d[\textbf{127}]}{dt} = -k_5[\textbf{127}] \tag{7.67}$$

$$\frac{d[\textbf{126}]}{dt} = k_3[\textbf{135}] + k_z([(-)\textbf{-125}][\mathrm{K_3PO_4}] + [(+)\textbf{-125}][\mathrm{K_3PO_4}]) \tag{7.68}$$

$$[\mathrm{cat}]_\mathrm{T} = 2[\textbf{139}] + [\textbf{140}] + [\textbf{135}] + [\textbf{136}] + [\textbf{127}] \tag{7.69}$$

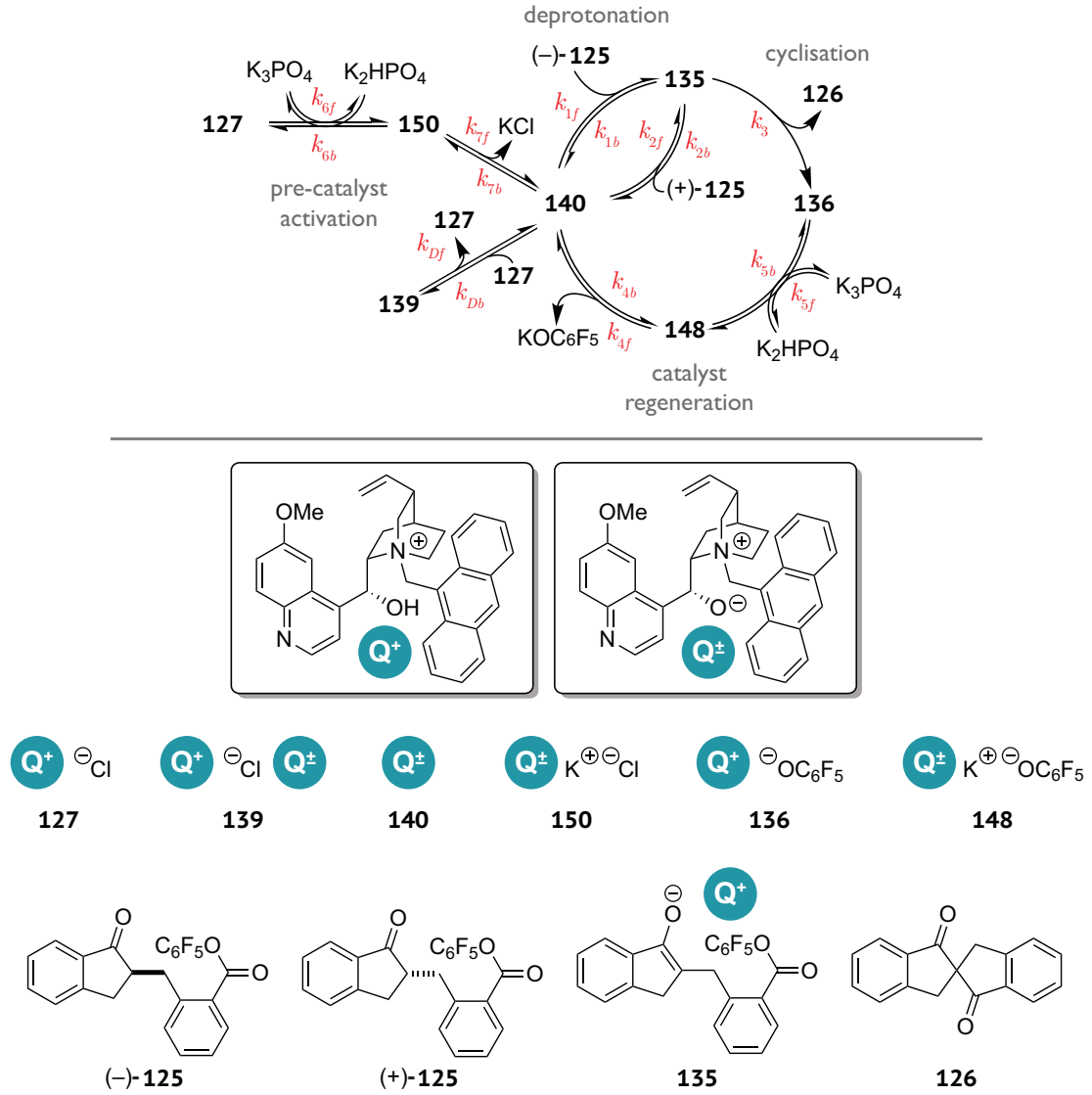
The parameters for each of the steps described by Scheme 7.5 were obtained (Table 7.19).

**Table 7.19: Parameters obtained from fitting model 5 to experimental data.** Data are reported to 4 significant figures.

| Entry | Parameter | Value |
|---|---|---|
| 1 | $k_{Df}$ | 0.2000 $min^{-1}$ |
| 2 | $k_{Db}$ | 20.00 $min^{-1}$ |
| 3 | $k_{1f}$ | 30.53 $M^{-1}$ $min^{-1}$ |
| 4 | $k_{1b}$ | 0.000 $min^{-1}$ |
| 5 | $k_{2f}$ | 55.80 $M^{-1}$ $min^{-1}$ |
| 6 | $k_{2b}$ | 0.000 $min^{-1}$ |
| 7 | $k_3$ | 354.6 $min^{-1}$ |
| 8 | $k_4$ | 0.004550 $min^{-1}$ |
| 9 | $k_5$ | 0.00424 $min^{-1}$ |
| 10 | $k_z$ | 0.0003500 $M^{-1}$ $min^{-1}$ |

### 7.22.7 Model 6

The corresponding differential rate equations for each step in Scheme 7.6 and the two regimes (pre-stirring and normal) are described by equations 7.70 to 7.92. The solution for the whole system was evaluated numerically. Fitting of the data was carried out against selected experimental results. If pre-stirring was carried out, the model evaluated the normal reaction (i.e. that in the presence of substrates (−)-**125** and (+)-**125**) using initial conditions dictated by the results of the pre-stirring protocol. The background reactions were included as follows: (+)-**125** + $K_3PO_4$ $\xrightarrow{k_z}$ **126** and (−)-**125** + $K_3PO_4$ $\xrightarrow{k_z}$ **126**.




**Scheme 7.6: System used to evaluate model 6.** The red text corresponds to the rate constant for the associated step.

### Pre-stirring reaction

$$\frac{d[\mathrm{K_3PO_4}]}{dt} = -k_{6f}[\mathrm{K_3PO_4}][\mathbf{127}] + k_{6b}[\mathrm{K_2HPO_4}][\mathbf{150}] \tag{7.70}$$

$$\frac{d[\mathrm{K_2HPO_4}]}{dt} = k_{6f}[\mathrm{K_3PO_4}][\mathbf{127}] - k_{6b}[\mathrm{K_2HPO_4}][\mathbf{150}] \tag{7.71}$$

$$\frac{d[\mathrm{KCl}]}{dt} = k_{7f}[\mathbf{150}] - k_{7b}[\mathbf{140}][\mathrm{KCl}] \tag{7.72}$$

$$\frac{d[\mathbf{139}]}{dt} = -k_{Df}[\mathbf{139}] + k_{Db}[\mathbf{140}][\mathbf{127}] \tag{7.73}$$

$$\frac{d[\mathbf{140}]}{dt} = k_{Df}[\mathbf{139}] - k_{Db}[\mathbf{140}][\mathbf{127}] + k_{7f}[\mathbf{150}] - k_{7b}[\mathbf{140}][\mathrm{KCl}] \tag{7.74}$$

$$\frac{d[\mathbf{127}]}{dt} = k_{Df}[\mathbf{139}] - k_{Db}[\mathbf{140}][\mathbf{127}] - k_{6f}[\mathrm{K_3PO_4}][\mathbf{127}] + k_{6b}[\mathrm{K_2HPO_4}][\mathbf{150}] \tag{7.75}$$

$$\frac{d[\mathbf{150}]}{dt} = k_{6f}[\mathrm{K_3PO_4}][\mathbf{127}] - k_{6b}[\mathrm{K_2HPO_4}][\mathbf{150}] - k_{7f}[\mathbf{150}] + k_{7b}[\mathbf{140}][\mathrm{KCl}] \tag{7.76}$$

$$[\mathrm{cat}]_\mathrm{T} = 2[\mathbf{139}] + [\mathbf{140}] + [\mathbf{127}] + [\mathbf{150}] \tag{7.77}$$

**Normal reaction**

$$\frac{d[\mathrm{K_3PO_4}]}{dt} = -k_{5f}[\mathrm{K_3PO_4}][\mathbf{136}] + k_{5b}[\mathrm{K_2HPO_4}][\mathbf{148}] - k_{6f}[\mathrm{K_3PO_4}][\mathbf{127}] + k_{6b}[\mathrm{K_2HPO_4}][\mathbf{150}] \tag{7.78}$$

$$\frac{d[\mathrm{K_2HPO_4}]}{dt} = k_{5f}[\mathrm{K_3PO_4}][\mathbf{136}] - k_{5b}[\mathrm{K_2HPO_4}][\mathbf{148}] + k_{6f}[\mathrm{K_3PO_4}][\mathbf{127}] - k_{6b}[\mathrm{K_2HPO_4}][\mathbf{150}] \tag{7.79}$$

$$\frac{d[\mathrm{KOC_6F_5}]}{dt} = k_{4f}[\mathbf{148}] - k_{4b}[\mathbf{140}][\mathrm{KOC_6F_5}] \tag{7.80}$$

$$\frac{d[\mathrm{KCl}]}{dt} = k_{7f}[\mathbf{150}] - k_{7b}[\mathbf{140}][\mathrm{KCl}] \tag{7.81}$$

$$\frac{d[\mathbf{139}]}{dt} = -k_{Df}[\mathbf{139}] + k_{Db}[\mathbf{140}][\mathbf{127}] \tag{7.82}$$

$$\frac{d[\mathbf{140}]}{dt} = k_{Df}[\mathbf{139}] - k_{Db}[\mathbf{140}][\mathbf{127}] - k_{1f}[\mathbf{140}][(-)\text{-}\mathbf{125}] + k_{1b}[\mathbf{135}] - k_{2f}[\mathbf{140}][(+)\text{-}\mathbf{125}] + k_{2b}[\mathbf{135}] + k_{4f}[\mathbf{148}] - k_{4b}[\mathbf{140}][\mathrm{KOC_6F_5}] + k_{7f}[\mathbf{150}] - k_{7b}[\mathbf{140}][\mathrm{KCl}] \tag{7.83}$$

$$\frac{d[(-)\text{-}\mathbf{125}]}{dt} = -k_{1f}[\mathbf{140}][(-)\text{-}\mathbf{125}] + k_{1b}[\mathbf{135}] - k_z[(-)\text{-}\mathbf{125}][\mathrm{K_3PO_4}] \tag{7.84}$$

$$\frac{d[(+)\text{-}\mathbf{125}]}{dt} = -k_{2f}[\mathbf{140}][(+)\text{-}\mathbf{125}] + k_{2b}[\mathbf{135}] - k_z[(+)\text{-}\mathbf{125}][\mathrm{K_3PO_4}] \tag{7.85}$$

$$\frac{d[\mathbf{135}]}{dt} = k_{1f}[\mathbf{140}][(-)\text{-}\mathbf{125}] - k_{1b}[\mathbf{135}] + k_{2f}[\mathbf{140}][(+)\text{-}\mathbf{125}] - k_{2b}[\mathbf{135}] - k_3[\mathbf{135}] \tag{7.86}$$

$$\frac{d[\mathbf{136}]}{dt} = k_3[\mathbf{135}] - k_{5f}[\mathrm{K_3PO_4}][\mathbf{136}] + k_{5b}[\mathrm{K_2HPO_4}][\mathbf{148}] \tag{7.87}$$

$$\frac{d[\mathbf{127}]}{dt} = k_{Df}[\mathbf{139}] - k_{Db}[\mathbf{140}][\mathbf{127}] - k_{6f}[\mathrm{K_3PO_4}][\mathbf{127}] + k_{6b}[\mathrm{K_2HPO_4}][\mathbf{150}] \tag{7.88}$$

$$\frac{d[\mathbf{148}]}{dt} = k_{5f}[\mathrm{K_3PO_4}][\mathbf{136}] - k_{5b}[\mathrm{K_2HPO_4}][\mathbf{148}] - k_{4f}[\mathbf{148}] + k_{4b}[\mathbf{140}][\mathrm{KOC_6F_5}] \tag{7.89}$$

$$\frac{d[\mathbf{150}]}{dt} = k_{6f}[\mathrm{K_3PO_4}][\mathbf{127}] - k_{6b}[\mathrm{K_2HPO_4}][\mathbf{150}] - k_{7f}[\mathbf{150}] + k_{7b}[\mathbf{140}][\mathrm{KCl}] \tag{7.90}$$

$$\frac{d[\mathbf{126}]}{dt} = k_3[\mathbf{135}] + k_z([(-)\text{-}\mathbf{125}][\mathrm{K_3PO_4}] + [(+)\text{-}\mathbf{125}][\mathrm{K_3PO_4}]) \tag{7.91}$$

$$[\mathrm{cat}]_\mathrm{T} = 2[\mathbf{139}] + [\mathbf{140}] + [\mathbf{135}] + [\mathbf{136}] + [\mathbf{127}] + [\mathbf{148}] + [\mathbf{150}] \tag{7.92}$$

The parameters for each of the steps described by Scheme 7.6 were obtained (Table 7.20).

**Table 7.20: Parameters obtained from fitting model 6 to experimental data.** Data are reported to 4 significant figures.

| Entry | Parameter | Value |
|---|---|---|
| 1 | $k_{Df}$ | 0.0002150 $\mathrm{min^{-1}}$ |
| 2 | $k_{Db}$ | 150000 $\mathrm{M^{-1}\ min^{-1}}$ |
| 3 | $k_{1f}$ | 700.0 $\mathrm{M^{-1}\ min^{-1}}$ |
| 4 | $k_{1b}$ | 0.000 $\mathrm{min^{-1}}$ |
| 5 | $k_{2f}$ | 1400 $\mathrm{M^{-1}\ min^{-1}}$ |
| 6 | $k_{2b}$ | 0.000 $\mathrm{min^{-1}}$ |
| 7 | $k_3$ | 354.6 $\mathrm{min^{-1}}$ |
| 8 | $k_{4f}$ | 0.01500 $\mathrm{min^{-1}}$ |
| 9 | $k_{4b}$ | 100.0 $\mathrm{M^{-1}\ min^{-1}}$ |
| 10 | $k_{5f}$ | 1.000 $\mathrm{M^{-1}\ min^{-1}}$ |
| 11 | $k_{5b}$ | 100.0 $\mathrm{M^{-1}\ min^{-1}}$ |
| 12 | $k_{6f}$ | 0.8000 $\mathrm{M^{-1}\ min^{-1}}$ |
| 13 | $k_{6b}$ | 0.0000 $\mathrm{M^{-1}\ min^{-1}}$ |
| 14 | $k_{7f}$ | 0.8000 $\mathrm{min^{-1}}$ |
| 15 | $k_{7b}$ | 0.8000 $\mathrm{M^{-1}\ min^{-1}}$ |
| 16 | $k_z$ | 0.00003000 $\mathrm{M^{-1}\ min^{-1}}$ |

# 8. R Scripts

## 8.1 General information

R Studio was used to create and run all R scripts. In general, a series of input files were required for each experiment: project files and reaction specific files. The project files were created globally and used for each experiment processed within the project. These files included general information of the reaction components (i.e. compounds and their properties, e.g. molecular weight, density, chirality), and the calibration factors as acquired from standard calibration curves. Additional reaction specific data were required from the user. These included the initial reaction conditions, and the signal integrals obtained from the HPLC chromatograms for each experiment. Following execution of a number of scripts, the result for each experiment was the outputted data, which contained temporal mmol and concentration data for analytes observed, in addition temporal ee data, and a summary of the initial reaction conditions of the experiment.

## 8.2 Processing data in project 1

The main file for inputting general parameters is located in:

```
"~/R/kinetics/functions/input/general-input-version-2.R"
```

In this file, the project is specified, in addition to the reaction code (*rxn.code*) for the experiment, the volume of aliquots extracted from the reaction mixtures, and whether conversion or concentration data are to be calculated.

The project specific parameters and calibration data are located in:

```
"~/R/kinetics/data/properties/prop-additions.csv"
"~/R/kinetics/data/processed/sc/additions/m-values.csv"
```

The output of the script, after running the contents of "~/R/kinetics/functions/input/general-input-version-2.R" is located in:

```
"~/R/kinetics/data/processed/rxn/additions"
```

In summary, the following R scripts were required to process each experiment based on the user input parameters, to generate the corresponding temporal concentration or conversion data:

```
"~/R/kinetics/functions/input/general-input-version-2.R"

if (project == "spirok"){
  data.types <- c("hplc.ratios.240e","conv","mmol","M", "ee")
  system.time(source(file="functions/spirok/spirok-rxn-conditions.R"))
  system.time(source(file="functions/spirok/wavelength-extrapolation-240-292.R"))
  system.time(source(file="functions/spirok/spirok-rxn-process.R"))
  system.time(source(file="functions/spirok/spirok-rxn-export.R"))
} else if (project == "snark"){
  data.types <- c("hplc.ratios","conv","mmol","M", "ee")
  system.time(source(file="functions/snark/snark-rxn-conditions.R"))
  system.time(source(file="functions/snark/snark-rxn-process.R"))
  system.time(source(file="functions/snark/snark-rxn-export.R"))
} else if (project == "additions") {
  if (conversion == TRUE){
  data.types <- c("hplc.ratios","conv","mmol","ee")
  system.time(source(file="functions/additions/additions-rxn-conditions.R"))
  system.time(source(file="functions/additions/additions-rxn-process.R"))
  system.time(source(file="functions/additions/additions-rxn-export.R"))
  }
  if (conversion == FALSE){
    data.types <- c("hplc.ratios","conv","mmol","M","ee")
    system.time(source(file="functions/additions/additions-rxn-conditions-conc.R"))
    system.time(source(file="functions/additions/additions-rxn-process-conc.R"))
    system.time(source(file="functions/additions/additions-rxn-export-conc.R"))
  }
}
```

### 8.2.1 Processing data according to conversion

Below are examples of the R scripts and user input data that were used to generate rate data corresponding to *amount in mmol* of substrate **49** to product **97** enantiomers; in addition, conversion and ee data were subsequently calculated.

In the following example, the project is designated "additions" which corresponds to theme of project 1. In this particular example, the reaction designated "additions-25" is being processed.

To process the data, the end user is required to input some parameters. For example in the

general parameters page:

```
rxn.code <- "additions-25"

replicates <- 1
# a minimum of 2 replicates for snark and spirok projects
# this MUST be 1 for additions projects

aliquot <- 1.50
# in uL, the volume of aliquots removed from the rxn mixture

conversion <- TRUE
# for additions project ONLY , if TRUE then only looking
# at conversion and not concentration of species

data.types <- c("hplc.ratios","conv","mmol","ee")
```

Additional data are required in the relevant "input" files, e.g.:

```
# additions-25

which_rep <- 1

base_added <- 3.8
# in uL

base_conc <- 8.9117663834
# in M (corresponds to 50 %(w/v) solution)

catalyst_added <- 7.6
# in mg

catalyst_MW <- 451.00
# in g/mol

catalyst_code <- "QD1"

limiting <- "substrate1"

stock.amount.standard <- 15
# amount of standard present in rxn in uL
```

The bulk processing then occurs in the following script, the outcome of which is exported temporal reaction data:

```
rm(list = ls())
setwd("~/Documents/R/kinetics")

library(abind)
library(arm)
library(gdata)
library(ggplot2)
library(gtools)
library(reshape2)
library(magrittr)
library(modelr)
  options(na.action = na.warn)
library(purrr)
library(deSolve)
library(tidyverse)

#simple functions

calc_mmol <- function(mass, MW) {
```

```
  mmol <- mass / MW
  return(mmol)}

ratio <- function(num,den){
  frac <- num/den
  return(frac)}

molecular <- function(molecular){
  names(molecular) <- c("code", "weight","density")
  return(molecular)}

insertRow <- function(existingDF, newrow, r) {
  existingDF[seq(r+1,nrow(existingDF)+1),] <- existingDF[seq(r,nrow(existingDF)),]
  existingDF[r,] <- newrow
  existingDF}

#simple functions

calc_mmol <- function(mass, MW) {
  mmol <- mass / MW
  return(mmol)
}

ratio <- function(num,den){
  frac <- num/den
  return(frac)
}

molecular <- function(molecular){
  names(molecular) <- c("code", "weight","density")
  return(molecular)
}

insertRow <- function(existingDF, newrow, r) {
  existingDF[seq(r+1,nrow(existingDF)+1),] <- existingDF[seq(r,nrow(existingDF)),]
  existingDF[r,] <- newrow
  existingDF
}

#data fetch commands

dataFetchPath <- function(rxn.data.type) {
  if (rxn.data.type == "user-input"){
    user.input.path <- paste("data/input/rxn/",project,sep="")
    user.input.path <- paste(user.input.path,rxn.code,sep="/")
    user.input.path <- paste(user.input.path,"user-input",sep="/")
    user.get.path <- paste(user.input.path, paste(c(1:replicates),".R",sep="") , sep="")
    user.get.path
  }
  else if (rxn.data.type == "sc-hplc"){
    hplc_data_path <- paste("data/raw/sc/",project,sep="")
    hplc_data_path <- paste(hplc_data_path,"hplc",sep="/")
    hplc_data_path <- paste(hplc_data_path,"sc-hplc",sep="/")
    get.path <- paste(hplc_data_path, paste(c(1:replicates),".csv",sep="") , sep="")
    get.path
  }
  else if (rxn.data.type == "rxn-hplc"){
    hplc_data_path <- paste("data/raw/rxn/",project,sep="")
    hplc_data_path <- paste(hplc_data_path,"hplc",sep="/")
    hplc_data_path <- paste(hplc_data_path,rxn.code,"hplc-data",sep="/")
    get.path <- paste(hplc_data_path, paste(c(1:replicates),".csv",sep="") , sep="")
    get.path
  } else if(rxn.data.type == "user-input-csv"){
    user.input.path <- paste("data/input/rxn/",project,sep="")
    user.input.path <- paste(user.input.path,rxn.code,sep="/")
    user.input.path <- paste(user.input.path,"user-input",sep="/")
    user.get.path <- paste(user.input.path, paste(c(1:replicates),".csv",sep="") , sep="")
    user.get.path
  } else if (rxn.data.type == "rxn-hplc-240"){
    hplc_data_path <- paste("data/raw/rxn/",project,sep="")
    hplc_data_path <- paste(hplc_data_path,"hplc",sep="/")
    hplc_data_path <- paste(hplc_data_path,rxn.code,"240-hplc-data",sep="/")
    get.path <- paste(hplc_data_path, paste(c(1:replicates),".csv",sep="") , sep="")
```

```
    get.path
  } else if (rxn.data.type == "rxn-hplc-292"){
    hplc_data_path <- paste("data/raw/rxn/",project,sep="")
    hplc_data_path <- paste(hplc_data_path,"hplc",sep="/")
    hplc_data_path <- paste(hplc_data_path,rxn.code,"292-hplc-data",sep="/")
    get.path <- paste(hplc_data_path, paste(c(1:replicates),".csv",sep="") , sep="")
    get.path
  } else if (rxn.data.type == "model-pars"){
    user.input.path <- paste("models",project,model,"input",sep="/") %>%
      paste(.,"/mod-pars",which.pars,".csv",sep="" )
    get.path <- user.input.path
    get.path
  } else if (rxn.data.type == "model-scheme"){
    user.input.path <- paste("models",project,model,"input",sep="/") %>%
      paste(.,"/mod-scheme",which.pars,".csv",sep="" )
    get.path <- user.input.path
    get.path
  }
}

getCoef <- function(numberInList)
{
temp <- as.character(mtype.list[numberInList])
temp <- gsub("\\."," ", temp)
temp <- unlist(strsplit(temp, " "))
temp <- unique(temp)
analyte.coordinate <- all.analytes[all.analytes %in% temp]
reps.coordinate <- all.reps[all.reps %in% temp]
mtype.coordinate <- all.ratios[all.ratios %in% temp]

temp <- m.all[mtype.coordinate,analyte.coordinate,reps.coordinate]
a <- temp[[1]]['coefficients',]
a <- simplify2array(a)
a[mtype.coordinate,1]
}

getSCurveData <- function(numberInList)
{
  temp <- as.character(mtype.list[numberInList])
  temp <- gsub("\\."," ", temp)
  temp <- unlist(strsplit(temp, " "))
  temp <- unique(temp)
  analyte.coordinate <- all.analytes[all.analytes %in% temp]
  reps.coordinate <- all.reps[all.reps %in% temp]
  mtype.coordinate <- all.ratios[all.ratios %in% temp]

  temp <- m.all[mtype.coordinate,analyte.coordinate,reps.coordinate]
  simplify2array(temp)

}

std <- function(x) sd(x)/sqrt(length(x))

### Imports the compound data specific to the project
all_compounds <- paste("data/properties/prop-", project, sep="") %>%
  paste(".csv",sep="") %>%
  read.csv() #Call in the data file with the compound properties, eg molecular weight

#sort data to be used
compounds <- all_compounds[!all_compounds$include == "FALSE",]

#checks if the compound is to be included in the processing table, if so,
# adds an appropriate header, then checks if chiral, if so, adds the enantiomer fields
n <- 1
headers_chiral <- c("")
repeat {
  if (n != length(compounds$identity)+1) {
    if (compounds$include[n] == TRUE && compounds$chiral[n] == TRUE){
      headers_chiral <- append(headers_chiral,
      (toString(compounds$identity[n])), after=length(headers_chiral))
      headers_chiral <- append(headers_chiral,
      paste(compounds$identity[n],"a",sep=""), after=length(headers_chiral))
      headers_chiral <- append(headers_chiral,
```

```
      paste(compounds$identity[n],"b",sep=""), after=length(headers_chiral))
    }
    if  (compounds$include[n] == TRUE && compounds$chiral[n] == FALSE){
      headers_chiral <- append(headers_chiral,
      (toString(compounds$identity[n])), after=length(headers_chiral))       }
  }
  n <- n + 1
  if (n == length(compounds$include)+1){
    headers_chiral <- headers_chiral[-1]
    rm(n)
    break
  }
}

##gets the ISC slope data for that project.
# For the moment, this needs to be created manually.
m.values <- paste("data/processed/sc/",project,"/m-values.csv",sep="")
m.values <- read.csv(file = m.values)
rownames(m.values) <- m.values[,'identity']
m.values <- m.values[,-c(1)]

all.reps <- paste("rep",c(1:replicates),sep="")
all.analytes <- headers_chiral[-1]
all.mtype <- colnames(m.values)

rxn.user.input.path <- dataFetchPath("user-input")
source(rxn.user.input.path)

## amount of standard added in mmol
standard.added <- stock.amount.standard*1.48/207.07

hplc.get.path <- dataFetchPath("rxn-hplc")
hplc_data <- read.csv(hplc.get.path)
names(hplc_data) <- c("time","standard","substrate1","product1a","product1b")
inj <- nrow(hplc_data)

hplc.data <- hplc_data

rxn.combined <- array(NA, dim = c(inj,length(all.analytes),
length(data.types),length(all.reps)))

dimnames(rxn.combined)[[1]] <- c(1:inj)
dimnames(rxn.combined)[[2]] <- all.analytes
dimnames(rxn.combined)[[4]] <- all.reps
dimnames(rxn.combined)[[3]] <- data.types
names(dimnames(rxn.combined)) <- list("time","analyte","data.type","reps")

# ###### calculating mmol from hplc integrals
a <- compounds$identity[which(compounds$chiral == "TRUE")]
for (i in all.analytes) {
  if (!(i %in% a)){
rxn.combined[,i,'hplc.ratios',] <- (hplc.data[,i,]/hplc.data[,'standard',])
}}

temp.analytes <- all.analytes[-(2)]
for (i in temp.analytes){
  for (n in all.reps){
    rxn.combined[,i,"mmol",n] <- rxn.combined[,i,'hplc.ratios',n]/
    m.values[i,"m.umol"]*standard.added}
}

###Adding up enantiomer mmol and calculating ee
for (i in all.analytes) {
  if (i %in% a){
    target.a <- c(paste(i,"a",sep=""))
    target.b <- c(paste(i,"b",sep=""))
    rxn.combined[,i,'mmol',] <- (rxn.combined[,target.a,'mmol',] +
    rxn.combined[,target.b,'mmol',])
    rxn.combined[,i,'ee',] <- (rxn.combined[,target.a,'hplc.ratios',] -
    rxn.combined[,target.b,'hplc.ratios',])/
    (rowSums(rxn.combined[,c(target.a,target.b),'hplc.ratios',]))*100

    #rxn.combined[,i,'hplc.ratios',] <- rxn.combined[,target.a,'hplc.ratios',]
```

```
    #target.a <- rxn.combined[,target.,'ee',]
    #rxn.combined[,i,'hplc.ratios',] <- (rxn.combined[,i,'hplc.ratios',] +
    rxn.combined[,target.b,'hplc.ratios',])
  }
}
rm(i, target.a, target.b)

# Calculating concentration and total conversion of substrate to product and
 in.total.conv <- all.analytes[!grepl("[a,b]$", all.analytes)]
 for(i in all.reps){
  total.conv <- rowSums(rxn.combined[,in.total.conv,'mmol',i])
  rxn.combined[,,'conv',i] <- (rxn.combined[,,'mmol',i]/total.conv)
}
 rm(total.conv, in.total.conv)

path <- paste("data/processed/rxn/",project,"/",rxn.code,"/", sep="")
if (file.exists(path)){
} else {
  dir.create(path)
}

for (i in all.reps){
  #inserts the time field into the exported data
  temp2 <- as.data.frame(hplc.data)
  temp2 <- temp2[1]
  temp <- as.data.frame(rxn.combined[,,'mmol',i])
  temp <- cbind (time = c(1:nrow(rxn.combined)), temp)
  temp[1] <- temp2
  #exports the data
  path <- i
  export_name <- paste(path,"mmol",sep="-")
  export_name <- paste(export_name,"csv",sep=".")
  write_csv(temp,paste("data/processed/rxn/",project,"/",rxn.code,"/",export_name,sep=""))
}

for (i in all.reps){
  #inserts the time field into the exported data
  temp2 <- as.data.frame(hplc.data)
  temp2 <- temp2[1]
  temp <- as.data.frame(rxn.combined[,,'ee',i])
  temp <- cbind (time = c(1:nrow(rxn.combined)), temp)
  temp[1] <- temp2
  #exports the data
  path <- i
  export_name <- paste(path,"ee",sep="-")
  export_name <- paste(export_name,"csv",sep=".")
  write_csv(temp,paste("data/processed/rxn/",project,"/",rxn.code,"/",export_name,sep=""))
}
rm(i)

for (i in all.reps){
  #inserts the time field into the exported data
  temp2 <- as.data.frame(hplc.data)
  temp2 <- temp2[1]
  temp <- as.data.frame(rxn.combined[,,'conv',i])
  temp <- cbind (time = c(1:nrow(rxn.combined)), temp)
  temp[1] <- temp2
  #exports the data
  path <- i
  export_name <- paste(path,"conv",sep="-")
  export_name <- paste(export_name,"csv",sep=".")
  write_csv(temp,paste("data/processed/rxn/",project,"/",rxn.code,"/",export_name,sep=""))
}
```

### 8.2.2 Processing data according to concentration

Below are examples of the R scripts and user input data that were used to generate rate data corresponding to *concentration* of substrate **49** to product **97** enantiomers; in addition, ee data were subsequently calculated.

In the following example, the project is designated "additions" which corresponds to theme of project 1. In this particular example, the reaction designated "additions-80" is being processed.

To process the data, the end user is required to input some parameters. For example in the general parameters page:

```
rxn.code <- "additions-80"

replicates <- 1
# a minimum of 2 replicates for snark and spirok projects
# this MUST be 1 for additions projects

aliquot <- 1.50
# in uL, the volume of aliquots removed from the rxn mixture

conversion <- FALSE
# for additions project ONLY , if TRUE then only looking
# at conversion and not concentration of species

data.types <- c("hplc.ratios","conv","mmol","M","ee")
```

Additional data are required in the relevant "input" files, e.g.:

```
#Reaction code additions-80

which_rep <- 1

base_added <- 3.8
#in uL

base_conc <- 8.911766          '
#in M (corresponds to 50 %(w/v) solution)

catalyst_added <- 3.8
#in mg

catalyst_MW <- 450
#in g/mol

catalyst_code <- "QD1"

limiting <- "substrate1"

solvent <- 0.9
#in mL

stock_volume <- 1
#in mL
```

```
#volume of the volumetric flask

stock_added <- 0.8
#in mL
# how much of the stock solution is added to the rxn

stock.amount.standard <- 21.7
#BrNaph is added as mass, not by volume. SO units are in mg.

stock.amount.substrate1 <- 49.8

stock.amount.substrate2 <- 19.6
```

The bulk processing then occurs in the following script, the outcome of which is exported temporal reaction data:

```
rm(list = ls())
setwd("~/Documents/R/kinetics")

library(abind)
library(arm)
library(gdata)
library(ggplot2)
library(gtools)
library(reshape2)
library(magrittr)
library(modelr)
  options(na.action = na.warn)
library(purrr)
library(deSolve)
library(tidyverse)

#simple functions

calc_mmol <- function(mass, MW) {
  mmol <- mass / MW
  return(mmol)}

ratio <- function(num,den){
  frac <- num/den
  return(frac)}

molecular <- function(molecular){
  names(molecular) <- c("code", "weight","density")
  return(molecular)}

insertRow <- function(existingDF, newrow, r) {
  existingDF[seq(r+1,nrow(existingDF)+1),] <- existingDF[seq(r,nrow(existingDF)),]
  existingDF[r,] <- newrow
  existingDF}

#simple functions

calc_mmol <- function(mass, MW) {
  mmol <- mass / MW
  return(mmol)
}

ratio <- function(num,den){
  frac <- num/den
  return(frac)
}

molecular <- function(molecular){
  names(molecular) <- c("code", "weight","density")
  return(molecular)
}
```

```
insertRow <- function(existingDF, newrow, r) {
  existingDF[seq(r+1,nrow(existingDF)+1),] <- existingDF[seq(r,nrow(existingDF)),]
  existingDF[r,] <- newrow
  existingDF
}

#data fetch commands

dataFetchPath <- function(rxn.data.type) {
  if (rxn.data.type == "user-input"){
    user.input.path <- paste("data/input/rxn/",project,sep="")
    user.input.path <- paste(user.input.path,rxn.code,sep="/")
    user.input.path <- paste(user.input.path,"user-input",sep="/")
    user.get.path <- paste(user.input.path, paste(c(1:replicates),".R",sep="") , sep="")
    user.get.path
  }
  else if (rxn.data.type == "sc-hplc"){
    hplc_data_path <- paste("data/raw/sc/",project,sep="")
    hplc_data_path <- paste(hplc_data_path,"hplc",sep="/")
    hplc_data_path <- paste(hplc_data_path,"sc-hplc",sep="/")
    get.path <- paste(hplc_data_path, paste(c(1:replicates),".csv",sep="") , sep="")
    get.path
  }
  else if (rxn.data.type == "rxn-hplc"){
    hplc_data_path <- paste("data/raw/rxn/",project,sep="")
    hplc_data_path <- paste(hplc_data_path,"hplc",sep="/")
    hplc_data_path <- paste(hplc_data_path,rxn.code,"hplc-data",sep="/")
    get.path <- paste(hplc_data_path, paste(c(1:replicates),".csv",sep="") , sep="")
    get.path
  } else if(rxn.data.type == "user-input-csv"){
    user.input.path <- paste("data/input/rxn/",project,sep="")
    user.input.path <- paste(user.input.path,rxn.code,sep="/")
    user.input.path <- paste(user.input.path,"user-input",sep="/")
    user.get.path <- paste(user.input.path, paste(c(1:replicates),".csv",sep="") , sep="")
    user.get.path
  } else if (rxn.data.type == "rxn-hplc-240"){
    hplc_data_path <- paste("data/raw/rxn/",project,sep="")
    hplc_data_path <- paste(hplc_data_path,"hplc",sep="/")
    hplc_data_path <- paste(hplc_data_path,rxn.code,"240-hplc-data",sep="/")
    get.path <- paste(hplc_data_path, paste(c(1:replicates),".csv",sep="") , sep="")
    get.path
  } else if (rxn.data.type == "rxn-hplc-292"){
    hplc_data_path <- paste("data/raw/rxn/",project,sep="")
    hplc_data_path <- paste(hplc_data_path,"hplc",sep="/")
    hplc_data_path <- paste(hplc_data_path,rxn.code,"292-hplc-data",sep="/")
    get.path <- paste(hplc_data_path, paste(c(1:replicates),".csv",sep="") , sep="")
    get.path
  } else if (rxn.data.type == "model-pars"){
    user.input.path <- paste("models",project,model,"input",sep="/") %>%
      paste(.,"/mod-pars",which.pars,".csv",sep="" )
    get.path <- user.input.path
    get.path
  } else if (rxn.data.type == "model-scheme"){
    user.input.path <- paste("models",project,model,"input",sep="/") %>%
      paste(.,"/mod-scheme",which.pars,".csv",sep="" )
    get.path <- user.input.path
    get.path
  }
}

getCoef <- function(numberInList)
{
temp <- as.character(mtype.list[numberInList])
temp <- gsub("\\."," ", temp)
temp <- unlist(strsplit(temp, " "))
temp <- unique(temp)
analyte.coordinate <- all.analytes[all.analytes %in% temp]
reps.coordinate <- all.reps[all.reps %in% temp]
mtype.coordinate <- all.ratios[all.ratios %in% temp]

temp <- m.all[mtype.coordinate,analyte.coordinate,reps.coordinate]
a <- temp[[1]]['coefficients',]
a <- simplify2array(a)
```

```
a[mtype.coordinate,1]
}

getSCurveData <- function(numberInList)
{
  temp <- as.character(mtype.list[numberInList])
  temp <- gsub("\\."," ", temp)
  temp <- unlist(strsplit(temp, " "))
  temp <- unique(temp)
  analyte.coordinate <- all.analytes[all.analytes %in% temp]
  reps.coordinate <- all.reps[all.reps %in% temp]
  mtype.coordinate <- all.ratios[all.ratios %in% temp]

  temp <- m.all[mtype.coordinate,analyte.coordinate,reps.coordinate]
  simplify2array(temp)

}

std <- function(x) sd(x)/sqrt(length(x))

##gets the ISC slope data for that project. For the moment, this needs to be created manually.
m.values <- paste("data/processed/sc/",project,"/m-values.csv",sep="")
m.values <- read.csv(file = m.values)
rownames(m.values) <- m.values[,'identity']
m.values <- m.values[,-c(1)]

all.reps <- paste("rep",c(1:replicates),sep="")
all.analytes <- headers_chiral[-1]
all.mtype <- colnames(m.values)

rxn.user.input.path <- dataFetchPath("user-input")
source(rxn.user.input.path)
#standard.added <- stock.amount.standard/207.07 ## amount of standard added in mmol

### specific for additions project - gets the variables from the input file
rxn_stock_amount <- c(stock.amount.standard, stock.amount.substrate1,
stock.amount.substrate2)
user.input <- list(base_added,base_conc,catalyst_added,catalyst_MW,
catalyst_code,limiting,solvent,stock_volume, stock_added)
stock_amount <- list(rxn_stock_amount)

## organising the user.input files into one list
names(stock_amount) <- all.reps
names(user.input) <- c("base_added","base_conc","catalyst_added",
"catalyst_MW","catalyst_code","limiting","solvent","stock_volume", "stock_added")

### Calculating the initial reaction volume
initial_volume <- (sum(unlist(user.input[c('solvent','stock_added')]))) +
(unlist(user.input['base_added']))/1000 )
names(initial_volume) <- "initial_volume"
 rm(base_added,base_conc,catalyst_added,catalyst_MW,
 catalyst_code,limiting,solvent,stock_volume)

### sorting which compounds to use in rxn compounds
rxn_compounds <- all_compounds
rxn_stock <- rxn_compounds[all_compounds$rxn_stock == "TRUE",]
rxn_stock <- rxn_stock[(1:4)]
rxn_stock <- cbind(rxn_stock, volume = NA, amount = NA,
conc_M = NA,added_mL = NA,mmol_added=NA)
#

### sorting data so that compounds added as a stock solution
# in the reaction mixture are findable by their analyte name.
# "stock.general" is general information about the stock solutions
stock.general <- rxn_compounds[all_compounds$rxn_stock == "TRUE",]
rownames(stock.general) <- unlist(stock.general['identity'])
stock.general <- stock.general[,-which(names(stock.general) %in% 'identity')]

variables.list <- names(stock.general)
variables.list <- variables.list[which(variables.list %in% c("weight","density"))]
variables.list <- append(variables.list, c("volume",
"amount", "conc_M","added_mL","mmol_added"))
```

```
## starting to organise the data that describe what went into the reactions
rxn.input <- array(NA, dim = c(length
(rownames(stock.general)),length(variables.list)))
dimnames(rxn.input)[[1]] <- rownames(stock.general)
dimnames(rxn.input)[[2]] <- variables.list
names(dimnames(rxn.input)) <- list("analyte","variable")

common <- variables.list[variables.list %in% names(stock.general)]
rm(variables.list)

####Filling in the reaction input table.
  rxn.input[, common] <- as.matrix(stock.general[common])
  rxn.input[,'amount'] <- unlist(stock_amount)
  rxn.input[,'volume'] <- unlist(user.input['stock_volume'])
  rxn.input[,'added_mL'] <- unlist(user.input['stock_added'])

  rm(common, stock_amount)


  for (i in rownames(rxn.input)){
      rxn.input[i,'conc_M'] <- ((rxn.input[i,'amount'])/
      (rxn.input[i,'weight'])/(rxn.input[i,'volume']))
    rxn.input[i,'mmol_added'] <- (rxn.input[i,'conc_M'])*
    (rxn.input[i,'added_mL'])
  }
    rxn.compounds <- factor(rxn_compounds[,1])
  rxn.conditions <- array(NA, c(length(rxn.compounds),3,replicates))
  dimnames(rxn.conditions)[[1]] <- rxn.compounds
  dimnames(rxn.conditions)[[2]] <- list("mmol","M", "equiv")
  dimnames(rxn.conditions)[[3]] <- all.reps
  names(dimnames(rxn.conditions)) <- list("analyte","measurement","reps")

  stock.compounds <- dimnames(rxn.conditions)[[1]]
  [dimnames(rxn.conditions)[[1]] %in% dimnames(rxn.input)[[1]]]
  rxn.conditions[stock.compounds,'mmol',] <-
  rxn.input[stock.compounds,'mmol_added']
  rm(stock.compounds)

  limiting <- user.input['limiting']

  for (i in all.reps){
    if (length(unlist(user.input['base_added'])) > 0){
      rxn.conditions['base','mmol',i] <-(unlist(user.input
      ['base_added'])*unlist(user.input['base_conc']))/1000
    } else {rxn.conditions['base','mmol',i] <- 0}

    if (length(unlist(user.input['catalyst_added'])) > 0){
      rxn.conditions['catalyst','mmol',i] <-(unlist(user.input
      ['catalyst_added'])/(unlist(user.input['catalyst_MW'])))
    } else {rxn.conditions['catalyst','mmol',i] <- 0}
    rxn.conditions[,'equiv',i] <- (rxn.conditions[,'mmol',i])/
    (rxn.conditions[as.character(limiting),'mmol',i])
  }

  for (i in all.reps){
    temp <- as.double(initial_volume)
    rxn.conditions[,'M',i] <- rxn.conditions[,'mmol',i]/temp
  }
  rm(limiting, i)

  hplc.get.path <- dataFetchPath("rxn-hplc")
hplc_data <- read.csv(hplc.get.path)
names(hplc_data) <- c("time","standard","substrate1","product1a","product1b")
inj <- nrow(hplc_data)

hplc.data <- hplc_data

rxn.combined <- array(NA, dim = c(inj,length(all.analytes),
length(data.types),length(all.reps)))
dimnames(rxn.combined)[[1]] <- c(1:inj)
dimnames(rxn.combined)[[2]] <- all.analytes
dimnames(rxn.combined)[[4]] <- all.reps
dimnames(rxn.combined)[[3]] <- data.types
```

```
names(dimnames(rxn.combined)) <- list("time","analyte","data.type","reps")

aliquot <- as.double(aliquot/1000) #aliquot volume in mL

cumulative.aliquots <- as.numeric(1:inj)
cumulative.aliquots <- cumulative.aliquots*aliquot
cumulative.volume <- initial_volume-cumulative.aliquots

###### calculating mmol from hplc integrals
a <- compounds$identity[which(compounds$chiral == "TRUE")]
for (i in all.analytes) {
  if (!(i %in% a)){
rxn.combined[,i,'hplc.ratios',] <- (hplc.data[,i,]/hplc.data[,'standard',])
}}

temp.analytes <- all.analytes[-(2)]
for (i in temp.analytes){
  for (n in all.reps){
    rxn.combined[,i,"mmol",n] <- rxn.combined[,i,'hplc.ratios',n]/
    m.values[i,"m.umol"]*standard.added}
}

###Adding up enantiomer mmol and calculating ee
for (i in all.analytes) {
  if (i %in% a){
    target.a <- c(paste(i,"a",sep=""))
    target.b <- c(paste(i,"b",sep=""))
    rxn.combined[,i,'mmol',] <- (rxn.combined[,target.a,'mmol',] +
    rxn.combined[,target.b,'mmol',])
    rxn.combined[,i,'ee',] <- (rxn.combined[,target.a,'hplc.ratios',]-
    rxn.combined[,target.b,'hplc.ratios',])/(rowSums(rxn.combined[,
    c(target.a,target.b),'hplc.ratios',]))*100

    #rxn.combined[,i,'hplc.ratios',] <- rxn.combined[,target.a,'hplc.ratios',]
    #target.a <- rxn.combined[,target.,'ee',]
    #rxn.combined[,i,'hplc.ratios',] <- (rxn.combined[,i,'hplc.ratios',] +
    rxn.combined[,target.b,'hplc.ratios',])
  }
}
rm(i, target.a, target.b)

cumulative.volume <- list(cumulative.volume)

# Calculating concentration and total conversion of substrate to product and
 in.total.conv <- all.analytes[!grepl("[a,b]$", all.analytes)]
 for(i in all.reps){
   names(cumulative.volume) <- i
     total.conv <- rowSums(rxn.combined[,in.total.conv,'mmol',i])
  rxn.combined[,,'conv',i] <- (rxn.combined[,,'mmol',i]/total.conv)
  rxn.combined[,,'M',i] <- (rxn.combined[,,'mmol',i]/cumulative.volume$rep1)
}
 rm(total.conv, in.total.conv)

path <- paste("data/processed/rxn/",project,"/",rxn.code,"/", sep="")
if (file.exists(path)){
} else {
  dir.create(path)
}

for (i in all.reps){
  #inserts the time field into the exported data
  temp2 <- as.data.frame(hplc.data)
  temp2 <- temp2[1]
  temp <- as.data.frame(rxn.combined[,,'mmol',i])
  temp <- cbind (time = c(1:nrow(rxn.combined)), temp)
  temp[1] <- temp2
  #exports the data
  path <- i
  export_name <- paste(path,"mmol",sep="-")
  export_name <- paste(export_name,"csv",sep=".")
  write_csv(temp,paste
  ("data/processed/rxn/",project,"/",rxn.code,"/",export_name,sep=""))
}
```

```
for (i in all.reps){
  #inserts the time field into the exported data
  temp2 <- as.data.frame(hplc.data)
  temp2 <- temp2[1]
  temp <- as.data.frame(rxn.combined[,,'ee',i])
  temp <- cbind (time = c(1:nrow(rxn.combined)), temp)
  temp[1] <- temp2
  #exports the data
  path <- i
  export_name <- paste(path,"ee",sep="-")
  export_name <- paste(export_name,"csv",sep=".")
  write_csv(temp,paste
  ("data/processed/rxn/",project,"/",rxn.code,"/",export_name,sep=""))
}
rm(i)

for (i in all.reps){
  #inserts the time field into the exported data
  temp2 <- as.data.frame(hplc.data)
  temp2 <- temp2[1]
  temp <- as.data.frame(rxn.combined[,,'conv',i])
  temp <- cbind (time = c(1:nrow(rxn.combined)), temp)
  temp[1] <- temp2
  #exports the data
  path <- i
  export_name <- paste(path,"conv",sep="-")
  export_name <- paste(export_name,"csv",sep=".")
  write_csv(temp,paste
  ("data/processed/rxn/",project,"/",rxn.code,"/",export_name,sep=""))
}

for (i in all.reps){
  #inserts the time field into the exported data
  temp2 <- as.data.frame(hplc.data)
  temp2 <- temp2[1]
  temp <- as.data.frame(rxn.combined[,,'M',i])
  temp <- cbind (time = c(1:nrow(rxn.combined)), temp)
  temp[1] <- temp2
  #exports the data
  path <- i
  export_name <- paste(path,"conc",sep="-")
  export_name <- paste(export_name,"csv",sep=".")
  write_csv(temp,paste
  ("data/processed/rxn/",project,"/",rxn.code,"/",export_name,sep=""))
}

path <- paste("data/processed/rxn/",project,"/",rxn.code,"/", sep="")
export_name <- paste(rxn.code,"rxn",sep="-")
export_name <- paste(export_name,"csv",sep=".")

rxn.conditions.df <- as.data.frame(rownames(rxn.conditions))
rxn.conditions.df <- cbind(rxn.conditions.df, rxn.conditions)
write_csv(rxn.conditions.df,paste(path,"",export_name,sep=""))
rm(temp, temp2)
```

## 8.3 Processing data in project 2

Data processing in project 2 was carried out analogously to project 1. The exception was in the specified project: "spirok" and the nested folders referenced during processing.

### 8.3.1 Example of processing data in project 2

In the following example, the project is designated "spirok" which corresponds to theme of project 2. In this particular example, the reaction designated "spirok-63" is being processed.

To process the data, the end user is required to input some parameters. For example in the general parameters page:

```
rxn.code <- "spirok-63"

replicates <- 2
# a minimum of 2 replicates for snark and spirok projects

aliquot <- 2.0
# in uL, aliquots removed from the rxn mixture

organic <- FALSE
# whether to calculate concentration as purely from
#the organic phase and disregards the aqueous phase

conversion <- TRUE
#for additions project ONLY, if TRUE then only
#looking at conversion and not concentration of species

data.types <- c("hplc.ratios.240e","conv","mmol","M", "ee")
```

Additional data are required in the relevant "input" files, e.g.:

```
#Reaction code spirok-63

which_protocol <- 2
#0 = n/a, 1 = srp, 2 = mrp, 3 = misc

which_rep <- 1

base_added <- 305
# in uL

base_conc <- 4.77
# in M

catalyst_added <- 10.6
# in mg

catalyst_MW <- 698.734
# in g/mol

catalyst_code <- "KAB157"

limiting <- "substrate1"

solvent <- 0.56
# in mL

stock_volume <- 1
# in mL #volume of the volumetric flask containing the stock solutions

stock_added <- 0.9
# in mL # how much of the stock solution is added to the rxn
```

```
stock.amount.standard <- 3.1
# amount (mg) of standard in the stock solution

stock.amount.substrate1 <- 70
# amount (mg) of substrate1 in the stock solution
```

The bulk processing then occurs in the following script, the outcome of which is exported temporal reaction data:

```
rm(list = ls())
setwd("~/Documents/R/kinetics")

library(abind)
library(arm)
library(gdata)
library(ggplot2)
library(gtools)
library(reshape2)
library(magrittr)
library(modelr)
  options(na.action = na.warn)
library(purrr)
library(deSolve)
library(tidyverse)

#simple functions

calc_mmol <- function(mass, MW) {
  mmol <- mass / MW
  return(mmol)}

ratio <- function(num,den){
  frac <- num/den
  return(frac)}

molecular <- function(molecular){
  names(molecular) <- c("code", "weight","density")
  return(molecular)}

insertRow <- function(existingDF, newrow, r) {
  existingDF[seq(r+1,nrow(existingDF)+1),] <- existingDF[seq(r,nrow(existingDF)),]
  existingDF[r,] <- newrow
  existingDF}

#data fetch commands

dataFetchPath <- function(rxn.data.type) {
  if (rxn.data.type == "user-input"){
    user.input.path <- paste("data/input/rxn/",project,sep="")
    user.input.path <- paste(user.input.path,rxn.code,sep="/")
    user.input.path <- paste(user.input.path,"user-input",sep="/")
    user.get.path <- paste(user.input.path, paste(c(1:replicates),".R",sep="") , sep="")
    user.get.path} else if (rxn.data.type == "sc-hplc"){
    hplc_data_path <- paste("data/raw/sc/",project,sep="")
    hplc_data_path <- paste(hplc_data_path,"hplc",sep="/")
    hplc_data_path <- paste(hplc_data_path,"sc-hplc",sep="/")
    get.path <- paste(hplc_data_path, paste(c(1:replicates),".csv",sep="") , sep="")
    get.path} else if (rxn.data.type == "rxn-hplc"){
    hplc_data_path <- paste("data/raw/rxn/",project,sep="")
    hplc_data_path <- paste(hplc_data_path,"hplc",sep="/")
    hplc_data_path <- paste(hplc_data_path,rxn.code,"hplc-data",sep="/")
    get.path <- paste(hplc_data_path, paste(c(1:replicates),".csv",sep="") , sep="")
    get.path} else if(rxn.data.type == "user-input-csv"){
    user.input.path <- paste("data/input/rxn/",project,sep="")
    user.input.path <- paste(user.input.path,rxn.code,sep="/")
    user.input.path <- paste(user.input.path,"user-input",sep="/")
    user.get.path <- paste(user.input.path, paste(c(1:replicates),".csv",sep="") , sep="")
    user.get.path} else if (rxn.data.type == "rxn-hplc-240"){
```

```
    hplc_data_path <- paste("data/raw/rxn/",project,sep="")
    hplc_data_path <- paste(hplc_data_path,"hplc",sep="/")
    hplc_data_path <- paste(hplc_data_path,rxn.code,"240-hplc-data",sep="/")
    get.path <- paste(hplc_data_path, paste(c(1:replicates),".csv",sep="") , sep="")
    get.path} else if (rxn.data.type == "rxn-hplc-292"){
    hplc_data_path <- paste("data/raw/rxn/",project,sep="")
    hplc_data_path <- paste(hplc_data_path,"hplc",sep="/")
    hplc_data_path <- paste(hplc_data_path,rxn.code,"292-hplc-data",sep="/")
    get.path <- paste(hplc_data_path, paste(c(1:replicates),".csv",sep="") , sep="")
    get.path} else if (rxn.data.type == "model-pars"){
    user.input.path <- paste("models",project,model,"input",sep="/") %>%
      paste(.,"/mod-pars",which.pars,".csv",sep="" )
    get.path <- user.input.path
    get.path} else if (rxn.data.type == "model-scheme"){
    user.input.path <- paste("models",project,model,"input",sep="/") %>%
      paste(.,"/mod-scheme",which.pars,".csv",sep="" )
    get.path <- user.input.path
    get.path}

 getCoef <- function(numberInList)
{
temp <- as.character(mtype.list[numberInList])
temp <- gsub("\\."," ", temp)
temp <- unlist(strsplit(temp, " "))
temp <- unique(temp)
analyte.coordinate <- all.analytes[all.analytes %in% temp]
reps.coordinate <- all.reps[all.reps %in% temp]
mtype.coordinate <- all.ratios[all.ratios %in% temp]

temp <- m.all[mtype.coordinate,analyte.coordinate,reps.coordinate]
a <- temp[[1]]['coefficients',]
a <- simplify2array(a)
a[mtype.coordinate,1]}

getSCurveData <- function(numberInList)
{
  temp <- as.character(mtype.list[numberInList])
  temp <- gsub("\\."," ", temp)
  temp <- unlist(strsplit(temp, " "))
  temp <- unique(temp)
  analyte.coordinate <- all.analytes[all.analytes %in% temp]
  reps.coordinate <- all.reps[all.reps %in% temp]
  mtype.coordinate <- all.ratios[all.ratios %in% temp]

  temp <- m.all[mtype.coordinate,analyte.coordinate,reps.coordinate]
  simplify2array(temp)}
std <- function(x) sd(x)/sqrt(length(x))
}

### Imports the compound data specific to the project
all_compounds <- paste("data/properties/prop-", project, sep="") %>%
  paste(".csv",sep="") %>%
  read.csv() #Call in the data file with the compound properties, eg molecular weight

#sort data to be used
compounds <- all_compounds[!all_compounds$include == "FALSE",]

#checks if the compound is to be included in the processing table, if so,
#adds an appropriate header, then checks if chiral, if so, adds the enantiomer fields
n <- 1
headers_chiral <- c("")
repeat {
  if (n != length(compounds$identity)+1) {
    if (compounds$include[n] == TRUE && compounds$chiral[n] == TRUE){
      headers_chiral <- append(headers_chiral,
      (toString(compounds$identity[n])), after=length(headers_chiral))
      headers_chiral <- append(headers_chiral,
      paste(compounds$identity[n],"a",sep=""), after=length(headers_chiral))
      headers_chiral <- append(headers_chiral,
      paste(compounds$identity[n],"b",sep=""), after=length(headers_chiral))
    }
    if  (compounds$include[n] == TRUE && compounds$chiral[n] == FALSE){
      headers_chiral <- append(headers_chiral,
```

```
      (toString(compounds$identity[n])), after=length(headers_chiral))      }
  }
  n <- n + 1
  if (n == length(compounds$include)+1){
    headers_chiral <- headers_chiral[-1]
    rm(n)
    break}}

## gets the ISC slope data for that project.
## For the moment, this needs to be created manually.
m.values <- paste("data/processed/sc/",project,"/m-values.csv",sep="")
m.values <- read.csv(file = m.values)
rownames(m.values) <- m.values[,'identity']
m.values <- m.values[,-c(1)]

all.reps <- paste("rep",c(1:replicates),sep="")
all.analytes <- headers_chiral[-1]
all.mtype <- colnames(m.values)

rxn.user.input.path <- dataFetchPath("user-input")

### specific for spirok project - gets the variables from the input file
for (i in rxn.user.input.path) {
  source(i)
    rxn_stock_amount <- c(stock.amount.standard, stock.amount.substrate1)
  rm(stock.amount.standard, stock.amount.substrate1)
  if (which_rep == 1){
    user.input <- list(base_added,base_conc,catalyst_added,catalyst_MW,
    catalyst_code,limiting,solvent,stock_volume, stock_added)
    stock_amount <- list(rxn_stock_amount)
  } else {
    temp <- list(base_added,base_conc,catalyst_added,catalyst_MW,
    catalyst_code,limiting,solvent,stock_volume, stock_added)
    user.input <- cbind(user.input,temp)
    stock_amount <- append(stock_amount,list(rxn_stock_amount))
    rm(temp)
  }
  rm(rxn_stock_amount, which_rep, stock_added)
}
rm(rxn.user.input.path)
if (length(all.reps)>1) {
## organising the user.input files into one list
names(stock_amount) <- all.reps
colnames(user.input) <- all.reps
rownames(user.input) <- c("base_added","base_conc","catalyst_added",
"catalyst_MW","catalyst_code","limiting","solvent","stock_volume", "stock_added")
} else if (length(all.reps) == 1) {
  print("just 1")}

## Calculating the initial reaction volume
initial_volume<- as.list(c(all.reps))
names(initial_volume) <- all.reps
if (organic == FALSE){
for (i in all.reps){
  initial_volume[i] <- (sum(unlist(user.input[c('solvent','stock_added'),i]))
  + (unlist(user.input['base_added',i]))/1000 )}
} else if (organic == TRUE){
  for (i in all.reps){
    initial_volume[i] <- (sum(unlist(user.input[c('solvent','stock_added'),i])))}}

rm(base_added,base_conc,catalyst_added,catalyst_MW,
catalyst_code,limiting,solvent,stock_volume)

### sorting which compounds to use in rxn compounds
rxn_compounds <- all_compounds
rxn_stock <- rxn_compounds[all_compounds$rxn_stock == "TRUE",]
rxn_stock <- rxn_stock[(1:4)]
rxn_stock <- cbind(rxn_stock, volume = NA, amount = NA,
        conc_M = NA,added_mL = NA,mmol_added=NA)

#source(file="functions/global/rxn-input-container.R")

### sorting data so that compounds added as a stock solution in the
```

```
## reaction mixture are findable by their analyte name.
## "stock.general" is general information about the stock solutions
stock.general <- rxn_compounds[all_compounds$rxn_stock == "TRUE",]
rownames(stock.general) <- unlist(stock.general['identity'])
stock.general <- stock.general[,-which(names(stock.general) %in% 'identity')]

variables.list <- names(stock.general)
variables.list <- variables.list[which(variables.list %in% c("weight","density"))]
variables.list <- append(variables.list,
c("volume", "amount", "conc_M","added_mL","mmol_added"))

## starting to organise the data that describe what went into the reactions
rxn.input <- array(NA, dim = c(length(rownames(stock.general)),
length(variables.list),length(all.reps)))
dimnames(rxn.input)[[1]] <- rownames(stock.general)
dimnames(rxn.input)[[2]] <- variables.list
dimnames(rxn.input)[[3]] <- all.reps
names(dimnames(rxn.input)) <- list("analyte","variable","reps")

common <- variables.list[variables.list %in% names(stock.general)]
rm(variables.list)

####Filling in the reaction input table.
for (i in all.reps) {
  rxn.input[, common, i] <- as.matrix(stock.general[common])
  rxn.input[,'amount',i] <- unlist(stock_amount[i])
  rxn.input[,'volume',i] <- unlist(user.input['stock_volume',i])
  rxn.input[,'added_mL',i] <- unlist(user.input['stock_added',i])}

rm(common, stock_amount)

for (i in rownames(rxn.input)){
  if (stock.general[i,'density'] > 0) {
    rxn.input[i,'conc_M',] <- (rxn.input[i,'density',]*(rxn.input[i,'amount',])/
    (rxn.input[i,'weight',])/(rxn.input[i,'volume',]))
  } else if (stock.general[i,'density'] == 0){
    rxn.input[i,'conc_M',] <- ((rxn.input[i,'amount',])/(rxn.input[i,'weight',])/
    (rxn.input[i,'volume',]))}
  rxn.input[i,'mmol_added',] <- (rxn.input[i,'conc_M',])*(rxn.input[i,'added_mL',])}

#####This is assuming all replicates use the same catalyst
rxn.compounds <- factor(rxn_compounds[,1])
rxn.conditions <- array(NA, c(length(rxn.compounds),3,replicates))
dimnames(rxn.conditions)[[1]] <- rxn.compounds
dimnames(rxn.conditions)[[2]] <- list("mmol","M", "equiv")
dimnames(rxn.conditions)[[3]] <- all.reps
names(dimnames(rxn.conditions)) <- list("analyte","measurement","reps")

stock.compounds <- dimnames(rxn.conditions)
[[1]][dimnames(rxn.conditions)[[1]] %in% dimnames(rxn.input)[[1]]]
rxn.conditions[stock.compounds,'mmol',] <- rxn.input[stock.compounds,'mmol_added',]
rm(stock.compounds)

limiting <- user.input['limiting',]

for (i in all.reps){
  if (length(unlist(user.input['base_added',i])) > 0){
    rxn.conditions['base','mmol',i] <-(unlist(user.input['base_added',i])
    *unlist(user.input['base_conc',i]))/1000
  } else {rxn.conditions['base','mmol',i] <- 0}

  if (length(unlist(user.input['catalyst_added',i])) > 0){
    rxn.conditions['catalyst','mmol',i] <-(unlist(user.input['catalyst_added',i])/
    (unlist(user.input['catalyst_MW',i])))
  } else {rxn.conditions['catalyst','mmol',i] <- 0}
  rxn.conditions[,'equiv',i] <- (rxn.conditions[,'mmol',i])/
  (rxn.conditions[as.character(limiting[i]),'mmol',i])
}

for (i in all.reps){
  temp <- as.double(initial_volume[i])
  rxn.conditions[,'M',i] <- rxn.conditions[,'mmol',i]/temp
}
```

```
rm(limiting, i,initial_volume)

#### import the hplc files to get the number of injections
hplc.get.path <- dataFetchPath("rxn-hplc-240")
hplc_data_240 <-lapply(hplc.get.path, read.csv, stringsAsFactors = FALSE)
names(hplc_data_240) <- all.reps
hplc_data_240 <- lapply(hplc_data_240, setNames, nm =
c('time',unlist(unique(lapply(hplc_data_240, names)))[-1]))

hplc.get.path <- dataFetchPath("rxn-hplc-292")
hplc_data_292 <-lapply(hplc.get.path, read.csv, stringsAsFactors = FALSE)
names(hplc_data_292) <- all.reps
hplc_data_292 <- lapply(hplc_data_292, setNames, nm =
c('time',unlist(unique(lapply(hplc_data_292, names)))[-1]))

inj <- nrow(hplc_data_240[[1]])

#### put the hplc in an easier to edit format
hplc.data.240 <- array(NA, dim = c(inj,ncol(hplc_data_240[[1]]),length(all.reps)))
dimnames(hplc.data.240)[[1]] <- c(1:inj)
dimnames(hplc.data.240)[[2]] <- names((hplc_data_240[[1]]))
dimnames(hplc.data.240)[[3]] <- all.reps

for (i in all.reps) {
  hplc.data.240[,,i] <- suppressWarnings(as.numeric(unlist(hplc_data_240[i])))
}

hplc.data.292 <- array(NA, dim = c(inj,ncol(hplc_data_292[[1]]),length(all.reps)))
dimnames(hplc.data.292)[[1]] <- c(1:inj)
dimnames(hplc.data.292)[[2]] <- names((hplc_data_292[[1]]))
dimnames(hplc.data.292)[[3]] <- all.reps

for (i in all.reps) {
  hplc.data.292[,,i] <- suppressWarnings(as.numeric(unlist(hplc_data_292[i])))
}

### calculates ratios of substrate1b:substrate1a and product1a:product1b at 292 nm
ratios.292 <- array(NA, dim = c(inj,analytes,length(all.reps)))
dimnames(ratios.292)[[1]] <- c(1:inj)
dimnames(ratios.292)[[2]] <- analyte
dimnames(ratios.292)[[3]] <- all.reps
ratios.292 <- ratios.292[,-c(1),]

for (i in all.reps) {
  ratios.292[,'substrate1',i] <- hplc.data.292[,'substrate1b',i]/
        hplc.data.292[,'substrate1a',i]
  ratios.292[,'product1',i] <- hplc.data.292[,'product1a',i]/
        hplc.data.292[,'product1b',i]
}

### creates container for holding extrapolated values at 240 nm,
### then adds the extrapolated data from 292 nm
hplc.data.240e <- hplc.data.240
for (i in all.reps) { hplc.data.240e[,'substrate1b',i] <-
hplc.data.240e[,'substrate1a',i]*ratios.292[,'substrate1',i]
hplc.data.240e[,'product1a',i] <- hplc.data.240e[,'product1b',i]*ratios.292[,'product1',i]}
rm(i)

#### Create the container to hold the hplc data, with length of number of injections
rxn.combined <- array(NA, dim = c(inj,length(all.analytes),
length(data.types),length(all.reps)))
dimnames(rxn.combined)[[1]] <- c(1:inj)
dimnames(rxn.combined)[[2]] <- all.analytes
dimnames(rxn.combined)[[3]] <- data.types
dimnames(rxn.combined)[[4]] <- all.reps
names(dimnames(rxn.combined)) <- list("time","analyte","data.type","reps")

initial.volume<- as.list(c(all.reps))
names(initial.volume) <- all.reps

aliquot <- as.double(aliquot/1000)

cumulative.aliquots <- as.numeric(1:inj)
```

```
cumulative.aliquots <- cumulative.aliquots*aliquot
cumulative.volume <- rep(list(cumulative.aliquots),replicates)
names(cumulative.volume) <- all.reps

if (organic == FALSE){
for (i in all.reps){
  initial.volume[i] <- (sum(unlist(user.input[c('solvent','stock_added'),i]))
  + (unlist(user.input['base_added',i]))/1000 )
  cumulative.volume[[i]] <- (initial.volume[[i]]-cumulative.aliquots)
}} else if (organic == TRUE){
  for (i in all.reps){
    initial.volume[i] <- (sum(unlist(user.input[c('solvent','stock_added'),i])) )
    cumulative.volume[[i]] <- (initial.volume[[i]]-cumulative.aliquots)}}

#start to fill in the hplc ratios data
a <- compounds$identity[which(compounds$chiral == "TRUE")]
for (i in all.analytes) {
  if (!(i %in% a)){
    rxn.combined[,i,'hplc.ratios.240e',] <-
    (hplc.data.240e[,i,]/hplc.data.240e[,'standard',])}}
rm(a)


# #fill in the rest of the hplc ratios data
# rxn.combined[,'substrate1','hplc.ratios.240e',] <-
rxn.combined[,'substrate1a','hplc.ratios.240e',]+
rxn.combined[,'substrate1b','hplc.ratios.240e',]
# rxn.combined[,'product1','hplc.ratios.240e',] <-
rxn.combined[,'product1a','hplc.ratios.240e',]+
rxn.combined[,'product1b','hplc.ratios.240e',]


###### calculating mmol from hplc integrals
temp.analytes <- all.analytes[-(1)]
temp.analytes <- temp.analytes[-(3)]
for (i in temp.analytes){
  for (n in all.reps){
    rxn.combined[,i,"mmol",n] <- rxn.combined[,i,'hplc.ratios.240e',n]/
    m.values[i,"m.umol"]*rxn.input['standard','mmol_added',n]}}

rxn.combined[,'substrate1','mmol',] <- rxn.combined[,'substrate1a','mmol',]+
rxn.combined[,'substrate1b','mmol',]
rxn.combined[,'product1','mmol',] <- rxn.combined[,'product1a','mmol',]+
rxn.combined[,'product1b','mmol',]

rm(temp.analytes)

# #fill in the rest of the mmol, conv and conc data.
in.total.conv <- all.analytes[!grepl("[a,b]$", all.analytes)]
for(i in all.reps){
  total.conv <- rowSums(rxn.combined[,in.total.conv,'mmol',i])
  rxn.combined[,,'conv',i] <- (rxn.combined[,,'mmol',i]/total.conv)
  rxn.combined[,,'M',i] <- (rxn.combined[,,'mmol',i]/cumulative.volume[[i]])}

### Assumes allllll time points are the same!!!
dimnames(rxn.combined)['time'] <- list(hplc.data.240e[,'time',1])

# # Otherwise, this works too:
# mod.rxn <- c(inj, length(all.analytes)+1, length(data.types), length(all.reps))
# mod.rxn <- array(NA, dim = mod.rxn)
# dimnames(mod.rxn)[[1]] <- c(1:inj)
# dimnames(mod.rxn)[[2]] <- append('time',all.analytes)
# dimnames(mod.rxn)[[4]] <- all.reps
# dimnames(mod.rxn)[[3]] <- data.types
# names(dimnames(mod.rxn)) <- list("injection","analyte","data.type","reps")
#
# common <- dimnames(mod.rxn)
[[2]][dimnames(mod.rxn)[[2]] %in% dimnames(rxn.combined)[[2]]]
# mod.rxn[,common,,] <- rxn.combined[,common,,]
# for (i in all.reps){
#   mod.rxn[,'time',,i]<- hplc.data[,'time',i]
# }
```

```
## Calculates the ee of substrate1 and product1
for (i in all.reps) {
for (n in in.total.conv) {
  target.a <- paste(n,"a",sep="")
  target.b <- paste(n,"b",sep="")
  rxn.combined[,n,'ee',i] <- (rxn.combined[,target.b,'mmol',i]
  -rxn.combined[,target.a,'mmol',i])/
  (rxn.combined[,target.a,'mmol',i]+
  rxn.combined[,target.b,'mmol',i])*100}}

rm(in.total.conv, cumulative.volume, total.conv,cumulative.aliquots)
rm(i,initial.volume,replicates)

path <- paste("data/processed/rxn/",project,"/",rxn.code,"/", sep="")
if (file.exists(path)){
} else {
  dir.create(path)}

for (i in all.reps){
  #inserts the time field into the exported data
  temp2 <- as.data.frame(hplc_data_240)
  temp2 <- temp2[1]
  temp <- as.data.frame(rxn.combined[,,'mmol',i])
  temp <- cbind (time = c(1:nrow(rxn.combined)), temp)
  temp[1] <- temp2
  #exports the data
  path <- i
  export_name <- paste(path,"mmol",sep="-")
  export_name <- paste(export_name,"csv",sep=".")
  write_csv(temp,paste
  ("data/processed/rxn/",project,"/",rxn.code,"/",export_name,sep=""))
}

for (i in all.reps){
  #inserts the time field into the exported data
  temp2 <- as.data.frame(hplc_data_240)
  temp2 <- temp2[1]
  temp <- as.data.frame(rxn.combined[,,'ee',i])
  temp <- cbind (time = c(1:nrow(rxn.combined)), temp)
  temp[1] <- temp2
    #exports the ee data
  path <- i
  export_name <- paste(path,"ee",sep="-")
  export_name <- paste(export_name,"csv",sep=".")
  write_csv(temp,paste
  ("data/processed/rxn/",project,"/",rxn.code,"/",export_name,sep=""))}
rm(i)

for (i in all.reps){
  #inserts the time field into the exported data
  temp2 <- as.data.frame(hplc_data_240)
  temp2 <- temp2[1]
  temp <- as.data.frame(rxn.combined[,,'M',i])
  temp <- cbind (time = c(1:nrow(rxn.combined)), temp)
  temp[1] <- temp2

  #exports the conc data
   path <- i
  export_name <- paste(path,"conc",sep="-")
  export_name <- paste(export_name,"csv",sep=".")
  write_csv(temp,paste
  ("data/processed/rxn/",project,"/",rxn.code,"/",export_name,sep=""))}
rm(i,path)

path <- paste("data/processed/rxn/",project,"/",rxn.code,"/", sep="")
export_name <- paste(rxn.code,"rxn",sep="-")
export_name <- paste(export_name,"csv",sep=".")

rxn.conditions.df <- as.data.frame(rownames(rxn.conditions))
rxn.conditions.df <- cbind(rxn.conditions.df, rxn.conditions)
write_csv(rxn.conditions.df,paste(path,"",export_name,sep=""))
rm(temp, temp2)
```

# 9. Mathematica Scripts

## 9.1 General information

All Mathematica scripts were created and optimised by MRG and are described below. The working notebooks for each of the described models (1 to 6) are available electronically in .nb format.

## 9.2 Mathematica scripts for model 1

The Mathematica model was constructed according to the system described in 7.22.2. In the script below, the naming conventions were as follows: Q = **127**, B = $K_3PO_4$, I1 = **139**, I2 = **140**, I3 = **135**, I4 = **136**, S1 = (−)-**125**, S2 = (+)-**125**, P = **126**.

```
  Remove["Global`*"]

Manipulate[
solution=NDSolve[{
Q'[t]==-kQ Q[t] B[t],
B'[t]==- kQ Q[t]B[t]-k5 I4[t]B[t] ,
I1'[t]==kQ Q[t] B[t] -2 k1f I1[t]^2 + 2k1b I2[t],
I2'[t]==k1f I1[t]^2 - k1b I2[t]-k2f I2[t] S1[t] + k2b I3[t] -
        k3f I2[t] S2[t] + k3b I3[t]+k5 I4[t]B[t] ,
S1'[t]==-k2f I2[t] S1[t] + k2b I3[t],
S2'[t]==-k3f I2[t] S2[t] + k3b I3[t],
I3'[t]==k2f I2[t] S1[t] - k2b I3[t] +k3f I2[t] S2[t] - k3b I3[t]-k4 I3[t] ,
I4'[t]==k4 I3[t] -k5 I4[t]B[t] ,
P'[t]== k4 I3[t],
Q[0]==q0x,
B[0]==b0x,
I1[0]==0,
I2[0]==0,
I3[0]==0,
I4[0]==0,
S1[0]==s10x,
S2[0]==s20x,
P[0]==0}/.{kQ->kQx,k1f->k1fx,k1b->k1bx,k2f->k2fx,
        k2b->k2bx, k3f->k3fx,k3b->k3bx,k4-> k4x,k5->k5x},
{Q,B,I1,I2,I3,I4,S1,S2,P},
{t,0,tmax}];
Plot[{
Legended[Evaluate[Q[t]/.solution],Q],
Legended[Evaluate[B[t]/.solution],B],
Legended[Evaluate[I1[t]/.solution],I1],
Legended[Evaluate[I2[t]/.solution],I2],
Legended[Evaluate[I3[t]/.solution],I3],
Legended[Evaluate[I4[t]/.solution],I4],
Legended[Evaluate[S1[t]/.solution],S1],
Legended[Evaluate[S2[t]/.solution],S2],
Legended[Evaluate[P[t]/.solution],P]
```

```
}
,{t,0,tmax},AxesLabel->{t,conc},AxesStyle->Directive[Thick,Medium],
        PlotRange->Full,PlotStyle->{LightMagenta,LightRed,Red,Green,
                Blue,Pink,Orange,Magenta,Purple},ImageSize->500]
,{{tmax,100000,"tmax"},1,1000000},{{q0x,0.1,"Q[0]"},0,1},{{b0x,0.1,"B[0]"},0,10},
        {{s10x,0.1,"s1[0]"},0,1},{{s20x,0.1,"s2[0]"},0,1},{{kQx,0.01,"kQ"},0,0.01},
        {{k1fx,0.01,"k1f"},0,0.1},{{k1bx,0.01,"k1b"},0,0.1},{{k2fx,0.01,"k2f"},0,0.1},
        {{k2bx,0.01,"k2b"},0,0.1},{{k3fx,0.01,"k3f"},0,0.1},{{k3bx,0.01,"k3b"},0,0.1},
        {{k4x,0.01,"k4"},0,0.1},{{k5x,0.01,"k5"},0,0.1},

Button["Export CSV",
dataExport=Table[{t,
Evaluate[Q[t]/.solution][[1]],
Evaluate[B[t]/.solution][[1]],
Evaluate[I1[t]/.solution][[1]],
Evaluate[I2[t]/.solution][[1]],
Evaluate[I3[t]/.solution][[1]],
Evaluate[I4[t]/.solution][[1]],
Evaluate[S1[t]/.solution][[1]],
Evaluate[S2[t]/.solution][[1]],
Evaluate[P[t]/.solution][[1]]
},{t,0,tmax,100}];
PrependTo[dataExport,{"t","Q","B","I1","I2","I3","I4","S1","S2","P"}];
Export[NotebookDirectory[]<>"results.csv",dataExport]
]
]
Manipulate[solution = NDSolve[{Derivative[1][Q][t] == ((-kQ)*Q[t])*B[t],
       Derivative[1][B][t] == ((-kQ)*Q[t])*B[t] - (k5*I4[t])*B[t],
       Derivative[1][I1][t] == (kQ*Q[t])*B[t] - (2*k1f)*I1[t]^2 +
         (2*k1b)*I2[t], Derivative[1][I2][t] == k1f*I1[t]^2 - k1b*I2[t] -
         (k2f*I2[t])*S1[t] + k2b*I3[t] - (k3f*I2[t])*S2[t] + k3b*I3[t] +
         (k5*I4[t])*B[t], Derivative[1][S1][t] == ((-k2f)*I2[t])*S1[t] +
         k2b*I3[t], Derivative[1][S2][t] == ((-k3f)*I2[t])*S2[t] + k3b*I3[t],
       Derivative[1][I3][t] == (k2f*I2[t])*S1[t] - k2b*I3[t] +
         (k3f*I2[t])*S2[t] - k3b*I3[t] - k4*I3[t], Derivative[1][I4][t] ==
        k4*I3[t] - (k5*I4[t])*B[t], Derivative[1][P][t] == k4*I3[t],
       Q[0] == q0x, B[0] == b0x, I1[0] == 0, I2[0] == 0, I3[0] == 0,
       I4[0] == 0, S1[0] == s10x, S2[0] == s20x, P[0] == 0} /.
      {kQ -> kQx, k1f -> k1fx, k1b -> k1bx, k2f -> k2fx, k2b -> k2bx,
       k3f -> k3fx, k3b -> k3bx, k4 -> k4x, k5 -> k5x},
     {Q, B, I1, I2, I3, I4, S1, S2, P}, {t, 0, tmax}];
   Plot[{Legended[Evaluate[Q[t] /. solution], Q],
     Legended[Evaluate[B[t] /. solution], B],
     Legended[Evaluate[I1[t] /. solution], I1],
     Legended[Evaluate[I2[t] /. solution], I2],
     Legended[Evaluate[I3[t] /. solution], I3],
     Legended[Evaluate[I4[t] /. solution], I4],
     Legended[Evaluate[S1[t] /. solution], S1],
     Legended[Evaluate[S2[t] /. solution], S2],
     Legended[Evaluate[P[t] /. solution], P]}, {t, 0, tmax},
    AxesLabel -> {t, conc}, AxesStyle -> Directive[Thick, Medium],
    PlotRange -> Full, PlotStyle -> {LightMagenta, LightRed, Red, Green,
      Blue, Pink, Orange, Magenta, Purple}, ImageSize -> 500],
  {{tmax, 23000., "tmax"}, 1, 1000000}, {{q0x, 0.1, "Q[0]"}, 0, 1},
  {{b0x, 0.1, "B[0]"}, 0, 10}, {{s10x, 0.1, "s1[0]"}, 0, 1},
  {{s20x, 0.1, "s2[0]"}, 0, 1}, {{kQx, 0.01, "kQ"}, 0, 0.01},
  {{k1fx, 0.01, "k1f"}, 0, 0.1}, {{k1bx, 0.01, "k1b"}, 0, 0.1},
  {{k2fx, 0.01, "k2f"}, 0, 0.1}, {{k2bx, 0.01, "k2b"}, 0, 0.1},
  {{k3fx, 0.01, "k3f"}, 0, 0.1}, {{k3bx, 0.01, "k3b"}, 0, 0.1},
  {{k4x, 0.01, "k4"}, 0, 0.1}, {{k5x, 0.01, "k5"}, 0, 0.1},
  Button["Export CSV",
   dataExport = Table[{t, Evaluate[Q[t] /. solution][[1]],
       Evaluate[B[t] /. solution][[1]], Evaluate[I1[t] /. solution][[1]],
       Evaluate[I2[t] /. solution][[1]], Evaluate[I3[t] /. solution][[1]],
       Evaluate[I4[t] /. solution][[1]], Evaluate[S1[t] /. solution][[1]],
       Evaluate[S2[t] /. solution][[1]], Evaluate[P[t] /. solution][[1]]},
      {t, 0, tmax, 10}]; PrependTo[dataExport, {"t", "Q", "B", "I1", "I2",
      "I3", "I4", "S1", "S2", "P"}]; Export[StringJoin[NotebookDirectory[],
      "results.csv"], dataExport]]]
```

## 9.3 Mathematica scripts for model 2

The Mathematica model was constructed according to the system described in 7.22.3. In the script below, the naming conventions were as follows: B = $K_3PO_4$, I1 = **139**, I2 = **140**, I3 = **135**, I4 = **136**, I5 = **142** (unknown), S1 = (−)-**125**, S2 = (+)-**125**, P = **126**.

```
In[780]:= Remove["Global`*"]

tmax=3000;
LARGE=100;

In[783]:= solution=ParametricNDSolve[{
B'[t]==-k5 I5[t]B[t]+kDb I2[t]^2 ,
I1'[t]== - (1/2)kDf I1[t]B[t] + (1/2)kDb I2[t]^2,
I2'[t]==kDf I1[t] B[t]- kDb I2[t]^2-k1f I2[t] S1[t] +
        k1b I3[t] -k2f I2[t] S2[t] + k2b I3[t]+k5 I5[t]B[t],
S1'[t]==-k1f I2[t] S1[t] + k1b I3[t],
S2'[t]==-k2f I2[t] S2[t] + k2b I3[t],
I3'[t]==k1f I2[t] S1[t] - k1b I3[t] +k2f I2[t] S2[t] - k2b I3[t]-k3 I3[t] ,
I4'[t]==k3 I3[t] -k4 I4[t],
I5'[t]==k4 I4[t]-k5 I5[t]B[t],
P'[t]== k3 I3[t],
I1[0]==q0,
B[0]==b0,
I2[0]==0,
I3[0]==0,
I4[0]==0,
I5[0]==0,
S1[0]==s10,
S2[0]==s20,
P[0]==0},

{B,I1,I2,I3,I4,I5,S1,S2,P},{t,0,3000},{kDf,kDb,k1f,
        k1b,k2f,k2b,k3,k4,k5,q0,b0,s10,s20}];

In[784]:= (* assumes that experimental data are in the folder
        "spirok-collated-data 20180504", which is in the same folder as this notebook *)
In[785]:= (* select file and repetition *)
folder1="2 catalyst-order"; (* some defaults *)
folder2="spirok -8";
datafile="rep2-conc.csv";
PopupMenu[Dynamic[folder1],Map[FileNameTake,
        FileNames[NotebookDirectory[]<>"spirok-collated-data 20180504\\* *"]]]
Dynamic[PopupMenu[Dynamic[folder2],SortBy[Map[FileNameTake,
        FileNames[NotebookDirectory[]<>"spirok-collated-data 20180504\\"
                <>folder1<>"\\*"]],ToExpression[StringDrop[#,7]]&]]]
Dynamic[PopupMenu[Dynamic[datafile],Map[FileNameTake,FileNames
        [NotebookDirectory[]<>"spirok-collated-data 20180504\\"<>folder1
                <>"\\"<>folder2<>"\\rep*-conc.csv"]]]]
Out[788]= BoxData[2 catalyst-order]
Out[789]= BoxData[spirok -8]
Out[790]= BoxData[rep2-conc.csv]
In[791]:=
In[792]:= (* import data from CSV and extract relevant columns *)
Dynamic[SetDirectory[NotebookDirectory[]<>
        "spirok-collated-data 20180504\\"<>folder1<>"\\"<>folder2];
dataCSV=Import[datafile,"CSV",HeaderLines->1];
dataS1=Map[{#[[1]],#[[3]]}&,dataCSV];
dataS2=Map[{#[[1]],#[[4]]}&,dataCSV];
dataP=Map[{#[[1]],#[[5]]}&,dataCSV];
datarxnCSV=Import[FileNames["spirok-*-rxn.csv"][[1]],"CSV",HeaderLines->1];
rep=ToExpression[StringTake[datafile,{4,4}]];
rxndata=Transpose[datarxnCSV][[1+3(rep-1)+2]];
rxndatacols=Transpose[datarxnCSV][[1]];
TableForm[{rxndatacols,rxndata}]
]
```

```
Out[792]= standard       substrate1       product1         solvent base    catalyst
0.0085755        0.082559         NA       NA       0.824278         0.00863536


In[793]:= fitparameters={kDf->3.451738555626276`,k1f->
         33.957156952981876`,k2f->89.53596178350551`,
         k3->443.365854190246`,k4->0.020807211004514263`,
         k5->117.97678946539892`}

Out[793]= {kDf->3.45174,k1f->33.9572,k2f->89.536,
         k3->443.366,k4->0.0208072,k5->117.977}

In[794]:= Dynamic[Manipulate[
parms={kDfx,kDbx,k1fx,k1bx,k2fx,k2bx,k3x,k4x,k5x,q0x,b0x,s10x,s20x};
Show[ListPlot[{dataS1,dataS2,dataP},PlotStyle->
         {Orange,Magenta,Purple},AxesLabel->{t,conc},AxesStyle->
         Directive[Thick,Medium],PlotRange->{If[autot,Full,{0,tmax}],
         If[autoconc,Full,{0,concmax}]},ImageSize->500],
Plot[{
(Apply[S1,parms][t]/.solution),
(Apply[S2,parms][t]/.solution),
(Apply[P,parms][t]/.solution)
}
,{t,0,3000},PlotStyle->{Orange,Magenta,Purple}]
]
,{{autoconc,True,"Show full conc range"},{True,False}},{{autot,True,
         "Show full time range"},{True,False}},{{concmax,0.05,"concmax"},
         0.0001,1},{{tmax,60,"tmax"},1,1000000},{{q0x,rxndata[[6]]/7,"I1[0]"},
         0,rxndata[[6]]/3,Appearance->"Open"},{{b0x,rxndata[[5]],"B[0]"},
         0,2rxndata[[5]]},{{s10x,rxndata[[2]]/2,"s1[0]"},0,rxndata[[2]],Appearance->"Open"},
         {{s20x,rxndata[[2]]/2,"s2[0]"},0,rxndata[[2]],Appearance->"Open"},
         {{kDfx,kDf/.fitparameters,"kDf"},0,2(kDf/.fitparameters)},{{kDbx,0,"kDb"},
         0,2000},{{k1fx,k1f/.fitparameters,"k1f"},0,2(k1f/.fitparameters)},
         {{k1bx,0,"k1b"},0,20},{{k2fx,k2f/.fitparameters,"k2f"},0,2(k2f/.fitparameters)},
         {{k2bx,0,"k2b"},0,20},{{k3x,k3/.fitparameters,"k3"},0,2(k3/.fitparameters)},
         {{k4x,k4/.fitparameters,"k4"},0,2(k4/.fitparameters)},
         {{k5x,k5/.fitparameters,"k5"},0,2(k5/.fitparameters)},
Button["Export CSV",
dataExport=Table[{t,
(Apply[S1,parms][t]/.solution),
(Apply[S2,parms][t]/.solution),
(Apply[P,parms][t]/.solution)
},{t,0,tmax,0.1}];
PrependTo[dataExport,{"t","S1","S2","P"}];
Export[NotebookDirectory[]<>"results.csv",dataExport]
]
,AppearanceElements->"ResetButton"
]]
Out[794]= Manipulate[parms = {kDfx, kDbx, k1fx, k1bx, k2fx, k2bx, k3x, k4x, k5x, q0x,
     b0x, s10x, s20x}; Show[ListPlot[{dataS1, dataS2, dataP},
     PlotStyle -> {Orange, Magenta, Purple}, AxesLabel -> {t, conc},
     AxesStyle -> Directive[Thick, Medium], PlotRange ->
      {If[autot, Full, {0, tmax}], If[autoconc, Full, {0, concmax}]},
     ImageSize -> 500], Plot[{(S1 @@ parms)[t] /. solution,
      (S2 @@ parms)[t] /. solution, (P @@ parms)[t] /. solution},
     {t, 0, 3000}, PlotStyle -> {Orange, Magenta, Purple}]],
  {{autoconc, True, "Show full conc range"}, {True, False}},
  {{autot, True, "Show full time range"}, {True, False}},
  {{concmax, 0.05, "concmax"}, 0.0001, 1}, {{tmax, 60, "tmax"}, 1, 1000000},
  {{q0x, 0.001233623075413075, "I1[0]"}, 0, 0.0028784538426305083,
   Appearance -> "Open"}, {{b0x, 0.8242776203966006, "B[0]"}, 0,
   1.6485552407932011}, {{s10x, 0.04127949719842606, "s1[0]"}, 0,
   0.08255899439685212, Appearance -> "Open"},
  {{s20x, 0.04127949719842606, "s2[0]"}, 0, 0.08255899439685212,
   Appearance -> "Open"}, {{kDfx, 3.451738555626276, "kDf"}, 0,
   6.903477111252552}, {{kDbx, 0, "kDb"}, 0, 2000},
  {{k1fx, 33.957156952981876, "k1f"}, 0, 67.91431390596375},
  {{k1bx, 0, "k1b"}, 0, 20}, {{k2fx, 89.53596178350551, "k2f"}, 0,
   179.07192356701103}, {{k2bx, 0, "k2b"}, 0, 20},
  {{k3x, 443.365854190246, "k3"}, 0, 886.731708380492},
  {{k4x, 0.020807211004514263, "k4"}, 0, 0.041614422009028526},
  {{k5x, 117.97678946539892, "k5"}, 0, 235.95357893079785},
  Button["Export CSV", dataExport = Table[{t, (S1 @@ parms)[t] /. solution,
```

```
      (S2 @@ parms)[t] /. solution, (P @@ parms)[t] /. solution},
     {t, 0, tmax, 0.1}]; PrependTo[dataExport, {"t", "S1", "S2", "P"}];
   Export[StringJoin[NotebookDirectory[], "results.csv"], dataExport]],
  AppearanceElements -> "ResetButton"]
```

## 9.4 Mathematica scripts for model 3

The Mathematica model was constructed according to the system described in 7.22.4. In the script below, the naming conventions were as follows: B = $K_3PO_4$, I1 = **139**, I2 = **140**, I3 = **135**, I4 = **136**, I5 = **142** (unknown), S1 = (−)-**125**, S2 = (+)-**125**, P = **126**.

```
In[805]:= Remove["Global`*"]
In[806]:= solution=ParametricNDSolve[{
B'[t]==-k5 I5[t]B[t]+kDb I2[t]^2 ,
I1'[t]== - (1/2)kDf I1[t]B[t] + (1/2)kDb I2[t]^2,
I2'[t]==kDf I1[t] B[t]- kDb I2[t]^2-k1f I2[t] S1[t] + k1b I3[t] -
        k2f I2[t] S2[t] + k2b I3[t]+k5 I5[t]B[t],
S1'[t]==-k1f I2[t] S1[t] + k1b I3[t],
S2'[t]==-k2f I2[t] S2[t] + k2b I3[t],
I3'[t]==k1f I2[t] S1[t] - k1b I3[t] +k2f I2[t] S2[t] - k2b I3[t]-k3 I3[t] ,
I4'[t]==k3 I3[t] -k4 I4[t],
I5'[t]==k4 I4[t]-k5 I5[t]B[t],
P'[t]== k3 I3[t],
I1[0]==q0,
B[0]==b0,
I2[0]==0,
I3[0]==0,
I4[0]==0,
I5[0]==0,
S1[0]==s10,
S2[0]==s20,
P[0]==0},
{B,I1,I2,I3,I4,I5,S1,S2,P},{t,0,3000},{kDf,kDb,k1f,k1b,
        k2f,k2b,k3,k4,k5,q0,b0,s10,s20}];
In[807]:= datafolder="spirok-collated-data 20180525";
In[808]:= (* select file and repetition *)
folder1="2 catalyst-order"; (* some defaults *)
folder2="spirok -12";
datafile="rep2-conc.csv";
PopupMenu[Dynamic[folder1],Map[FileNameTake,
        FileNames[NotebookDirectory[]<>datafolder<>"\\* *"]]]
Dynamic[PopupMenu[Dynamic[folder2],SortBy[Map[FileNameTake,
        FileNames[NotebookDirectory[]<>datafolder<>"\\"<>
        folder1<>"\\*"]],ToExpression[StringDrop[#,7]]&]]]
Dynamic[PopupMenu[Dynamic[datafile],Map[FileNameTake,
        FileNames[NotebookDirectory[]<>datafolder<>"\\"<>
        folder1<>"\\"<>folder2<>"\\rep*-conc.csv"]]]]
Out[811]= BoxData[2 catalyst-order]
Out[812]= BoxData[spirok -12]
Out[813]= BoxData[rep2-conc.csv]
In[814]:= (* import data from CSV and extract relevant columns *)
Dynamic[SetDirectory[NotebookDirectory[]<>"\\"<>
        datafolder<>"\\"<>folder1<>"\\"<>folder2];
dataCSV=Import[datafile,"CSV",HeaderLines->1];
dataS1=Map[{#[[1]],#[[3]]}&,dataCSV];
dataS2=Map[{#[[1]],#[[4]]}&,dataCSV];
dataP=Map[{#[[1]],#[[5]]}&,dataCSV];
datarxnCSV=Import[FileNames["spirok-*-rxn.csv"][[1]],"CSV",HeaderLines->1];
rep=ToExpression[StringTake[datafile,{4,4}]];
rxndata=Transpose[datarxnCSV][[1+3(rep-1)+2]];
rxndatacols=Transpose[datarxnCSV][[1]];
TableForm[{rxndatacols,rxndata}]
]
```

```
Out[814]= standard       substrate1       product1         solvent base     catalyst
0.00848709       0.082559         NA       NA       0.824278         0.0257005


In[815]:= (*model[index_,tx_,kDf_,kDb_,k1f_,k1b_,k2f_,k2b_,
        k3_,k4_,k5_,q0_,b0_,s10_,s20_]=
KroneckerDelta[index,1] (S1[kDf,kDb,k1f,k1b,k2f,k2b,k3,k4,k5,
        q0,b0,s10,s20][tx+0.5]/.solution)+
KroneckerDelta[index,2] (S2[kDf,kDb,k1f,k1b,k2f,k2b,k3,k4,k5,
        q0,b0,s10,s20][tx+0.5]/.solution)+
KroneckerDelta[index,3] (P[kDf,kDb,k1f,k1b,k2f,k2b,k3,k4,k5,
        q0,b0,s10,s20][tx+0.5]/.solution);
fitdata=Join[Map[{1,#[[1]],#[[2]]}&,dataS1],Map[{2,#[[1]],
        #[[2]]}&,dataS2],Map[{3,#[[1]],#[[2]]}&,dataP]];
fitdata=Select[fitdata,#[[2]]<500&];
fitspecified={};
fit=NonlinearModelFit[fitdata,
{model[index,tx,kDf,0,k1f,0,k2f,0,k3,k4,k5,rxndata[[6]]*
        catfactor,rxndata[[5]],s0,s0],kDf>0,k1f>0,k2f>0,k3>0,k4>0,k5>0,s0>0,catfactor>0}
,
{{kDf,3},{k1f,7.88},{k2f,16},{k3,78},{k4,0.01},{k5,10},
        {s0,rxndata[[2]]/2},{catfactor,1/7}},{index,tx},Method
        {"NMinimize",Method?"NelderMead"},MaxIterations?500];ListPlot[fit["FitResiduals"]]
fit["BestFitParameters"];
allparameters=Join[fit["BestFitParameters"],fitspecified]*)

In[816]:= allparameters={kDf->4.214230611118172`,k1f->
        9.667151387892016`,k2f->19.808941409316443`,
        k3->97.66956123561947`,k4->0.016836837525126127`,
        k5->12.645210174152666`,s0->0.03785632395737685`,
        catfactor->0.16455927322239033`}
Out[816]= {kDf->4.21423,k1f->9.66715,k2f->19.8089,
        k3->97.6696,k4->0.0168368,k5->12.6452,
        s0->0.0378563,catfactor->0.164559}
In[817]:= (*fitspecified={kDf?(kDf/.allparameters),k1f?(k1f/.allparameters),
k2f?(k2f/.allparameters),k3?(k3/.allparameters),k4?(k4/.allparameters),
k5?(k5/.allparameters),catfactor?(catfactor/.allparameters)};
fit=NonlinearModelFit[fitdata,
{model[index,tx,(kDf/.allparameters),0,(k1f/.allparameters),0,
        (k2f/.allparameters),0,(k3/.allparameters),(k4/.allparameters),
        (k5/.allparameters),rxndata[[6]]*       (catfactor/.allparameters),
        rxndata[[5]],s0,s0],s0>0}
,
{{s0,rxndata[[2]]/2}},{index,tx},Method?{"NMinimize",
Method?"NelderMead"},MaxIterations?1000];ListPlot[fit["FitResiduals"]]
fit["BestFitParameters"];
allparameters=Join[fit["BestFitParameters"],fitspecified]*)
In[818]:= Dynamic[Manipulate[
parms={kDfx,kDbx,k1fx,k1bx,k2fx,k2bx,k3x,k4x,k5x,q0x,b0x,s10x,s20x};
Show[ListPlot[{dataS1,dataS2,dataP},PlotStyle->{Orange,Magenta,Purple},
AxesLabel->{t,conc},AxesStyle->Directive[Thick,Medium],PlotRange->
{If[autot,Full,{0,tmax}],If[autoconc,Full,{0,concmax}]},ImageSize->500],
Plot[{
(Apply[S1,parms][t-toff]/.solution),
(Apply[S2,parms][t-toff]/.solution),
(Apply[P,parms][t-toff]/.solution)
},{t,0,3000}
,PlotStyle->{Orange,Magenta,Purple}]
]
,{{autoconc,True,"Show full conc range"},{True,False}},
{{concmax,0.05,"concmax"},0.0001,1},{{autot,True,"Show full time range"},
{True,False}},{{tmax,60,"tmax"},1,1000000},{{q0x,rxndata[[6]]*
(catfactor/.allparameters),"I1[0]"},0,rxndata[[6]]/3},{{b0x,rxndata[[5]],
"B[0]"},0,10},{{s10x,rxndata[[2]]/2,"s1[0]"},0,rxndata[[2]]},
{{s20x,rxndata[[2]]/2,"s2[0]"},0,rxndata[[2]]},{{kDfx,(kDf/.allparameters),"kDf"},
0,2(kDf/.allparameters)},{{kDbx,0,"kDb"},0,2000},{{k1fx,(k1f/.allparameters),"k1f"},
0,2(k1f/.allparameters)},{{k1bx,0,"k1b"},0,20},{{k2fx,(k2f/.allparameters),"k2f"},
0,2(k2f/.allparameters)},{{k2bx,0,"k2b"},0,20},{{k3x,(k3/.allparameters),"k3"},
0,2(k3/.allparameters)},{{k4x,(k4/.allparameters),"k4"},
0,(k4/.allparameters)},{{k5x,(k5/.allparameters),"k5"},
0,2(k5/.allparameters)},{{toff,-0.5,"t offset"},-1,0}
]]
```

```
Out[818]= Manipulate[parms = {kDfx, kDbx, k1fx, k1bx, k2fx, k2bx, k3x, k4x, k5x, q0x,
     b0x, s10x, s20x}; Show[ListPlot[{dataS1, dataS2, dataP},
     PlotStyle -> {Orange, Magenta, Purple}, AxesLabel -> {t, conc},
     AxesStyle -> Directive[Thick, Medium], PlotRange ->
      {If[autot, Full, {0, tmax}], If[autoconc, Full, {0, concmax}]},
     ImageSize -> 500], Plot[{(S1 @@ parms)[t - toff] /. solution,
      (S2 @@ parms)[t - toff] /. solution, (P @@ parms)[t - toff] /.
       solution}, {t, 0, 3000}, PlotStyle -> {Orange, Magenta, Purple}]],
  {{autoconc, True, "Show full conc range"}, {True, False}},
  {{concmax, 0.05, "concmax"}, 0.0001, 1},
  {{autot, True, "Show full time range"}, {True, False}},
  {{tmax, 60, "tmax"}, 1, 1000000}, {{q0x, 0.004229252431673868, "I1[0]"}, 0,
   0.008566826912590798}, {{b0x, 0.8242776203966006, "B[0]"}, 0, 10},
  {{s10x, 0.04127949719842606, "s1[0]"}, 0, 0.08255899439685212},
  {{s20x, 0.04127949719842606, "s2[0]"}, 0, 0.08255899439685212},
  {{kDfx, 4.214230611118172, "kDf"}, 0, 8.428461222236344},
  {{kDbx, 0, "kDb"}, 0, 2000}, {{k1fx, 9.667151387892016, "k1f"}, 0,
   19.334302775784032}, {{k1bx, 0, "k1b"}, 0, 20},
  {{k2fx, 19.808941409316443, "k2f"}, 0, 39.617882818632886},
  {{k2bx, 0, "k2b"}, 0, 20}, {{k3x, 97.66956123561947, "k3"}, 0,
   195.33912247123894}, {{k4x, 0.016836837525126127, "k4"}, 0,
   0.016836837525126127}, {{k5x, 12.645210174152666, "k5"}, 0,
   25.290420348305332}, {{toff, -0.5, "t offset"}, -1, 0}]
```

## 9.5 Mathematica scripts for model 4

The Mathematica model was constructed according to the system described in 7.22.5. In the script below, the naming conventions were as follows: B = $K_3PO_4$, I1 = **139**, I2 = **140**, I3 = **135**, I4 = **136**, I5 = **142** (unknown), S1 = (−)-**125**, S2 = (+)-**125**, P = **126**.

```
In[853]:= Remove["Global`*"]

In[854]:= solution=ParametricNDSolve[{
B'[t]==-k5 I5[t]B[t]-kDf I1[t]B[t]+kDb I2[t]^2 ,
I1'[t]== - (1/2)kDf I1[t]B[t] + (1/2)kDb I2[t]^2,
I2'[t]==kDf I1[t] B[t]- kDb I2[t]^2-k1f I2[t] S1[t] + k1b I3[t]
        -k2f I2[t] S2[t] + k2b I3[t]+k5 I5[t]B[t],
S1'[t]==-k1f I2[t] S1[t] + k1b I3[t]-kx S1[t]I5[t]-ky S1[t] I4[t]-kz S1[t]B[t],
S2'[t]==-k2f I2[t] S2[t] + k2b I3[t]-kx S2[t]I5[t]-ky S2[t] I4[t]-kz S2[t]B[t],
I3'[t]==k1f I2[t] S1[t] - k1b I3[t] +k2f I2[t] S2[t] - k2b I3[t]-k3 I3[t] ,
I4'[t]==k3 I3[t] -k4 I4[t]+kx S1[t]I5[t]+kx S2[t]I5[t],
I5'[t]==k4 I4[t]-k5 I5[t]B[t]-kx S1[t]I5[t]-kx S2[t]I5[t],
P'[t]== k3 I3[t]+kx S1[t]I5[t]+kx S2[t]I5[t]+
        ky( S1[t] I4[t]+S2[t] I4[t]) + kz(S1[t]B[t] + S2[t]B[t]),
cat[t]==2I1[t]+I2[t]+I3[t]+I4[t]+I5[t],
I1[0]==i10,
B[0]==b0,
I2[0]==0,
I3[0]==0,
I4[0]==i40,
I5[0]==0,
S1[0]==s10,
S2[0]==s20,
P[0]==0
},

{B,I1,I2,I3,I4,I5,S1,S2,P,cat},{t,0,3000},{kDf,kDb,k1f,k1b,
        k2f,k2b,k3,k4,k5,kx,ky,kz,i10,i40,b0,s10,s20}];
In[855]:= datafolder="spirok-collated-data 20180525";
In[856]:= (* select file and repetition *)
folder1="2 catalyst-order"; (* some defaults *)
folder2="spirok-12";
datafile="rep2-conc.csv";
```

```
PopupMenu[Dynamic[folder1],Map[FileNameTake,
        FileNames[NotebookDirectory[]<>datafolder<>"\\* *"]]]
Dynamic[PopupMenu[Dynamic[folder2],SortBy[Map[
        FileNameTake,FileNames[NotebookDirectory[]
                <>datafolder<>"\\"<>folder1<>"\\*"]],
                        ToExpression[StringDrop[#,7]]&]]]
Dynamic[PopupMenu[Dynamic[datafile],Map[FileNameTake,
        FileNames[NotebookDirectory[]<>datafolder<>"\\"
        <>folder1<>"\\"<>folder2<>"\\rep*-conc.csv"]]]]
Out[859]= BoxData[2 catalyst-order]
Out[860]= BoxData[spirok-12]
Out[861]= BoxData[rep2-conc.csv]
In[862]:= (* import data from CSV and extract relevant columns *)
Dynamic[SetDirectory[NotebookDirectory[]<>"\\"<>
        datafolder<>"\\"<>folder1<>"\\"<>folder2];
dataCSV=Import[datafile,"CSV",HeaderLines->1];
dataS1=Map[{#[[1]],#[[3]]}&,dataCSV];
dataS2=Map[{#[[1]],#[[4]]}&,dataCSV];
dataP=Map[{#[[1]],#[[5]]}&,dataCSV];
datatot=Map[{#[[1]],#[[3]]+#[[4]]+#[[5]]}&,dataCSV];
datarxnCSV=Import[FileNames["spirok-*-rxn.csv"][[1]],"CSV",HeaderLines->1];
rep=ToExpression[StringTake[datafile,{4,4}]];
rxndata=Transpose[datarxnCSV][[1+3(rep-1)+2]];
rxndatacols=Transpose[datarxnCSV][[1]];
TableForm[{rxndatacols,rxndata}]
]

Out[862]= standard       substrate1       product1         solvent base     catalyst
0.00848709       0.082559         NA       NA       0.824278         0.0257005


In[863]:= (*fit assuming catalyst starts as I1*)
(*FrontEndExecute[FrontEndToken["ToggleDynamicUpdating"]]
model[index_,tx_,kDf_,kDb_,k1f_,k1b_,k2f_,k2b_,k3_,
        k4_,k5_,kx_,q0_,b0_,s10_,s20_]=
KroneckerDelta[index,1] (S1[kDf,kDb,k1f,k1b,k2f,k2b,
        k3,k4,k5,kx,q0/2,0,b0,s10,s20][tx+0]/.solution)+
KroneckerDelta[index,2] (S2[kDf,kDb,k1f,k1b,k2f,k2b,
        k3,k4,k5,kx,q0/2,0,b0,s10,s20][tx+0]/.solution)+
KroneckerDelta[index,3] (P[kDf,kDb,k1f,k1b,k2f,k2b,
        k3,k4,k5,kx,q0/2,0,b0,s10,s20][tx+0]/.solution);
fitdata=Join[Map[{1,#[[1]],#[[2]]}&,dataS1],Map
        [{2,#[[1]],#[[2]]}&,dataS2],Map[{3,#[[1]],#[[2]]}&,dataP]];
fitdata=Select[fitdata,#[[2]]<1000&];
fitspecified={kx?0.004};
fit=NonlinearModelFit[fitdata,
{model[index,tx,kDf,kDb,k1f,0,k2f,0,k3,k4,k5,kx/.fitspecified,rxndata[[6]]*catfactor,
        rxndata[[5]],s0,s0],kDf>0,kDb>0,k1f>0,k2f>0,
                k3>0,k4>0,k5>0,s0>0,catfactor>0}
,
{{kDf,1.1},{kDb,2.9},{k1f,9.66},{k2f,19.8},{k3,97.7},
        {k4,44.5},{k5,0.01},{s0,rxndata[[2]]/2},{catfactor,0.32}},
        {index,tx},Method?{"NMinimize",Method
        "NelderMead"},MaxIterations?500];ListPlot[fit["FitResiduals"]]
fit["BestFitParameters"];
allparameters=Join[fit["BestFitParameters"],fitspecified]
FrontEndExecute[FrontEndToken["ToggleDynamicUpdating"]]*)
In[864]:= (*fit assuming catalyst starts as I4*)
(*FrontEndExecute[FrontEndToken["ToggleDynamicUpdating"]]
model[index_,tx_,kDf_,kDb_,k1f_,k1b_,k2f_,k2b_,
        k3_,k4_,k5_,kx_,q0_,b0_,s10_,s20_]=
KroneckerDelta[index,1] (S1[kDf,kDb,k1f,k1b,k2f,
        k2b,k3,k4,k5,kx,0,q0,b0,s10,s20][tx+0]/.solution)+
KroneckerDelta[index,2] (S2[kDf,kDb,k1f,k1b,
        k2f,k2b,k3,k4,k5,kx,0,q0,b0,s10,s20][tx+0]/.solution)+
KroneckerDelta[index,3] (P[kDf,kDb,k1f,k1b,
        k2f,k2b,k3,k4,k5,kx,0,q0,b0,s10,s20][tx+0]/.solution);
fitdata=Join[Map[{3,#[[1]],#[[2]]}&,dataP]];
fitdata=Select[fitdata,#[[2]]<1000&];
fitdata=Select[fitdata,#[[3]]?"NA"&];
fitspecified={k1f?9.667151387892016`,k2f?
19.808941409316443`,k3?97.66956123561947`,
        kx?0.004,catfactor?1, s0->rxndata[[2]]/2};
```

```
fit=NonlinearModelFit[fitdata,
{model[index,tx,kDf,kDb,k1f/.fitspecified,0,k2f/
        .fitspecified,0,k3/.fitspecified,k4,k5,kx/.fitspecified,
        rxndata[[6]]*catfactor/.fitspecified,rxndata[[5]],
        rxndata[[2]]/2,rxndata[[2]]/2],kDf>0,kDb>0,k4>0,k5>0}
,
{{kDf,2},{kDb,2.74},{k4,67.2},{k5,0.0093}},{index,tx},
        Method?{"NMinimize",Method?"NelderMead"},
        MaxIterations?500];ListPlot[fit["FitResiduals"]]
fit["BestFitParameters"];
allparameters=Join[fit["BestFitParameters"],fitspecified]
FrontEndExecute[FrontEndToken["ToggleDynamicUpdating"]]*)

In[865]:= allparameters={kDf->3.7458598145115705`,
        kDb->12.695911215785163`,k1f->30.52580182727398`,
        k2f->69.06504486786915`,k3->354.61765435181513`,
        k4->159.71386624437037`,k5->0.01885530240868606`,
        s0->0.037746900262685415`,catfactor->0.32913736994956755`,
        kx->0,ky->0,kz->0.00035}

Out[865]= {kDf->3.74586,kDb->12.6959,k1f->30.5258,
        k2f->69.065,k3->354.618,k4->159.714,k5->0.0188553,
        s0->0.0377469,catfactor->0.329137,kx->0,ky->0,kz->0.00035}

In[866]:= Dynamic[Manipulate[
parms={kDfx,kDbx,k1fx,k1bx,k2fx,k2bx,k3x,k4x,k5x,
        kxx,kyx,kzx,If[cati1==True,i10x*(catfactor/.allparameters)/2,0],
        If[cati1==False,i10x,0],b0x,s10x,s20x};
Column[{
{Show[ListPlot[If[showtot,{dataS1,dataS2,dataP,datatot},
        {dataS1,dataS2,dataP}],PlotStyle->{Orange,Magenta,Purple,Brown},
        AxesLabel->{t,conc},AxesStyle->Directive[Thick,Medium],
        PlotRange->{If[autot,Full,{0,tmax}],If[autoconc,Full,{0,concmax}]}],
ImageSize->500],
Plot[{
(Apply[S1,parms][t-toff]/.solution),
(Apply[S2,parms][t-toff]/.solution),
(Apply[P,parms][t-toff]/.solution)
},{t,0,3000}
,PlotStyle->{Orange,Magenta,Purple,Brown}]
]},
Plot[{
Legended[(Apply[I0,parms][t-toff]/.solution),"I0"],
Legended[(Apply[I1,parms][t-toff]/.solution),"I1"],
Legended[(Apply[I2,parms][t-toff]/.solution),"I2"],
Legended[(Apply[I3,parms][t-toff]/.solution),"I3"],
Legended[(Apply[I4,parms][t-toff]/.solution),"I4"],
Legended[(Apply[I5,parms][t-toff]/.solution),"I5"]
},{t,0,tmax}
,PlotStyle->{Orange,Magenta,Purple,Brown,Green,Pink},
        AxesLabel->{t,conc},AxesStyle->Directive[Thick,Medium],
        PlotRange->{If[autot,Full,{0,tmax}],If[autoconc,Full,{0,concmax}]},ImageSize->500],
Plot[{
Legended[(Apply[B,parms][t-toff]/.solution),"B"]
},{t,0,tmax}
,PlotStyle->{Orange,Magenta,Purple,Brown,Green,Black},
        AxesLabel->{t,conc},AxesStyle->Directive[Thick,Medium],
        PlotRange->{If[autot,Full,{0,tmax}],If[autoconc,Full,Full]},ImageSize->500],
"ln k = "<>ToString[Log[(Apply[P,parms][gradmax]-
        Apply[P,parms][gradmin])/(gradmax-gradmin)/.solution]]
},ImageSize->500]
,
{{showtot,True,"Show S1 + S2 + P conc"},{True,False}},
{{autoconc,False,"Show full conc range"},{True,False}},
        {{concmax,0.008,"concmax"},0.0001,1},
        {{autot,True,"Show full time range"},{True,False}},{{tmax,60,"tmax"},1,1000000},
{{cati1,True,"Catalyst is I1"},{True,False}},
{{i10x,rxndata[[6]],"cat[0]"},0,2rxndata[[6]]},
{{b0x,rxndata[[5]],"B[0]"},0,10},{{s10x,rxndata[[2]]/2,"s1[0]"},
        0,rxndata[[2]]},{{s20x,rxndata[[2]]/2,"s2[0]"},0,rxndata[[2]]},
        {{kDfx,(kDf/.allparameters),"kDf"},0,2(kDf/.allparameters)},
        {{kDbx,0,"kDb"},0,2000},{{k1fx,(k1f/.allparameters),"k1f"},
        0,2(k1f/.allparameters)},{{k1bx,0,"k1b"},0,20},
```

```
        {{k2fx,(k2f/.allparameters),"k2f"},0,2(k2f/.allparameters)},
        {{k2bx,0,"k2b"},0,20},{{k3x,(k3/.allparameters),"k3"},
        0,2(k3/.allparameters)},{{k4x,(k4/.allparameters),"k4"},
        0,(k4/.allparameters)},{{k5x,(k5/.allparameters),"k5"},0,2(k5/.allparameters)},
{{kxx,(kx/.allparameters),"kx"},0,2(kx/.allparameters)},
{{kyx,(ky/.allparameters),"ky"},0,2(ky/.allparameters)},
{{kzx,(kz/.allparameters),"kz"},0,2(kz/.allparameters)},
{{toff,0,"t offset"},-1,0},
{{gradmin,20,"gradient Subscript[t, 0]"},0,60},
{{gradmax,50,"gradient Subscript[t, 1]"},0,60},

Button["Export CSV",
dataExport=Table[{t,
(Apply[cat,parms][t]/.solution),
(Apply[I1,parms][t]/.solution),
(Apply[I2,parms][t]/.solution),
(Apply[I3,parms][t]/.solution),
(Apply[I4,parms][t]/.solution),
(Apply[I5,parms][t]/.solution),
(Apply[B,parms][t]/.solution),
(Apply[S1,parms][t]/.solution),
(Apply[S2,parms][t]/.solution),
(Apply[P,parms][t]/.solution)
},{t,0,tmax,0.2}];
PrependTo[dataExport,{"t","cat","I1","I2","I3","I4","I5","B","S1","S2","P"}];
Export[NotebookDirectory[]<>"results.csv",dataExport]
]

]]
Out[866]= Manipulate[parms = {kDfx, kDbx, k1fx, k1bx, k2fx, k2bx, k3x, k4x, k5x, kxx,
     kyx, kzx, If[cati1 == True, i10x*((catfactor /. allparameters)/2), 0],
     If[cati1 == False, i10x, 0], b0x, s10x, s20x};
   Column[{{Show[ListPlot[If[showtot, {dataS1, dataS2, dataP, datatot},
         {dataS1, dataS2, dataP}], PlotStyle -> {Orange, Magenta, Purple,
          Brown}, AxesLabel -> {t, conc}, AxesStyle -> Directive[Thick,
          Medium], PlotRange -> {If[autot, Full, {0, tmax}],
          If[autoconc, Full, {0, concmax}]}, ImageSize -> 500],
       Plot[{(S1 @@ parms)[t - toff] /. solution, (S2 @@ parms)[t - toff] /.
          solution, (P @@ parms)[t - toff] /. solution}, {t, 0, 3000},
        PlotStyle -> {Orange, Magenta, Purple, Brown}]]},
     Plot[{Legended[(I0 @@ parms)[t - toff] /. solution, "I0"],
       Legended[(I1 @@ parms)[t - toff] /. solution, "I1"],
       Legended[(I2 @@ parms)[t - toff] /. solution, "I2"],
       Legended[(I3 @@ parms)[t - toff] /. solution, "I3"],
       Legended[(I4 @@ parms)[t - toff] /. solution, "I4"],
       Legended[(I5 @@ parms)[t - toff] /. solution, "I5"]}, {t, 0, tmax},
      PlotStyle -> {Orange, Magenta, Purple, Brown, Green, Pink},
      AxesLabel -> {t, conc}, AxesStyle -> Directive[Thick, Medium],
      PlotRange -> {If[autot, Full, {0, tmax}], If[autoconc, Full,
         {0, concmax}]}, ImageSize -> 500],
     Plot[{Legended[(B @@ parms)[t - toff] /. solution, "B"]}, {t, 0, tmax},
      PlotStyle -> {Orange, Magenta, Purple, Brown, Green, Black},
      AxesLabel -> {t, conc}, AxesStyle -> Directive[Thick, Medium],
      PlotRange -> {If[autot, Full, {0, tmax}], If[autoconc, Full, Full]},
      ImageSize -> 500], StringJoin["ln k = ",
      ToString[Log[((P @@ parms)[gradmax] - (P @@ parms)[gradmin])/
          (gradmax - gradmin) /. solution]]]}, ImageSize -> 500],
  {{showtot, True, "Show S1 + S2 + P conc"}, {True, False}},
  {{autoconc, False, "Show full conc range"}, {True, False}},
  {{concmax, 0.008, "concmax"}, 0.0001, 1},
  {{autot, True, "Show full time range"}, {True, False}},
  {{tmax, 60, "tmax"}, 1, 1000000}, {{cati1, True, "Catalyst is I1"},
   {True, False}}, {{i10x, 0.025700480737772397, "cat[0]"}, 0,
   0.05140096147554479}, {{b0x, 0.8242776203966006, "B[0]"}, 0, 10},
  {{s10x, 0.04127949719842606, "s1[0]"}, 0, 0.08255899439685212},
  {{s20x, 0.04127949719842606, "s2[0]"}, 0, 0.08255899439685212},
  {{kDfx, 3.7458598145115705, "kDf"}, 0, 7.491719629023141},
  {{kDbx, 0, "kDb"}, 0, 2000}, {{k1fx, 30.52580182727398, "k1f"}, 0,
   61.05160365454796}, {{k1bx, 0, "k1b"}, 0, 20},
  {{k2fx, 69.06504486786915, "k2f"}, 0, 138.1300897357383},
  {{k2bx, 0, "k2b"}, 0, 20}, {{k3x, 354.61765435181513, "k3"}, 0,
   709.2353087036303}, {{k4x, 159.71386624437037, "k4"}, 0,
   159.71386624437037}, {{k5x, 0.01885530240868606, "k5"}, 0,
```

```
 0.03771060481737212}, {{kxx, 0, "kx"}, 0, 0}, {{kyx, 0, "ky"}, 0, 0},
{{kzx, 0.00035, "kz"}, 0, 0.0007}, {{toff, 0, "t offset"}, -1, 0},
{{gradmin, 20, "gradient \!\(\*SubscriptBox[\(t\), \(0\)]\)"}, 0, 60},
{{gradmax, 50, "gradient \!\(\*SubscriptBox[\(t\), \(1\)]\)"}, 0, 60},
Button["Export CSV", dataExport = Table[{t, (cat @@ parms)[t] /. solution,
     (I1 @@ parms)[t] /. solution, (I2 @@ parms)[t] /. solution,
     (I3 @@ parms)[t] /. solution, (I4 @@ parms)[t] /. solution,
     (I5 @@ parms)[t] /. solution, (B @@ parms)[t] /. solution,
     (S1 @@ parms)[t] /. solution, (S2 @@ parms)[t] /. solution,
     (P @@ parms)[t] /. solution}, {t, 0, tmax, 0.2}];
  PrependTo[dataExport, {"t", "cat", "I1", "I2", "I3", "I4", "I5", "B",
    "S1", "S2", "P"}]; Export[StringJoin[NotebookDirectory[],
    "results.csv"], dataExport]]]
```

## 9.6 Mathematica scripts for model 5

The Mathematica model was constructed according to the system described in 7.22.6. In the script below, the naming conventions were as follows: B = $K_3PO_4$, I1 = **139**, I2 = **140**, I3 = **135**, I4 = **136**, I5 = **127**, S1 = (−)-**125**, S2 = (+)-**125**, P = **126**.

```
In[878]:= Remove["Global`*"]
In[879]:= prestirsolution=ParametricNDSolve[{
B'[t]==0,
I1'[t]== - (1/2)kDf I1[t] + (1/2)kDb I2[t]^2,
I2'[t]==kDf I1[t] - kDb I2[t]^2+k5 I5[t],
I5'[t]==-k5 I5[t],
cat[t]==2I1[t]+I2[t]+I5[t],
I1[0]==0,
B[0]==b0,
I2[0]==0,
I5[0]==i50
},
{B,I1,I2,I5,cat},{t,0,3000},{kDf,kDb,k5,b0,i50}];
In[880]:=
In[881]:= solution=ParametricNDSolve[{
B'[t]==0,
I1'[t]== - (1/2)kDf I1[t] + (1/2)kDb I2[t]^2,
I2'[t]==kDf I1[t] - kDb I2[t]^2-k1f I2[t] S1[t] + k1b I3[t] -
        k2f I2[t] S2[t] + k2b I3[t]+k4 I4[t]+k5 I5[t] ,
S1'[t]==-k1f I2[t] S1[t] + k1b I3[t]-kz S1[t]B[t],
S2'[t]==-k2f I2[t] S2[t] + k2b I3[t]-kz S2[t]B[t],
I3'[t]==k1f I2[t] S1[t] - k1b I3[t] +k2f I2[t] S2[t] - k2b I3[t]-k3 I3[t] ,
I4'[t]==k3 I3[t] -k4 I4[t],
I5'[t]==-k5 I5[t],
P'[t]== k3 I3[t]+ kz(S1[t]B[t] + S2[t]B[t]),
cat[t]==2I1[t]+I2[t]+I3[t]+I4[t]+I5[t],
I1[0]==i10,
B[0]==b0,
I2[0]==i20,
I3[0]==0,
I4[0]==i40,
I5[0]==i50,
S1[0]==s10,
S2[0]==s20,
P[0]==0
},
{B,I1,I2,I3,I4,I5,S1,S2,P,cat},{t,0,3000},{kDf,kDb,k1f,k1b,k2f,k2b,k3,
        k4,k5,kz,i10,i20,i40,i50,b0,s10,s20}];
In[882]:= datafolder="spirok-collated-data 20180525";
In[883]:= (* select file and repetition *)
folder1="2 catalyst-order"; (* some defaults *)
folder2="spirok-12";
datafile="rep2-conc.csv";
```

```
PopupMenu[Dynamic[folder1],Map[FileNameTake,FileNames
        [NotebookDirectory[]<>datafolder<>"\\* *"]]]
Dynamic[PopupMenu[Dynamic[folder2],SortBy[Map
        [FileNameTake,FileNames[NotebookDirectory[]<>datafolder
        <>"\\"<>folder1 <>"\\*"],ToExpression[StringDrop[#,7]]&]]]
Dynamic[PopupMenu[Dynamic[datafile],Map[FileNameTake,
        FileNames[NotebookDirectory[]<>datafolder
        <>"\\"<>folder1 <>"\\"<>folder2 <>"\\rep*-conc.csv"]]]]
Out[886]= BoxData[2 catalyst-order]
Out[887]= BoxData[spirok-12]
Out[888]= BoxData[rep2-conc.csv]
In[889]:= (* import data from CSV and extract relevant columns *)
Dynamic[SetDirectory[NotebookDirectory[]
        <>"\\"<>datafolder<>"\\"<>folder1<>"\\"<>folder2];
dataCSV=Import[datafile,"CSV",HeaderLines->1];
dataS1=Map[{#[[1]],#[[3]]}&,dataCSV];
dataS2=Map[{#[[1]],#[[4]]}&,dataCSV];
dataP=Map[{#[[1]],#[[5]]}&,dataCSV];
datatot=Map[{#[[1]],#[[3]]+#[[4]]+#[[5]]}&,dataCSV];
datarxnCSV=Import[FileNames["spirok-*-rxn.csv"][[1]],"CSV",HeaderLines->1];
rep=ToExpression[StringTake[datafile,{4,4}]];
rxndata=Transpose[datarxnCSV][[1+3(rep-1)+2]];
rxndatacols=Transpose[datarxnCSV][[1]];
TableForm[{rxndatacols,rxndata}]
]

Out[889]= standard      substrate1      product1        solvent base    catalyst
0.00848709      0.082559        NA      NA      0.824278        0.0257005


In[890]:= (*fit assuming catalyst starts as I1*)
(*FrontEndExecute[FrontEndToken["ToggleDynamicUpdating"]]
model[index_,tx_,kDf_,kDb_,k1f_,k1b_,k2f_,k2b_,k3_,
        k4_,k5_,kx_,q0_,b0_,s10_,s20_]=
KroneckerDelta[index,1] (S1[kDf,kDb,k1f,k1b,k2f,k2b,k3,
        k4,k5,kx,q0/2,0,b0,s10,s20][tx+0]/.solution)+
KroneckerDelta[index,2] (S2[kDf,kDb,k1f,k1b,k2f,k2b,k3,
        k4,k5,kx,q0/2,0,b0,s10,s20][tx+0]/.solution)+
KroneckerDelta[index,3] (P[kDf,kDb,k1f,k1b,k2f,k2b,k3,
        k4,k5,kx,q0/2,0,b0,s10,s20][tx+0]/.solution);
fitdata=Join[Map[{1,#[[1]],#[[2]]}&,dataS1],Map[{2,#[[1]],
        #[[2]]}&,dataS2],Map[{3,#[[1]],#[[2]]}&,dataP]];
fitdata=Select[fitdata,#[[2]]<1000&];
fitspecified={kx?0.004};
fit=NonlinearModelFit[fitdata,
{model[index,tx,kDf,kDb,k1f,0,k2f,0,k3,k4,k5,kx/.fitspecified,
        rxndata[[6]]*catfactor,rxndata[[5]],s0,s0],
        kDf>0,kDb>0,k1f>0,k2f>0,k3>0,k4>0,k5>0,s0>0,catfactor>0}
,
{{kDf,1.1},{kDb,2.9},{k1f,9.66},{k2f,19.8},{k3,97.7},
        {k4,44.5},{k5,0.01},{s0,rxndata[[2]]/2},{catfactor,0.32}},
        {index,tx},Method?{"NMinimize",Method?"NelderMead"},
        MaxIterations?500];ListPlot[fit["FitResiduals"]]
fit["BestFitParameters"];
allparameters=Join[fit["BestFitParameters"],fitspecified]
FrontEndExecute[FrontEndToken["ToggleDynamicUpdating"]]*)
In[891]:= (*fit assuming catalyst starts as I4*)
(*FrontEndExecute[FrontEndToken["ToggleDynamicUpdating"]]
model[index_,tx_,kDf_,kDb_,k1f_,k1b_,k2f_,k2b_,k3_,
        k4_,k5_,kx_,q0_,b0_,s10_,s20_]=
KroneckerDelta[index,1] (S1[kDf,kDb,k1f,k1b,k2f,k2b,k3,
        k4,k5,kx,0,q0,b0,s10,s20][tx+0]/.solution)+
KroneckerDelta[index,2] (S2[kDf,kDb,k1f,k1b,k2f,k2b,k3,
        k4,k5,kx,0,q0,b0,s10,s20][tx+0]/.solution)+
KroneckerDelta[index,3] (P[kDf,kDb,k1f,k1b,k2f,k2b,k3,
        k4,k5,kx,0,q0,b0,s10,s20][tx+0]/.solution);
fitdata=Join[Map[{3,#[[1]],#[[2]]}&,dataP]];
fitdata=Select[fitdata,#[[2]]<1000&];
fitdata=Select[fitdata,#[[3]]?"NA"&];
fitspecified={k1f?9.667151387892016`,
        k2f?19.808941409316443`,k3?97.66956123561947`,
        kx?0.004,catfactor?1, s0->rxndata[[2]]/2};
fit=NonlinearModelFit[fitdata,
```

```
{model[index,tx,kDf,kDb,k1f/.fitspecified,0,k2f/.fitspecified,0,k3/
        .fitspecified,k4,k5,kx/.fitspecified,rxndata[[6]]
        *catfactor/.fitspecified,rxndata[[5]],rxndata[[2]]/
        2,rxndata[[2]]/2],kDf>0,kDb>0,k4>0,k5>0}
,
{{kDf,2},{kDb,2.74},{k4,67.2},{k5,0.0093}},
        {index,tx},Method?{"NMinimize",Method?
"NelderMead"},MaxIterations?500];ListPlot[fit["FitResiduals"]]
fit["BestFitParameters"];
allparameters=Join[fit["BestFitParameters"],fitspecified]
FrontEndExecute[FrontEndToken["ToggleDynamicUpdating"]]*)
In[892]:= allparameters={kDf->0.2,kDb->20,
        k1f->30.52580182727398`,k2f->55.8(*69.06504486786915`*),
        k3->354.61765435181513`,k4->0.00455,k5->0.00424,
        s0->0.037746900262685415`,catfactor->0.32913736994956755`,
        kx->0,ky->0,kz->0.00035(*0.000068*)}

Out[892]= {kDf->0.2,kDb->20,k1f->30.5258,k2f->55.8,
        k3->354.618,k4->0.00455,k5->0.00424,s0->0.0377469,
        catfactor->0.329137,kx->0,ky->0,kz->0.00035}

In[893]:= Dynamic[Manipulate[

i10c=I1[kDfx,kDbx,k5x,b0x,i10x][tstir]/.prestirsolution;
i20c=I2[kDfx,kDbx,k5x,b0x,i10x][tstir]/.prestirsolution;
i50c=I5[kDfx,kDbx,k5x,b0x,i10x][tstir]/.prestirsolution;
parms=If[cati1==False,{kDfx,kDbx,k1fx,k1bx,k2fx,k2bx,
        k3x,k4x,k5x,kzx,i10c,i20c,0,i50c,b0x,s10x,s20x},
{kDfx,kDbx,k1fx,k1bx,k2fx,k2bx,k3x,k4x,k5x,kzx,0,0,i10x,0,b0x,s10x,s20x}];
Column[{
{Show[ListPlot[If[showtot,{dataS1,dataS2,dataP,datatot},
        {dataS1,dataS2,dataP}],PlotStyle->{Orange,Magenta,Purple,Brown},
        AxesLabel->{t,conc},AxesStyle->Directive[Thick,Medium],
        PlotRange->{If[autot,Full,{0,tmax}],If[autoconc,Full,{0,concmax}]},
ImageSize->500],
Plot[{
(Apply[S1,parms][t]/.solution),
(Apply[S2,parms][t]/.solution),
(Apply[P,parms][t]/.solution)
},{t,0,3000}
,PlotStyle->{Orange,Magenta,Purple,Brown}]
]},
Show[If[cati1==False,Plot[{
(I1[kDfx,kDbx,k5x,b0x,i10x][t+tstir]/.prestirsolution),
(I2[kDfx,kDbx,k5x,b0x,i10x][t+tstir]/.prestirsolution),
(I5[kDfx,kDbx,k5x,b0x,i10x][t+tstir]/.prestirsolution),
(cat[kDfx,kDbx,k5x,b0x,i10x][t+tstir]/.prestirsolution)
},{t,-tstir,0}
,PlotStyle->{Magenta,Purple,Pink,Red},AxesLabel->{t,conc},
        AxesStyle->Directive[Thick,Medium],
        PlotRange->{If[autot,Full,{-tstir,0}],If[autoconc,Full,{0,concmax}]},
        ImageSize->500,PlotRangePadding->{tmax,Automatic}],{}],
Plot[{
Legended[(Apply[I0,parms][t]/.solution),"I0"],
Legended[(Apply[I1,parms][t]/.solution),"I1"],
Legended[(Apply[I2,parms][t]/.solution),"I2"],
Legended[(Apply[I3,parms][t]/.solution),"I3"],
Legended[(Apply[I4,parms][t]/.solution),"I4"],
Legended[(Apply[I5,parms][t]/.solution),"I5"],
Legended[(Apply[cat,parms][t]/.solution),"cat"]
},{t,0,tmax}
,PlotStyle->{Orange,Magenta,Purple,Brown,Green,Pink,Red},
                AxesLabel->{t,conc},AxesStyle->Directive[Thick,Medium],
                PlotRange->{If[autot,Full,{0,tmax}],If[autoconc,Full,{0,concmax}]},
                ImageSize->500]
],

Show[If[cati1==False,
Plot[{
(B[kDfx,kDbx,k5x,b0x,i10x][t+tstir]/.prestirsolution)
},{t,-tstir,0}
,PlotStyle->{Orange,Magenta,Purple,Brown,Green,Black},
        AxesLabel->{t,conc},AxesStyle->Directive[Thick,Medium],
```

```
        PlotRange->{If[autot,Full,{-tstir,0}],{0,Automatic}},
        ImageSize->500,PlotRangePadding->{tmax,Automatic}],{}],
Plot[{
Legended[(Apply[B,parms][t]/.solution),"B"]
},{t,0,tmax}
,PlotStyle->{Orange,Magenta,Purple,Brown,Green,Black},
        AxesLabel->{t,conc},AxesStyle->Directive[Thick,Medium],
        PlotRange->{If[autot,Full,{0,tmax}],If[autoconc,Full,Full]},
        ImageSize->500]
],
"ln k = "<>ToString[Log[(Apply[P,parms][gradmax]-Apply[P,parms]
        [gradmin])/(gradmax-gradmin)/.solution]]
},ImageSize->500]


,
{{showtot,False,"Show S1 + S2 + P conc"},{True,False}},
{{autoconc,True,"Show full conc range"},{True,False}},
        {{concmax,0.008,"concmax"},0.0001,1},{{autot,True,"Show full time range"},
        {True,False}},{{tmax,60,"tmax"},1,1000000},
{{cati1,False,"Catalyst added as I4"},{True,False}},
{{i10x,rxndata[[6]],"cat[0]"},0,2rxndata[[6]]},
{{b0x,rxndata[[5]],"B[0]"},0,2rxndata[[5]]},{{s10x,rxndata[[2]]/2,"s1[0]"},
        0,rxndata[[2]]},{{s20x,rxndata[[2]]/2,"s2[0]"},0,rxndata[[2]]},
        {{kDfx,(kDf/.allparameters),"kDf"},0,2(kDf/.allparameters)},
        {{kDbx,kDb/.allparameters,"kDb"},0,2000},{{k1fx,(k1f/.allparameters),"k1f"},
        0,2(k1f/.allparameters)},{{k1bx,0,"k1b"},0,20},
        {{k2fx,(k2f/.allparameters),"k2f"},0,2(k2f/.allparameters)},
        {{k2bx,0,"k2b"},0,20},{{k3x,(k3/.allparameters),"k3"},
        0,2(k3/.allparameters)},{{k4x,(k4/.allparameters),"k4"},
        0,2(k4/.allparameters)},{{k5x,(k5/.allparameters),"k5"},0,2(k5/.allparameters)},
{{kxx,(kx/.allparameters),"kx"},0,2(kx/.allparameters)},
{{kyx,(ky/.allparameters),"ky"},0,2(ky/.allparameters)},
{{kzx,(kz/.allparameters),"kz"},0,2(kz/.allparameters)},
{{tstir,94,"prestirring time"},1,300},
{{gradmin,20,"gradient Subscript[t, 0]"},0,60},
{{gradmax,50,"gradient Subscript[t, 1]"},0,60},
Button["Export CSV",
dataExport=Table[{t,
0,
(Apply[I1,parms][t]/.solution),
(Apply[I2,parms][t]/.solution),
(Apply[I3,parms][t]/.solution),
(Apply[I4,parms][t]/.solution),
(Apply[I5,parms][t]/.solution),
(Apply[B,parms][t]/.solution),
(Apply[S1,parms][t]/.solution),
(Apply[S2,parms][t]/.solution),
(Apply[P,parms][t]/.solution)
},{t,0,tmax,0.1}];
If[cati1==False,
dataExport=Join[Table[{t,
0,
(I1[kDfx,kDbx,k5x,b0x,i10x][t+tstir]/.prestirsolution),
(I2[kDfx,kDbx,k5x,b0x,i10x][t+tstir]/.prestirsolution),
0,
0,
(I5[kDfx,kDbx,k5x,b0x,i10x][t+tstir]/.prestirsolution),
(B[kDfx,kDbx,k5x,b0x,i10x][t+tstir]/.prestirsolution),
0,
0,
0
},{t,-tstir,0-0.1,0.1}],dataExport]];
PrependTo[dataExport,{"t","cat","I1","I2","I3","I4","I5","B","S1","S2","P"}];
Export[NotebookDirectory[]<>"results.csv",dataExport]

]
]]
Out[893]= Manipulate[i10c = I1[kDfx, kDbx, k5x, b0x, i10x][tstir] /. prestirsolution;
   i20c = I2[kDfx, kDbx, k5x, b0x, i10x][tstir] /. prestirsolution;
   i50c = I5[kDfx, kDbx, k5x, b0x, i10x][tstir] /. prestirsolution;
   parms = If[cati1 == False, {kDfx, kDbx, k1fx, k1bx, k2fx, k2bx, k3x, k4x,
      k5x, kzx, i10c, i20c, 0, i50c, b0x, s10x, s20x},
     {kDfx, kDbx, k1fx, k1bx, k2fx, k2bx, k3x, k4x, k5x, kzx, 0, 0, i10x, 0,
```

```
    b0x, s10x, s20x}];
 Column[{{Show[ListPlot[If[showtot, {dataS1, dataS2, dataP, datatot},
       {dataS1, dataS2, dataP}], PlotStyle -> {Orange, Magenta, Purple,
        Brown}, AxesLabel -> {t, conc}, AxesStyle -> Directive[Thick,
        Medium], PlotRange -> {If[autot, Full, {0, tmax}],
        If[autoconc, Full, {0, concmax}]}, ImageSize -> 500],
      Plot[{(S1 @@ parms)[t] /. solution, (S2 @@ parms)[t] /. solution,
        (P @@ parms)[t] /. solution}, {t, 0, 3000},
       PlotStyle -> {Orange, Magenta, Purple, Brown}]]},
   Show[If[cati1 == False, Plot[{I1[kDfx, kDbx, k5x, b0x, i10x][
         t + tstir] /. prestirsolution, I2[kDfx, kDbx, k5x, b0x, i10x][
         t + tstir] /. prestirsolution, I5[kDfx, kDbx, k5x, b0x, i10x][
         t + tstir] /. prestirsolution, cat[kDfx, kDbx, k5x, b0x, i10x][
         t + tstir] /. prestirsolution}, {t, -tstir, 0},
       PlotStyle -> {Magenta, Purple, Pink, Red}, AxesLabel -> {t, conc},
       AxesStyle -> Directive[Thick, Medium], PlotRange ->
        {If[autot, Full, {-tstir, 0}], If[autoconc, Full, {0, concmax}]},
       ImageSize -> 500, PlotRangePadding -> {tmax, Automatic}], {}],
     Plot[{Legended[(I0 @@ parms)[t] /. solution, "I0"],
       Legended[(I1 @@ parms)[t] /. solution, "I1"],
       Legended[(I2 @@ parms)[t] /. solution, "I2"],
       Legended[(I3 @@ parms)[t] /. solution, "I3"],
       Legended[(I4 @@ parms)[t] /. solution, "I4"],
       Legended[(I5 @@ parms)[t] /. solution, "I5"],
       Legended[(cat @@ parms)[t] /. solution, "cat"]}, {t, 0, tmax},
      PlotStyle -> {Orange, Magenta, Purple, Brown, Green, Pink, Red},
      AxesLabel -> {t, conc}, AxesStyle -> Directive[Thick, Medium],
      PlotRange -> {If[autot, Full, {0, tmax}], If[autoconc, Full,
         {0, concmax}]}, ImageSize -> 500]],
   Show[If[cati1 == False, Plot[{B[kDfx, kDbx, k5x, b0x, i10x][
         t + tstir] /. prestirsolution}, {t, -tstir, 0},
       PlotStyle -> {Orange, Magenta, Purple, Brown, Green, Black},
       AxesLabel -> {t, conc}, AxesStyle -> Directive[Thick, Medium],
       PlotRange -> {If[autot, Full, {-tstir, 0}], {0, Automatic}},
       ImageSize -> 500, PlotRangePadding -> {tmax, Automatic}], {}],
     Plot[{Legended[(B @@ parms)[t] /. solution, "B"]}, {t, 0, tmax},
      PlotStyle -> {Orange, Magenta, Purple, Brown, Green, Black},
      AxesLabel -> {t, conc}, AxesStyle -> Directive[Thick, Medium],
      PlotRange -> {If[autot, Full, {0, tmax}], If[autoconc, Full, Full]},
      ImageSize -> 500]], StringJoin["ln k = ",
     ToString[Log[((P @@ parms)[gradmax] - (P @@ parms)[gradmin])/
        (gradmax - gradmin) /. solution]]]}, ImageSize -> 500],
{{showtot, False, "Show S1 + S2 + P conc"}, {True, False}},
{{autoconc, True, "Show full conc range"}, {True, False}},
{{concmax, 0.008, "concmax"}, 0.0001, 1},
{{autot, True, "Show full time range"}, {True, False}},
{{tmax, 60, "tmax"}, 1, 1000000}, {{cati1, False, "Catalyst added as I4"},
 {True, False}}, {{i10x, 0.025700480737772397, "cat[0]"}, 0,
 0.05140096147554479}, {{b0x, 0.8242776203966006, "B[0]"}, 0,
 1.6485552407932011}, {{s10x, 0.04127949719842606, "s1[0]"}, 0,
 0.08255899439685212}, {{s20x, 0.04127949719842606, "s2[0]"}, 0,
 0.08255899439685212}, {{kDfx, 0.2, "kDf"}, 0, 0.4},
{{kDbx, 20, "kDb"}, 0, 2000}, {{k1fx, 30.52580182727398, "k1f"}, 0,
 61.05160365454796}, {{k1bx, 0, "k1b"}, 0, 20},
{{k2fx, 55.8, "k2f"}, 0, 111.6}, {{k2bx, 0, "k2b"}, 0, 20},
{{k3x, 354.61765435181513, "k3"}, 0, 709.2353087036303},
{{k4x, 0.00455, "k4"}, 0, 0.0091}, {{k5x, 0.00424, "k5"}, 0, 0.00848},
{{kxx, 0, "kx"}, 0, 0}, {{kyx, 0, "ky"}, 0, 0},
{{kzx, 0.00035, "kz"}, 0, 0.0007}, {{tstir, 94, "prestirring time"}, 1,
 300}, {{gradmin, 20, "gradient \!\(\*SubscriptBox[\(t\), \(0\)]\)"}, 0,
 60}, {{gradmax, 50, "gradient \!\(\*SubscriptBox[\(t\), \(1\)]\)"}, 0,
 60}, Button["Export CSV",
 dataExport = Table[{t, 0, (I1 @@ parms)[t] /. solution,
     (I2 @@ parms)[t] /. solution, (I3 @@ parms)[t] /. solution,
     (I4 @@ parms)[t] /. solution, (I5 @@ parms)[t] /. solution,
     (B @@ parms)[t] /. solution, (S1 @@ parms)[t] /. solution,
     (S2 @@ parms)[t] /. solution, (P @@ parms)[t] /. solution},
    {t, 0, tmax, 0.1}]; If[cati1 == False, dataExport =
    Join[Table[{t, 0, I1[kDfx, kDbx, k5x, b0x, i10x][t + tstir] /.
        prestirsolution, I2[kDfx, kDbx, k5x, b0x, i10x][t + tstir] /.
        prestirsolution, 0, 0, I5[kDfx, kDbx, k5x, b0x, i10x][t + tstir] /.
        prestirsolution, B[kDfx, kDbx, k5x, b0x, i10x][t + tstir] /.
        prestirsolution, 0, 0, 0}, {t, -tstir, 0 - 0.1, 0.1}],
```

```
    dataExport]]; PrependTo[dataExport, {"t", "cat", "I1", "I2", "I3",
   "I4", "I5", "B", "S1", "S2", "P"}];
  Export[StringJoin[NotebookDirectory[], "results.csv"], dataExport]]]
```

## 9.7 Mathematica scripts for model 6

The Mathematica model was constructed according to the system described in 7.22.7. In the script below, the naming conventions were as follows: B = $K_3PO_4$, B2 = $K_2HPO_4$, B3 = **160**, B4 = **161**, I1 = **139**, I2 = **140**, I3 = **135**, I4 = **136**, I5 = **127**, I6 = **148**, I7 = **150**, S1 = (−)-**125**, S2 = (+)-**125**, P = **126**.

```
Remove["Global`*"]
p=0.5;p2=0.5;
prestirsolution=ParametricNDSolve[{
B'[t]==-k6f B[t]I5[t] + k6b B2[t] I7[t],
B2'[t]==k6f B[t]I5[t]-k6b B2[t]I7[t],
B4'[t]==k7f I7[t]-k7b I2[t]B4[t],
I1'[t]== - kDf I1[t] + kDb I2[t]I5[t],
I2'[t]==kDf I1[t] - kDb I2[t]I5[t]+k7f I7[t]-k7b I2[t]B4[t],
I5'[t]==kDf I1[t]-kDb I2[t]I5[t] -k6f B[t]I5[t] + k6b B2[t] I7[t],
I7'[t]==k6f B[t]I5[t] - k6b B2[t] I7[t]-k7f I7[t]+k7b I2[t]B4[t],
cat[t]==2I1[t]+I2[t]+I5[t]+I7[t],
I1[0]==0,
B[0]==b0,
B2[0]==0,
B4[0]==0,
I2[0]==0,
I5[0]==i50,
I7[0]==0
},
{B,B2,B4,I1,I2,I5,I7,cat},{t,0,3000},{kDf,kDb,k6f,k6b,k7f,k7b,b0,i50}];
solution=ParametricNDSolve[{
B'[t]==-k5f B[t]I4[t] + k5b B2[t] I6[t]-k6f B[t]I5[t] + k6b B2[t] I7[t],
B2'[t]==k5f B[t]I4[t]-k5b B2[t]I6[t]+k6f B[t]I5[t]-k6b B2[t]I7[t],
B3'[t]==k4f I6[t]-k4b I2[t]B3[t],
B4'[t]==k7f I7[t]-k7b I2[t]B4[t],
I1'[t]== - kDf I1[t] + kDb I2[t]I5[t],
I2'[t]==kDf I1[t] - kDb I2[t]I5[t]-k1f I2[t] S1[t] + k1b I3[t] -k2f I2[t] S2[t] +
         k2b I3[t]+k4f I6[t]-k4b I2[t]B3[t]+k7f I7[t]-k7b I2[t]B4[t],
S1'[t]==-k1f I2[t] S1[t] + k1b I3[t]-kz S1[t]B[t],
S2'[t]==-k2f I2[t] S2[t] + k2b I3[t]-kz S2[t]B[t],
I3'[t]==k1f I2[t] S1[t] - k1b I3[t] +k2f I2[t] S2[t] - k2b I3[t]-k3 I3[t] ,
I4'[t]==k3 I3[t]  -k5f B[t]I4[t]+k5b B2[t]I6[t],
I5'[t]==kDf I1[t]-kDb I2[t]I5[t]-k6f B[t]I5[t] + k6b B2[t] I7[t],
I6'[t]==k5f B[t]I4[t] - k5b B2[t] I6[t]-k4f I6[t]+k4b I2[t]B3[t],
I7'[t]==k6f B[t]I5[t] - k6b B2[t] I7[t]-k7f I7[t]+k7b I2[t]B4[t],
P'[t]== k3 I3[t]+ kz(S1[t]B[t] + S2[t]B[t]),
cat[t]==2I1[t]+I2[t]+I3[t]+I4[t]+I5[t]+I6[t]+I7[t],
I1[0]==i10,
B[0]==b0,
B2[0]==0,
B3[0]==0,
B4[0]==0,
I2[0]==i20,
I3[0]==0,
I4[0]==i40,
I5[0]==i50,
I6[0]==0,
I7[0]==i70,
S1[0]==s10,
S2[0]==s20,
```

```
P[0]==0
},
{B,B2,B3,B4,I1,I2,I3,I4,I5,I6,I7,S1,S2,P,cat},{t,0,3000},
        {kDf,kDb,k1f,k1b,k2f,k2b,k3,k4f,k4b,k5f,k5b,k6f,
        k6b,k7f,k7b,kz,i10,i20,i40,i50,i70,b0,s10,s20}];
datafolder="spirok-data 20181211";

allparameters7={kDf->0.001,kDb->1000,k1f->10,k2f->10,
        k3->354.6,k4f->0.015,k4b->100,k5f->1,k5b->100,
        k6f->1,k6b->100,k7f->2,k7b->100,kz->0.00035};
allparameters9={kDf->0.0011,kDb->150000,k1f->700,
        k2f->1400,k3->354.6,k4f->0.015,k4b->100,k5f->1,
        k5b->100,k6f->0.8,k6b->0,k7f->0.8,k7b->0,kz->0.00035};
allparameters10={kDf->0.000215,kDb->150000,k1f->700,
        k2f->1400,k3->354.6,k4f->0.015,k4b->100,k5f->1,
        k5b->100,k6f->0.8,k6b->0,k7f->0.8,k7b->0,kz->0.00003};

allparameters=allparameters10;

(*fit assuming catalyst starts as I1*)
(*model[tx_,kDf_,kDb_,k1f_,k5f_]=
(P[kDf,kDb,k1f,0,k1f,0,354.61,0.012,0,k5f,0,0.00035,0,0,0,rxndata[[6]],
        rxndata[[5]],rxndata[[2]]/2,rxndata[[2]]/2][tx+0]/.solution);
fitdata=dataP;
(*fitdata=Select[fitdata,#[[1]]<60&];*)
fit=NonlinearModelFit[fitdata,
{model[tx,kDf,kDb,k1f,k5f],kDf>0,kDb>0,k1f>0,k5f>0}
,
{{kDf,0},{kDb,72},{k1f,2},{k5f,0.5}},tx,Method?{"NMinimize",
        Method?"DifferentialEvolution"},MaxIterations?10];*)
(*ListPlot[fit["FitResiduals"]]
Show[ListPlot[fitdata,PlotStyle->Black],Plot[fit[t],{t,0,150}]]
fit["BestFitParameters"]*)
Manipulate[

prestirparms={kDfx,kDbx,k6fx,k6bx,k7fx,k7bx,baseconcBefore,catconcBefore};
volratio=(solventbasevol/totalvol);
i10c=volratio *Apply[I1,prestirparms][tstir]/.prestirsolution;
i20c=volratio *Apply[I2,prestirparms][tstir]/.prestirsolution;
i50c=volratio *Apply[I5,prestirparms][tstir]/.prestirsolution;
i70c=volratio *Apply[I7,prestirparms][tstir]/.prestirsolution;

parms=If[cati1==True,{kDfx,kDbx,k1fx,k1bx,k2fx,k2bx,k3x,k4fx,
        k4bx,k5fx,k5bx,k6fx,k6bx,k7fx,k7bx,kzx,0,0,rxndata[[6]],
        0,0,rxndata[[5]],s10x*rxndata[[2]]/2,s20x*rxndata[[2]]/2},
If[prestir==True,
{kDfx,kDbx,k1fx,k1bx,k2fx,k2bx,k3x,k4fx,k4bx,k5fx,
        k5bx,k6fx,k6bx,k7fx,k7bx,kzx,i10c,i20c,0,i50c,i70c,
        rxndata[[5]],s10x*rxndata[[2]]/2,s20x*rxndata[[2]]/2},
{kDfx,kDbx,k1fx,k1bx,k2fx,k2bx,k3x,k4fx,k4bx,k5fx,k5bx,
        k6fx,k6bx,k7fx,k7bx,kzx,0,0,0,rxndata[[6]],0,
        rxndata[[5]],s10x*rxndata[[2]]/2,s20x*rxndata[[2]]/2}]
];

tdata = 1.05 Last[dataP][[1]];
Column[{
Show[ListPlot[If[showtot,{dataS1,dataS2,dataP,datatot},
        {dataS1,dataS2,dataP}],PlotStyle->{Orange,Magenta,Purple,Brown},
        AxesLabel->{t,conc},AxesStyle->Directive[Thick,Medium],
        PlotRange->{If[autot,{If[prestir,-tstir,0],tdata},
        {If[prestir,-tstir,0],tmax}],If[autoconc,Full,{0,concmax}]},
ImageSize->500],
Plot[{
Legended[(Apply[S1,parms][t]/.solution),"S1"],
Legended[(Apply[S2,parms][t]/.solution),"S2"],
Legended[(Apply[P,parms][t]/.solution),"P"],
Legended[(Apply[S1,parms][t]/.solution)+
        (Apply[S2,parms][t]/.solution)+(Apply[P,parms][t]/.solution),"Tot"]
},{t,0,3000}
,PlotStyle->{Orange,Magenta,Purple,Brown}]
]
,
Show[If[And[cati1==False,prestir==True],Plot[{
```

```
(Apply[cat,prestirparms][t+tstir]/.prestirsolution),
(Apply[I1,prestirparms][t+tstir]/.prestirsolution),
(Apply[I2,prestirparms][t+tstir]/.prestirsolution),
(Apply[I5,prestirparms][t+tstir]/.prestirsolution),
(Apply[I7,prestirparms][t+tstir]/.prestirsolution)
},{t,-tstir,0}
,PlotStyle->{Orange,Magenta,Purple,Pink,Red},
        AxesLabel->{t,conc},AxesStyle->Directive[Thick,Medium],
        PlotRange->{If[autot,{-tstir,tdata},{-tstir,tmax}],
        If[autoconc,Full,{0,concmax}]},ImageSize->500],{}],
Plot[{
Legended[(Apply[cat,parms][t]/.solution),"cat"],
Legended[(Apply[I1,parms][t]/.solution),"I1"],
Legended[(Apply[I2,parms][t]/.solution),"I2"],
Legended[(Apply[I3,parms][t]/.solution),"I3"],
Legended[(Apply[I4,parms][t]/.solution),"I4"],
Legended[(Apply[I5,parms][t]/.solution),"I5"],
Legended[(Apply[I6,parms][t]/.solution),"I6"],
Legended[(Apply[I7,parms][t]/.solution),"I7"]
},{t,0,If[autot,tdata,tmax]}
,PlotStyle->{Orange,Magenta,Purple,Brown,Green,Pink,Yellow,Red},
        AxesLabel->{t,conc},AxesStyle->Directive[Thick,Medium],
        PlotRange->{If[autot,{0,tdata},{0,tmax}],If[autoconc,Full,{0,concmax}]},
        ImageSize->500]
]
,
Show[If[prestir==True,
Plot[{
(Apply[B,prestirparms][t+tstir]/.prestirsolution),
(Apply[B2,prestirparms][t+tstir]/.prestirsolution),
(Apply[B4,prestirparms][t+tstir]/.prestirsolution)
},{t,-tstir,0}
,PlotStyle->{Orange,Magenta,Brown},AxesLabel->{t,conc},
        AxesStyle->Directive[Thick,Medium],PlotRange->{If[autot,{-tstir,tdata},
        {-tstir,tmax}],{0,Automatic}},ImageSize->500],{}],
Plot[{
Legended[(Apply[B,parms][t]/.solution),"B"],
Legended[(Apply[B2,parms][t]/.solution),"B2"],
Legended[(Apply[B3,parms][t]/.solution),"B3"],
Legended[(Apply[B4,parms][t]/.solution),"B4"]
},{t,0,If[autot,tdata,tmax]}
,PlotStyle->{Orange,Magenta,Purple,Brown,Green,Black},
        AxesLabel->{t,conc},AxesStyle->Directive[Thick,Medium],
        PlotRange->{If[autot,{0,tdata},{0,tmax}],{0,Automatic}},
        ImageSize->500]
],
"ln k = "<>ToString[Log[(Apply[P,parms][gradmax]-
        Apply[P,parms][gradmin])/(gradmax-gradmin)/.solution]],"",
TableForm[{rxndatacols,rxndata}],"",
TableForm[Transpose[kvPairs[[1;;5]]]],"",
TableForm[Transpose[kvPairs[[6;;10]]]],"",
TableForm[Transpose[kvPairs[[11;;]]]],"",
TableForm[{{"baseconcBefore","catconcBefore"},{baseconcBefore,catconcBefore}}],"",
TableForm[{{"baseconcAfter","catconcAfter","substrateconcAfter"},
        {baseconcAfter,catconcAfter,substrateconcAfter}}]
},ImageSize->500]


,
{{folder1,"00 all reactions data","Category"},Map[FileNameTake,
        FileNames[NotebookDirectory[]<>datafolder<>"\\* *"]],PopupMenu},
{{folder2,"spirok-12","Folder"},SortBy[Map[FileNameTake,
        FileNames[NotebookDirectory[]<>datafolder<>"\\"<>
        folder1<>"\\*"]],ToExpression[StringDrop[#,7]]&],PopupMenu},
{{datafile,"rep1-conc.csv","Repetition"},
Map[FileNameTake,FileNames[NotebookDirectory[]<>
        datafolder<>"\\"<>folder1<>"\\"<>folder2<>"\\rep*-conc.csv"]],PopupMenu},
Button["Load data",
SetDirectory[NotebookDirectory[]<>"\\"<>datafolder<>"\\"<>folder1<>"\\"<>folder2];
dataCSV=Import[datafile,"CSV",HeaderLines->1];
dataS1=Map[{#[[1]],#[[3]]}&,dataCSV];
dataS2=Map[{#[[1]],#[[4]]}&,dataCSV];
dataP=Map[{#[[1]],#[[5]]}&,dataCSV];
datatot=Map[{#[[1]],#[[3]]+#[[4]]+#[[5]]}&,dataCSV];
```

```
datarxnCSV=Import[FileNames["spirok-*-rxn.csv"][[1]],"CSV",HeaderLines->1];
rep=ToExpression[StringTake[datafile,{4,4}]];
rxndata=Transpose[datarxnCSV][[1+3(rep-1)+2]];
rxndatacols=Transpose[datarxnCSV][[1]];


SetDirectory[NotebookDirectory[]<>"\\"<>datafolder<>"\\00 all reactions input\\"<>folder2];
dataInput=Import["user-input"<>ToString[rep]<>".R","Text"];
dataInput=StringReplace[dataInput,Shortest["#"~~__~~"\n"]->"\n"] ;(*strip comments*)
dataInput=StringReplace[dataInput,"#"~~__->"\n"] ;(*strip last comment*)
StringTrim[dataInput];
kvPairs=StringCases[dataInput,RegularExpression["(\\S*)\\s*
        <-\\s*(\\S*)\\s*\n"]:>{"$1","$2"}];
inputParams=AssociationThread[Transpose[kvPairs][[1]],Transpose[kvPairs][[2]]];

baseadded=ToExpression[({"base_added"}/.inputParams)[[1]]];
baseconc=ToExpression[({"base_conc"}/.inputParams)[[1]]];
basemoles = (baseadded/10^6)baseconc;
catadded=ToExpression[({"catalyst_added"}/.inputParams)[[1]]];
catmw=ToExpression[({"catalyst_MW"}/.inputParams)[[1]]];
catmoles = (catadded/10^3)/catmw;
solventvol=ToExpression[({"solvent"}/.inputParams)[[1]]];
stockvol=ToExpression[({"stock_volume"}/.inputParams)[[1]]];
stockadded=ToExpression[({"stock_added"}/.inputParams)[[1]]];
stockamountsubstrate1=ToExpression[({"stock.amount.substrate1"}/.inputParams)[[1]]];
submoles=(stockadded/stockvol)*(stockamountsubstrate1/10^3)/432.346;
solventbasevol=(solventvol+baseadded/10^3)/10^3;
totalvol=(solventvol+baseadded/10^3+stockadded)/10^3;
baseconcBefore=basemoles/solventbasevol;
catconcBefore=catmoles/solventbasevol;
baseconcAfter=basemoles/totalvol;
catconcAfter=catmoles/totalvol;
substrateconcAfter=submoles/totalvol;
],
{{showtot,False,"Show S1 + S2 + P conc"},{True,False}},
{{autoconc,True,"Show full conc range"},{True,False}},{{concmax,0.008,
        "concmax"},0.0001,1},{{autot,True,"Show full time range"},
        {True,False}},{{tmax,60,"tmax"},1,1000000},
{{cati1,False,"Catalyst added as I4"},{True,False}},
{{prestir,False,"Prestirred catalyst and base"},{True,False}},
(*{{i10x,rxndata[[6]],"cat[0]"},0,2rxndata[[6]]},
{{b0x,rxndata[[5]],"B[0]"},0,2rxndata[[5]]},*)
{{s10x,1,"s1 adjust"},0.8,1.2},{{s20x,1,"s2 adjust"},0.8,1.2},
        {{kDfx,(kDf/.allparameters),"kDf"},0,2(kDf/.allparameters)},
        {{kDbx,kDb/.allparameters,"kDb"},0,2(kDb/.allparameters)},
        {{k1fx,(k1f/.allparameters),"k1f"},0,2(k1f/.allparameters)},
        {{k1bx,0,"k1b"},0,20},{{k2fx,(k2f/.allparameters),"k2f"},
        0,2(k2f/.allparameters)},{{k2bx,0,"k2b"},0,20},
        {{k3x,(k3/.allparameters),"k3"},0,2(k3/.allparameters)},
        {{k4fx,(k4f/.allparameters),"k4f"},0,2(k4f/.allparameters)},
        {{k4bx,(k4b/.allparameters),"k4b"},0,2(k4b/.allparameters)},
        {{k5fx,(k5f/.allparameters),"k5f"},0,2(k5f/.allparameters)},
{{k5bx,(k5b/.allparameters),"k5b"},0,2(k5b/.allparameters)},
{{k6fx,(k6f/.allparameters),"k6f"},0,2(k6f/.allparameters)},
        {{k6bx,(k6b/.allparameters),"k6b"},0,2(k6b/.allparameters)},
        {{k7fx,(k7f/.allparameters),"k7f"},0,2(k7f/.allparameters)},
{{k7bx,(k7b/.allparameters),"k7b"},0,2(k7b/.allparameters)},
{{kxx,(kx/.allparameters),"kx"},0,2(kx/.allparameters)},
{{kyx,(ky/.allparameters),"ky"},0,2(ky/.allparameters)},
{{kzx,(kz/.allparameters),"kz"},0,2(kz/.allparameters)},
{{tstir,50,"prestirring time"},1,300},
{{gradmin,20,"gradient Subscript[t, 0]"},0,60},
{{gradmax,50,"gradient Subscript[t, 1]"},0,60},
Button["Export CSV",
dataExport=Table[{t,
(Apply[cat,parms][t]/.solution),
(Apply[I1,parms][t]/.solution),
(Apply[I2,parms][t]/.solution),
(Apply[I3,parms][t]/.solution),
(Apply[I4,parms][t]/.solution),
(Apply[I5,parms][t]/.solution),
(Apply[I6,parms][t]/.solution),
(Apply[I7,parms][t]/.solution),
```

```
(Apply[B,parms][t]/.solution),
(Apply[S1,parms][t]/.solution),
(Apply[S2,parms][t]/.solution),
(Apply[P,parms][t]/.solution)
},{t,0,tmax,0.1}];
If[And[cati1==False,prestir==True],
dataExport=Join[Table[{t,
(Apply[cat,prestirparms][t+tstir]/.prestirsolution),
(Apply[I1,prestirparms][t+tstir]/.prestirsolution),
(Apply[I2,prestirparms][t+tstir]/.prestirsolution),
0,
0,
(Apply[I5,prestirparms][t+tstir]/.prestirsolution),
0,
(Apply[I7,prestirparms][t+tstir]/.prestirsolution),
(Apply[B,prestirparms][t+tstir]/.prestirsolution),
0,
0,
0
},{t,-tstir,0-0.1,0.1}],dataExport]];
PrependTo[dataExport,{"t","cat","I1","I2","I3","I4","I5","I6","I7","B","S1","S2","P"}];
Export[NotebookDirectory[]<>"results.csv",dataExport]

],Initialization:>{
folder1="00 all reactions data";
folder2="spirok-36";
datafile="rep1-conc.csv";
SetDirectory[NotebookDirectory[]<>"\\"<>datafolder<>"\\"<>folder1<>"\\"<>folder2];
dataCSV=Import[datafile,"CSV",HeaderLines->1];
dataS1=Map[{#[[1]],#[[3]]}&,dataCSV];
dataS2=Map[{#[[1]],#[[4]]}&,dataCSV];
dataP=Map[{#[[1]],#[[5]]}&,dataCSV];
datatot=Map[{#[[1]],#[[3]]+#[[4]]+#[[5]]}&,dataCSV];
datarxnCSV=Import[FileNames["spirok-*-rxn.csv"][[1]],"CSV",HeaderLines->1];
rep=ToExpression[StringTake[datafile,{4,4}]];
rxndata=Transpose[datarxnCSV][[1+3(rep-1)+2]];
rxndatacols=Transpose[datarxnCSV][[1]];


SetDirectory[NotebookDirectory[]<>"\\"<>datafolder<>"\\00 all reactions input\\"<>folder2];
dataInput=Import["user-input"<>ToString[rep]<>".R","Text"];
dataInput=StringReplace[dataInput,Shortest["#"~~__~~"\n"]->"\n"] ;(*strip comments*)
dataInput=StringReplace[dataInput,"#"~~__->"\n"] ;(*strip last comment*)
StringTrim[dataInput];
kvPairs=StringCases[dataInput,RegularExpression["(\\S*)\\s*<-\\s*(\\S*)\\s*\n"]:>{"$1","$2"}];
inputParams=AssociationThread[Transpose[kvPairs][[1]],Transpose[kvPairs][[2]]];

baseadded=ToExpression[({"base_added"}/.inputParams)[[1]]];
baseconc=ToExpression[({"base_conc"}/.inputParams)[[1]]];
basemoles = (baseadded/10^6)baseconc;
catadded=ToExpression[({"catalyst_added"}/.inputParams)[[1]]];
catmw=ToExpression[({"catalyst_MW"}/.inputParams)[[1]]];
catmoles = (catadded/10^3)/catmw;
solventvol=ToExpression[({"solvent"}/.inputParams)[[1]]];
stockvol=ToExpression[({"stock_volume"}/.inputParams)[[1]]];
stockadded=ToExpression[({"stock_added"}/.inputParams)[[1]]];
stockamountsubstrate1=ToExpression[({"stock.amount.substrate1"}/.inputParams)[[1]]];
submoles=(stockadded/stockvol)*(stockamountsubstrate1/10^3)/432.346;
solventbasevol=(solventvol+baseadded/10^3)/10^3;
totalvol=(solventvol+baseadded/10^3+stockadded)/10^3;
baseconcBefore=basemoles/solventbasevol;
catconcBefore=catmoles/solventbasevol;
baseconcAfter=basemoles/totalvol;
catconcAfter=catmoles/totalvol;
substrateconcAfter=submoles/totalvol;

}
]
Manipulate[prestirparms = {kDfx, kDbx, k6fx, k6bx, k7fx, k7bx,
     baseconcBefore, catconcBefore}; volratio = solventbasevol/totalvol;
   i10c = volratio*(I1 @@ prestirparms)[tstir] /. prestirsolution;
   i20c = volratio*(I2 @@ prestirparms)[tstir] /. prestirsolution;
   i50c = volratio*(I5 @@ prestirparms)[tstir] /. prestirsolution;
```

```
i70c = volratio*(I7 @@ prestirparms)[tstir] /. prestirsolution;
parms = If[cati1 == True, {kDfx, kDbx, k1fx, k1bx, k2fx, k2bx, k3x, k4fx,
   k4bx, k5fx, k5bx, k6fx, k6bx, k7fx, k7bx, kzx, 0, 0, rxndata[[6]], 0,
   0, rxndata[[5]], s10x*(rxndata[[2]]/2), s20x*(rxndata[[2]]/2)},
  If[prestir == True, {kDfx, kDbx, k1fx, k1bx, k2fx, k2bx, k3x, k4fx,
    k4bx, k5fx, k5bx, k6fx, k6bx, k7fx, k7bx, kzx, i10c, i20c, 0, i50c,
    i70c, rxndata[[5]], s10x*(rxndata[[2]]/2), s20x*(rxndata[[2]]/2)},
   {kDfx, kDbx, k1fx, k1bx, k2fx, k2bx, k3x, k4fx, k4bx, k5fx, k5bx, k6fx,
    k6bx, k7fx, k7bx, kzx, 0, 0, 0, rxndata[[6]], 0, rxndata[[5]],
    s10x*(rxndata[[2]]/2), s20x*(rxndata[[2]]/2)}]];
tdata = 1.05*Last[dataP][[1]];
Column[{Show[ListPlot[If[showtot, {dataS1, dataS2, dataP, datatot},
     {dataS1, dataS2, dataP}], PlotStyle -> {Orange, Magenta, Purple,
      Brown}, AxesLabel -> {t, conc}, AxesStyle -> Directive[Thick,
      Medium], PlotRange -> {If[autot, {If[prestir, -tstir, 0], tdata},
       {If[prestir, -tstir, 0], tmax}], If[autoconc, Full, {0, concmax}]},
    ImageSize -> 500], Plot[{Legended[(S1 @@ parms)[t] /. solution, "S1"],
     Legended[(S2 @@ parms)[t] /. solution, "S2"],
     Legended[(P @@ parms)[t] /. solution, "P"],
     Legended[((S1 @@ parms)[t] /. solution) + ((S2 @@ parms)[t] /.
        solution) + ((P @@ parms)[t] /. solution), "Tot"]}, {t, 0, 3000},
    PlotStyle -> {Orange, Magenta, Purple, Brown}]],
  Show[If[cati1 == False && prestir == True,
    Plot[{(cat @@ prestirparms)[t + tstir] /. prestirsolution,
      (I1 @@ prestirparms)[t + tstir] /. prestirsolution,
      (I2 @@ prestirparms)[t + tstir] /. prestirsolution,
      (I5 @@ prestirparms)[t + tstir] /. prestirsolution,
      (I7 @@ prestirparms)[t + tstir] /. prestirsolution}, {t, -tstir, 0},
     PlotStyle -> {Orange, Magenta, Purple, Pink, Red},
     AxesLabel -> {t, conc}, AxesStyle -> Directive[Thick, Medium],
     PlotRange -> {If[autot, {-tstir, tdata}, {-tstir, tmax}],
       If[autoconc, Full, {0, concmax}]}, ImageSize -> 500], {}],
   Plot[{Legended[(cat @@ parms)[t] /. solution, "cat"],
     Legended[(I1 @@ parms)[t] /. solution, "I1"],
     Legended[(I2 @@ parms)[t] /. solution, "I2"],
     Legended[(I3 @@ parms)[t] /. solution, "I3"],
     Legended[(I4 @@ parms)[t] /. solution, "I4"],
     Legended[(I5 @@ parms)[t] /. solution, "I5"],
     Legended[(I6 @@ parms)[t] /. solution, "I6"],
     Legended[(I7 @@ parms)[t] /. solution, "I7"]},
    {t, 0, If[autot, tdata, tmax]}, PlotStyle -> {Orange, Magenta, Purple,
      Brown, Green, Pink, Yellow, Red}, AxesLabel -> {t, conc},
    AxesStyle -> Directive[Thick, Medium], PlotRange ->
     {If[autot, {0, tdata}, {0, tmax}], If[autoconc, Full, {0, concmax}]},
    ImageSize -> 500]], Show[If[prestir == True,
    Plot[{(B @@ prestirparms)[t + tstir] /. prestirsolution,
      (B2 @@ prestirparms)[t + tstir] /. prestirsolution,
      (B4 @@ prestirparms)[t + tstir] /. prestirsolution}, {t, -tstir, 0},
     PlotStyle -> {Orange, Magenta, Brown}, AxesLabel -> {t, conc},
     AxesStyle -> Directive[Thick, Medium], PlotRange ->
      {If[autot, {-tstir, tdata}, {-tstir, tmax}], {0, Automatic}},
     ImageSize -> 500], {}], Plot[{Legended[(B @@ parms)[t] /. solution,
      "B"], Legended[(B2 @@ parms)[t] /. solution, "B2"],
     Legended[(B3 @@ parms)[t] /. solution, "B3"],
     Legended[(B4 @@ parms)[t] /. solution, "B4"]},
    {t, 0, If[autot, tdata, tmax]}, PlotStyle -> {Orange, Magenta, Purple,
      Brown, Green, Black}, AxesLabel -> {t, conc},
    AxesStyle -> Directive[Thick, Medium], PlotRange ->
     {If[autot, {0, tdata}, {0, tmax}], {0, Automatic}},
    ImageSize -> 500]], StringJoin["ln k = ",
   ToString[Log[((P @@ parms)[gradmax] - (P @@ parms)[gradmin])/
      (gradmax - gradmin) /. solution]]], "",
  TableForm[{rxndatacols, rxndata}], "",
  TableForm[Transpose[kvPairs[[1 ;; 5]]]], "",
  TableForm[Transpose[kvPairs[[6 ;; 10]]]], "",
  TableForm[Transpose[kvPairs[[11 ;; All]]]], "",
  TableForm[{{"baseconcBefore", "catconcBefore"},
    {baseconcBefore, catconcBefore}}], "",
  TableForm[{{"baseconcAfter", "catconcAfter", "substrateconcAfter"},
    {baseconcAfter, catconcAfter, substrateconcAfter}}]},
 ImageSize -> 500], {{folder1, "00 all reactions data", "Category"},
{"00 all reactions data", "00 all reactions input"},
ControlType -> PopupMenu}, {{folder2, "spirok-36", "Folder"},
```

```
 Dynamic[SortBy[FileNameTake /@ FileNames[StringJoin[NotebookDirectory[],
      datafolder, "\\", folder1, "\\*"]],
    ToExpression[StringDrop[#1, 7]] & ]], ControlType -> PopupMenu},
{{datafile, "rep1-conc.csv", "Repetition"},
 Dynamic[FileNameTake /@ FileNames[StringJoin[NotebookDirectory[],
     datafolder, "\\", folder1, "\\", folder2, "\\rep*-conc.csv"]]],
 ControlType -> PopupMenu}, Button["Load data",
 SetDirectory[StringJoin[NotebookDirectory[], "\\", datafolder, "\\",
    folder1, "\\", folder2]]; dataCSV = Import[datafile, "CSV",
    HeaderLines -> 1]; dataS1 = ({#1[[1]], #1[[3]]} & ) /@ dataCSV;
  dataS2 = ({#1[[1]], #1[[4]]} & ) /@ dataCSV;
  dataP = ({#1[[1]], #1[[5]]} & ) /@ dataCSV;
  datatot = ({#1[[1]], #1[[3]] + #1[[4]] + #1[[5]]} & ) /@ dataCSV;
  datarxnCSV = Import[FileNames["spirok-*-rxn.csv"][[1]], "CSV",
    HeaderLines -> 1]; rep = ToExpression[StringTake[datafile, {4, 4}]];
  rxndata = Transpose[datarxnCSV][[1 + 3*(rep - 1) + 2]];
  rxndatacols = Transpose[datarxnCSV][[1]];
  SetDirectory[StringJoin[NotebookDirectory[], "\\", datafolder,
    "\\00 all reactions input\\", folder2]];
  dataInput = Import[StringJoin["user-input", ToString[rep], ".R"],
    "Text"]; dataInput = StringReplace[dataInput,
    Shortest["#"~~__~~"\n"] -> "\n"]; dataInput =
   StringReplace[dataInput, "#"~~__ -> "\n"]; StringTrim[dataInput];
  kvPairs = StringCases[dataInput,
    RegularExpression["(\\S*)\\s*<-\\s*(\\S*)\\s*\n"] :> {"$1", "$2"}];
  inputParams = AssociationThread[Transpose[kvPairs][[1]],
    Transpose[kvPairs][[2]]]; baseadded = ToExpression[
    ({"base_added"} /. inputParams)[[1]]];
  baseconc = ToExpression[({"base_conc"} /. inputParams)[[1]]];
  basemoles = (baseadded/10^6)*baseconc;
  catadded = ToExpression[({"catalyst_added"} /. inputParams)[[1]]];
  catmw = ToExpression[({"catalyst_MW"} /. inputParams)[[1]]];
  catmoles = catadded/10^3/catmw; solventvol =
   ToExpression[({"solvent"} /. inputParams)[[1]]];
  stockvol = ToExpression[({"stock_volume"} /. inputParams)[[1]]];
  stockadded = ToExpression[({"stock_added"} /. inputParams)[[1]]];
  stockamountsubstrate1 = ToExpression[({"stock.amount.substrate1"} /.
      inputParams)[[1]]]; submoles = (stockadded/stockvol)*
    (stockamountsubstrate1/10^3/432.346); solventbasevol =
   (solventvol + baseadded/10^3)/10^3;
  totalvol = (solventvol + baseadded/10^3 + stockadded)/10^3;
  baseconcBefore = basemoles/solventbasevol;
  catconcBefore = catmoles/solventbasevol; baseconcAfter =
   basemoles/totalvol; catconcAfter = catmoles/totalvol;
  substrateconcAfter = submoles/totalvol; ],
{{showtot, False, "Show S1 + S2 + P conc"}, {True, False}},
{{autoconc, True, "Show full conc range"}, {True, False}},
{{concmax, 0.008, "concmax"}, 0.0001, 1},
{{autot, True, "Show full time range"}, {True, False}},
{{tmax, 60, "tmax"}, 1, 1000000}, {{cati1, False, "Catalyst added as I4"},
 {True, False}}, {{prestir, False, "Prestirred catalyst and base"},
 {True, False}}, {{s10x, 1, "s1 adjust"}, 0.8, 1.2},
{{s20x, 1, "s2 adjust"}, 0.8, 1.2}, {{kDfx, 0.000215, "kDf"}, 0, 0.00043},
{{kDbx, 150000, "kDb"}, 0, 300000}, {{k1fx, 700, "k1f"}, 0, 1400},
{{k1bx, 0, "k1b"}, 0, 20}, {{k2fx, 1400, "k2f"}, 0, 2800},
{{k2bx, 0, "k2b"}, 0, 20}, {{k3x, 354.6, "k3"}, 0, 709.2},
{{k4fx, 0.015, "k4f"}, 0, 0.03}, {{k4bx, 100, "k4b"}, 0, 200},
{{k5fx, 1, "k5f"}, 0, 2}, {{k5bx, 100, "k5b"}, 0, 200},
{{k6fx, 0.8, "k6f"}, 0, 1.6}, {{k6bx, 0, "k6b"}, 0, 0},
{{k7fx, 0.8, "k7f"}, 0, 1.6}, {{k7bx, 0, "k7b"}, 0, 0},
{{kxx, kx, "kx"}, 0, 2*kx}, {{kyx, ky, "ky"}, 0, 2*ky},
{{kzx, 0.00003, "kz"}, 0, 0.00006}, {{tstir, 50, "prestirring time"}, 1,
 300}, {{gradmin, 20, "gradient \!\(\*SubscriptBox[\(t\), \(0\)]\)"}, 0,
 60}, {{gradmax, 50, "gradient \!\(\*SubscriptBox[\(t\), \(1\)]\)"}, 0,
 60}, Button["Export CSV",
 dataExport = Table[{t, (cat @@ parms)[t] /. solution,
     (I1 @@ parms)[t] /. solution, (I2 @@ parms)[t] /. solution,
     (I3 @@ parms)[t] /. solution, (I4 @@ parms)[t] /. solution,
     (I5 @@ parms)[t] /. solution, (I6 @@ parms)[t] /. solution,
     (I7 @@ parms)[t] /. solution, (B @@ parms)[t] /. solution,
     (S1 @@ parms)[t] /. solution, (S2 @@ parms)[t] /. solution,
     (P @@ parms)[t] /. solution}, {t, 0, tmax, 0.1}];
  If[cati1 == False && prestir == True, dataExport =
```

```
    Join[Table[{t, (cat @@ prestirparms)[t + tstir] /. prestirsolution,
       (I1 @@ prestirparms)[t + tstir] /. prestirsolution,
       (I2 @@ prestirparms)[t + tstir] /. prestirsolution, 0, 0,
       (I5 @@ prestirparms)[t + tstir] /. prestirsolution, 0,
       (I7 @@ prestirparms)[t + tstir] /. prestirsolution,
       (B @@ prestirparms)[t + tstir] /. prestirsolution, 0, 0, 0},
      {t, -tstir, 0 - 0.1, 0.1}], dataExport]];
  PrependTo[dataExport, {"t", "cat", "I1", "I2", "I3", "I4", "I5", "I6",
    "I7", "B", "S1", "S2", "P"}]; Export[StringJoin[NotebookDirectory[],
    "results.csv"], dataExport]], Initialization :>
 {folder1 = "00 all reactions data"; folder2 = "spirok-36";
   datafile = "rep1-conc.csv"; SetDirectory[StringJoin[NotebookDirectory[],
     "\\", datafolder, "\\", folder1, "\\", folder2]];
   dataCSV = Import[datafile, "CSV", HeaderLines -> 1];
   dataS1 = ({#1[[1]], #1[[3]]} & ) /@ dataCSV;
   dataS2 = ({#1[[1]], #1[[4]]} & ) /@ dataCSV;
   dataP = ({#1[[1]], #1[[5]]} & ) /@ dataCSV;
   datatot = ({#1[[1]], #1[[3]] + #1[[4]] + #1[[5]]} & ) /@ dataCSV;
   datarxnCSV = Import[FileNames["spirok-*-rxn.csv"][[1]], "CSV",
     HeaderLines -> 1]; rep = ToExpression[StringTake[datafile, {4, 4}]];
   rxndata = Transpose[datarxnCSV][[1 + 3*(rep - 1) + 2]];
   rxndatacols = Transpose[datarxnCSV][[1]];
   SetDirectory[StringJoin[NotebookDirectory[], "\\", datafolder,
     "\\00 all reactions input\\", folder2]];
   dataInput = Import[StringJoin["user-input", ToString[rep], ".R"],
     "Text"]; dataInput = StringReplace[dataInput,
     Shortest["#"~~__~~"\n"] -> "\n"]; dataInput = StringReplace[dataInput,
     "#"~~__ -> "\n"]; StringTrim[dataInput];
   kvPairs = StringCases[dataInput, RegularExpression[
      "(\\S*)\\s*<-\\s*(\\S*)\\s*\n"] :> {"$1", "$2"}];
   inputParams = AssociationThread[Transpose[kvPairs][[1]],
     Transpose[kvPairs][[2]]]; baseadded = ToExpression[
     ({"base_added"} /. inputParams)[[1]]];
   baseconc = ToExpression[({"base_conc"} /. inputParams)[[1]]];
   basemoles = (baseadded/10^6)*baseconc;
   catadded = ToExpression[({"catalyst_added"} /. inputParams)[[1]]];
   catmw = ToExpression[({"catalyst_MW"} /. inputParams)[[1]]];
   catmoles = catadded/10^3/catmw; solventvol =
    ToExpression[({"solvent"} /. inputParams)[[1]]];
   stockvol = ToExpression[({"stock_volume"} /. inputParams)[[1]]];
   stockadded = ToExpression[({"stock_added"} /. inputParams)[[1]]];
   stockamountsubstrate1 = ToExpression[({"stock.amount.substrate1"} /.
      inputParams)[[1]]]; submoles = (stockadded/stockvol)*
     (stockamountsubstrate1/10^3/432.346); solventbasevol =
    (solventvol + baseadded/10^3)/10^3;
   totalvol = (solventvol + baseadded/10^3 + stockadded)/10^3;
   baseconcBefore = basemoles/solventbasevol; catconcBefore =
    catmoles/solventbasevol; baseconcAfter = basemoles/totalvol;
   catconcAfter = catmoles/totalvol; substrateconcAfter =
    submoles/totalvol; }]
```

## 10. References


[1] C. M. Starks, C. L. Liotta, M. Halpern, *Phase-Transfer Catalysis: Fundamentals, Applications and Industrial Perspectives*, Chapman & Hall, inc., New York, **1994**.

[2] E. V. Dehmlow, S. S. Dehmlow, *Phase Transfer Catalysis*, VCH, Weinheim, **1993**.

[3] J. Tan, N. Yasuda, *Org. Process Res. Dev.* **2015**, *19*, 1731.

[4] D. L. Hughes, *Org. Process Res. Dev.* **2018**, *22*, 574.

[5] C. M. Starks, *J. Am. Chem. Soc.* **1971**, *93*, 195.

[6] C. M. Starks, R. M. Owens, *J. Am. Chem. Soc.* **1973**, *95*, 3613.

[7] R. A. Jones, *Quaternary Ammonium Salts: Their Use in Phase-Transfer Catalysed Reactions*, Academic Press, London, **2001**.

[8] T. Hashimoto, K. Maruoka, *Chem. Rev.* **2007**, *107*, 5656.

[9] S. Shirakawa, K. Maruoka, *Angew. Chem., Int. Ed.* **2013**, *52*, 4312.

[10] M. Mąkosza, W. Lasek, *Tetrahedron* **1991**, *47*, 2843.

[11] D. C. M. Albanese, F. Foschi, M. Penso, *Org. Process Res. Dev.* **2016**, *20*, 129.

[12] V. Gevorgyan, E. Lukevics, *J. Chem. Soc., Chem. Commun.* **1985**, 1234.

[13] F. Rolla, *J. Org. Chem.* **1982**, *47*, 4327.

[14] S. Colonna, R. Fornasier, *J. Chem. Soc., Perkin Trans. 1* **1978**, 371.

[15] M. Rabinovitz, Y. Cohen, M. Halpern, *Angew. Chem., Int. Ed. Engl.* **1986**, *25*, 960.

[16] D. Albanese, *Catal. Rev.* **2003**, *45*, 369.

[17] H.-M. Yang, H.-S. Wu, *Catal. Rev.* **2003**, *45*, 463.

[18] M. Mąkosza, M. Fedoryński, *Catal. Rev.* **2003**, *45*, 321.

[19] S. E. Denmark, R. C. Weintraub, N. D. Gould, *J. Am. Chem. Soc.* **2012**, *134*, 13415.

[20] A. W. Herriott, D. Picker, *Tetrahedron Lett.* **1972**, *13*, 4521.

[21] A. W. Herriott, D. Picker, *J. Am. Chem. Soc.* **1975**, *97*, 2345.

[22] D. Landini, A. Maia, F. Montanari, *J. Chem. Soc., Chem. Commun.* **1977**, 112.

[23] J. E. Gordon, R. E. Kutina, *J. Am. Chem. Soc.* **1977**, *99*, 3903.

[24] D. Landini, A. Maia, F. Montanari, *J. Am. Chem. Soc.* **1978**, *100*, 2796.

[25] W. Lasek, M. Makosza, *J. Phys. Org. Chem.* **1993**, *6*, 412.

[26] C. M. Starks, *Tetrahedron* **1999**, *55*, 6261.

[27] M. Hamkalo, P. Fita, M. Fedorynski, M. Makosza, *Chem.–Eur. J.* **2018**, *24*, 3975.

[28] P. Fita, *J. Phys. Chem. C* **2014**, *118*, 23147.

[29] D. L. Hughes, U. H. Dolling, K. M. Ryan, E. F. Schoenewaldt, E. J. J. Grabowski, *J. Org. Chem.* **1987**, *52*, 4745.

[30] R. Solaro, S. D'Antone, E. Chiellini, *J. Org. Chem.* **1980**, *45*, 4179.

[31] T. Kano, Y. Aota, K. Maruoka, *Adv. Synth. Catal.* **2016**, *358*, 2996.

[32] K. Brak, E. N. Jacobsen, *Angew. Chem., Int. Ed.* **2013**, *52*, 534.

[33] K. Maruoka, T. Ooi, *Chem. Rev.* **2003**, *103*, 3013.

[34] K. Maruoka (ed.), *Asymmetric Phase Transfer Catalysis*, WILEY-VCH Verlag GmbH & Co., Weinheim, **2008**.

[35] M. J. O'Donnell, *Acc. Chem. Res.* **2004**, *37*, 506.

[36] B. Lygo, B. I. Andrews, *Acc. Chem. Res.* **2004**, *37*, 518.

[37] R. J. Armstrong, M. D. Smith, *Angew. Chem., Int. Ed.* **2014**, *53*, 12822.

[38] C. P. Johnston, A. Kothari, T. Sergeieva, S. I. Okovytyy, K. E. Jackson, R. S. Paton, M. D. Smith, *Nat. Chem.* **2015**, *7*, 171.

[39] A. J. Fugard, A. S. K. Lahdenperä, J. S. J. Tan, A. Mekareeya, R. S. Paton, M. D. Smith, *Angew. Chem., Int. Ed.* **2019**, *58*, 2795.

[40] U. H. Dolling, P. Davis, E. J. J. Grabowski, *J. Am. Chem. Soc.* **1984**, *106*, 446.

[41] R. S. E. Conn, A. V. Lovell, S. Karady, L. M. Weinstock, *J. Org. Chem.* **1986**, *51*, 4710.

[42] K. Maruoka, *Org. Process Res. Dev.* **2008**, *12*, 679.

[43] T. Ooi, T. Miki, M. Taniguchi, M. Shiraishi, M. Takeuchi, K. Maruoka, *Angew. Chem., Int. Ed.* **2003**, *42*, 3796.

[44] S. Shirakawa, K. Koga, T. Tokuda, K. Yamamoto, K. Maruoka, *Angew. Chem., Int. Ed.* **2014**, *53*, 6220.

[45] B. Xiang, K. M. Belyk, R. A. Reamer, N. Yasuda, *Angew. Chem., Int. Ed.* **2014**, *53*, 8375.

[46] E. Gomez-Bengoa, A. Linden, R. López, I. Múgica-Mendiola, M. Oiarbide, C. Palomo, *J. Am. Chem. Soc.* **2008**, *130*, 7955.

[47] K. M. Johnson, M. S. Rattley, F. Sladojevich, D. M. Barber, M. G. Nuñez, A. M. Goldys, D. J. Dixon, *Org. Lett.* **2012**, *14*, 2492.

[48] S.-s. Jew, H.-g. Park, *Chem. Commun.* **2009**, 7090.

[49] B. Lygo, B. Allbutt, S. R. James, *Tetrahedron Lett.* **2003**, *44*, 5629.

[50] T. Ooi, M. Kameda, K. Maruoka, *J. Am. Chem. Soc.* **2003**, *125*, 5139.

[51] A. E. Sheshenev, E. V. Boltukhina, A. J. P. White, K. K. M. Hii, *Angew. Chem., Int. Ed.* **2013**, *52*, 6988.

[52] J. Miguélez, H. Miyamura, S. Kobayashi, *Adv. Synth. Catal.* **2017**, *359*, 2897.

[53] M. Waser, K. Gratzer, R. Herchl, N. Müller, *Org. Biomol. Chem.* **2012**, *10*, 251.

[54] G. Gururaja, R. Herchl, A. Pichler, K. Gratzer, M. Waser, *Molecules* **2013**, *18*, 4357.

[55] S. E. Denmark, N. D. Gould, L. M. Wolf, *J. Org. Chem.* **2011**, *76*, 4260.

[56] S. E. Denmark, N. D. Gould, L. M. Wolf, *J. Org. Chem.* **2011**, *76*, 4337.

[57] T. Shibuguchi, Y. Fukuta, Y. Akachi, A. Sekine, T. Ohshima, M. Shibasaki, *Tetrahedron Lett.* **2002**, *43*, 9539.

[58] T. Ohshima, V. Gnanadesikan, T. Shibuguchi, Y. Fukuta, T. Nemoto, M. Shibasaki, *J. Am. Chem. Soc.* **2003**, *125*, 11206.

[59] T. Ohshima, T. Shibuguchi, Y. Fukuta, M. Shibasaki, *Tetrahedron* **2004**, *60*, 7743.

[60] A. Okada, T. Shibuguchi, T. Ohshima, H. Masu, K. Yamaguchi, M. Shibasaki, *Angew. Chem., Int. Ed.* **2005**, *44*, 4564.

[61] D. Uraguchi, Y. Asai, Y. Seto, T. Ooi, *Synlett* **2009**, *2009*, 658.

[62] D. Enders, T. V. Nguyen, *Org. Biomol. Chem.* **2012**, *10*, 5327.

[63] S. Liu, Y. Kumatabara, S. Shirakawa, *Green Chem.* **2016**, *18*, 331.

[64] S. Liu, K. Maruoka, S. Shirakawa, *Angew. Chem., Int. Ed.* **2017**, *129*, 4897.

[65] M. J. O'Donnell, T. M. Eckrich, *Tetrahedron Lett.* **1978**, 4625.

[66] M. J. O'Donnell, W. D. Bennett, S. Wu, *J. Am. Chem. Soc.* **1989**, *111*, 2353.

[67] M. J. O'Donnell, S. Wu, J. C. Huffman, *Tetrahedron* **1994**, *50*, 4507.

[68] A. Bhattacharya, U. H. Dolling, E. J. J. Grabowski, S. Karady, K. M. Ryan, L. M. Weinstock, *Angew. Chem., Int. Ed. Engl.* **1986**, *25*, 476.

[69] B. Lygo, P. G. Wainwright, *Tetrahedron Lett.* **1997**, *38*, 8595.

[70] E. J. Corey, F. Xu, M. C. Noe, *J. Am. Chem. Soc.* **1997**, *119*, 12414.

[71] S. E Denmark, R. C. Weintraub, *Heterocycles* **2011**, *82*, 1527.

[72] B. Wang, Y. He, X. Fu, Z. Wei, Y. Lin, H. Duan, *Synlett* **2015**, *26*, 2588.

[73] R. Chinchilla, C. Nájera, F. J. Ortega, *Tetrahedron: Asymmetry* **2006**, *17*, 3423.

[74] A. Claraz, S. Oudeyer, V. Levacher, *Adv. Synth. Catal.* **2013**, *355*, 841.

[75] J. Godemert, S. Oudeyer, V. Levacher, *ChemCatChem* **2015**, *8*, 74.

[76] B. Lygo, J. Crosby, T. R. Lowdon, P. G. Wainwright, *Tetrahedron* **2001**, *57*, 2391.

[77] B. Lygo, J. Crosby, T. R. Lowdon, J. A. Peterson, P. G. Wainwright, *Tetrahedron* **2001**, 2403.

[78] B. A. Jones, T. Balan, J. D. Jolliffe, C. D. Campbell, M. D. Smith, *Angew. Chem., Int. Ed.* **2019**, *58*, 4596.

[79] H. Li, Y. Wang, L. Tang, L. Deng, *J. Am. Chem. Soc.* **2004**, *126*, 9906.

[80] T. Tozawa, Y. Yamane, T. Mukaiyama, *Chem. Lett.* **2006**, *35*, 56.

[81] M.-S. Yoo, B.-S. Jeong, J.-H. Lee, H.-g. Park, S.-s. Jew, *Org. Lett.* **2005**, *7*, 1129.

[82] S.-s. Jew, M.-S. Yoo, B.-S. Jeong, I. Y. Park, H.-g. Park, *Org. Lett.* **2002**, *4*, 4245.

[83] K. B. Lipkowitz, M. W. Cavanaugh, B. Baker, M. J. O'Donnell, *J. Org. Chem.* **1991**, *56*, 5181.

[84] E. F. Martins, J. R. Pliego Jr, *J. Mol. Catal. A: Chem.* **2016**, *417*, 192.

[85] C. Q. He, A. Simon, Y.-h. Lam, A. P. J. Brunskill, N. Yasuda, J. Tan, A. M. Hyde, E. C. Sherer, K. N. Houk, *J. Org. Chem.* **2017**, *82*, 8645.

[86] K. Sharma, J. R. Wolstenhulme, P. P. Painter, D. Yeo, F. Grande-Carmona, C. P. Johnston, D. J. Tantillo, M. D. Smith, *J. Am. Chem. Soc.* **2015**, *137*, 13414.

[87] E. de Freitas Martins, J. R. Pliego Jr., *ACS Catal.* **2013**, *3*, 613.

[88] R. J. Armstrong, *Catalytic Asymmetric Reactions Employing Chiral Cations*, DPhil thesis, University of Oxford, Oxford, **2016**.

[89] E. Díez-Barra, A. de la Hoz, S. Merino, A. Rodríguez, P. Sánchez-Verdú, *Tetrahedron* **1998**, *54*, 1835.

[90] D. Almaşi, D. A. Alonso, C. Nájera, *Tetrahedron: Asymmetry* **2007**, *18*, 299.

[91] M.-Q. Hua, L. Wang, H.-F. Cui, J. Nie, X.-L. Zhang, J.-A. Ma, *Chem. Commun.* **2011**, *47*, 1631.

[92] M. Tiffner, J. Novacek, A. Busillo, K. Gratzer, A. Massa, M. Waser, *RSC Adv.* **2015**, *5*, 78941.

[93] T. Ooi, D. Ohara, K. Fukumoto, K. Maruoka, *Org. Lett.* **2005**, *7*, 3195.

[94] T. Ma, X. Fu, C. W. Kee, L. Zong, Y. Pan, K.-W. Huang, C.-H. Tan, *J. Am. Chem. Soc.* **2011**, *133*, 2828.

[95] B. Lygo, C. Beynon, C. Lumley, M. C. McLeod, C. E. Wade, *Tetrahedron Lett.* **2009**, *50*, 3363.

[96] S. Arai, K. Tokumaru, T. Aoyama, *Chem. Pharm. Bull.* **2004**, *52*, 646.

[97] U. Filp, A. L. Pees, C. Taddei, A. Pekošak, A. D. Gee, A. D. Windhorst, A. J. Poot, *Eur. J. Org. Chem.* **2017**, *2017*, 5154.

[98] S. Wen, X. Li, W. Yao, A. Waheed, N. Ullah, Y. Lu, *Eur. J. Org. Chem.* **2016**, *2016*, 4298.

[99] L. Bernardi, J. López-Cantarero, B. Niess, K. A. Jørgensen, *J. Am. Chem. Soc.* **2007**, *129*, 5772.

[100] T. Cadart, V. Levacher, S. Perrio, J.-F. Brière, *Adv. Synth. Catal.* **2018**, *360*, 1499.

[101] W. Nerinckx, M. Vandewalle, *Tetrahedron: Asymmetry* **1990**, *1*, 265.

[102] According to a Reaxys® search carried out in August 2018.

[103] J. S. Bandar, A. Tanaset, T. H. Lambert, *Chem.–Eur. J.* **2015**, *21*, 7365.

[104] E. J. Corey, Y. Bo, J. Busch-Petersen, *J. Am. Chem. Soc.* **1998**, *120*, 13000.

[105] E. J. Corey, M. C. Noe, F. Xu, *Tetrahedron Lett.* **1998**, *39*, 5347.

[106] C. M. Gasparski, M. J. Miller, *Tetrahedron* **1991**, *47*, 5367.

[107] S. Mettath, G. S. C. Srikanth, B. S. Dangerfield, S. L. Castle, *J. Org. Chem.* **2004**, *69*, 6489.

[108] T. Ooi, M. Kameda, M. Taniguchi, K. Maruoka, *J. Am. Chem. Soc.* **2004**, *126*, 9685.

[109] B. Lygo, B. Allbutt, E. H. M. Kirton, *Tetrahedron Lett.* **2005**, *46*, 4461.

[110] M. A. Watzky, R. G. Finke, *J. Am. Chem. Soc.* **1997**, *119*, 10382.

[111] S. A. Bartlett, K. A. Badiola, H. Arandiyan, A. F. Masters, T. Maschmeyer, *Eur. J. Inorg. Chem.* **2018**, *2018*, 3384.

[112] L. Bentea, M. A. Watzky, R. G. Finke, *J. Phys. Chem. C* **2017**, *121*, 5302.

[113] E. V. Anslyn, D. A. Dougherty, *Modern Physical Organic Chemistry*, University Science Books, **2006**.

[114] B. F. Rahemtulla, H. F. Clark, M. D. Smith, *Angew. Chem., Int. Ed.* **2016**, *55*, 13180.

[115] B. F. Rahemtulla, *Development of Cation-Directed Acylation Reactions*, DPhil thesis, University of Oxford, Oxford, **2018**.

[116] R Core Team, *R: A Language and Environment for Statistical Computing*, R Foundation for Statistical Computing, Vienna, **2019**.

[117] F. G. Bordwell, *Acc. Chem. Res.* **1988**, *21*, 456.

[118] W. N. Olmstead, Z. Margolin, F. G. Bordwell, *J. Org. Chem.* **1980**, *45*, 3295.

[119] J. Burés, *Angew. Chem., Int. Ed.* **2016**, *55*, 2068.

[120] M. Li, D. Constantinescu, L. Wang, A. Mohs, J. Gmehling, *Ind. Eng. Chem. Res.* **2010**, *49*, 4981.

[121] S. S. Yufit, S. S. Zinovyev, *Tetrahedron* **1999**, *55*, 6319.

[122] S. S. Yufit, S. S. Zinovyev, *J. Phys. Org. Chem.* **2001**, *14*, 343.

[123] T. Okino, Y. Takemoto, *Org. Lett.* **2001**, *3*, 1515.

[124] S.-s. Jew, J.-H. Lee, B.-S. Jeong, M.-S. Yoo, M.-J. Kim, Y.-J. Lee, J. Lee, S.-h. Choi, K. Lee, M. S. Lah, H.-g. Park, *Angew. Chem., Int. Ed.* **2005**, *44*, 1383.

[125] A. S. Abramovitz, V. Massey, *J. Biol. Chem.* **1976**, *251*, 5321.

[126] K. Kaupmees, A. Trummal, I. Leito, *Croat. Chem. Acta* **2014**, *87*, 385.

[127] R. Schwesinger, H. Schlemper, C. Hasenfratz, J. Willaredt, T. Dambacher, T. Breuer, C. Ottaway, M. Fletschinger, J. Boele, H. Fritz, D. Putzas, H. W. Rotter, F. G. Bordwell, A. V. Satish, G.-Z. Ji, E.-M. Peters, K. Peters, H. G. von Schnering, L. Walz, *Liebigs*

*Ann.* **1996**, 1055.

[128] R. W. Alder, P. S. Bowman, W. R. S. Steele, D. R. Winterman, *Chem. Commun.* **1968**, 723.

[129] W. M. Haynes, D. R. Lide, T. J. Bruno, *CRC Handbook of Chemistry and Physics : A Ready-reference Book of Chemical and Physical Data*, CRC Press, Boca Raton, 95th edition, **2014**.

[130] D. C. Warhurst, J. C. Craig, I. S. Adagu, D. J. Meyer, S. Y. Lee, *Malar. J.* **2003**, *2*, 26.

[131] E. A. Castro, M. Aliaga, P. R. Campodonico, J. R. Leis, L. García-Río, J. G. Santos, *J. Phys. Org. Chem.* **2008**, *21*, 102.

[132] W. M. Haynes, D. R. Lide, T. J. Bruno, *CRC Handbook of Chemistry and Physics : A Ready-reference Book of Chemical and Physical Data*, CRC Press, Boca Raton, 97th edition, **2016**.

[133] A. B. Pangborn, M. A. Giardello, R. H. Grubbs, R. K. Rosen, F. J. Timmers, *Organometallics* **1996**, *15*, 1518.

[134] D. B. G. Williams, M. Lawton, *J. Org. Chem.* **2010**, *75*, 8351.

[135] W. C. Still, M. Kahn, A. Mitra, *J. Org. Chem.* **1978**, *43*, 2923.

[136] P. Danner, M. Bauer, P. Phukan, M. E. Maier, *Eur. J. Org. Chem.* **2005**, *2005*, 317.

[137] P. Nun, V. Pérez, M. Calmès, J. Martinez, F. Lamaty, *Chem.–Eur. J.* **2012**, *18*, 3773.

[138] M. J. O'Donnell, R. L. Polt, *J. Org. Chem.* **1982**, *47*, 2663.

[139] T. Perrard, J.-C. Plaquevent, J.-R. Desmurs, D. Hébrault, *Org. Lett.* **2000**, *2*, 2959.

[140] M. R. Crampton, I. A. Robotham, *J. Chem. Res.* **1997**, 22.